DYNAMIC PROPERTIES OF FROZEN COHESIONLESS SOILS UNDER CYCLIC TRIAXIAL LOADING CONDITIONS

by

Ted S. Vinson, Ronald L. Czajkowski, and John C. Li
Department of Civil Engineering

Volume II of II
Final Report of Research Conducted Under Research Grant ENG74-13506
SHEAR MODULI AND DAMPING FACTORS IN FROZEN SOILS
for the Period October 1, 1974 to September 30, 1976

sponsored by the
NATIONAL SCIENCE FOUNDATION
Washington, D.C. 20550

Report No. MSU-CE-77-1

January 1977

Division of Engineering Research
MICHIGAN STATE UNIVERSITY
East Lansing, Michigan 48824

BIBLIOGRAPHIC DATA SHEET	1. Report No. MSU-CE-77-1	2.	3. Recipient's Accession No. PB284952

4. Title and Subtitle

DYNAMIC PROPERTIES OF FROZEN COHESIONLESS SOILS UNDER CYCLIC TRIAXIAL LOADING CONDITIONS

5. Report Date: January 1977

6.

7. Author(s) Ronald L. Czajkowski, Ted S. Vinson (Oregon State University), and John C. Li

8. Performing Organization Rept. No.

9. Performing Organization Name and Address

Division of Engineering Research
Michigan State University
East Lansing, Michigan 48824

10. Project/Task/Work Unit No.

11. Contract/Grant No. ENG74-13506

12. Sponsoring Organization Name and Address

National Science Foundation
Washington, D.C. 20550

13. Type of Report & Period Covered Final Oct 1,1974 to Sept. 30,19

14.

15. Supplementary Notes Volume II of II; Final Report of research conducted under project entitled "Shear Moduli and Damping Factors in Frozen Soils"

16. Abstracts As part of a long-term study to evaluate dynamic properties of frozen soils under simulated earthquake and low frequency loading conditions, cyclic triaxial tests were performed on laboratory prepared samples of frozen silt and sand. Two types of silt were used in the research program: Hanover and Alaska. The samples were tested at axial strain amplitudes from approximately 2 x 10^{-3} to 8 x 10^{-2}%, temperatures from -1 to -10°C, frequencies from 0.05 to 10.0 cps, and confining pressures from 0 to 200 psi. Values of dynamic Young's modulus obtained ranged from 1 to 10^5 to 35 x 10^5 psi for Hanover silt and from 1 x 10^5 to 22 x 10^5 psi for Alaska silt; values of damping ratio obtained ranged from .02 to .36 for Hanover silt and from .02 to .32 for Alaska silt. The frozen Ottawa sand samples were prepared at three sand contents: 20, 45 and 65% (by volume). The samples were tested at axial strain amplitudes from approximately 2 x 10^{-3} to 4 x 10^{-2}%, temperatures from -1 to -10°C, frequencies from 0.05 to 5.0 cps, and confining pressures from 0 to 200 psi. Values of dynamic Young's modulus obtained ranged from 2 x 10^5 to 38 x 10^5 psi; values of damping ratio ranged from .02 to .27.

17. Key Words and Document Analysis. 17a. Descriptors

* Geotechnical Engineering
* Dynamics
* Earthquakes
* Permafrost
* Cohesionless soils
* Silt
* Sand

Cyclic Loading
Damping
Young's Modulus
Triaxial tests
Frozen soils

17b. Identifiers/Open-Ended Terms

17c. COSATI Field/Group 8/13; 8/12; 8/11

18. Availability Statement No restriction on distribution.

[redacted] National Technical Information Service

NSF approved 08/19/78

19. Security Class (This Report) UNCLASSIFIED

20. Security Class (This Page) UNCLASSIFIED

22. Price PCA14/MF A01

FORWARD

This report presents the results from a research project entitled "Shear Moduli and Damping Factors in Frozen Soils" sponsored by the National Science Foundation under Grant ENG74-13506. The Principal Investigator for the research project was Dr. Ted S. Vinson, Associate Professor of Civil Engineering, Michigan State University. Mr. Thira Chaichanavong, Mr. Ronald L. Czajkowski, and Mr. John C. Li, Graduate Research Assistants in the Division of Engineering Research, conducted the laboratory tests associated with the study. Ms. Charlene Burns, Ms. Sheila Eddington, and Ms. Geraldine Wright, Undergraduate Research Aides in the Division of Engineering Research, assisted in the data reduction and presentation. Mr. Dave Aditays and Mr. Elbert Mills, Undergraduate Research Aides in the Division of Engineering Research, assisted in the development and fabrication of the electronic instrumentation associated with the test system. Mr. Don Childs, Shop Supervisor in the Division of Engineering Research, assisted in the design and construction of the mechanical and hydraulic components associated with the test system. Ms. Charlene Burns and Ms. Connie Schweitz typed the final draft of the report. Finally, Dr. O.B. Andersland offered many helpful suggestions during the course of the study. His contribution is sincerely appreciated.

The results of the research project are presented in two volumes entitled: "Dynamic Properties of Ice and Frozen Clay Under Cylic Triaxial Loading Conditions" and "Dynamic Properties of Frozen Cohesionless Soils Under Cyclic Triaxial Loading Conditions." The work presented in this volume is associated with the experimental techniques employed to evaluate dynamic properties of frozen cohesionless soils, a discussion of the experimental results, and a comparison of the experimental results of the present study to those of previous studies.

ABSTRACT

As part of a long-term study to evaluate dynamic properties of frozen soils under simulated earthquake and low frequency loading conditions, cyclic triaxial tests were performed on laboratory prepared samples of frozen silt and sand. The cyclic triaxial test setup consists of four basic components: (1) an MTS electrohydraulic closed loop test system which applies a cyclic deviator stress to the sample, (2) a triaxial cell which contains the sample and noncirculating coolant, (3) a refrigeration unit and cold bath which circulates the coolant around the triaxial cell, (4) output recording devices to monitor the load (stress) and displacement (strain) of the sample during the test.

Two types of silt were used in the research program: Hanover and Alaska. The silt samples were generally prepared at two water contents to assess the influence of water content and dry density on the dynamic properties of silts. The samples were tested at axial strain amplitudes from approximately 2×10^{-3} to 8×10^{-2}%, temperatures from -1 to -10°C, frequencies from 0.05 to 10.0 cps, and confining pressures from 0 to 200 psi. Values of dynamic Young's modulus obtained ranged from 1×10^5 to 35×10^5 psi for Hanover silt and from 1×10^5 to 22×10^5 psi for Alaska silt. The test results indicate that dynamic Young's modulus decreases with increasing frequency and descending temperature. The relationship between dynamic Young's modulus and water content varies; in some cases dynamic Young's modulus increases with increasing water content and in other cases it decreases. Dynamic Young's modulus is apparently not affected by confining pressure. Values of damping ratio obtained ranged from .02 to .36 for Hanover silt and from .02 to .32 for Alaska silt. The test results indicate that damping ratio generally increases with increasing axial strain amplitude and decreases with increasing frequency, increasing water content and descending temperature. Damping ratio is generally not significantly influenced by confining pressure.

The frozen Ottawa sand samples were prepared at three sand contents: 20, 45, and 65% (by volume). This allowed the influence of dry density on the dynamic properties of sand-ice systems to be assessed. The samples were tested at axial strain amplitudes from approximately 2×10^{-3} to 4×10^{-2}%, temperatures from -1 to -10°C, frequencies

from 0.05 to 5.0 cps, and confining pressures from 0 to 200 psi. Values of dynamic Young's modulus obtained ranged from 2×10^5 to 38×10^5 psi. The test results indicate that dynamic Young's modulus decreases in general, with increasing axial strain amplitude and increases, in general, with increasing confining pressure, sand content and frequency and descending temperature. The test results indicate that, in general, damping ratio decreases with increasing confining pressure and descending temperature and increases with increasing sand content. There appears to be no well-defined relationship between damping ratio of frozen sand and strain amplitude or confining pressure.

The dynamic properties of the frozen cohesionless soils tested in the present study were compared to those obtained in previous studies. In general, there is good agreement between the wave velocity-temperature relationships obtained in the present study to those obtained in previous studies. The values of damping ratio determined in the present study are higher than those obtained in a previous study.

TABLE OF CONTENTS

LIST OF TABLES

LIST OF FIGURES

LIST OF SYMBOLS

cp	confining pressure
D	damping ratio
e	void ratio
E_d	dynamic Young's modulus
E*	complex Young's modulus
F, f	frequency
G	(dynamic) shear modulus or dynamic modulus of rigidity
G*	complex shear modulus
S	degree of saturation
T	temperature
V_L	longitudinal wave velocity
V_p,P-wave	compression wave velocity
V_S,S-wave	shear wave velocity
δ	lag angle between stress vector and strain vector
ε_A	axial strain
θ	temperature
λ	damping ratio
μ	Poisson's ratio
ρ	density
σ_D, σ_o	dynamic stress
σ_1,σ_2,σ_3	major, intermediate and minor principal stress

CHAPTER 1

INTRODUCTION

1.1 Purpose and Scope of Studies

As part of a long-term study to evaluate dynamic properties of frozen soils under simulated earthquake and low frequency loading conditions, dynamic Young's moduli and damping ratios of several types of artifically frozen soils and ice at two densities have been evaluated using cyclic triaxial test equipment. The scope of studies associated with the research program includes the development of the cyclic triaxial test system and experimental techniques employed to evaluate dynamic properties of frozen soils and ice, a discussion of the experimental results, and a comparison of the experimental results obtained in the present study to those obtained by previous investigators.

The results of the research work are presented in two volumes entitled: "Dynamic Properties of Ice and Frozen Clay Under Cyclic Triaxial Loading Conditions" and "Dynamic Properties of Frozen Cohesionless Soils Under Cyclic Triaxial Loading Conditions." The work presented in this volume is associated with the experimental techniques employed to evaluate dynamic properties of frozen cohesionless soils, a discussion of the experimental results, and a comparison of the experimental results of the present study to those obtained by previous investigators. Specifically, in Chapter 2 a thorough review of previous studies to evaluate dynamic properties of frozen cohesionless soils is presented. All of the information given in Chapter 2 is associated with field or laboratory experimental methods which are significantly different from the method employed in the research program. Chapter 3 provides information on the laboratory preparation of samples of frozen cohesionless soils, installation of the samples in a triaxial cell, and the procedure used to test the samples. Chapter 4 presents the experimental results on the dynamic properties of frozen silt. The influence on dynamic properties caused by changes in temperature, confining pressure, frequency, strain amplitude and water content is included. In Chapter 5 the experimental results on the dynamic properties of frozen sand are presented. The influence on dynamic properties caused by changes in temperature, confining pressure, frequency, strain amplitude, and sand content is included. Chapter 6 presents a comparison of the dynamic properties of frozen cohesionless soils obtained

in the research program to those obtained by previous investigators. Chapter 7 summarizes the results of the research program and presents conclusions that can be reached.

1.2 Background

An understanding of the research work is enhanced by a knowledge of the mechanical properties of frozen soils and thermal characteristics of frozen soil deposits, the dynamic properties of unfrozen soils, and fundamentals of cyclic triaxial testing. This is presented in Volume I. To better understand the extent to which the soils tested in the research program are representative of those occurring in frozen soil deposits, the remainder of this chapter provides information on the distribution of various soil deposits in Alaska.

1.2.1 Distribution of Frozen Soil Deposits in Alaska

The unconsolidated surficial deposits in Alaska consist of soils of all types and of all origins. They have been described and mapped by many investigators and are summarized by Woods et al (1962) and Williams and Waller (1963). An evaluation of the various soil deposits in Alaska is best made on a regional basis; the basic physiographic regions of Alaska and corresponding soil deposits associated with each region are summarized in Figures 1.1 and 1.2.

Northern Alaska as discussed here includes three physiographic regions: the Arctic Rockies, the Arctic Foothills, and the Arctic Coastal Plain. The Arctic Rockies, loosely synonymous with the Brooks Range, is generally a mountainous area with little or no soil cover. The Arctic Foothills lie between the Arctic Rockies to the south and the Arctic Coastal Plain to the north and are characterized by erosional rather than depositional features; soil deposits are thin and generally consist of sand and silt, with some gravel associated with streams. The Arctic Coastal Plain is the northernmost region and contains extensive deposits of fluvial and marine sediments up to 150 feet thick. The sediments consist primarily of sands and silts with occasional gravel, clay, and peat. The soils are generally permanently frozen over their entire depth, with permafrost extending from 600 to 1300 feet beneath the ground surface.

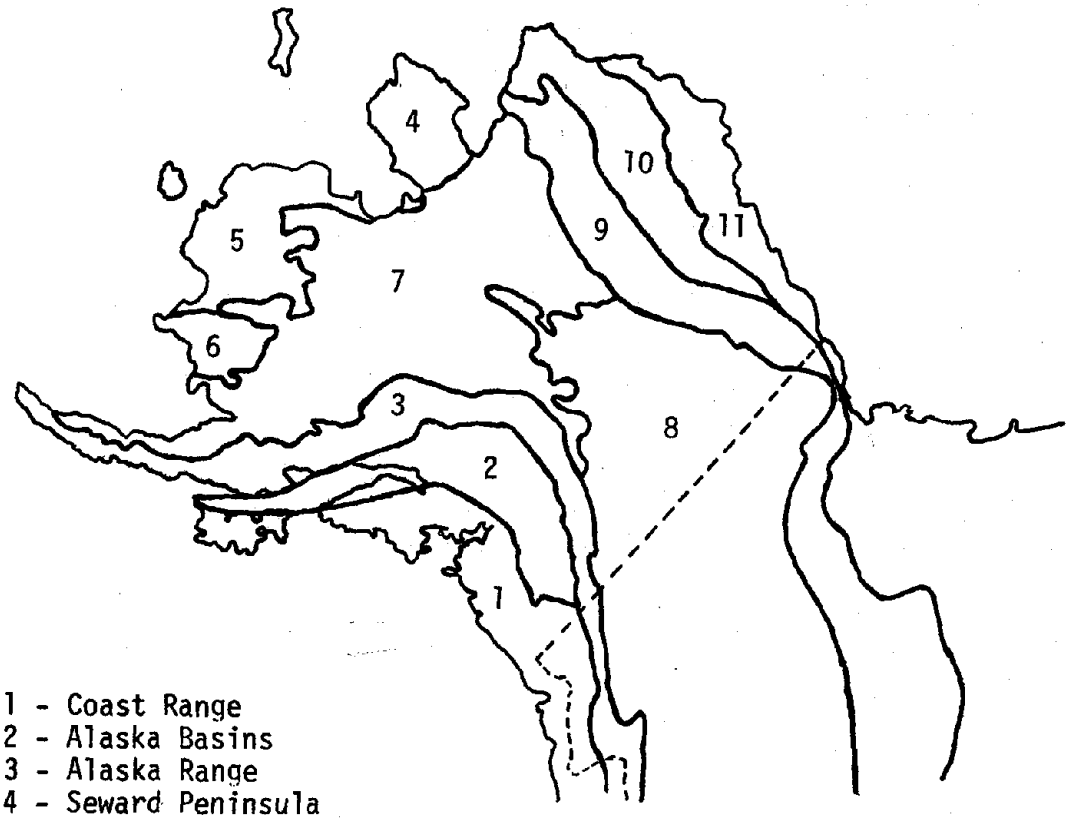

1 - Coast Range
2 - Alaska Basins
3 - Alaska Range
4 - Seward Peninsula
5 - Bering Shelf
6 - Ahklun Mountains
7 - Western Alaska
8 - Northern Plateau
9 - Arctic Rockies
10 - Arctic Foothills
11 - Arctic Coastal Plain

Figure 1.1 PHYSIOGRAPHIC REGIONS OF ALASKA (after Lovell and Roberts, 1975)

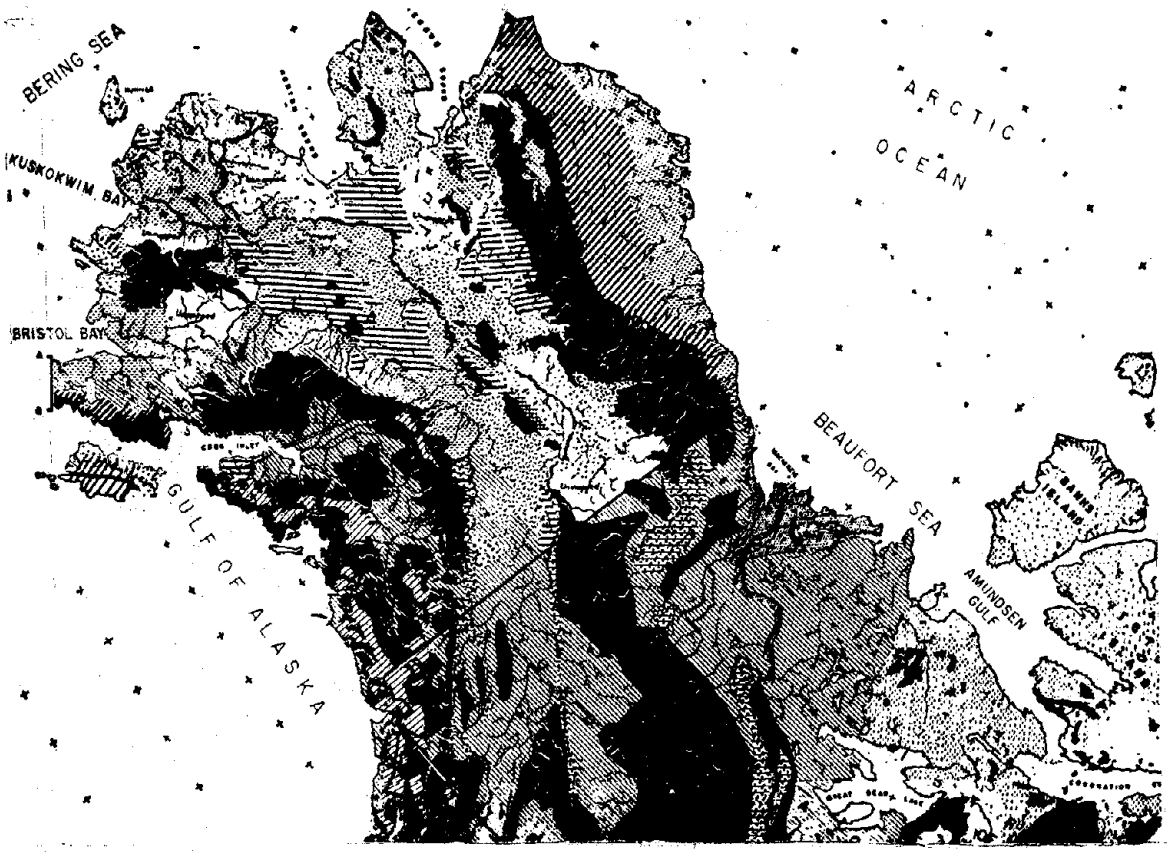

Residual Soils

Soils developed from:

- Limestone
- Sandstone; sandstone and shale
- Clay shale (with some limestone)
- Metamorphic and intrusive rocks (schist, gneiss, slate, granite, etc.)
- Extrusive rocks (basalt and lava)

Glacial Soils

- Young drift (Wisconsin and Iowan Ages)

Water-deposited Soils

- Gravel and sand
- Valley fill, consolidated to unconsolidated sands, silts, gravels, clays, tuffs, volcanic ash
- Sand-clay; interbedded and intermixed sands, clays, gravels, and silts of the Coastal Plain (includes semigranular deposits in the interior of Alaska with muskeg cover)

Miscellaneous

- Glacial ice
- Nonsoil areas (locations in which the soil is very thin or otherwise has little engineering significance because of rough topography or exposed rock; including mountains, canyons, scablands, or badlands and ice-scoured areas of the Laurentian upland)

Figure 1.2 GENERALIZED SOILS MAP OF ALASKA (after Woods et al, 1962)

Central Alaska as discussed here includes the area of Alaska between the Brooks Range in the north and the Alaska Range in the south and between the Canada-Alaska boundary in the east and the Bering Sea in the west. The area can be divided into the following physiographic regions: Northern Plateau, Western Alaska, Seward Peninsula, Bering Shelf, and Ahklun Mountains.

The most extensive soil deposits in Central Alaska are alluvial deposits associated with the Yukon and Kuskokwim drainage basins in the Northern Plateau, Western Alaska, and Bering Shelf regions. The deposits are generally thick and consist primarily of silt, gravel, and sand. The soil deposits generally occur in flood plains and terraces of valleys and outwash plains and alluvial fans fronting the mountains. The Yukon-Kuskokwim delta in the Bearing Shelf region consists of silt, sand and gravel to a depth of almost 1000 ft. Coastal plain deposits occur over the entire Bering Sea coast; on the Seward Peninsula the deposits consist primarily of gravel on the southern coast and silt on the northern coast. Additional soil deposits which occur in local areas include lacustrine deposits, glacial drift in mountainous areas which had been glaciated, and eolian deposits of silt and sand, generally less than 60 ft. thick, over alluvial deposits and upland areas.

Central Alaska is generally an area of discontinuous permafrost. The depth of permafrost varies considerably throughout the area; deposits in the Yukon-Kuskokwim delta are frozen to depths of 350 to 600 ft. while deposits bordering Bristol Bay farther south are frozen in some places to depths of 150 ft. Alluvial deposits in Central Alaska are generally unfrozen beneath river and stream channels and oxbow lakes and are frozen to depths ranging up to 300 ft. and more elsewhere. The depth and areal extent of permafrost is generally greater in higher flood-plain deposits than in lower deposits and is also greater in northern regions than in southern regions.

Southern Alaska includes the Alaska and Coast Ranges and the Alaska Basins. The Alaska and Coast Ranges consist of rugged mountainous topography and contain little or no soil cover except in low places, where gravelly glacial outwash occurs. The Alaska Basins lie between the Alaska and Coast Ranges and include the Copper River Valley in the eastern section and the Matanuska Valley in the western section. The

Copper River Valley contains deposits of granular material up to several hundred feet in thickness; silt and sand cover the granular material in the flood plain and silty glacial till occurs in areas closer to mountains. The Matanuska Valley contains thick deposits of granular outwash covered in many places by thin deposits of fluvial and eolian silt.

Southern Alaska is near the southern boundary of the permafrost zone; permafrost in the area is thus discontinuous and generally thin. In the Matanuska Valley permafrost is sporadic; in the center of the Copper River Valley, sediments are frozen to depths of 100 to 200 ft.

CHAPTER 2

DYNAMIC PROPERTIES OF FROZEN COHESIONLESS SOILS

2.1 General

This chapter provides information on the results of previous investigations to evaluate the dynamic properties of frozen cohesionless soils. The dynamic properties that have been evaluated by various investigators using different testing techniques fall into two categories:

(1) dynamic elastic properties and

(2) damping properties.

Dynamic elastic properties are given in terms of dynamic Young's and shear moduli, complex Young's and shear moduli, sound velocity, and compression, dilatational, longitudinal, irrotational, primary, bulk, or "P" and shear, transverse, secondary, rotational, or "S" wave velocities. Damping properties are expressed in terms of angle of phase lag, attenuation coefficient, damping coefficient, loss factor, quality factor, log decrement, and damping ratio. Conversion equations between the various terms can be used to allow direct comparisons to be made between the results obtained by different investigators. These equations are given in Table 2.1 of Volume I.

2.2 Previous Research on the Dynamic Properties of Frozen Soils

Field techniques have been widely used to evaluate the dynamic elastic properties of frozen soils. The most common method used is the seismic method, which involves the measurement of compressional and shear wave velocities in naturally frozen soil deposits. A summary of wave velocities in frozen cohesionless soil deposits obtained by several investigators is given in Table 2.1.

The dynamic properties of frozen cohesionless soils have been investigated using various laboratory techniques by Kaplar (1969), Nakano and Froula (1973), and Stevens (1973). Cohesionless soil samples tested in the laboratory have generally been artificially prepared; Stevens (1973), however, has tested silt which had been cored in a naturally frozen state. Kaplar (1969) and Stevens (1973) used a resonant frequency method in their testing programs; Nakano and Froula (1973) used an

Table 2.1 FIELD MEASUREMENTS OF WAVE VELOCITY IN FROZEN COHESIONLESS SOILS

Soil Types	Locality	Compression Wave Velocity (km/s) Frozen	Unfrozen	Estimated Ground Temperature °C	Reference
Coarse-Grained					
Floodplain alluvium	Fairbanks Area, Alaska	2.4 - 4.3	1.9 - 2.1	-1	Barnes, 1963
Gravel	Fairbanks Area, Alaska	4.0 - 4.6	1.8 - 2.3	-1	Barnes, 1963
Glacier moraine	Delta Junction, Alaska	2.3 - 4.0		-2	Barnes, 1963
Aeolian sand	Tetlin Junction, Alaska	2.4		-3	Barnes, 1963
Outwash gravel	Tanacross, Alaska	2.3 - 3.0		-3	Barnes, 1963
Glacier outwash	Thule, Greenland	4.5 - 4.7		-11	Roethlisberger, 1961
Glacier till	Thule, Greenland	4.7 - 4.8		-11	Roethlisberger, 1961
Glacier till	McMurdo Sound, Antarctica	3.0 - 4.3	0.5 - 1.5	-20	Bell, 1966
Till	Norman Wells, N.W.T.	2.2 - 3.6			King, et al, 1974
Saturated sand		3.2 - 4.0			Hunter, 1973
Water-saturated gravel		3.6 - 4.0			Hunter, 1973
Gravel	Klondike Area, Yukon	5.5			Hobson, 1966
Outwash with relatively thick ice lenses	Lake Vida, Antarctica	5.7 - 5.9			McGinnis, et al, 1973
Outwash	Meirs Valley, Antarctica	3.6 - 4.0			Bell, 1966
Fine-Grained					
Silt and gravel	Fairbanks Area, Alaska	2.3 - 3.0		-1	Barnes, 1963
Silt and organic matter	Fairbanks Area, Alaska	1.5 - 3.0	0.6 - 1.2	-1	Barnes, 1963
Silt with ice lenses	Eielson AFB, Alaska	2.0 - 2.8		-1.5	Blouin, 1976
Silt	Glen Creek Valley, Alaska	2.7 - 3.3		-4.2	Hunter, 1974

ultrasonic method. The apparatus and experimental technique used by each investigator is described in detail in Volume I.

2.3 Dynamic Elastic Properties of Frozen Cohesionless Soils

The influence of various parameters on the dynamic elastic properties of frozen cohesionless soils has been investigated by Kaplar (1969), Nakano and Froula (1973), and Stevens (1973). The parameters considered include stress or strain amplitude, frequency of loading, temperature, void ratio or water content, and degree of ice saturation.

2.3.1 Effect of Void Ratio

The effect of void ratio on the dynamic elastic properties of frozen cohesionless soils has been investigated by Stevens (1973) and is summarized in Figure 2.1. The complex shear modulus decreases as the void ratio increases; as the volume of ice becomes significantly greater than the volume of soil, the modulus approaches the value for ice.

2.3.2 Effect of Ice Saturation

The effect of ice saturation on the dynamic elastic properties of frozen cohesionless soils has been investigated by Stevens (1973). As shown in Figure 2.2, the complex shear modulus increases significantly as the degree of ice saturation in the voids increases. The complex shear modulus of frozen Manchester silt increases from about 0.1 GN/m^2 at 0% ice saturation to about 7.0 GN/m^2 at 100% ice saturation; the comple shear modulus of frozen Ottawa sand increases from about 0.1 GN/m^2 at 0% ice saturation to about 13.0 GN/m^2 at 100% ice saturation.

2.3.3 Effect of Temperature

The dynamic elastic properties of frozen cohesionless soils tend to decrease with increasing temperature. The decrease is generally more pronounced at higher temperatures than at lower temperatures. Kaplar (1969) has determined the longitudinal wave velocity in beams of frozen cohesionless soils as a function of temperature; the relationships for frozen New Hampshire silt, Fairbanks silt, and Yukon silt are shown in Figure 2.3. The longitudinal wave velocity decreases between -10°F

Design.		f kHz	σ_D kN/m²	e_{min}
PG	Peabody Gravel (Kaplar[3])	4	–	0.27
MCS	McNamara Concrete Sand (Kaplar[3])	3.7	–	0.38
OS	20-30 Ottawa Sand	5	0.7	0.49
MS	Manchester Silt	5	0.7	0.65
HS	Hanover Silt	5	0.7	0.65
NHS	New Hampshire Silt (Kaplar[3])	3	–	0.57
FS	Fairbanks Silt (Stevens, Kaplar[3])	5	0.7	0.50

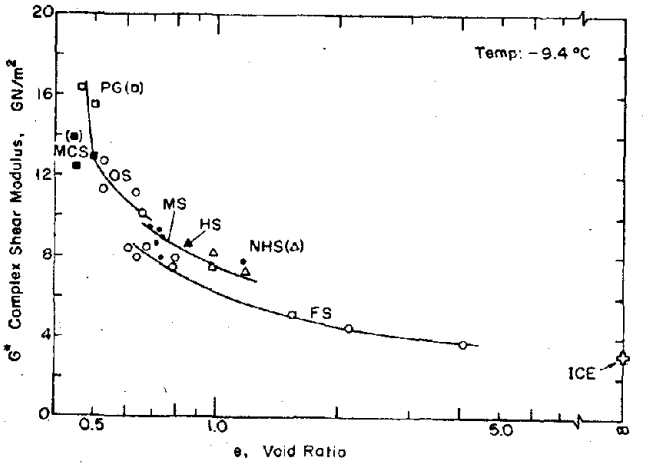

Figure 2.1 COMPLEX SHEAR MODULUS VERSUS VOID RATIO FOR FROZEN COHESIONLESS SOILS

Point Design.	Non-frozen Soils f=1kHz σ_D=34.4 kN/m²	W.C. %
A	20-30 Ottawa Sand	Dry
B'	Manchester Silt	18.3

Point Design.	Frozen Soils	f kHz	Temp °C
B	Manchester Silt	1	-3.9
D	20-30 Ottawa Sand (Nakano and Arnold[7])	1000	-10

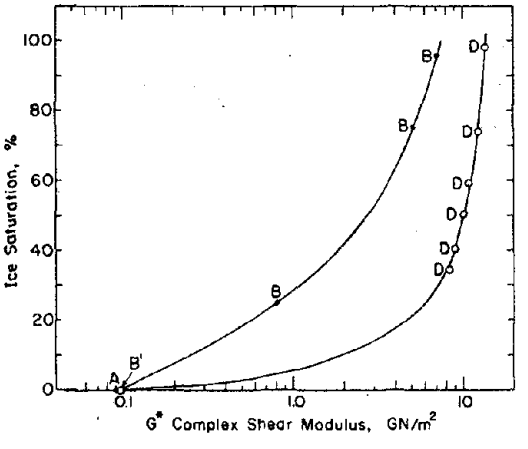

Figure 2.2 EFFECT OF ICE SATURATION ON COMPLEX SHEAR MODULUS OF FROZEN MANCHESTER SILT AND OTTAWA SAND (after Stevens, 1973)

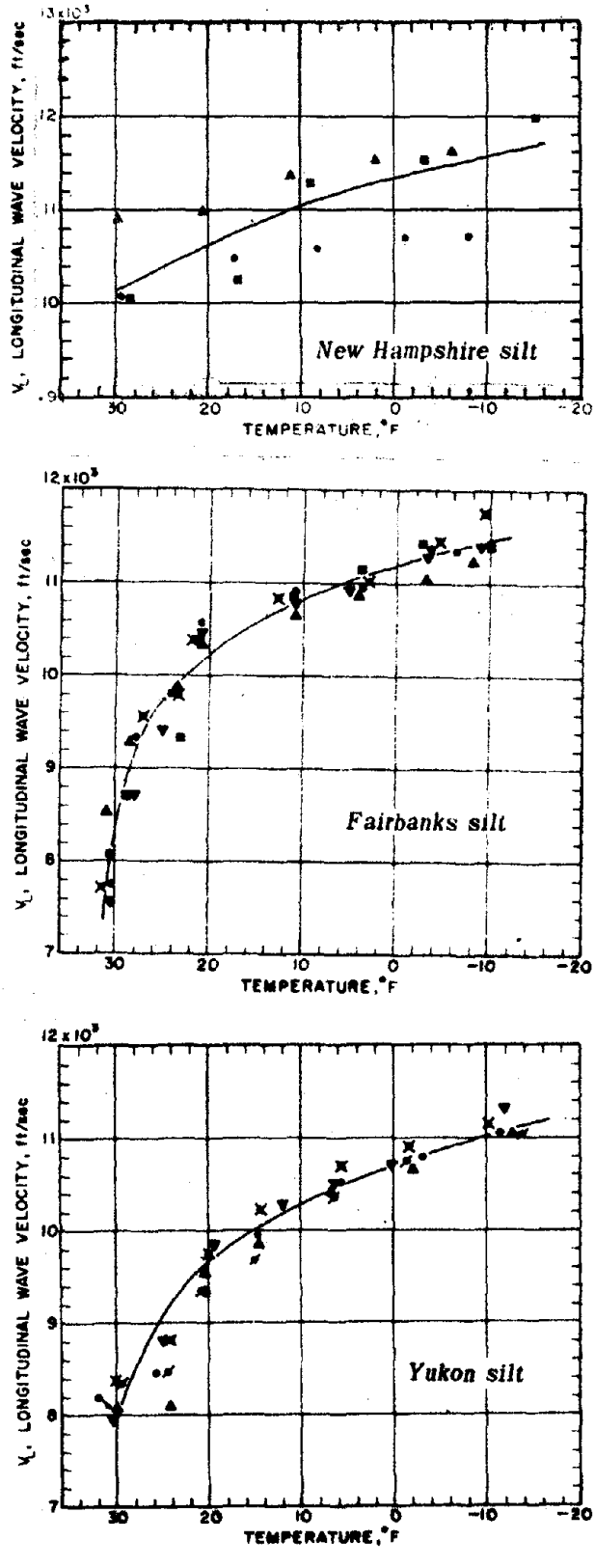

Figure 2.3 LONGITUDINAL WAVE VELOCITY VERSUS TEMPERATURE FOR FROZEN NEW HAMPSHIRE SILT, FAIRBANKS SILT, AND YUKON SILT (after Kaplar, 1969)

and 30°F from 11.6 x 10^3 to 10.1 x 10^3 ft/sec for New Hampshire silt, from 11.5 x 10^3 to 8.0 x 10^3 ft/sec for Fairbanks silt, and from 11.0 x 10^3 to 8.0 x 10^3 ft/sec for Yukon silt. The relationships for frozen Peabody gravelly sand, McNamara Concrete sand, and East Boston till are shown in Figure 2.4. The longitudinal wave velocity decreases between -10°F and 30°F from 14.8 x 10^3 to 13.4 x 10^3 ft/sec for Peabody gravelly sand, from 13.3 x 10^3 to 11.7 x 10^3 ft/sec for McNamara concrete sand, and from 11.9 x 10^3 to approximately 7.7 x 10^3 ft/sec for East Boston till.

Nakano and Froula (1973) have determined the shear wave velocity of frozen Hanover silt and Ottawa sand as a function of temperature. The results are summarized in Figure 2.5; the shear wave velocity of Hanover silt decreases from 2.1 km/sec at -14°C to 1.9 km/sec at -1°C; the shear wave velocity of Ottawa sand decreases from 2.55 km/sec at -14°C to 2.45 km/sec at -1°C.

Stevens (1973) has studied the influence of temperature on the dynamic complex Young's and shear moduli of Manchester silt and Ottawa sand. The results are shown in Figure 2.6. The dynamic complex Young's modulus of Manchester silt decreases from 2.5 x 10^3 MN/m^2 at -18°C to 1.9 x 10^3 MN/m^2 at -4°C and to 11.0 MN/m^2 in the unfrozen state. The dynamic complex shear modulus decreases from 9.5 x 10^2 MN/m^2 at -18°C to 7.5 x 10^2 MN/m^2 at -4°C and to 5.5 MN/m^2 in the unfrozen state. The dynamic complex Young's modulus of Ottawa sand decreases from 3.5 x 10^3 MN/m^2 at -18°C to 3.0 x 10^3 MN/m^2 at -4°C and to 10 MN/m^2 in the unfrozen state. The dynamic complex shear modulus decreases from 1.5 x 10^3 MN/m^2 at -18°C to 1.4 x 10^3 MN/m^2 at -4°C and to 4 MN/m^2 in the unfrozen state.

2.3.4 Effect of Frequency

The influence of frequency on the dynamic elastic properties of frozen cohesionless soils has been studied by Stevens (1973). As shown in Figure 2.7, the complex shear modulus of frozen Hanover-Manchester silt increases slightly with increasing frequency between 1.0 kHz and 1000 kHz, with much of the increase occurring in the 1-5 kHz range. Similar results are shown for Ottawa sand. Stevens suggests that a significant decrease in shear modulus might result if testing was done at much lower frequencies.

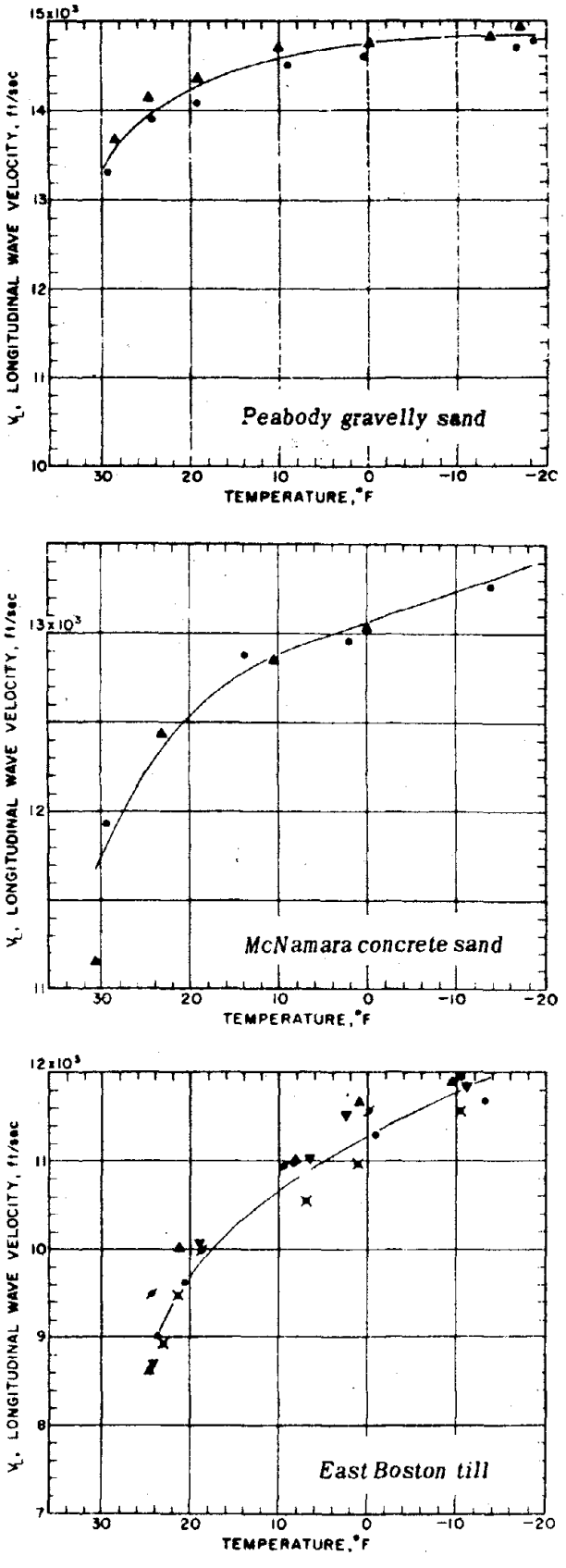

Figure 2.4 LONGITUDINAL WAVE VELOCITY VERSUS TEMPERATURE FOR FROZEN PEABODY GRAVELLY SAND, McNAMARA CONCRETE SAND, AND EAST BOSTON TILL (after Kaplar, 1969)

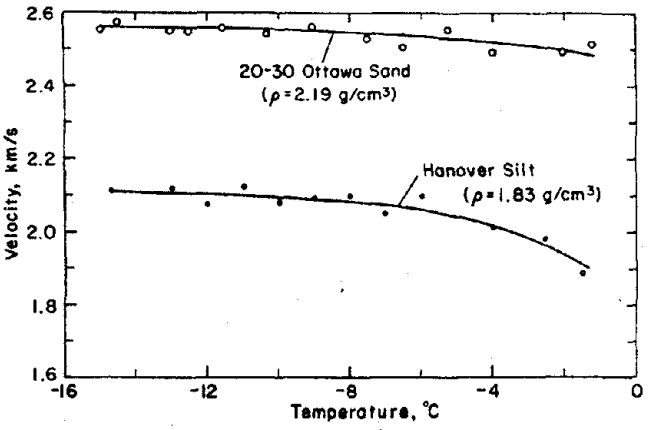

Figure 2.5 S-WAVE VELOCITY VERSUS TEMPERATURE FOR FROZEN HANOVER SILT AND OTTAWA SAND (after Nakano and Froula, 1973)

Design.	S_i %	S_w %	e	
A	99.1	–	0.53	E*20-30 Ottawa Sand
A'	–	93.8	0.60	
A''	Dry		0.50	
B	97.2	–	0.73	E*Manchester Silt
B'	–	91.4	0.73	
D	99.1	–	0.53	G*20-30 Ottawa Sand
D'	–	93.8	0.60	
D''	Dry		0.50	
E	97.2	–	0.73	G*Manchester Silt
E'	–	91.4	0.73	

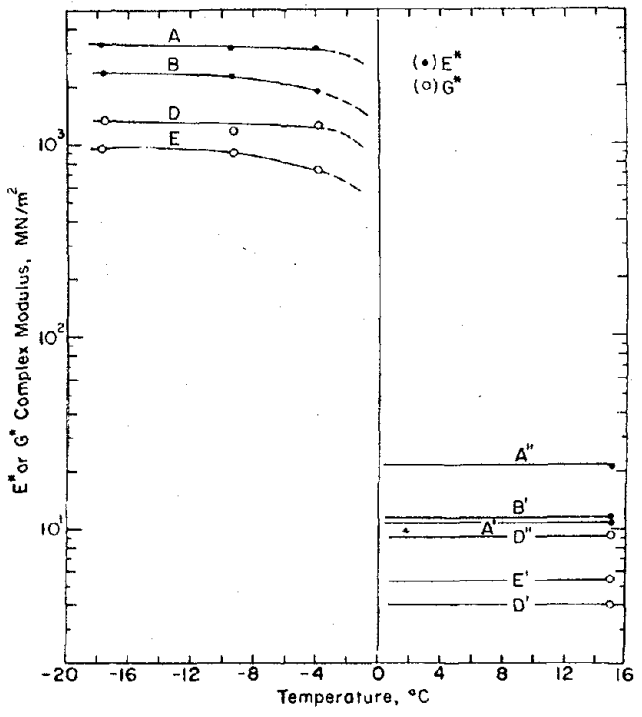

Figure 2.6 EFFECT OF TEMPERATURE ON COMPLEX MODULI OF FROZEN MANCHESTER SILT AND OTTAWA SAND (after Stevens, 1973)

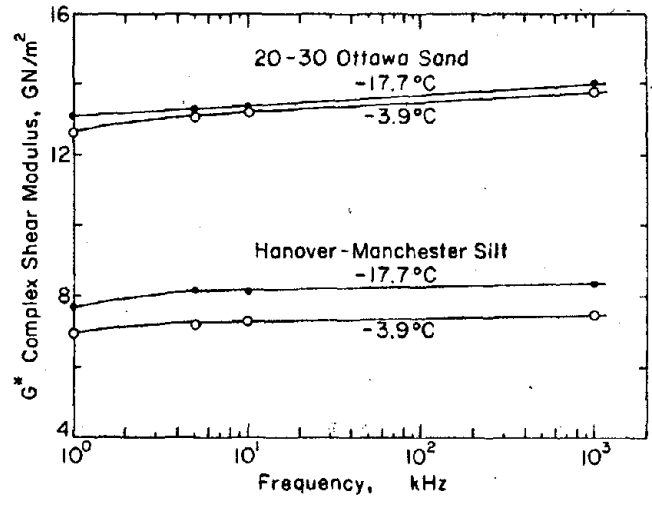

Figure 2.7 COMPLEX SHEAR MODULUS VERSUS FREQUENCY FOR FROZEN HANOVER-MANCHESTER SILT AND OTTAWA SAND (after Stevens, 1973)

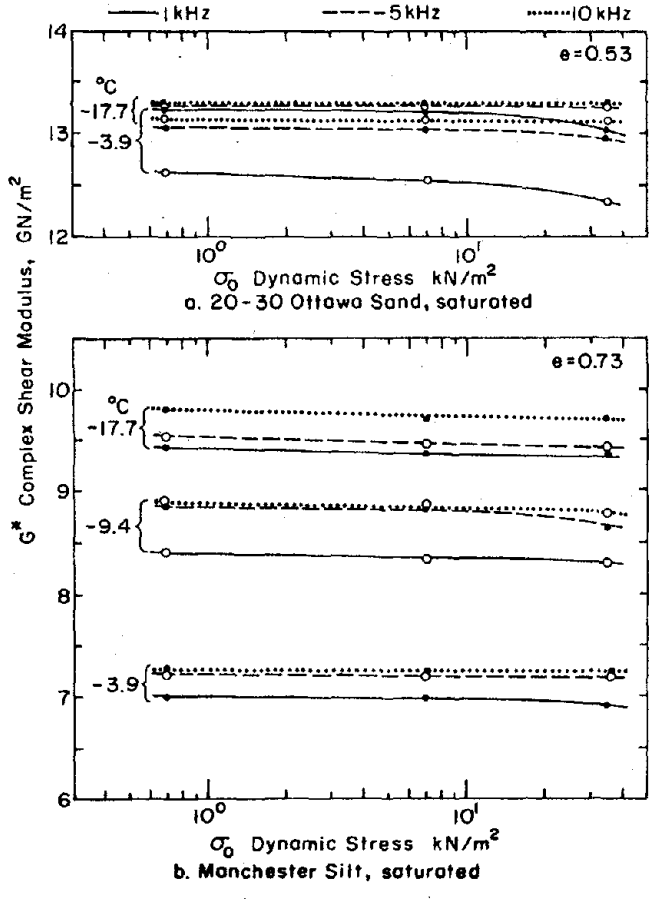

Figure 2.8 COMPLEX SHEAR MODULUS VERSUS DYNAMIC STRESS FOR FROZEN MANCHESTER SILT AND OTTAWA SAND (after Stevens, 1973)

2.3.5 Effect of Dynamic Stress or Strain

Information on the effect of dynamic stress on the dynamic elastic properties of frozen cohesionless soils is given by Stevens (1973). As shown in Figure 2.8, the complex shear modulus of Manchester silt decreases slightly with increasing dynamic stress between 0.7 and 34.5 kN/m^2. Similar results are shown for Ottawa sand. In general, the influence of stress is greater at higher temperatures, lower frequencies, and higher stress levels.

2.4 Damping Properties of Frozen Cohesionless Soils

The damping properties of frozen cohesionless soils have been studied by Stevens (1973). The influence of temperature on damping (in terms of tan δ) for Manchester silt is shown in Figure 2.9. The overall relationship between damping and temperature is not entirely clear; it appears that longitudinal damping in frozen silt is less than in unfrozen silt and decreases with increasing temperature while torsional damping in frozen silt is greater than in unfrozen silt and increases with increasing temperature. Similar results are shown for Ottawa sand although the relationships are again not obvious.

The influence of frequency on damping has been studied by Stevens (1973). As shown in Figure 2.10, damping of frozen Manchester silt and Ottawa sand decreases with increasing frequency between 1 and 10 kHz. The decrease is pronounced for Ottawa sand.

The influence of dynamic stress on damping of frozen silt has been studied by Stevens (1973) and is shown in Figure 2.11. At temperatures of -3.9 to -9.4°C damping of frozen Manchester silt increases slightly with increasing dynamic stress between 0.7 and 34.5 kN/m^2, the influence of dynamic stress on damping is generally greater at higher stress levels than at lower stress levels. At a temperature of -17.7°C damping decreases with increasing dynamic stress.

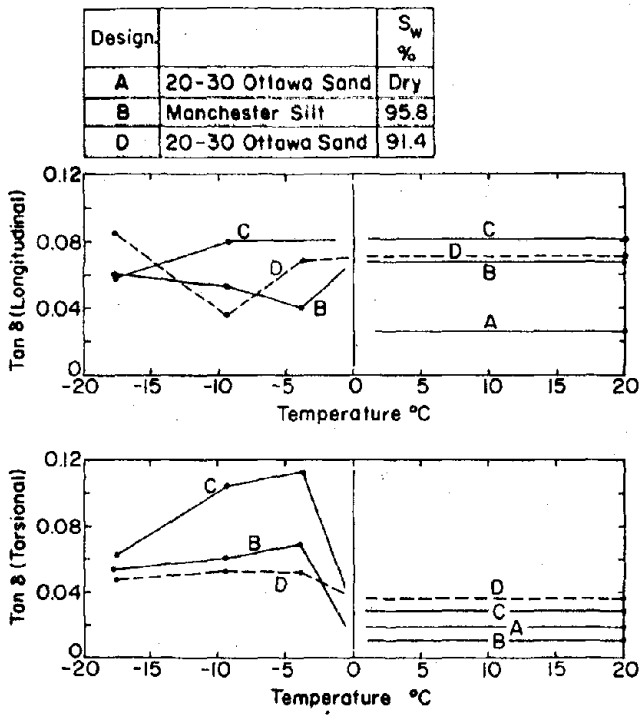

Figure 2.9 EFFECT OF TEMPERATURE ON TAN δ OF FROZEN MANCHESTER SILT AND OTTAWA SAND (after Stevens, 1973)

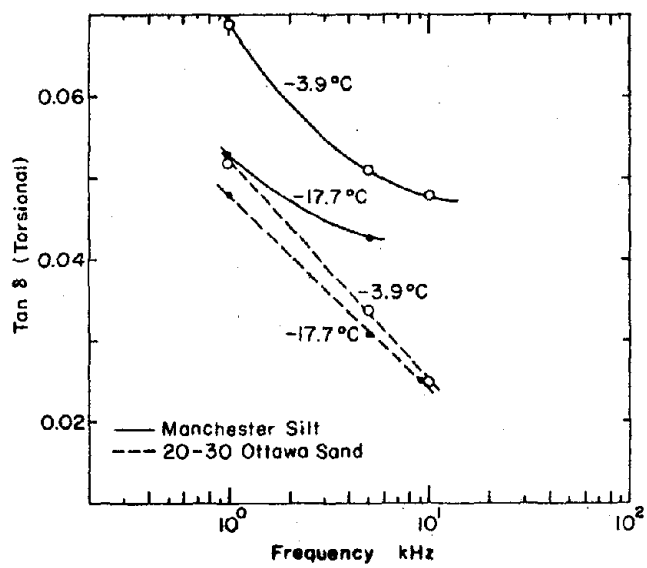

Figure 2.10 EFFECT OF FREQUENCY ON TAN δ OF FROZEN MANCHESTER SILT AND OTTAWA SAND (after Stevens, 1973)

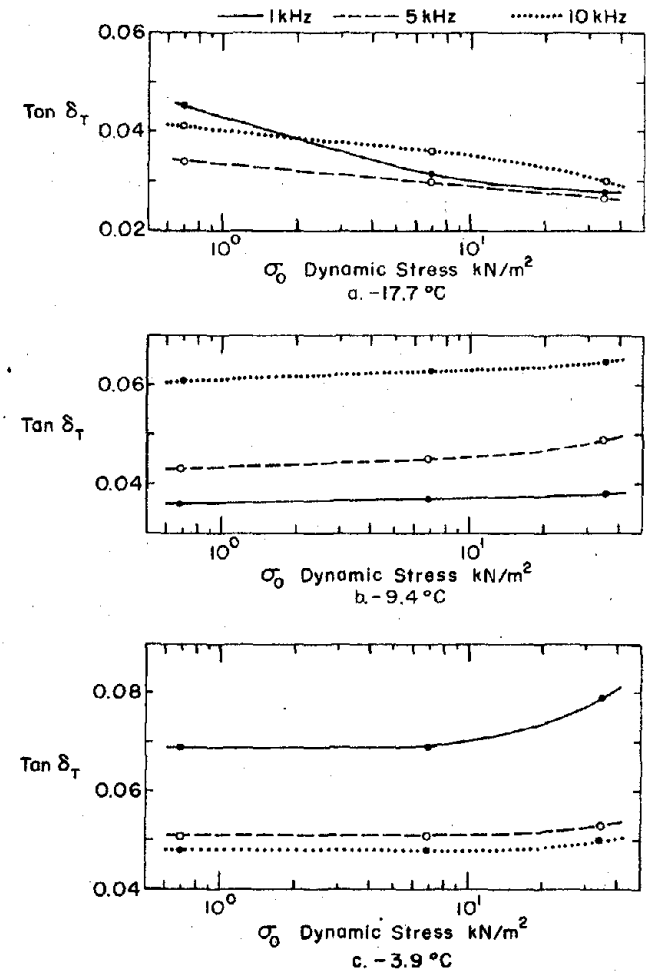

Figure 2.11 EFFECT OF DYNAMIC STRESS ON TAN δ OF FROZEN MANCHESTER SILT (after Stevens, 1973)

CHAPTER 3

SAMPLE PREPARATION, SAMPLE INSTALLATION, TRIAXIAL CELL ASSEMBLY, AND TEST PROCEDURE

3.1 General

This chapter deals with the laboratory preparation of frozen silt and sand samples, installation of the samples in a triaxial cell, triaxial cell assembly, and the test procedure used in the program. A basic knowledge of the components of the test system is assumed. The MTS electrohydraulic closed-loop test system, the refrigeration unit, the triaxial cell, and the output recording devices used in the testing program are described in detail in Volume I.

3.2 Preparation of Frozen Silt Samples

Two types of silt were used in the testing program: Hanover silt, termed HS, and Alaska silt, termed AS. The gradations and physical properties of both silts are given in Figure 3.1. Samples were prepared at two water contents for each of the two silts to assess the influence of water content and dry density on the dynamic properties of silts. All samples were formed and frozen to aluminum coupling devices in a hollow cylindrical teflon mold 30.5 cm high, 7.1 cm in inside diameter, and 1.3 cm thick.

The high density (low water content) samples for both Hanover silt and Alaska silt were prepared as follows:

(1) A silt slurry with a water content of approximately 36% was made by adding distilled water to oven-dried silt and mixing thoroughly. The slurry was then placed in a triaxial cell and consolidated isotropically under a cell pressure of 40 psi for for 24 hours.

(2) The sample was removed from the consolidation cell and trimmed to a diameter approximately equal to the inside diameter of the mold. Material trimmed from the sample was packed tightly around the couplings on the caps; the sample and the caps were then placed in the mold. The caps were then hammered vigorously to assure a good bond between the main portion of the sample

Design.	Soil	LL	PL	PI
HS	Hanover Silt	22	--	NP
AS	Alaska Silt	28	23	5
OS	Ottawa Sand	NP	NP	NP

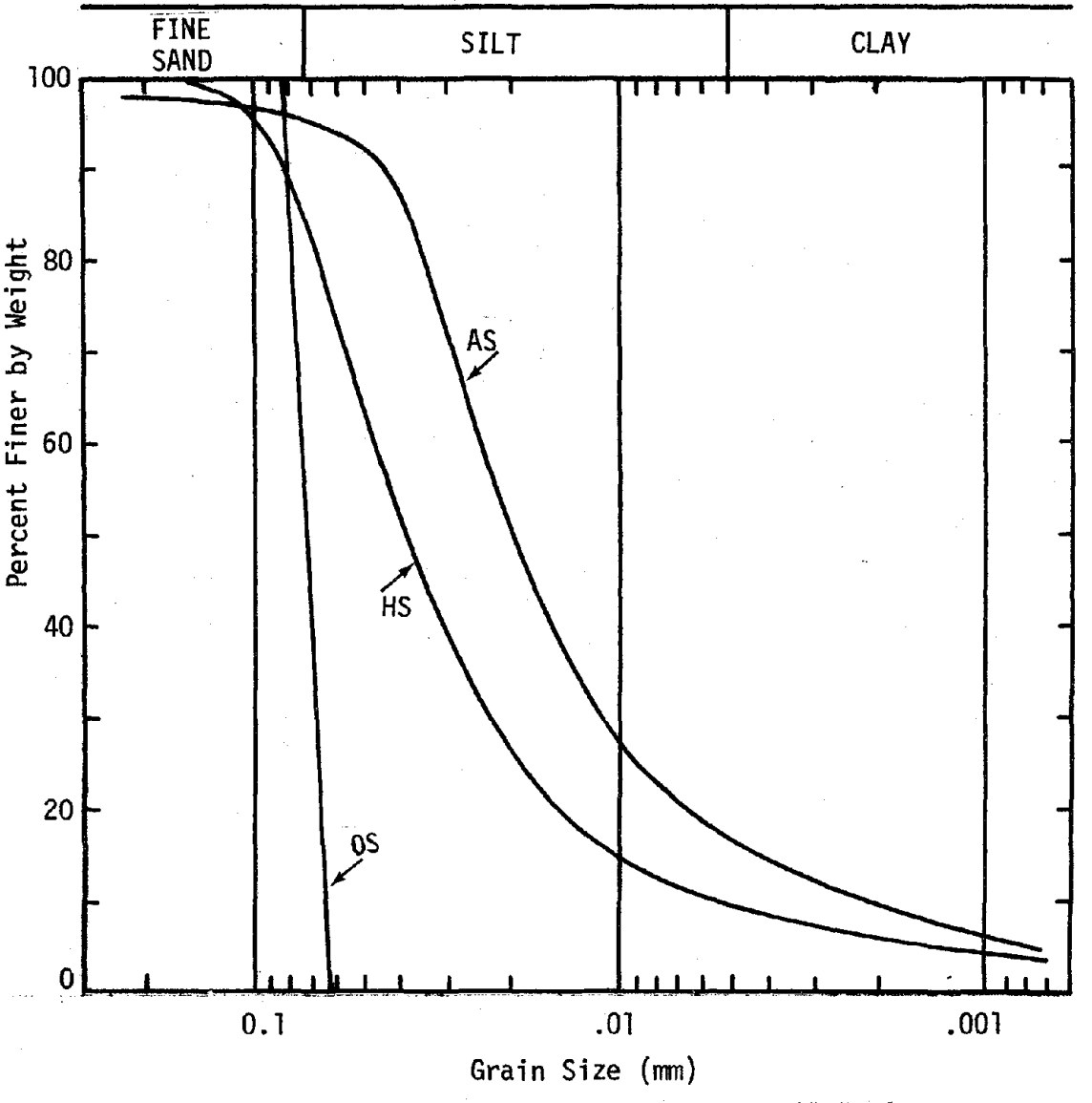

Figure 3.1 GRAIN SIZE DISTRIBUTION OF HANOVER SILT, ALASKA SILT, AND OTTAWA SAND

and the material around the couplings and to allow any entrapped air to escape. A small hole near the top of the mold facilitated the removal of air. The mold was then placed in a freezer at -30 ± 1°C for approximately 24 hours.

(3) The mold was removed from the freezer. The sample was extruded from the mold as quickly as possible, weighed, transferred to a freezer, and jacketed with two rubber membranes. The sample was now ready for installation in the triaxial cell.

The high density frozen silt samples were uniform in appearance with occasional ice lenses in the outer portion of the sample and were classified as ML, Nbn (Linell and Kaplar, 1966). The water content was reasonably uniform over the length of the sample, with a slightly higher water content in the vicinity of the caps. Average water contents were 21.4% for Hanover silt and 20.5% for Alaska silt.

The low density (high water content) samples for both Hanover silt and Alaska silt were prepared as follows:

(1) A silt slurry with a water content of 51% was made by adding the appropriate amount of distilled water to oven-dried silt and mixing thoroughly. The slurry was stored at a temperature slightly above 0°C for 24 hours.

(2) The teflon mold and aluminim caps were precooled to -30°C. The slurry was mixed again and poured into the mold with the bottom cap in place. Additional slurry was packed around the coupling of the top cap, which was then set in the mold and hammered to remove any entrapped air. The mold was then placed on its side in a freezer at -30°C for 24 hours. In order to prevent settling of the silt particles before freezing, the sample was rotated 180° every 10 minutes for the first three hours after being placed in the freezer.

(3) The mold was removed from the freezer and the sample was extruded, weighed, and jacketed with membranes as described above.

The resulting low density frozen silt samples were classified ML, Nbe. They contained a layer approximately .1" thick consisting of silt with ice lenses around the entire sample. While the interior of the sample appeared to be uniformly frozen with no ice lenses, the water content

varied significantly from the center to the ends of the sample. The distribution of water content over the effective length of the sample (between top and bottom coupling) for both Hanover silt and Alaska silt is shown in Figure 3.2.

It is apparent that the permeability of both silts was great enough to allow significant migration of water in both a radial direction and along the length of the sample during the freezing process. This movement occurred despite efforts to freeze the sample as quickly as possible by precooling the slurry, mold, and caps. Since a uniform water content could not be obtained, the water content was taken as the weighted average water content of the material over the effective length of the sample excluding the silt-ice layer around the outside of the sample. Average water contents determined using this technique were 35.5% for Hanover silt and 38.9% for Alaska silt.

Two samples of Alaska silt were prepared at water contents intermediate between high and low water contents. The procedure used was similar to the method used in preparation of the high water content samples, with the major difference being the use of a slurry with a water content of 36%. The frozen sample was similar in appearance to the high water content sample and had an average water content of 29.2%.

A summary of the water contents and densities of the frozen silt samples tested in the research program is given in Table 3.1.

3.3 Preparation of Frozen Sand Samples

The sand used in the testing program was commercial Ottawa sand, termed OS. The gradation and physical properties of the sand are given in Figure 3.1. Test samples were prepared at three sand contents: 20, 45, and 65% (by volume). This allowed the influence of dry density on the dynamic properties of sand-ice systems to be assessed. All samples were formed and frozen to aluminum coupling devices in a hollow cylindrical teflon mold 30.5 cm high, 7.1 cm in inside diameter, and 1.3 cm thick.

The sand-ice samples at a sand content of 20 and 45% (by volume) were prepared as follows:

(1) The mold, with the bottom cap inserted at one end, and the top cap, were placed in a large freezer box maintained at a temper-

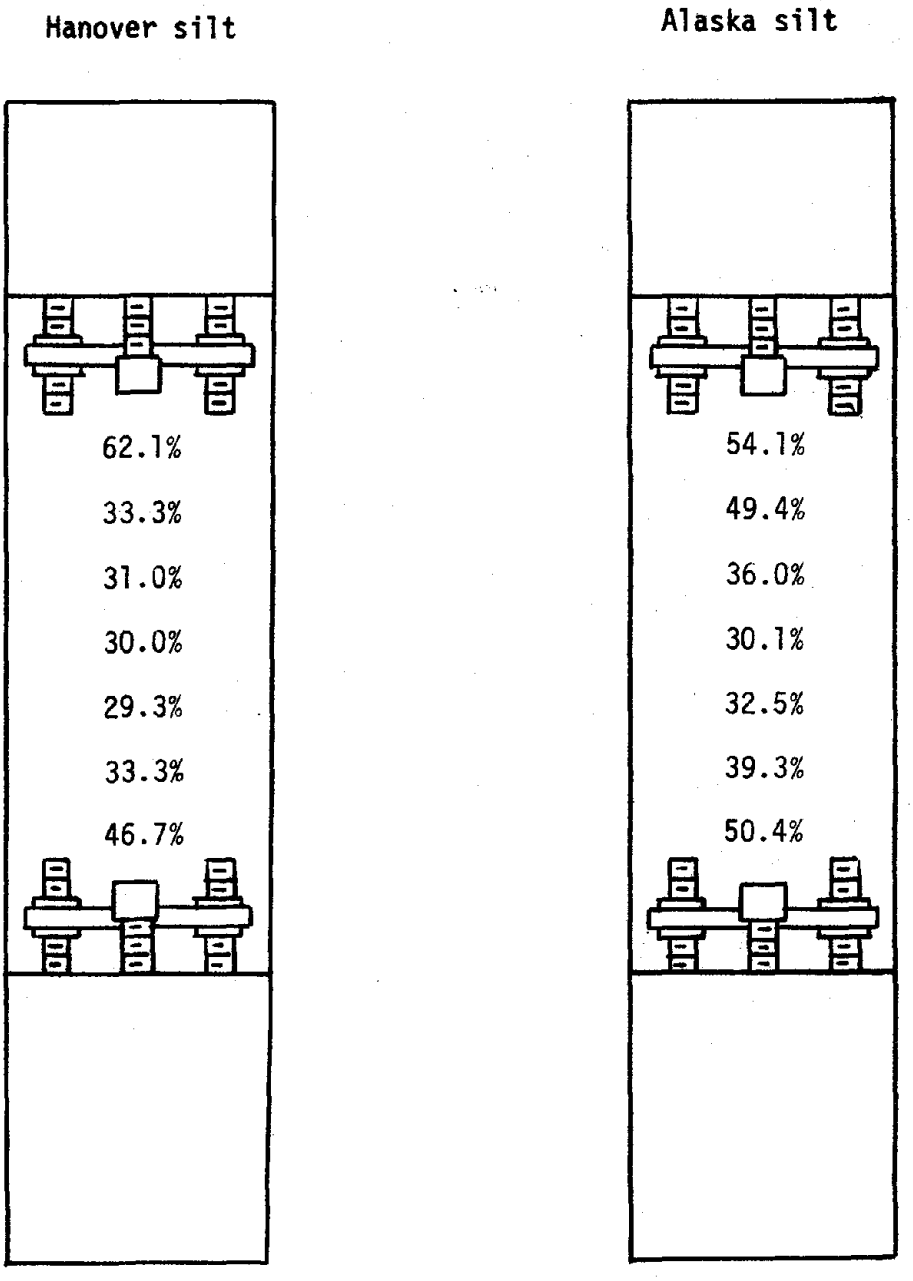

Figure 3.2 DISTRIBUTION OF WATER CONTENT OVER LENGTH OF HIGH WATER CONTENT FROZEN SILT SAMPLES

Table 3.1 WATER CONTENT AND DENSITY OF SILT SAMPLES

Soil	Average water content (%)	Testing temperature (°C)	Sample number	Water content (%)	Density (g/cc)
Hanover silt	21.4	-1	HS-14	21.7	2.04
			HS-15	22.1	2.08
		-4	HS-6	24.5	2.01
			HS-7	24.5	2.04
			HS-11	24.2	2.05
		-10	HS-21	20.9	2.06
			HS-22	21.8	2.05
	35.5	-1	HS-13	*	1.74
			HS-16	*	1.67
			HS-17	*	1.66
		-4	HS-3	*	1.87
			HS-4	*	1.85
			HS-5	*	1.78
			HS-8	*	1.77
			HS-10	*	1.72
			HS-12	*	1.72
			HS-18	*	1.71
		-10	HS-19	*	1.67
			HS-20	*	1.68
Alaska silt	20.5	-1	AS-3	22.1	2.07
			AS-4	21.9	2.06
		-4	AS-10	20.8	2.06
			AS-11	21.5	2.06
		-10	AS-13	19.7	2.09
			AS-15	19.8	2.09
	29.2	-1	AS-5	27.1	1.90
			AS-6	31.2	1.86
			AS-7	31.7	1.74
	38.9	-1	AS-1	*	1.59
			AS-2	*	1.65
		-4	AS-8	*	1.69
			AS-9	*	1.69
		-10	AS-12	*	1.66
			AS-14	*	1.66

* Average water content determined from weighted average technique using single sample rather than individual samples.

ature of -30 ± 1°C for approximately one hour.

(2) Air-dried Ottawa sand, passing a No. 20 sieve and retained on a No. 40 sieve, was cooled in a freezer box to -30°C and then mixed thoroughly with loose, dry clean snow (passing a No. 4 sieve). The amount of sand and snow were controlled by weight to insure the samples would have a 20 or 45% sand content by volume.

(3) The mold was filled to within two inches from the top with the mixture prepared in (2) and left in the freezer for approximately one hour.

(4) Precooled distilled water (close to 0°C) was poured into the mixture from the top up to the surface of the mixture and the top cap was inserted. A small hole near the top of the mold facilitated the removal of air. The mold and sample were placed in a freezer maintained at -30 ± 1°C for approximately 24 hours.

(5) The mold was removed from the freezer and the sample was extruded from the mold with a hydraulic jack. The sample was weighed, transferred to another freezer, and jacketed with two rubber membranes.

The sand-ice samples at a sand content of 20 and 45% (by volume) were classified as SP, Vs (Linell and Kaplar, 1966). They had a transverse layered structure formed by slight differences in the sand content along the longitudinal axis of the sample.

The sand-ice samples at a sand content of 65% (by volume) were prepared as follows:

(1) The mold, with the bottom cap inserted at one end, and the top cap, were placed in a large freezer box maintained at a temperature of -30 ± 1°C for approximately one hour.

(2) The mold was filled to within 2 inches from the top with a mixture of precooled Ottawa sand and water.

(3) The sample cap was forced into contact with the Ottawa sand-water mixture. The excess water was released through a small hole in the cap. The mold was vibrated to achieve a high density. The mold and sample were placed in a freezer maintained at -30 ± 1°C for approximately 24 hours.

(4) The mold was removed from the freezer and the sample was extruded from the mold with a hydraulic jack. The sample was weighed, transferred to another freezer, and jacketed with two rubber membranes.

The sand-ice samples at a sand content of 65% were classified as SP, Nb (Linell and Kaplar, 1966). The structure appeared to be very homogeneous.

A summary of the sand contents and densities of the frozen Ottawa sand-ice samples tested in the research program is given in Table 3.2.

3.4 Sample Installation, Triaxial Cell Assembly and Test Procedure

The sample installation, triaxial cell assembly, and test procedure for the frozen silt and Ottawa sand samples is essentially the same as that for the ice and frozen clay samples. The reader is referred to Sections 3.4 and 3.5 of Volume I for this information.

Table 3.2 SAND CONTENT AND DENSITY OF SAND SAMPLES

Testing temperature (°C)	Sample number	Sand content (%)	Density (g/cc)
-1	OS-8	21.3	1.28
	OS-9	21.6	1.28
	OS-10	21.1	1.29
	OS-12	20.4	1.28
	OS-11	44.8	1.67
	OS-13	48.7	1.74
	OS-14	43.0	1.64
	OS-16	43.9	1.53
	OS-15	64.2	2.04
	OS-17	63.5	2.00
-4	OS-2	20.7	1.28
	OS-3	21.3	1.28
	OS-4	19.5	1.28
	OS-5	38.3	1.50
	OS-6	45.5	1.71
	OS-18	48.1	1.69
	OS-19	46.3	1.70
	OS-20	62.9	1.99
	OS-21	59.1	2.00
	OS-31	65.0	2.04
-10	OS-22	21.2	1.30
	OS-23	21.0	1.29
	OS-24	47.0	1.71
	OS-25	47.0	1.72
	OS-26	44.8	1.69
	OS-27	65.0	2.03
	OS-28	64.4	2.00
	OS-29	64.5	2.02
	OS-30	64.4	2.04

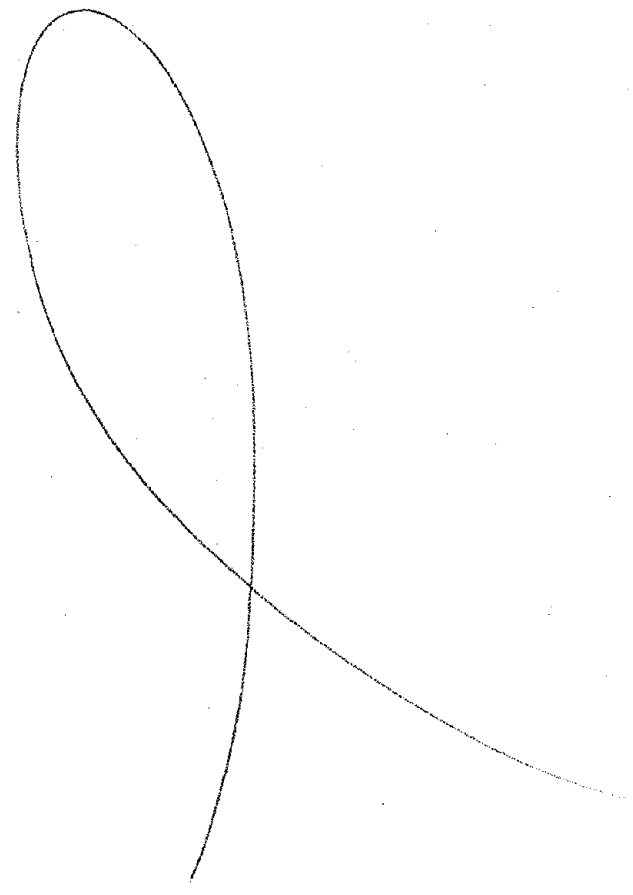

CHAPTER 4

DYNAMIC PROPERTIES OF FROZEN SILT UNDER CYCLIC TRIAXIAL LOADING CONDITIONS

4.1 General

Cyclic triaxial tests were conducted on the frozen Hanover and Alaska silt samples described in Chapter 3. Samples of both silts were tested at two water contents to determine the influence of sample density on the dynamic properties. To determine the influence of other parameters which might affect the dynamic properties of frozen silts, samples were tested at temperatures of -1, -4, and -10°C, confining pressures of 0, 50, and 200 psi, frequencies of 0.05, 0.3, 1.0, 5.0, and 10.0 cps, and over a range of axial strain amplitudes from .002 to .08%.

4.2 Testing Sequence

The test history (i.e., the sequence in which the various test condition parameters - confining pressure, frequency, and strain amplitude - were applied) used on the frozen silt samples in the research program is shown in Figure 4.1. The test history was similar to that used for frozen clay given in Volume I. With a test sequence similar to that used for frozen clay, the influence of sample disturbance on the measured dynamic properties was felt to be negligible.

The ranges of the various test condition parameters were as follows:

(1) Temperature - three temperatures (-1, -4, and -10°C) were used in the testing program; each sample was tested at only one temperature.

(2) Strain amplitude - each sample was tested at four strain amplitudes ranging from approximately .002 to .08% axial strain. In general, the strain amplitude of .08% was applied only at 200 psi confining pressure; the strain amplitude at 0 and 50 psi was limited to approximately .02% axial strain.

(3) Confining pressure - the samples were tested at three confining pressures (0, 50, and 200 psi).

(4) Frequency - each sample was tested at five loading frequencies (.05, .3, 1.0, 5.0, and 1.0 cps).

Constant temperature

Approximate axial strain = $2.0 \times 10^{-3}\%$

- cp=200 psi → f=0.05 cps → f=0.3 cps → f=1.0 cps → f=5.0 cps → f=10.0 cps
- cp= 50 psi → f=0.05 cps → f=0.3 cps → f=1.0 cps → f=5.0 cps → f=10.0 cps
- cp= 0 psi → f=0.05 cps → f=0.3 cps → f=1.0 cps → f=5.0 cps → f=10.0 cps

Approximate axial strain = $5.0 \times 10^{-3}\%$

- cp=200 psi → f=0.05 cps → f=0.3 cps → f=1.0 cps → f=5.0 cps → f=10.0 cps
- cp= 50 psi → f=0.05 cps → f=0.3 cps → f=1.0 cps → f=5.0 cps → f=10.0 cps
- cp= 0 psi → f=0.05 cps → f=0.3 cps → f=1.0 cps → f=5.0 cps → f=10.0 cps

Approximate axial strain = $1.8 \times 10^{-2}\%$

- cp=200 psi → f=0.05 cps → f=0.3 cps → f=1.0 cps → f=5.0 cps → f=10.0 cps
- cp= 50 psi → f=0.05 cps → f=0.3 cps → f=1.0 cps → f=5.0 cps → f=10.0 cps
- cp= 0 psi → f=0.05 cps → f=0.3 cps → f=1.0 cps → f=5.0 cps → f=10.0 cps

Approximate axial strain = $8.0 \times 10^{-2}\%$

- cp=200 psi → f=0.05 cps → f=0.3 cps → f=1.0 cps → f=5.0 cps → f=10.0 cps

Figure 4.1 DIAGRAM OF TEST HISTORY FOR FROZEN SILT

(5) Number of cycles - each sample was generally subjected to a maximum of 10 cycles per loading condition.

(6) Water content - both silts were prepared at two water contents; average water contents were 21.4 and 35.6% for Hanover silt and 20.5 and 38.9% for Alaska silt. Two samples of Alaska silt tested at $-1^{o}C$ were prepared at an intermediate water content (29.2%).

The dynamic Young's modulus for each loading condition was evaluated from the amplitude of the load and deformation sine waves from the strip-chart recorder output. The results presented in Section 5.3, Volume I indicate that the dynamic Young's modulus does not vary significantly with the number of cycles of loading up to 20 cycles of loading. Therefore, a representative cycle of loading less than 20 was selected to determine the dynamic Young's modulus for each loading condition.

The damping ratio for each loading condition was evaluated from a hysteresis loop recorded on a storage oscilloscope. (An x-y recorder was used in the tests conducted on ice and frozen clay samples). A cycle of loading within the first ten cycles was chosen and recorded; the trace on the oscilloscope was then observed for subsequent cycles to assure that the loop recorded did not differ from loops at other cycles for the particular loading condition. The loops on the oscilloscope were then photographed, enlarged, and projected onto sheets of paper and traced; areas of the traced loops were found with a planimeter and damping ratios were calculated. Typical hysteresis loops recorded in this manner are shown in Figure 4.2. Any deviations from symmetry in the loops generally indicated imminent sample failure or melting at the couplings.

4.3 Dynamic Young's Modulus of Frozen Silt

Values of dynamic Young's modulus were plotted versus the log of axial strain expressed as a percent for all loading conditions. Plots for both silts at all water contents are given in Appendix A. Each plot represents a silt at a particular water content, temperature, and frequency. Data from at least two samples are included in each plot. It can be seen that, in general, data points from duplicate samples are in good agreement. There is somewhat more scatter in the data points for high water content samples; this is due perhaps to the lack of uniformity and the difficulty in reproducing the high water content

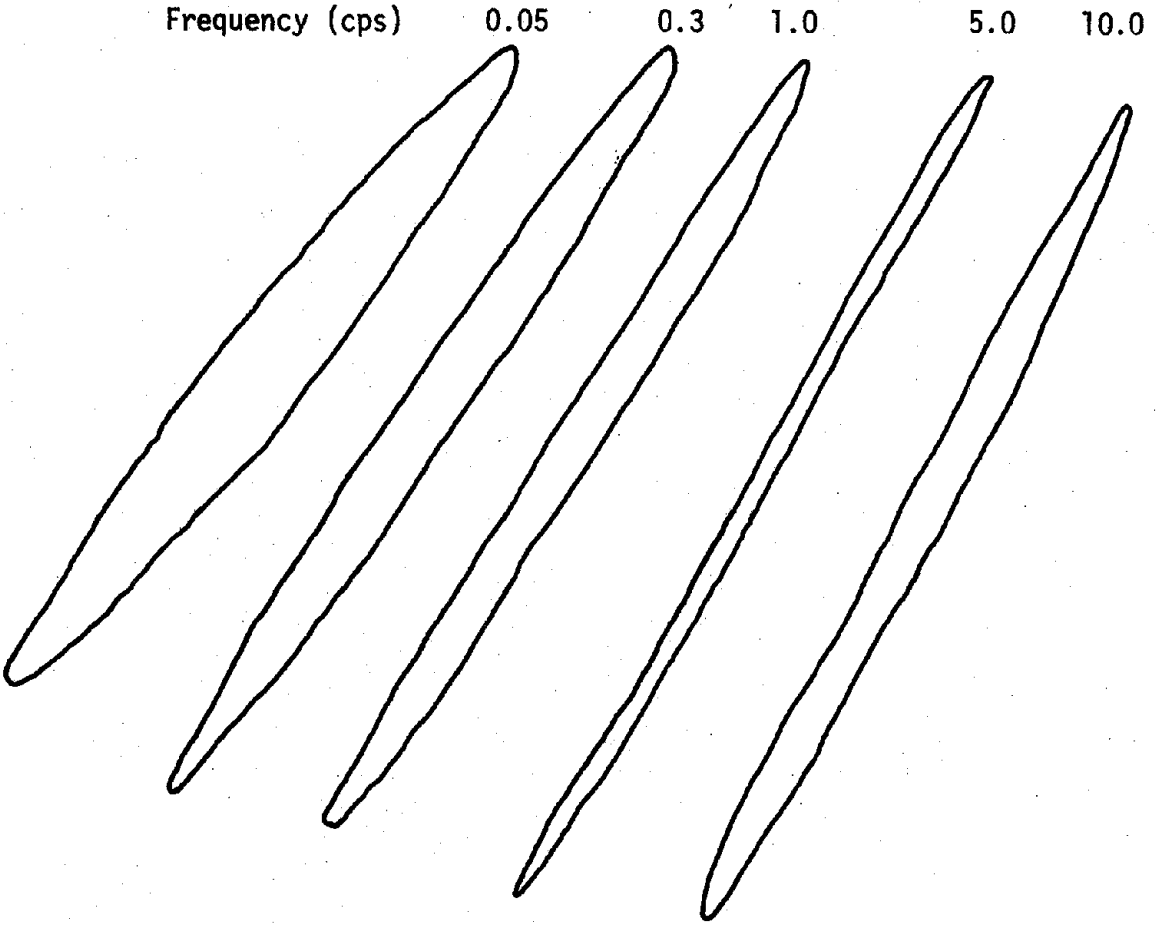

Figure 4.2 TYPICAL HYSTERESIS LOOPS OBTAINED DURING CYCLIC TRIAXIAL TESTING

samples. In general, however, the data is felt to be quite reliable.

It was apparent early in the testing program that confining pressure had a negligible influence on dynamic Young's modulus regardless of strain amplitude, frequency, temperature, or water content. A typical plot of dynamic Young's modulus versus confining pressure for a single sample is shown in Figure 4.3. Since dynamic Young's modulus was not influenced by confining pressure, data points for all confining pressures were plotted together in the graphs of dynamic Young's modulus versus axial strain amplitude.

4.3.1 Effect of Strain Amplitude

To assess the influence of strain amplitude on dynamic Young's modulus, a "best fit" line was drawn through the data points shown on the plots given in Appendix A. The relationships between dynamic Young's modulus and strain amplitudes for both silts are summarized in Figures 4.4 to 4.12. Each graph represents one silt at a given water content, at three temperatures, and at least two frequencies. Values for dynamic Young's modulus ranged from 1×10^5 to 35×10^5 psi for Hanover silt and 1×10^5 to 22×10^5 psi for Alaska silt.

The dynamic Young's modulus for both silts decreases as the axial strain amplitude increases; the decrease is more pronounced at -4 and -10^{o}C than at -1^{o}C. The relationship between dynamic Young's modulus and strain amplitude appears to be independent of water content and frequency.

To assess the influence of frequency, temperature, and water content on dynamic Young's modulus, values of dynamic Young's modulus were obtained from Figures 4.4. to 4.12 at axial strain amplitudes of 3.16×10^{-3}% (log axial strain = -2.50) and 3.16×10^{-2}% (log axial strain = -1.50). The modulus values were then plotted versus frequency, temperature, and water content.

4.3.2 Effect of Frequency

The relationship between dynamic Young's modulus and frequency for both silts is given in Figures 4.13 to 4.22; each plot represents the relationship for a silt at a single water content at three temperatures. Dynamic Young's modulus increases with increasing frequency. In

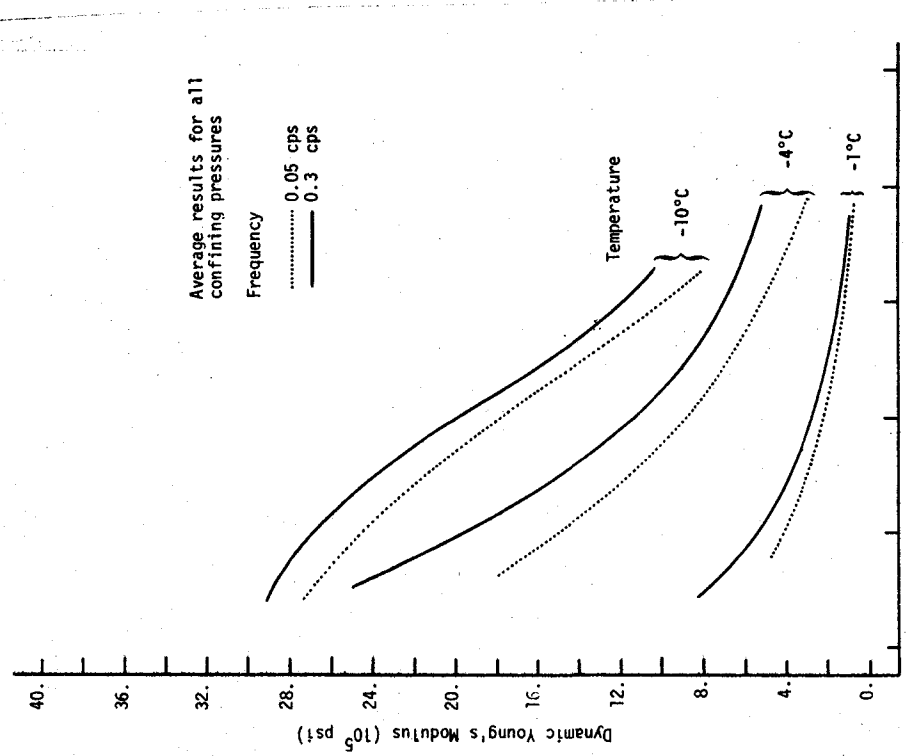

Figure 4.4 DYNAMIC YOUNG'S MODULUS VERSUS AXIAL STRAIN FOR HANOVER SILT AT 21.4% WATER CONTENT

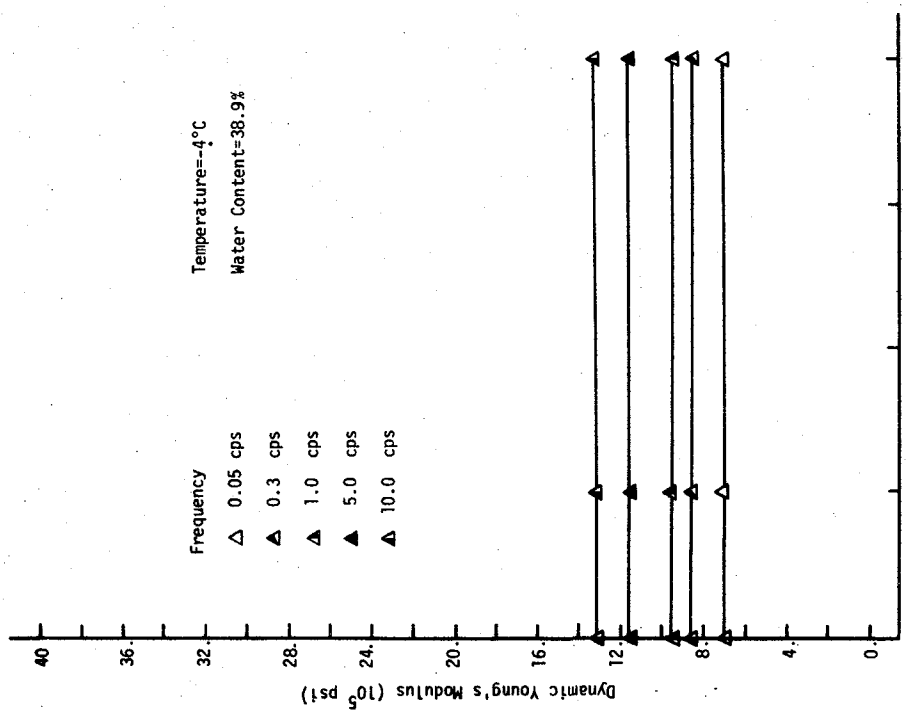

Figure 4.3 DYNAMIC YOUNG'S MODULUS VERSUS CONFINING PRESSURE FOR ALASKA SILT AT AN AXIAL STRAIN OF 5.0×10^{-3}%

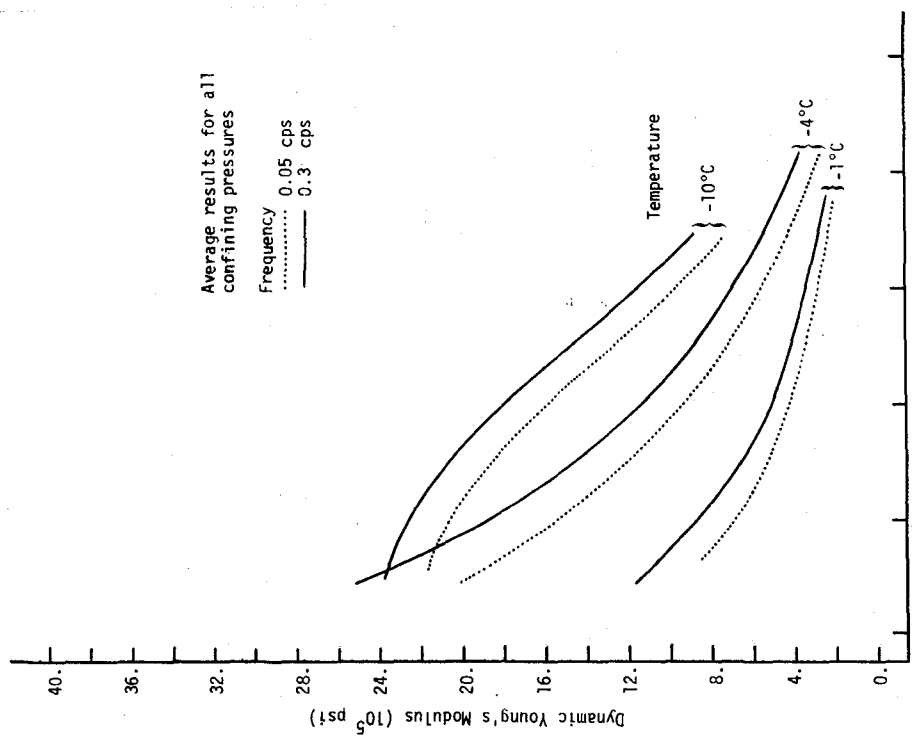

Figure 4.6 DYNAMIC YOUNG'S MODULUS VERSUS AXIAL STRAIN FOR HANOVER SILT AT 35.5% WATER CONTENT

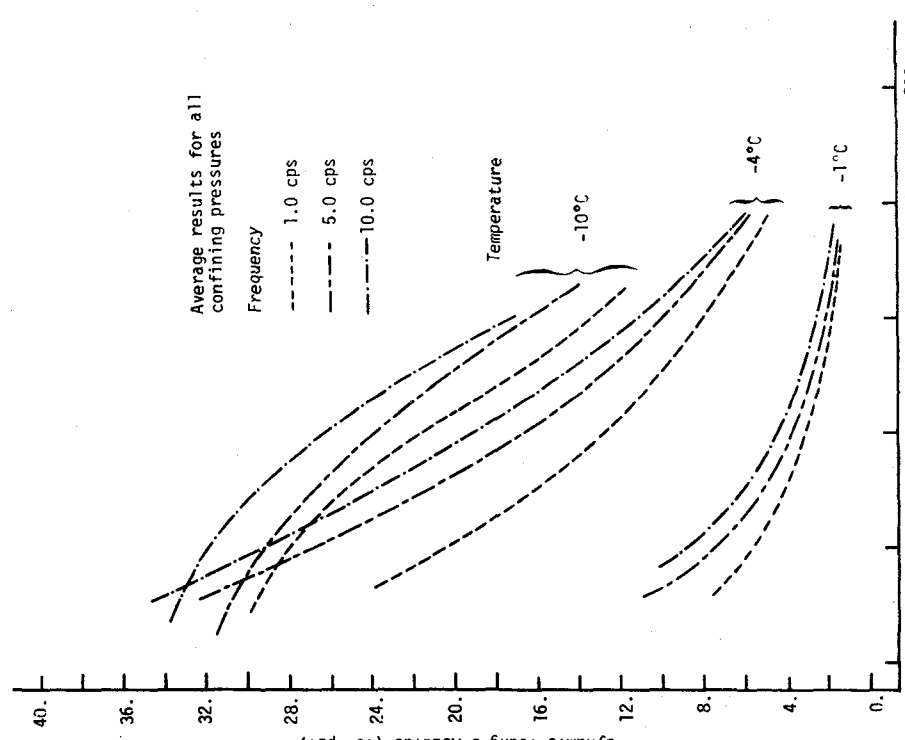

Figure 4.5 DYNAMIC YOUNG'S MODULUS VERSUS AXIAL STRAIN FOR HANOVER SILT AT 21.4% WATER CONTENT

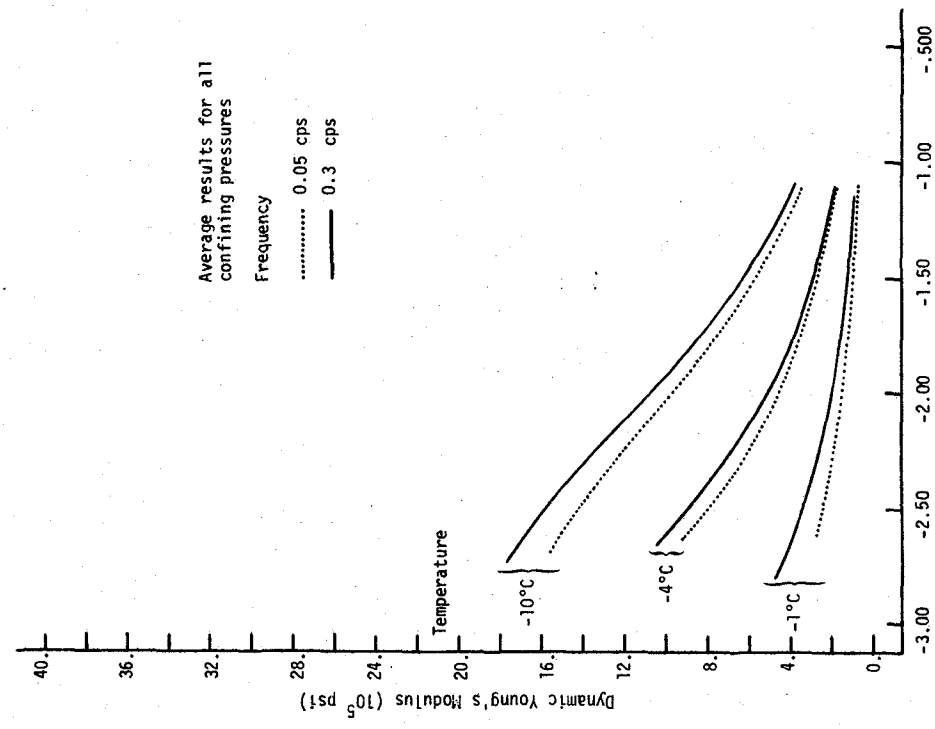

Figure 4.7 DYNAMIC YOUNG'S MODULUS VERSUS AXIAL STRAIN FOR HANOVER SILT AT 35.5% WATER CONTENT

Figure 4.8 DYNAMIC YOUNG'S MODULUS VERSUS AXIAL STRAIN FOR ALASKA SILT AT 20.5% WATER CONTENT

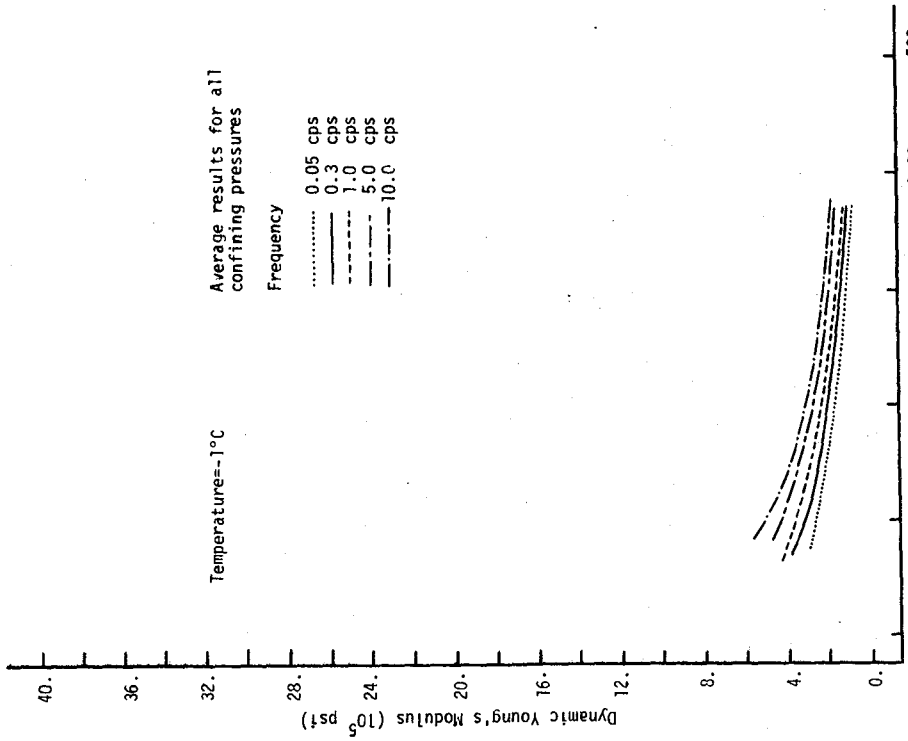

Figure 4.10 DYNAMIC YOUNG'S MODULUS VERSUS AXIAL STRAIN FOR ALASKA SILT AT 29.2% WATER CONTENT

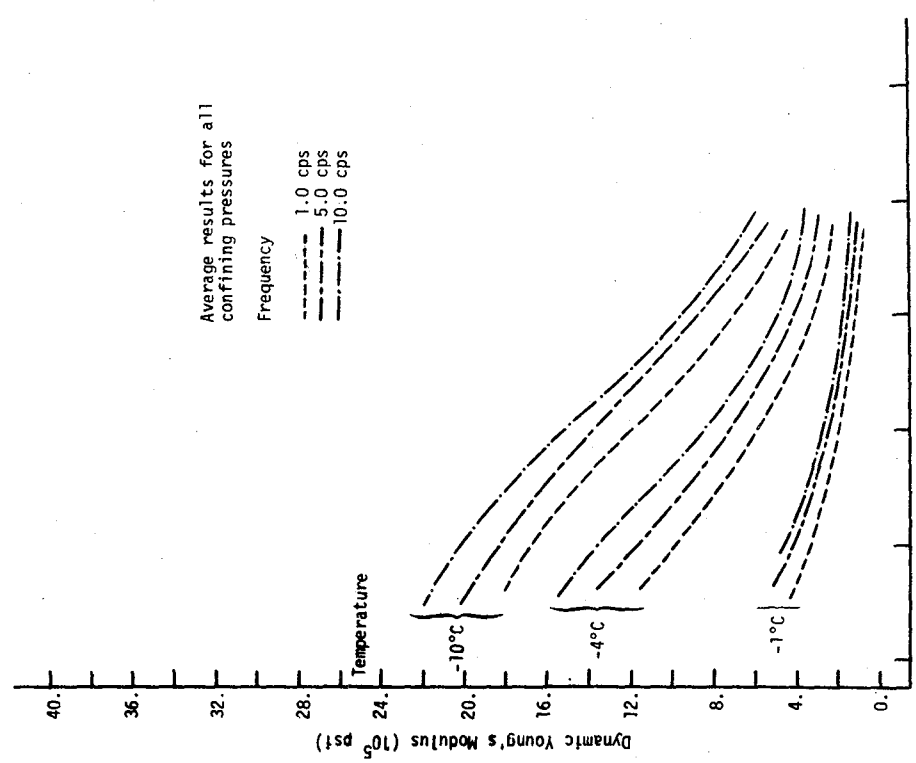

Figure 4.9 DYNAMIC YOUNG'S MODULUS VERSUS AXIAL STRAIN FOR ALASKA SILT AT 20.5% WATER CONTENT

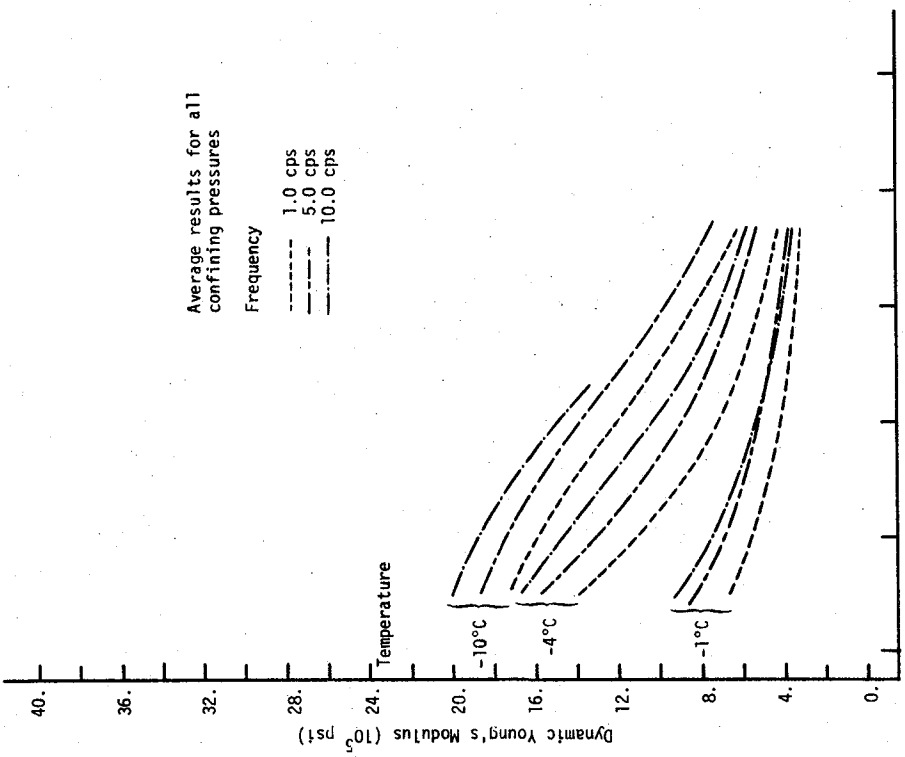

Figure 4.12 DYNAMIC YOUNG'S MODULUS VERSUS AXIAL STRAIN FOR ALASKA SILT AT 38.9% WATER CONTENT

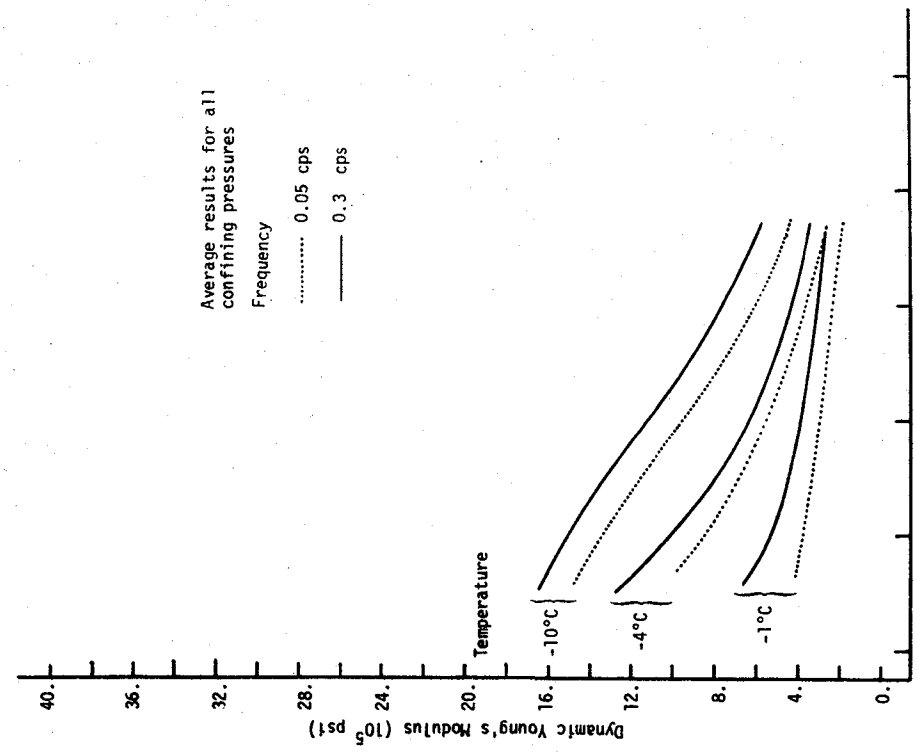

Figure 4.11 DYNAMIC YOUNG'S MODULUS VERSUS AXIAL STRAIN FOR ALASKA SILT AT 38.9% WATER CONTENT

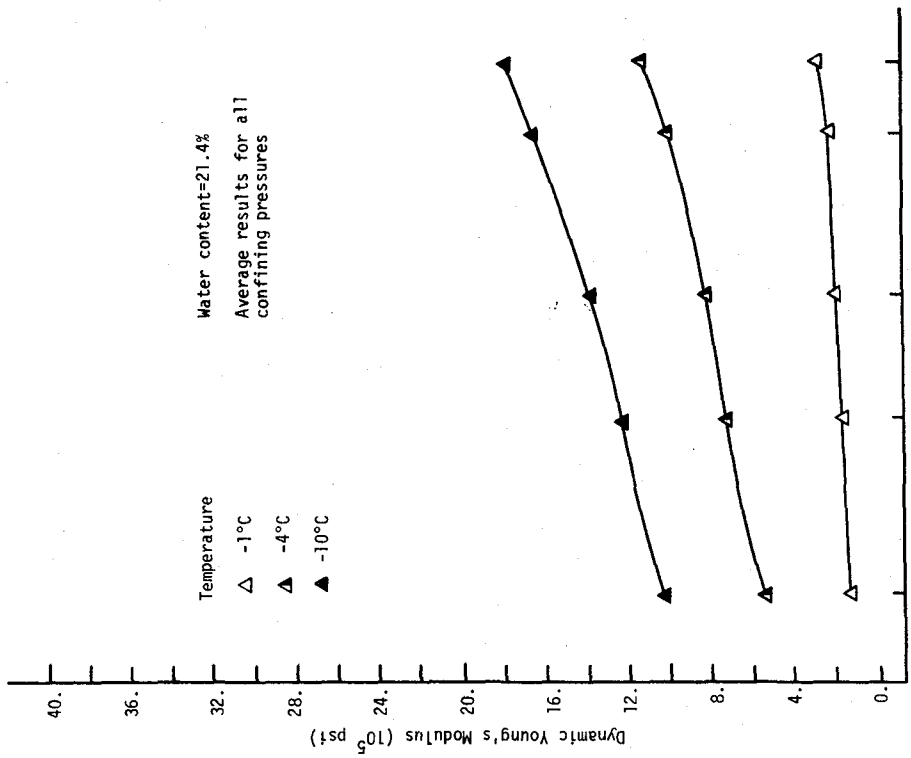

Figure 4.14 DYNAMIC YOUNG'S MODULUS VERSUS FREQUENCY FOR HANOVER SILT AT AN AXIAL STRAIN OF 3.16×10^{-2}%

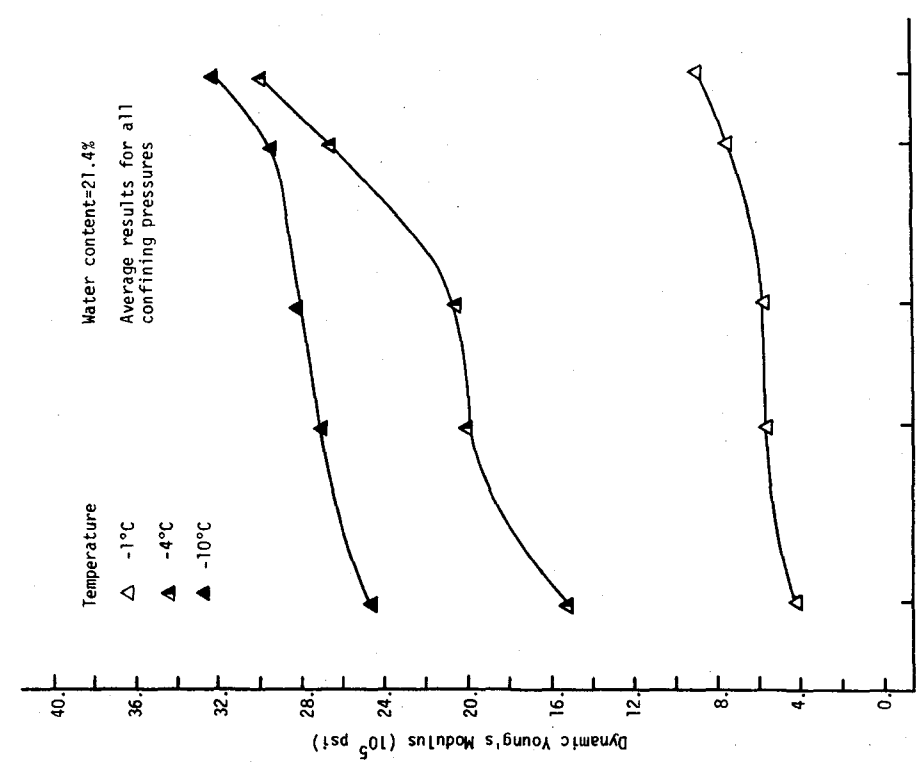

Figue 4.13 DYNAMIC YOUNG'S MODULUS VERSUS FREQUENCY FOR HANOVER SILT AT AN AXIAL STRAIN OF 3.16×10^{-3}%

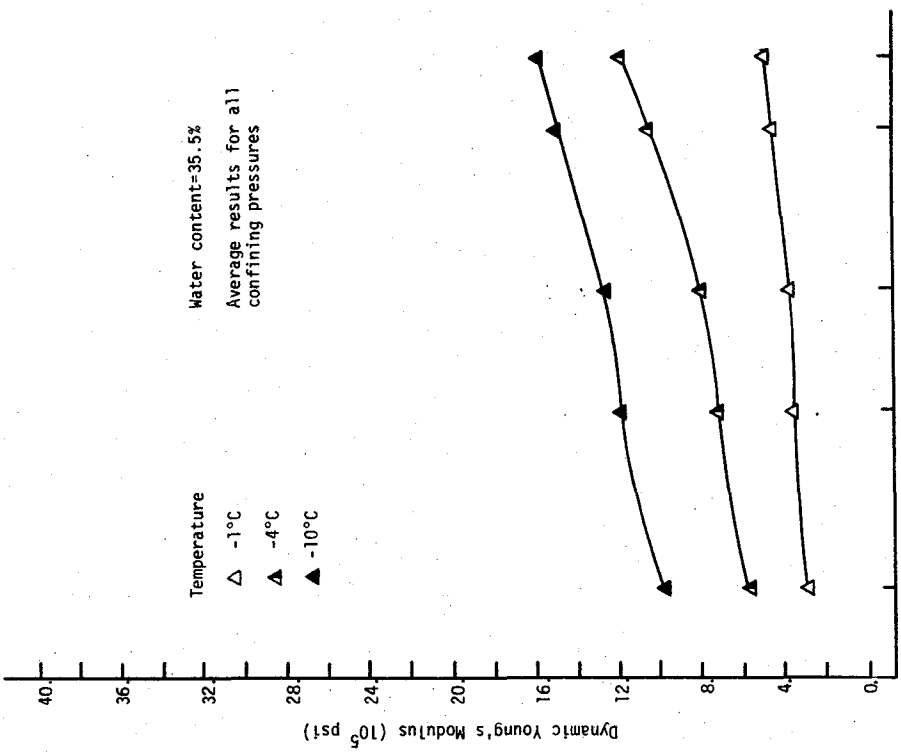

Figure 4.16 DYNAMIC YOUNG'S MODULUS VERSUS FREQUENCY FOR HANOVER SILT AT AN AXIAL STRAIN OF 3.16×10^{-2}%

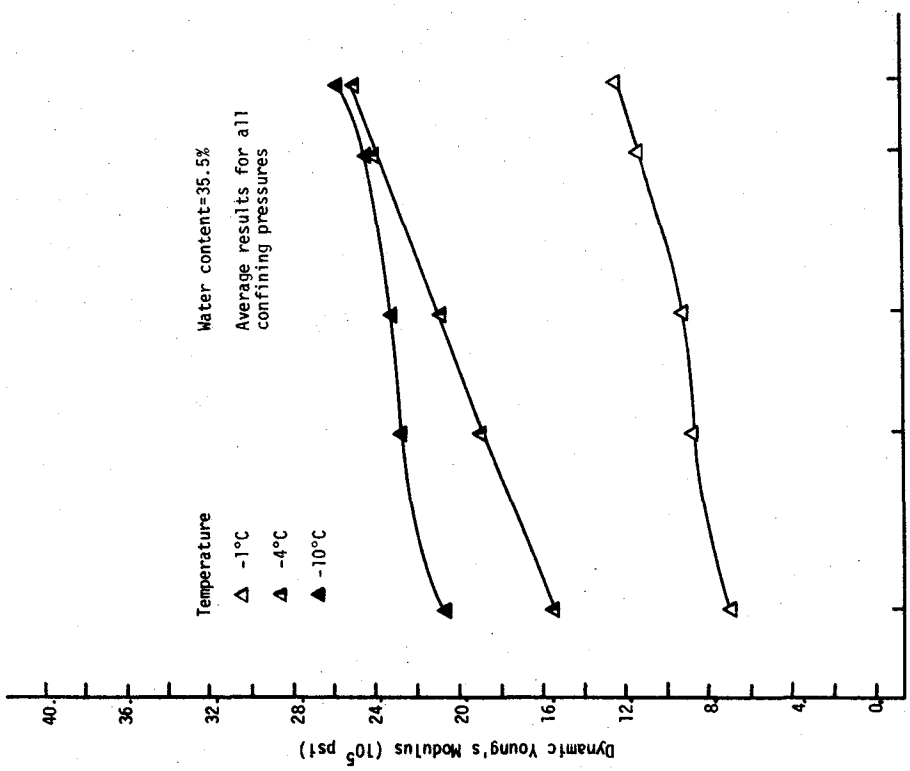

Figure 4.15 DYNAMIC YOUNG'S MODULUS VERSUS FREQUENCY FOR HANOVER SILT AT AN AXIAL STRAIN OF 3.16×10^{-3}%

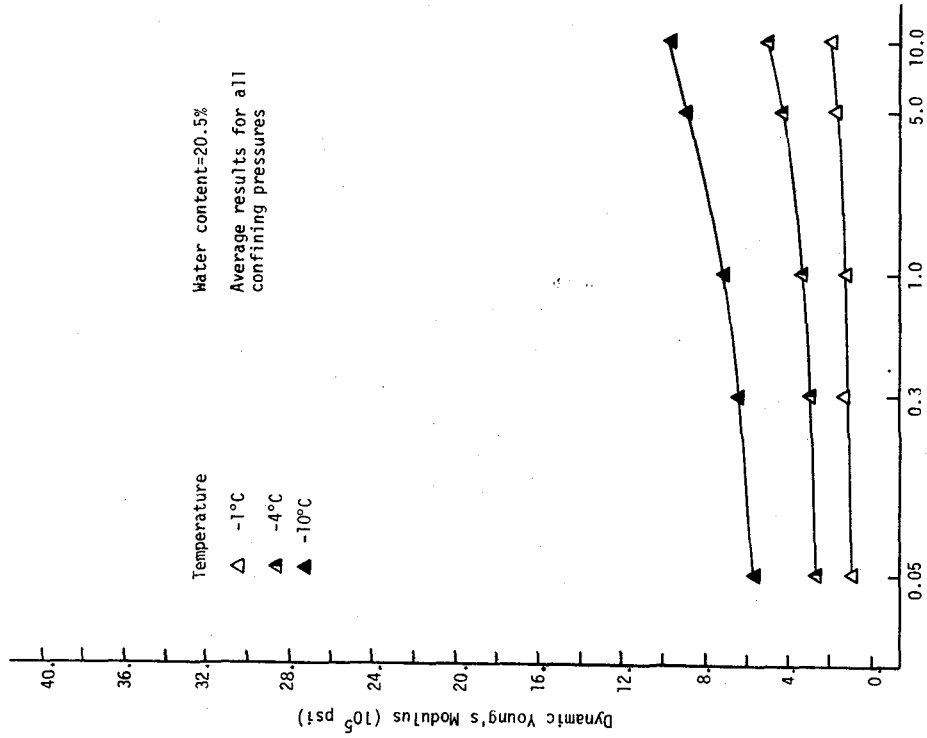

Figure 4.18 DYNAMIC YOUNG'S MODULUS VERSUS FREQUENCY FOR ALASKA SILT AT AN AXIAL STRAIN OF 3.16×10^{-2}%

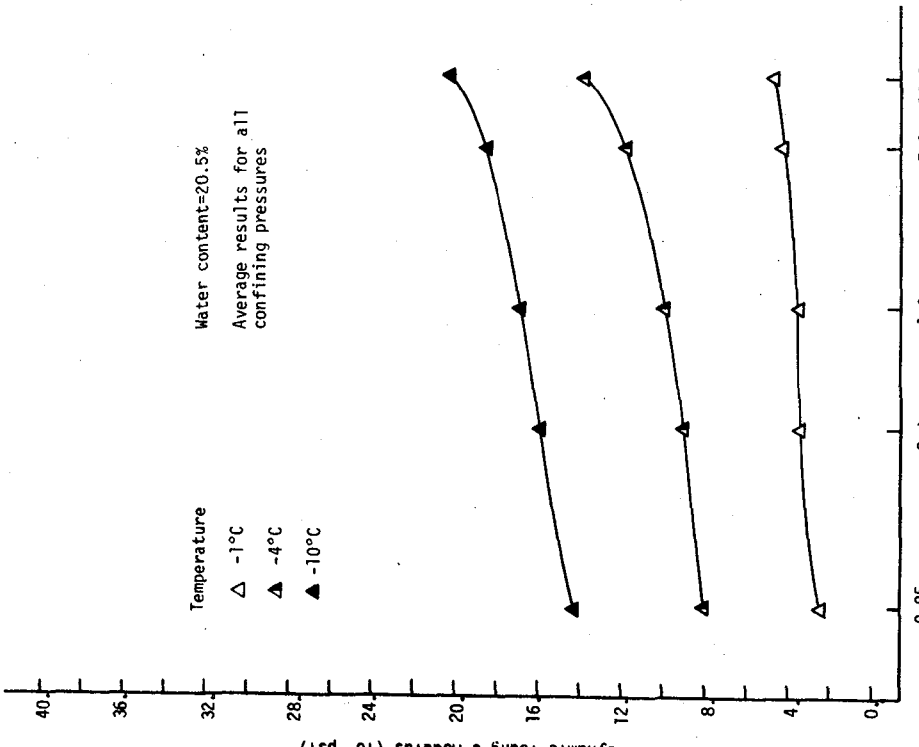

Figure 4.17 DYNAMIC YOUNG'S MODULUS VERSUS FREQUENCY FOR ALASKA SILT AT AN AXIAL STRAIN OF 3.16×10^{-3}%

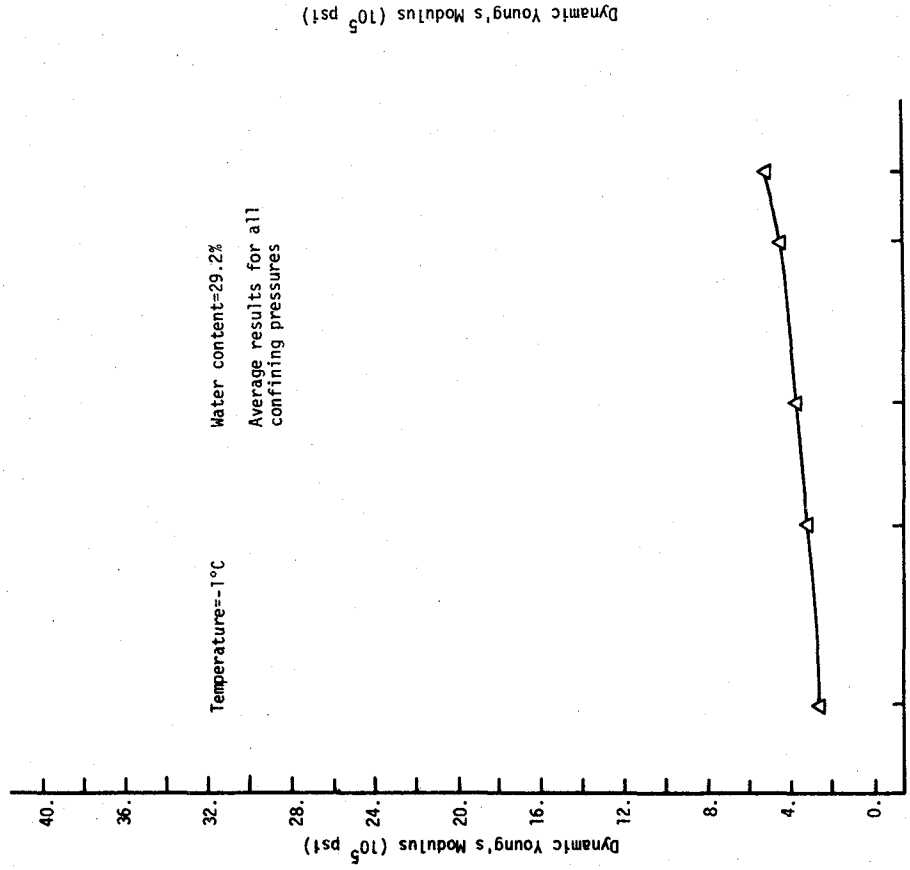

Figure 4.19 DYNAMIC YOUNG'S MODULUS VERSUS FREQUENCY FOR ALASKA SILT AT AN AXIAL STRAIN OF 3.16×10^{-3}%

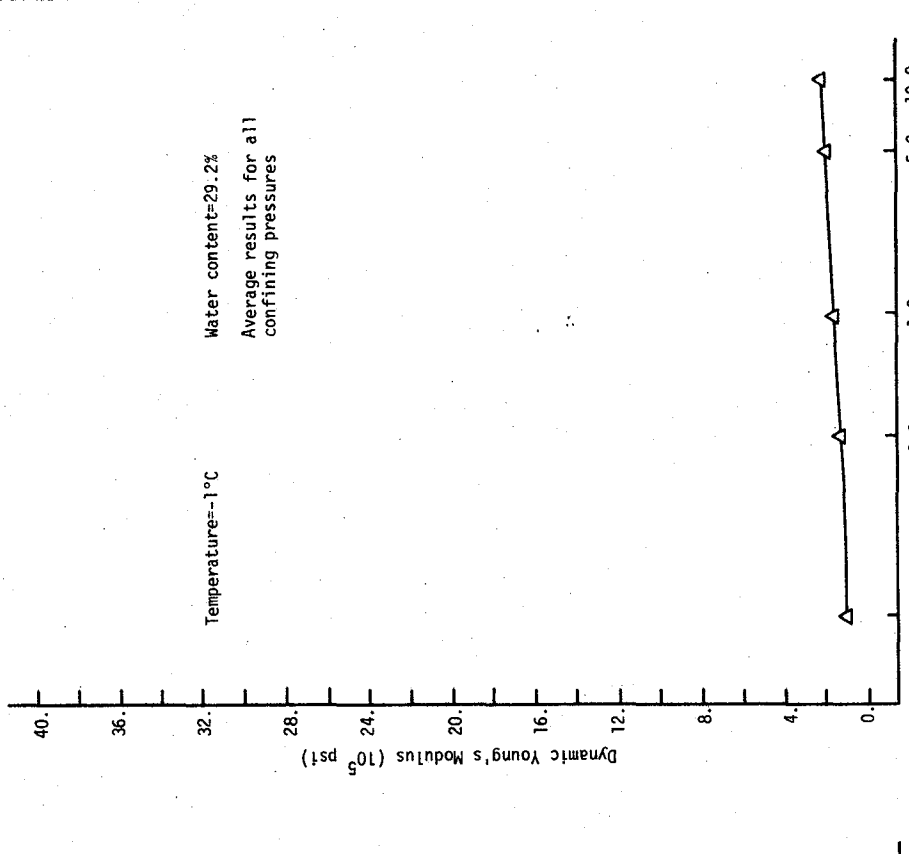

Figure 4.20 DYNAMIC YOUNG'S MODULUS VERSUS FREQUENCY FOR ALASKA SILT AT AN AXIAL STRAIN OF 3.16×10^{-2}%

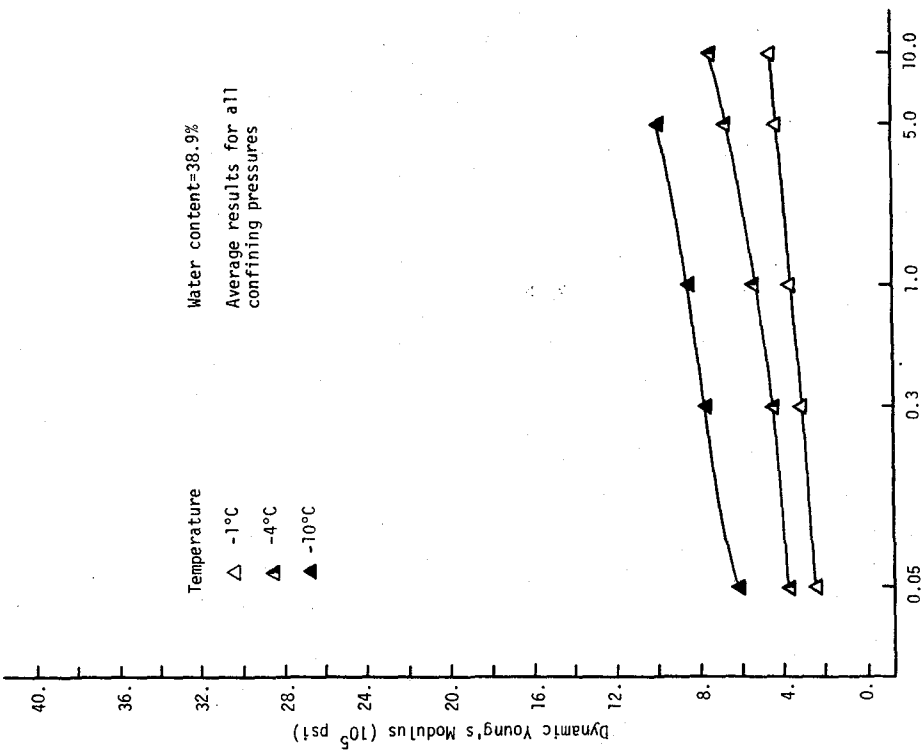

Figure 4.22 DYNAMIC YOUNG'S MODULUS VERSUS FREQUENCY FOR ALASKA SILT AT AN AXIAL STRAIN OF 3.16×10^{-2}%

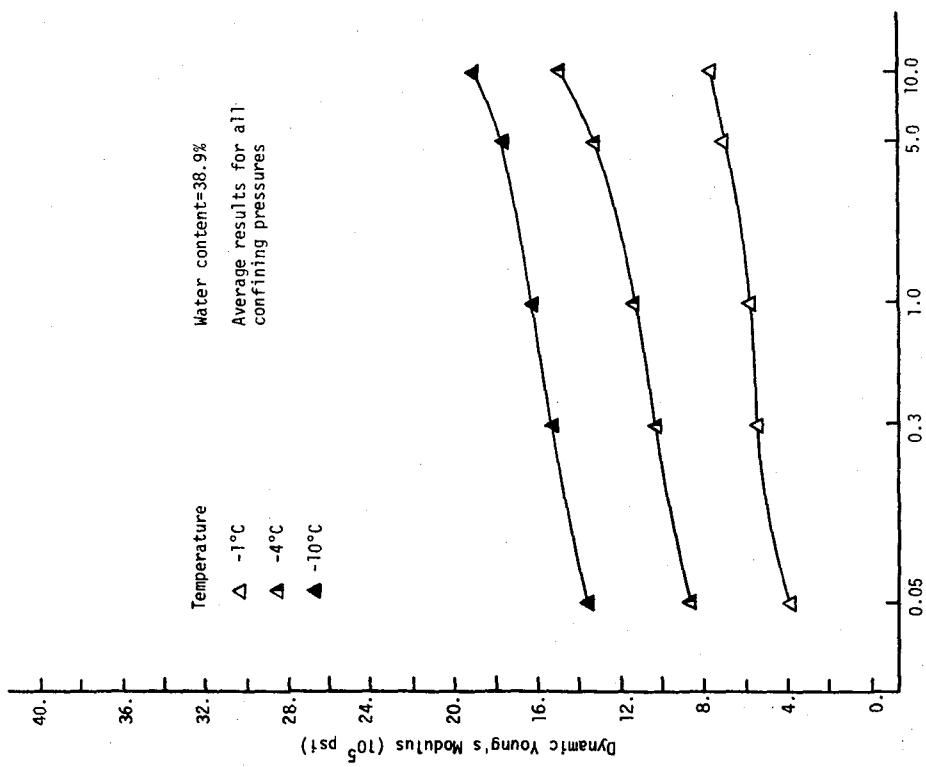

Figure 4.21 DYNAMIC YOUNG'S MODULUS VERSUS FREQUENCY FOR ALASKA SILT AT AN AXIAL STRAIN OF 3.16×10^{-3}%

general, the rate of increase is slightly greater at very low and very high frequencies than at intermediate frequencies. At a high strain amplitude, the relationship between dynamic Young's modulus and frequency appears to be independent of water content and temperature. At a low strain amplitude, the rate of increase of dynamic Young's modulus with frequency is somewhat greater at $-4^{o}C$ than at -1 and $-10^{o}C$. In the case of Hanover silt, the value of dynamic Young's modulus at $-4^{o}C$ approaches the value at $-10^{o}C$ at high frequencies.

4.3.3 Effect of Temperature

The relationship between dynamic Young's modulus and temperature for both silts is given in Figures 4.23 to 4.30. Each plot represents the relationship for a silt at a given water content, five frequencies, and at one of two axial strain amplitudes. In all cases, dynamic Young's modulus increases significantly with decreasing temperature. The rate of increase is fairly constant at a high strain amplitude ($3.16 \times 10^{-2}\%$), with a slightly greater rate of increase at higher temperatures (-1 to $-4^{o}C$) than at lower temperatures (-4 to $-10^{o}C$). At a lower strain amplitude ($3.16 \times 10^{-3}\%$) the rate of increase in generally significantly greater at higher temperatures (-1 to $-4^{o}C$) than at lower temperatures (-4 to $-10^{o}C$). The rate of increase of dynamic Young's modulus with decreasing temperature is generally more uniform over the entire range of temperatures (-1 to $-10^{o}C$) at lower frequencies than at higher frequencies.

4.3.4 Effect of Water Content

The relationship between dynamic Young's modulus and water content is given in Figures 4.31 to 4.36. Each graph represents a silt at a given temperature at two strain amplitudes and five frequencies. Each relationship shown is based on only two points with the exception of the relationship for Alaska silt at $-1^{o}C$ (Figure 4.34) which is based on three points. At a temperature of $-1^{o}C$, dynamic Young's modulus increases by a moderate amount as the water content increases (from 21.4 to 35.5% for Hanover silt and from 20.5 to 38.9% for Alaska silt) for both strain amplitudes (3.16×10^{-3} and $3.16 \times 10^{-2}\%$); this relationship does not appear to be affected by frequency. In the case of Alaska silt, most of the increase in dynamic Young's modulus with

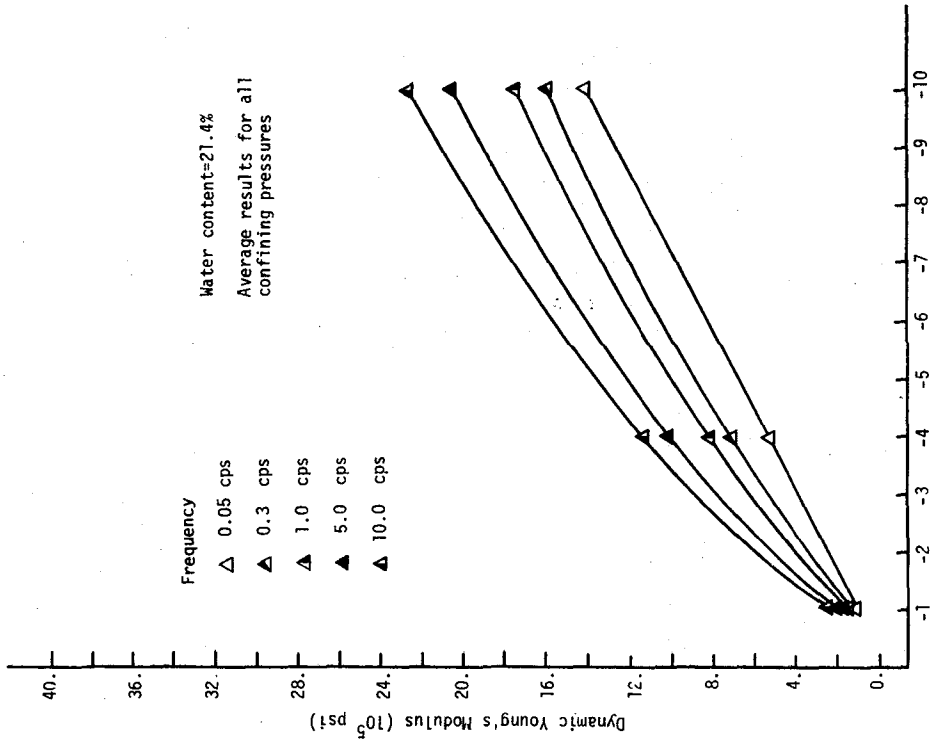

Figure 4.24 DYNAMIC YOUNG'S MODULUS VERSUS TEMPERATURE FOR HANOVER SILT AT AN AXIAL STRAIN OF 3.16×10^{-2}%

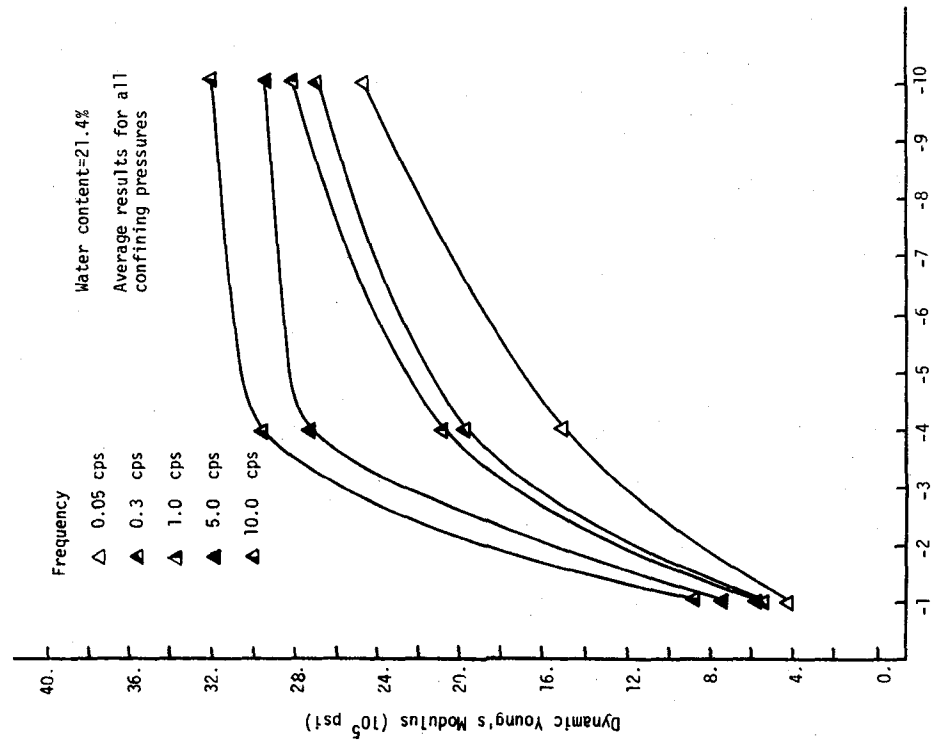

Figure 4.23 DYNAMIC YOUNG'S MODULUS VERSUS TEMPERATURE FOR HANOVER SILT AT AN AXIAL STRAIN OF 3.16×10^{-3}%

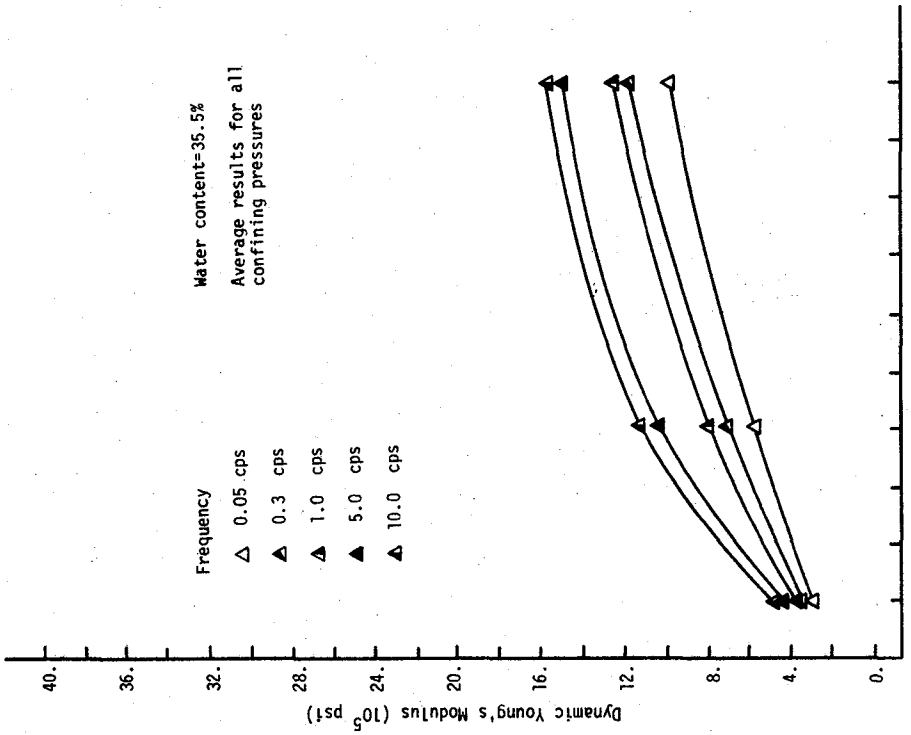

Figure 4.26 DYNAMIC YOUNG'S MODULUS VERSUS TEMPERATURE FOR HANOVER SILT AT AN AXIAL STRAIN OF 3.16×10^{-2}%

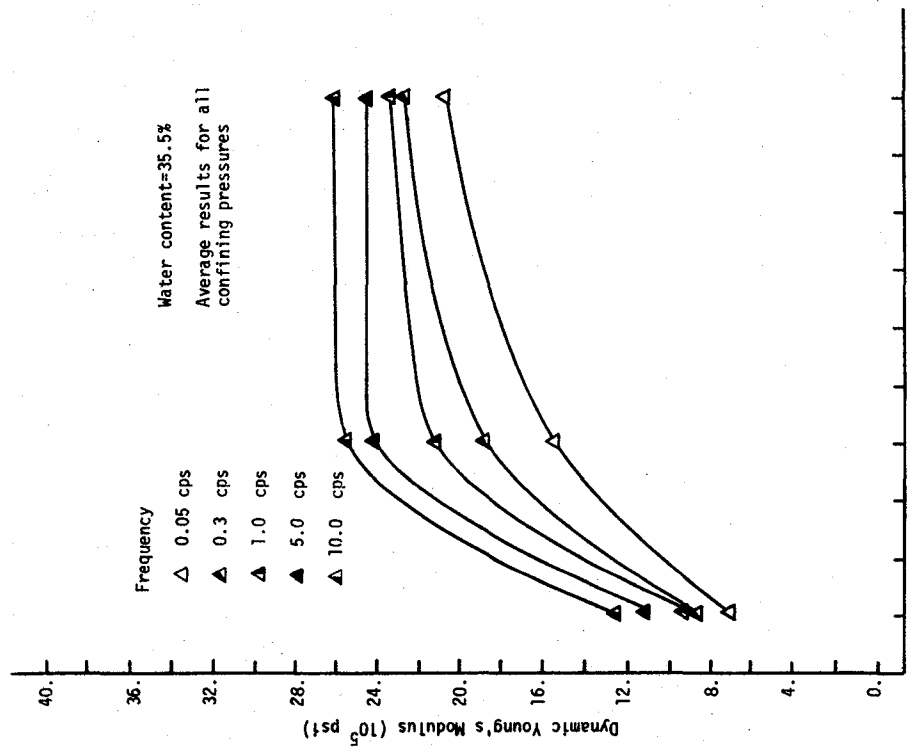

Figure 4.25 DYNAMIC YOUNG'S MODULUS VERSUS TEMPERATURE FOR HANOVER SILT AT AN AXIAL STRAIN OF 3.16×10^{-3}%

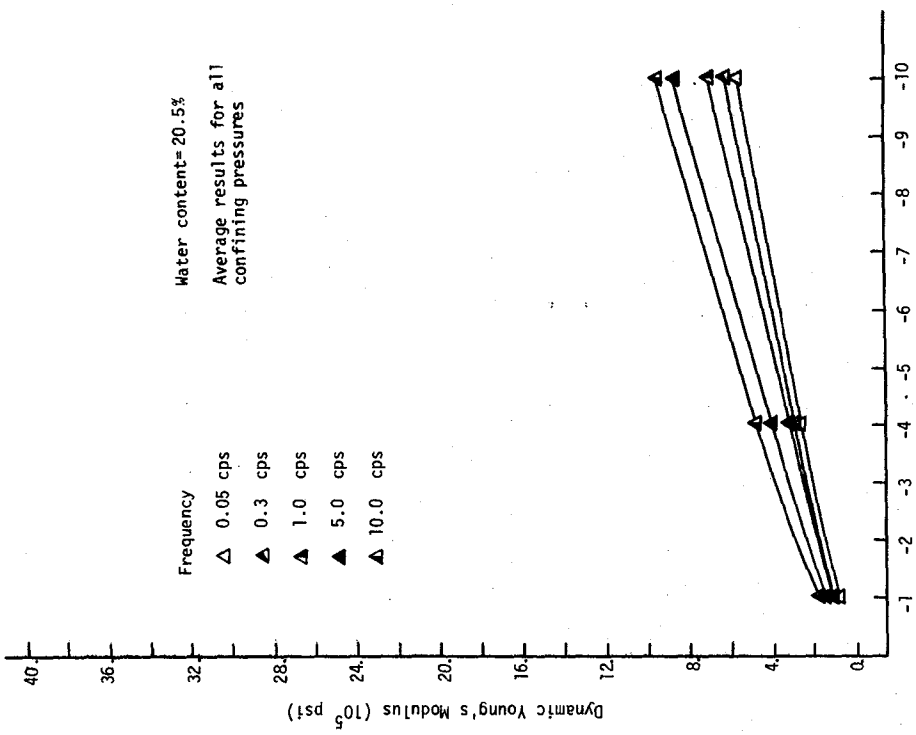

Figure 4.28 DYNAMIC YOUNG'S MODULUS VERSUS TEMPERATURE FOR ALASKA SILT AT AN AXIAL STRAIN OF 3.16×10^{-2}%

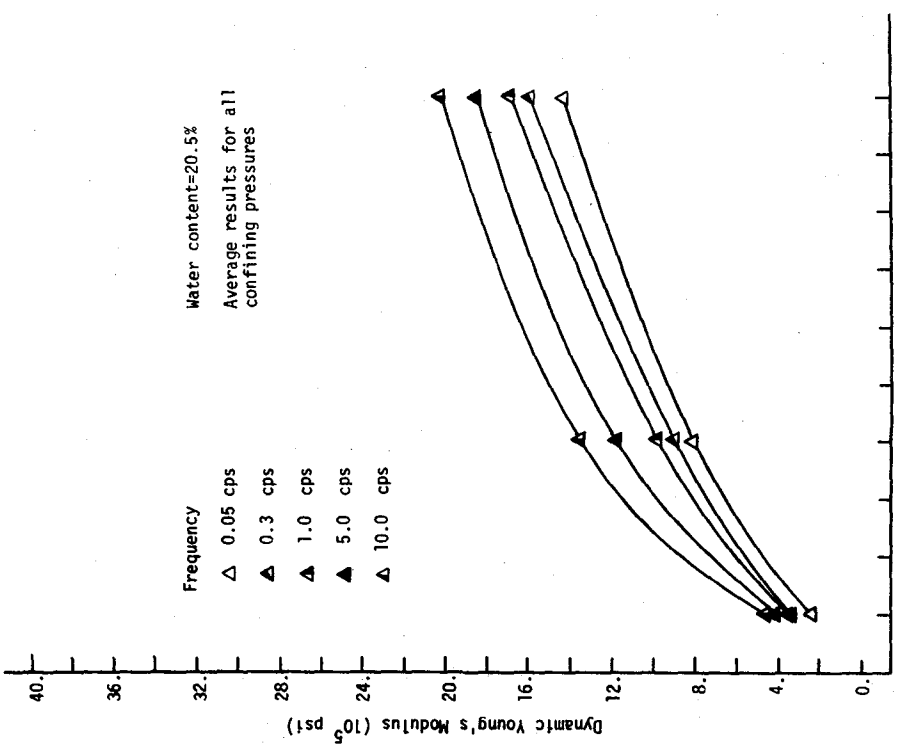

Figure 4.27 DYNAMIC YOUNG'S MODULUS VERSUS TEMPERATURE FOR ALASKA SILT AT AN AXIAL STRAIN OF 3.16×10^{-3}%

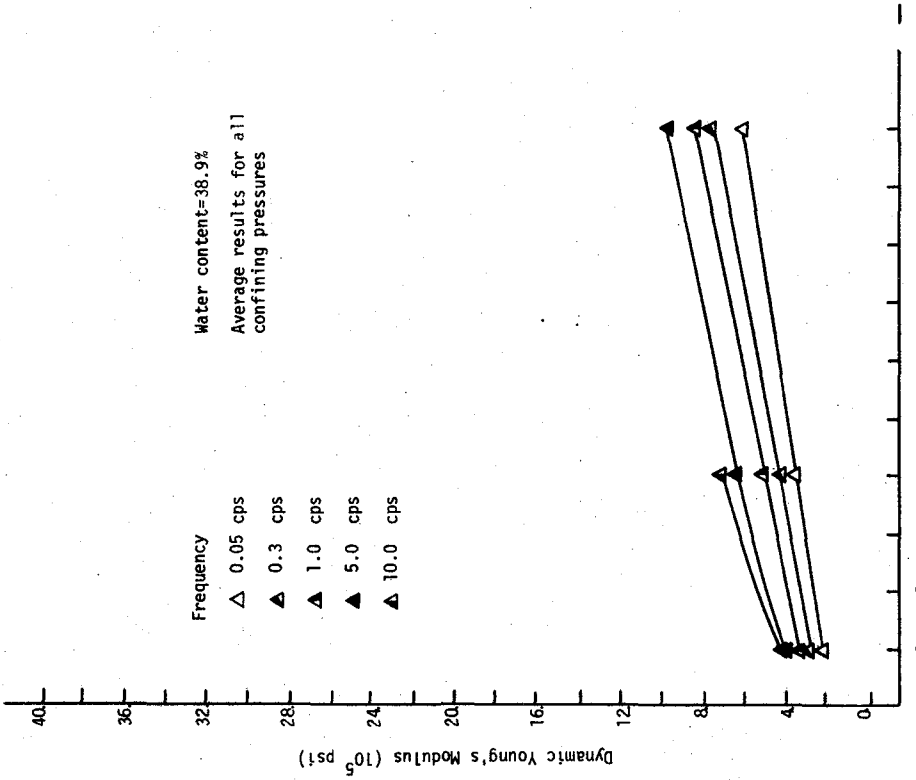

Figure 4.30 DYNAMIC YOUNG'S MODULUS VERSUS TEMPERATURE FOR ALASKA SILT AT AN AXIAL STRAIN OF 3.16×10^{-2}%

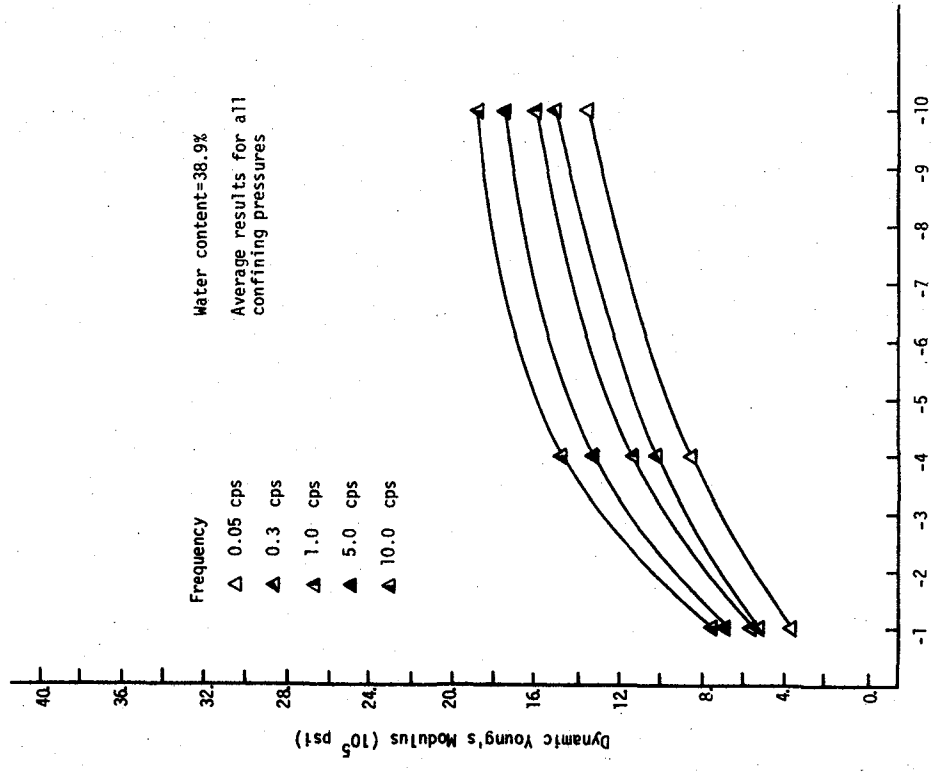

Figure 4.29 DYNAMIC YOUNG'S MODULUS VERSUS TEMPERATURE FOR ALASKA SILT AT AN AXIAL STRAIN OF 3.16×10^{-3}%

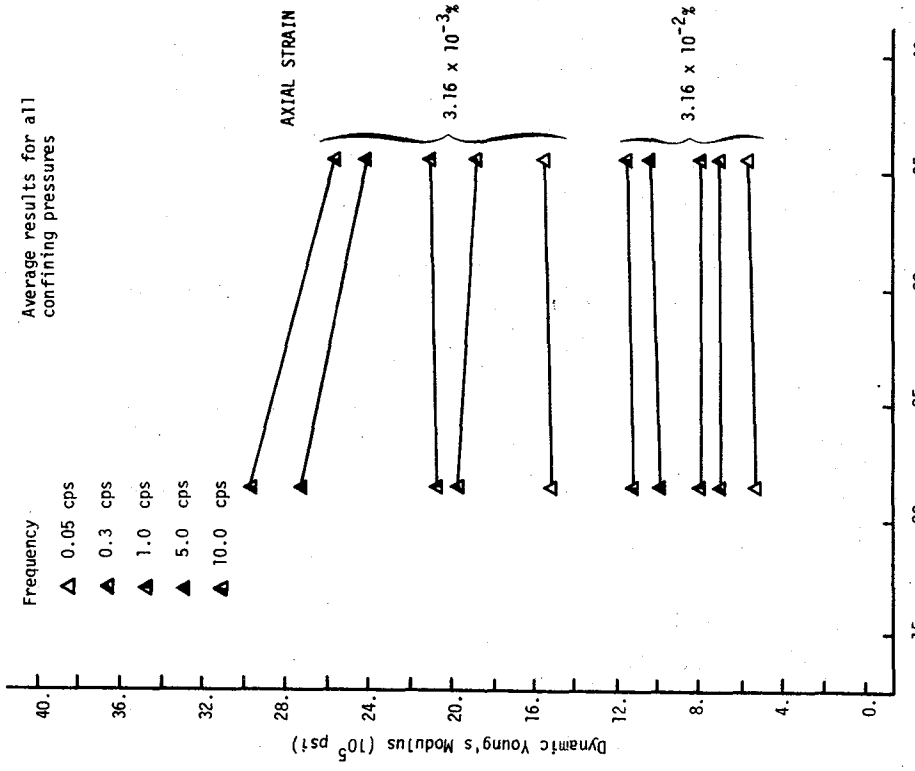

Figure 4.32 DYNAMIC YOUNG'S MODULUS VERSUS WATER CONTENT FOR HANOVER SILT AT A TEMPERATURE OF -4°C

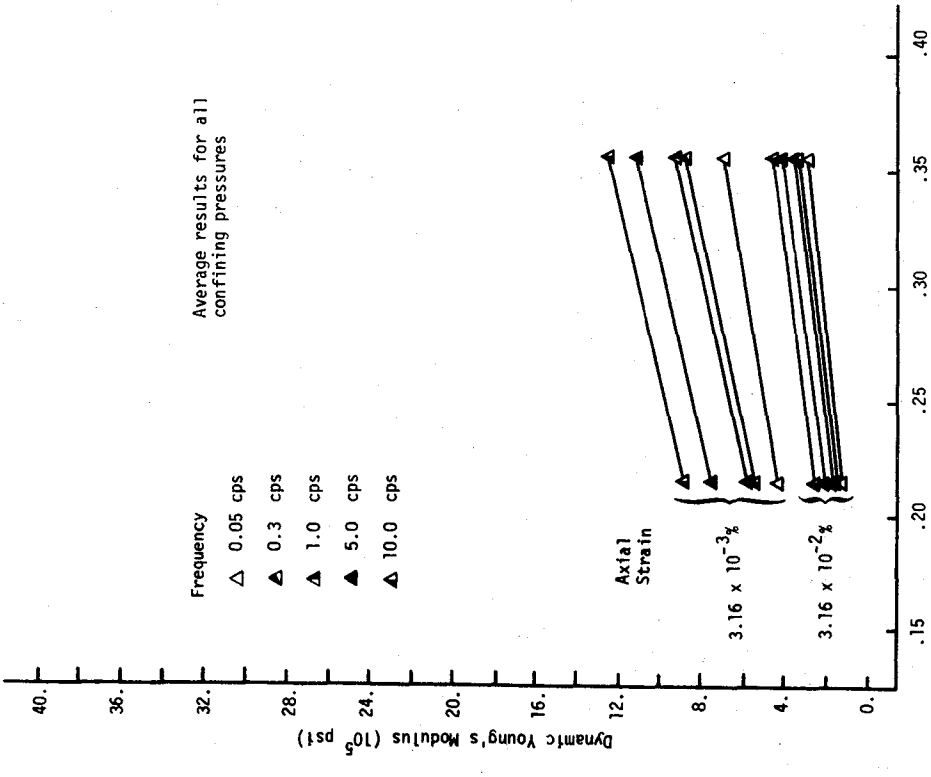

Figure 4.31 DYNAMIC YOUNG'S MODULUS VERSUS WATER CONTENT FOR HANOVER SILT AT A TEMPERATURE OF -1°C

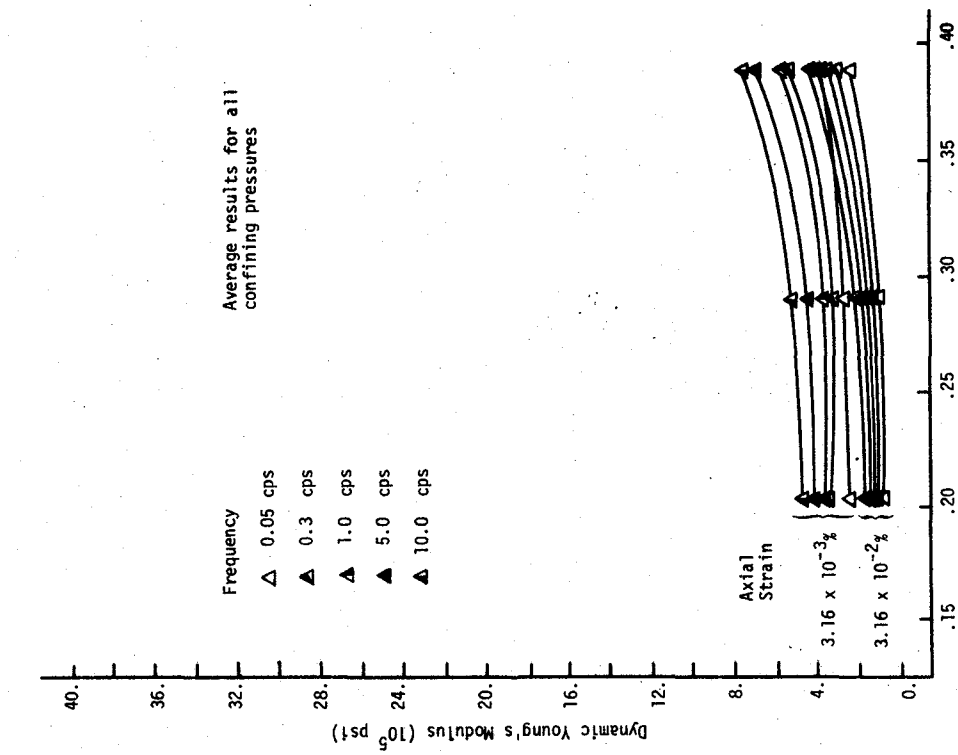

Figure 4.34 DYNAMIC YOUNG'S MODULUS VERSUS WATER CONTENT FOR ALASKA SILT AT A TEMPERATURE OF -1°C

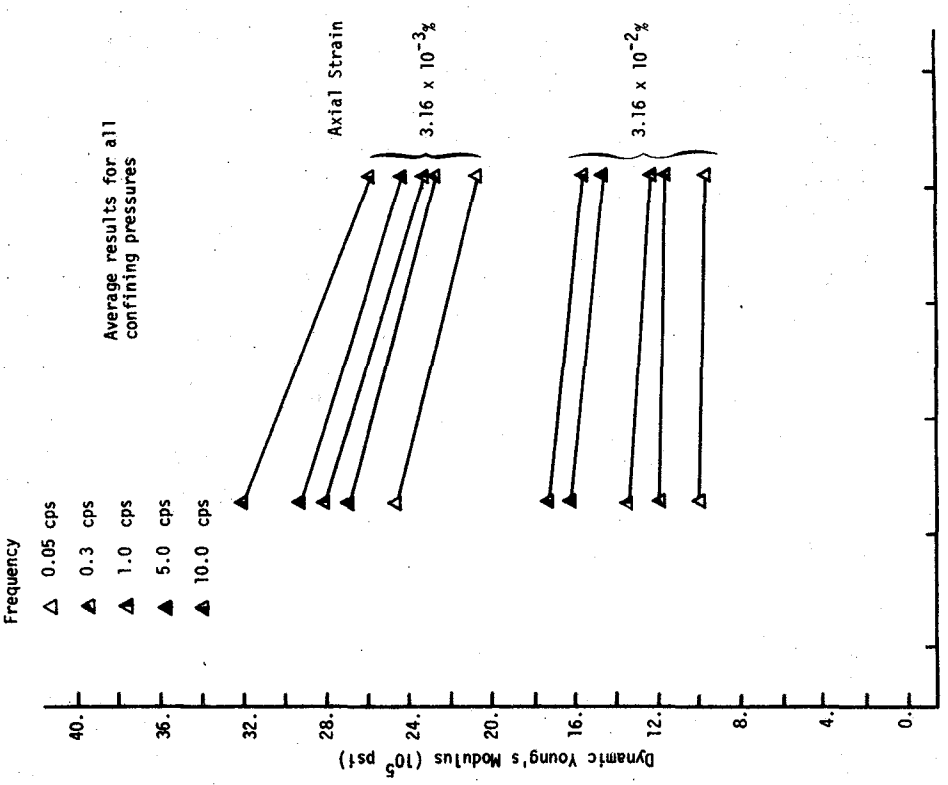

Figure 4.33 DYNAMIC YOUNG'S MODULUS VERSUS WATER CONTENT FOR HANOVER SILT AT A TEMPERATURE OF -10^{o}C

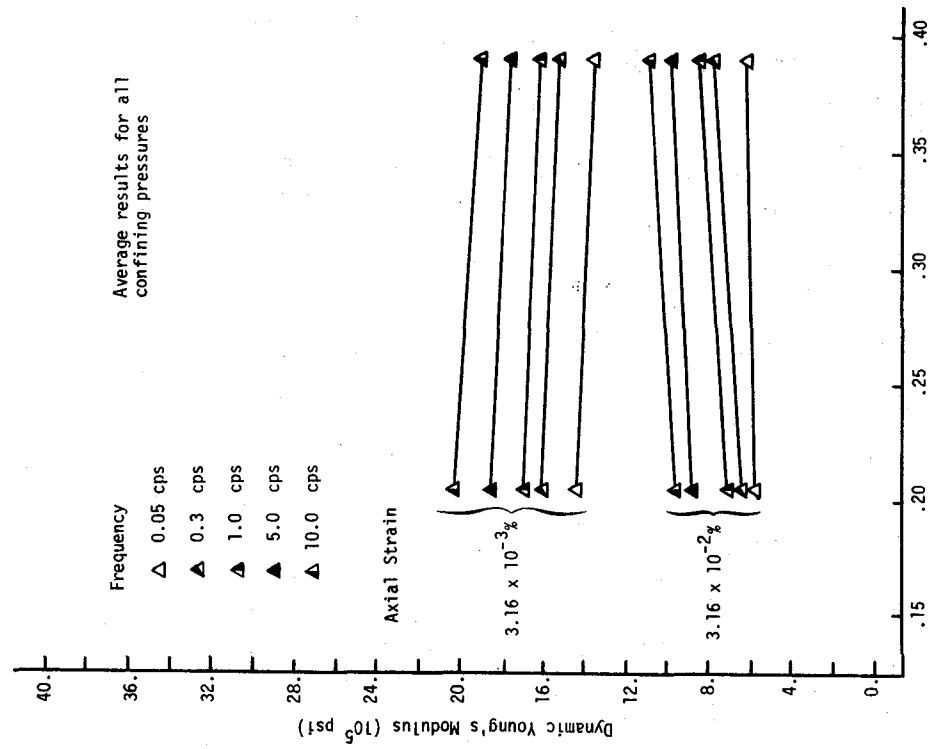

Figure 4.35 DYNAMIC YOUNG'S MODULUS VERSUS WATER CONTENT FOR ALASKA SILT AT A TEMPERATURE OF -4°C

Figure 4.36 DYNAMIC YOUNG'S MODULUS VERSUS WATER CONTENT FOR ALASKA SILT AT A TEMPERATURE OF -10°C

water content occurs in the higher water content range (29.2 to 38.9%).

At lower temperatures (-4 and -10°C) there appears to be little or no significant influence of water content on dynamic Young's modulus at a higher strain amplitude (3.16×10^{-2}%). At a lower strain amplitude (3.16×10^{-3}%) the relationship between dynamic Young's modulus and water content is not clear. In the case of Hanover silt, dynamic Young's modulus decreases by a small amount as the water content increases at both -4 and -10°C; in the case of Alaska silt, dynamic Young's modulus appears to increase by a small amount at -4°C and decrease by a small amount at -10°C as the water content increases.

The influence of temperature on the relationship between dynamic Young's modulus and water content may be a function of the unfrozen water content of the silt. At a low temperature (-10°C) where the influence of unfrozen water content is small, dynamic Young's modulus tends to decrease with increasing water content. At higher temperatures where the unfrozen water content is greater, dynamic Young's modulus increases with increasing water content; this may be due to the relatively larger proportion of water in the form of ice in the higher water content samples than in the lower water content samples.

4.4 Damping Ratio of Frozen Silt

Values of damping ratio were plotted against the log of axial strain amplitude expressed as a percent for all loading conditions. Plots for both silts at all water contents are given in Appendix B. Each plot represents data points for a silt at a particular water content, temperature, and frequency. Data points for all three confining pressures are included on each plot. Each plot represents at least two samples; in general, there is good agreement between data points from duplicate samples. At very low strains, the scatter of the data points is due to the influence of background "noise" during testing, which results in difficulty in accurately measuring damping from the hysteresis loops recorded. The scatter of data at the high water contents is due to the lack of uniformity and the difficulty in reproducing the high water content samples.

4.4.1 Effect of Strain Amplitude

To determine the influence of strain amplitude on damping ratio,

a "best fit" line was drawn through the data points given in the plots in Appendix B. The relationship between damping ratio and strain amplitude is summarized in Figures 4.37 to 4.58. Each graph represents a silt at a given loading frequency at each of three temperatures. In cases where damping ratio was felt to be influenced by confining pressure, a separate curve was drawn for each confining pressure.

In general, damping ratio increases as strain amplitude increases. At a temperature of $-1^{o}C$, the rate of increase is moderate at low frequencies and somewhat greater at higher frequencies for low water contents. For higher water contents, the rate of increase is moderate at all frequencies. At lower temperatures (-4 and $-10^{o}C$) damping increases significantly with increasing strain amplitude at low frequencies. At high frequencies, damping ratio increases by a smaller amount and in some cases decreases by a small amount with increasing strain amplitude. In some instances, the relationship becomes U-shaped with a slight decrease in damping followed by an increase with increasing strain amplitude.

To assess the influence of confining pressure, frequency, temperature, and water content on damping ratio, values of damping ratio were obtained from Figures 4.37 to 4.58 and Appendix B at axial strain amplitudes of $3.16 \times 10^{-3}\%$ (log axial strain = -2.50) and $3.16 \times 10^{-2}\%$ (log axial strain = -1.50). The damping ratio values were then plotted versus confining pressure, frequency, temperature, and water content.

4.4.2 Effect of Confining Pressure

The relationships between damping ratio and confining pressure are summarized in Figures 4.59 to 4.63. Since it was apparent that confining pressure did not influence damping ratio at low temperatures (-4 and $-10^{o}C$), plots were prepared only for a temperature of $-1^{o}C$. In general, at a temperature of $-1^{o}C$ and at a low strain amplitude ($3.16 \times 10^{-3}\%$) damping ratio decreases with increasing confining pressure at low frequencies and is not significantly affected by confining pressure at higher frequencies. At a high strain amplitude ($3.16 \times 10^{-2}\%$) damping ratio decreases slightly with increasing confining pressure at low frequencies and is not affected by confining pressure at higher frequencies. Since the change in damping ratio with confining pressure is small to negligible at a high strain amplitude, only one

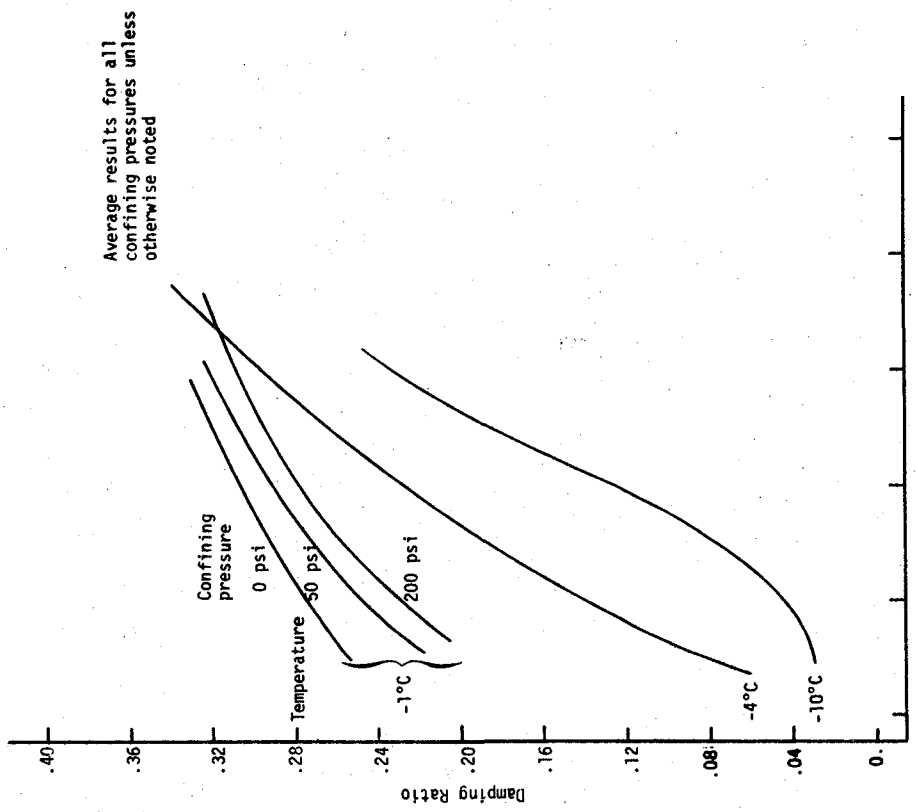

Figure 4.38 DAMPING RATIO VERSUS AXIAL STRAIN FOR HANOVER SILT AT 0.3 cps FREQUENCY AND 21.4% WATER CONTENT

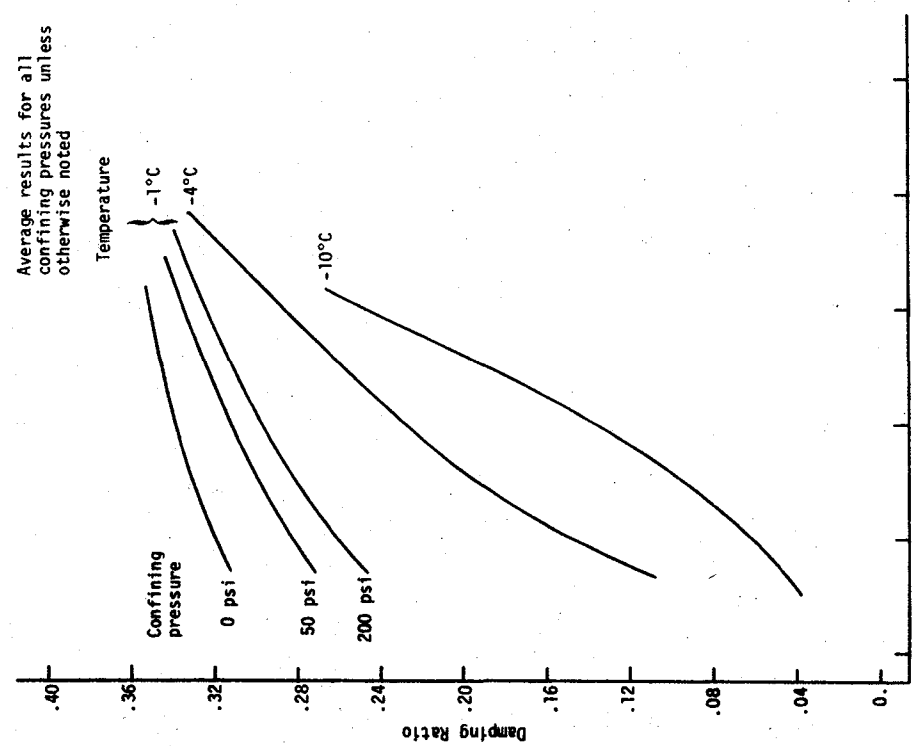

Figure 4.37 DAMPING RATIO VERSUS AXIAL STRAIN FOR HANOVER SILT AT 0.05cps FREQUENCY AND 21.4% WATER CONTENT

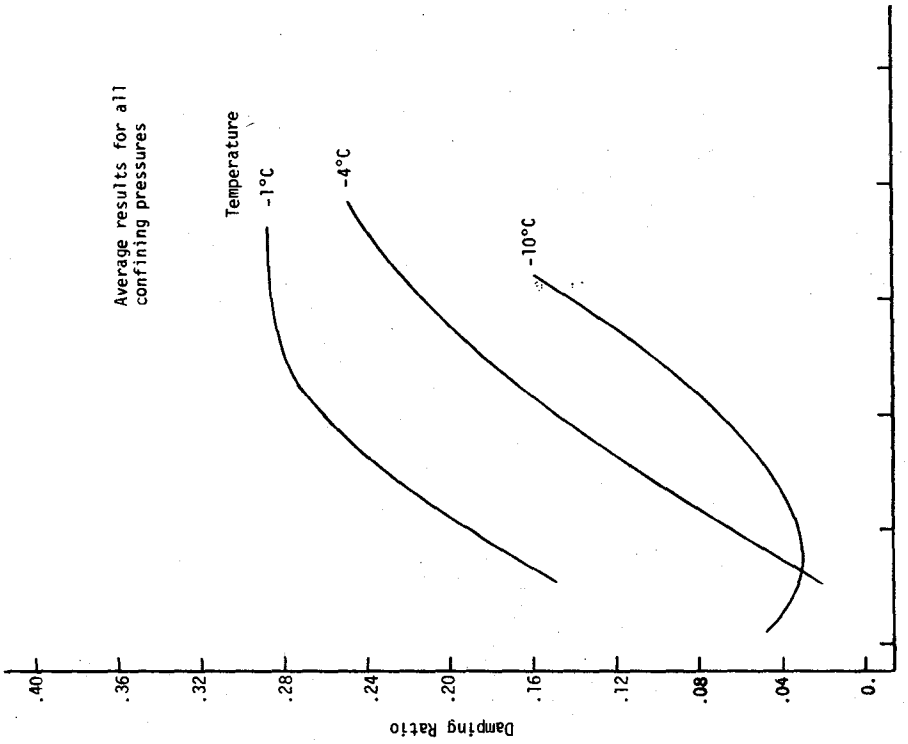

Figure 4.40 DAMPING RATIO VERSUS AXIAL STRAIN FOR HANOVER SILT AT 5.0 cps FREQUENCY AND 21.4% WATER CONTENT

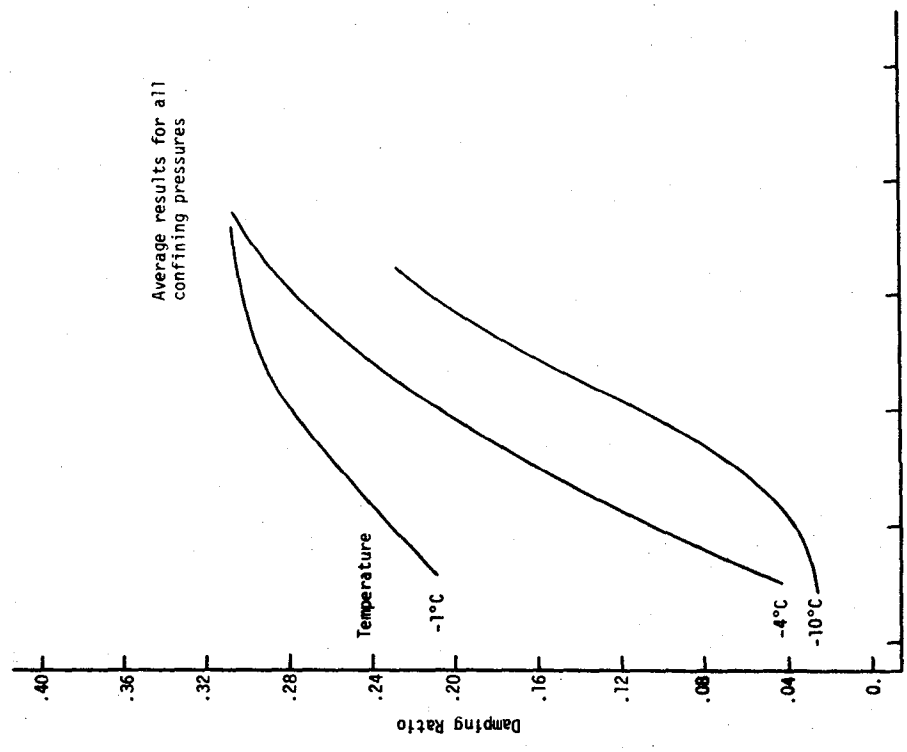

Figure 4.39 DAMPING RATIO VERSUS AXIAL STRAIN FOR HANOVER SILT AT 1.0 cps FREQUENCY AND 21.4% WATER CONTENT

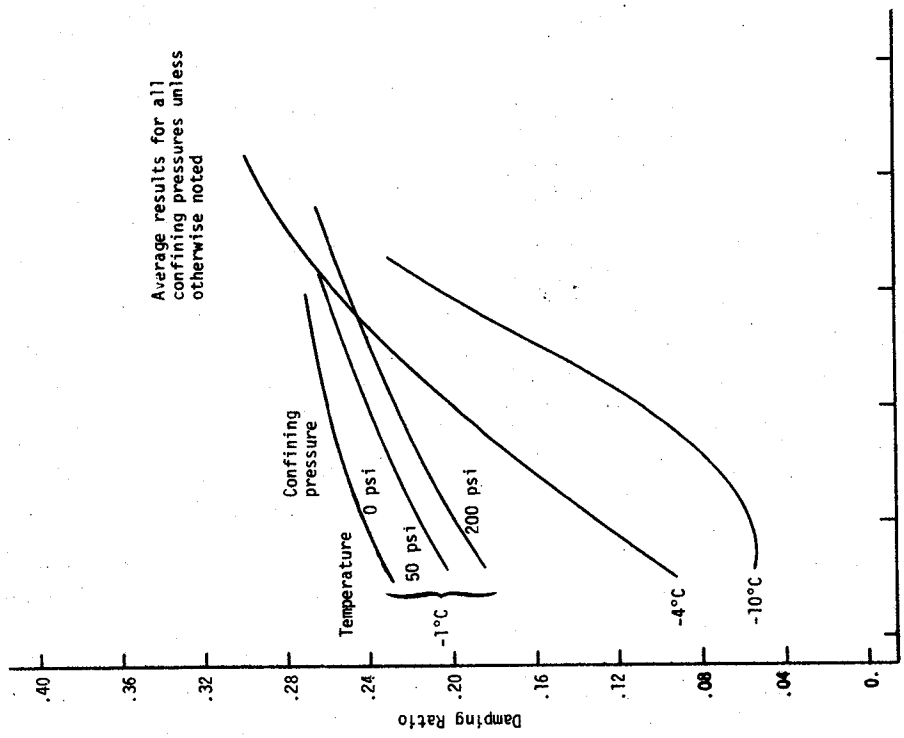

Figure 4.42 DAMPING RATIO VERSUS AXIAL STRAIN FOR HANOVER SILT AT 0.05 cps FREQUENCY AND 35.5% WATER CONTENT

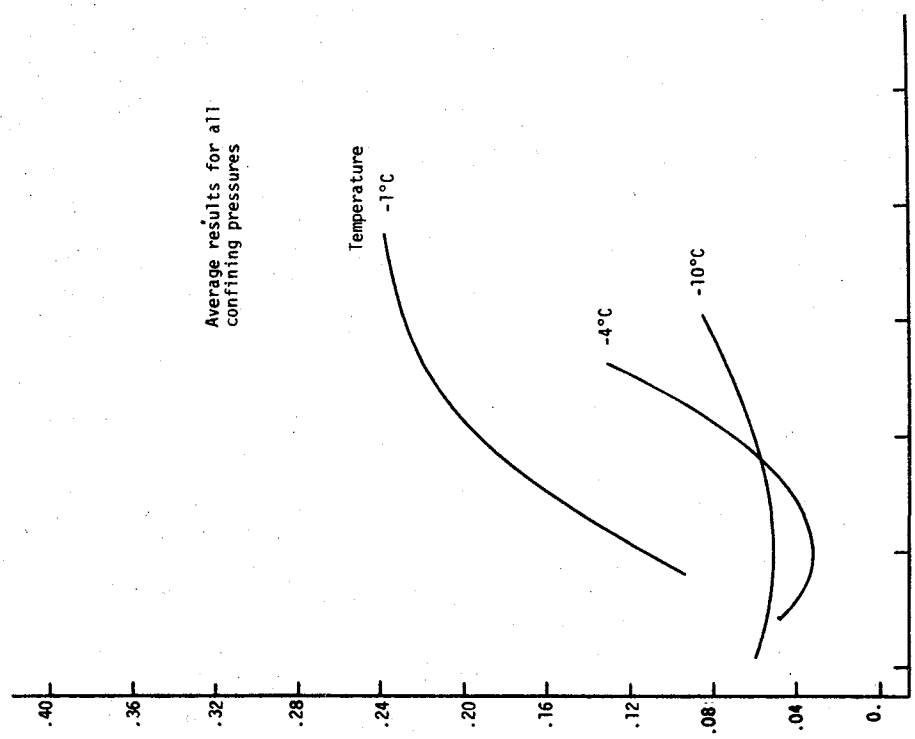

Figure 4.41 DAMPING RATIO VERSUS AXIAL STRAIN FOR HANOVER SILT AT 10.0 cps FREQUENCY AND 21.4% WATER CONTENT

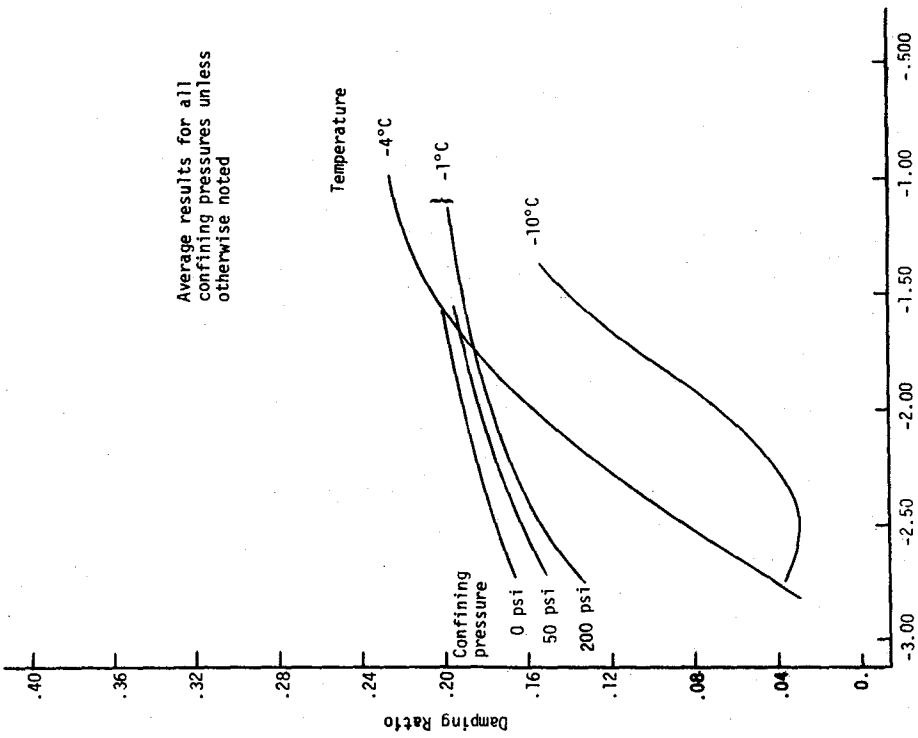

Figure 4.44 DAMPING RATIO VERSUS AXIAL STRAIN FOR HANOVER SILT AT 1.0 cps FREQUENCY AND 35.5% WATER CONTENT

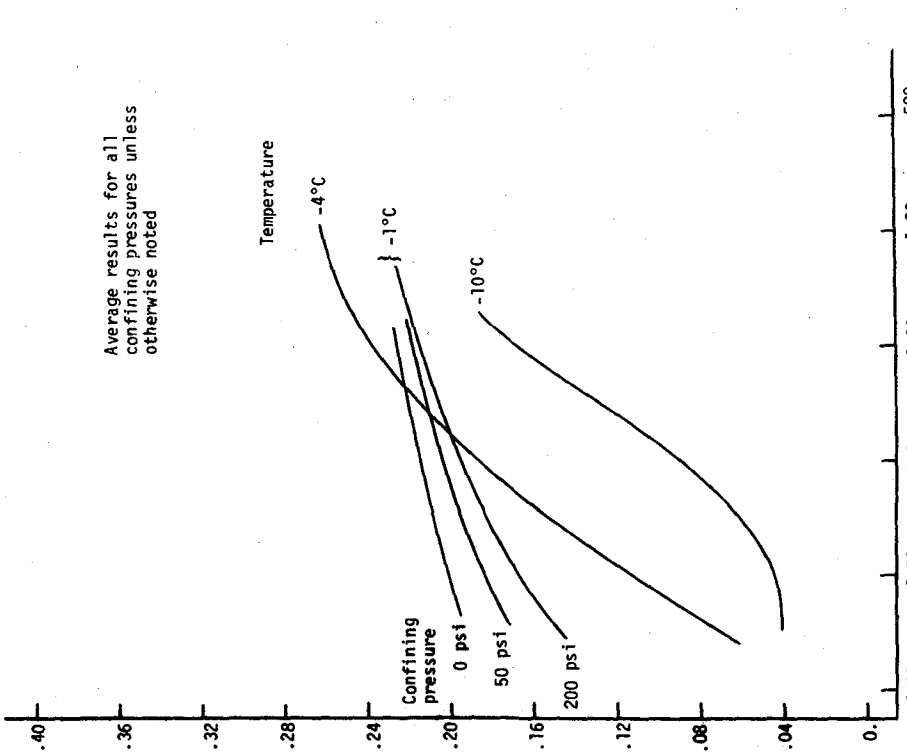

Figure 4.43 DAMPING RATIO VERSUS AXIAL STRAIN FOR HANOVER SILT AT 0.3 cps FREQUENCY AND 35.5% WATER CONTENT

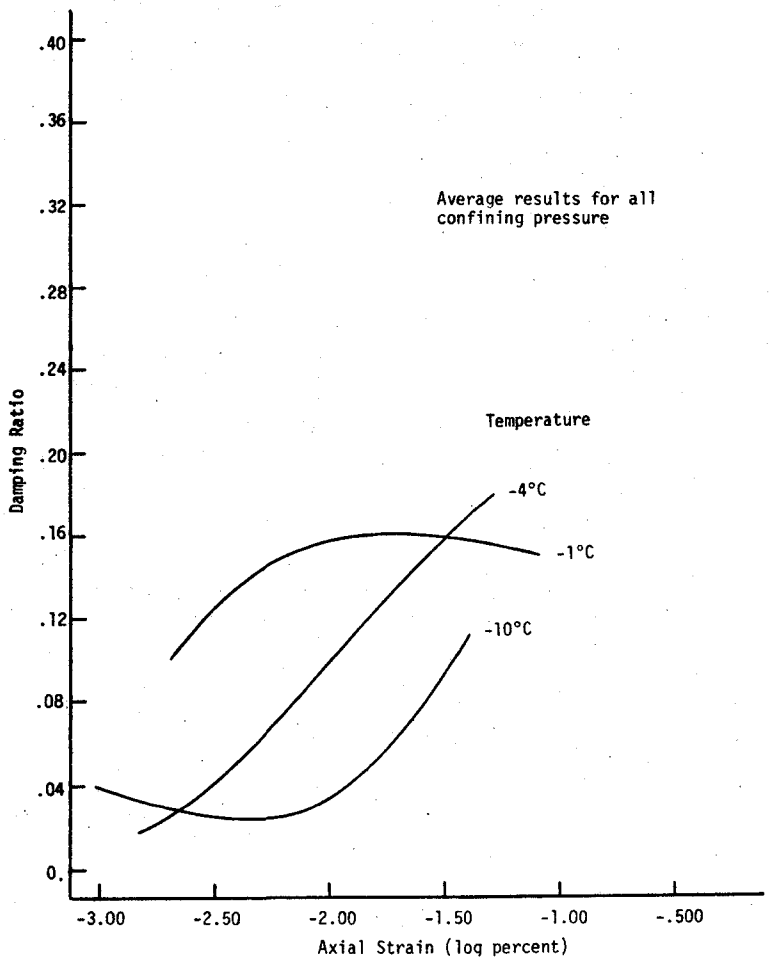

Figure 4.45 DAMPING RATIO VERSUS AXIAL STRAIN FOR HANOVER SILT AT 5.0 cps FREQUENCY AND 35.5% WATER CONTENT

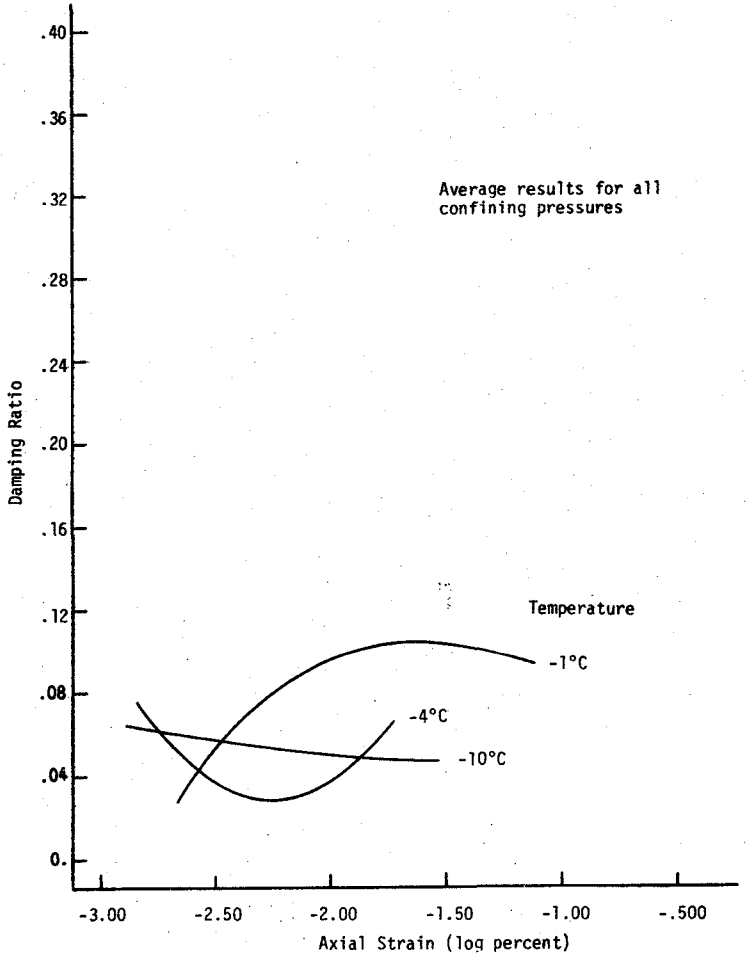

Figure 4.46 DAMPING RATIO VERSUS AXIAL STRAIN FOR HANOVER SILT AT 10.0 cps FREQUENCY AND 35.5% WATER CONTENT

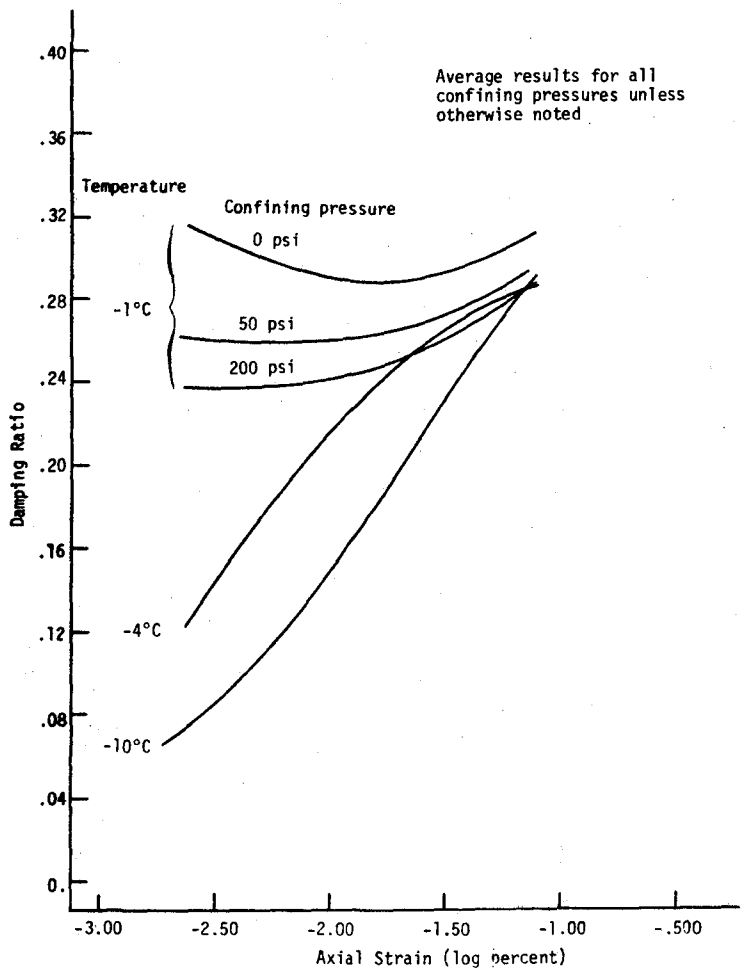

Figure 4.47 DAMPING RATIO VERSUS AXIAL STRAIN FOR ALASKA SILT AT 0.05 cps FREQUENCY AND 20.5% WATER CONTENT

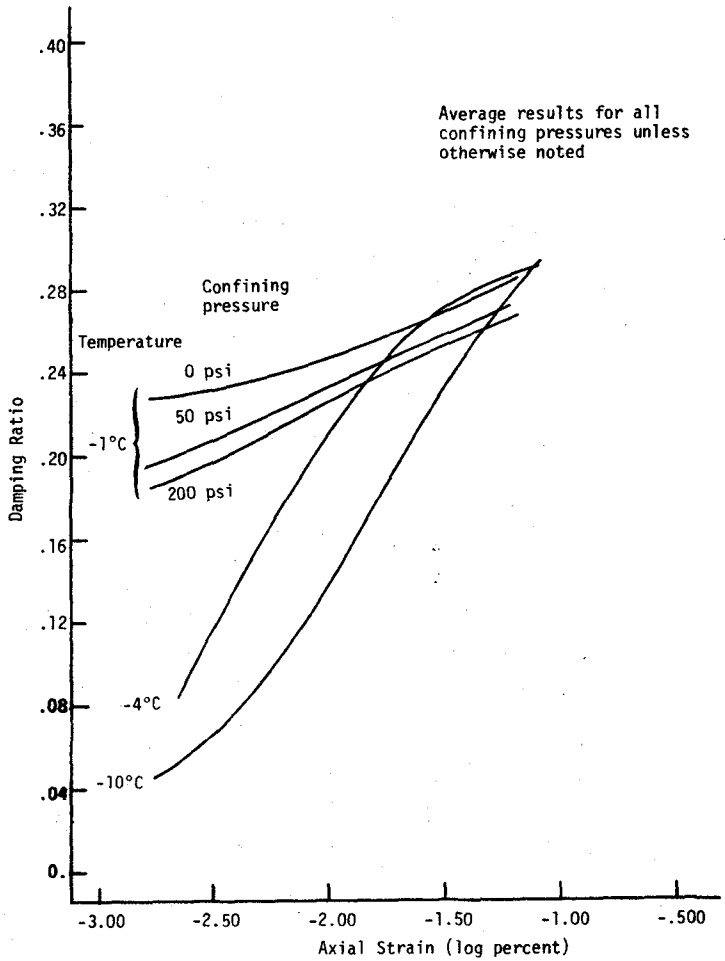

Figure 4.48 DAMPING RATIO VERSUS AXIAL STRAIN FOR ALASKA SILT AT 0.3 cps FREQUENCY AND 20.5% WATER CONTENT

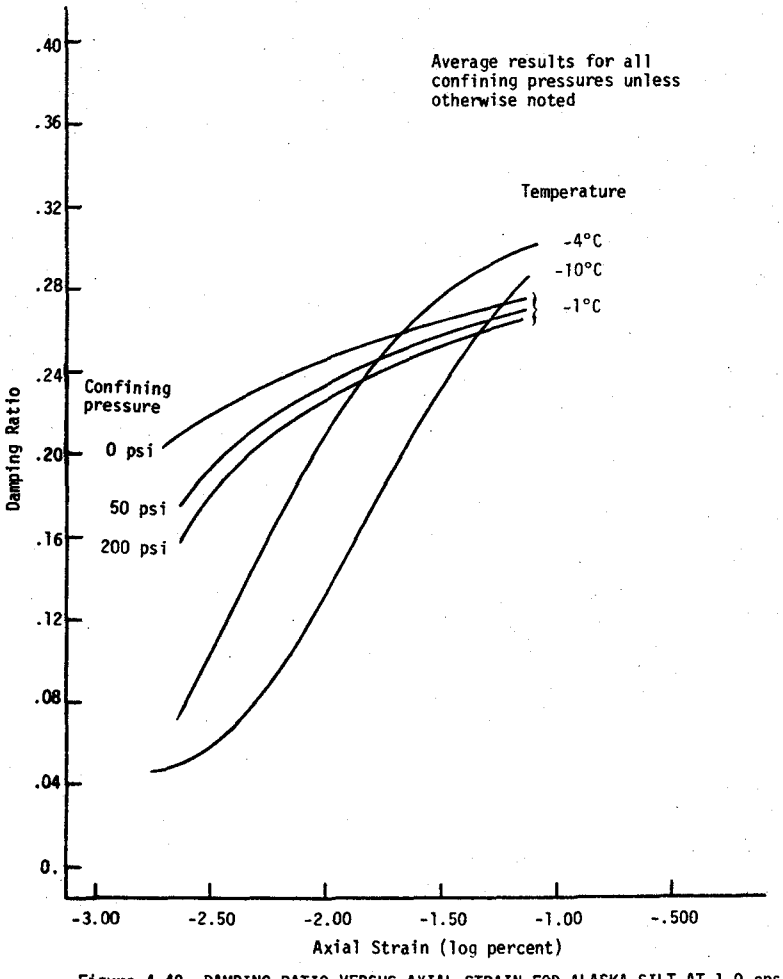

Figure 4.49 DAMPING RATIO VERSUS AXIAL STRAIN FOR ALASKA SILT AT 1.0 cps FREQUENCY AND 20.5% WATER CONTENT

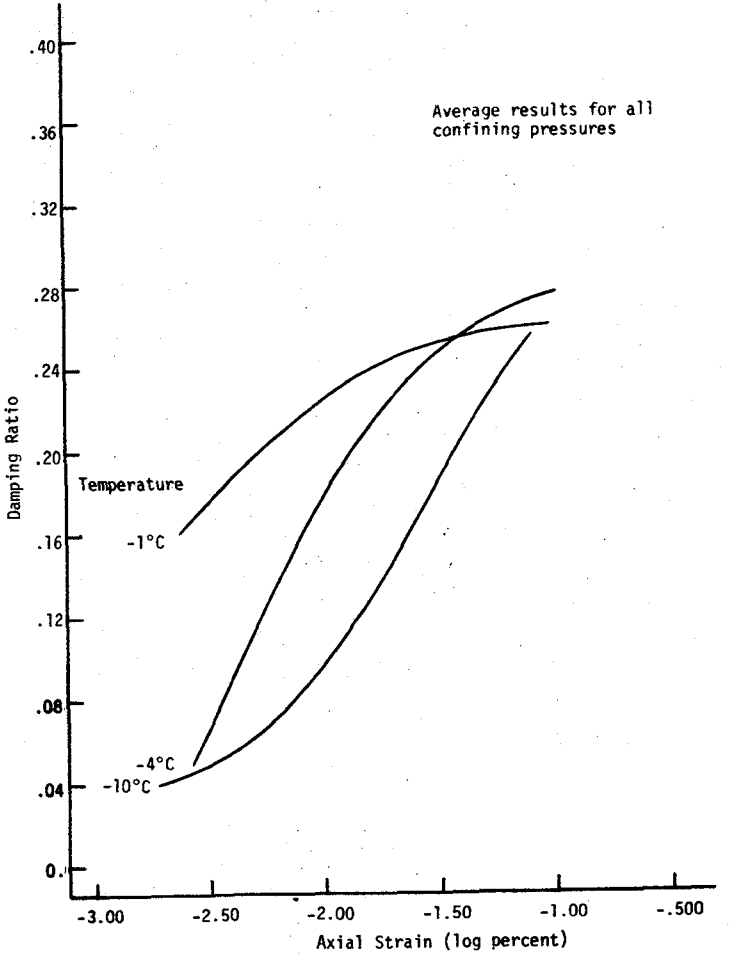

Figure 4.50 DAMPING RATIO VERSUS AXIAL STRAIN FOR ALASKA SILT AT 5.0 cps FREQUENCY AND 20.5% WATER CONTENT

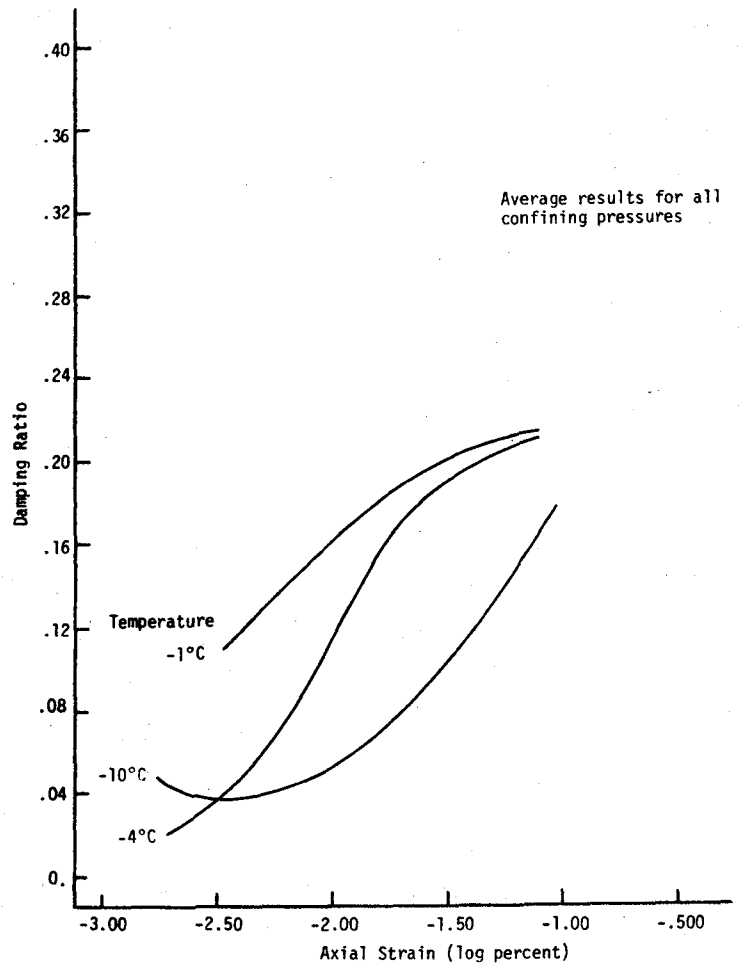

Figure 4.51 DAMPING RATIO VERSUS AXIAL STRAIN FOR ALASKA SILT AT 10.0 cps FREQUENCY AND 20.5% WATER CONTENT

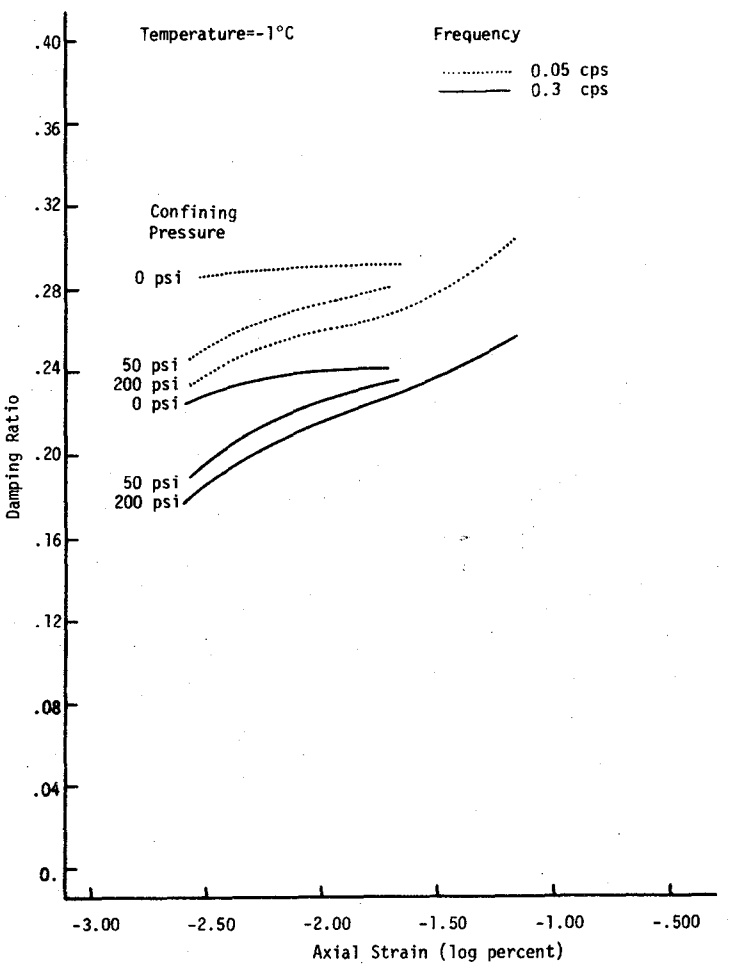

Figure 4.52 DAMPING RATIO VERSUS AXIAL STRAIN FOR ALASKA SILT AT 29.2% WATER CONTENT

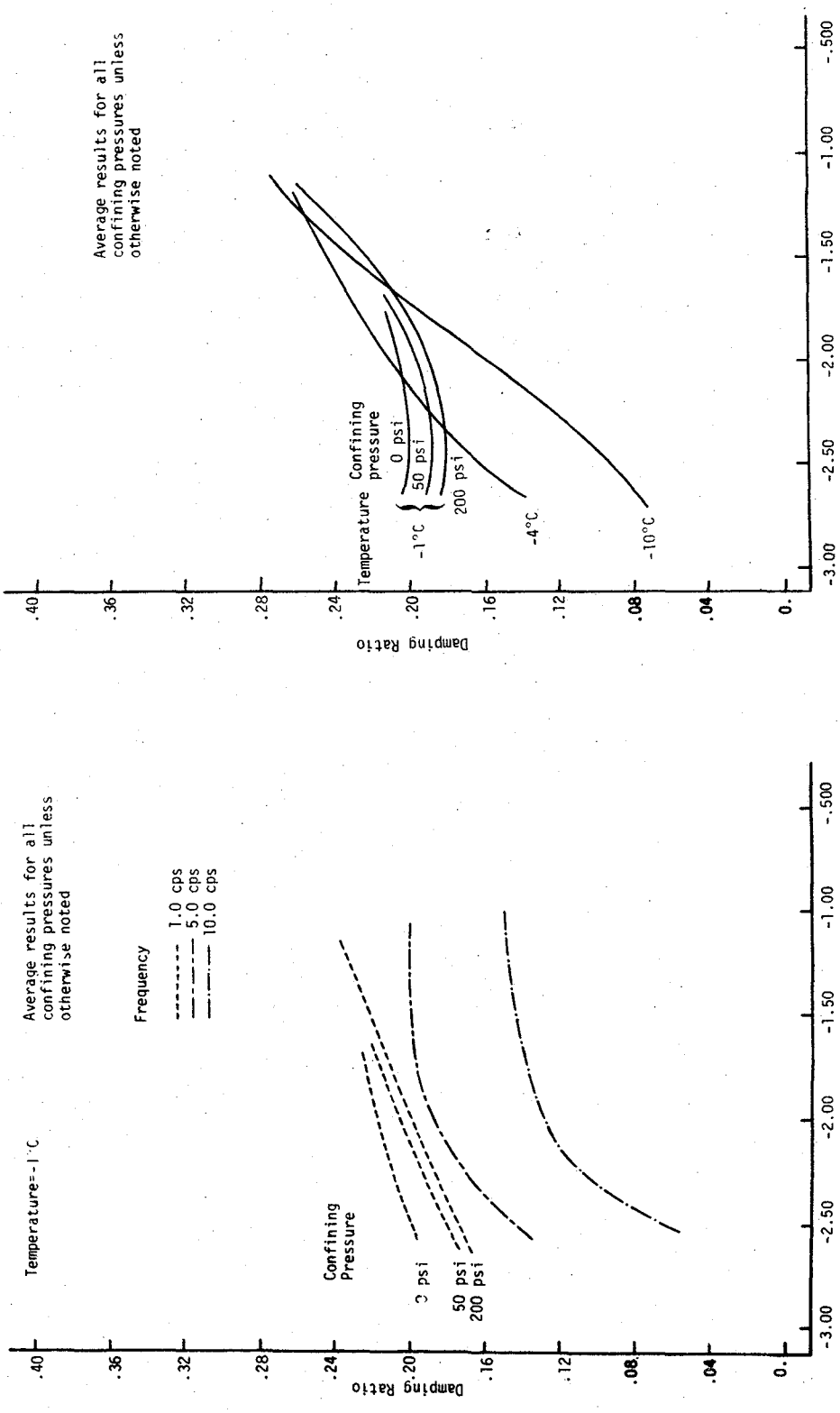

Figure 4.53 DAMPING RATIO VERSUS AXIAL STRAIN FOR ALASKA SILT AT 29.2% WATER CONTENT

Figure 4.54 DAMPING RATIO VERSUS AXIAL STRAIN FOR ALASKA SILT AT 0.05 cps FREQUENCY AND 38.9% WATER CONTENT

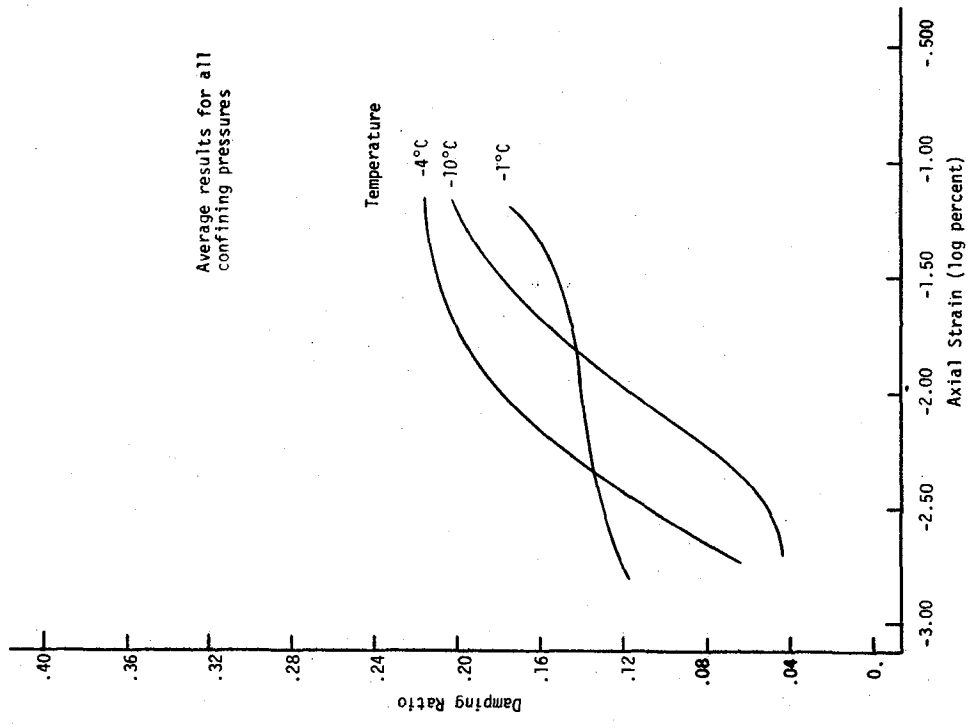

Figure 4.56 DAMPING RATIO VERSUS AXIAL STRAIN FOR ALASKA SILT AT 1.0 cps FREQUENCY AND 38.9% WATER CONTENT

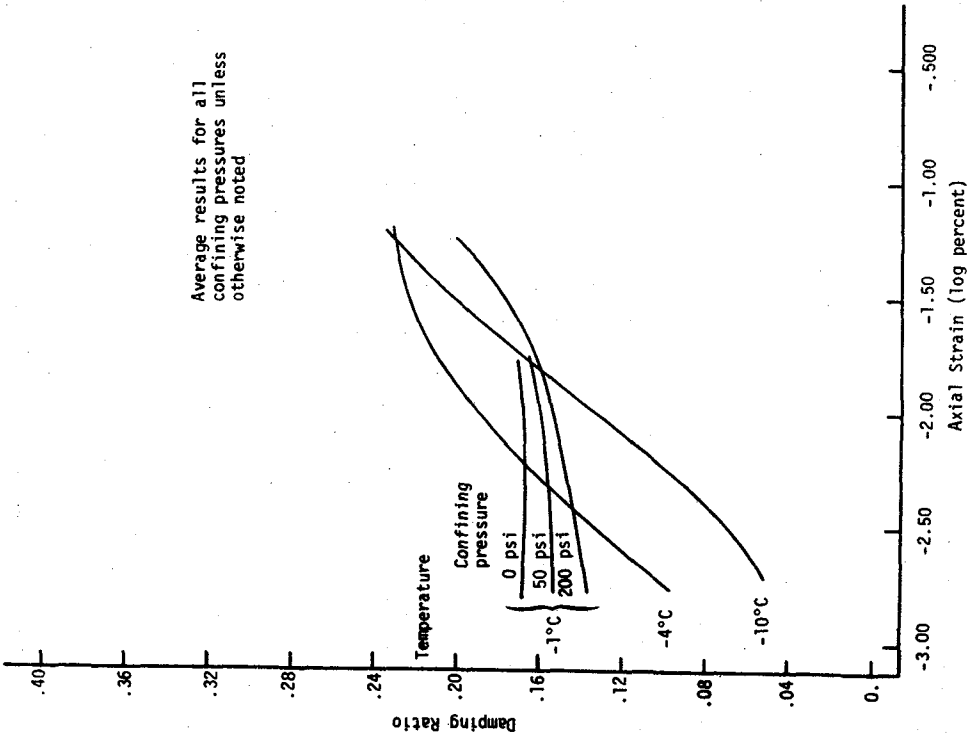

Figure 4.55 DAMPING RATIO VERSUS AXIAL STRAIN FOR ALASKA SILT AT 0.3 cps FREQUENCY AND 38.9% WATER CONTENT

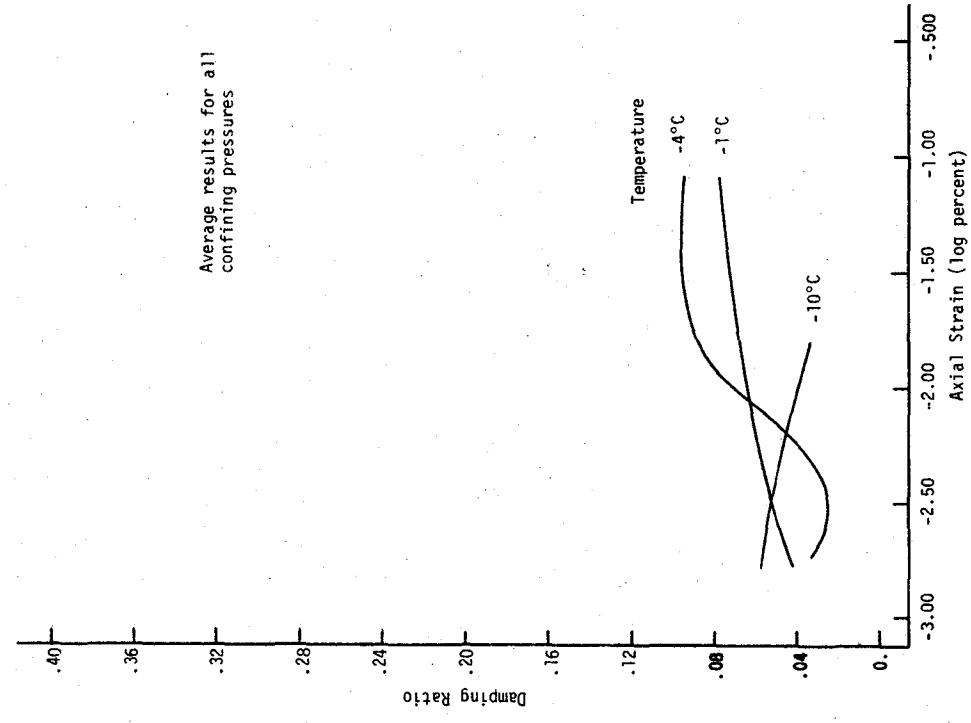

Figure 4.58 DAMPING RATIO VERSUS AXIAL STRAIN FOR ALASKA SILT AT 10 cps FREQUENCY AND 38.9% WATER CONTENT

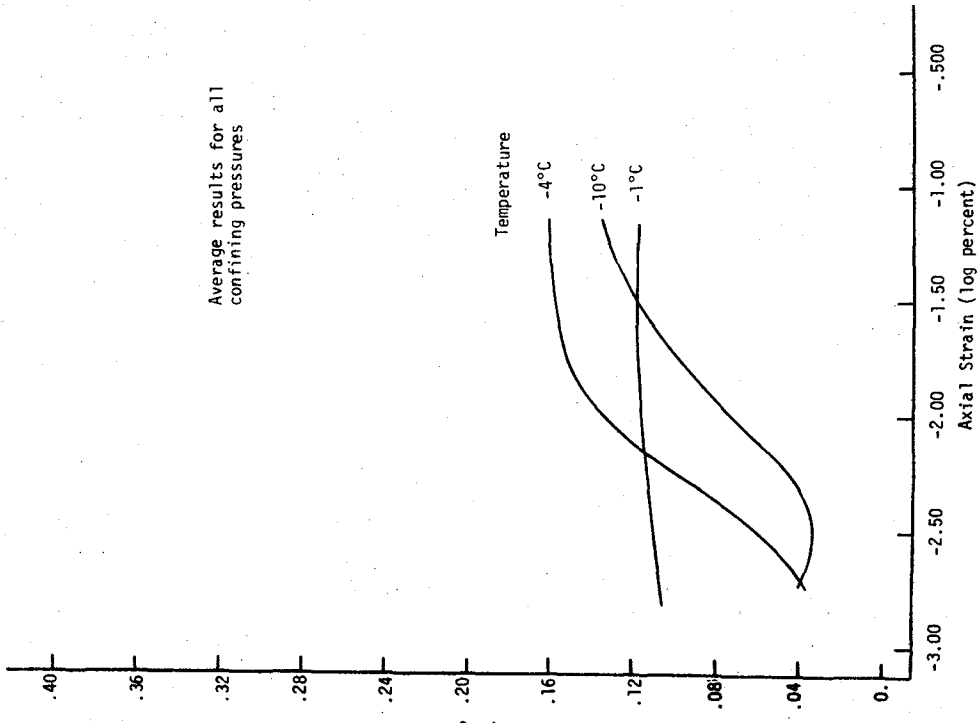

Figure 4.57 DAMPING RATIO VERSUS AXIAL STRAIN FOR ALASKA SILT AT 5.0 cps FREQUENCY AND 38.9% WATER CONTENT

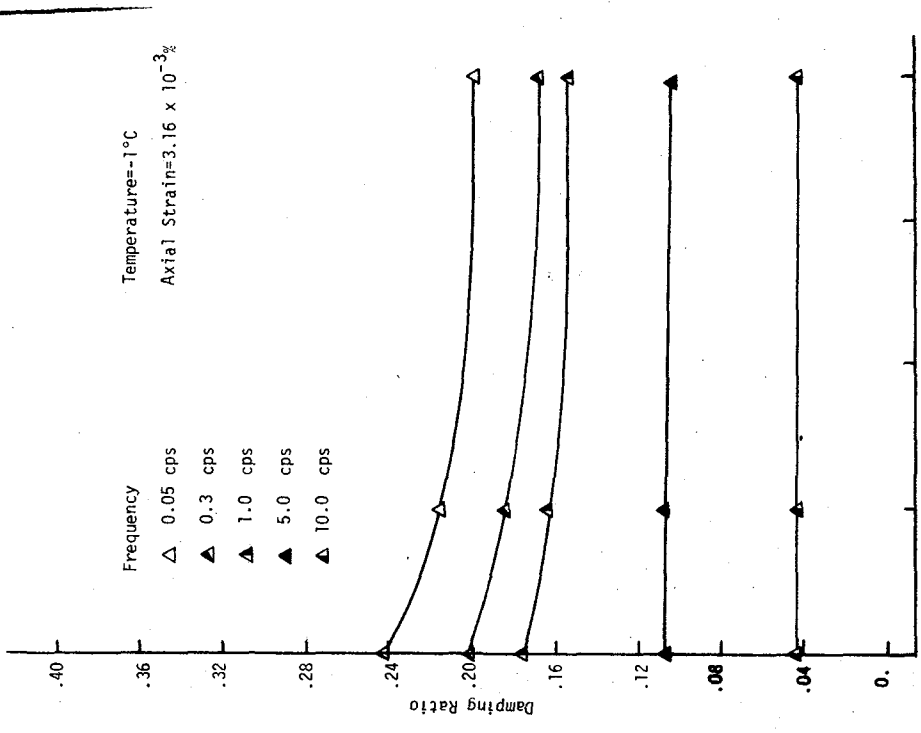

Figure 4.60 DAMPING RATIO VERSUS CONFINING PRESSURE FOR HANOVER SILT AT A WATER CONTENT OF 35.5%

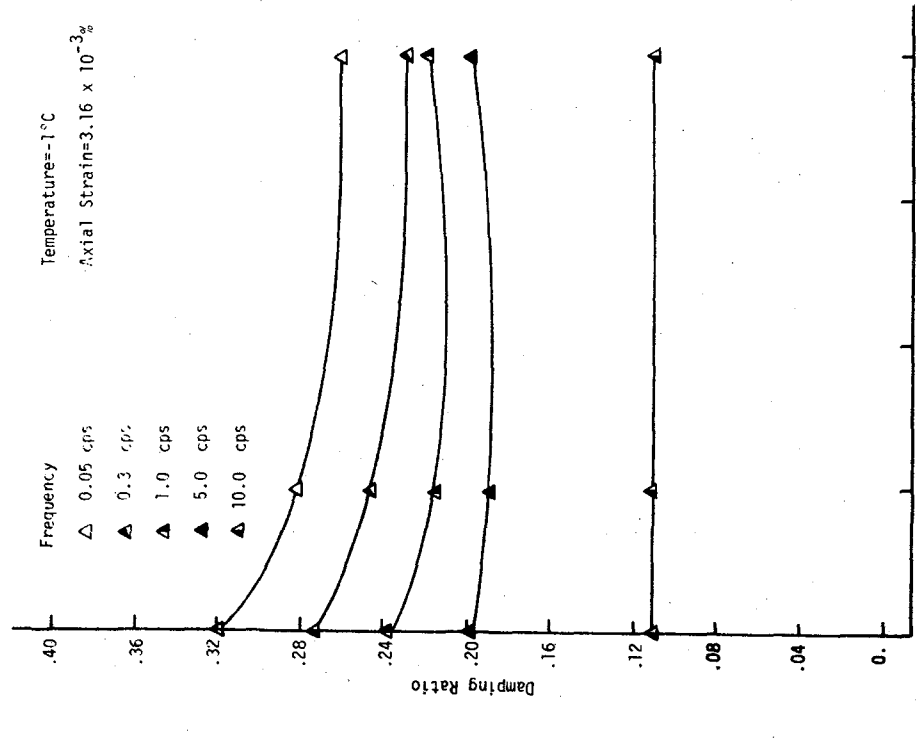

Figure 4.59 DAMPING RATIO VERSUS CONFINING PRESSURE FOR HANOVER SILT AT A WATER CONTENT OF 21.4%

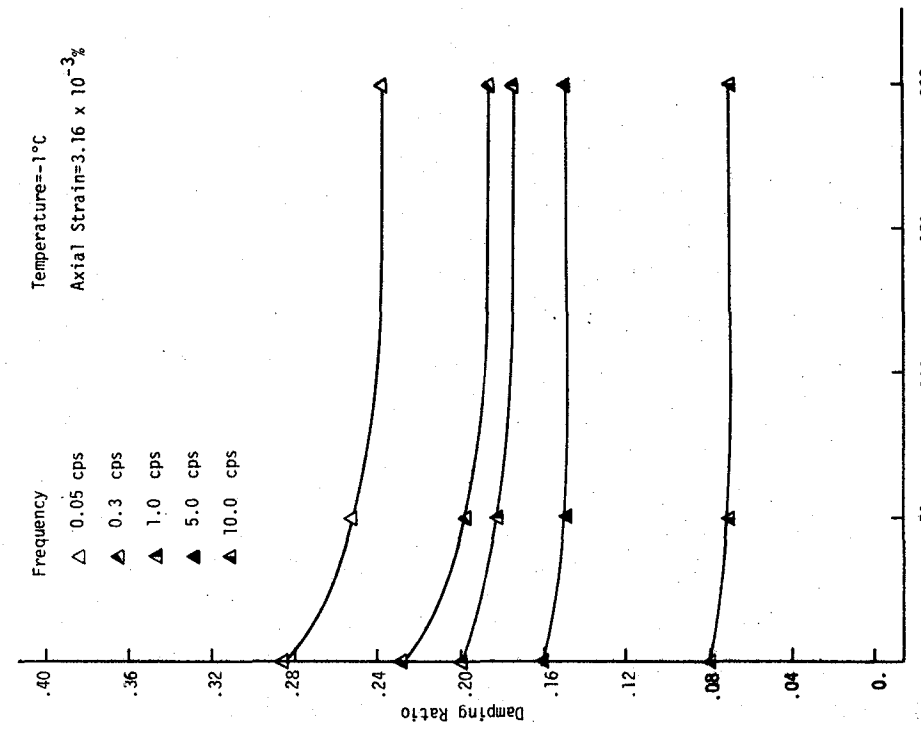

Figure 4.62 DAMPING RATIO VERSUS CONFINING PRESSURE FOR ALASKA SILT AT A WATER CONTENT OF 29.2%

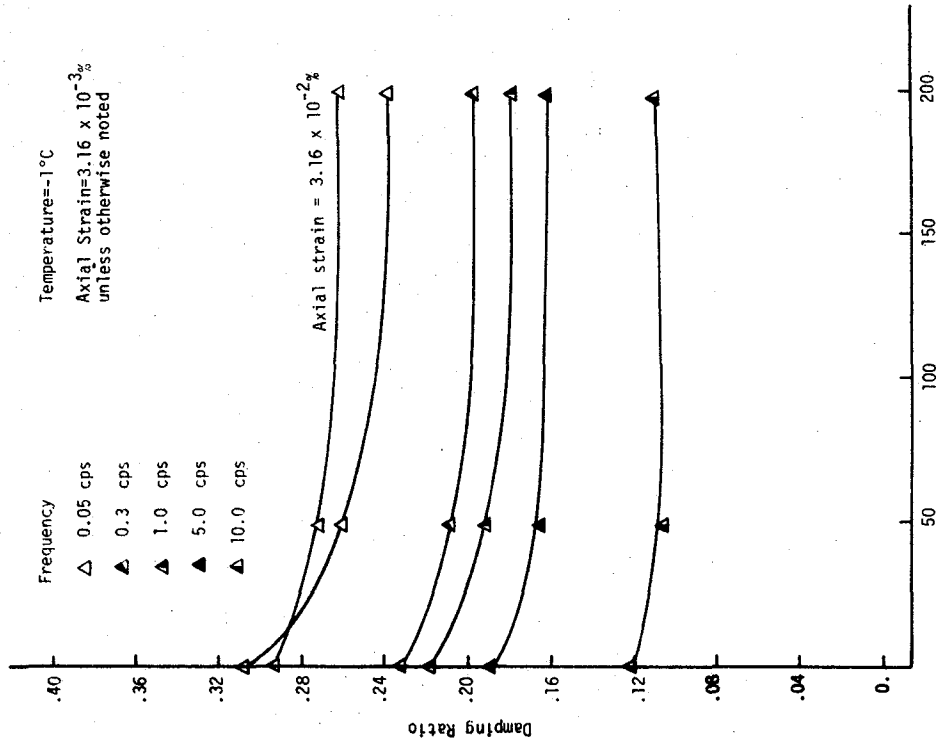

Figure 4.61 DAMPING RATIO VERSUS CONFINING PRESSURE FOR ALASKA SILT AT A WATER CONTENT OF 20.5%

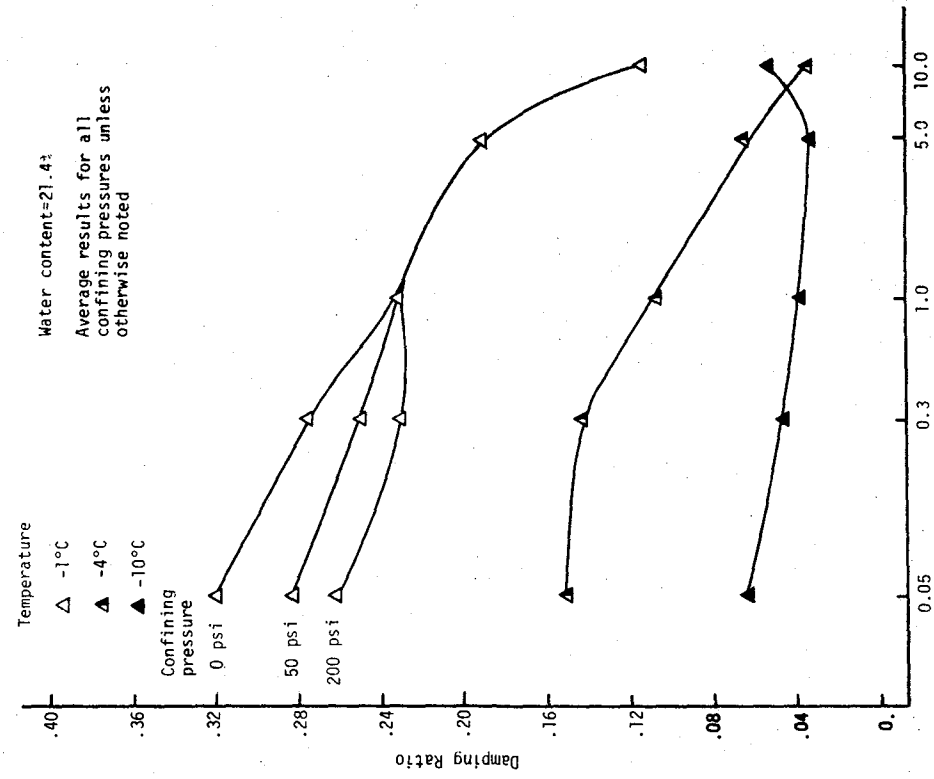

Figure 4.64 DAMPING RATIO VERSUS FREQUENCY FOR HANOVER SILT AT AN AXIAL STRAIN OF 3.16×10^{-3}%

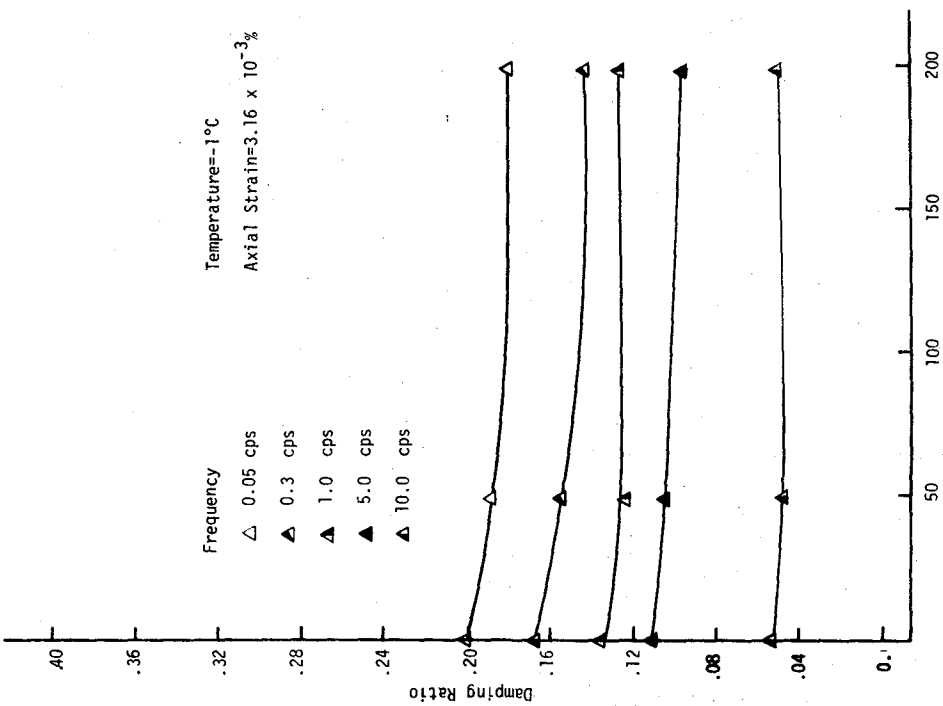

Figure 4.63 DAMPING RATIO VERSUS CONFINING PRESSURE FOR ALASKA SILT AT A WATER CONTENT OF 38.9%

curve has been shown for the damping ratio-confining pressure relationship at a high strain amplitude (Figure 4.61). In general, the rate of decrease of damping ratio is more pronounced at low confining pressures (0 to 50 psi) than at high confining pressures (50 to 200 psi). It appears that confining pressure has a more significant influence on damping ratio at low water contents than at high water contents.

4.4.3 Effect of Frequency

The relationships between damping ratio and frequency are given in Figures 4.64 to 4.73. Each graph represents the relationship for a silt at a particular water content at three temperatures and, where applicable, at three confining pressures. At a temperature of $-1^{o}C$, the damping ratio decreases by a moderate amount in the frequency range 0.05 to 5.0 cps and decreases sharply from 5.0 to 10.0 cps. In general, at low water contents the influence of frequency on damping ratio is more significant at a low strain amplitude ($3.16 \times 10^{-3}\%$) than at a high strain amplitude ($3.16 \times 10^{-2}\%$). At higher water contents, the rate of decrease of damping ratio with frequency is not significantly influenced by strain amplitude.

At a temperature of $-4^{o}C$, damping ratio decreases with increasing frequency at a low strain amplitude ($3.16 \times 10^{-3}\%$) at a rate somewhat more uniform than at $-1^{o}C$. At a higher strain amplitude ($3.16 \times 10^{-2}\%$) the damping ratio-frequency relationship is similar to that at $-1^{o}C$ with a more pronounced decline in damping ratio at high frequencies than at low frequencies. At a low water content for both silts, there appears to be an initial increase in damping ratio at low frequencies followed by a sharp decrease at high frequencies.

At a temperature of $-10^{o}C$ and at a low strain amplitude ($3.16 \times 10^{-3}\%$) damping ratio generally decreases by a small amount with increasing frequency at low frequencies (0.05 to 5.0 cps) and increases at higher frequencies (5.0 to 10.0 cps). At a high strain amplitude ($3.16 \times 10^{-2}\%$) the damping ratio-frequency relationship is similar to that at -1 and $-4^{o}C$. The rate of decrease of damping ratio is greater at high frequencies than at low frequencies.

4.4.4 Effect of Temperature

The relationship between damping ratio and temperature is given in Figures 4.74 to 4.90. Each graph represents the relationship for a silt

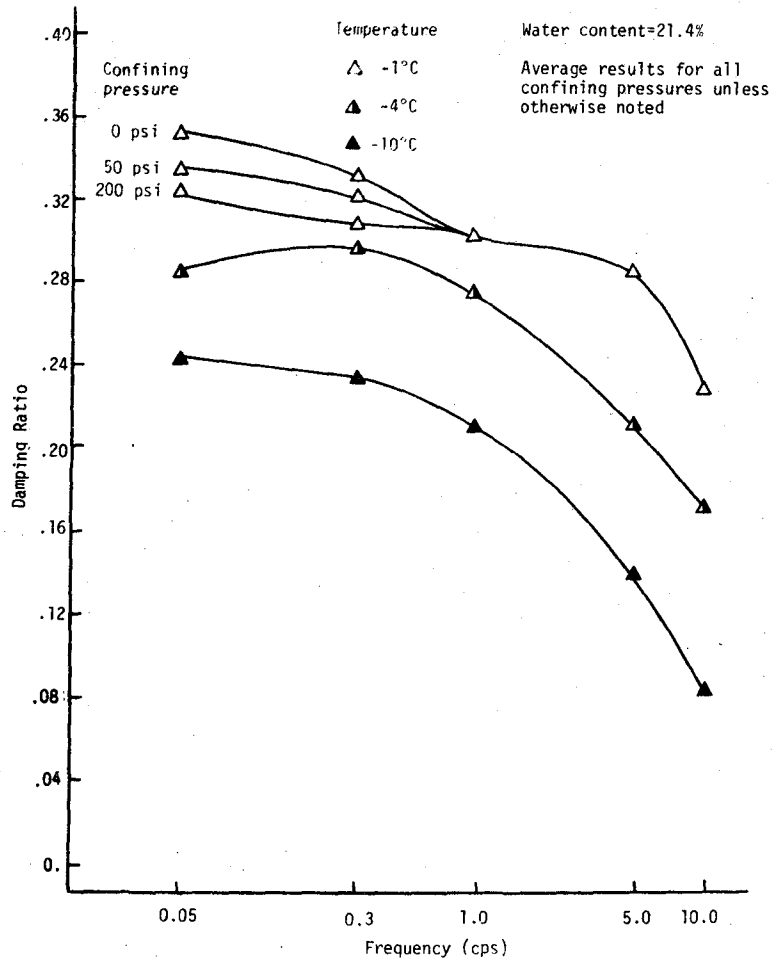

Figure 4.65 DAMPING RATIO VERSUS FREQUENCY FOR HANOVER SILT AT AN AXIAL STRAIN OF 3.16×10^{-2}%

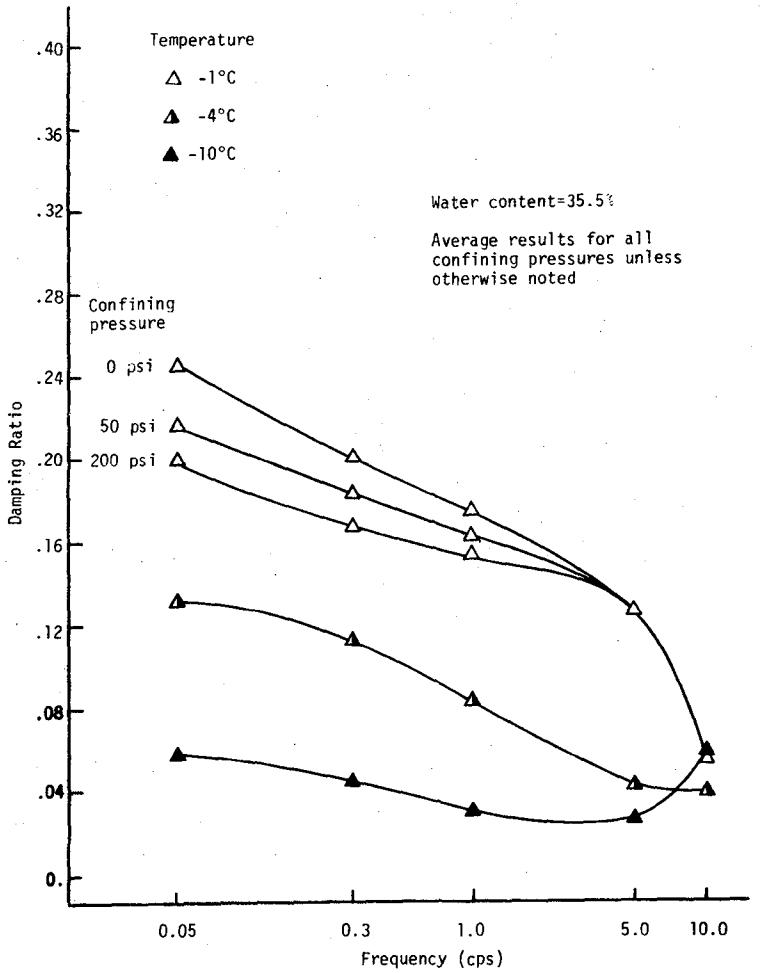

Figure 4.66 DAMPING RATIO VERSUS FREQUENCY FOR HANOVER SILT AT AN AXIAL STRAIN OF 3.16×10^{-3}%

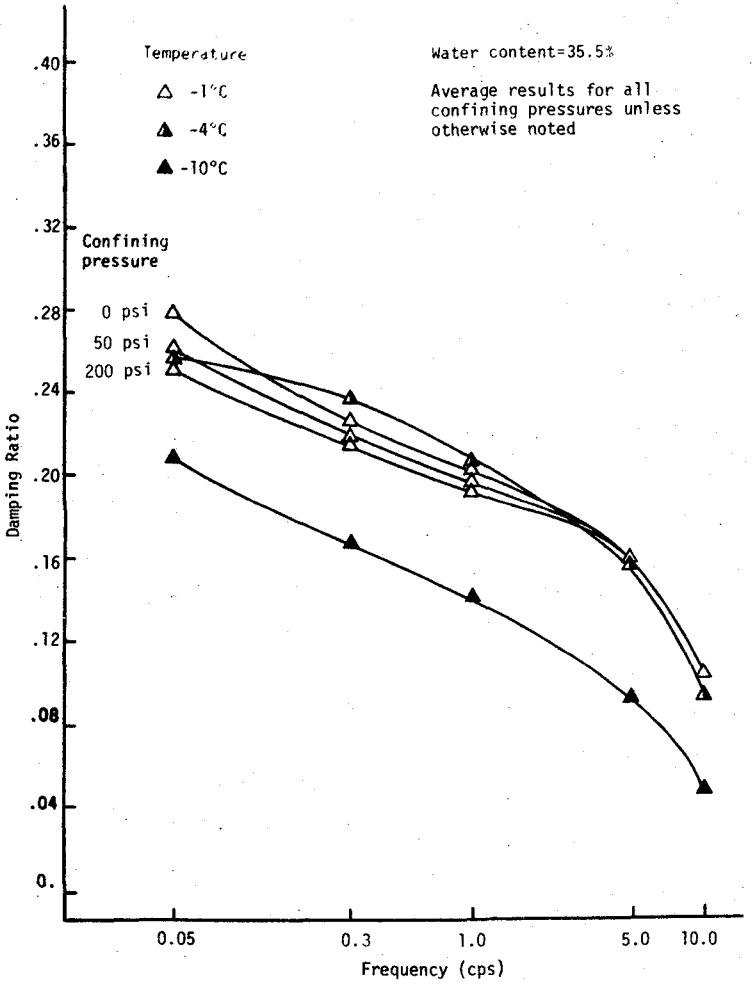

Figure 4.67 DAMPING RATIO VERSUS FREQUENCY FOR HANOVER SILT AT AN AXIAL STRAIN OF 3.16×10^{-2}%

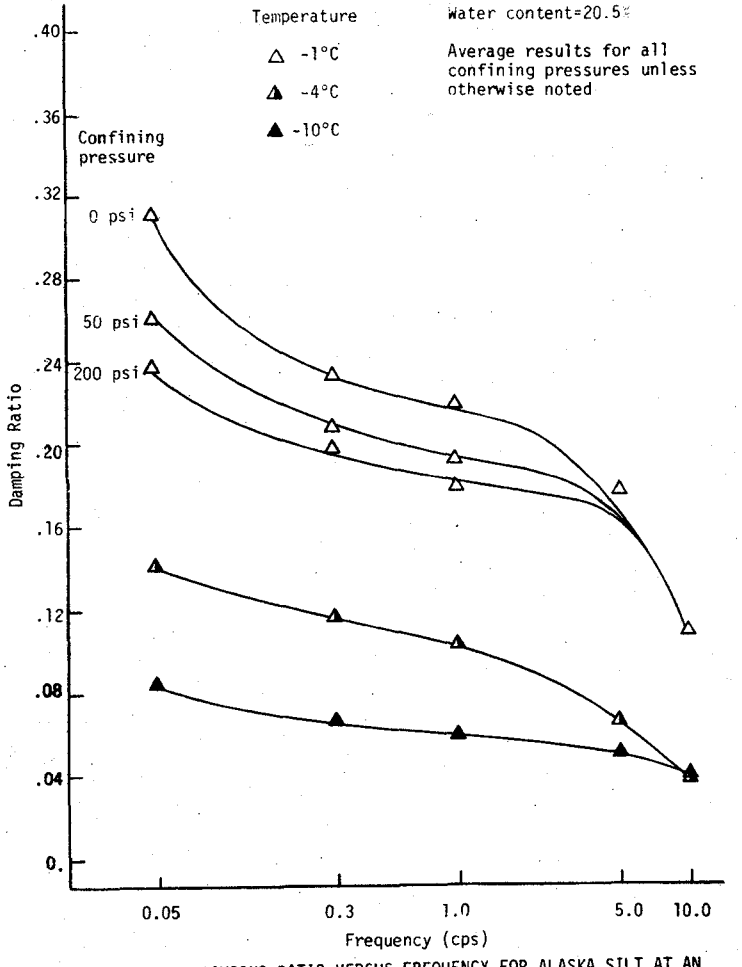

Figure 4.68 DAMPING RATIO VERSUS FREQUENCY FOR ALASKA SILT AT AN AXIAL STRAIN OF 3.16×10^{-3}%

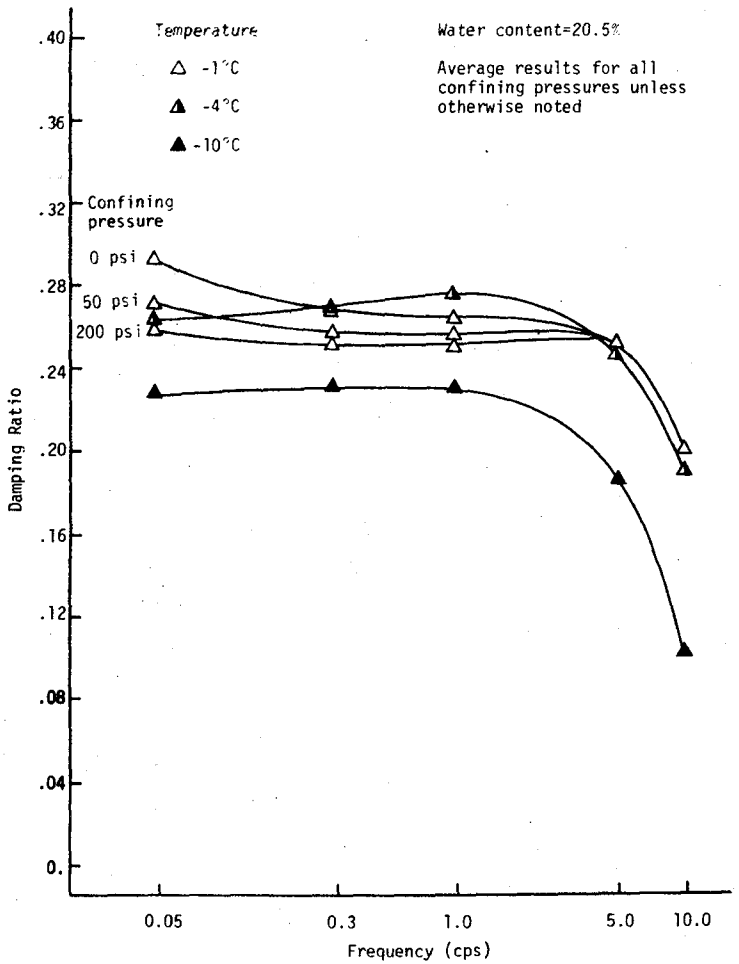

Figure 4.69 DAMPING RATIO VERSUS FREQUENCY FOR ALASKA SILT AT AN AXIAL STRAIN OF 3.16×10^{-2}%

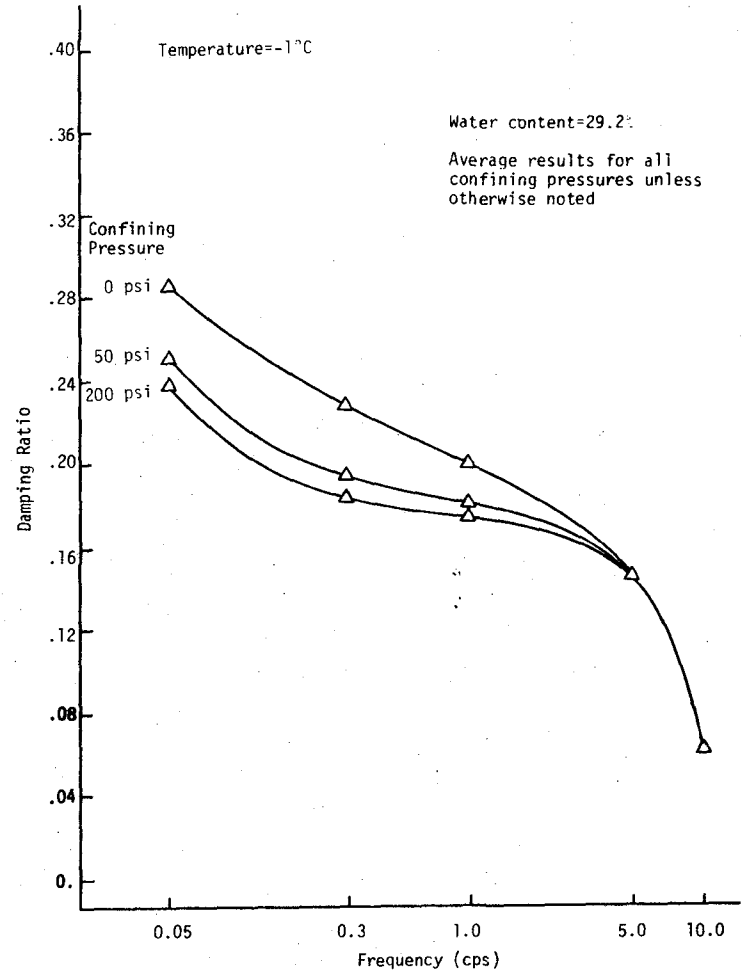

Figure 4.70 DAMPING RATIO VERSUS FREQUENCY FOR ALASKA SILT AT AN AXIAL STRAIN OF 3.16×10^{-3}%

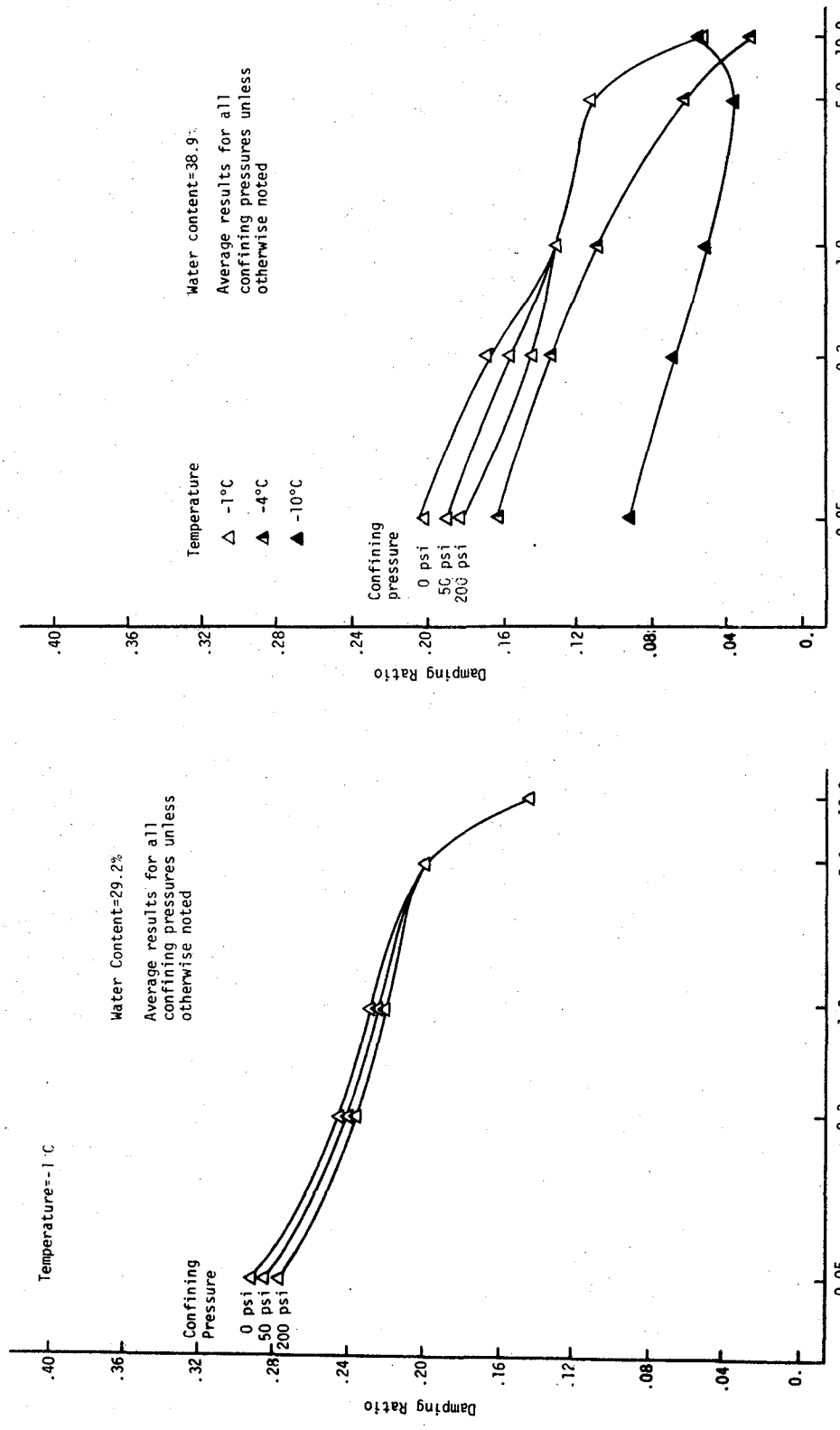

Figure 4.71 DAMPING RATIO VERSUS FREQUENCY FOR ALASKA SILT AT AN AXIAL STRAIN OF 3.16×10^{-2}%

Figure 4.72 DAMPING RATIO VERSUS FREQUENCY FOR ALASKA SILT AT AN AXIAL STRAIN OF 3.16×10^{-3}%

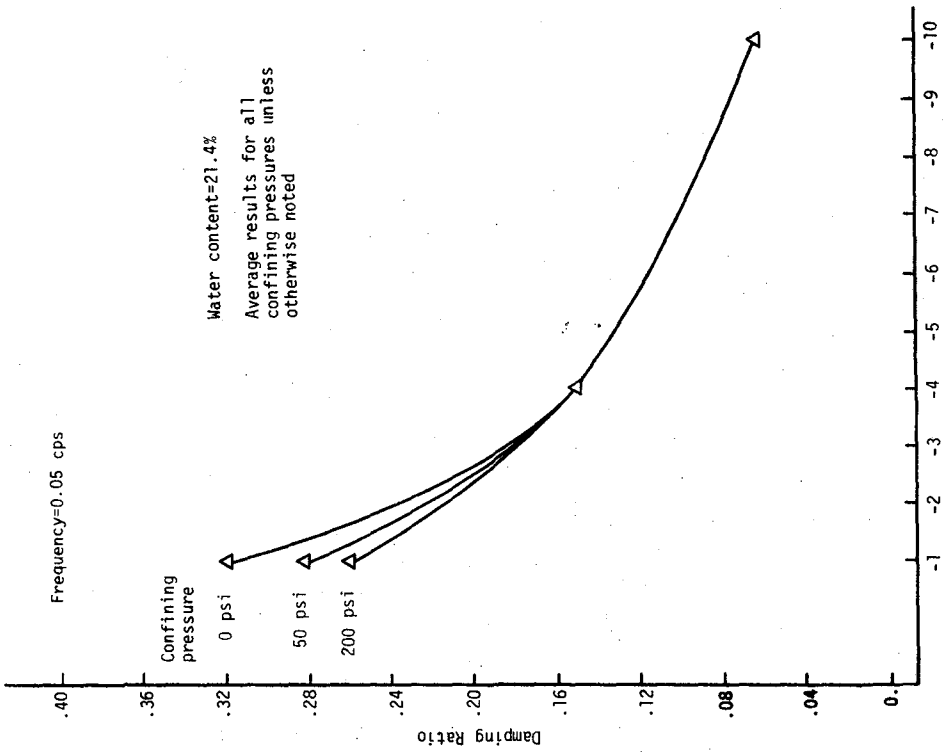

Figure 4.74 DAMPING RATIO VERSUS TEMPERATURE FOR HANOVER SILT AT AN AXIAL STRAIN OF 3.16×10^{-3}%

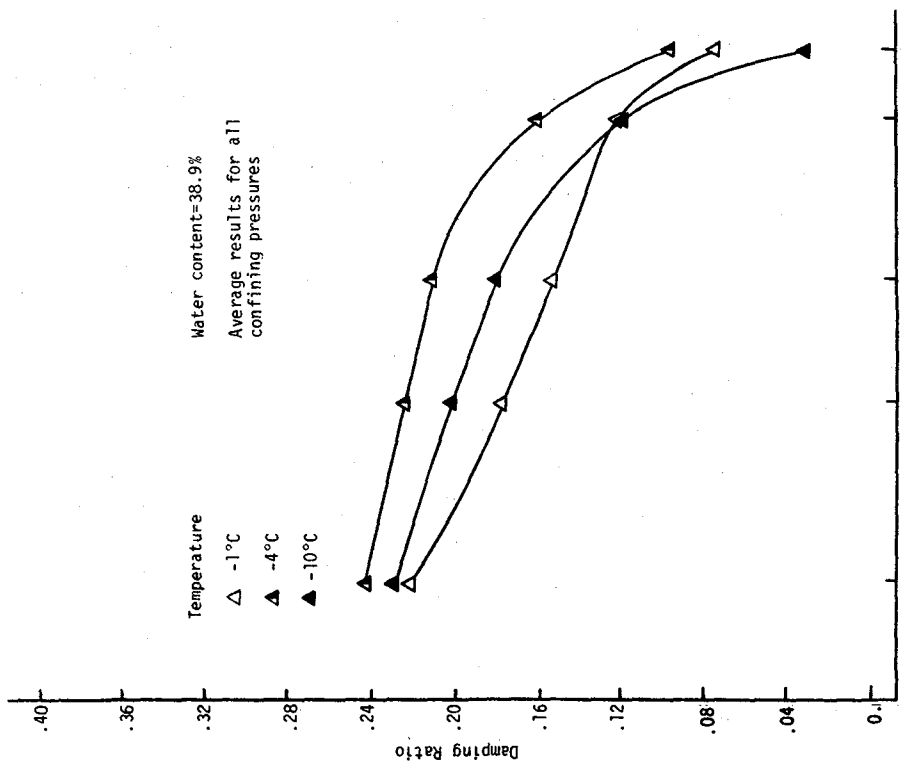

Figure 4.73 DAMPING RATIO VERSUS FREQUENCY FOR ALASKA SILT AT AN AXIAL STRAIN OF 3.16×10^{-2}%

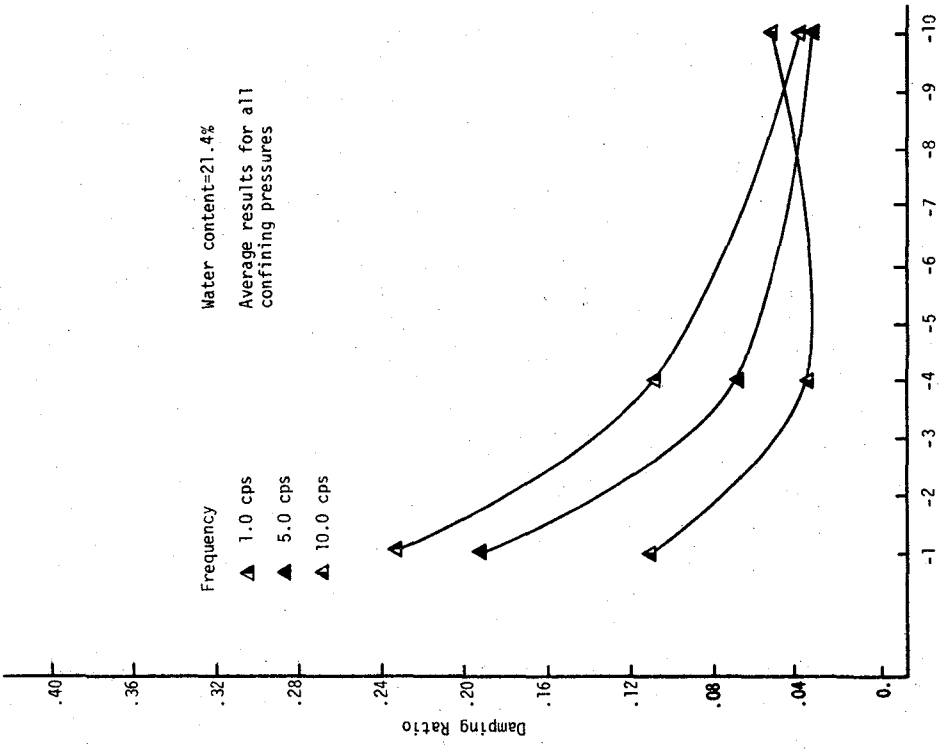

Figure 4.76 DAMPING RATIO VERSUS TEMPERATURE FOR HANOVER SILT AT AN AXIAL STRAIN OF 3.16×10^{-3}%

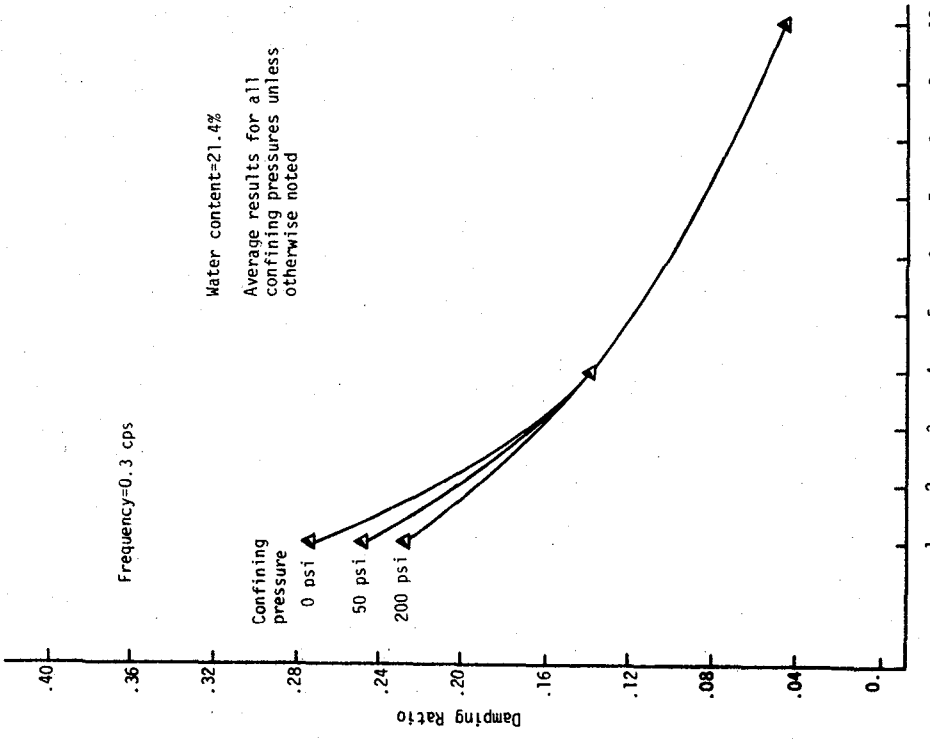

Figure 4.75 DAMPING RATIO VERSUS TEMPERATURE FOR HANOVER SILT AT AN AXIAL STRAIN OF 3.16×10^{-3}%

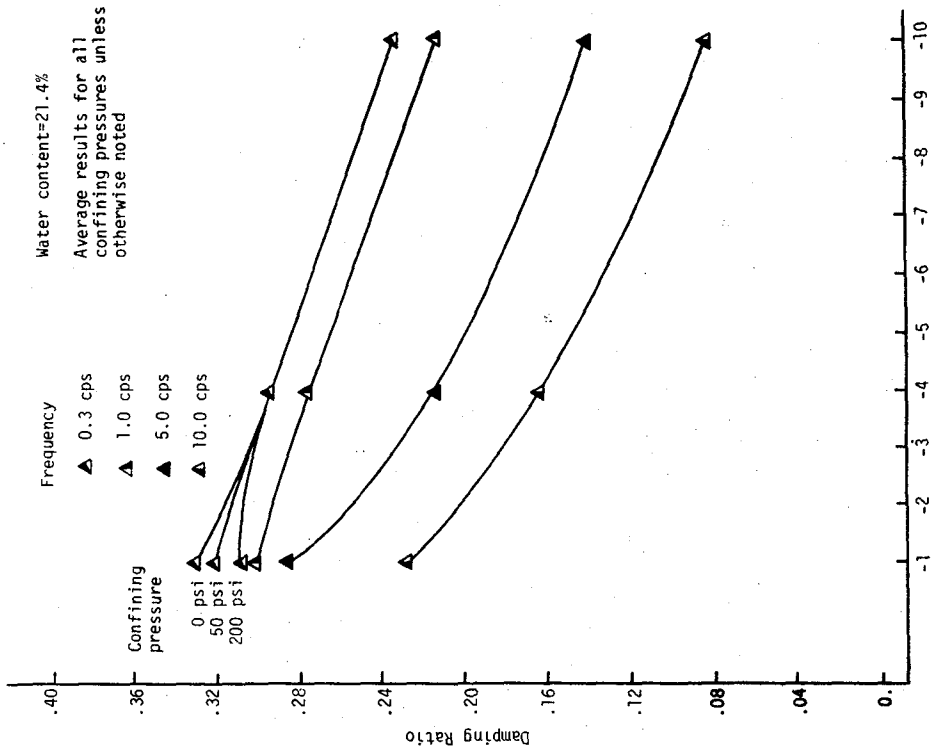

Figure 4.77 DAMPING RATIO VERSUS TEMPERATURE FOR HANOVER SILT AT AN AXIAL STRAIN OF 3.16×10^{-2}%

Figure 4.78 DAMPING RATIO VERSUS TEMPERATURE FOR HANOVER SILT AT AN AXIAL STRAIN OF 3.16×10^{-2}%

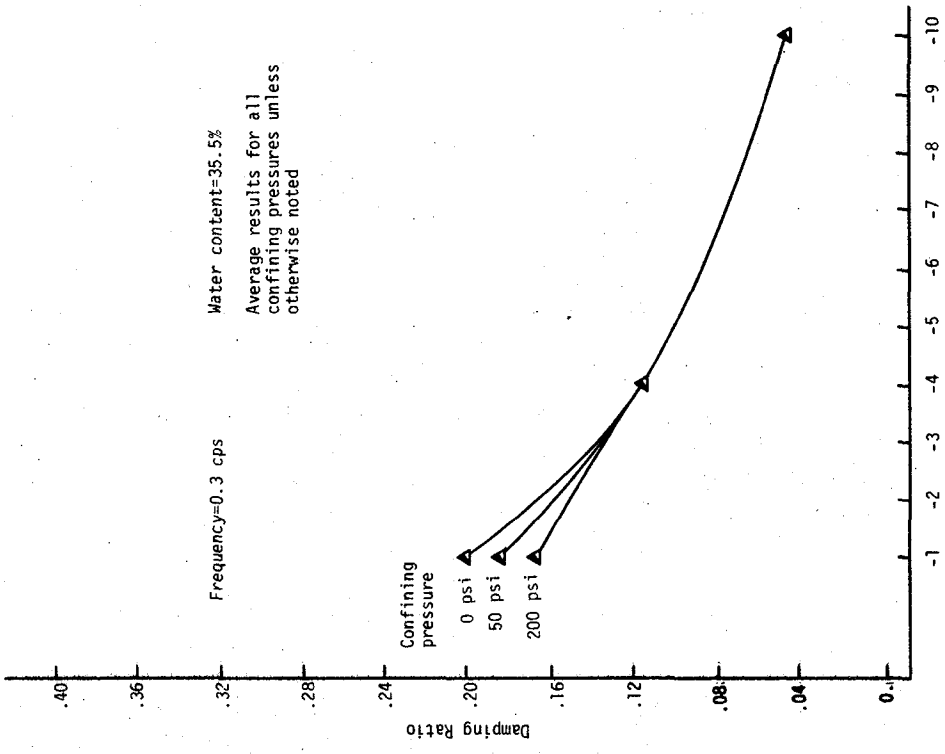

Figure 4.80 DAMPING RATIO VERSUS TEMPERATURE FOR HANOVER SILT AT AN AXIAL STRAIN OF 3.16×10^{-3}%

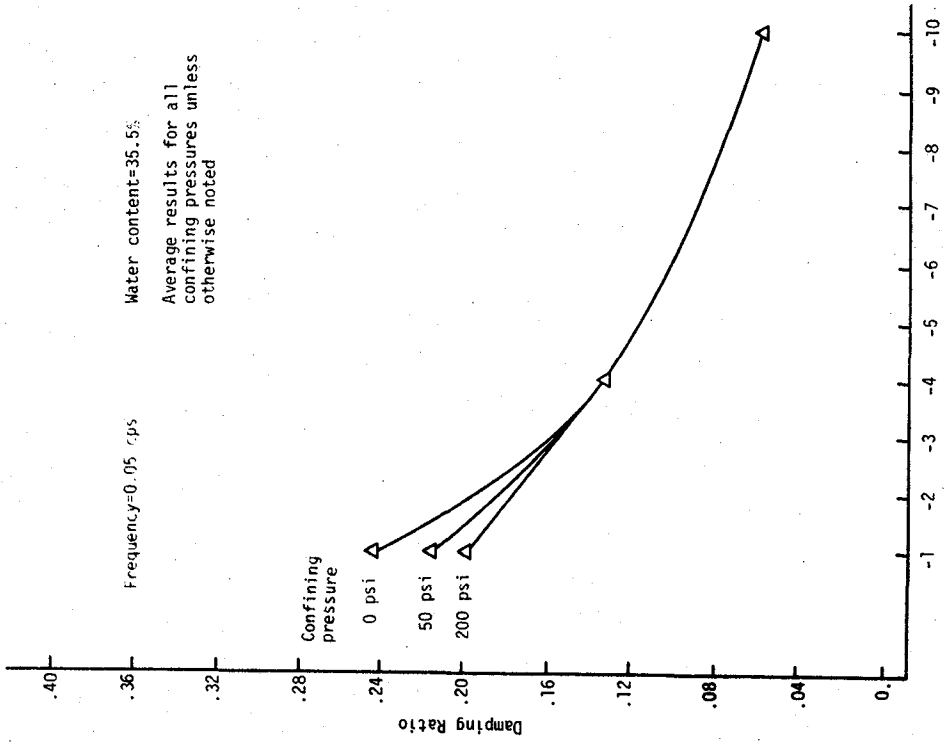

Figure 4.79 DAMPING RATIO VERSUS TEMPERATURE FOR HANOVER SILT AT AN AXIAL STRAIN OF 3.16×10^{-3}%

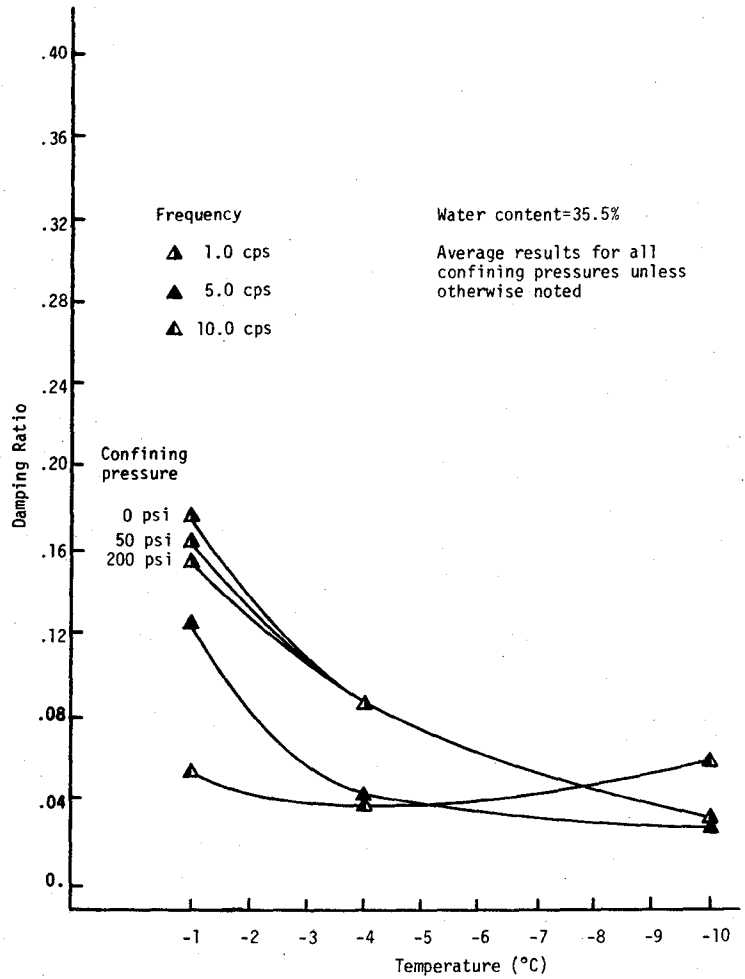

Figure 4.81 DAMPING RATIO VERSUS TEMPERATURE FOR HANOVER SILT AT AN AXIAL STRAIN OF $3.16 \times 10^{-3}\%$

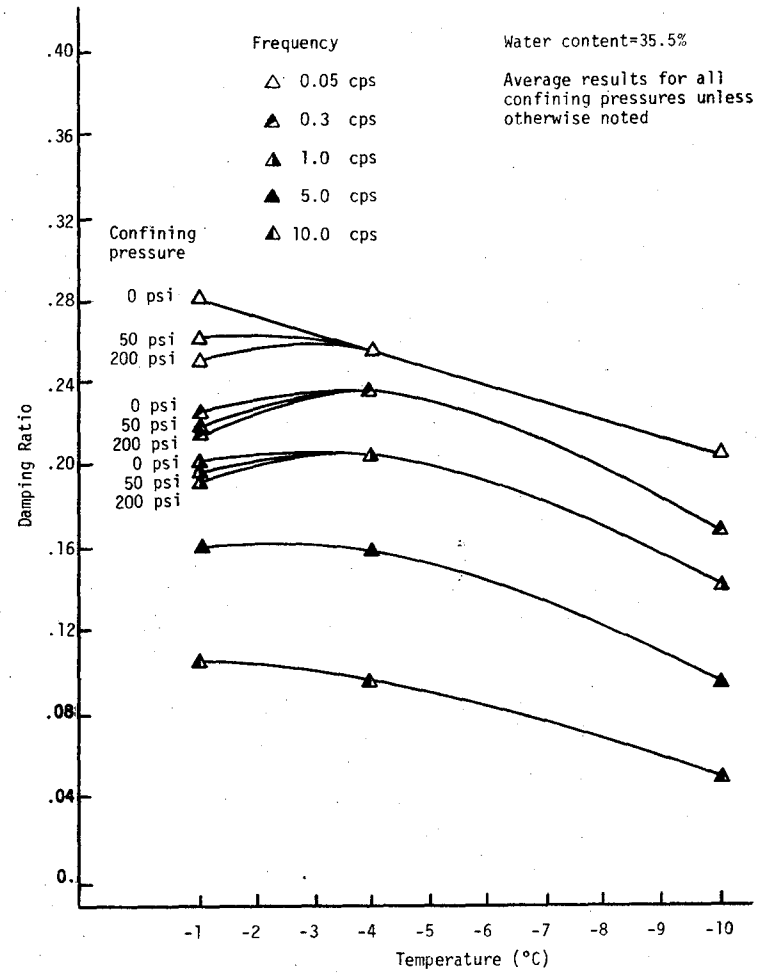

Figure 4.82 DAMPING RATIO VERSUS TEMPERATURE FOR HANOVER SILT AT AN AXIAL STRAIN OF $3.16 \times 10^{-2}\%$

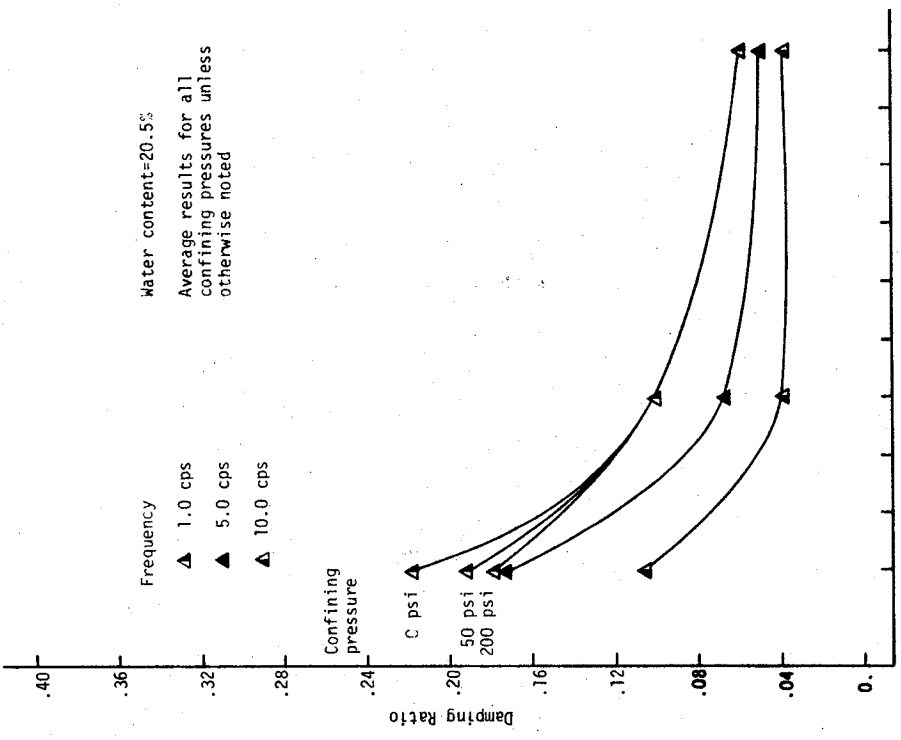

Figure 4.84 DAMPING RATIO VERSUS TEMPERATURE FOR ALASKA SILT AT AN AXIAL STRAIN OF 3.16×10^{-3}%

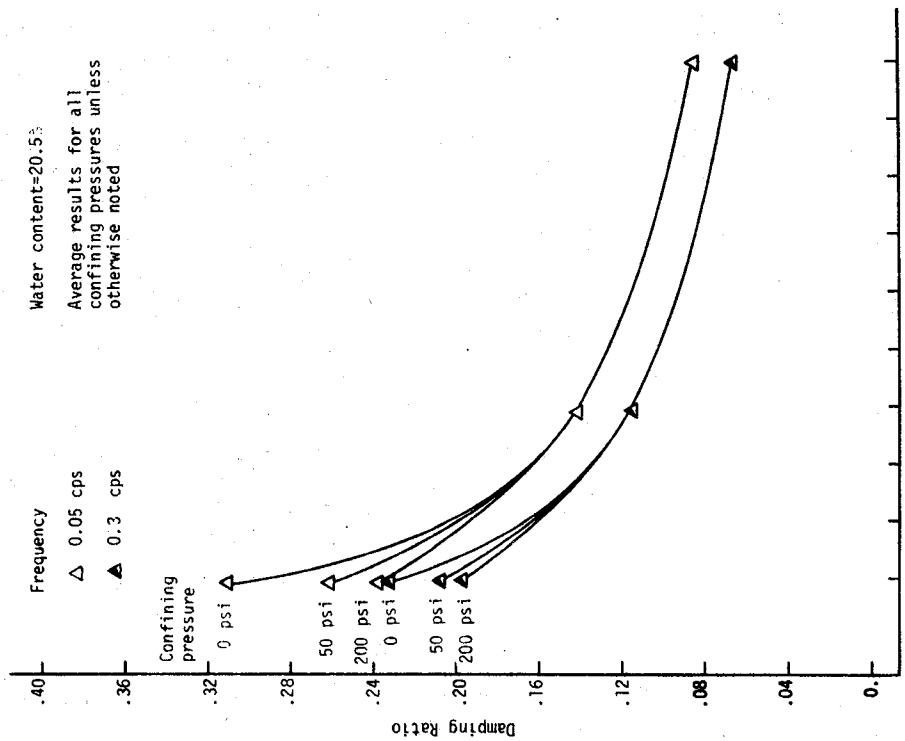

Figure 4.83 DAMPING RATIO VERSUS TEMPERATURE FOR ALASKA SILT AT AN AXIAL STRAIN OF 3.16×10^{-3}%

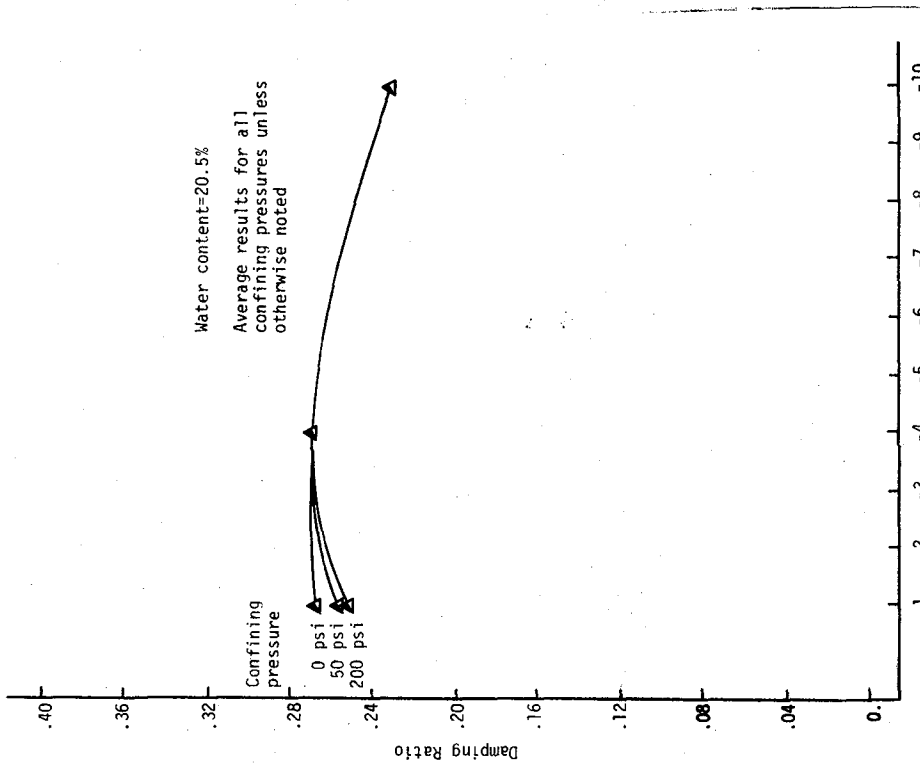

Figure 4.86 DAMPING RATIO VERSUS TEMPERATURE FOR ALASKA SILT AT AN AXIAL STRAIN OF 3.16×10^{-2}% AND 0.3 cps FREQUENCY

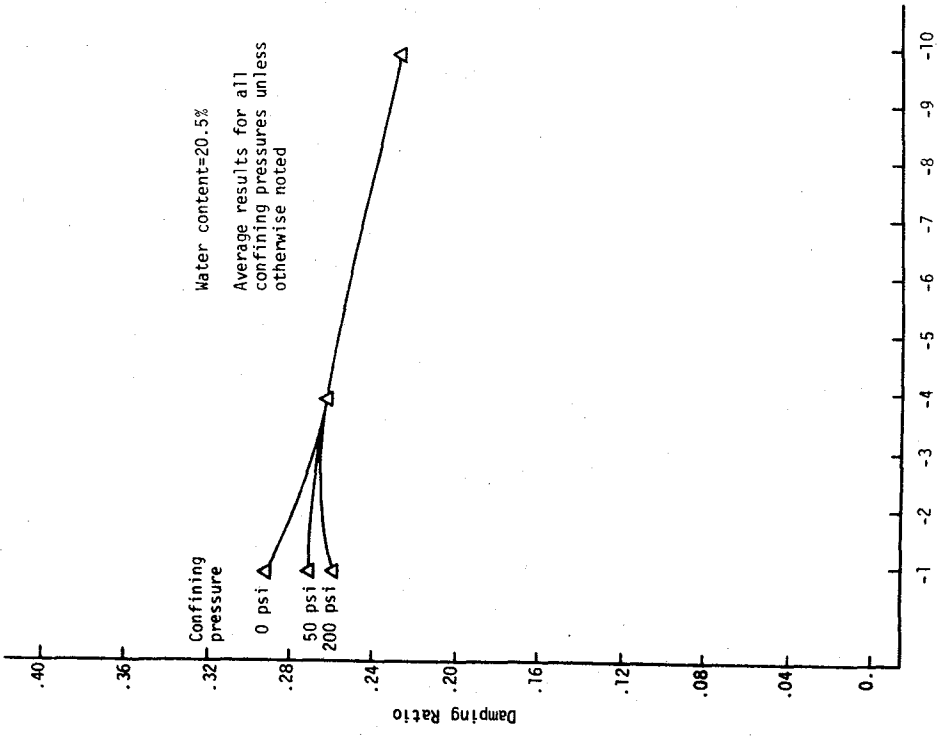

Figure 4.85 DAMPING RATIO VERSUS TEMPERATURE FOR ALASKA SILT AT AN AXIAL STRAIN OF 3.16×10^{-2}% AND 0.05 cps FREQUENCY

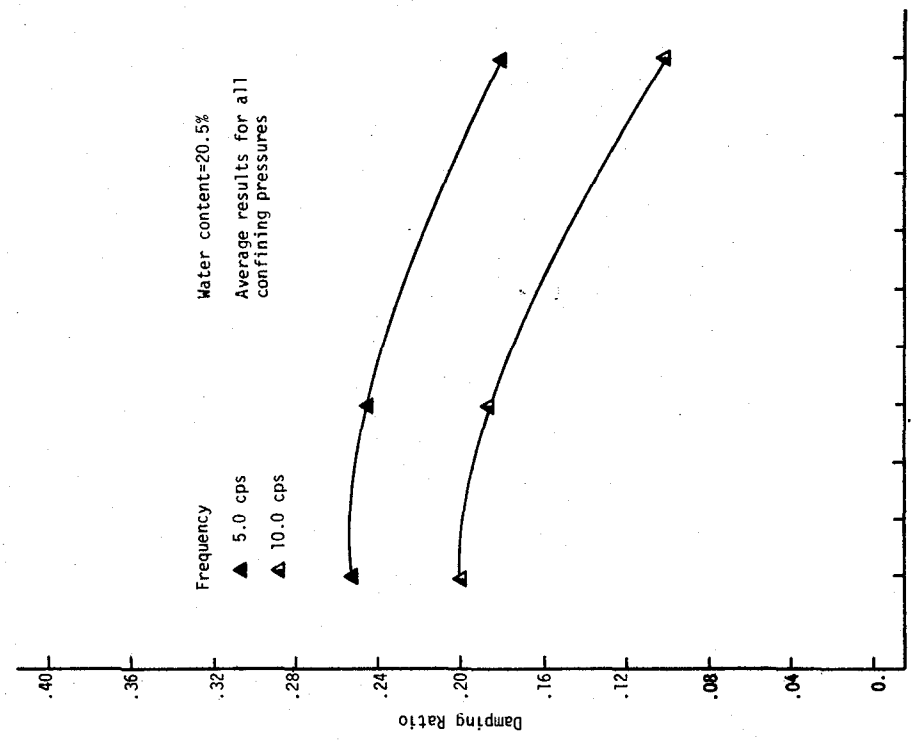

Figure 4.88 DAMPING RATIO VERSUS TEMPERATURE FOR ALASKA SILT AT AN AXIAL STRAIN OF 3.16×10^{-2}%

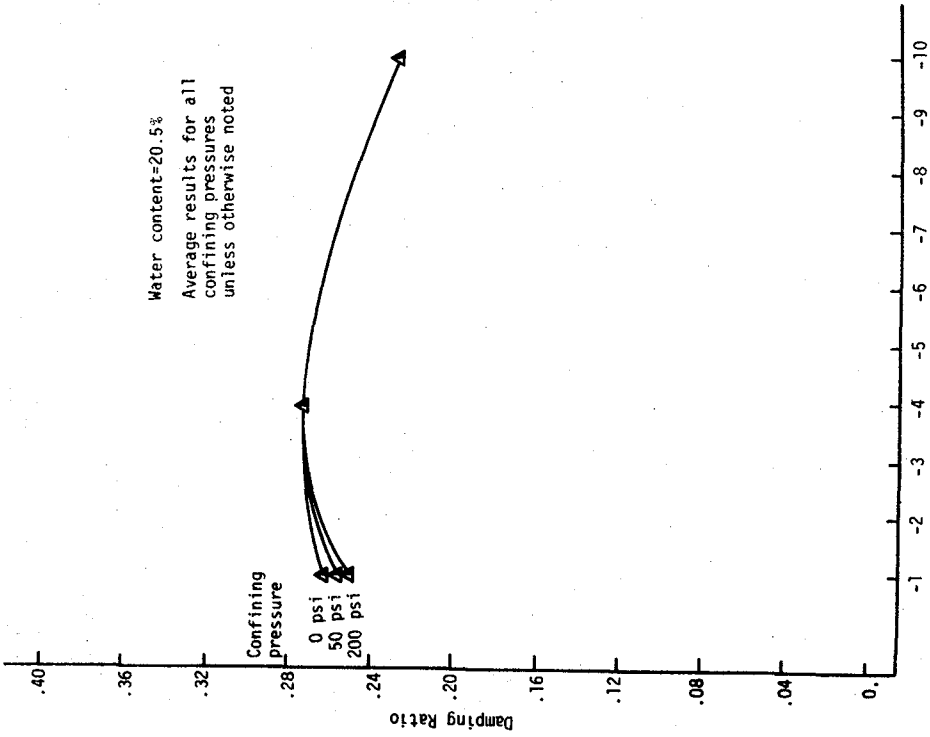

Figure 4.87 DAMPING RATIO VERSUS TEMPERATURE FOR ALASKA SILT AT AN AXIAL STRAIN OF 3.16×10^{-2}% AND 1.0 cps FREQUENCY

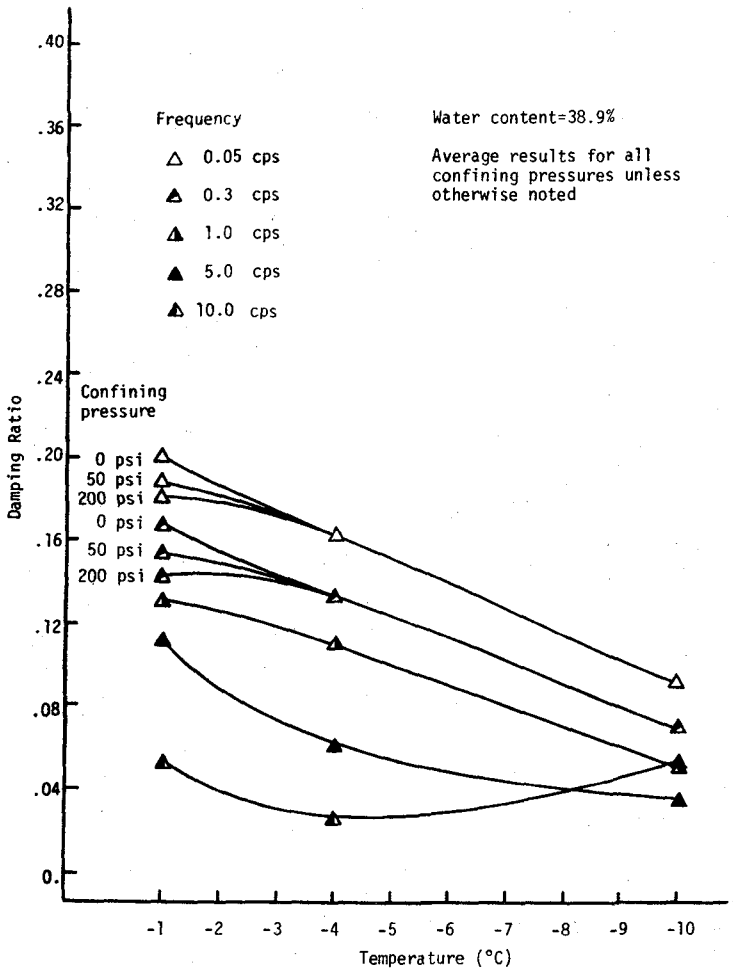

Figure 4.89 DAMPING RATIO VERSUS TEMPERATURE FOR ALASKA SILT AT AN AXIAL STRAIN OF 3.16×10^{-3}%

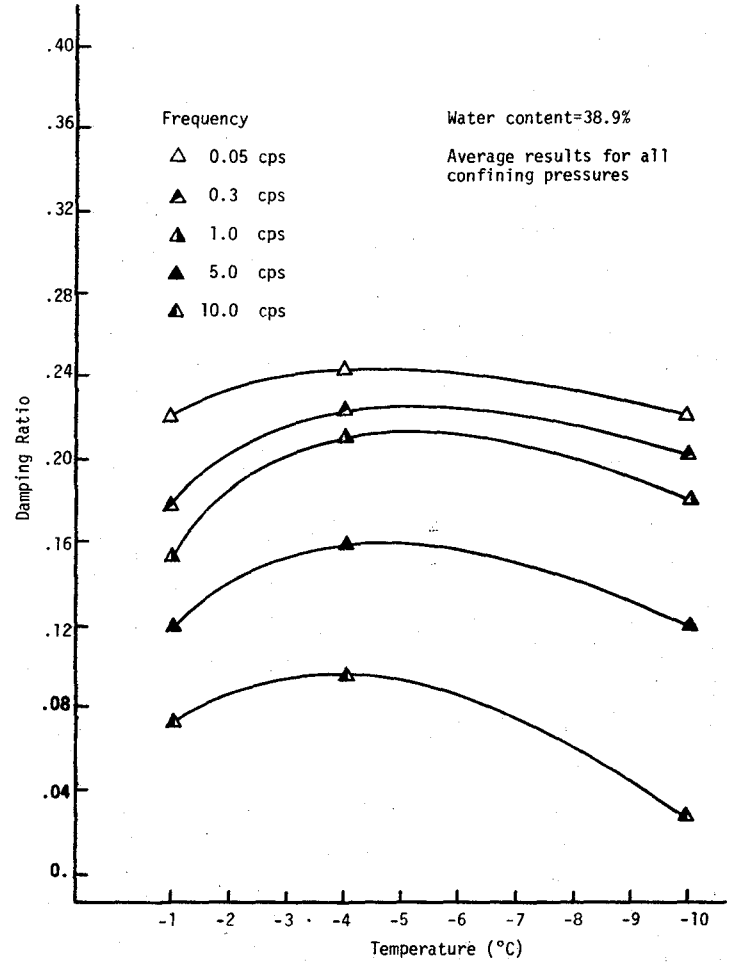

Figure 4.90 DAMPING RATIO VERSUS TEMPERATURE FOR ALASKA SILT AT AN AXIAL STRAIN OF 3.16×10^{-2}%

at a particular water content, at one of two axial strain amplitudes, and at one or more frequencies. In general, damping ratio decreases with decreasing temperature. The influence of temperature on damping ratio appears to be more significant at low water contents than at high water contents. At a low strain amplitude (3.16×10^{-3}%) at low water contents, the rate of decrease of damping ratio is generally greater in the high temperature range (-1 to -4°C) than in the low temperature range (-4 to -10°C); at high water contents the rate of decrease apepars to be more uniform over the entire range of temperatures (-1 to -10°C). At a very high frequency (10.0 cps) there is an initial decrease in damping ratio from -1 to -4°C followed by an increase from -4 to -10°C.

At a high strain amplitude (3.16×10^{-2}%) the rate of decrease in damping ratio with decreasing temperature is generally somewhat less than at a low strain amplitude (3.16×10^{-3}%). In many cases, there appears to be either little change or a slight increase in damping ratio from -1 to -4°C followed by a gradual decrease from -4 to -10°C.

4.4.5 Effect of Water Content

The relationship between damping ratio and water content is given in Figures 4.91 to 4.102. Each figure represents the relationship for a silt at a particular temperature, at two axial strain amplitudes, and at one or more frequencies. The relationships are based on only two data points with the exception of those for Alaska silt at a temperature of -1°C, which are based on three data points. At a temperature of -1°C, damping ratio decreases significantly with increasing water content. The relationship does not seem to be significantly affected by strain amplitude. It appears that at low frequencies most of the decrease in damping ratio occurs in the higher water content range while at high frequencies the rate of decrease is more uniform over the entire range of water contents.

At lower temperatures (-4 and -10°C) there appears to be no significant influence of water content on damping ratio at a low strain amplitude (3.16×10^{-3}%). At a high strain amplitude (3.16×10^{-2}%) damping ratio decreases with increasing water content; the relationship appears to be dependent on frequency, with a slight decrease occurring at low frequencies and a more significant decrease at high frequencies.

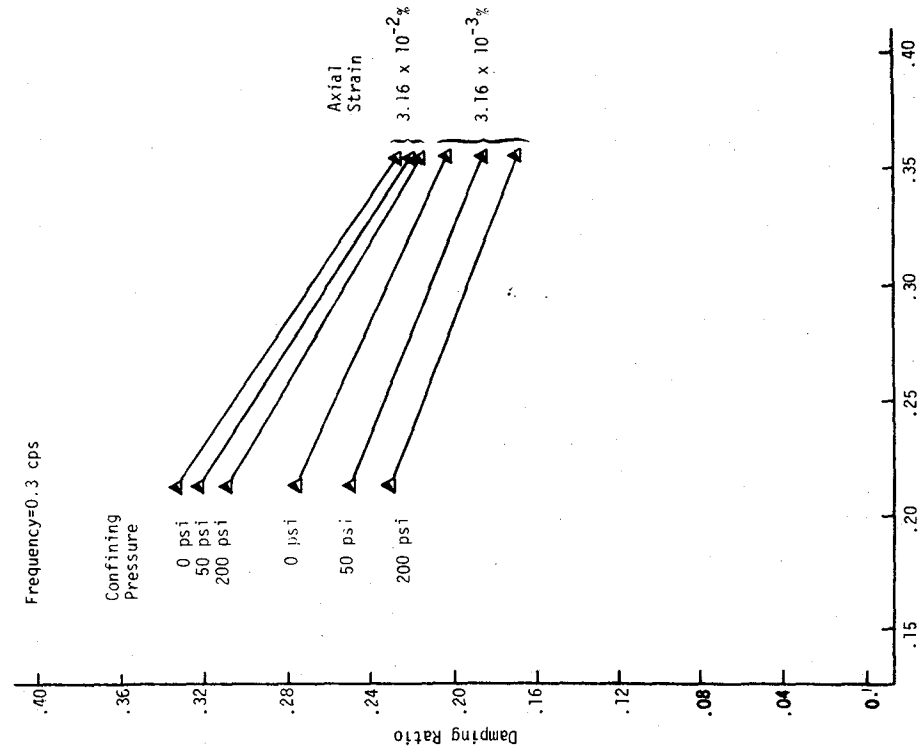

Figure 4.92 DAMPING RATIO VERSUS WATER CONTENT FOR HANOVER SILT AT A TEMPERATURE OF -1°C

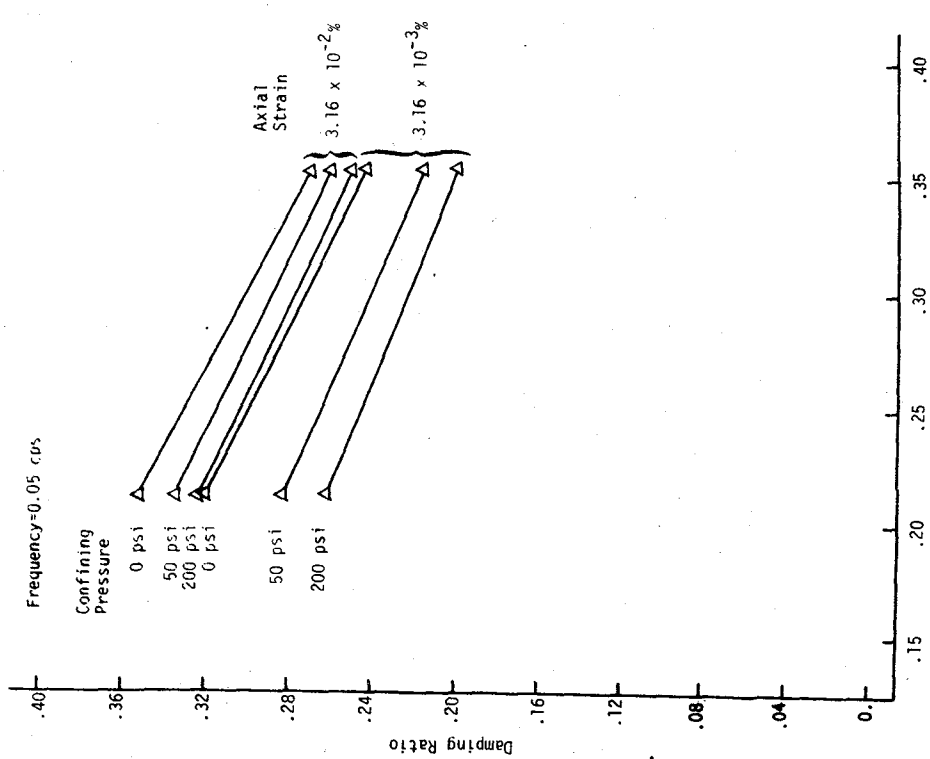

Figure 4.91 DAMPING RATIO VERSUS WATER CONTENT FOR HANOVER SILT AT A TEMPERATURE OF -1°C

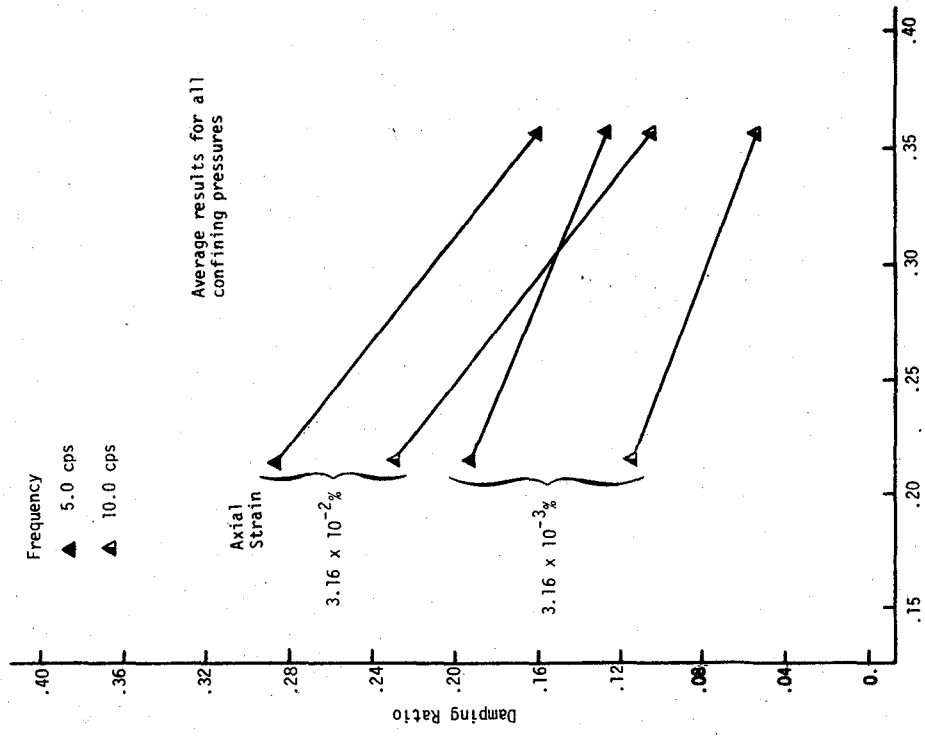

Figure 4.94 DAMPING RATIO VERSUS WATER CONTENT FOR HANOVER SILT AT A TEMPERATURE OF $-1^{o}C$

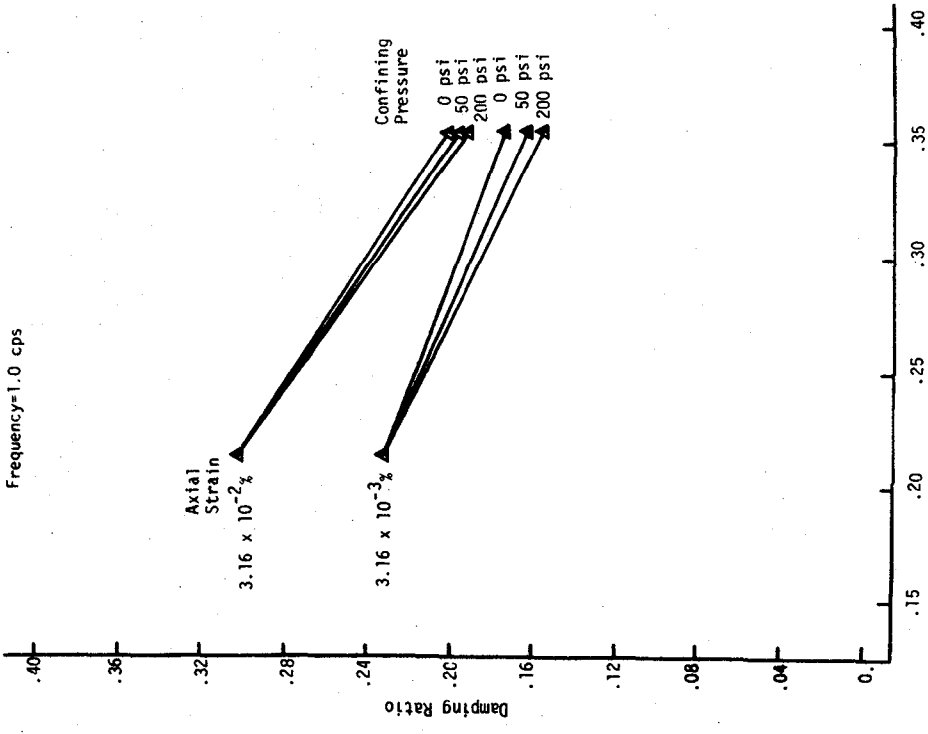

Figure 4.93 DAMPING RATIO VERSUS WATER CONTENT FOR HANOVER SILT AT A TEMPERATURE OF -1^{o}

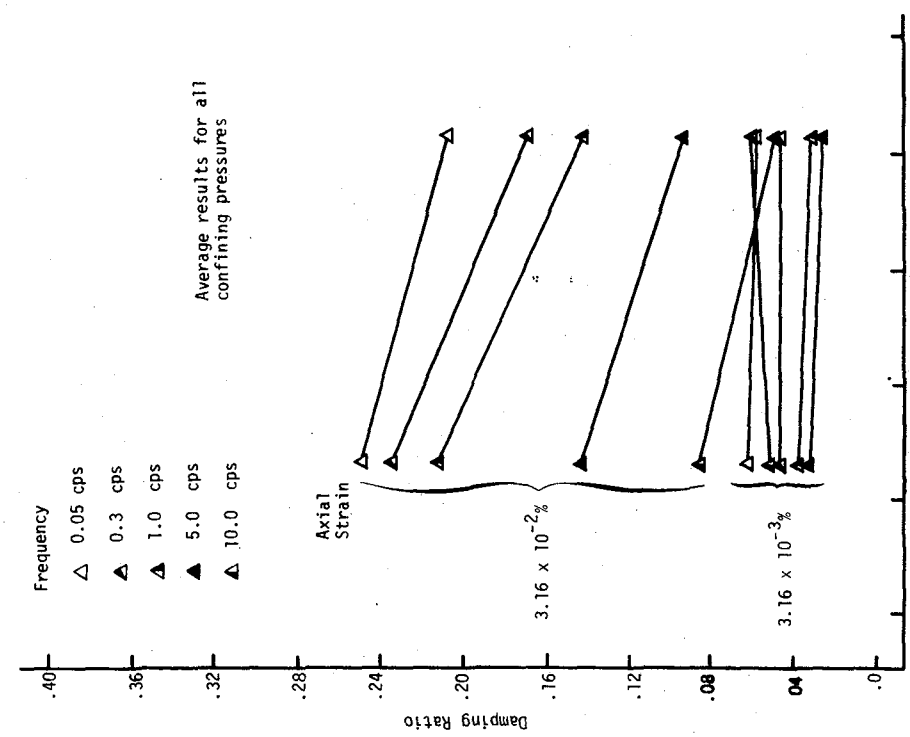

Figure 4.96 DAMPING RATIO VERSUS WATER CONTENT FOR HANOVER SILT AT A TEMPERATURE OF -10°C

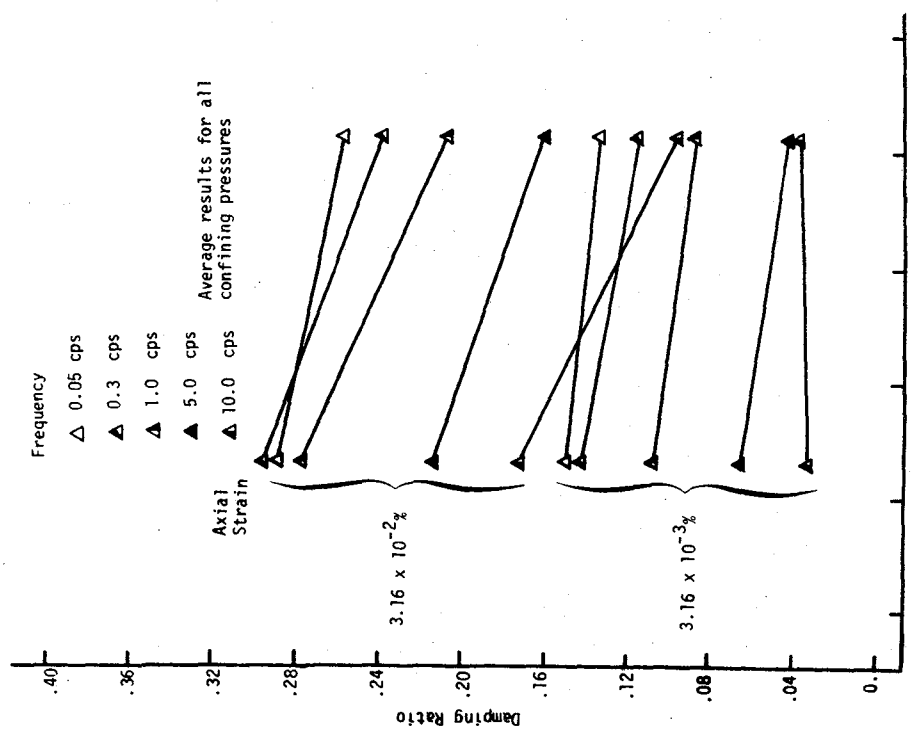

Figure 4.95 DAMPING RATIO VERSUS WATER CONTENT FOR HANOVER SILT AT A TEMPERATURE OF -4°C

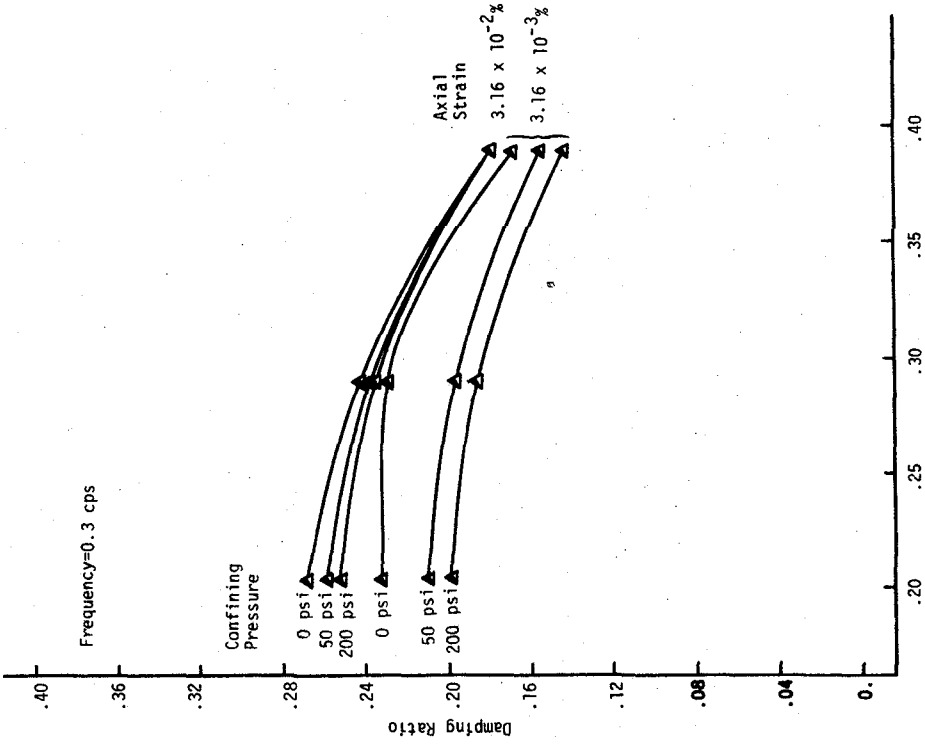

Figure 4.98 DAMPING RATIO VERSUS WATER CONTENT FOR ALASKA SILT AT A TEMPERATURE OF -1°C

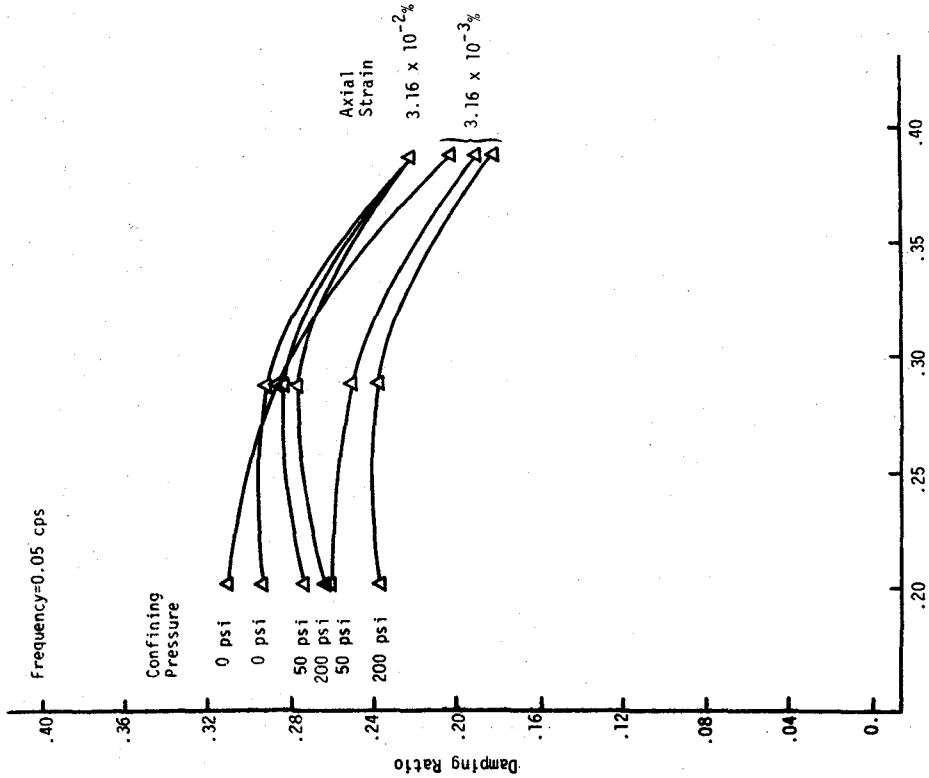

Figure 4.97 DAMPING RATIO VERSUS WATER CONTENT FOR ALASKA SILT AT A TEMPERATURE OF -1°C

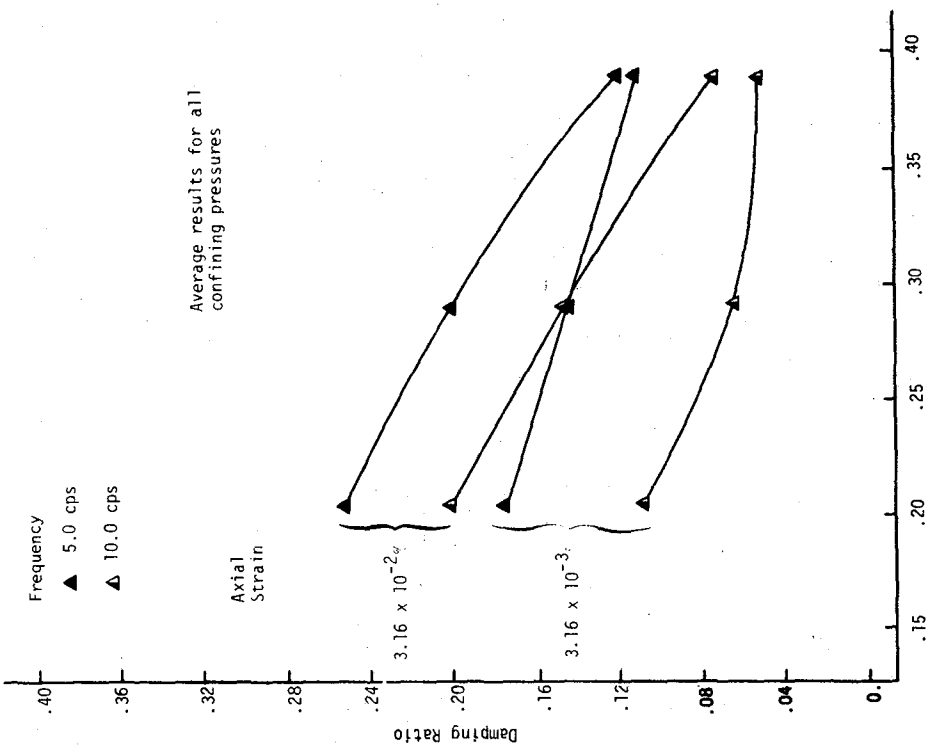

Figure 4.100 DAMPING RATIO VERSUS WATER CONTENT FOR ALASKA SILT AT A TEMPERATURE OF -1°C

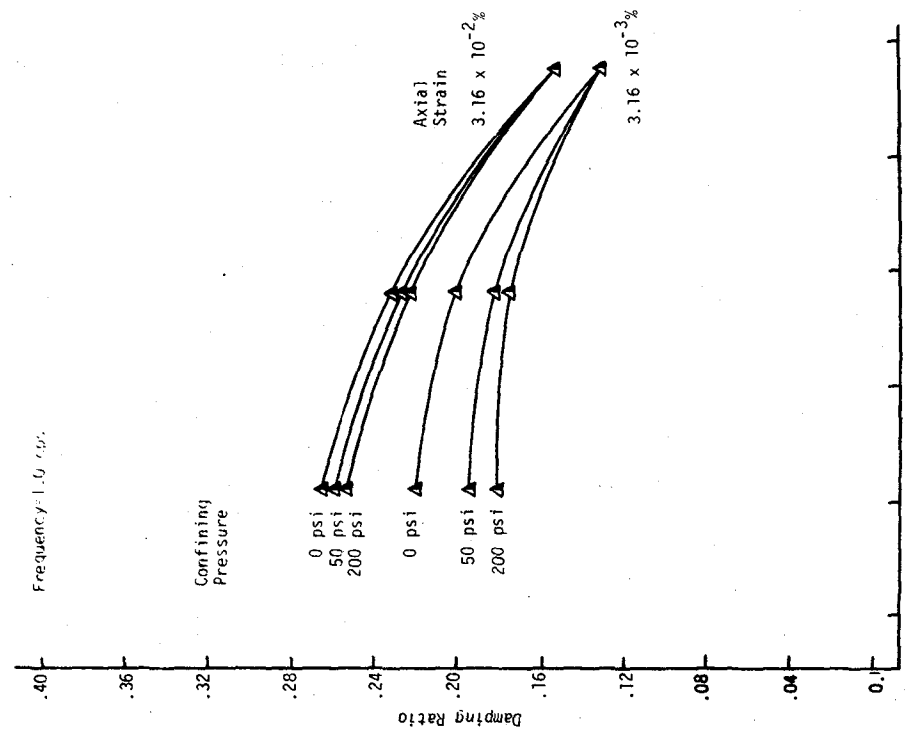

Figure 4.99 DAMPING RATIO VERSUS WATER CONTENT FOR ALASKA SILT AT A TEMPERATURE OF -1°C

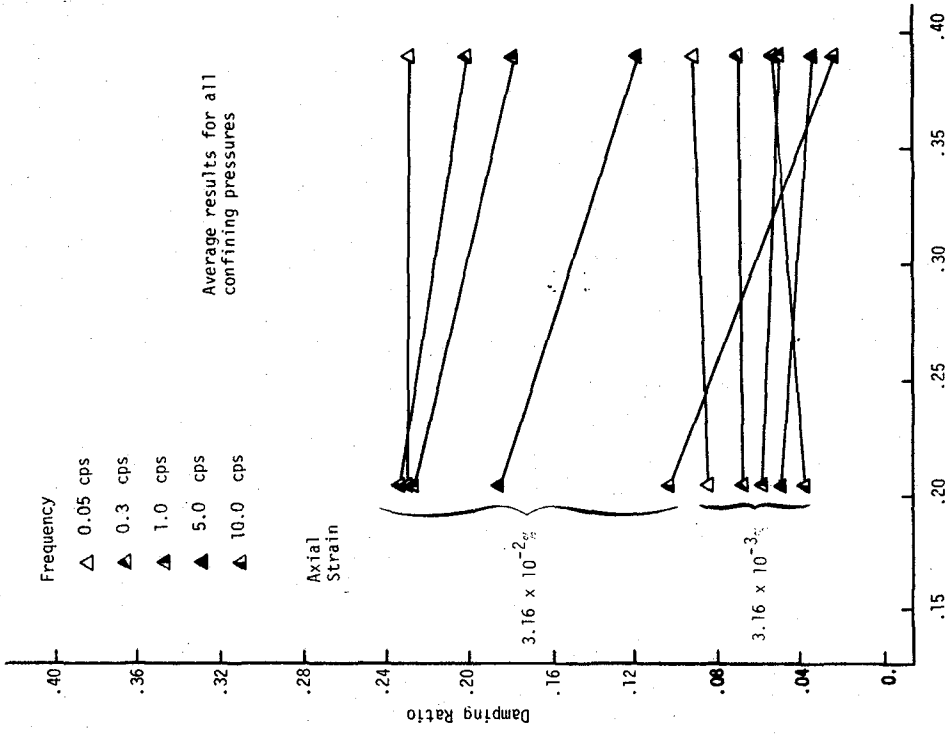

Figure 4.101 DAMPING RATIO VERSUS WATER CONTENT FOR ALASKA SILT AT A TEMPERATURE OF -4°C

Figure 4.102 DAMPING RATIO VERSUS WATER CONTENT FOR ALASKA SILT AT A TEMPERATURE OF -10°C

CHAPTER 5

DYNAMIC PROPERTIES OF FROZEN SAND UNDER CYCLIC TRIAXIAL LOADING CONDITIONS

5.1 General

Cyclic triaxial tests were conducted on the Frozen Ottawa sand samples described in Chapter 3. The Ottawa sand samples were tested at three sand contents to determine the influence of sample density on the dynamic properties. To determine the influence of other parameters which might affect the dynamic properties of frozen sand, samples were tested at temperatures of -1, -4, and -10^{o}C, confining pressures of 0, 50, and 200 psi, frequencies of 0.05, 0.3, 1.0, and 5.0, and over a range of axial strain amplitudes from .002 to .04%.

5.2 Testing Sequence

The test history used on the frozen Ottawa sand samples is given in Figure 5.1. The test sequence is similar to that used for frozen silt samples except the samples were not tested at a frequency of 10 cps.

The dynamic Young's modulus was evaluated from the load and displacement amplitude on a strip chart recording. The damping ratio was evaluated from a hysteresis loop recorded on a storage oscilloscope. The specific techniques employed are the same as for the frozen silt samples and are presented in Chapter 4.

5.3 Dynamic Young's Modulus of Frozen Sand

5.3.1 Effect of Strain Amplitude

The dynamic Young's modulus of frozen sand was plotted against the log of axial strain amplitude expressed as a percent. The plots are shown in Appendix C. Least squares best fit lines were determined and drawn through the data for a given test condition. These lines are summarized in Figures 5.2 to 5.37.

Dynamic Young's modulus decreases with increasing axial strain amplitude. The decrease varies from one test condition to another but does not follow any definite trend. Over the range of test conditions considered the value of dynamic Young's modulus ranged from 2×10^5 to 38×10^5 psi.

Constant temperature

Approximate axial strain = 2.0×10^{-3}%

- cp=200 psi → f=0.05 cps → f=0.3 cps → f=1.0 cps → f=5.0 cps
- cp= 50 psi → f=0.05 cps → f=0.3 cps → f=1.0 cps → f=5.0 cps
- cp= 0 psi → f=0.05 cps → f=0.3 cps → f=1.0 cps → f=5.0 cps

Approximate axial strain = 6.0×10^{-3}%

- cp=200 psi → f=0.05 cps → f=0.3 cps → f=1.0 cps → f=5.0 cps
- cp= 50 psi → f=0.05 cps → f=0.3 cps → f=1.0 cps → f=5.0 cps
- cp= 0 psi → f=0.05 cps → f=0.3 cps → f=1.0 cps → f=5.0 cps

Approximate axial strain = 2.0×10^{-2}%

- cp=200 psi → f=0.05 cps → f=0.3 cps → f=1.0 cps → f=5.0 cps
- cp= 50 psi → f=0.05 cps → f=0.3 cps → f=1.0 cps → f=5.0 cps
- cp= 0 psi → f=0.05 cps → f=0.3 cps → f=1.0 cps → f=5.0 cps

Approximate axial strain = 4.0×10^{-2}%

- cp=200 psi → f=0.05 cps → f=0.3 cps → f=1.0 cps → f=5.0 cps
- cp= 50 psi → f=0.05 cps → f=0.3 cps → f=1.0 cps → f=5.0 cps
- cp= 0 psi → f=0.05 cps → f=0.3 cps → f=1.0 cps → f=5.0 cps

Figure 5.1 DIAGRAM FOR TEST HISTORY OF FROZEN SAND

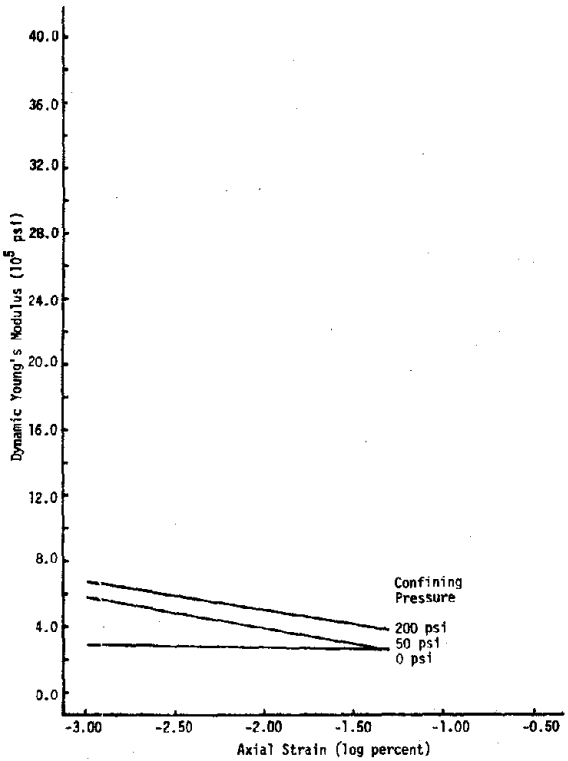

Figure 5.2 DYNAMIC YOUNG'S MODULUS VERSUS AXIAL STRAIN FOR SAND-ICE SAMPLES OF 20% SAND CONTENT AT -1°C AND 0.05 cps

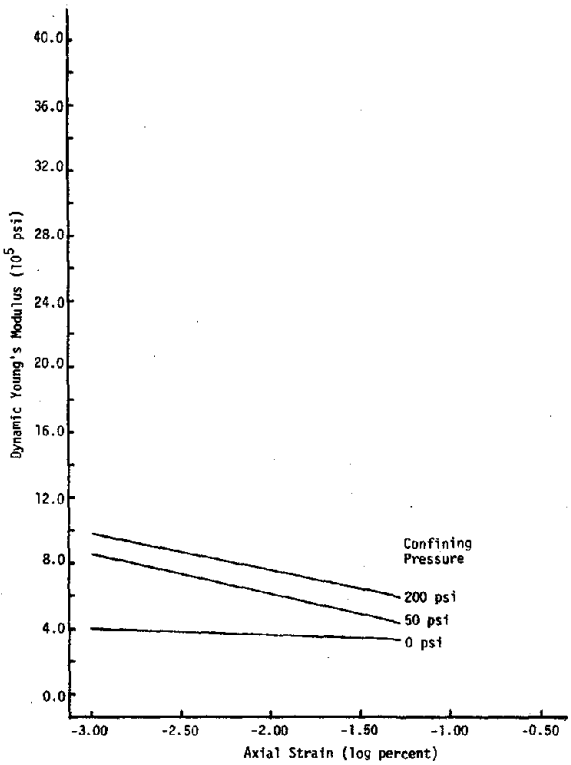

Figure 5.3 DYNAMIC YOUNG'S MODULUS VERSUS AXIAL STRAIN FOR SAND-ICE SAMPLES OF 20% SAND CONTENT AT -1°C AND 0.3 cps

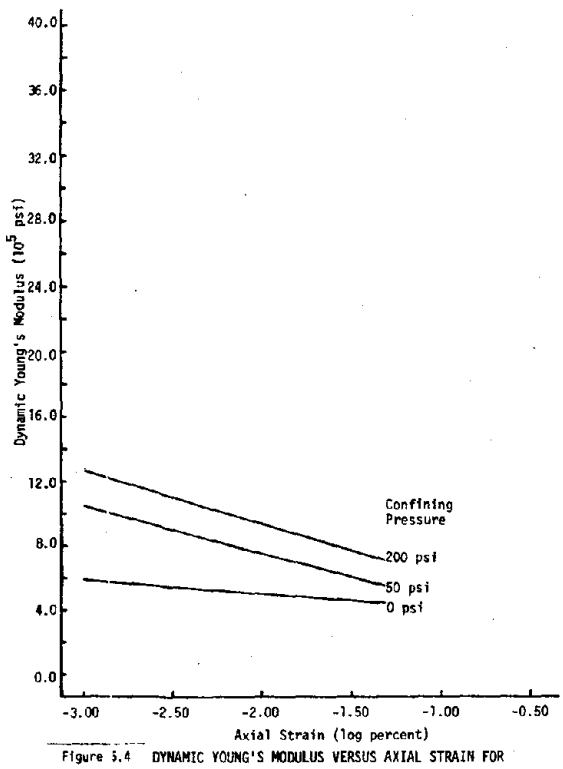

Figure 5.4 DYNAMIC YOUNG'S MODULUS VERSUS AXIAL STRAIN FOR SAND-ICE SAMPLES OF 20% SAND CONTENT AT -1°C AND 1.0 cps

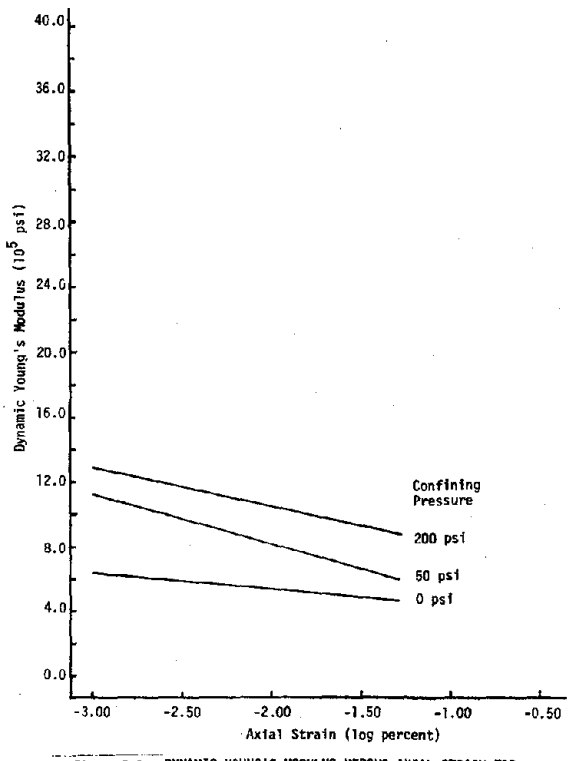

Figure 5.5 DYNAMIC YOUNG'S MODULUS VERSUS AXIAL STRAIN FOR SAND-ICE SAMPLES OF 20% SAND CONTENT AT -1°C AND 5.0 cps

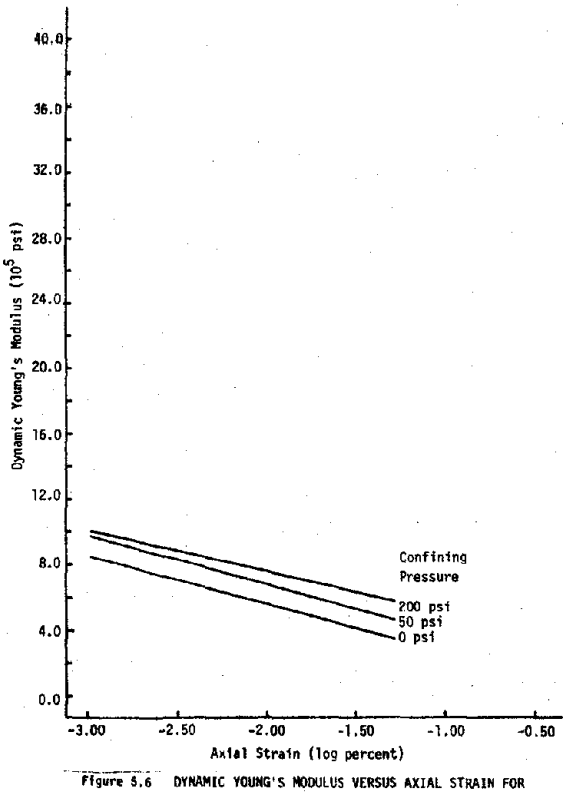

Figure 5.6 DYNAMIC YOUNG'S MODULUS VERSUS AXIAL STRAIN FOR SAND-ICE SAMPLES OF 20% SAND CONTENT AT -4°C AND 0.05 cps

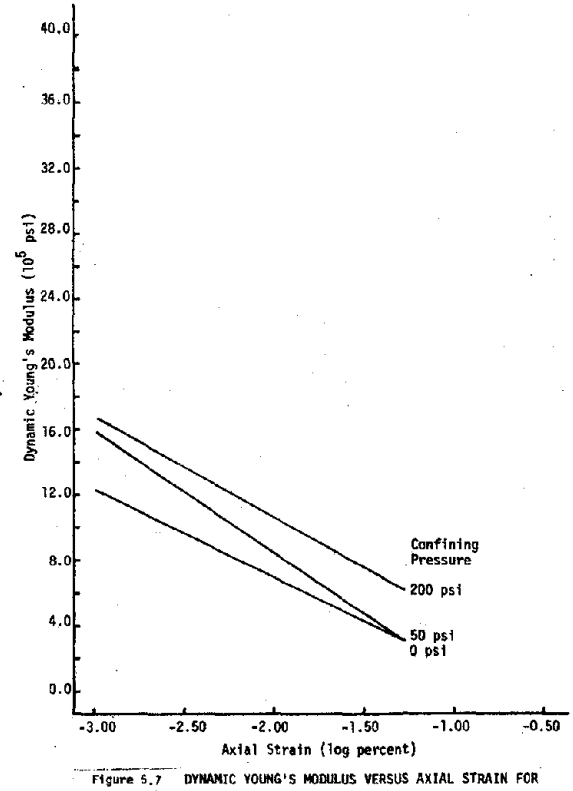

Figure 5.7 DYNAMIC YOUNG'S MODULUS VERSUS AXIAL STRAIN FOR SAND-ICE SAMPLES OF 20% SAND CONTENT AT -4°C AND 0.3 cps

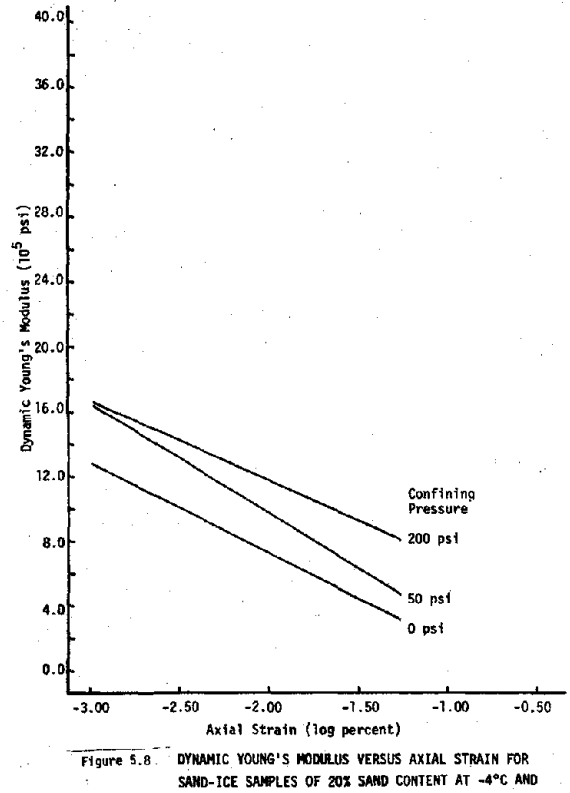

Figure 5.8 DYNAMIC YOUNG'S MODULUS VERSUS AXIAL STRAIN FOR SAND-ICE SAMPLES OF 20% SAND CONTENT AT -4°C AND 1.0 cps

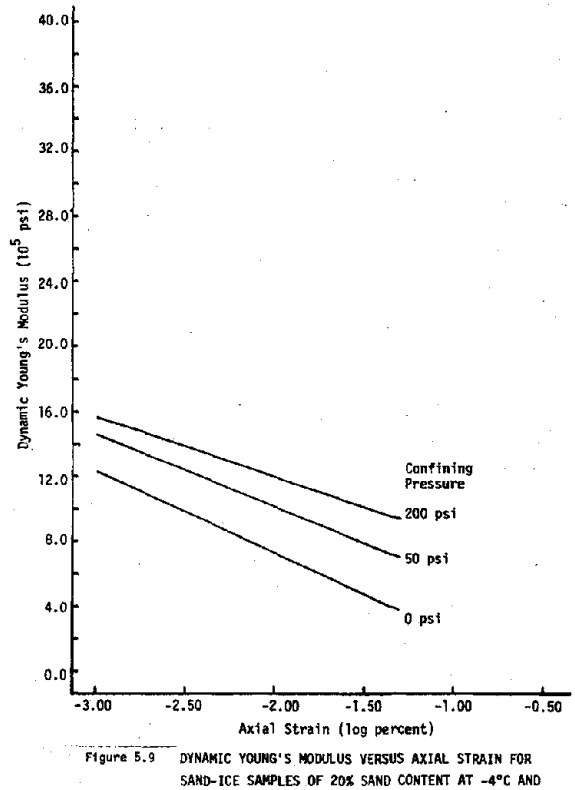

Figure 5.9 DYNAMIC YOUNG'S MODULUS VERSUS AXIAL STRAIN FOR SAND-ICE SAMPLES OF 20% SAND CONTENT AT -4°C AND 5.0 cps

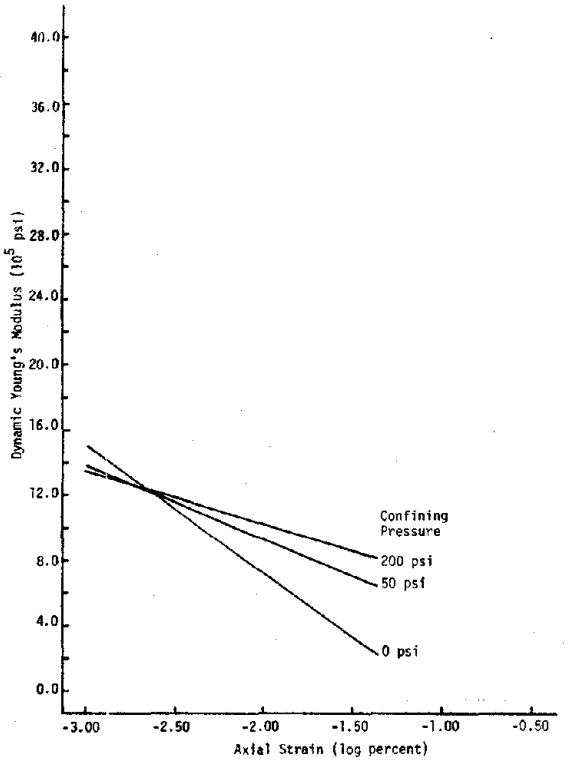

Figure 5.10 DYNAMIC YOUNG'S MODULUS VERSUS AXIAL STRAIN FOR SAND-ICE SAMPLES OF 20% SAND CONTENT AT -10°C AND 0.05 cps

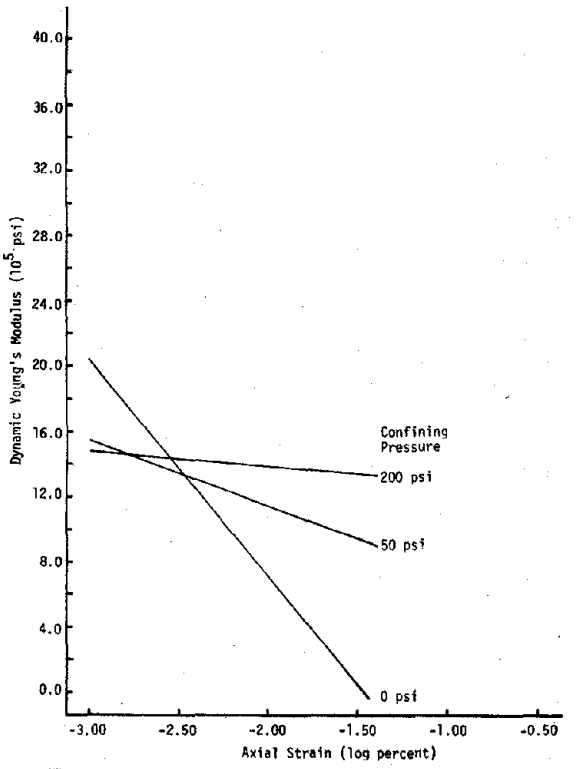

Figure 5.11 DYNAMIC YOUNG'S MODULUS VERSUS AXIAL STRAIN FOR SAND-ICE SAMPLES OF 20% SAND CONTENT AT -10°C AND 0.3 cps

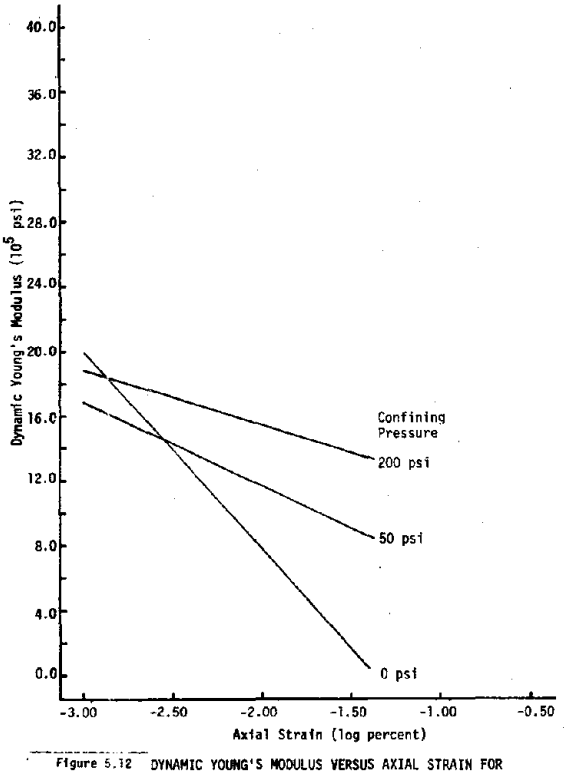

Figure 5.12 DYNAMIC YOUNG'S MODULUS VERSUS AXIAL STRAIN FOR SAND-ICE SAMPLES OF 20% SAND CONTENT AT -10°C AND 1.0 cps

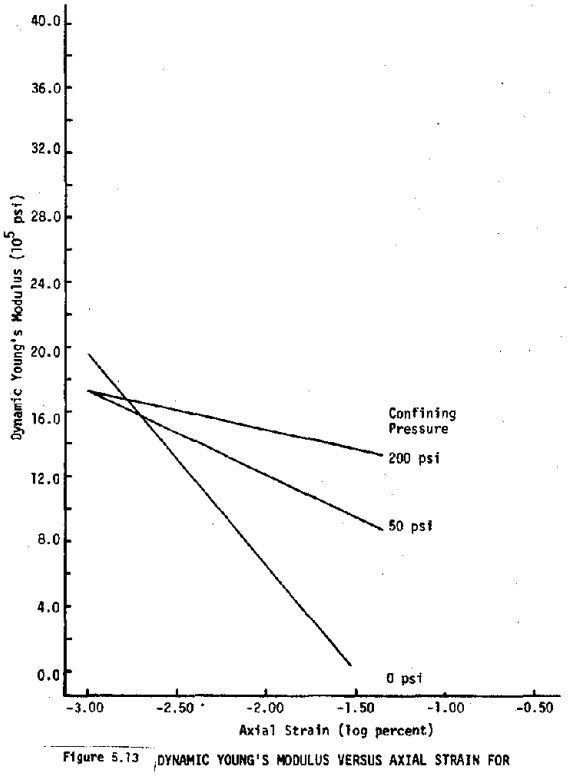

Figure 5.13 DYNAMIC YOUNG'S MODULUS VERSUS AXIAL STRAIN FOR SAND-ICE SAMPLES OF 20% SAND CONTENT AT -10°C AND 5.0 cps

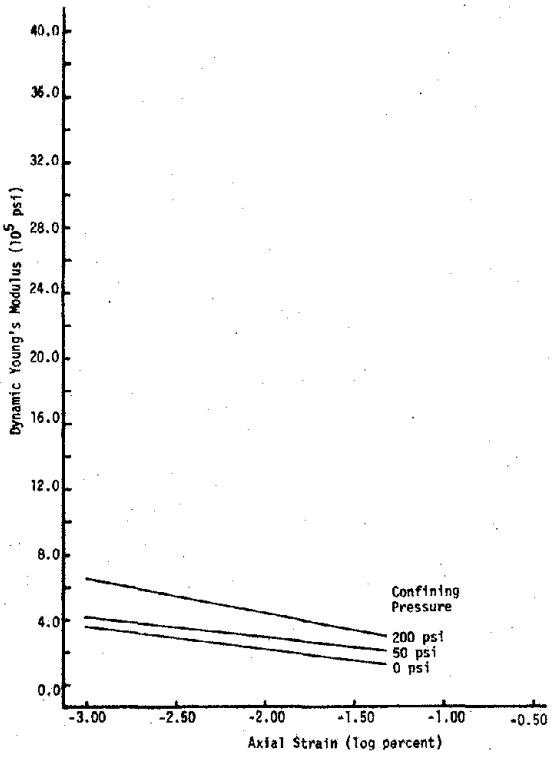

Figure 5.14 DYNAMIC YOUNG'S MODULUS VERSUS AXIAL STRAIN FOR SAND-ICE SAMPLES OF 45% SAND CONTENT AT -1°C AND 0.05 cps

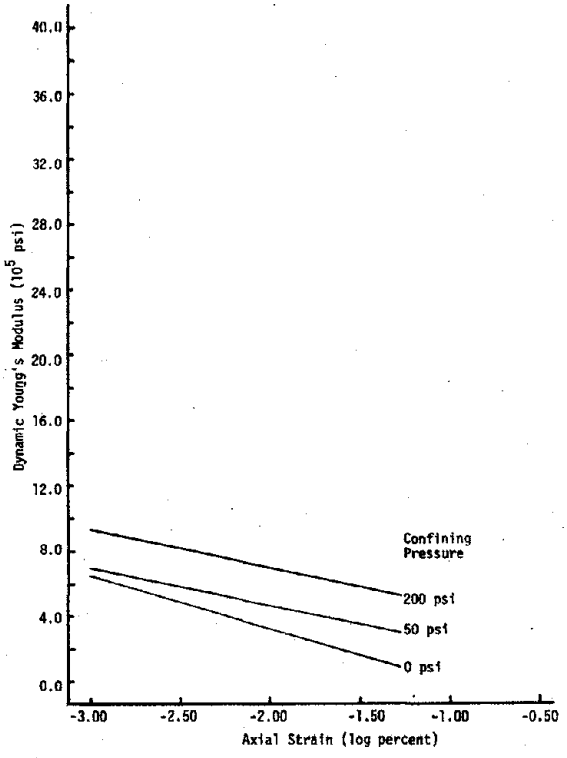

Figure 5.15 DYNAMIC YOUNG'S MODULUS VERSUS AXIAL STRAIN FOR SAND-ICE SAMPLES OF 45% SAND CONTENT AT -1°C AND 0.3 cps

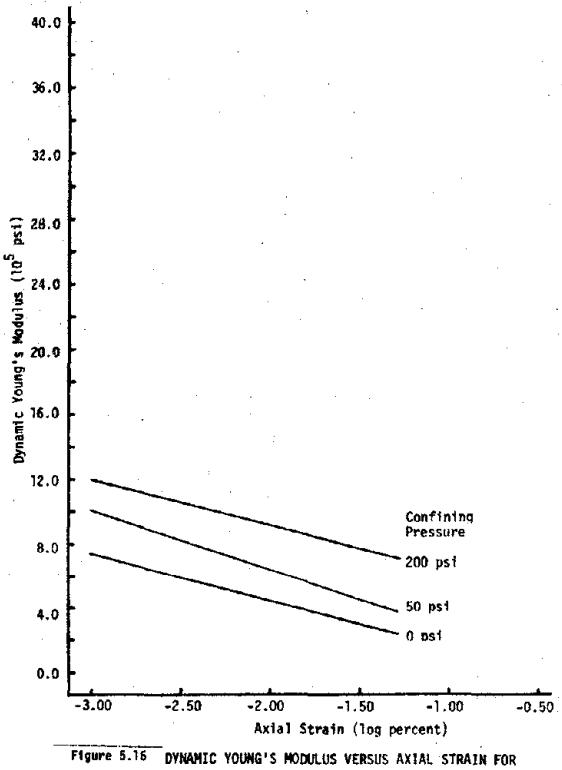

Figure 5.16 DYNAMIC YOUNG'S MODULUS VERSUS AXIAL STRAIN FOR SAND-ICE SAMPLES OF 45% SAND CONTENT AT -1°C AND 1.0 cps

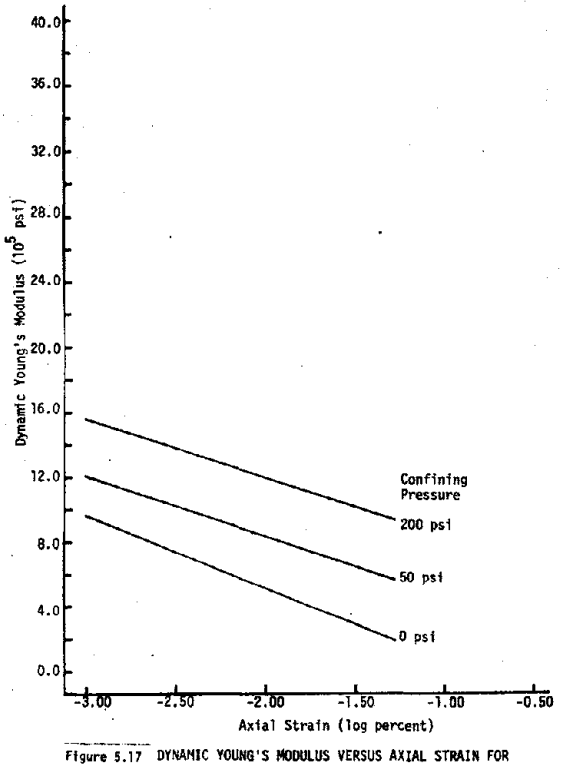

Figure 5.17 DYNAMIC YOUNG'S MODULUS VERSUS AXIAL STRAIN FOR SAND-ICE SAMPLES OF 45% SAND CONTENT AT -1°C AND 5.0 cps

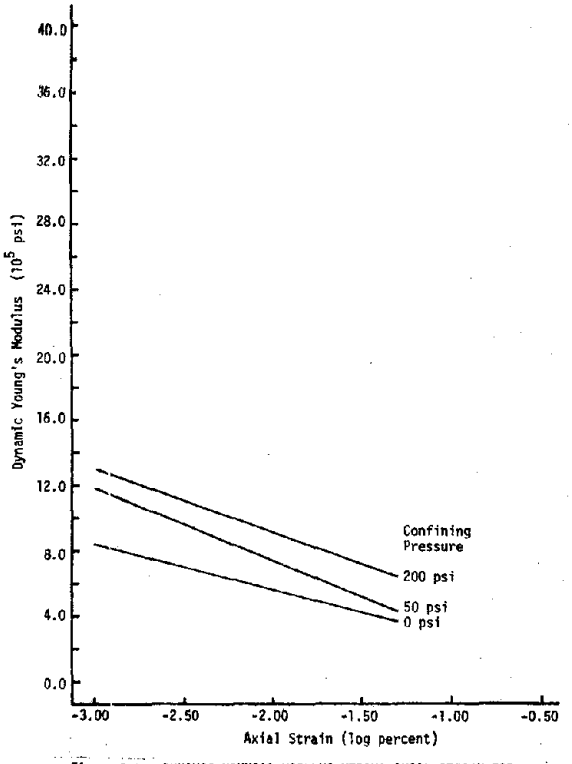

Figure 5.18 DYNAMIC YOUNG'S MODULUS VERSUS AXIAL STRAIN FOR SAND-ICE SAMPLES OF 45% SAND CONTENT AT -4°C AND 0.05 cps

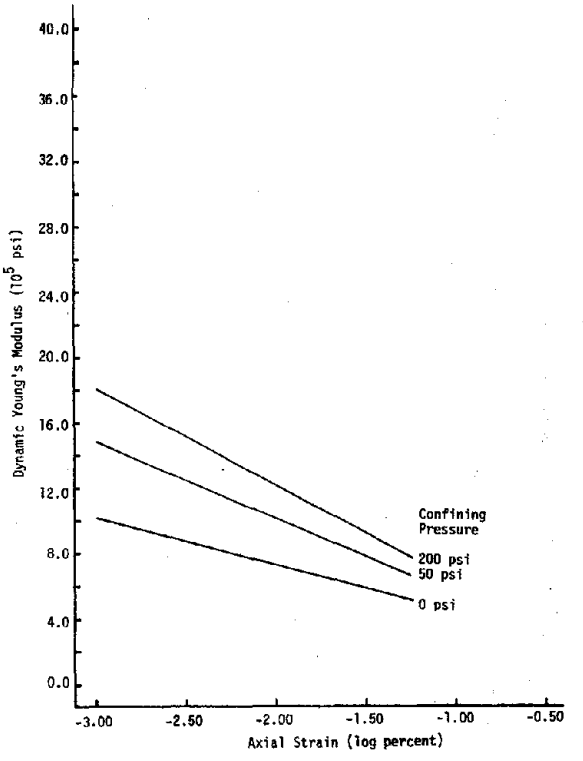

Figure 5.19 DYNAMIC YOUNG'S MODULUS VERSUS AXIAL STRAIN FOR SAND-ICE SAMPLES OF 45% SAND CONTENT AT -4°C AND 0.3 cps

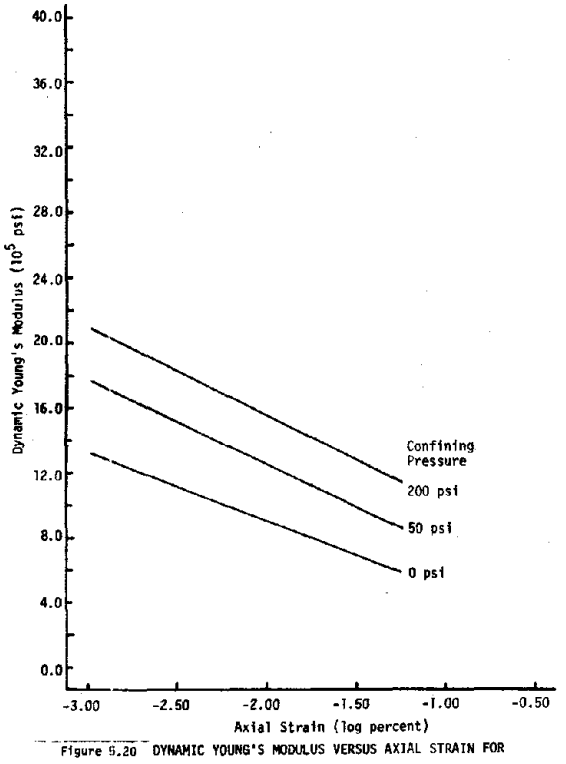

Figure 5.20 DYNAMIC YOUNG'S MODULUS VERSUS AXIAL STRAIN FOR SAND-ICE SAMPLES OF 45% SAND CONTENT AT -4°C AND 1.0 cps

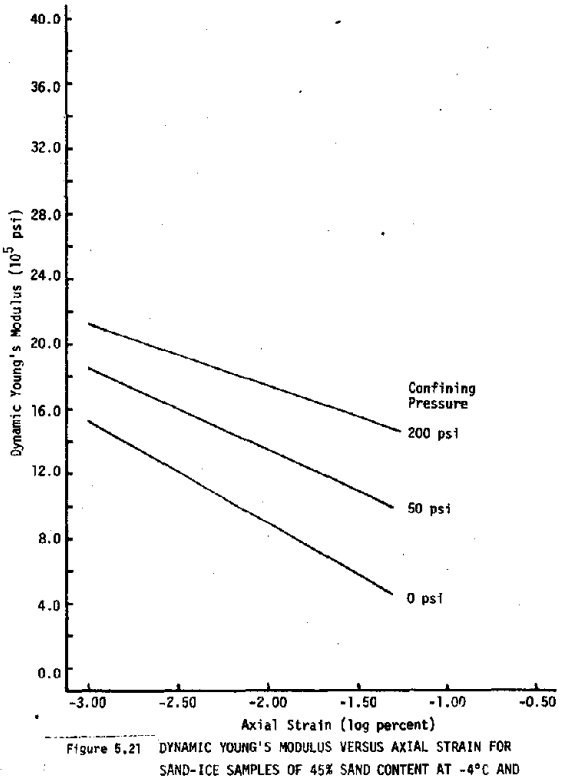

Figure 5.21 DYNAMIC YOUNG'S MODULUS VERSUS AXIAL STRAIN FOR SAND-ICE SAMPLES OF 45% SAND CONTENT AT -4°C AND 5.0 cps

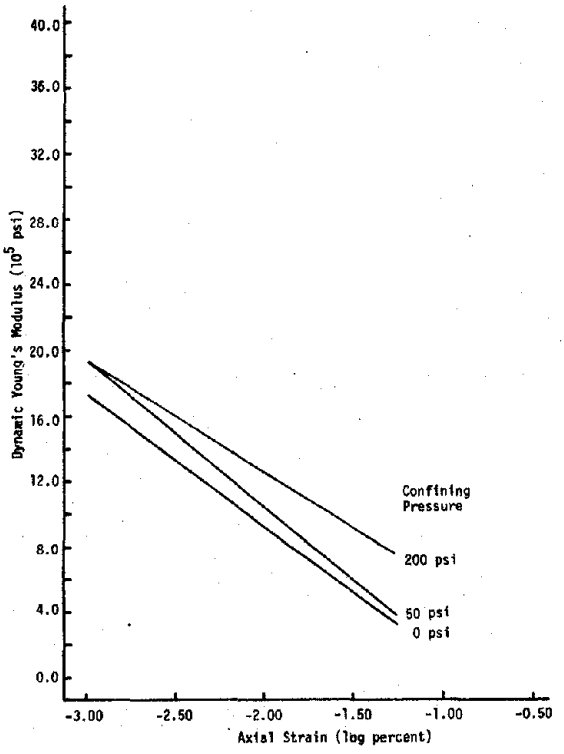

Figure 5.22 DYNAMIC YOUNG'S MODULUS VERSUS AXIAL STRAIN FOR SAND-ICE SAMPLES OF 45% SAND CONTENT AT -10°C AND 0.05 cps

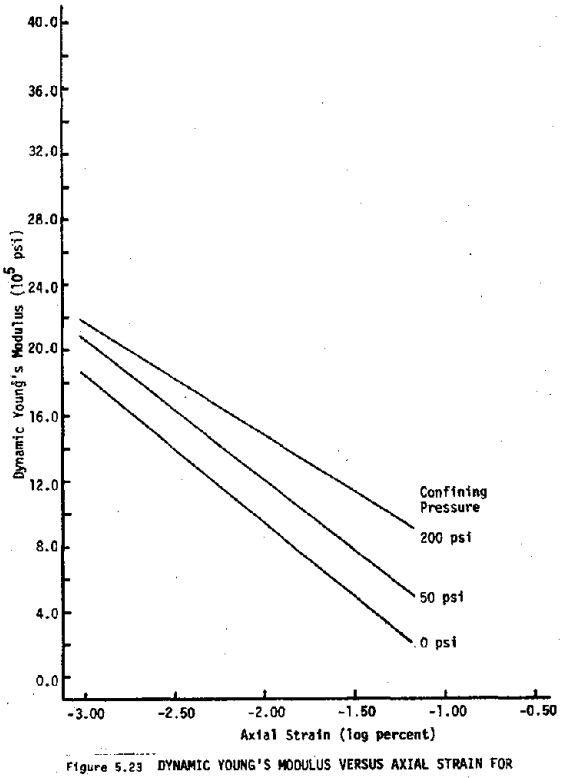

Figure 5.23 DYNAMIC YOUNG'S MODULUS VERSUS AXIAL STRAIN FOR SAND-ICE SAMPLES OF 45% SAND CONTENT AT -10°C AND 0.3 cps

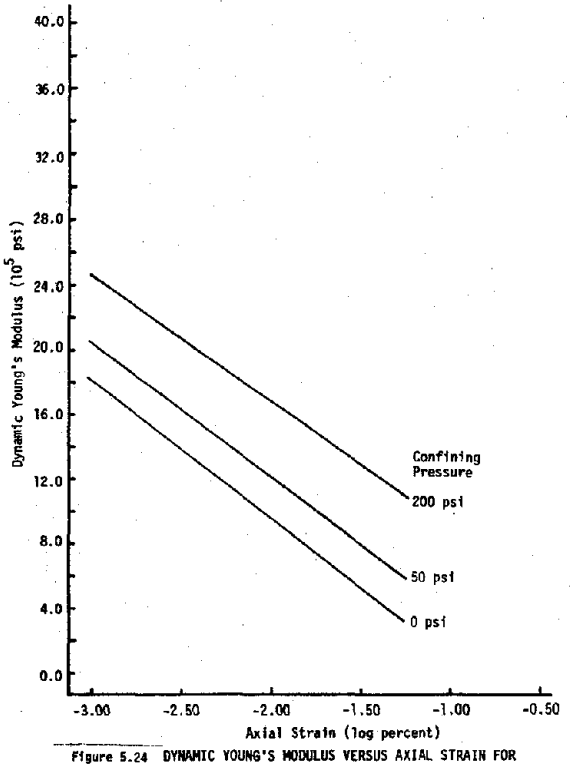

Figure 5.24 DYNAMIC YOUNG'S MODULUS VERSUS AXIAL STRAIN FOR SAND-ICE SAMPLES OF 45% SAND CONTENT AT -10°C AND 1.0 cps

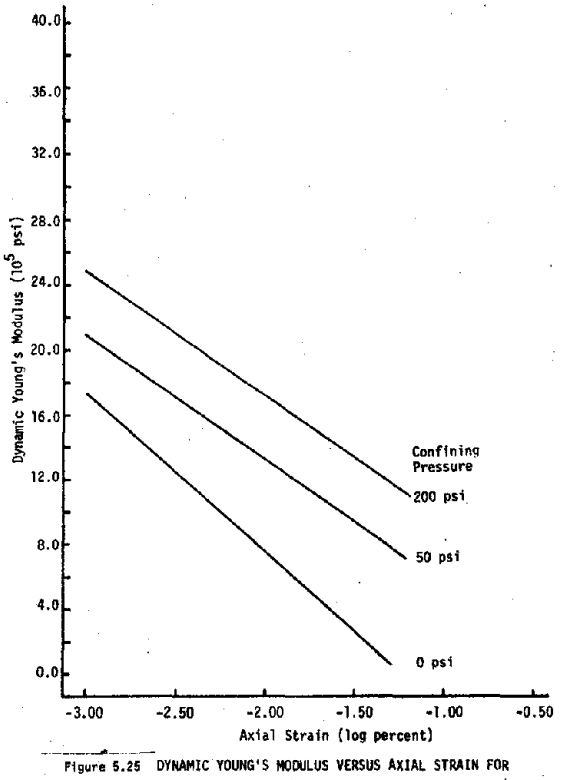

Figure 5.25 DYNAMIC YOUNG'S MODULUS VERSUS AXIAL STRAIN FOR SAND-ICE SAMPLES OF 45% SAND CONTENT AT -10°C AND 5.0 cps

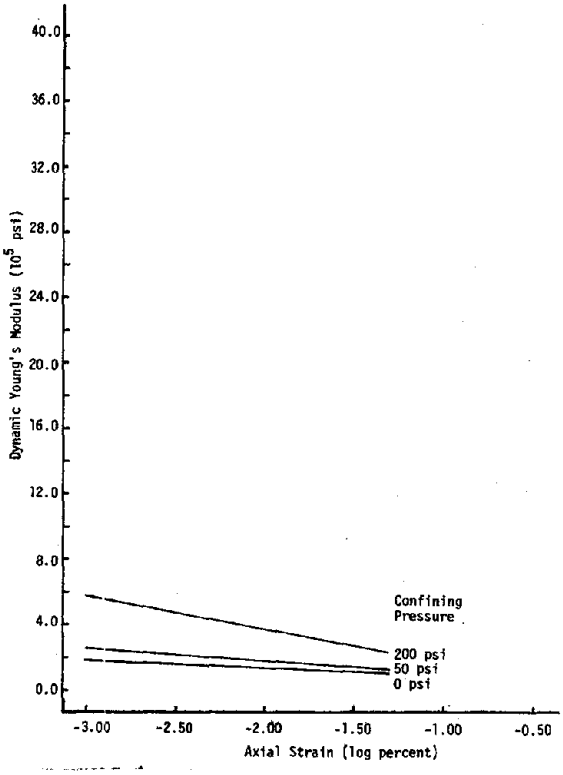

Figure 5.26 DYNAMIC YOUNG'S MODULUS VERSUS AXIAL STRAIN FOR SAND-ICE SAMPLES OF 65% SAND CONTENT AT -1°C AND 0.05 cps

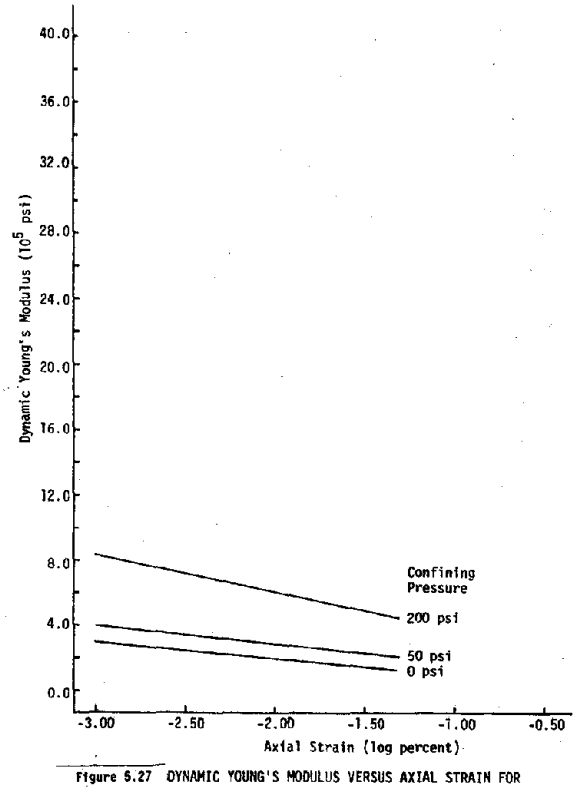

Figure 5.27 DYNAMIC YOUNG'S MODULUS VERSUS AXIAL STRAIN FOR SAND-ICE SAMPLES OF 65% SAND CONTENT AT -1°C AND 0.3 cps

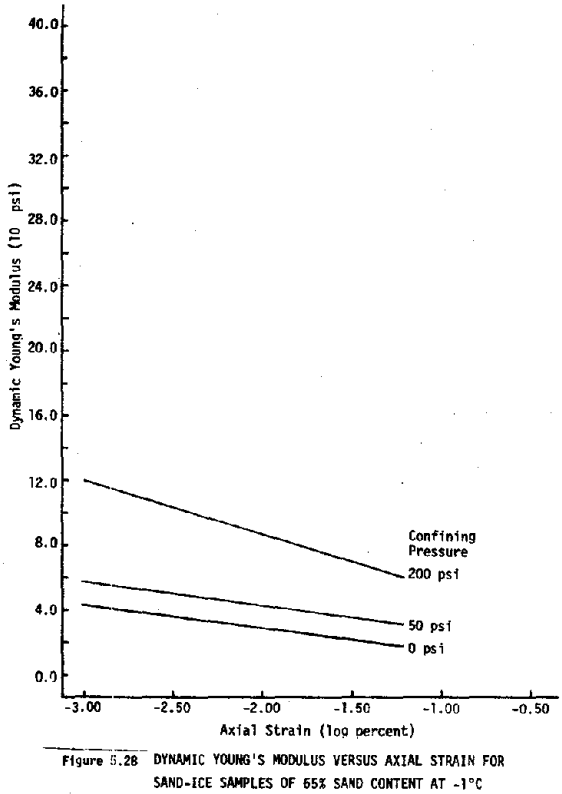

Figure 5.28 DYNAMIC YOUNG'S MODULUS VERSUS AXIAL STRAIN FOR SAND-ICE SAMPLES OF 65% SAND CONTENT AT -1°C AND 1.0 cps

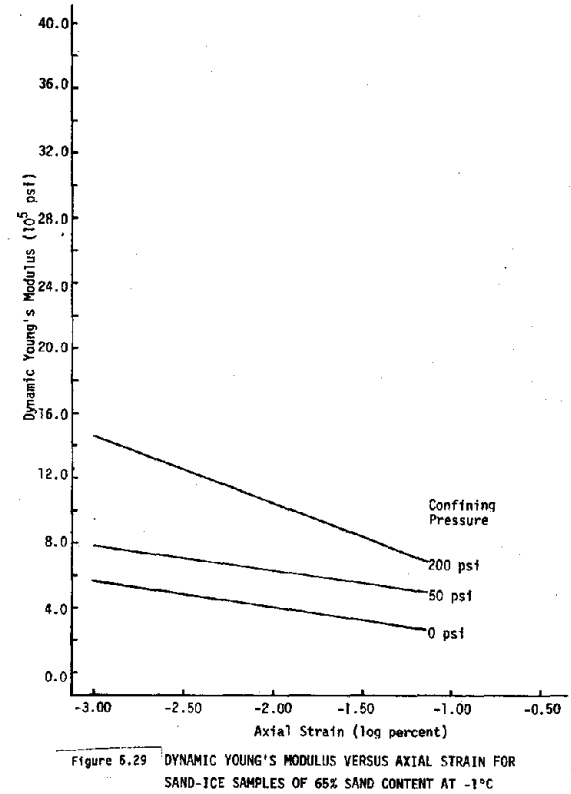

Figure 5.29 DYNAMIC YOUNG'S MODULUS VERSUS AXIAL STRAIN FOR SAND-ICE SAMPLES OF 65% SAND CONTENT AT -1°C AND 5.0 cps

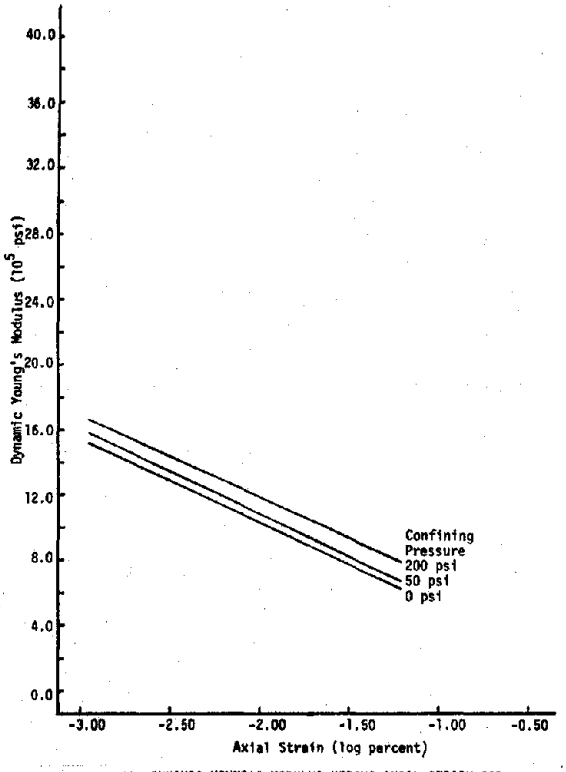

Figure 5.30 DYNAMIC YOUNG'S MODULUS VERSUS AXIAL STRAIN FOR SAND-ICE SAMPLES OF 65% SAND CONTENT AT -4°C AND 0.05 cps

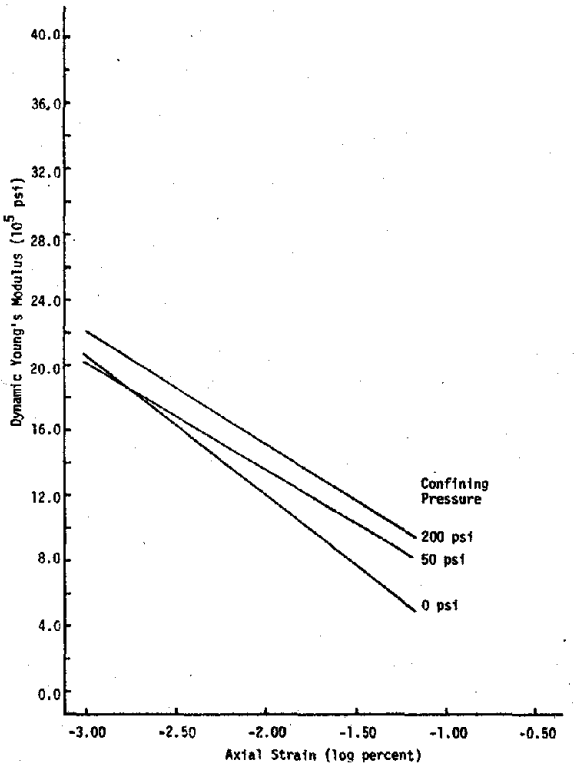

Figure 5.31 DYNAMIC YOUNG'S MODULUS VERSUS AXIAL STRAIN FOR SAND-ICE SAMPLES OF 65% SAND CONTENT AT -4°C AND 0.3 cps

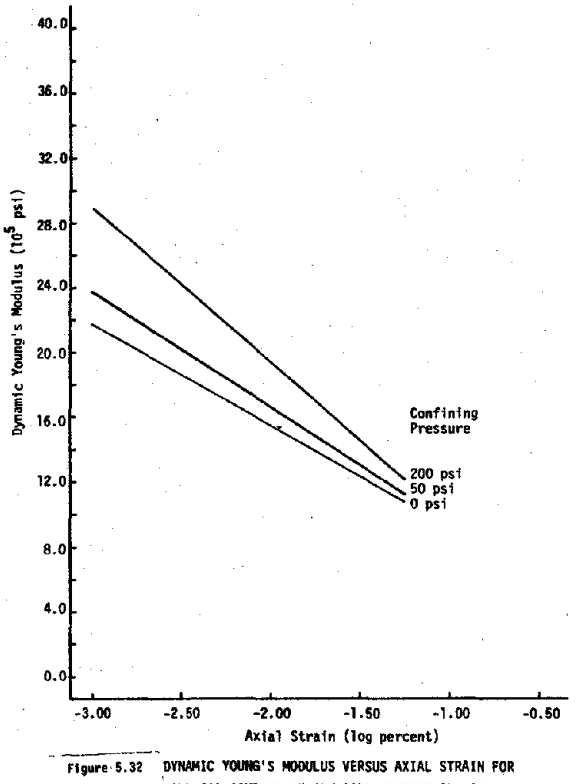

Figure 5.32 DYNAMIC YOUNG'S MODULUS VERSUS AXIAL STRAIN FOR SAND-ICE SAMPLES OF 65% SAND CONTENT AT -4°C AND 1.0 cps

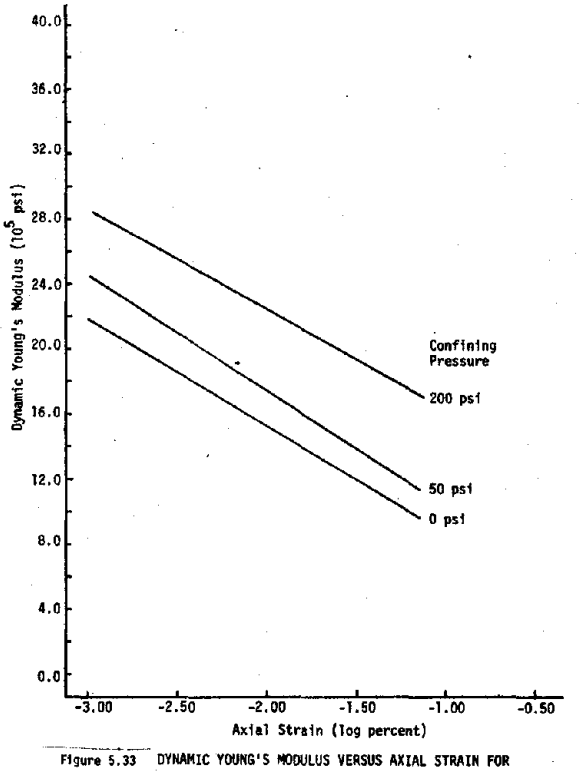

Figure 5.33 DYNAMIC YOUNG'S MODULUS VERSUS AXIAL STRAIN FOR SAND-ICE SAMPLES OF 65% SAND CONTENT AT -4°C AND 5.0 cps

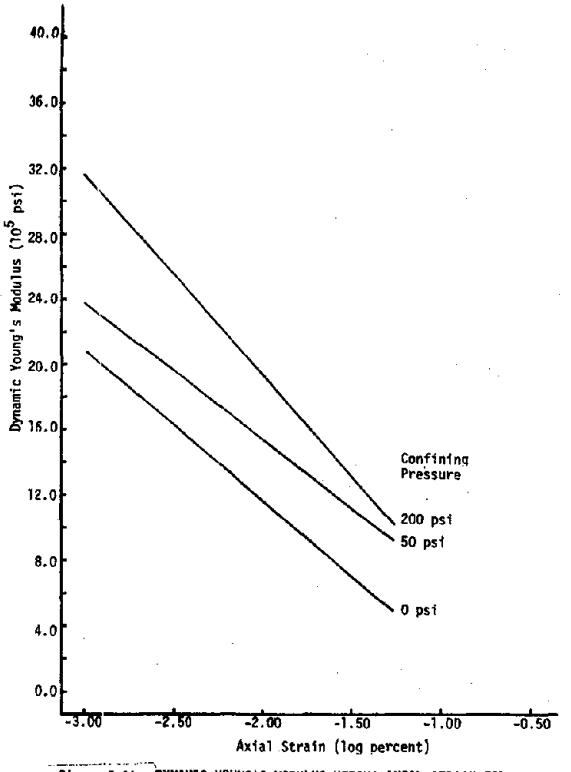

Figure 5.34 DYNAMIC YOUNG'S MODULUS VERSUS AXIAL STRAIN FOR SAND-ICE SAMPLES OF 65% SAND CONTENT AT -10°C AND 0.05 cps

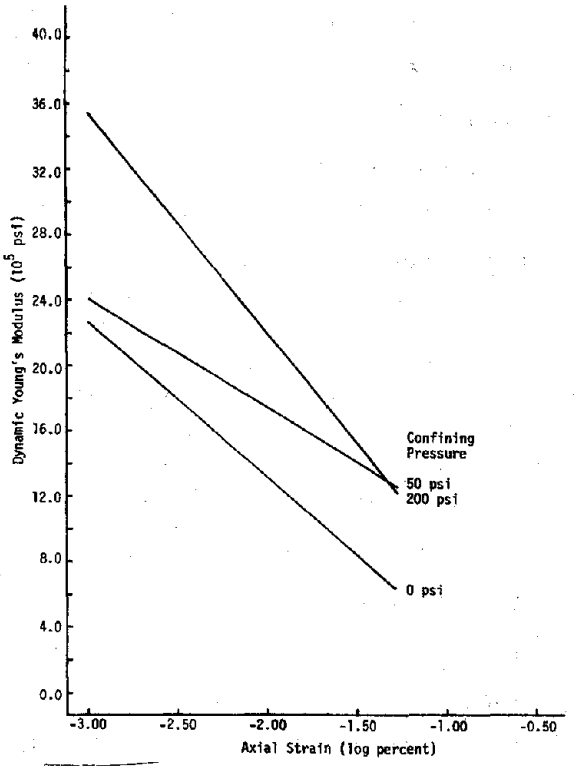

Figure 5.35 DYNAMIC YOUNG'S MODULUS VERSUS AXIAL STRAIN FOR SAND-ICE SAMPLES OF 65% SAND CONTENT AT -10°C AND 0.3 cps

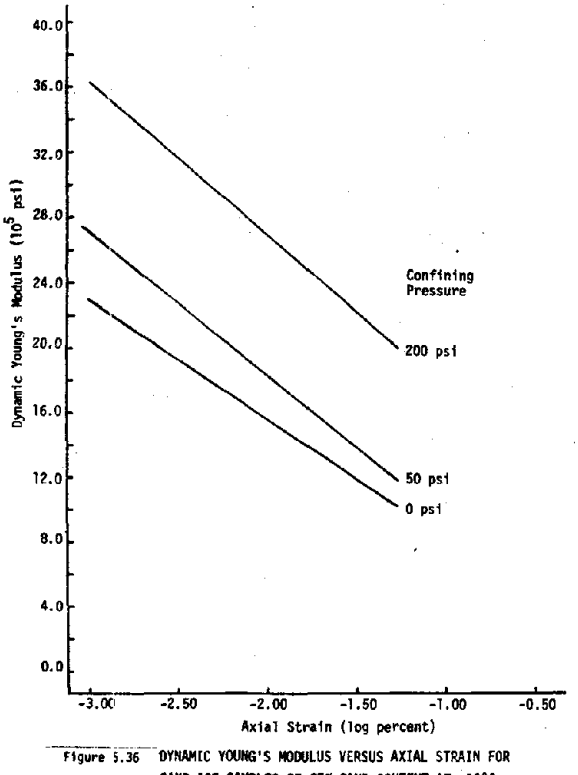

Figure 5.36 DYNAMIC YOUNG'S MODULUS VERSUS AXIAL STRAIN FOR SAND-ICE SAMPLES OF 65% SAND CONTENT AT -10°C AND 1.0 cps

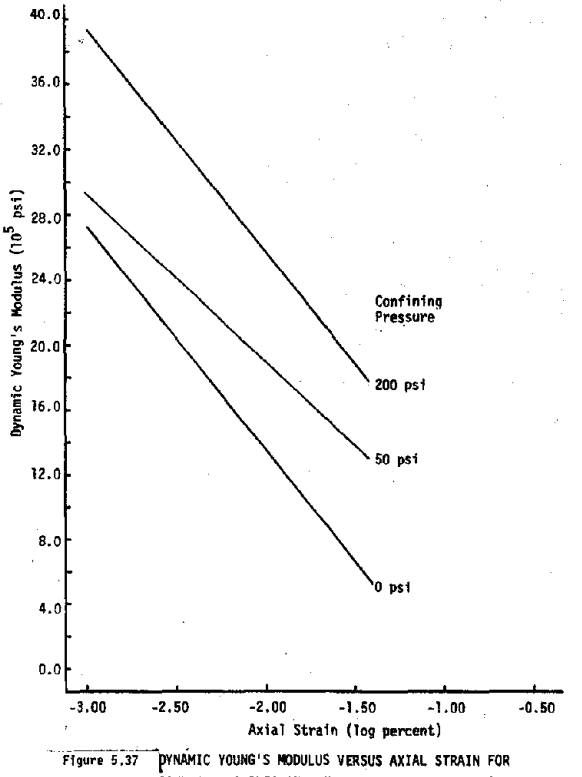

Figure 5.37 DYNAMIC YOUNG'S MODULUS VERSUS AXIAL STRAIN FOR SAND-ICE SAMPLES OF 65% SAND CONTENT AT -10 °C AND 5.0 cps

The relationship between dynamic Young's modulus and confining pressure, frequency, and temperature can be established by interpolation of the results presented in Figures 5.2 to 5.37 at a specified strain amplitude. A strain amplitude of .01% was selected for this purpose. Another strain amplitude could have been selected without significantly changing the conclusions reached in the following paragraphs.

5.3.2 Effect of Confining Pressure

The relationship between dynamic Young's modulus and confining pressure at an axial strain of .01% is shown in Figure 5.38 to 5.46. The relationship is shown at four frequencies at a given sand content and temperature. The results shown indicate dynamic Young's modulus increases with increasing confining pressure. The rate of increase appears to be greater at the highest sand content (65%). The frequency of loading and temperature do not appear to have a pronounced effect on the rate of increase.

At low sand contents (20%) the relationship between dynamic Young's modulus and confining pressure might be caused by changes in the microstructure of the ice under various confining pressures. Microfissures might close when a sample is subjected to a high confining pressure. This would lead to a sample with a higher dynamic modulus. At high sand contents (65%) the relationship between dynamic Young's modulus and confining pressure might be associated with an increase in the stress at the contact points between the sand particles. As the confining pressure is increased the stress at the contact point increases and dynamic Young's modulus would increase.

5.3.3 Effect of Frequency

The relationship between dynamic Young's modulus and frequency at an axial strain of .01% is shown in Figures 5.47 to 5.55. The relationship is shown at three temperatures at a given sand content and confining pressure. At temperatures of -1 and -4°C, dynamic Young's modulus increases with increasing frequency. At a temperature of -10°C dynamic Young's modulus increases to a frequency of 1.0 cps; between 1.0 and 5.0 cps dynamic Young's modulus either decreases or remains con-

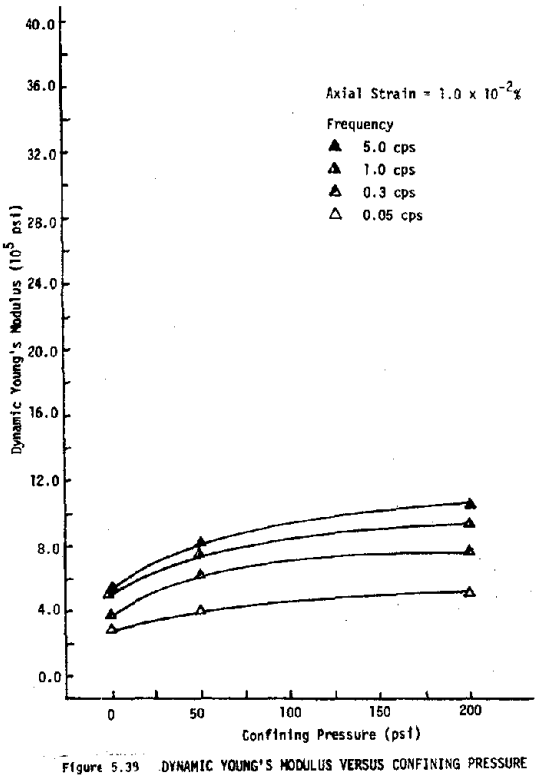

Figure 5.39 DYNAMIC YOUNG'S MODULUS VERSUS CONFINING PRESSURE FOR SAND-ICE SAMPLES OF 20% SAND CONTENT AT -1°C

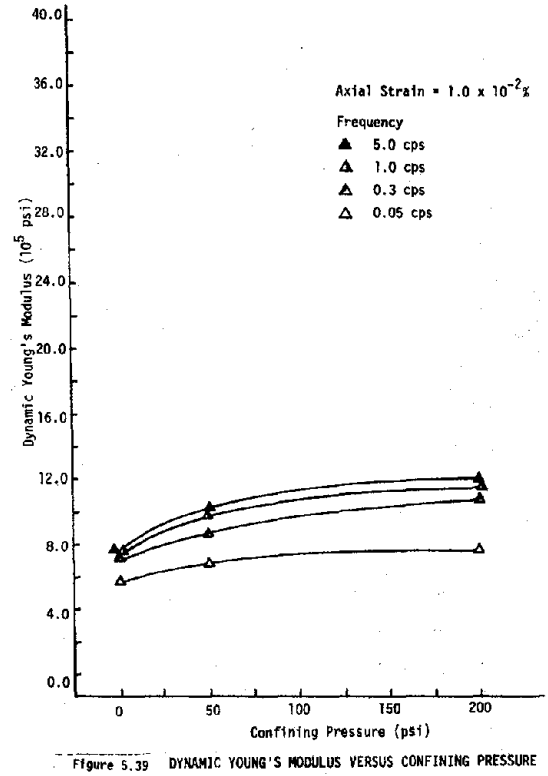

Figure 5.39 DYNAMIC YOUNG'S MODULUS VERSUS CONFINING PRESSURE FOR SAND-ICE SAMPLES OF 20% SAND CONTENT AT -4°C

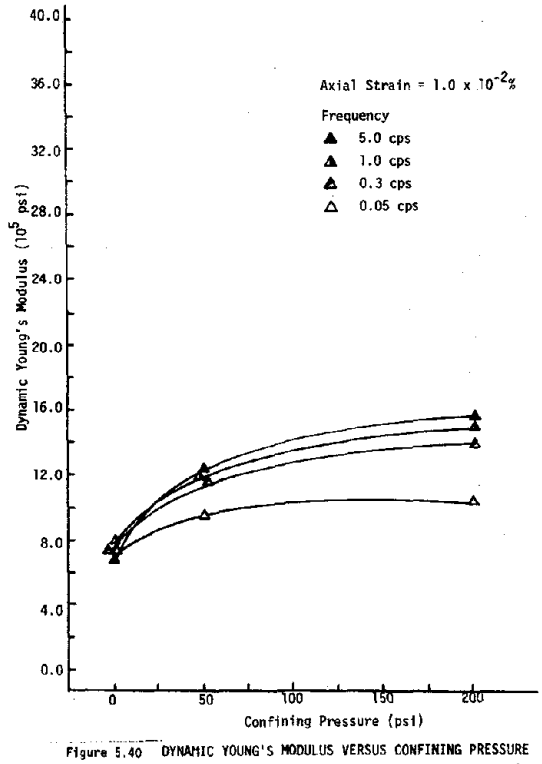

Figure 5.40 DYNAMIC YOUNG'S MODULUS VERSUS CONFINING PRESSURE FOR SAND-ICE SAMPLES OF 20% SAND CONTENT AT -10°C

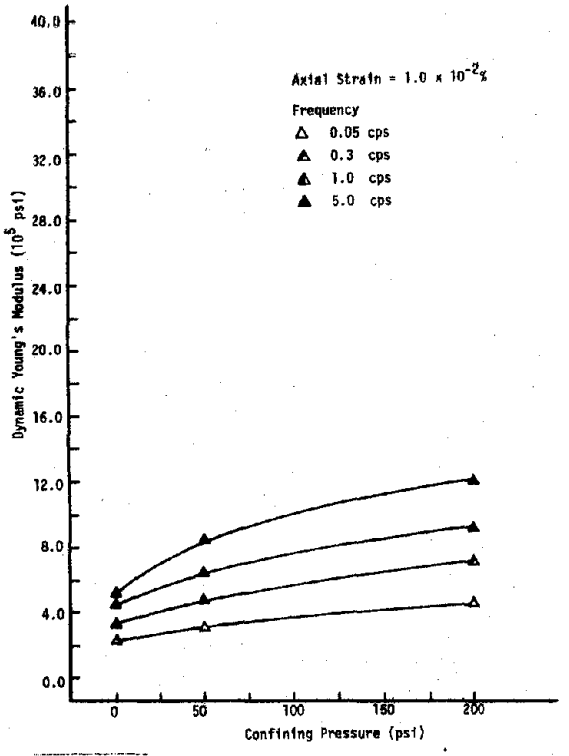

Figure 5.41 DYNAMIC YOUNG'S MODULUS VERSUS CONFINING PRESSURE FOR SAND-ICE SAMPLES OF 45% SAND CONTENT AT -1°C

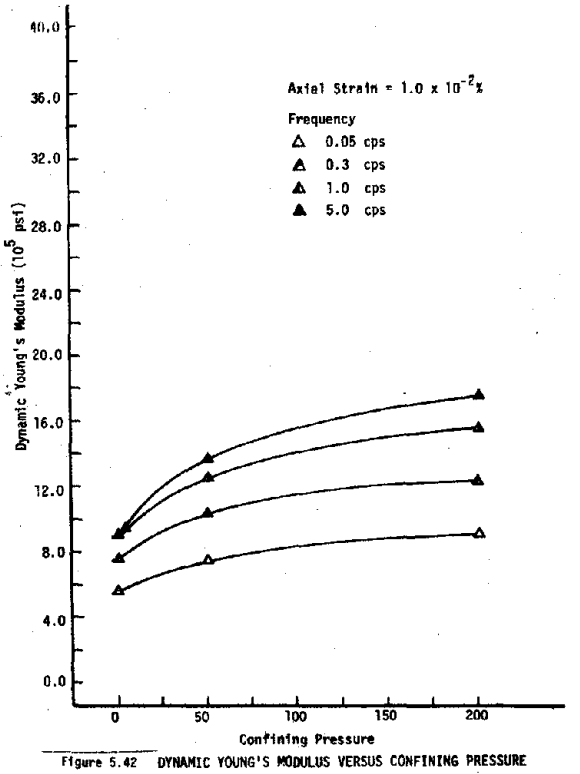

Figure 5.42 DYNAMIC YOUNG'S MODULUS VERSUS CONFINING PRESSURE FOR SAND-ICE SAMPLES OF 45% SAND CONTENT AT -4°C

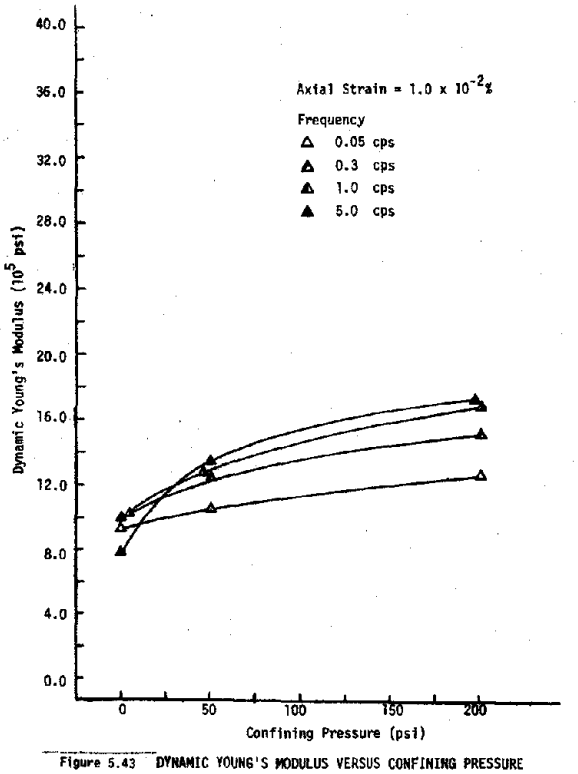

Figure 5.43 DYNAMIC YOUNG'S MODULUS VERSUS CONFINING PRESSURE FOR SAND-ICE SAMPLES OF 45% SAND CONTENT AT -10°C

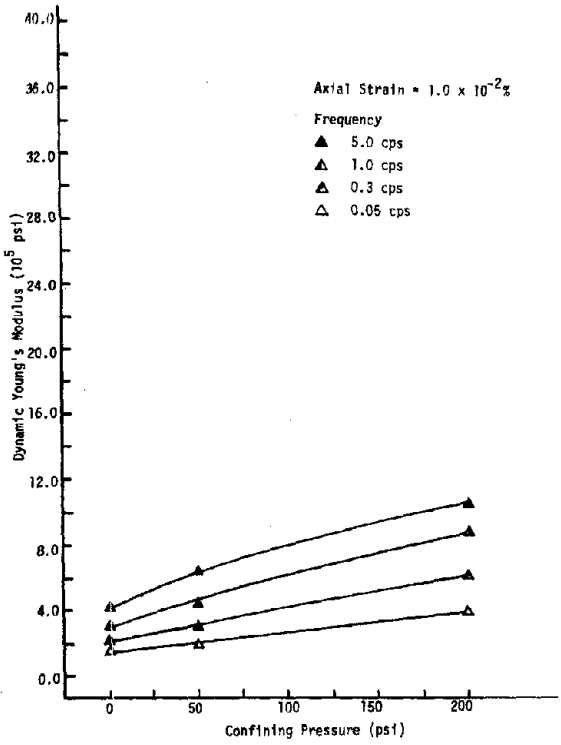

Figure 5.44 DYNAMIC YOUNG'S MODULUS VERSUS CONFINING PRESSURE FOR SAND-ICE SAMPLES OF 65% SAND CONTENT AT -1°C

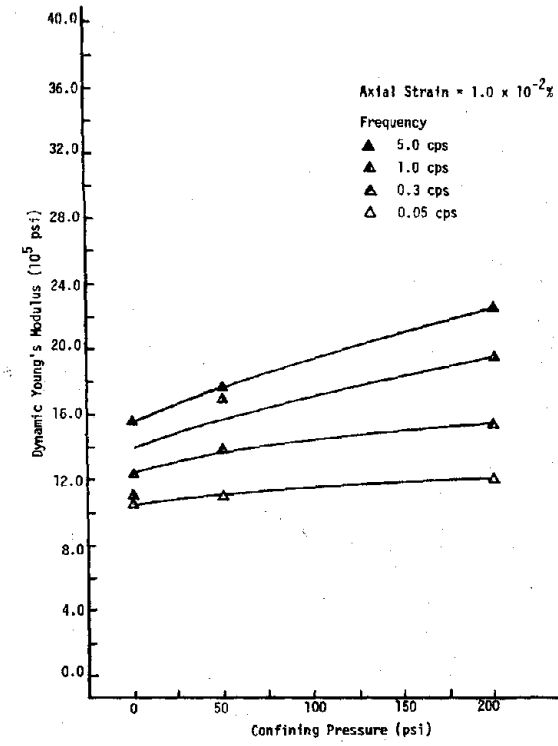

Figure 5.45 DYNAMIC YOUNG'S MODULUS VERSUS CONFINING PRESSURE FOR SAND-ICE SAMPLES OF 65% SAND CONTENT AT -4°C

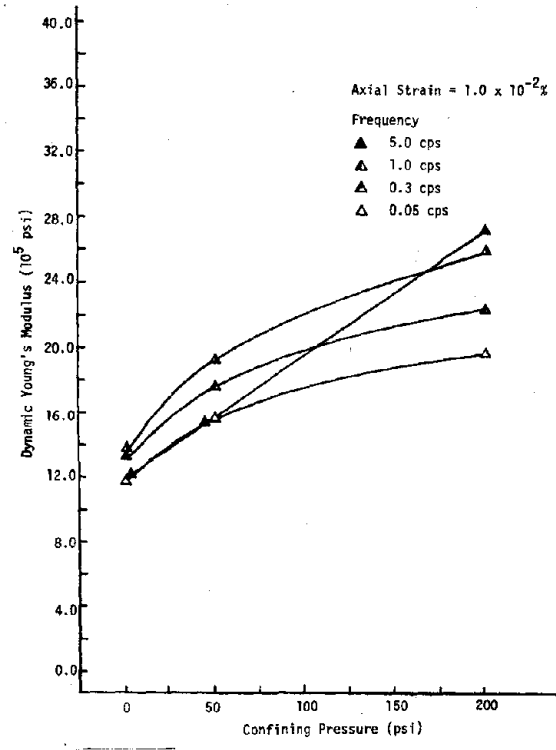

Figure 5.46 DYNAMIC YOUNG'S MODULUS VERSUS CONFINING PRESSURE FOR SAND-ICE SAMPLES OF 65% SAND CONTENT AT -10°C

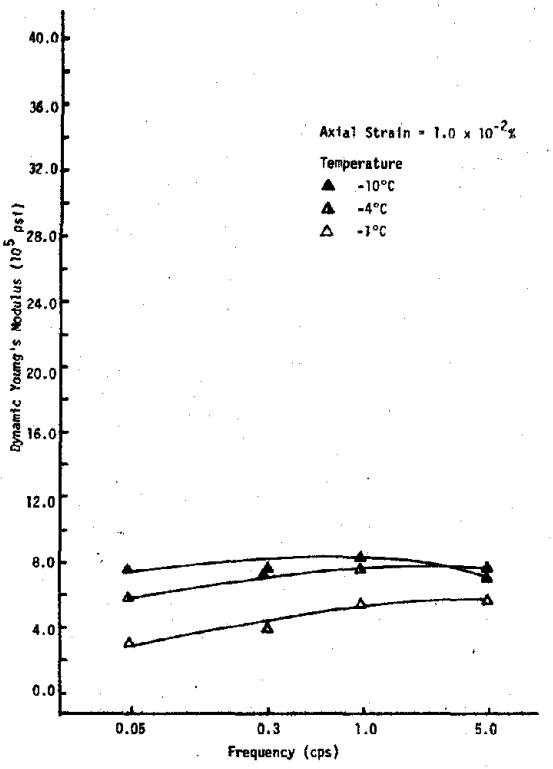

Figure 5.47 DYNAMIC YOUNG'S MODULUS VERSUS FREQUENCY FOR SAND-ICE SAMPLES OF 20% SAND CONTENT AT 0 psi CONFINING PRESSURE

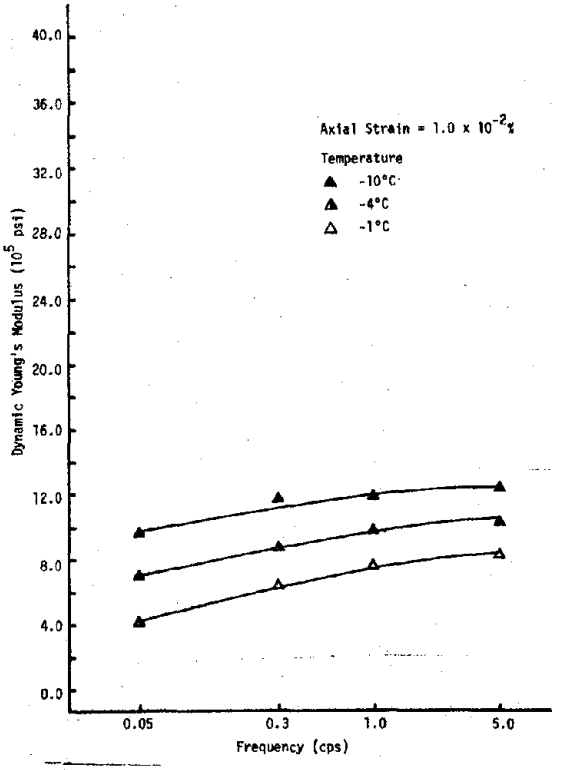

Figure 5.48 DYNAMIC YOUNG'S MODULUS VERSUS FREQUENCY FOR SAND-ICE SAMPLES OF 20% SAND CONTENT AT 50 psi CONFINING PRESSURE

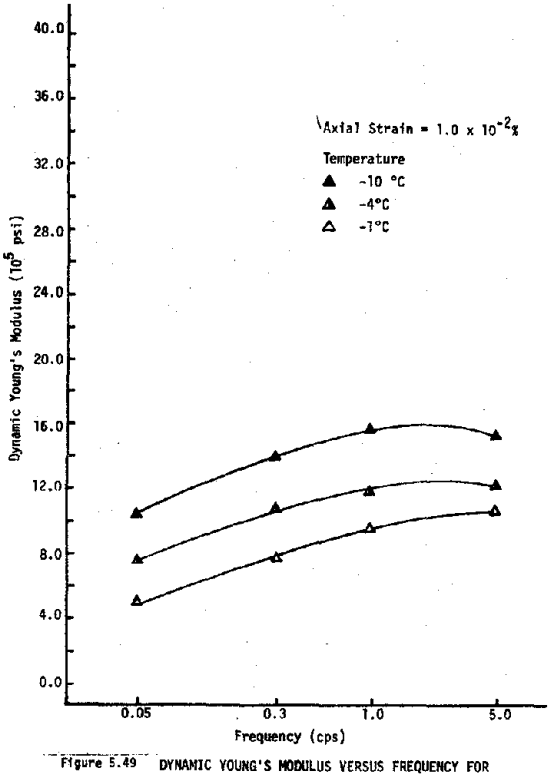

Figure 5.49 DYNAMIC YOUNG'S MODULUS VERSUS FREQUENCY FOR SAND-ICE SAMPLES OF 20% SAND CONTENT AT 200 psi CONFINING PRESSURE

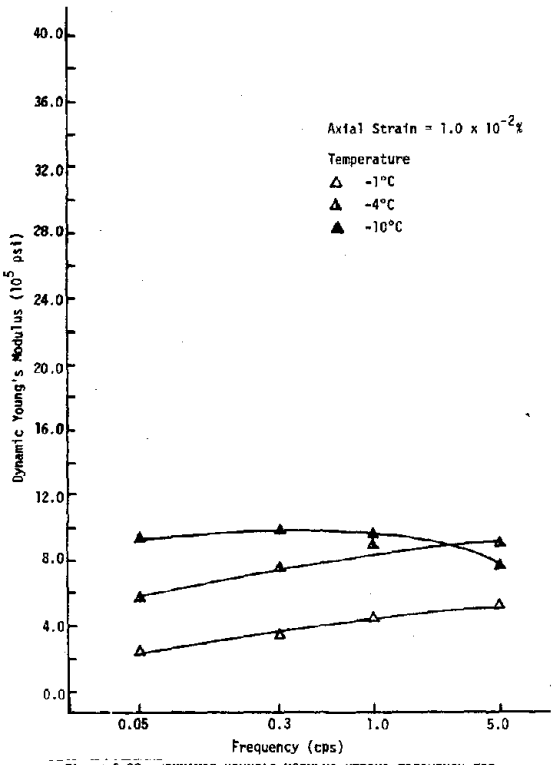

Figure 5.50 DYNAMIC YOUNG'S MODULUS VERSUS FREQUENCY FOR SAND-ICE SAMPLES OF 45% SAND CONTENT AT 0 psi CONFINING PRESSURE

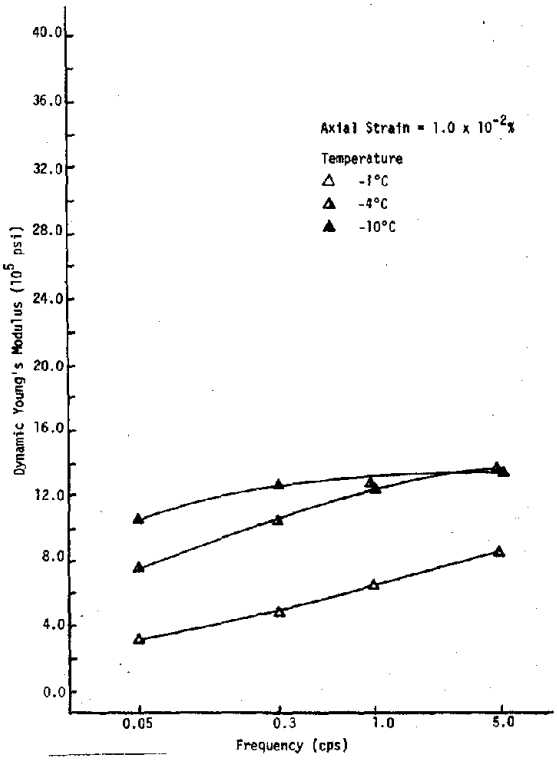

Figure 5.51 DYNAMIC YOUNG'S MODULUS VERSUS FREQUENCY FOR SAND-ICE SAMPLES OF 45% SAND CONTENT AT 50 psi CONFINING PRESSURE

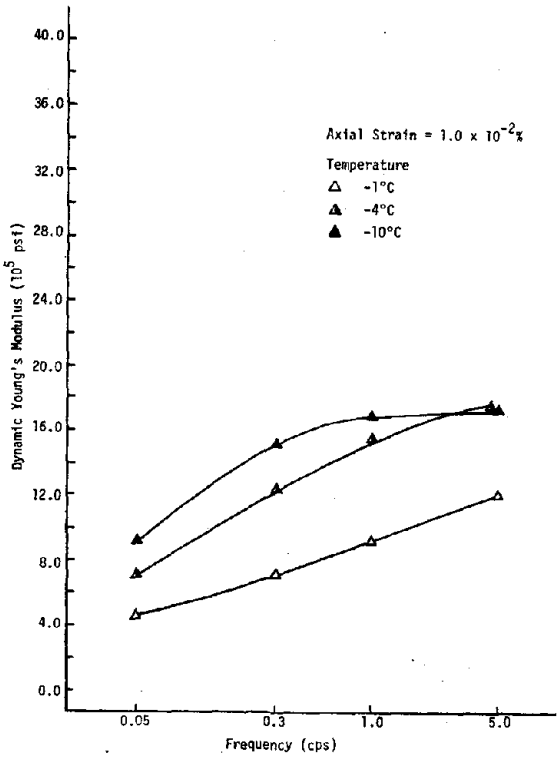

Figure 5.52 DYNAMIC YOUNG'S MODULUS VERSUS FREQUENCY FOR SAND-ICE SAMPLES OF 45% SAND CONTENT AT 200 psi CONFINING PRESSURE

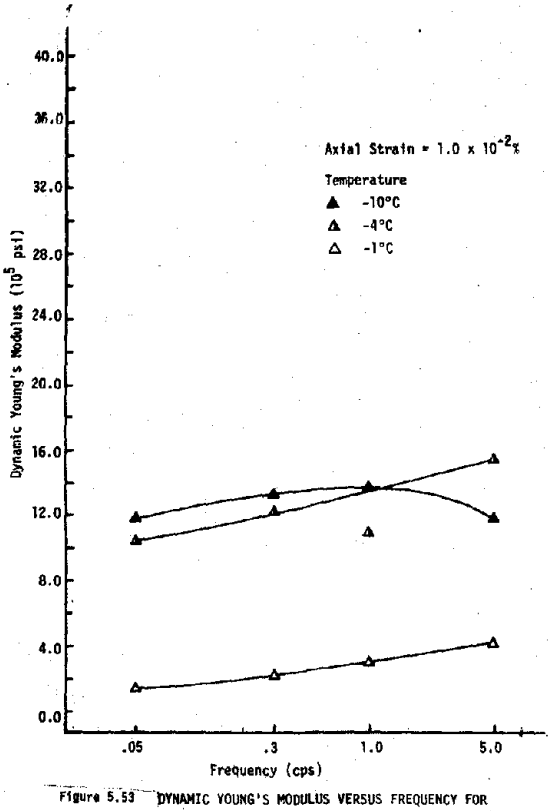

Figure 5.53 DYNAMIC YOUNG'S MODULUS VERSUS FREQUENCY FOR SAND-ICE SAMPLES OF 65% SAND CONTENT AT 0 psi CONFINING PRESSURE

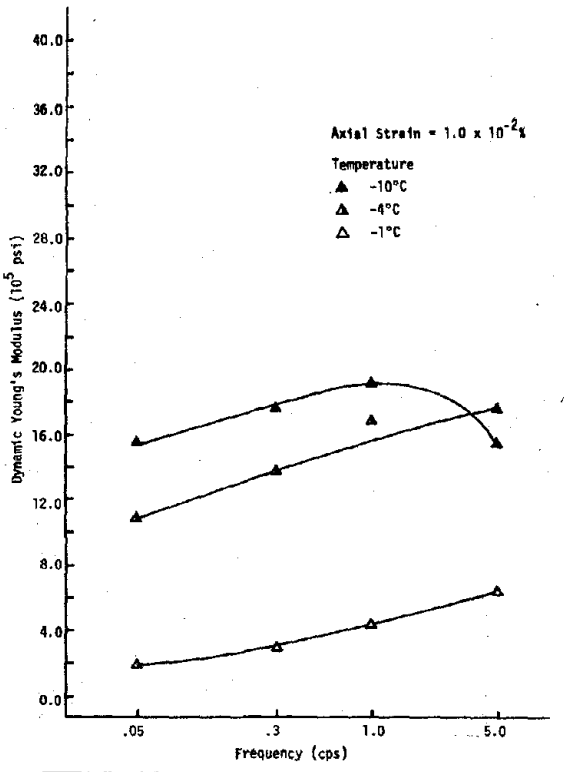

Figure 5.54 DYNAMIC YOUNG'S MODULUS VERSUS FREQUENCY FOR SAND-ICE SAMPLES OF 65% SAND CONTENT AT 50 psi CONFINING PRESSURE

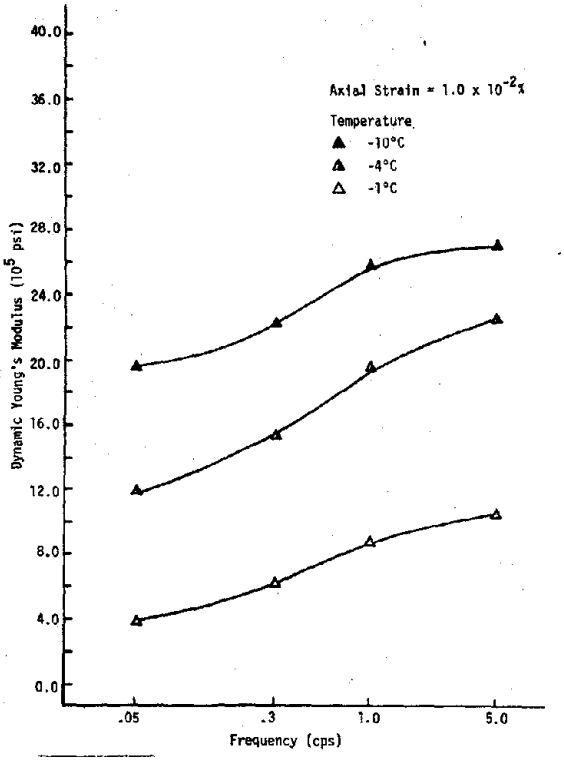

Figure 5.55 DYNAMIC YOUNG'S MODULUS VERSUS FREQUENCY FOR SAND-ICE SAMPLES OF 65% SAND CONTENT AT 200 psi CONFINING PRESSURE

stant. The relationship between dynamic Young's modulus and frequency appears to be independent of temperature and sand content.

5.3.4 Effect of Temperature

The relationship between dynamic Young's modulus and temperature at an axial strain of .01% is shown in Figures 5.56 to 5.64. The relationship is shown at four frequencies at a given sand content and confining pressure. Dynamic Young's modulus increases with descending temperature at frequencies of 0.05, 0.3, and 1.0 cps. The rate of increase appears to be greatest at a high confining pressure (200 psi) and high sand content (65%). At a frequency of 5.0 cps dynamic Young's modulus increases, in general, with descending temperature; however, at the low confining pressures (0 and 50 psi) dynamic Young's modulus was found to decrease between -4 and -10^{o}C.

The explanation of dynamic Young's modulus increasing with descending temperature for a cohesionless soil is not obvious. There is not a significant change in unfrozen water content of cohesionless soils with temperature nor is the dynamic modulus of the ice in the voids of the frozen soil mass strongly dependent on temperature. The explanation is possibly associated with the dependence of the dynamic elastic properties of cohesionless soils on confining pressure. It is well established that the dynamic elastic properties of cohesionless soils increase with increasing confining pressure (Seed and Idriss, 1970) owing to the increased stress at the contact points between particles. The ice in the voids of a frozen soil mass in which the soil grains are in contact must also increase the stress at the contact points between particles owing to the adhesive-attractive bond it has with the particles. The high stress at the contact points leads to high values of dynamic modulus. The adhesive attractive bond is apparently temperature dependent; the higher the temperature, the lower the adhesive attractive bond and the lower the stress at the contact points. Consequently, dynamic Young's modulus decreases with ascending temperature owing to the decrease in the adhesive-attractive bond. No explanation for the decrease in dynamic Young's modulus in the temperature range -4 to -10^{o}C at a frequency of 5.0 cps and low confining pressures is available at this time.

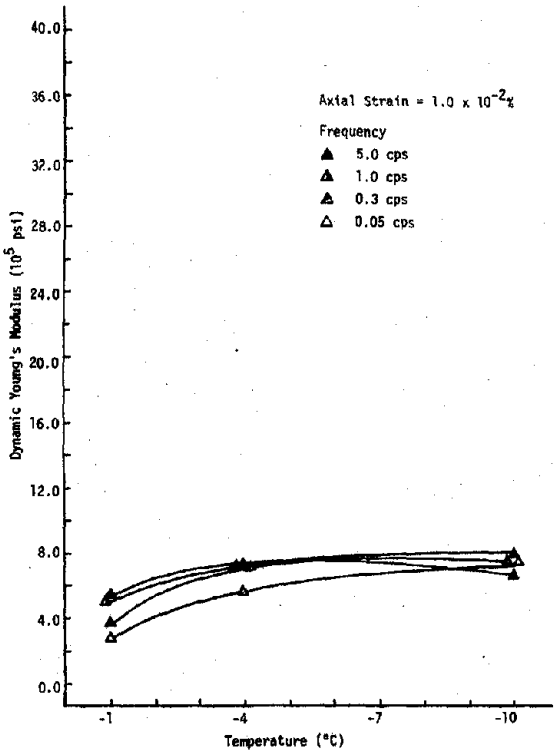

Figure 5.56 DYNAMIC YOUNG'S MODULUS VERSUS TEMPERATURE FOR SAND-ICE SAMPLES OF 20% SAND CONTENT AT 0 psi CONFINING PRESSURE

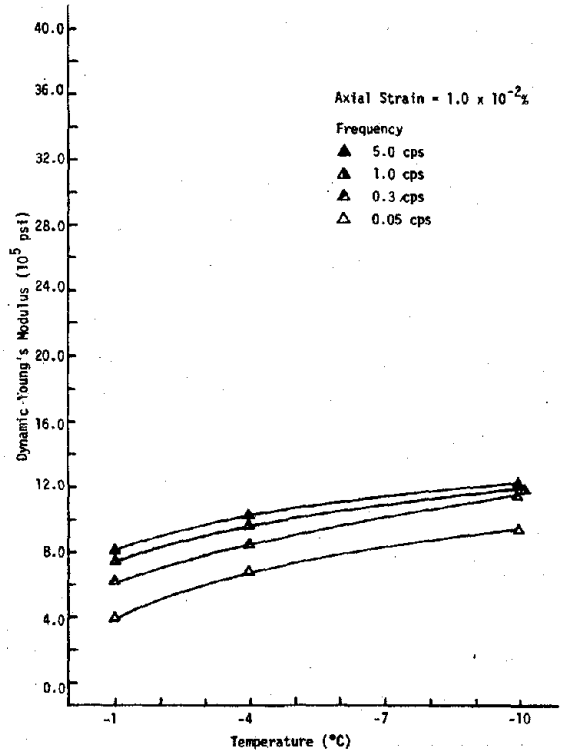

Figure 5.57 DYNAMIC YOUNG'S MODULUS VERSUS TEMPERATURE FOR SAND-ICE SAMPLES OF 20% SAND CONTENT AT 50 psi CONFINING PRESSURE

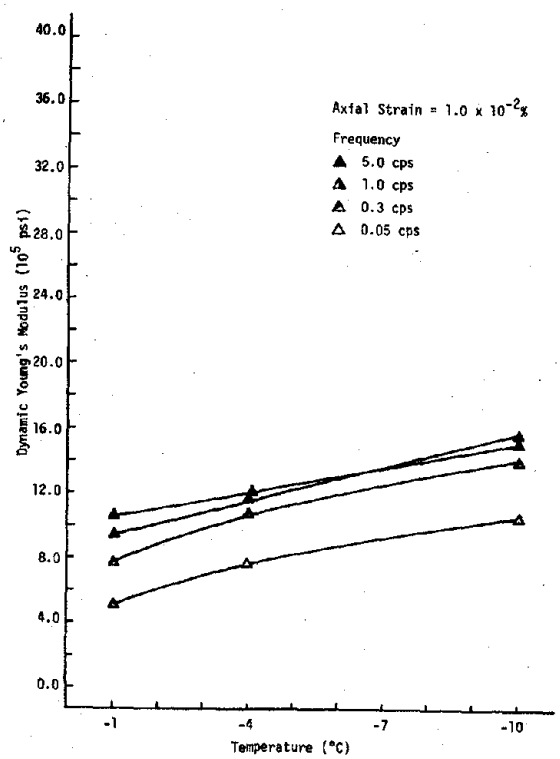

Figure 5.58 DYNAMIC YOUNG'S MODULUS VERSUS TEMPERATURE FOR SAND-ICE SAMPLES OF 20% SAND CONTENT AT 200 psi CONFINING PRESSURE

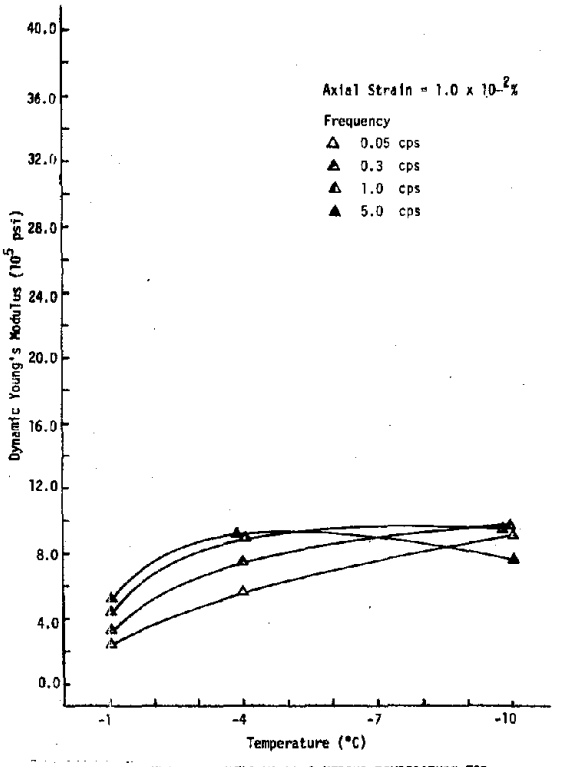

Figure 5.59 DYNAMIC YOUNG'S MODULUS VERSUS TEMPERATURE FOR SAND-ICE SAMPLES OF 45% SAND CONTENT AT 0 psi CONFINING PRESSURE

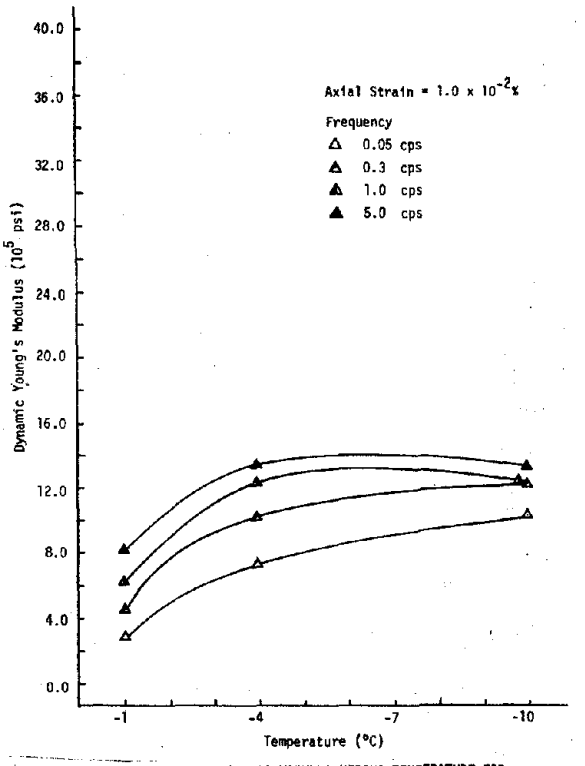

Figure 5.60 DYNAMIC YOUNG'S MODULUS VERSUS TEMPERATURE FOR SAND-ICE SAMPLES OF 45% SAND CONTENT AT 50 psi CONFINING PRESSURE

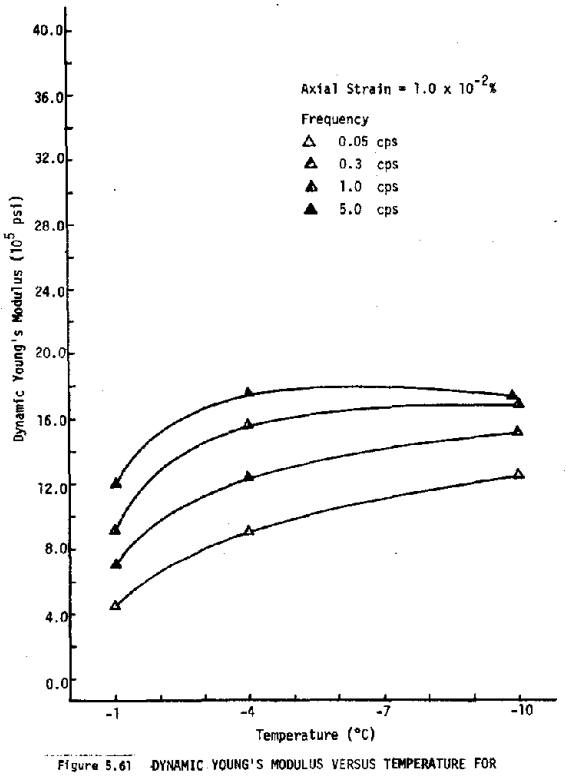

Figure 5.61 DYNAMIC YOUNG'S MODULUS VERSUS TEMPERATURE FOR SAND-ICE SAMPLES OF 45% SAND CONTENT AT 200 psi CONFINING PRESSURE

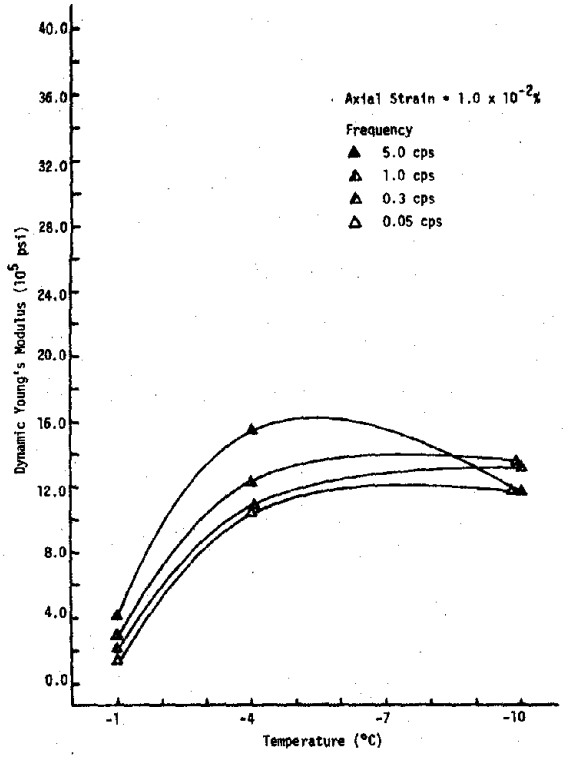

Figure 5.62 DYNAMIC YOUNG'S MODULUS VERSUS TEMPERATURE FOR SAND-ICE SAMPLES OF 65% SAND CONTENT AT 0 psi CONFINING PRESSURE

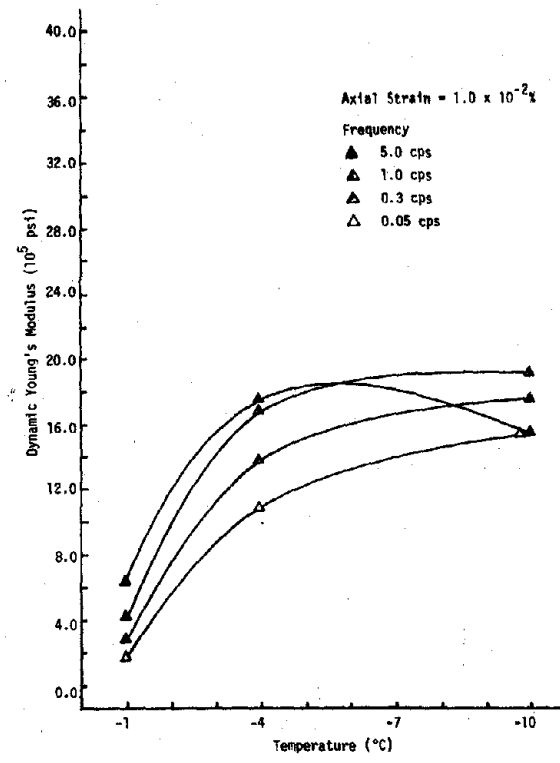

Figure 5.63 DYNAMIC YOUNG'S MODULUS VERSUS TEMPERATURE FOR SAND-ICE SAMPLES OF 65% SAND CONTENT AT 50 psi CONFINING PRESSURE

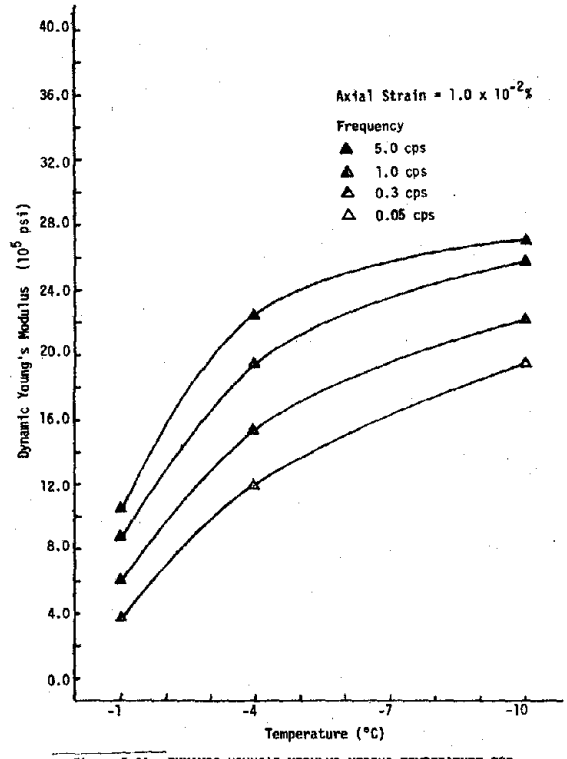

Figure 5.64 DYNAMIC YOUNG'S MODULUS VERSUS TEMPERATURE FOR SAND-ICE SAMPLES OF 65% SAND CONTENT AT 200 psi CONFINING PRESSURE

5.3.5 Effect of Sand Content

The relationship between dynamic Young's modulus and sand content at an axial strain of .01% is shown in Figures 5.65 to 5.70. In Figures 5.65 to 5.67 the relationship is shown at four frequencies at a given confining pressure and temperature; in Figures 5.68 to 5.70 the relationship is shown at three temperatures at a constant frequency and confining pressure.

Dynamic Young's modulus decreases with increasing sand content at a temperature of $-1^{o}C$; dynamic Young's modulus increases with sand content at temperatures of -4 and $-10^{o}C$. The increase in dynamic Young's modulus with increasing sand content may be attributed to the increase in density of the sand-ice mixture and, at a sand content of 65% the development of interparticle contacts. The decrease in dynamic Young's modulus with increasing sand content is puzzling. It is probably related to the temperature dependence of the adhesive-attractive bond the ice has with the sand particles (see Section 5.3.2).

5.4 Damping Ratio of Frozen Sand

5.4.1 Effect of Strain Amplitude

Values of damping ratio of frozen sand were plotted against the log of axial strain amplitude expressed as a percent. The data were plotted in two ways: (1) the data were plotted at separate confining pressures for a given test condition as shown in Appendix D, and (2) the data were plotted at all confining pressures for a given test condition as shown in Appendix E. Least squares best fit lines were drawn through the data for a given test condition.

The results presented in Appendix D or E indicate the relationship between damping ratio and axial strain amplitude appears to vary considerably. The results shown in Appendix E are summarized in Figures 5.71 to 5.79 and illustrate this fact. The value of damping ratio may increase, decrease, or remain constant with increasing axial strain amplitude. An explanation of these relationships is not available at this time.

The relationship between damping ratio and confining pressure, frequency, and temperature can be established by interpolation of the

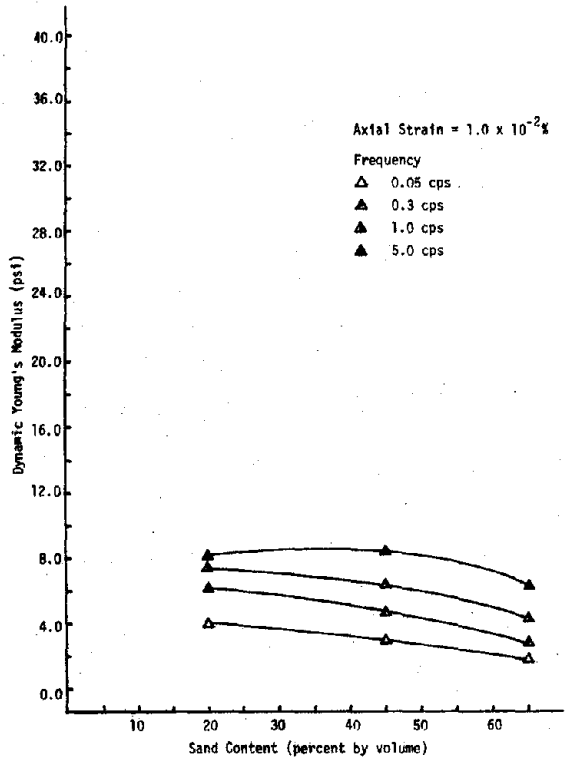

Figure 5.65 DYNAMIC YOUNG'S MODULUS VERSUS SAND CONTENT FOR SAND-ICE SAMPLES AT 50 psi AND -1°C

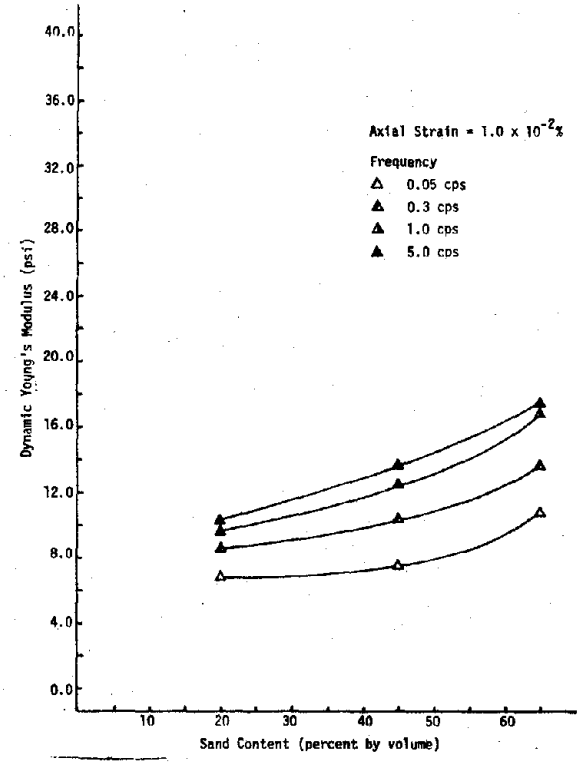

Figure 5.66 DYNAMIC YOUNG'S MODULUS VERSUS SAND CONTENT FOR SAND-ICE SAMPLES AT 50 psi AND -4°C

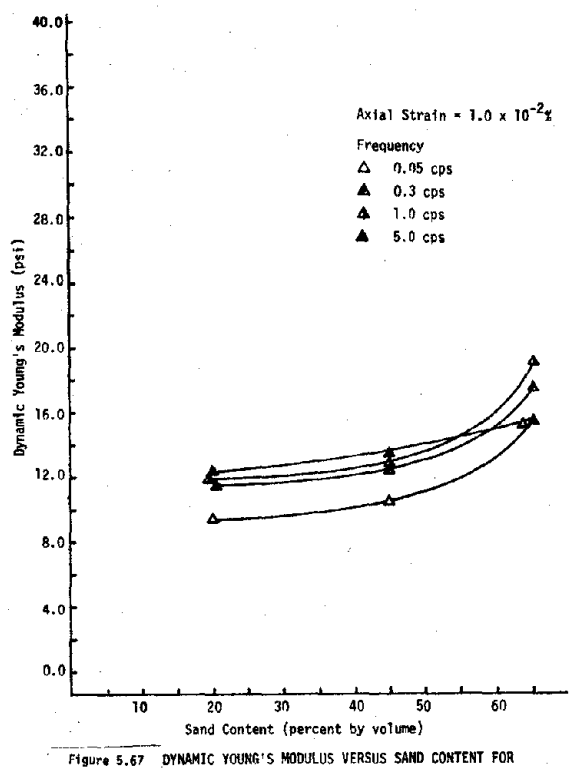

Figure 5.67 DYNAMIC YOUNG'S MODULUS VERSUS SAND CONTENT FOR SAND-ICE SAMPLES AT 50 psi AND -10°C

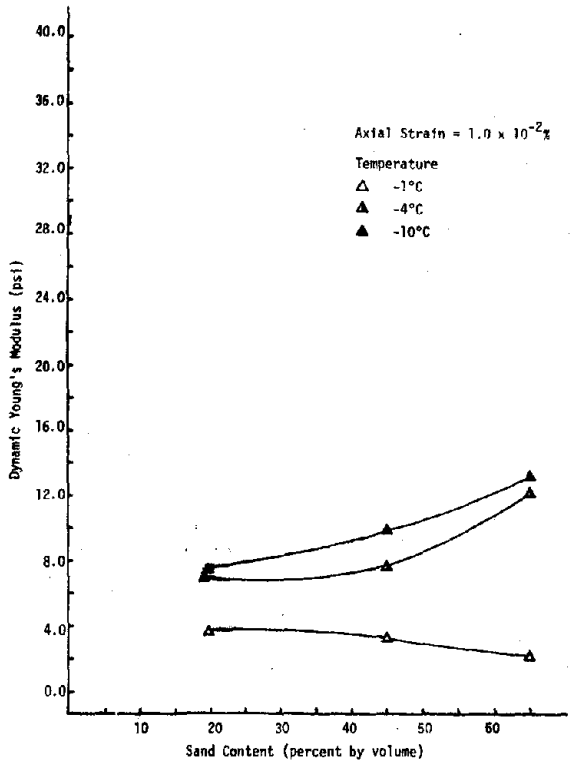

Figure 5.68 DYNAMIC YOUNG'S MODULUS VERSUS SAND CONTENT FOR SAND-ICE SAMPLES AT 0.3 cps AND 0 psi CONFINING PRESSURE

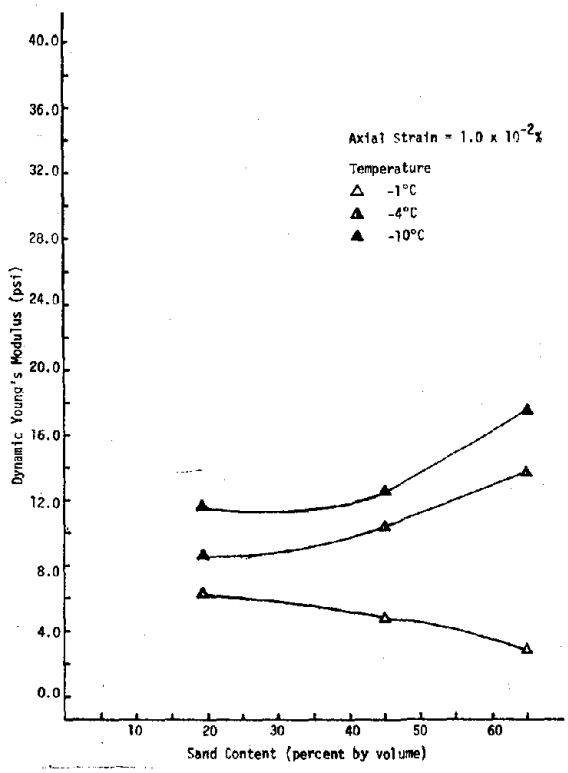

Figure 5.69 DYNAMIC YOUNG'S MODULUS VERSUS SAND CONTENT FOR SAND-ICE SAMPLES AT 0.3 cps AND 50 psi CONFINING PRESSURE

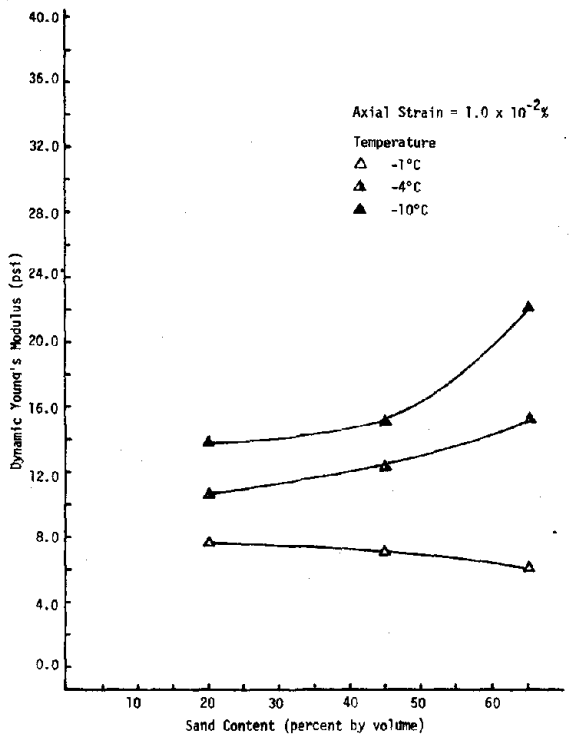

Figure 5.70 DYNAMIC YOUNG'S MODULUS VERSUS SAND CONTENT FOR SAND-ICE SAMPLES AT 0.3 cps AND 200 psi CONFINING PRESSURE

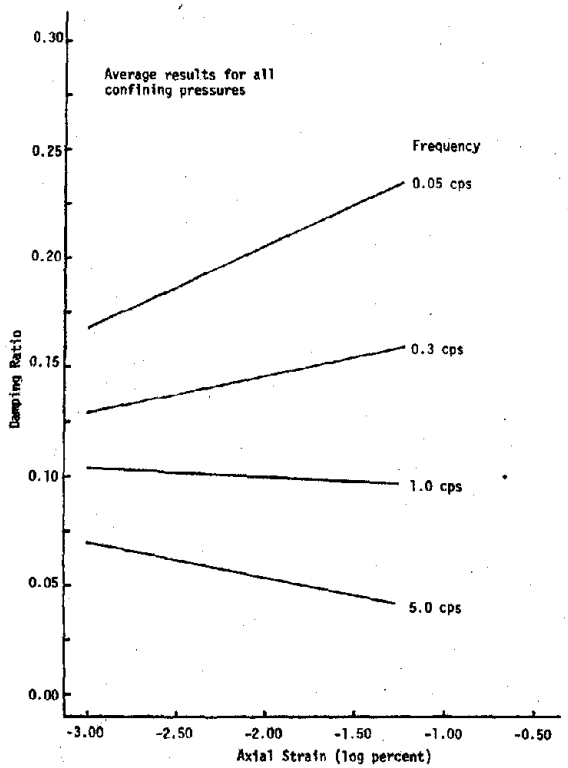

Figure 5.71 DAMPING RATIO VERSUS AXIAL STRAIN FOR SAND-ICE SAMPLES OF 20% SAND CONTENT AT -1°C

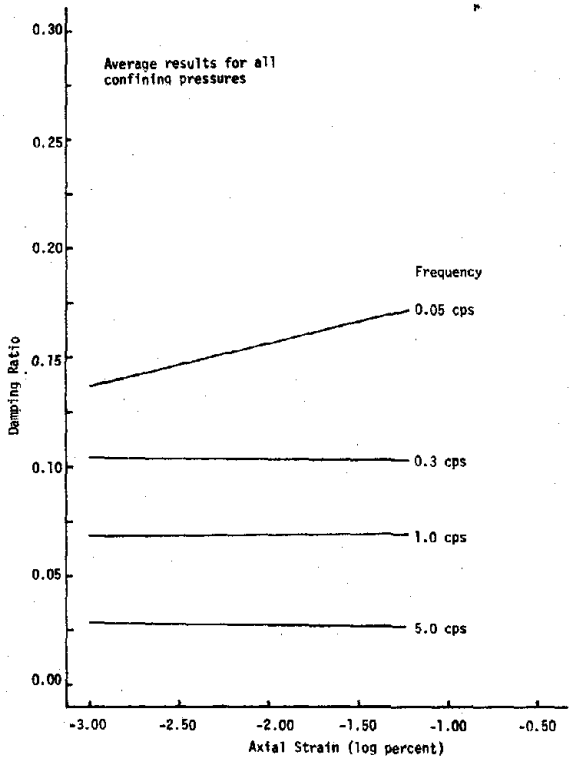

Figure 5.72 DAMPING RATIO VERSUS AXIAL STRAIN FOR SAND-ICE SAMPLES OF 20% SAND CONTENT AT -4°C

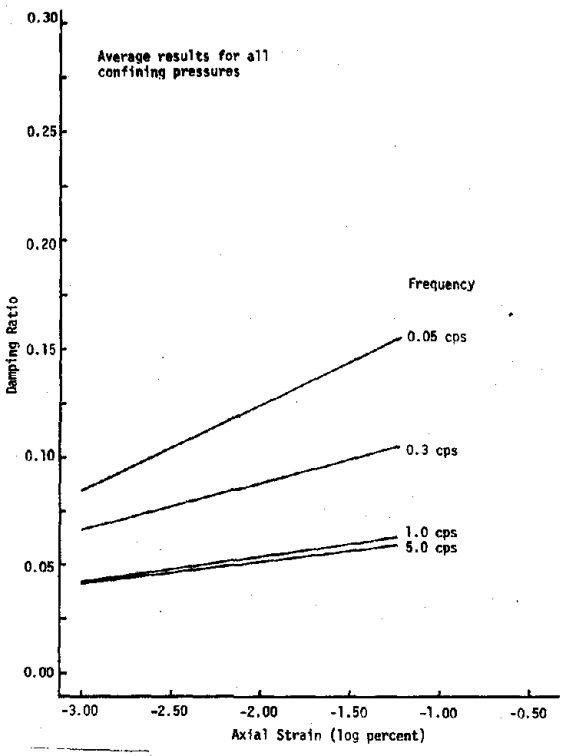

Figure 5.73 DAMPING RATIO VERSUS AXIAL STRAIN FOR SAND-ICE SAMPLES OF 20% SAND CONTENT AT -10°C

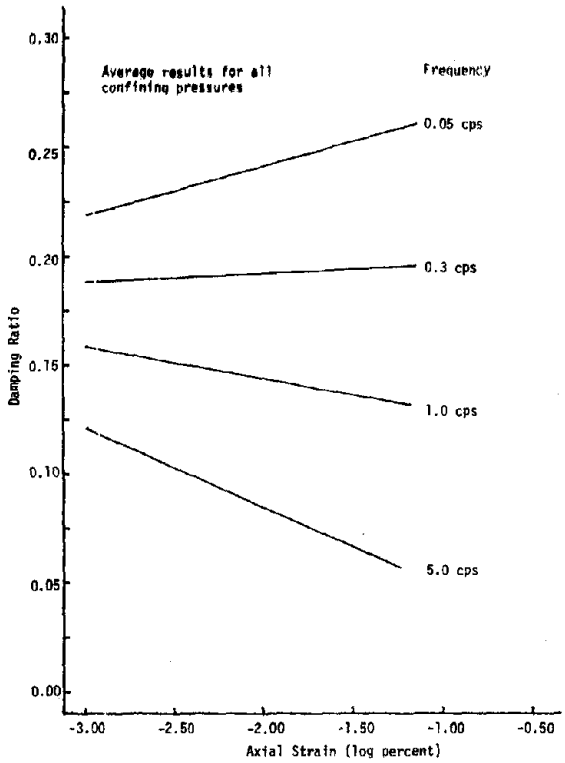

Figure 5.74 DAMPING RATIO VERSUS AXIAL STRAIN FOR SAND-ICE SAMPLES OF 45% SAND CONTENT AT -1°C

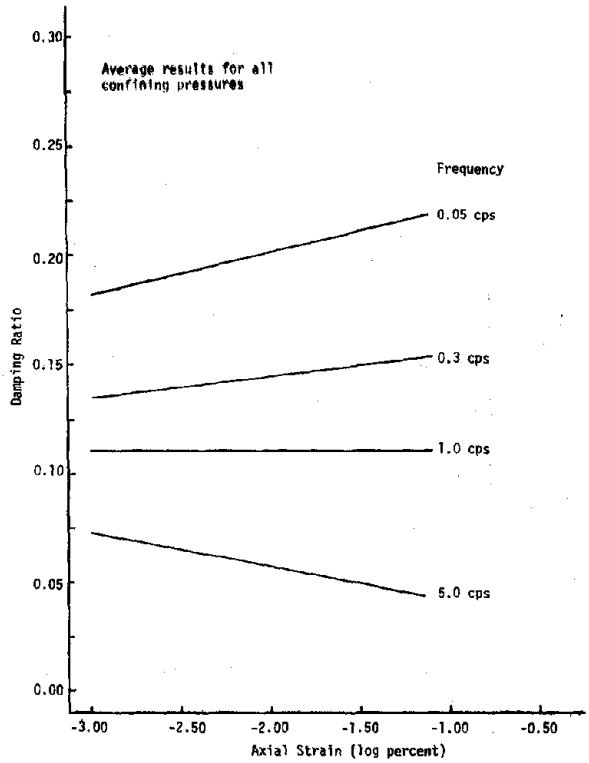

Figure 5.75 DAMPING RATIO VERSUS AXIAL STRAIN FOR SAND-ICE SAMPLES OF 45% SAND CONTENT AT -4°C

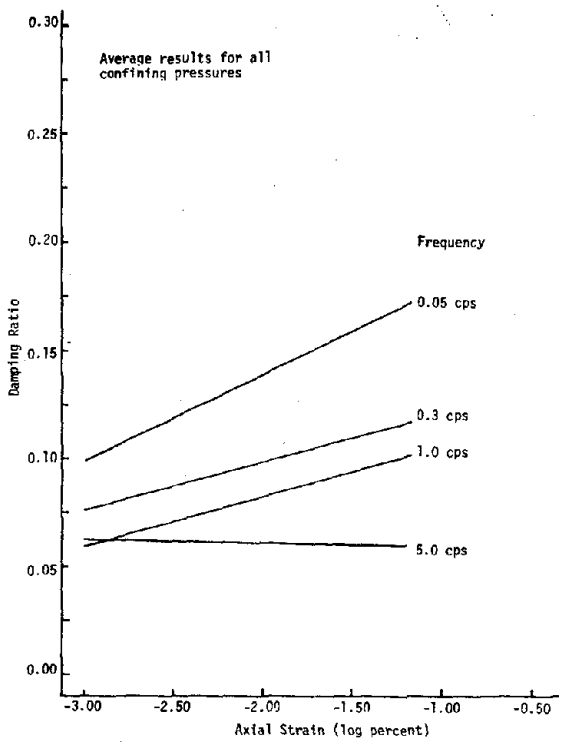

Figure 5.76 DAMPING RATIO VERSUS AXIAL STRAIN FOR SAND-ICE SAMPLES OF 45% SAND CONTENT AT -10°C

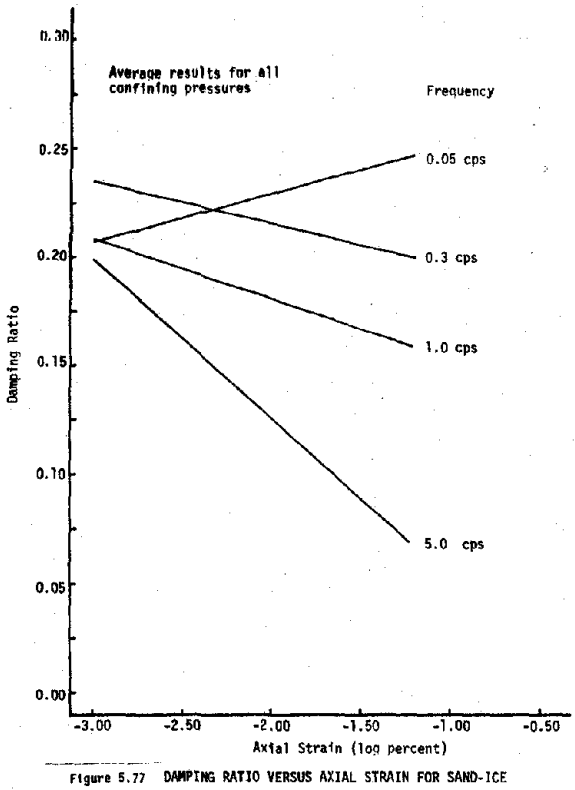

Figure 5.77 DAMPING RATIO VERSUS AXIAL STRAIN FOR SAND-ICE SAMPLES OF 65% SAND CONTENT AT -1°C

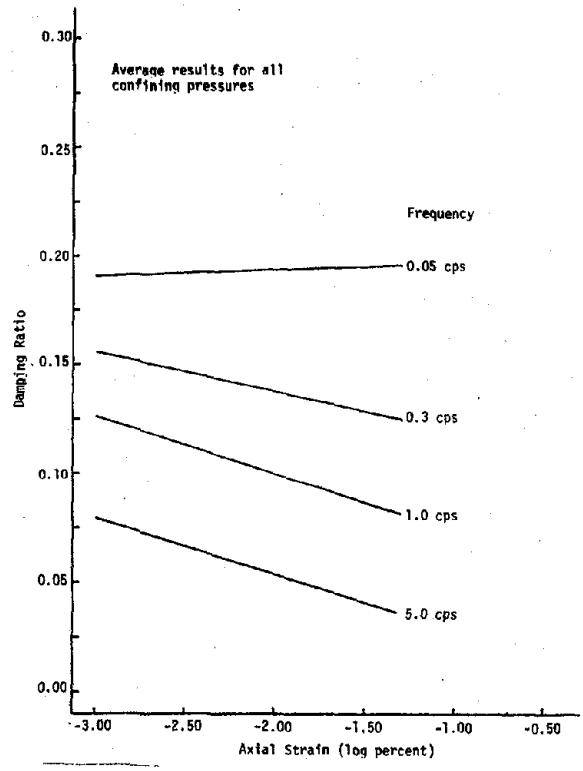

Figure 5.78 DAMPING RATIO VERSUS AXIAL STRAIN FOR SAND-ICE SAMPLES OF 65% SAND CONTENT AT -4°C

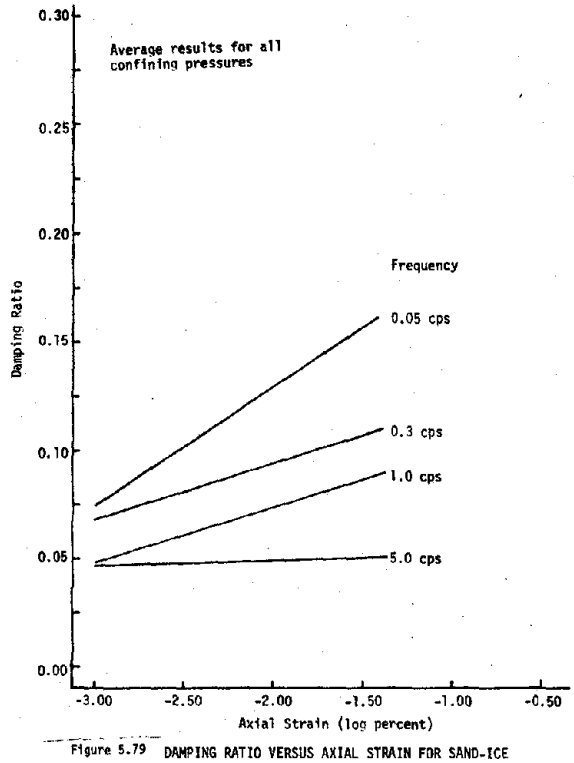

Figure 5.79 DAMPING RATIO VERSUS AXIAL STRAIN FOR SAND-ICE SAMPLES OF 65% SAND CONTENT AT -10°C

results presented in Appendix D at a specified strain amplitude. A strain amplitude of .01% was selected for this purpose. Another strain amplitude could have been selected without significantly changing the conclusions reached in the following paragraphs.

5.4.2 Effect of Confining Pressure

The relationship between damping ratio and confining pressure is shown in Figures 5.80 to 5.88. It is apparent that the relationship is not well-defined. Damping ratio can increase, decrease or remain constant with increasing confining pressure. It should be noted, however, that the change in damping ratio with confining pressure is generally quite small. Over the range of confining pressure from 0 to 200 psi it would appear that the change in damping ratio is less than 0.03 under most test conditions.

5.4.3 Effect of Frequency

The relationship between damping ratio and frequency at an axial strain amplitude of .01% is shown in Figures 5.89 to 5.97. The relationship is shown at three temperatures at a given sand content and confining pressure. Damping ratio decreases with increasing frequency. The rate of decrease appears to be independent of temperature, confining pressure at sand contents of 20 and 45%. At a sand content of 65%, a temperature of $-1^{o}C$, and low confining pressures there may be a slight decrease in the rate.

5.4.4 Effect of Temperature

The relationship between damping ratio and temperature at an axial strain amplitude of .01% is shown in Figures 5.98 to 5.106. The relationship is shown at four frequencies at a given sand content and confining pressure. At frequencies below 1.0 cps damping ratio decreases with descending temperature. The rate of decrease may be slightly less for a low sand content (20%) than high sand contents (45 and 65%). At a frequency of 5.0 cps and between -4 and $-10^{o}C$ the value of damping ratio was found to increase slightly with descending temperature.

5.4.5 Effect of Sand Content

The relationship between damping ratio and sand content at an

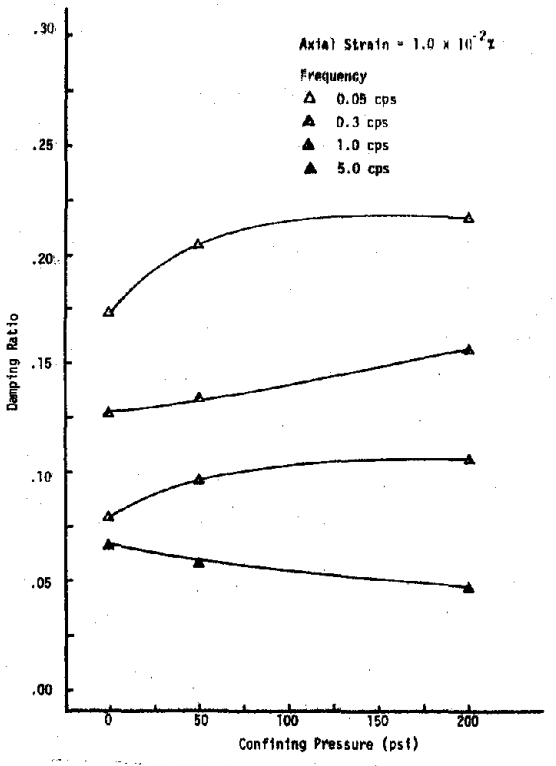

Figure 5.80 DAMPING RATIO VERSUS CONFINING PRESSURE FOR SAND-ICE SAMPLES OF 20% SAND CONTENT AT -1°C

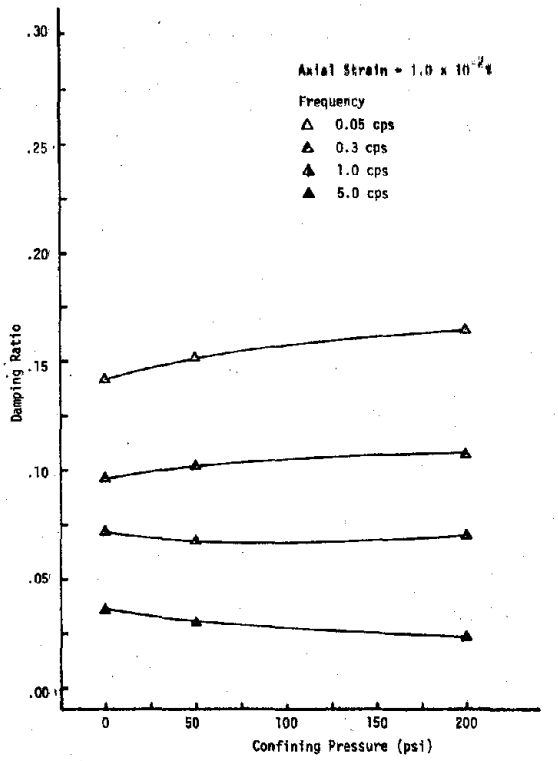

Figure 5.81 DAMPING RATIO VERSUS CONFINING PRESSURE FOR SAND-ICE SAMPLES OF 20% SAND CONTENT AT -4°C

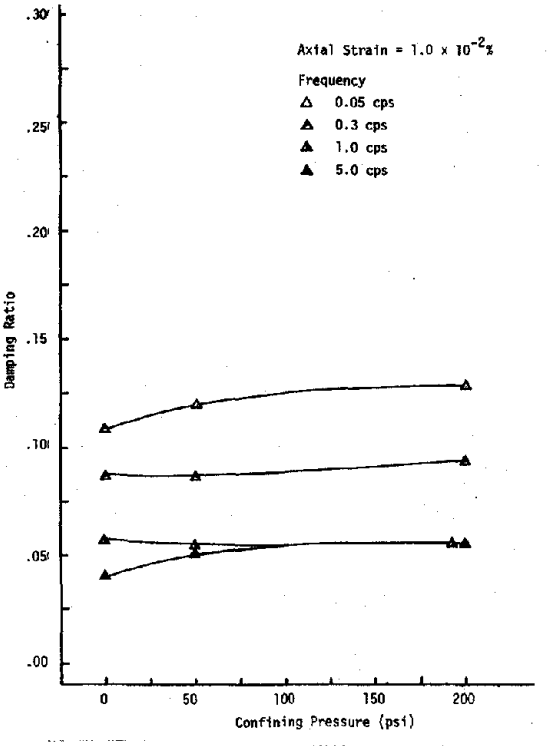

Figure 5.82 DAMPING RATIO VERSUS CONFINING PRESSURE FOR SAND-ICE SAMPLES OF 20% SAND CONTENT AT -10°C

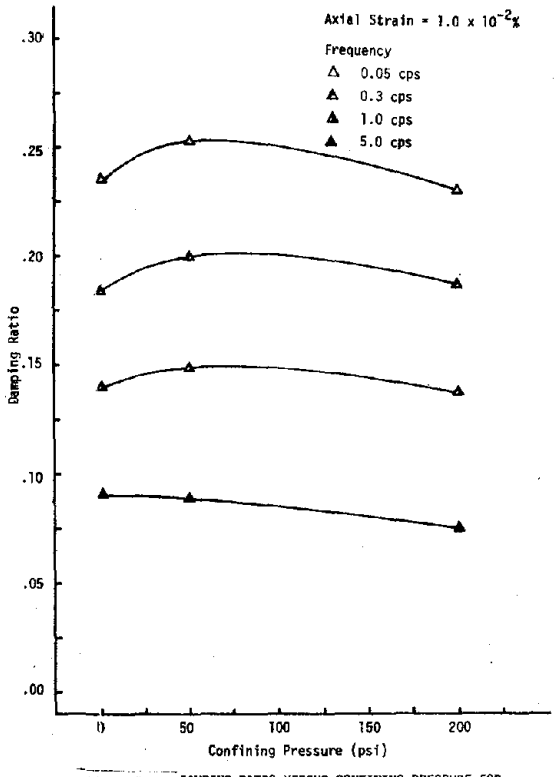

Figure 5.83 DAMPING RATIO VERSUS CONFINING PRESSURE FOR SAND-ICE SAMPLES OF 45% SAND CONTENT AT -1°C

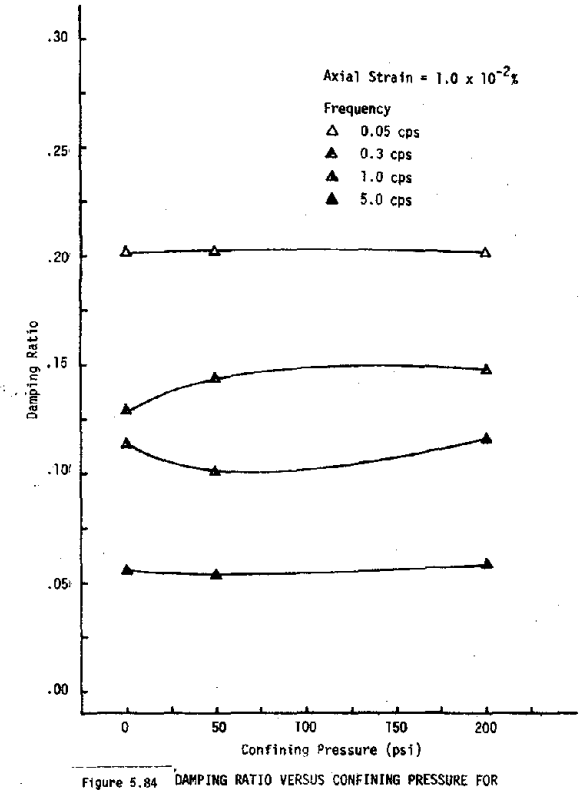

Figure 5.84 DAMPING RATIO VERSUS CONFINING PRESSURE FOR SAND-ICE SAMPLES OF 45% SAND CONTENT AT -4°C

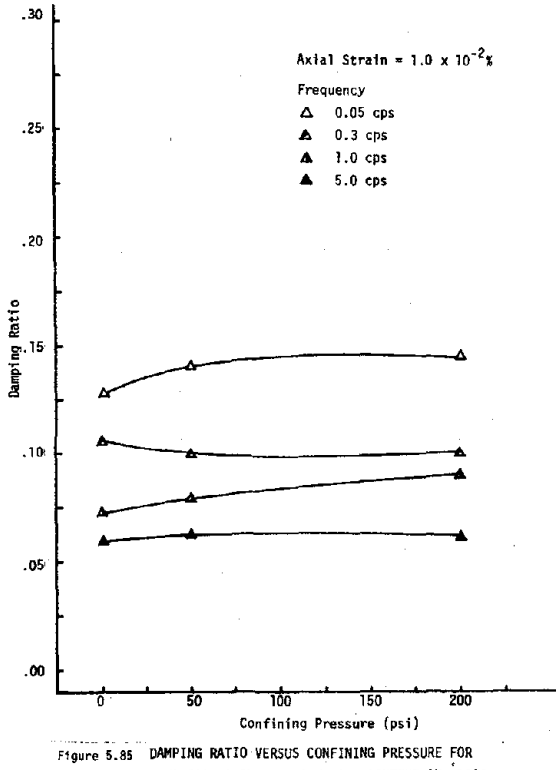

Figure 5.85 DAMPING RATIO VERSUS CONFINING PRESSURE FOR SAND-ICE SAMPLES OF 45% SAND CONTENT AT -10°C

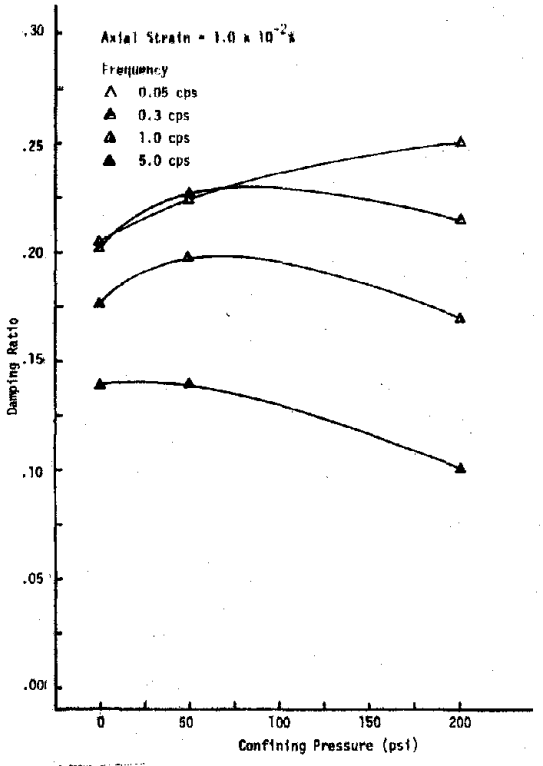

Figure 5.86 DAMPING RATIO VERSUS CONFINING PRESSURE FOR SAND-ICE SAMPLES OF 65% SAND CONTENT AT -1°C

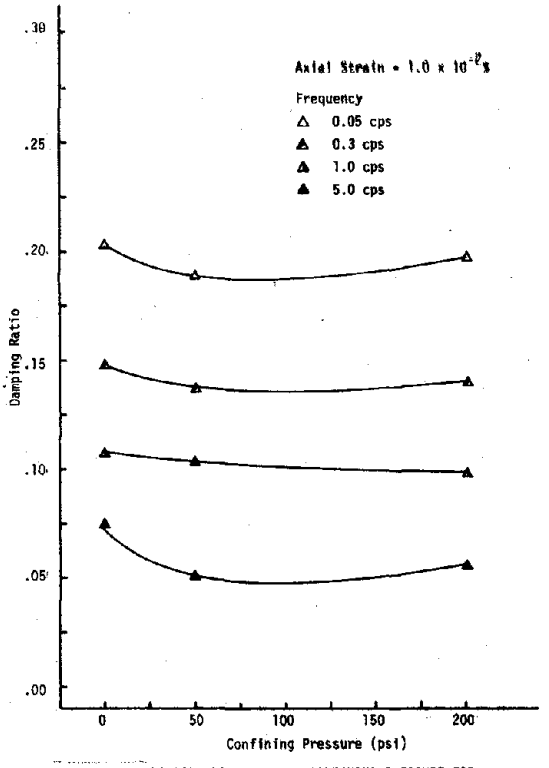

Figure 5.87 DAMPING RATIO VERSUS CONFINING PRESSURE FOR SAND-ICE SAMPLES OF 65% SAND CONTENT AT -4°C

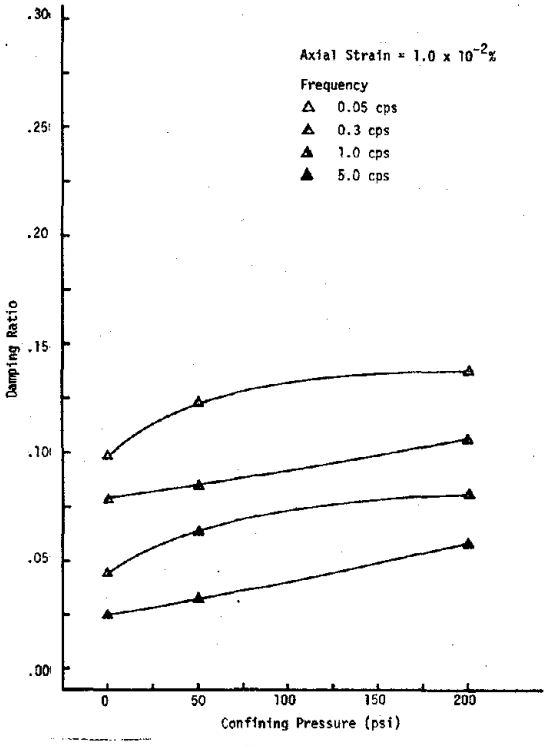

Figure 5.88 DAMPING RATIO VERSUS CONFINING PRESSURE FOR SAND-ICE SAMPLES OF 65% SAND CONTENT AT -10°C

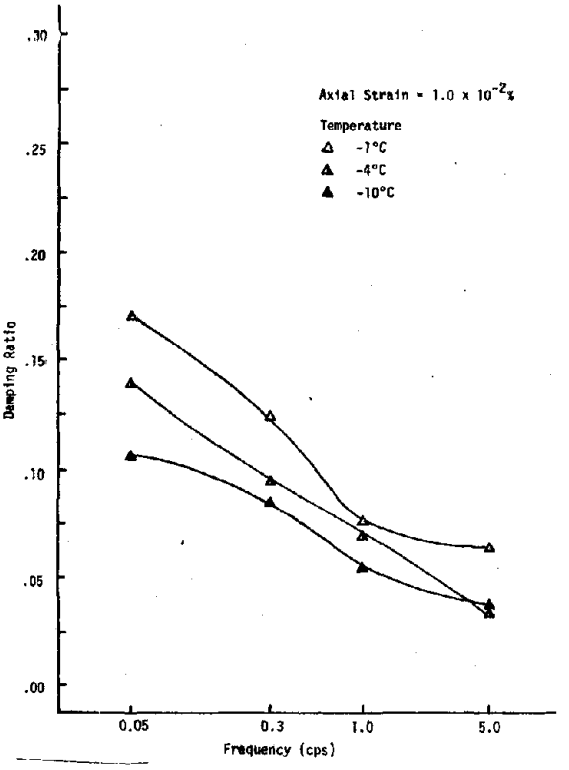

Figure 5.89 DAMPING RATIO VERSUS FREQUENCY FOR SAND-ICE SAMPLES OF 20% SAND CONTENT AT 0 psi CONFINING PRESSURE

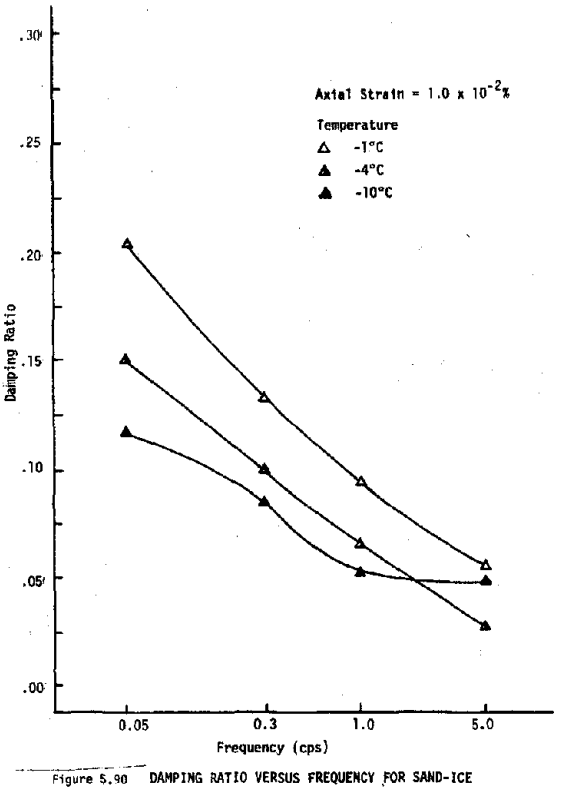

Figure 5.90 DAMPING RATIO VERSUS FREQUENCY FOR SAND-ICE SAMPLES OF 20% SAND CONTENT AT 50 psi CONFINING PRESSURE

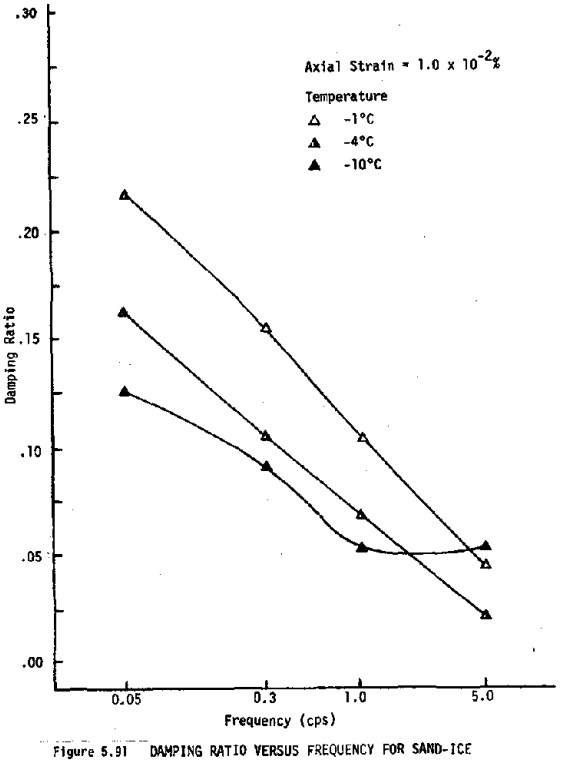

Figure 5.91 DAMPING RATIO VERSUS FREQUENCY FOR SAND-ICE SAMPLES OF 20% SAND CONTENT AT 200 psi CONFINING PRESSURE

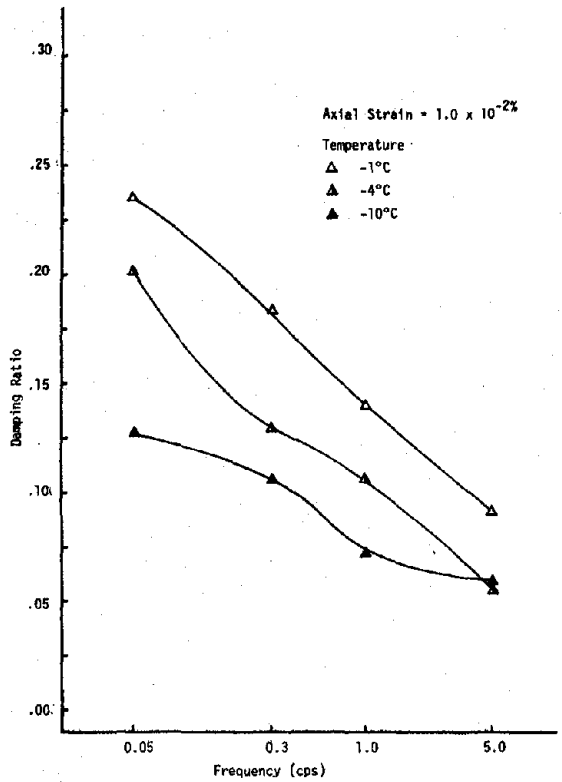

Figure 5.92 DAMPING RATIO VERSUS FREQUENCY FOR SAND-ICE SAMPLES OF 45% SAND CONTENT AT 0 psi CONFINING PRESSURE

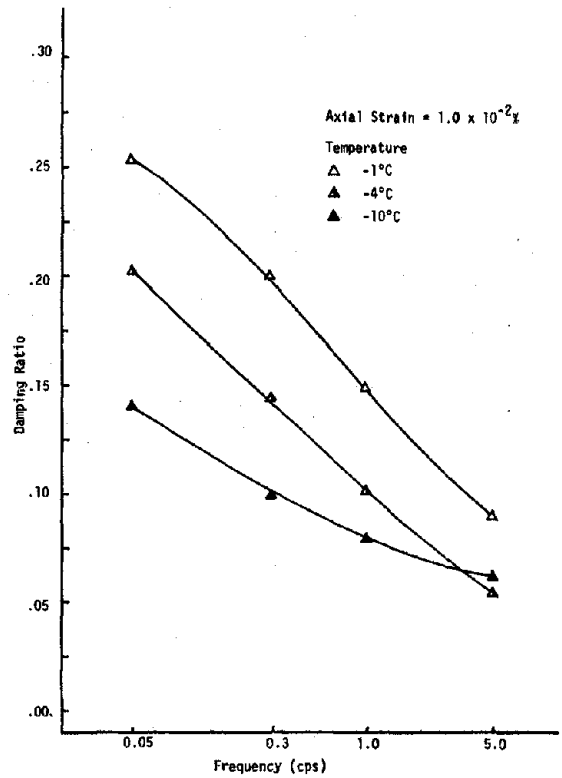

Figure 5.93 DAMPING RATIO VERSUS FREQUENCY FOR SAND-ICE SAMPLES OF 45% SAND CONTENT AT 50 psi CONFINING PRESSURE

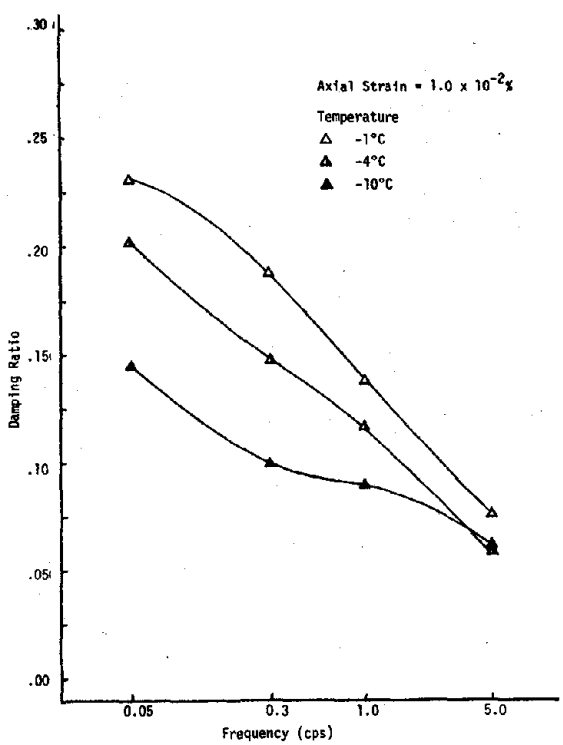

Figure 5.94 DAMPING RATIO VERSUS FREQUENCY FOR SAND-ICE SAMPLES OF 45% SAND CONTENT AT 200 psi CONFINING PRESSURE

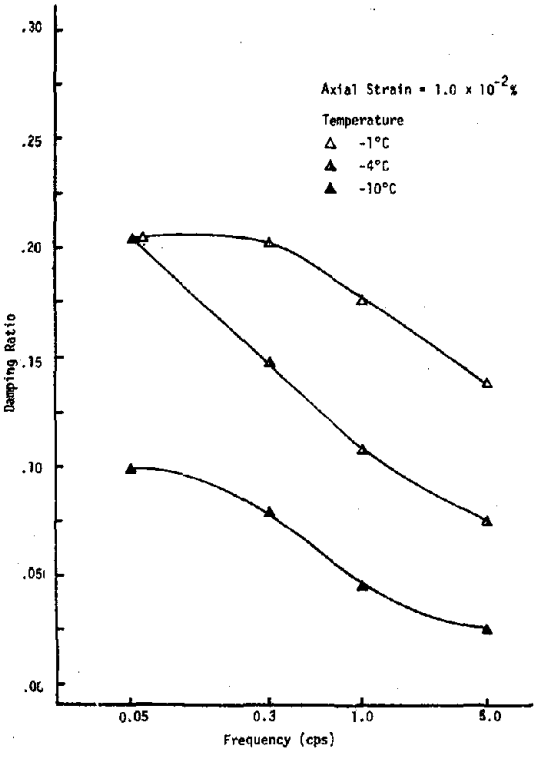

Figure 5.95 DAMPING RATIO VERSUS FREQUENCY FOR SAND-ICE SAMPLES OF 65% SAND CONTENT AT 0 psi CONFINING PRESSURE

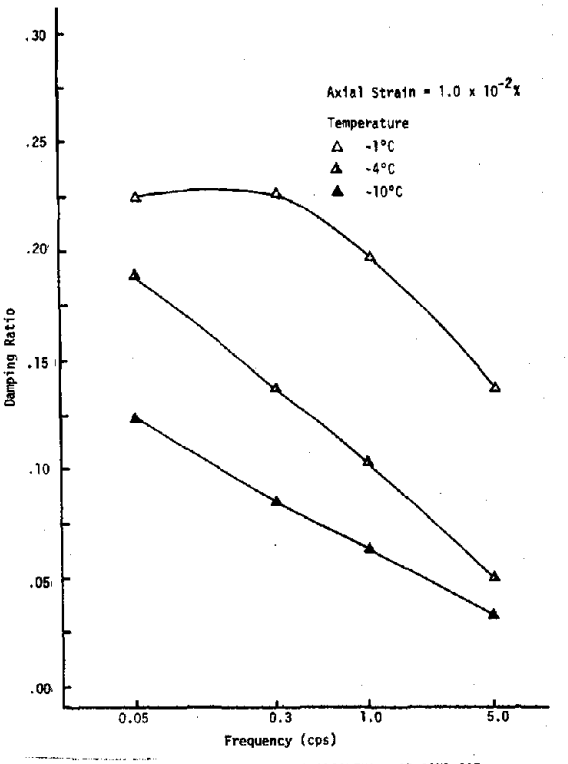

Figure 5.96 DAMPING RATIO VERSUS FREQUENCY FOR SAND-ICE SAMPLES OF 65% SAND CONTENT AT 50 psi CONFINING PRESSURE

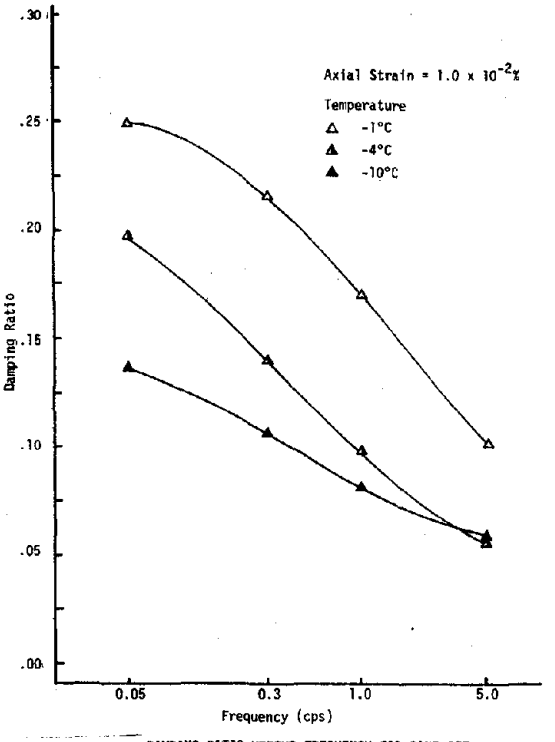

Figure 5.97 DAMPING RATIO VERSUS FREQUENCY FOR SAND-ICE SAMPLES OF 65% SAND CONTENT AT 200 psi CONFINING PRESSURE

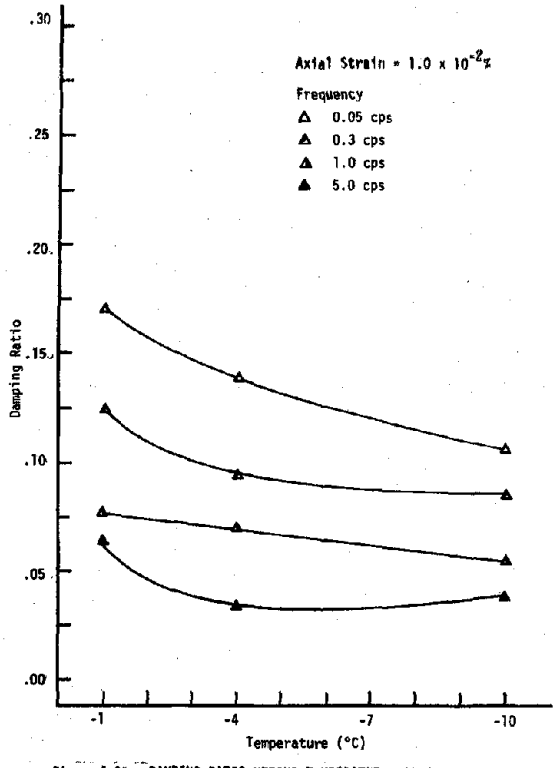

Figure 5.98 DAMPING RATIO VERSUS TEMPERATURE FOR SAND-ICE SAMPLES OF 20% SAND CONTENT AT 0 psi CONFINING PRESSURE

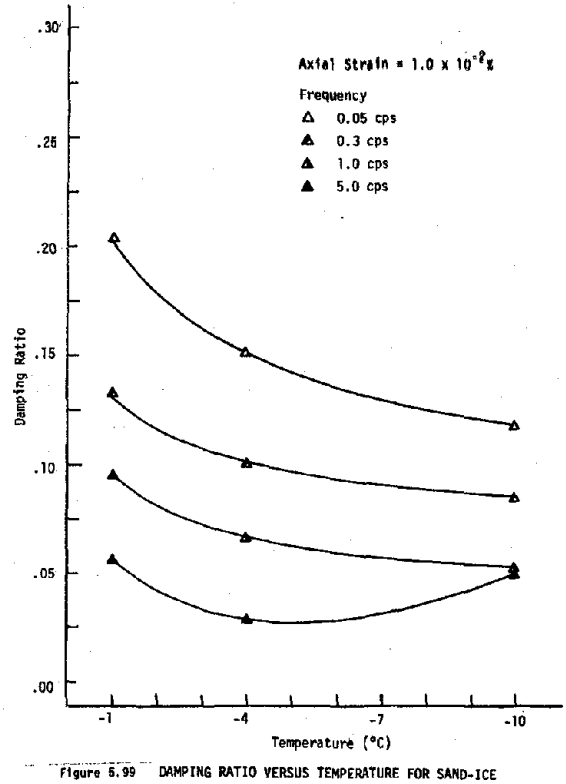

Figure 5.99 DAMPING RATIO VERSUS TEMPERATURE FOR SAND-ICE SAMPLES OF 20% SAND CONTENT AT 50 psi CONFINING PRESSURE

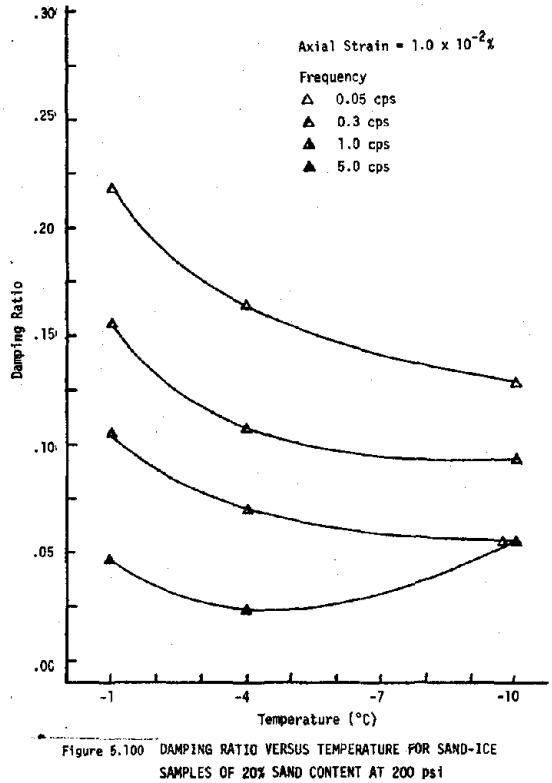

Figure 5.100 DAMPING RATIO VERSUS TEMPERATURE FOR SAND-ICE SAMPLES OF 20% SAND CONTENT AT 200 psi CONFINING PRESSURE

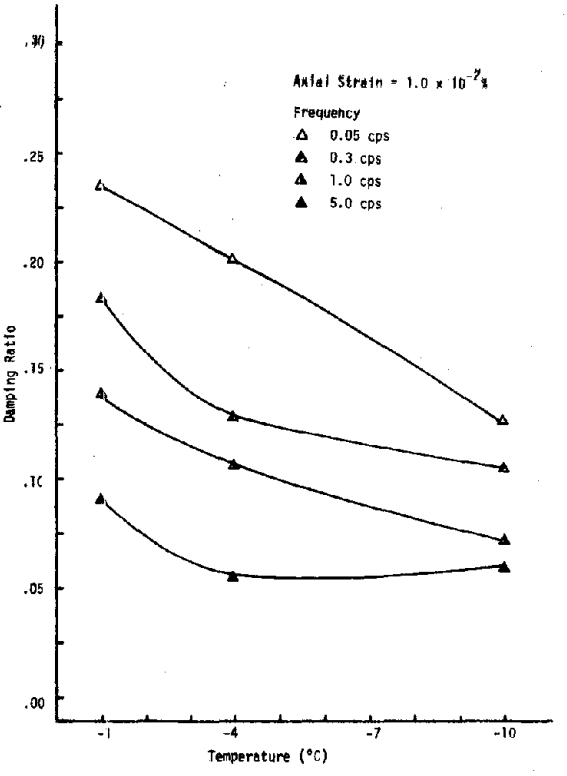

Figure 5.101 DAMPING RATIO VERSUS FREQUENCY FOR SAND-ICE SAMPLES OF 45% SAND CONTENT AT 0 psi CONFINING PRESSURE

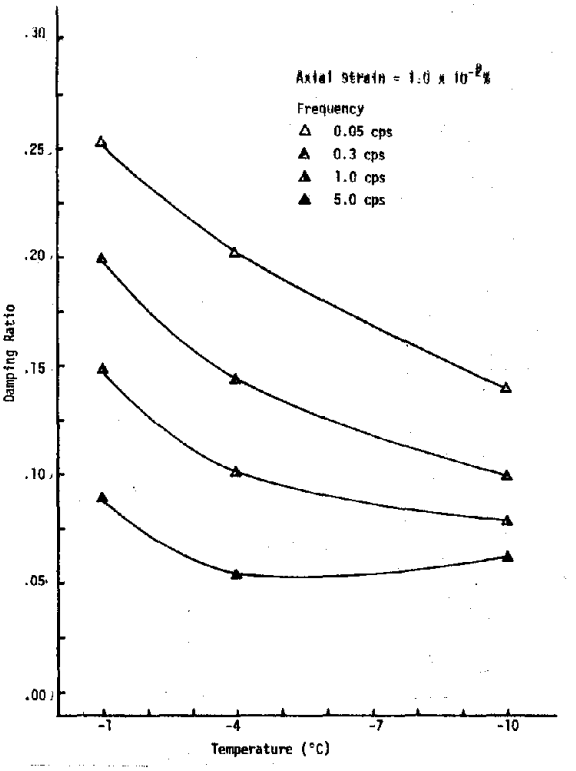

Figure 5.102 DAMPING RATIO VERSUS TEMPERATURE FOR SAND-ICE SAMPLES OF 45% SAND CONTENT AT 50 psi CONFINING PRESSURE

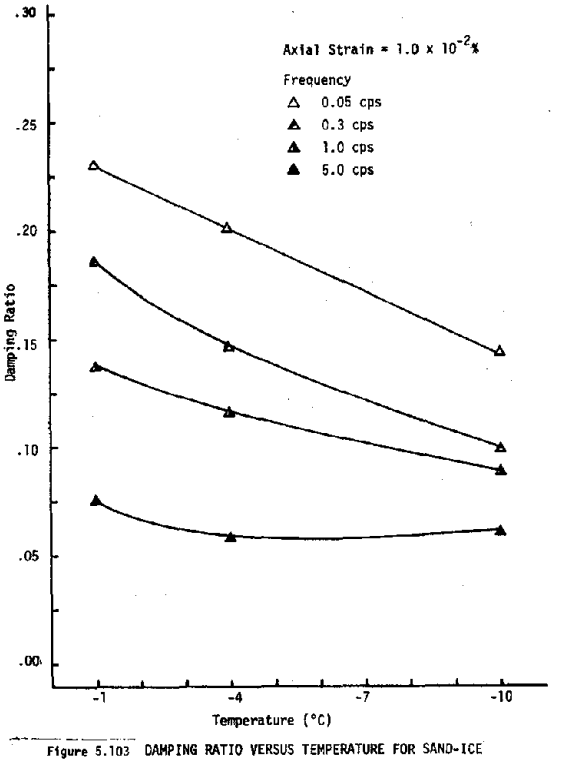

Figure 5.103 DAMPING RATIO VERSUS TEMPERATURE FOR SAND-ICE SAMPLES OF 45% SAND CONTENT AT 200 psi CONFINING PRESSURE

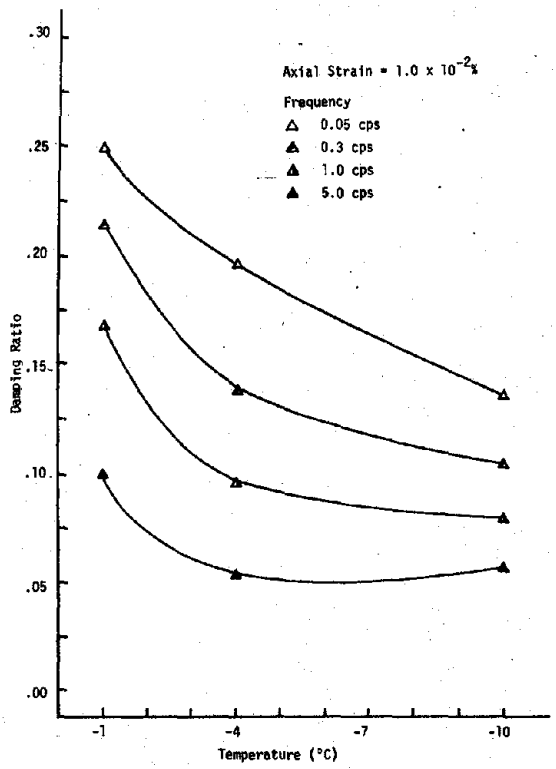

Figure 5.104 DAMPING RATIO VERSUS TEMPERATURE FOR SAND-ICE SAMPLES OF 65% SAND CONTENT AT 0 psi CONFINING PRESSURE

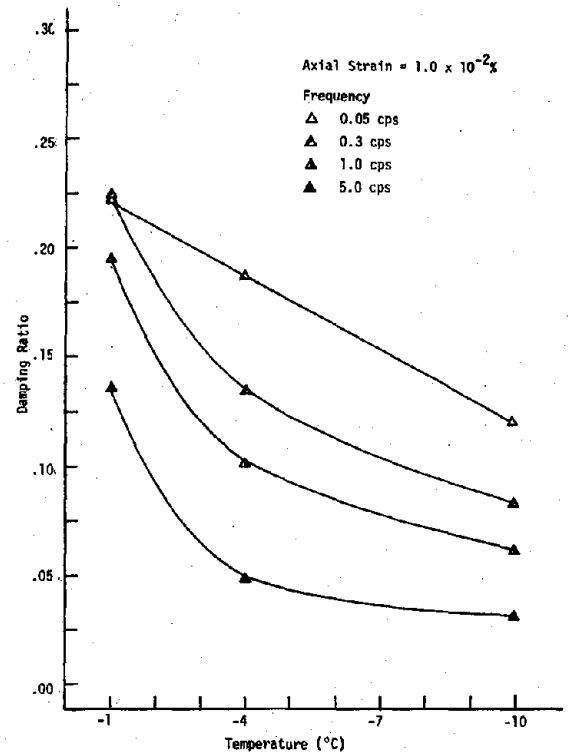

Figure 5.105 DAMPING RATIO VERSUS TEMPERATURE FOR SAND-ICE SAMPLES OF 65% SAND CONTENT AT 50 psi CONFINING PRESSURE

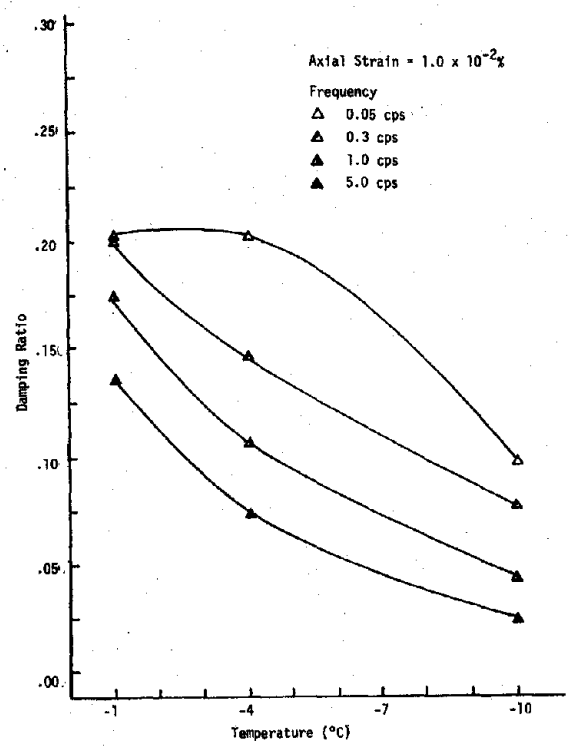

Figure 5.106 DAMPING RATIO VERSUS TEMPERATURE FOR SAND-ICE SAMPLES OF 65% SAND CONTENT AT 200 psi CONFINING PRESSURE

axial strain amplitude of .01% is shown in Figures 5.107 to 5.109. The relationship is shown at four frequencies at a given temperature. The relationship is based upon the average results for all confining pressures shown in Figures 5.71 to 5.79. Damping ratio increases with increasing sand content up to 45% sand content. Damping ratio appears to decrease slightly with an increase in sand content from 45 to 65% for -4 and -10°C. The change in damping ratio with sand content decreases as the test temperature descends from -1 to -10°C.

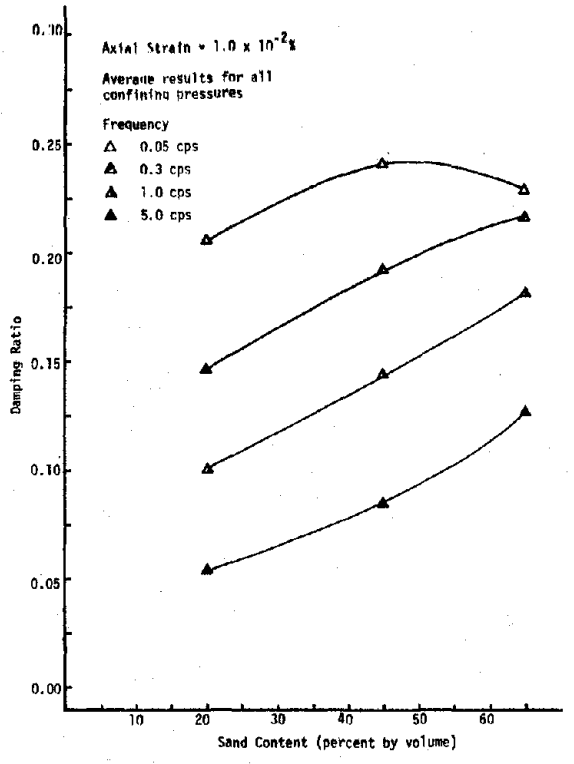

Figure 5.107 DAMPING RATIO VERSUS SAND CONTENT FOR SAND-ICE SAMPLES AT -1°C

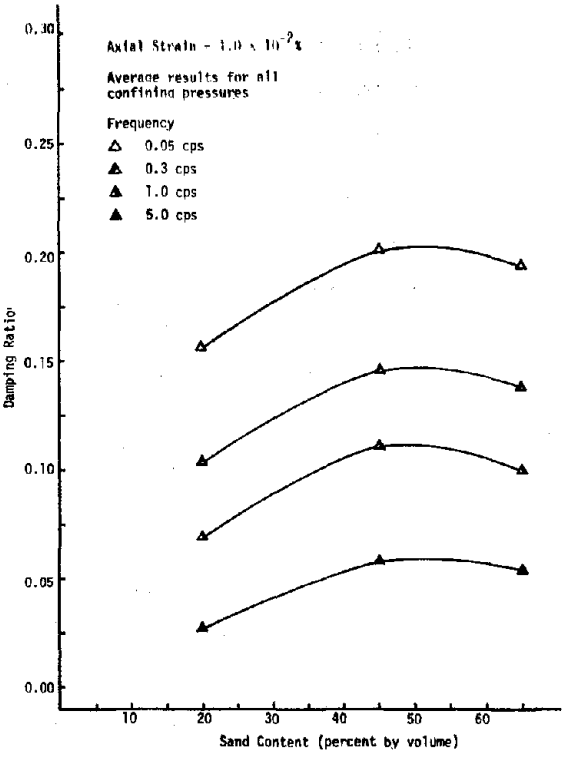

Figure 5.108 DAMPING RATIO VERSUS SAND CONTENT FOR SAND-ICE SAMPLES AT -4°C

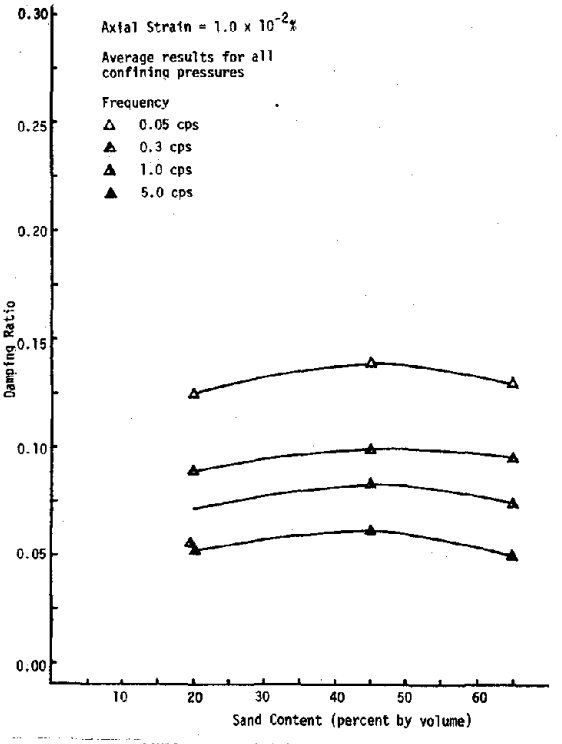

Figure 5.109 DAMPING RATIO VERSUS SAND CONTENT FOR SAND-ICE SAMPLES AT -10°C

CHAPTER 6

COMPARISONS OF DYNAMIC PROPERTIES OF FROZEN COHESIONLESS SOILS

6.1 General

This chapter presents a comparison of the dynamic properties of frozen silt and sand obtained in the present study with the results obtained in previous studies. To allow a direct comparison to be made, the dynamic properties obtained in all of the studies were converted to common units. Thus, dynamic elastic properties are presented in terms of compressional or longitudinal wave velocities and damping properties are presented in terms of damping ratios. Values of dynamic Young's modulus obtained in the present study were converted to longitudinal wave velocities using:

$$V_L = \sqrt{\frac{E_d}{\rho}} \qquad (6.1)$$

in which,

V_L = longitudinal wave velocity,

E_d = dynamic Young's modulus,

ρ = material density.

Results of field investigations are presented in terms of compressional wave velocities, which are related to longitudinal wave velocities as follows:

$$V_P = V_L \sqrt{\frac{(1 - \mu)}{(1 + \mu)(1 - 2\mu)}} \qquad (6.2)$$

in which,

V_P = compressional wave velocity

μ = Poisson's ratio.

Values of damping ratio were calculated from loss factors determined in previous studies using:

$$D = \sin \frac{\delta}{2} \qquad (6.3)$$

in which,

D = damping ratio

δ = phase lag.

6.2 Comparison of Dynamic Properties of Frozen Cohesionless Soils

6.2.1 Longitudinal and Compression Wave Velocity

The relationship between longitudinal or compressional wave velocity and temperature obtained in the present study and in previous studies is summarized in Figure 6.1 for frozen silt and Figure 6.2 for frozen sand. In general, there is fairly good agreement among the basic wave velocity-temperature relationships obtained in the several studies. The variation in the magnitude of the wave velocities may be attributed to differences in testing techniques and material characteristics and may be summarized as follows:

(1) Frequency - the range of frequencies associated with the present study using cyclic triaxial equipment (0.05 to 5.0 Hz) is significantly less than the frequencies associated with the testing techniques used in the previous studies (resonant frequency, approximately 1 to 10 kHz; seismic, approximately 150 Hz; ultrasonic, approximately 50 to 1000 kHz). It was shown in the present study that dynamic Young's modulus of frozen silt and Ottawa sand increases with increasing frequency between 0.05 and 5.0 cps. Stevens (1973; see Figure 2.7) found that dynamic shear modulus increases with increasing frequency from 1 to 1000 kHz. Based on these results it appears that dynamic elastic properties increase with increasing frequency over a considerable range of frequencies. Therefore, the longitudinal wave velocities obtained in the present study at low frequencies should be lower than those obtained in previous studies at much higher frequencies.

(2) Strain amplitude - the strain amplitudes associated with the cyclic traixial method (approximately 10^{-2}%) are greater than the strain amplitudes associated with the other methods (resonant frequency, approximately 10^{-6} to 10^{-3}%; ultrasonic and seismic methods, approximately 10^{-7} to 10^{-4}%). It was found in the present study that the dynamic Young's modulus of frozen silt and Ottawa sand decreases with increasing strain amplitude over the entire range of strain amplitudes in the testing program. For strain amplitudes less than 10^{-3}% it is felt that

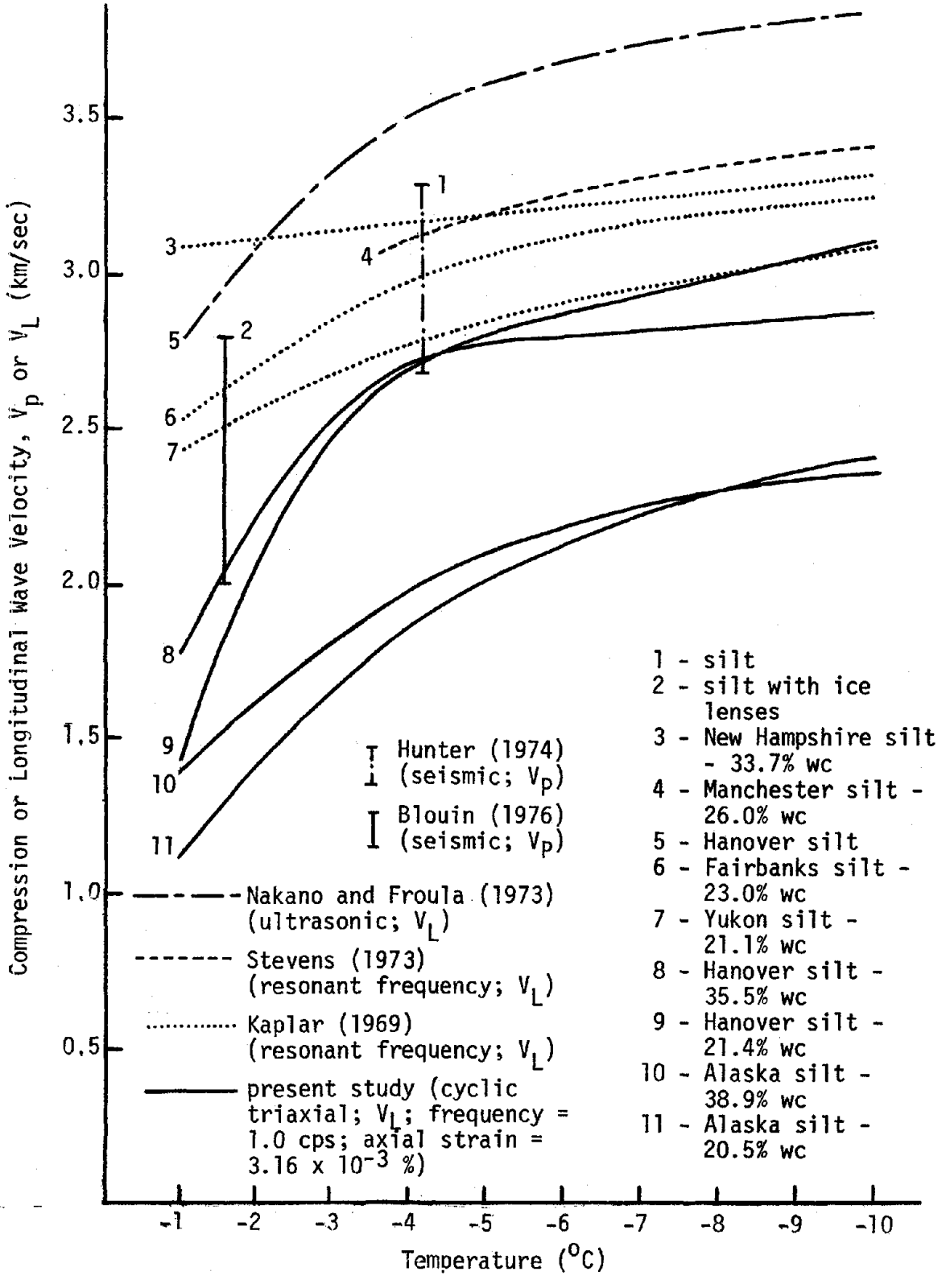

Figure 6.1 WAVE VELOCITY VERSUS TEMPERATURE OF FROZEN SILT

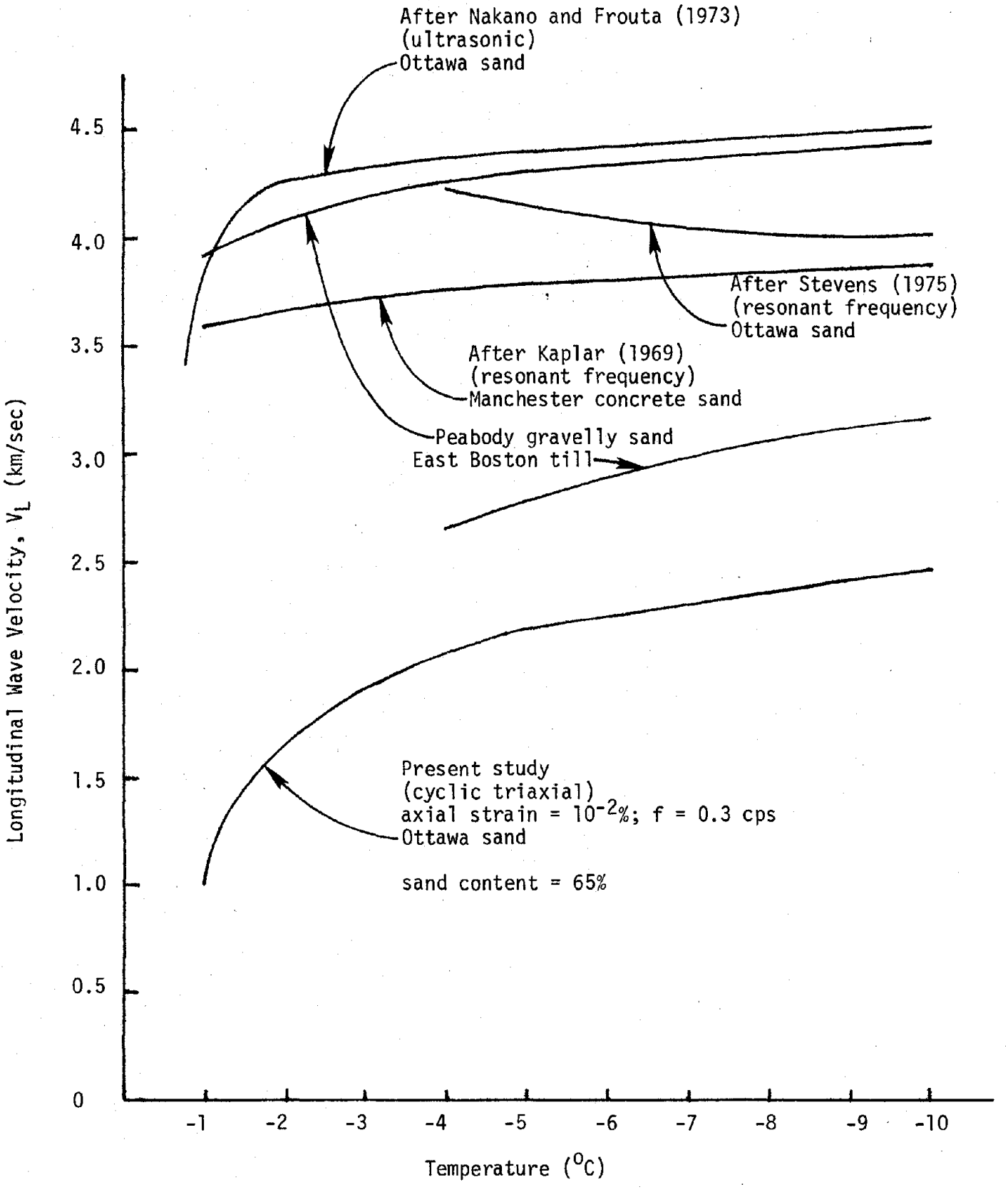

Figure 6.2 WAVE VELOCITY VERSUS TEMPERATURE OF FROZEN SAND

there is no change in dynamic elastic properties with strain amplitude. Since the results shown in Figure 6.1 for the present study are at strain amplitude of 3.16×10^{-3} the difference in the wave velocity associated with differences in the strain amplitudes of testing should be negligible. The results shown in Figure 6.2 for the present study are at a strain amplitude of 10^{-2}%. Therefore, the wave velocities obtained in previous studies should be slightly higher than those obtained in the present study.

(3) Material characteristics - in general, the wave-velocity-temperature relationships from the several studies shown in Figure 6.1 are associated with frozen silts over a relatively narrow range of water contents. It was found in the present study that water content did not influence the longitudinal wave velocities of Hanover and Alaska silt appreciably, at least over the range of water contents investigated in the study. It is, therefore, not likely that the differences in wave velocities among the several laboratory studies are due to the relatively small differences in water contents. On the other hand, it appears that the wave velocity can be influenced to a larger extent by the nature of the silt itself, such as the grain size characteristics. In the present study, for example, the lower longitudinal wave velocity for the Alaska silt compared to the Hanover silt may be a function of the finer grain size of the Alaska silt.

The Ottawa sand used in the present study is the same as that used in previous studies. The results from the present study shown in Figure 6.2 are for a sand content of 65%. This corresponds to a void ratio of 0.49. The void ratio of the Ottawa sand tested by Nakano (1973) was 0.38 while that tested by Stevens (1973) was 0.54 (average). The results from the present study indicate the dynamic elastic properties of Ottawa sand increase with decreasing void ratio (increasing sand content) at a temperature of $-4^{o}C$ (see Figure 5.66). Therefore, based on void ratio, the wave velocities obtained by Nakano should be higher than those obtained in the present study while those obtained by Stevens should be lower.

Kaplar (1969) has found dynamic Young's modulus increases with increasing D_{50} particle size. The D_{50} particle size for the Peabody gravelly sand, McNamara concrete sand, and East Boston till is greater than the D_{50} particle size of the Ottawa sand. Therefore, based on the particle size influence, the wave velocities obtained by Kaplar should be greater than those obtained in the present study. (Note: the wave velocities obtained by Kaplar should also be greater than those obtained by Nakano and Stevens; however, as can be seen in Figure 6.2, they are not. The explanation for the difference in wave velocities between these studies is not obvious).

The void ratios of the Peabody gravelly sand (0.48) and McNamara concrete sand (0.48) are close to the void ratio of the Ottawa sand (0.49) of the present study. The void ratio of the East Boston till (0.34) is lower than that of the Ottawa sand. Therefore, the wave velocity for the East Boston till should be greater than that of the Ottawa sand based on the difference in void ratio.

Overall, the wave velocities obtained in the present study appear to be in good agreement with the wave velocities obtained in the previous studies.

6.2.2 Damping Ratio

The relationship between damping ratio and temperature obtained in the present study and in a previous study by Stevens (1973) is summarized in Figure 6.3 for frozen silt and Figure 6.4 for frozen Ottawa sand. The values of damping ratio obtained by Stevens (1973) are lower than the values obtained in the present study. This difference may be attributed to differences in the testing techniques in the two studies and may be summarized as follows:

(1) Frequency - the frequency associated with Stevens' (1973) resonant frequency test is much greater than that associated with the present study. It was shown in the present study that the damping ratio of frozen silt and Ottawa sand decreases with increasing frequency between 0.05 and 5.0 cps. Since the damping ratio is smaller at high frequencies than at low frequencies, the values of damping ratio obtained in the present

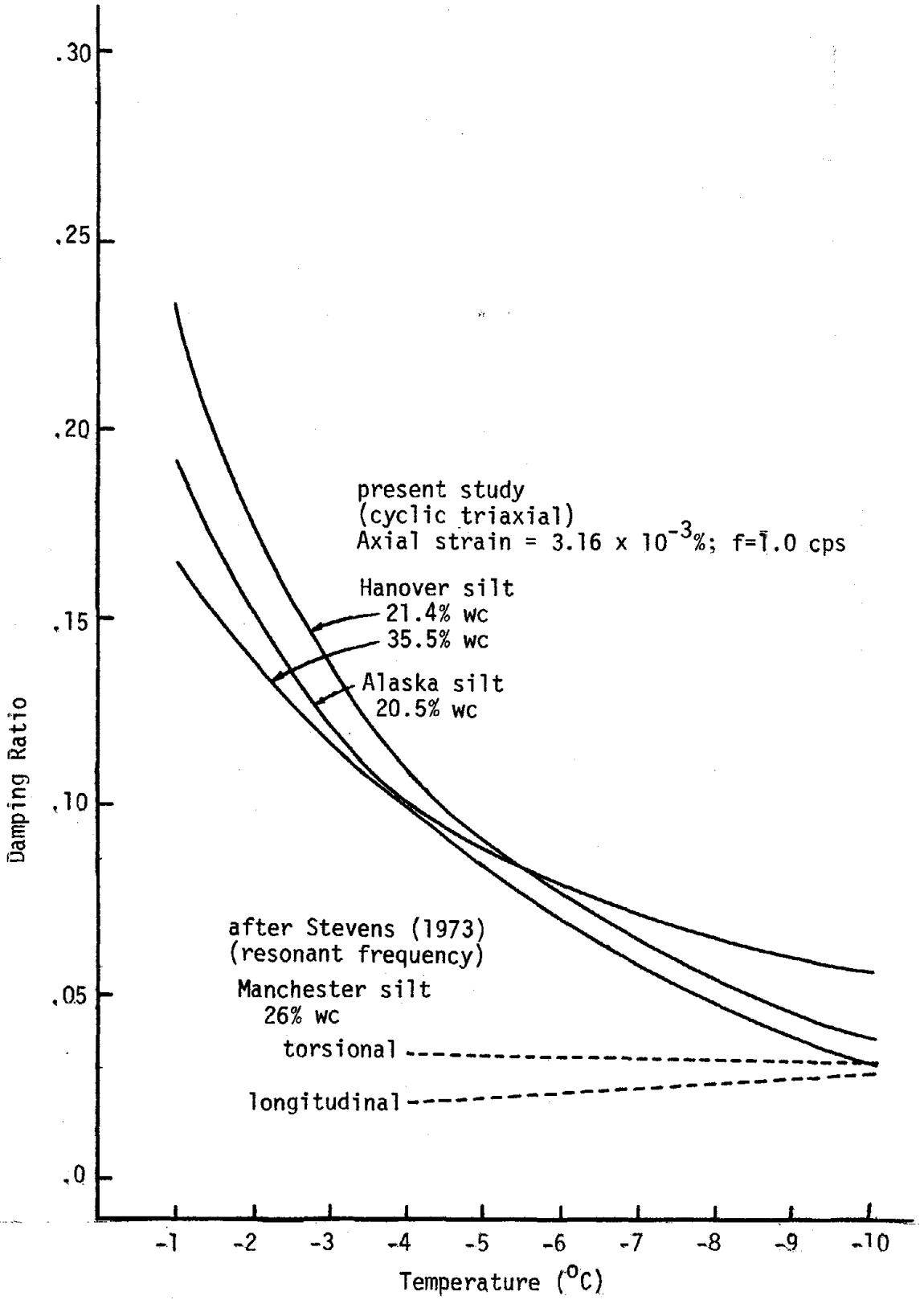

Figure 6.3 DAMPING RATIO VERSUS TEMPERATURE OF FROZEN SILT

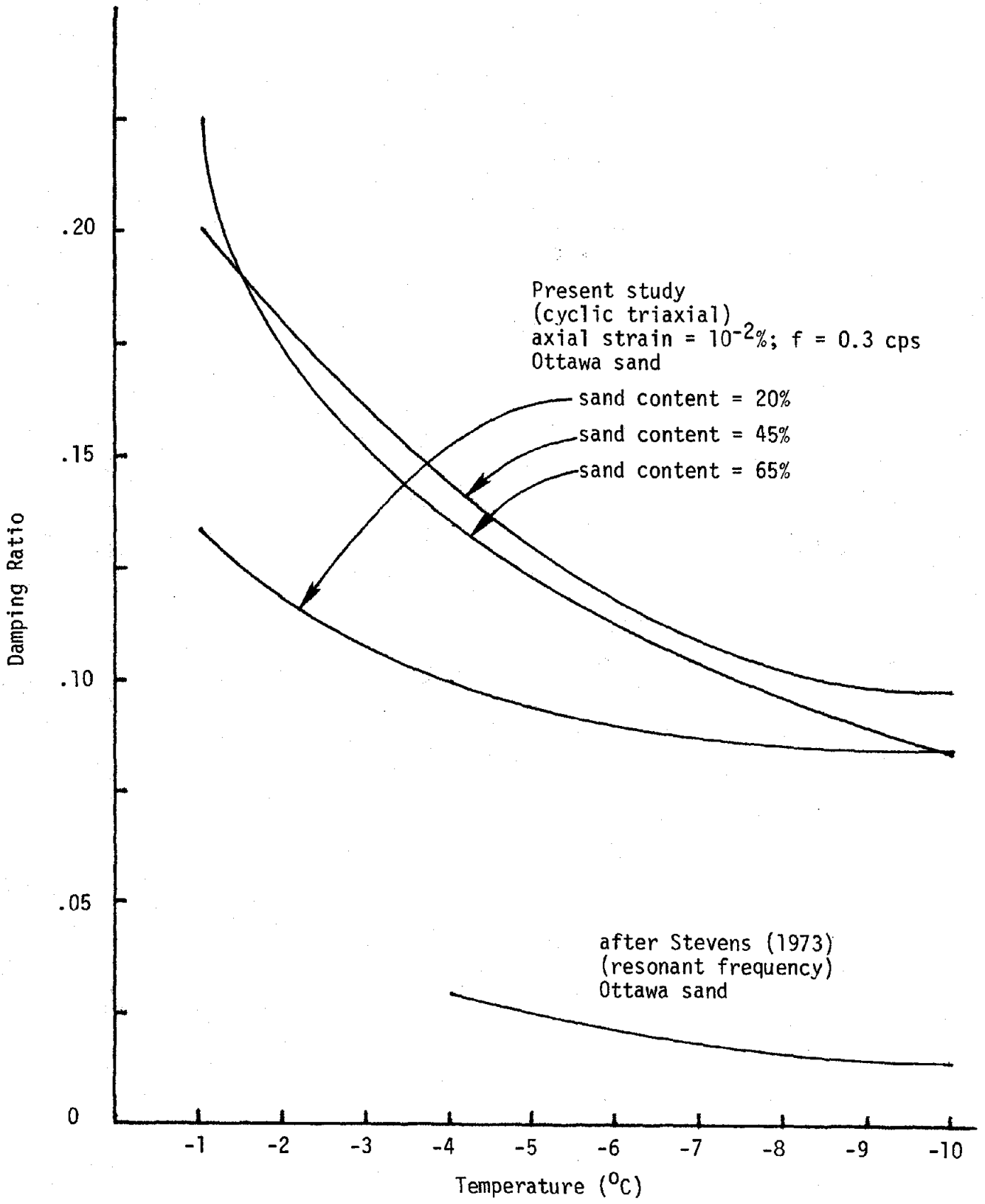

Figure 6.4 DAMPING RATIO VERSUS TEMPERATURE OF FROZEN SAND

study should be higher than those obtained by Stevens (1973).

(2) Strain amplitude - the strain amplitudes associated with the present study are greater than the strain amplitudes associated with the resonant frequency method. It was shown in the present study that the damping ratio of frozen silt increases with increasing axial strain amplitude between approximately 2×10^{-3} and 8×12^{-2}%. Since the damping ratio of frozen silt is lower at low strain amplitude than at high strain amplitudes, the values of damping ratio obtained in the present study should be greater than those obtained by Stevens (1973).

The relationship between damping ratio and axial strain amplitude for Ottawa sand was not well defined based on the results of the present study. Therefore, an explanation of the relative position of the results shown in Figure 6.4 on this basis is not possible at this time.

Overall, it is felt that the comparison between the damping ratios obtained in the present study and by Stevens (1973) is reasonable.

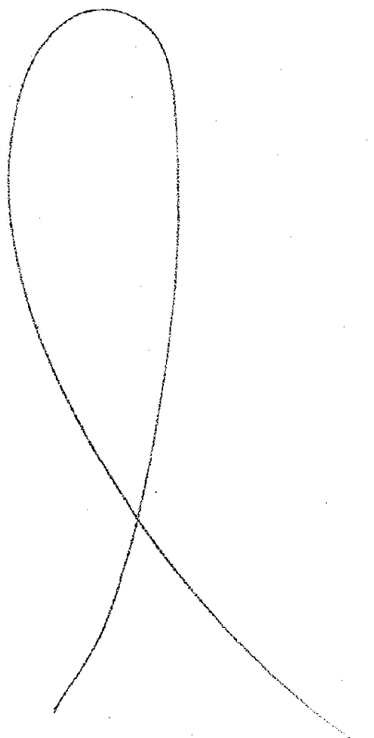

CHAPTER 7
SUMMARY AND CONCLUSIONS

Cyclic triaxial tests were performed on laboratory prepared samples of frozen silt and sand and dynamic Young's moduli and damping ratios were determined. The test results may be summarized as follows:

(1) Values of dynamic Young's modulus of frozen silt for the range of test strain amplitudes (approximately 2×10^{-3} to 8×10^{-2}%), frequencies (0.05 to 10.0 cps), temperatures (-1 to -10°C), confining pressure (0 to 200 psi), and sample water contents (21.4 and 35.5% for Hanover silt and 20.5, 29.2 and 38.9% for Alaska silt) ranged from 1×10^5 to 35×10^5 psi for Hanover silt and 1×10^5 to 22×10^5 psi for Alaska silt. Values of damping ratio ranged from .02 to .36 for Hanover silt and .02 to .32 for Alaska silt.

(2) The influence of the various parameters on the dynamic Young's modulus of frozen silt in the order of their importance is as follows:

   a. Strain amplitude - the dynamic Young's modulus of frozen silt decreases as the axial strain amplitude increases, with a more pronounced effect at low temperature (-4 and -10°C) than at high temperatures (-1°C). The relationship between dynamic Young's modulus and strain amplitude appears to be independent of frequency and water content.

   b. Temperature - the dynamic Young's modulus increases significantly with descending temperature. At a low strain amplitude (3.16×10^{-3}%) the rate of increase is generally greater at higher temperatures (-1 to -4°C) than at lower temperatures (-4 to -10°C); at a high strain amplitude (3.16×10^{-2}%), the rate of increase is more uniform over the entire temperature range. The rate of increase of dynamic Young's modulus with decreasing temperature is generally more uniform over the entire range of temperatures (-1 to -10°C) at low frequencies than at high frequencies.

c. Frequency - dynamic Young's modulus increases with increasing frequency. The rate of increase is slightly greater at very low and very high frequencies than at intermediate frequencies. At a high strain amplitude ($3.16 \times 10^{-2}\%$) the relationship between dynamic Young's modulus and frequency appears to be independent of water content and temperature . At a low strain amplitude ($3.16 \times 10^{-3}\%$) the rate of increase of dynamic Young's modulus with frequency is somewhat greater at -4°C than at -1 and -10°C.

d. Water content - dynamic Young's modulus increases by a moderate amount as the water content increases at a high temperature (-1°C); this relationship does not appear to be affected by frequency. At lower temperatures (-4 and -10°C) there appears to be little or no significant influence of water content on dynamic Young's modulus at a high strain amplitude ($3.16 \times 10^{-2}\%$). At a lower strain amplitude ($3.16 \times 10^{-3}\%$) the relationship between dynamic Young's modulus and water content is not clear. In the case of Hanover silt, dynamic Young's modulus decreases by a small amount as the water content increases at both -4 and -10°C; in the case of Alaska silt, dynamic Young's modulus appears to increase by a small amount at -4°C and decrease by a small amount at -10°C as the water content increases.

e. Confining pressure - the dynamic Young's modulus does not appear to be influenced by confining pressure under any test conditions.

(3) The influence of the various parameters on the damping ratio of frozen silt in the order of their importance is as follows:

a. Strain amplitude - in general, the damping ratio increases as strain amplitude increases. At a high temperature (-1°C) the rate of increase is moderate at low frequencies and somewhat greater at higher frequencies for low water contents; for higher water contents the rate of increase is moderate at all frequencies. At lower temperatures (-4 to -10°C) damping

increases significantly with increasing strain amplitude at low frequencies. At high frequencies the damping ratio increases by a smaller amount and in some cases decreases by a small amount with increasing strain amplitude; in some instances the relationship becomes U-shaped, with a slight decrease in damping followed by an increase with increasing strain amplitude.

b. Temperature - damping ratio generally decreases with decreasing temperature. The influence of temperature on damping ratio appears to be more significant at low water contents than at high water contents. At a low strain amplitude (3.16×10^{-3}%) at low water contents the rate of decrease of damping ratio is generally greater in the high temperature range (-1 to -4°C) than in the low temperature range (-4 to -10°C); at high water contents the rate of decrease appears to be more uniform over the entire temperature range (-1 to -10°C). At a high strain amplitude (3.16×10^{-2}%) the rate of decrease in damping ratio with decreasing temperature is generally somewhat less than at a low strain amplitude (3.16×10^{-3}%). In many cases, there appears to be either little change or a slight increase in damping ratio from -1 to -4°C followed by a gradual decrease from -4 to -10°C.

c. Frequency - damping ratio generally decreases with increasing frequency. At a high strain amplitude (3.16×10^{-2}%) at all temperatures and at a low strain amplitude (3.16×10^{-3}%) at a high temperature (-1°C) the damping ratio generally decreases by a smaller amount in the frequency range 0.05 to 5.0 cps than in the frequency range 5.0 to 10.0 cps. At a low strain amplitude (3.16×10^{-3}%) at a temperature of -4°C, the damping ratio decreases with increasing frequency at a rate somewhat more uniform than at -1°C. At a low temperature (-10°C) at a low strain amplitude (3.16×10^{-3}%) the damping ratio generally decreases by a small amount with increasing frequency at low frequencies (0.04 to 5.0 cps) and increases with increasing frequency at higher frequencies (5.0 to 10.0 cps).

d. Water content - damping ratio decreases significantly with increasing water content at a high temperature (-1°C); the relationship does not seem to be significantly affected by strain amplitude. It appears that at low frequencies most of the decrease in damping ratio occurs in the high water content range while at high frequencies the rate of decrease is more uniform over the entire range of water contents. At lower temperatures (-4 and -10°C) there appears to be no significant influence of water content on damping ratio at a low strain amplitude (3.16×10^{-3}%). At a high strain amplitude (3.16×10^{-2}%) the damping ratio decreases with increasing water content; the relationship appears to be dependent on frequency, with a slight decrease occurring at low frequencies and a more significant decrease at higher frequencies.

e. Confining pressure - damping ratio is not influenced by confining pressure at low temperatures (-4 and -10°C). At a high temperature (-1°C) and a low strain amplitude (3.16×10^{-3}%) damping ratio decreases with increasing confining pressure at low frequencies and is not significantly affected by confining pressure at higher frequencies. In general, the rate of decrease of damping ratio is greater at low confining pressures (0 to 50 psi) than at high confining pressures (50 to 200 psi). Confining pressure appears to have a more significant influence on damping ratio at low water contents than at high water contents.

(4) Values of dynamic Young's modulus of frozen sand for the range of test strain amplitudes (2×10^{-3} to 4×10^{-2}%), frequencies (0.05 to 50 cps), temperatures (-1 to -10°C), confining pressure (0 to 200 psi) and sand contents (20, 45 and 65% by volume) ranged from 2×10^{5} to 38×10^{5} psi; values of damping ratio were from .02 to .26.

(5) The influence of the various parameters on the dynamic Young's modulus of frozen sand in the order of their importance is as follows:

a. Strain amplitude - the dynamic Young's modulus of frozen sand decreases as the axial strain amplitude increases

with a more pronounced effect at low temperatures (-4 and -10°C) than at high temperaures (-1°C). The rate of decrease varies with frequency, confining pressure and sand content, but does not appear to follow any definite trends.

b. Temperature - the dynamic Young's modulus increases, in general, with descending temperature. The rate of increase appears to be greatest at a high confining pressure (200 psi) and a high sand content (65%).

c. Confining pressure - dynamic Young's modulus increases with increasing confining pressure. The rate of increase appears to be greater at the highest sand content (65%). The frequency of loading and temperature do not appear to have a pronounced effect on the rate of increase.

d. Sand content - dynamic Young's modulus increases, with increasing sand content at a temperature of -1°C. The relationship does not appear to be dependent on frequency or temperature.

e. Frequency - dynamic Young's modulus increases with increasing frequency at temperatures of -1 and -4°C; at a temperature of -10°C dynamic Young's modulus increases to a frequency of 1.0 cps; between 1.0 and 5.0 cps dynamic Young's modulus either decreases or remains constant. The relationship between dynamic Young's modulus and frequency appears to be independent of temperature and sand content.

5. There appears to be no well-defined relationship between damping ratio of frozen sand and strain amplitude or confining pressure. The influence of the other parameters on the damping ratio of frozen sand in the order of their importance is as follows:

   a. frequency - damping ratio decreases with increasing frequency, The rate of decrease appears to be independent, in general, of temperature and confining pressure.

b. temperature - damping ratio decreases, in general, with descending temperature. The rate of decrease may be slightly less for low sand content (20%) than for high sand contents (45 and 65%).

c. sand content - damping ratio increases with increasing sand content up to 45% sand content; it appears to decrease slightly with an increase in sand content from 45 to 65% for -4 to -10°C.

A comparison of the dynamic properties of frozen cohesionless soils obtained in the present study to those obtained in previous studies indicates:

1. In general, there is good agreement among the wave velocity-temperature relationships obtained in several studies.
2. The values of damping ratio determined in the present study are higher than those obtained in a previous study. It is felt that the values obtained in the present study compared to those obtained in a previous study are reasonable.

LIST OF REFERENCES

1. Barnes, D. F., "Geophysical Methods for Delineating Permafrost," Proceedings of the Permafrost International Conference, National Academy of Sciences, National Research Council Publication No. 1287, 1963, pp. 349-355.

2. Bell, R. A. I., "A Seismic Reconnaissance of the McMurdo Sound Region, Antarctica," Journal of Glaciology, Vol. 6, No. 44, 1966, pp. 209-221.

3. Blouin, S., personal communication with T. S. Vinson, 1976.

4. Gagne, R. M. and Hunter, J. S., "Hammer Seismic Studies of Surficial Materials, Banks Island, Ellesmere Island and Boothia Peninsula," Geol. Surv. Can. Paper 75-1B, 1975, pp. 13-18.

5. Hobson, G. D., "A Shallow Seismic Experiment in Permafrost, Klondike Area, Yukon Territory," Paper 66-2, Report of Activities November 1965 to April 1966, Geological Survey of Canada, Ottawa, 1966, pp. 10-14.

6. Hunter, J. A. A., "The Application of Shallow Seismic Methods to Mapping of Frozen Surficial Materials," North American Contribution to the Second International Conference on Permafrost, National Academy of Science, 1973.

7. Hunter, J. A. M., "Seismic Velocity Measurements in Permafrost, Fox Tunnel, Fairbanks, Alaska," Paper 74-1, Geological Survey of Canada, Part B, 1974, pp. 89-90.

8. Kaplar, C. W., "Laboratory Determination of the Dynamic Moduli of Frozen Soils and of Ice," Proceedings of the Permafrost International Conference, National Academy of Sciences, National Research Council Publication No. 1287, 1963, pp. 293-301.

9. Kaplar, C. W., "Laboratory Determination of Dynamic Moduli of Frozen Soils and of Ice," Research Report 163, USACRREL, Hanover, New Hampshire, January 1969.

10. King, M. S., T. S. Bamford, and P. J. Kurfurst, "Ultrasonic Velocity Measurements on Frozen Rocks and Soils," Proceedings of Symposium on Permafrost Hydrology and Geophysics, Calgary, February 1974, 8 pp.

11. Linell, K. A. and C. W. Kaplar, "Description and Classification of Frozen Soils," Technical Report 150, USACRREL, Hanover, New Hampshire, January 1969.

12. Lovell, C. W. and W. S. Roberts, "Physiographic Divisions, Provinces, Sections and Subsections of Alaska, Canada and the United States," Purdue University, 1975.

13. McGinnis, L. D., Nakao, K., and Clark, C. C., "Geophysical Identification of Frozen and Unfrozen Found," North American Contribution to the Second International Conference on Permafrost, National Academy of Sciences, 1973, pp. 136-136.

14. Nakano, Y., and Froula, N. H., "Sound and Shock Transmission in Frozen Soils," North American Contribution to the Second International Conference on Permafrost, National Academy of Science, 1973.

15. Roethlisberger, H., "The Applicability of Seismic Refraction Soundings in Permafrost near Thule, Greenland," USACRREL Technical Report 81, 1961.

16. Seed, H. B., and I. M. Idriss, "Soil Moduli and Damping Factors for Dynamic Response Analyses," Report No. EERC 70-10, Earthquake Engineering Research Center, University of California, Berkeley, Calif., 1970.

17. Stevens, H. W., "Viscoelastic Properties of Frozen Soil Under Vibratory Loads," North American Contribution to the Second International Conference on Permafrost, National Academy of Sciences, 1973, pp. 400-409.

18. Stevens, H. W., "The Response of Frozen Soils to Vibratory Loads," Technical Report 265, USACRREL, Hanover, New Hampshire, June, 1975.

19. Williams, J. R., and R. M. Waller, "Ground Water Occurrence in Permafrost Regions of Alaska," Proceedings of the Permafrost International Conference, National Academy of Sciences, National Research Council Publication No. 1287, 1963, pp. 159-64.

20. Woods, K. B., M. D. Miles and C. W. Lovell, Jr., "Origin, Formation, and Distribution of Soils in North American," Chapter I in Foundation Engineering by G. A. Leonards, McGraw-Hill Book Company, Inc., 1962.

APPENDICES

APPENDIX A

CYCLIC TRIAXIAL TEST RESULTS: DYNAMIC YOUNG'S MODULUS OF FROZEN SILT

Test results for Hanover silt are shown in Figures A.1 to A.30. Test results for Alaska silt are shown in Figures A.31 to A.65.

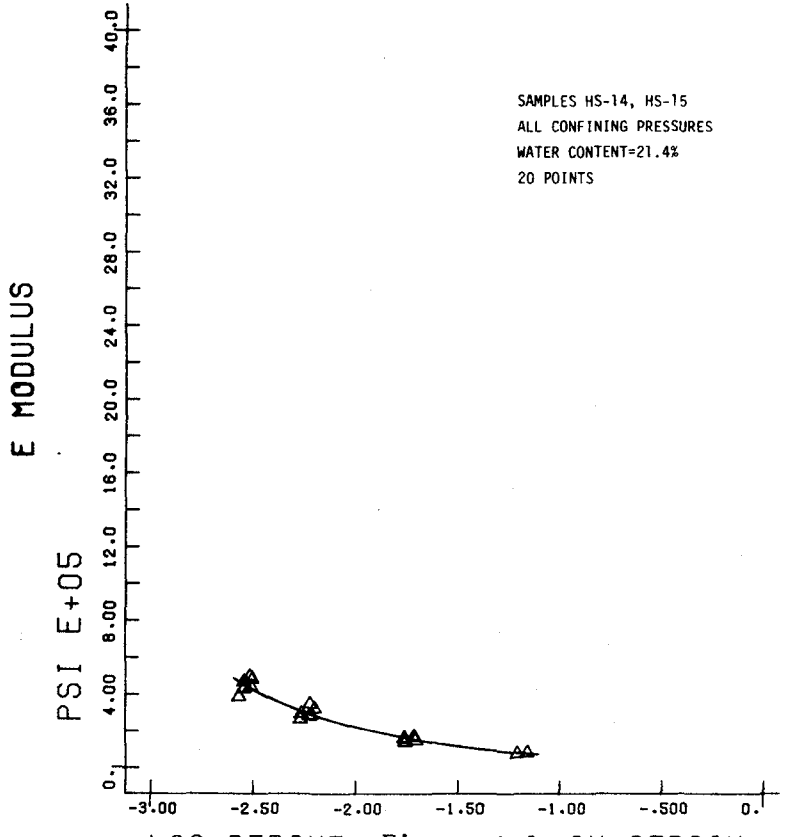

Figure A.1

H-SILTT-1F.05

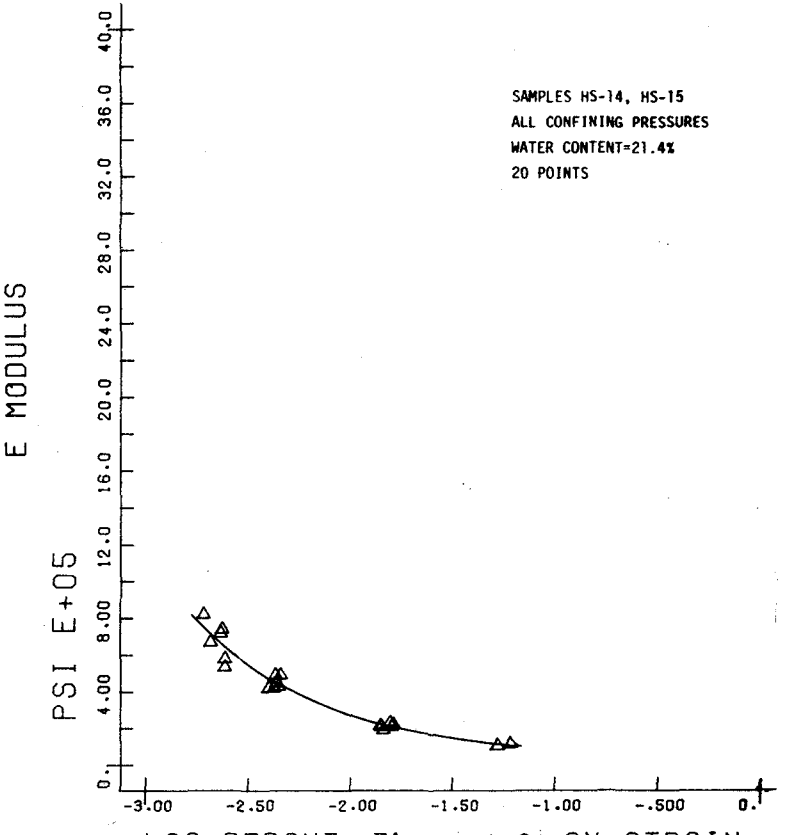

Figure A.2

H-SILTT-1F.3

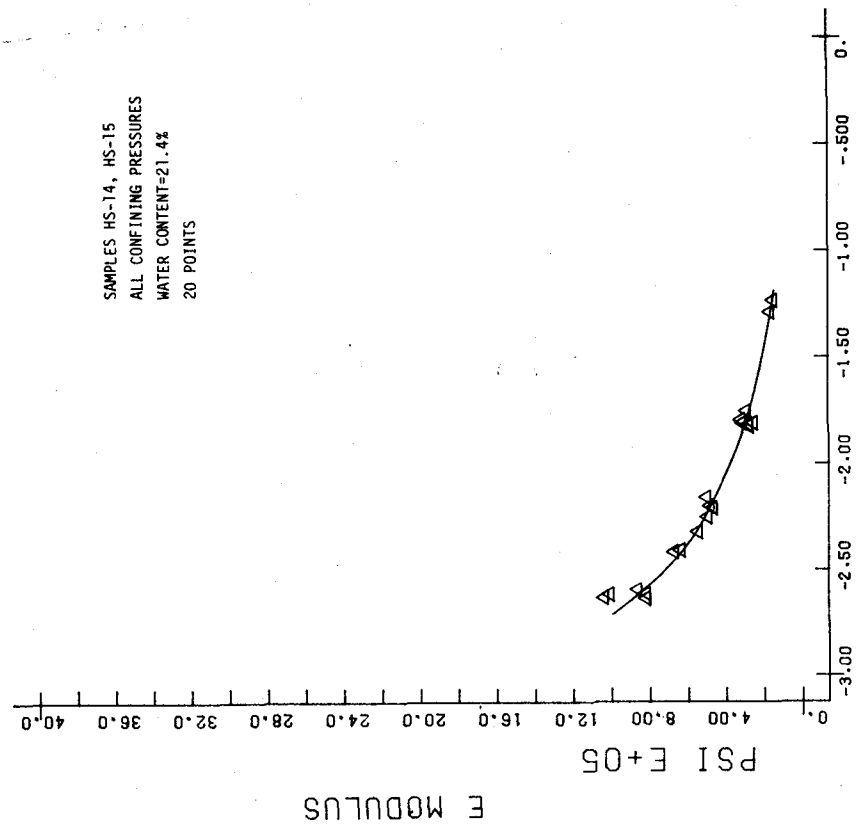

H-SILTT-1F5

Figure A.4

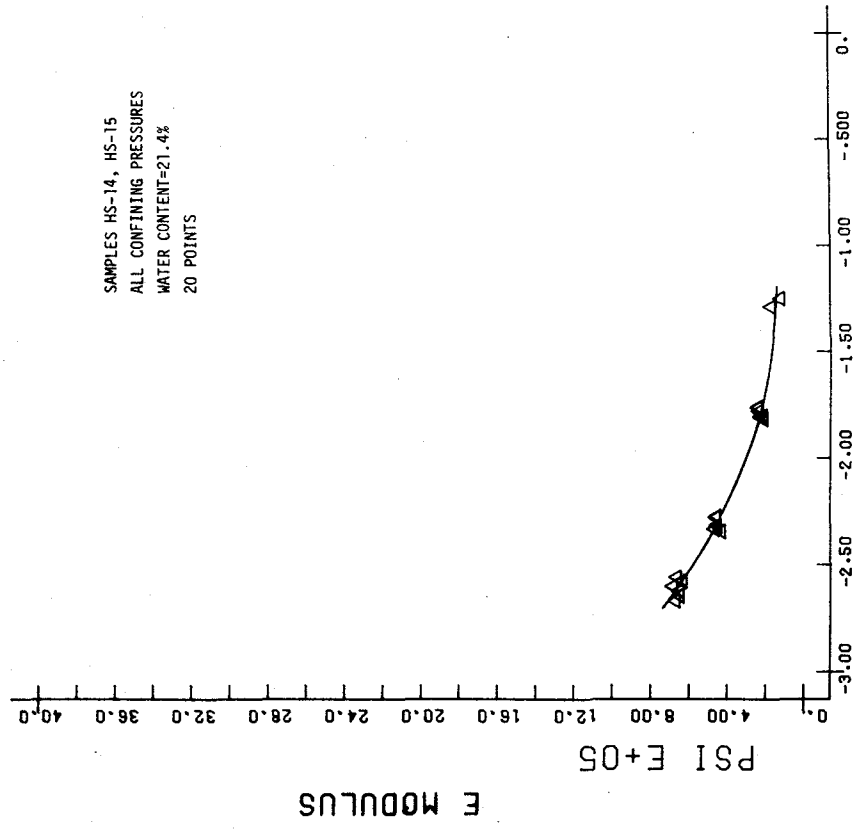

H-SILTT-1F1

Figure A.3

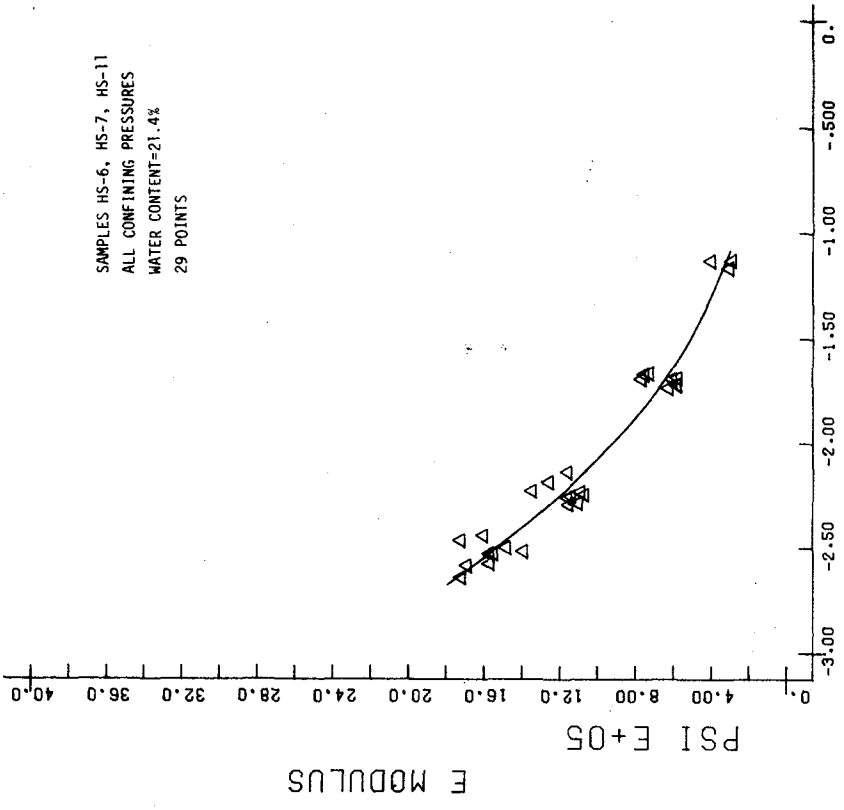

Figure A.5 H-SILTT-1F10

Figure A.6 H-SILTT-4F05

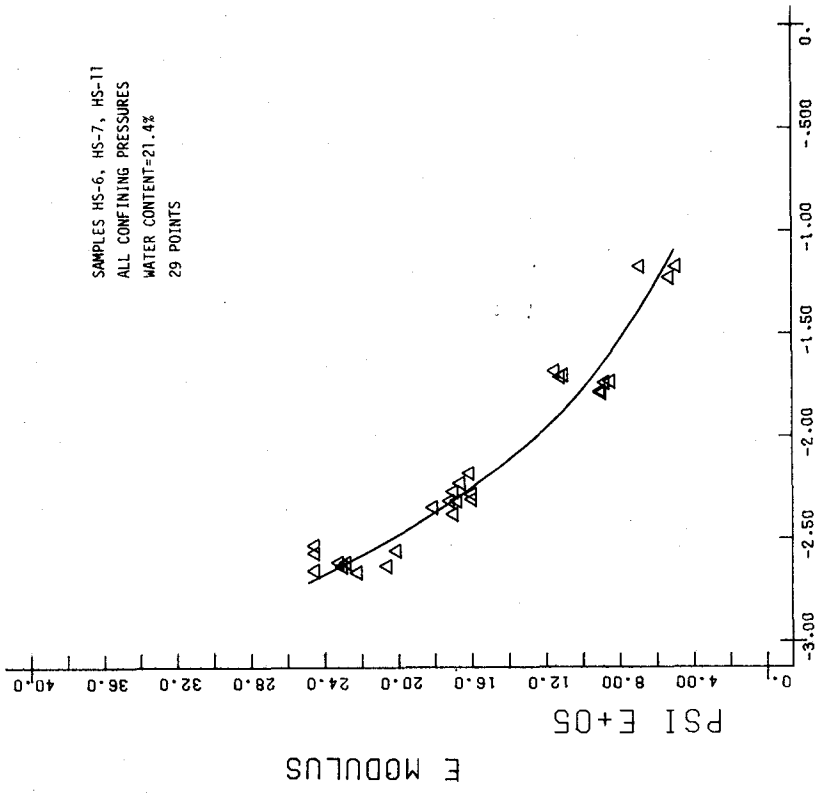

H-SILTT-4F1

Figure A.8

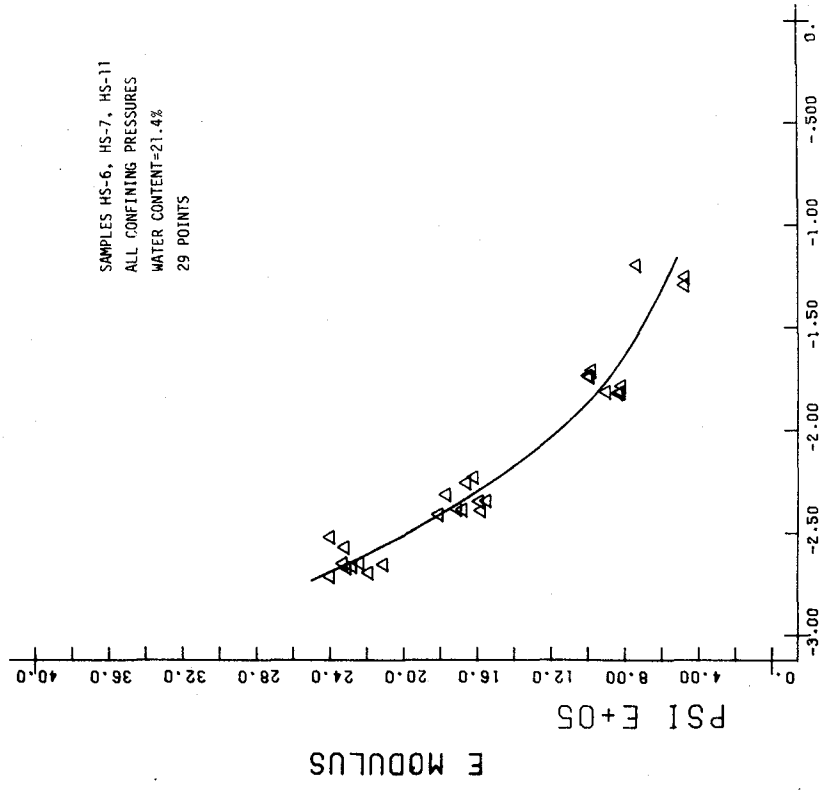

H-SILTT-4F3

Figure A.7

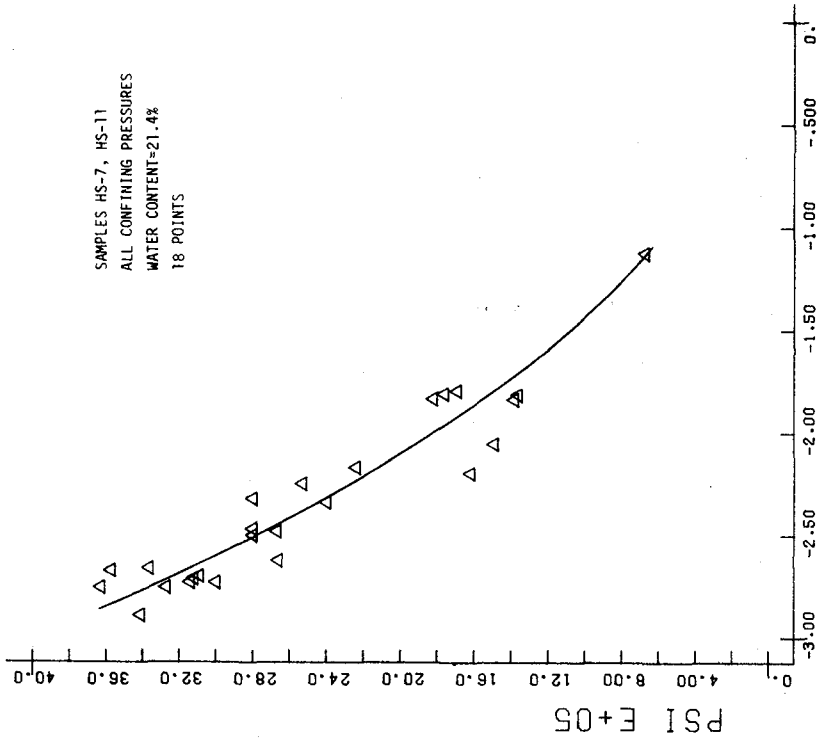

Figure A.10 AX STRAIN

H-SILTT-4F10

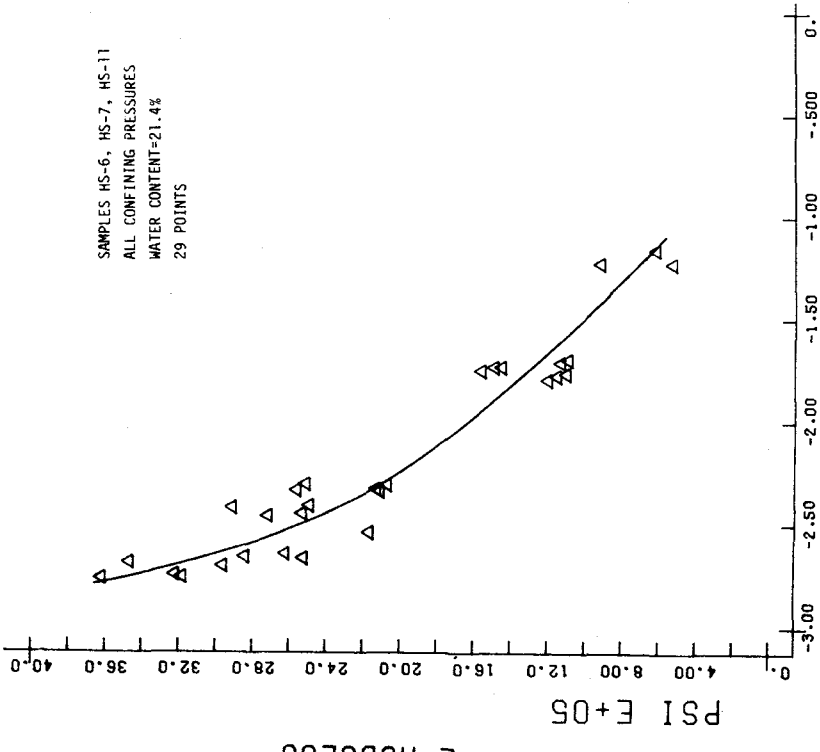

Figure A.9 AX STRAIN

H-SILTT-4F5

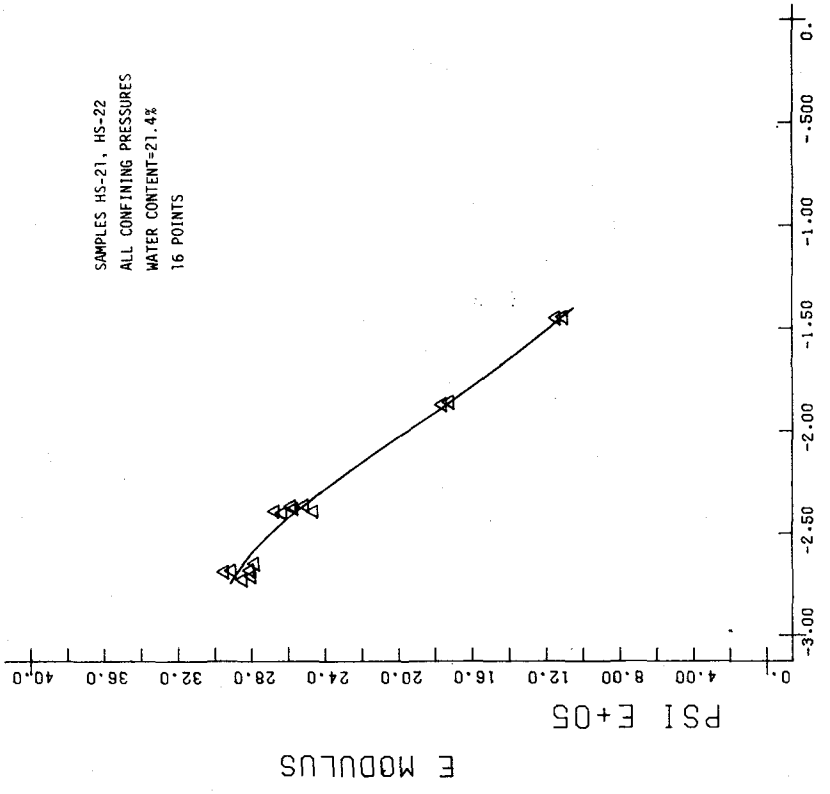

Figure A.12 AX STRAIN

H-SILTT-10F3

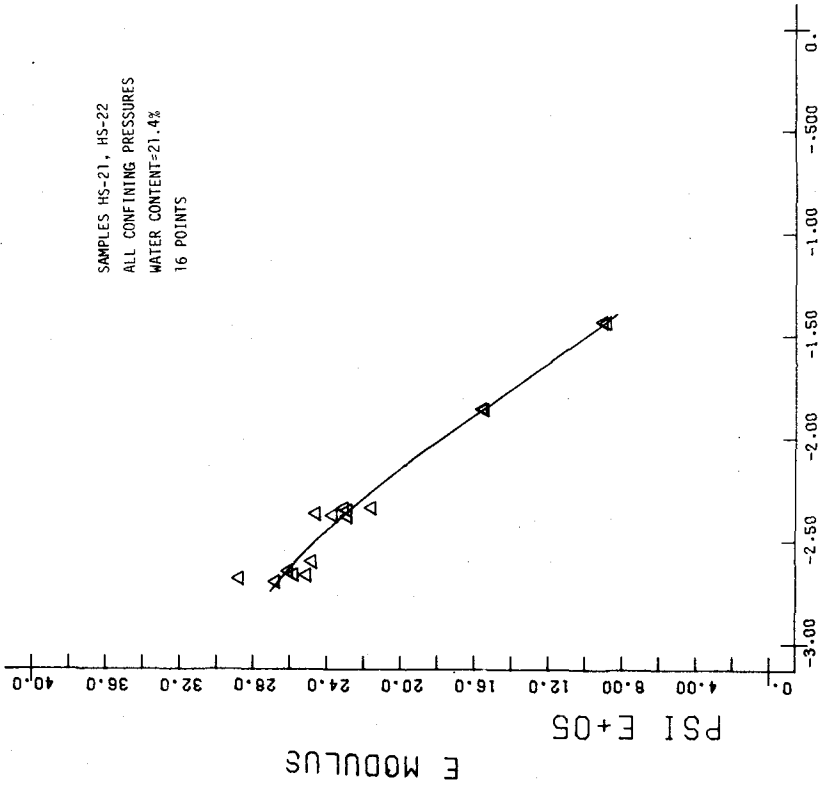

Figure A.11 AX STRAIN

H-SILTT-10F05

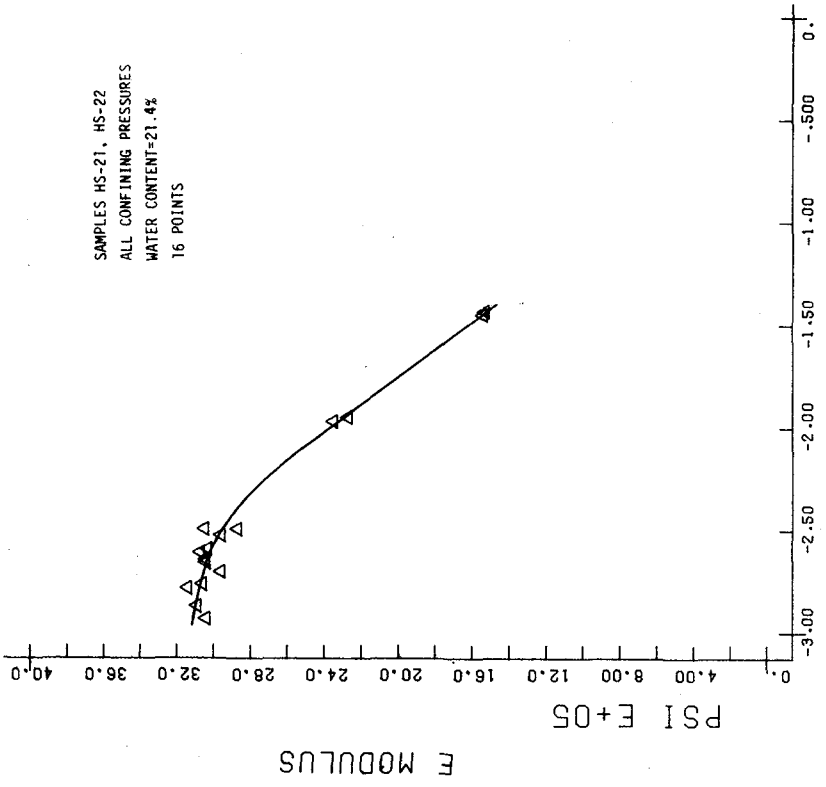

Figure A.14 H-SILTT-10F5

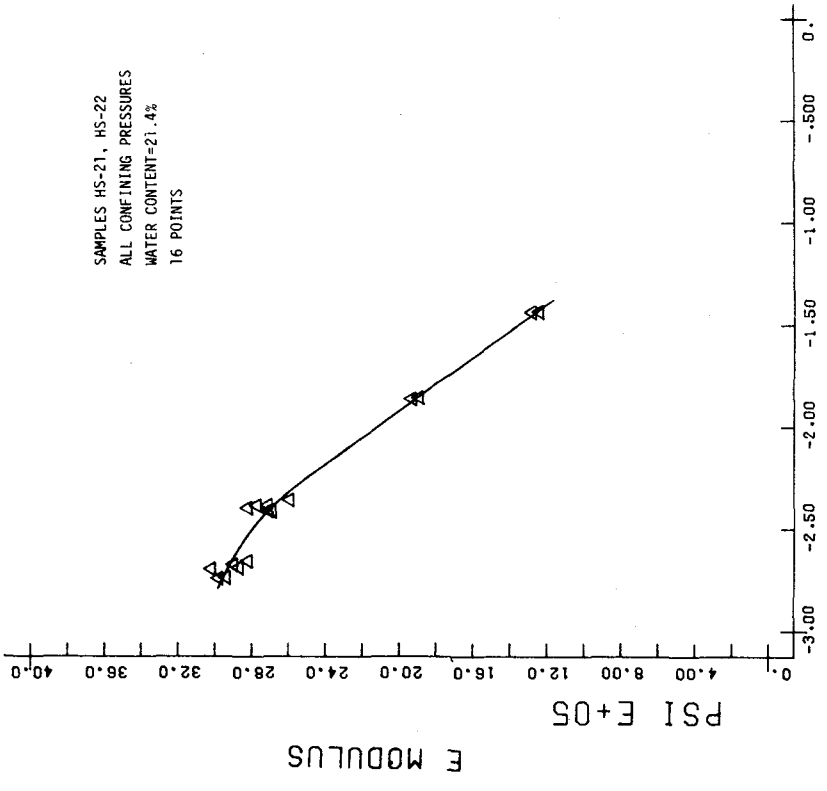

Figure A.13 H-SILTT-10F1

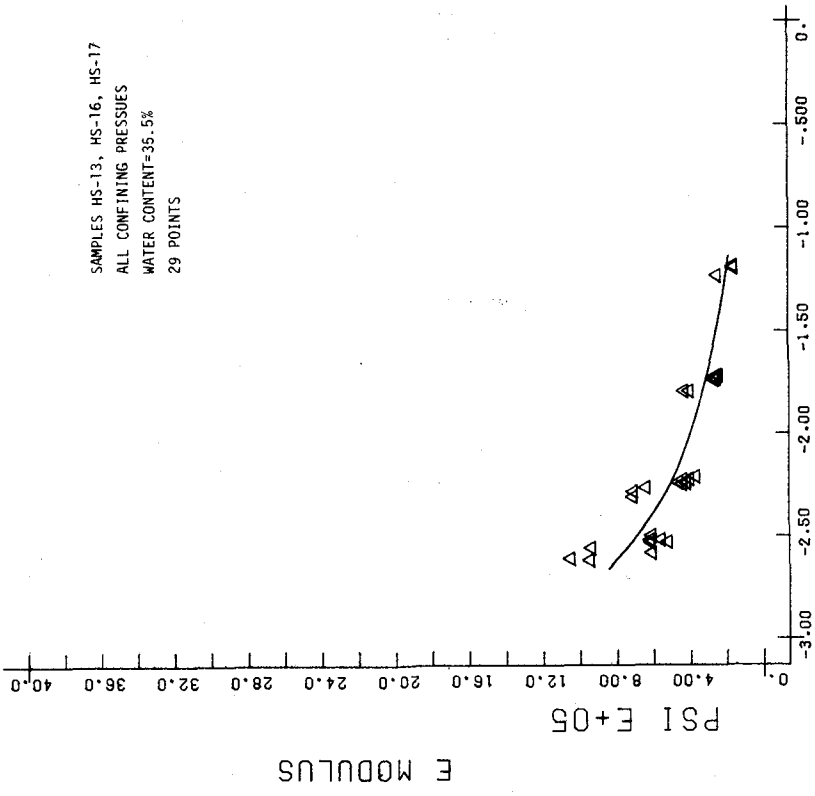

Figure A.16 AX STRAIN

H-SILTT-1F.05

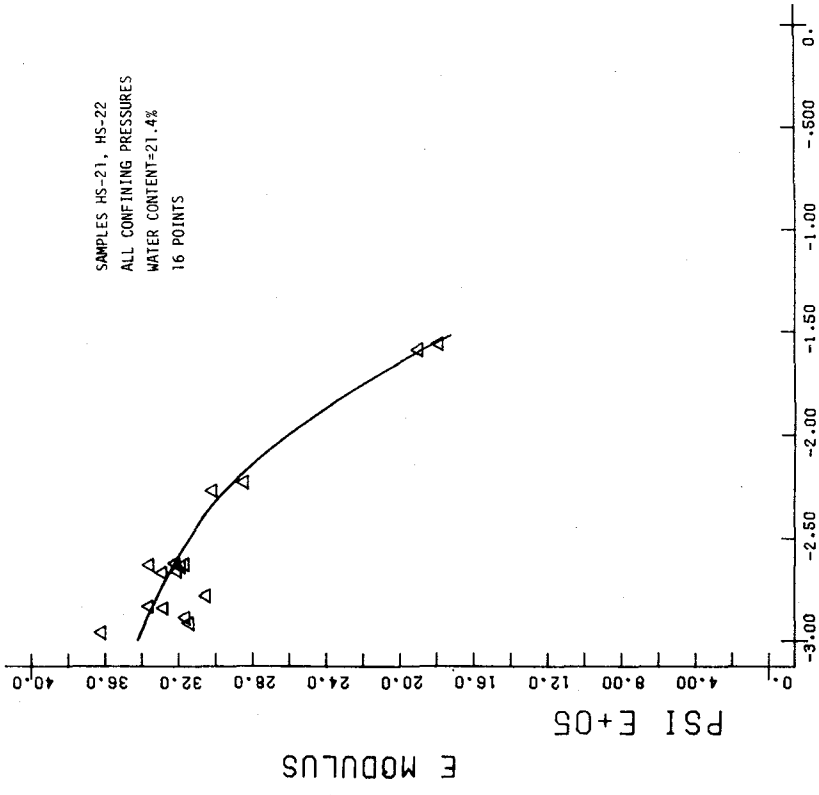

Figure A.15 AX STRAIN

H-SILTT-10F10

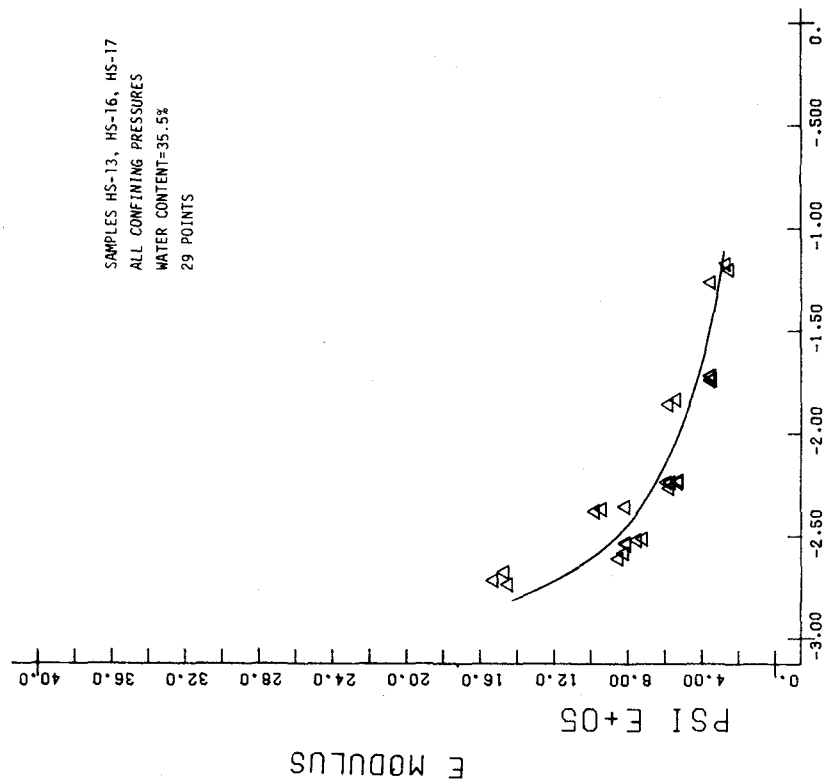

Figure A.18 AX STRAIN

H-SILTT-1F1

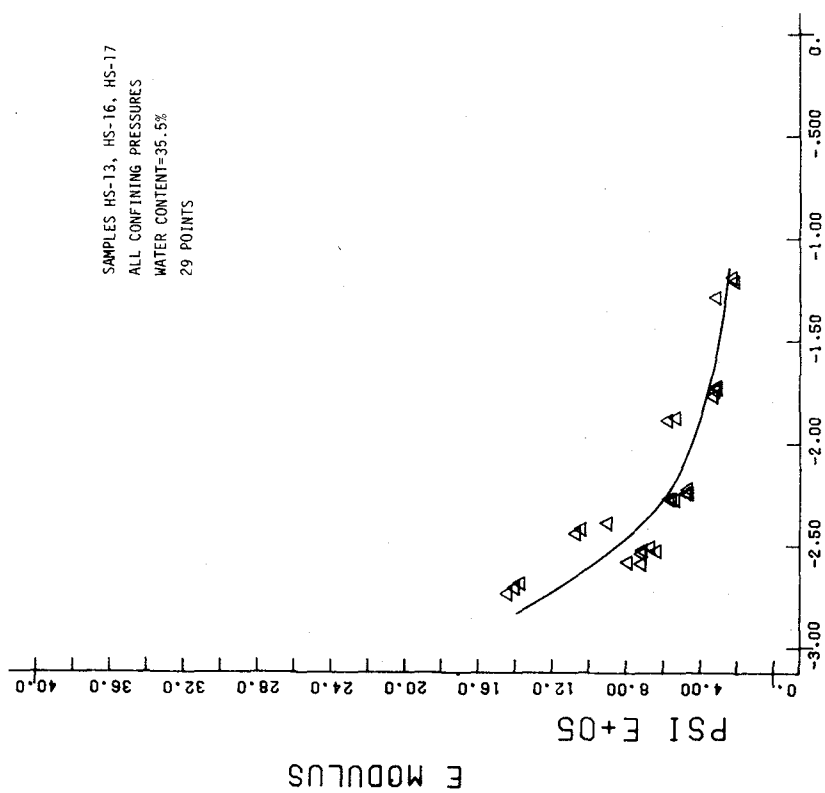

Figure A.17 AX STRAIN

H-SILTT-1F3

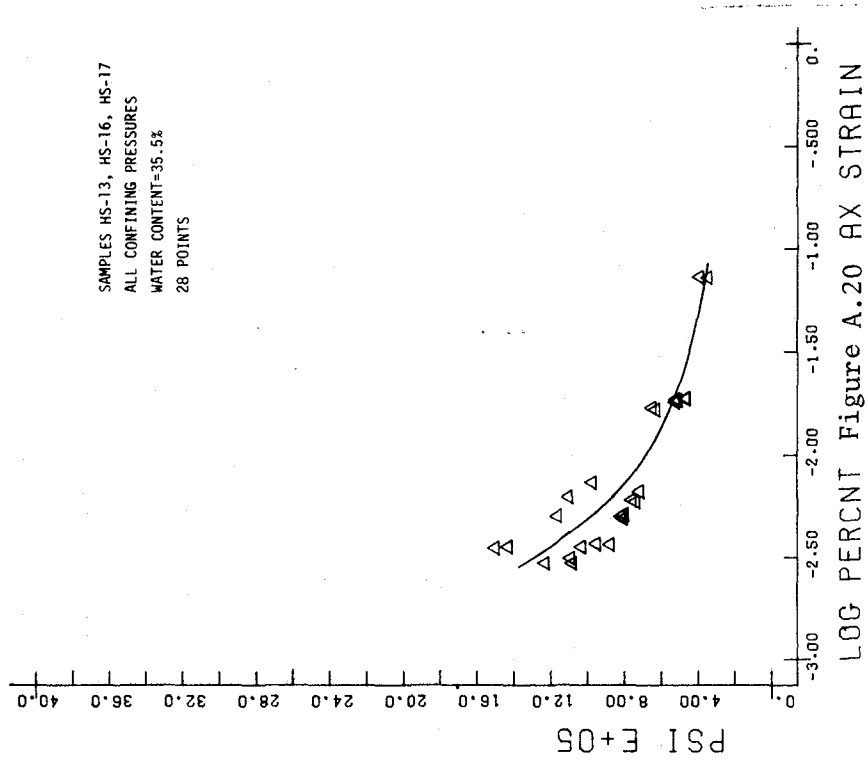

H-SILTT-1F10

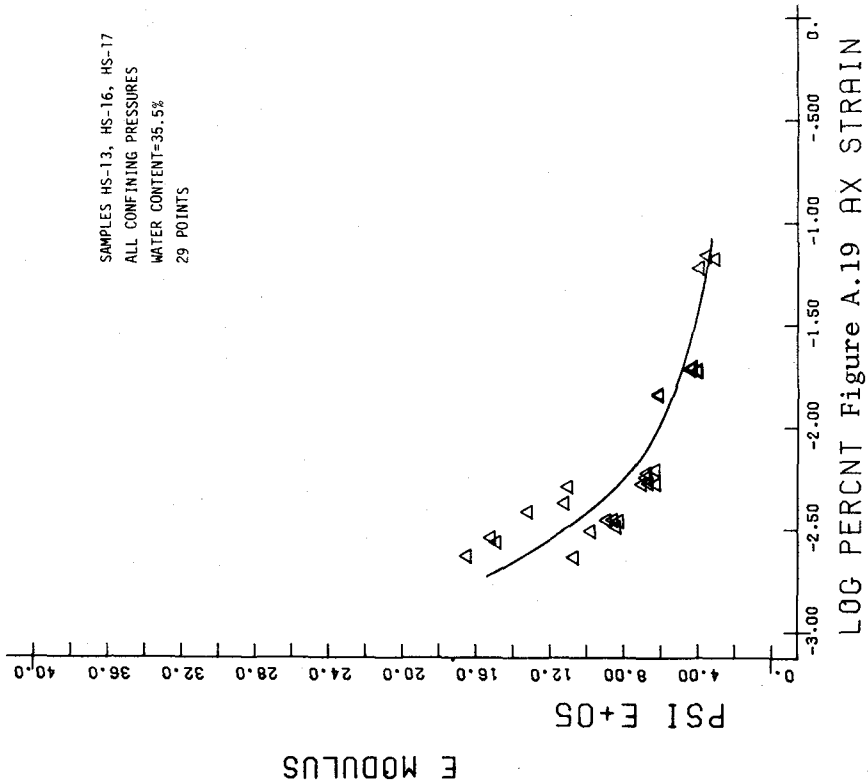

H-SILTT-1F5

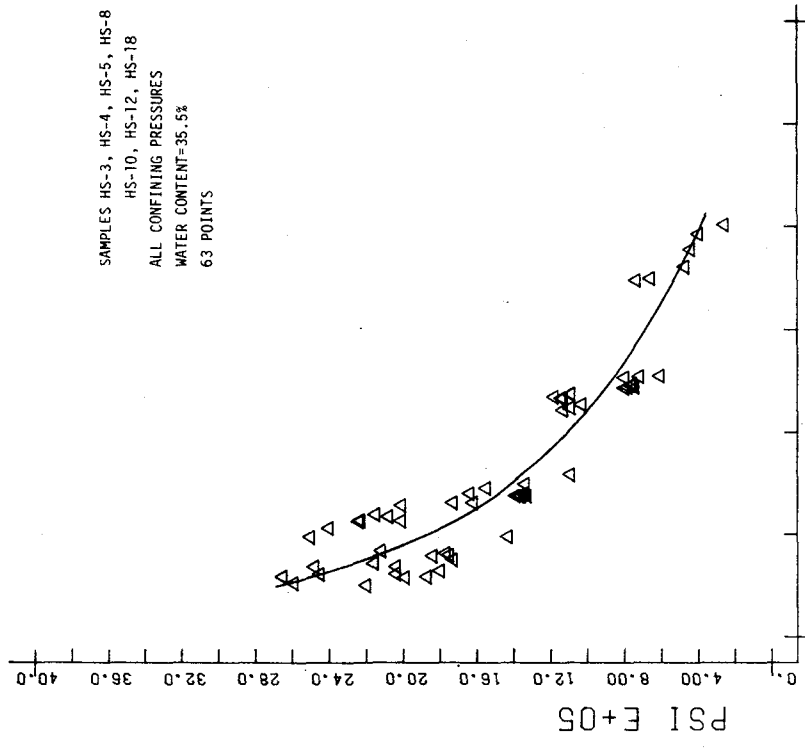

H-SILTT-4F.3

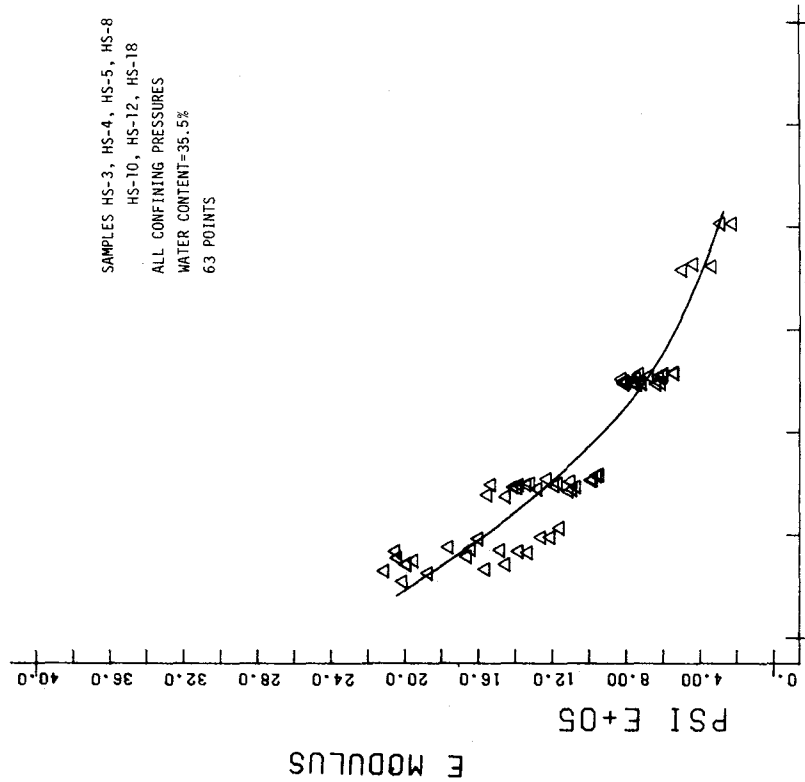

H-SILTT-4F.05

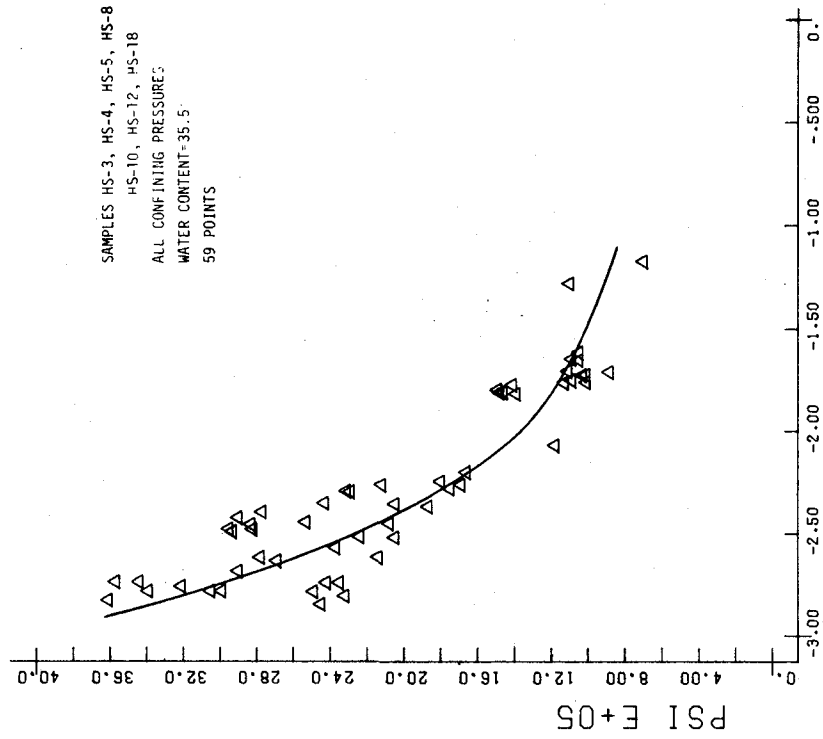

Figure A.24 H-SILTT-4F5

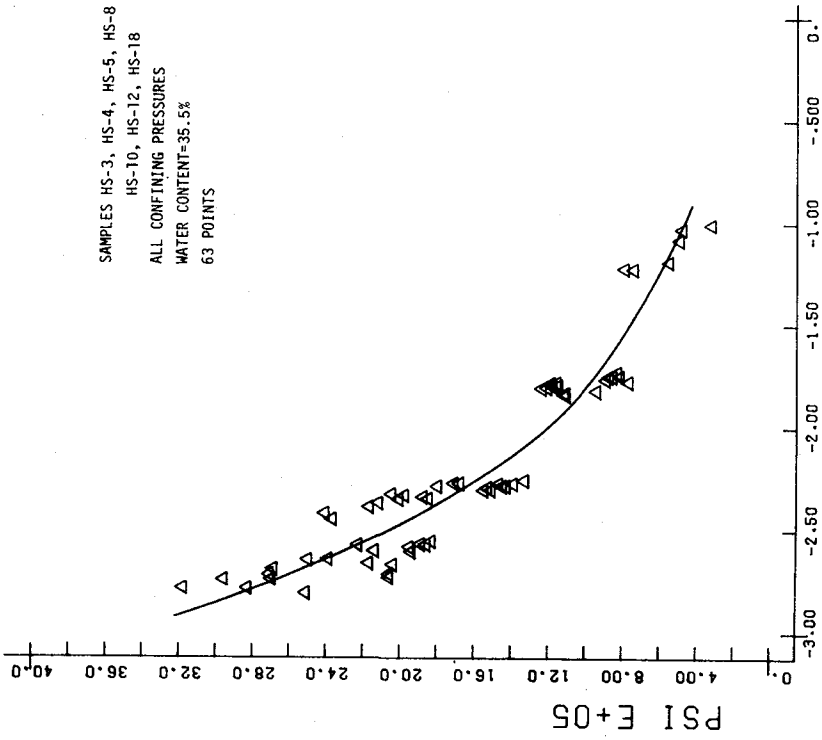

Figure A.23 H-SILTT-4F1

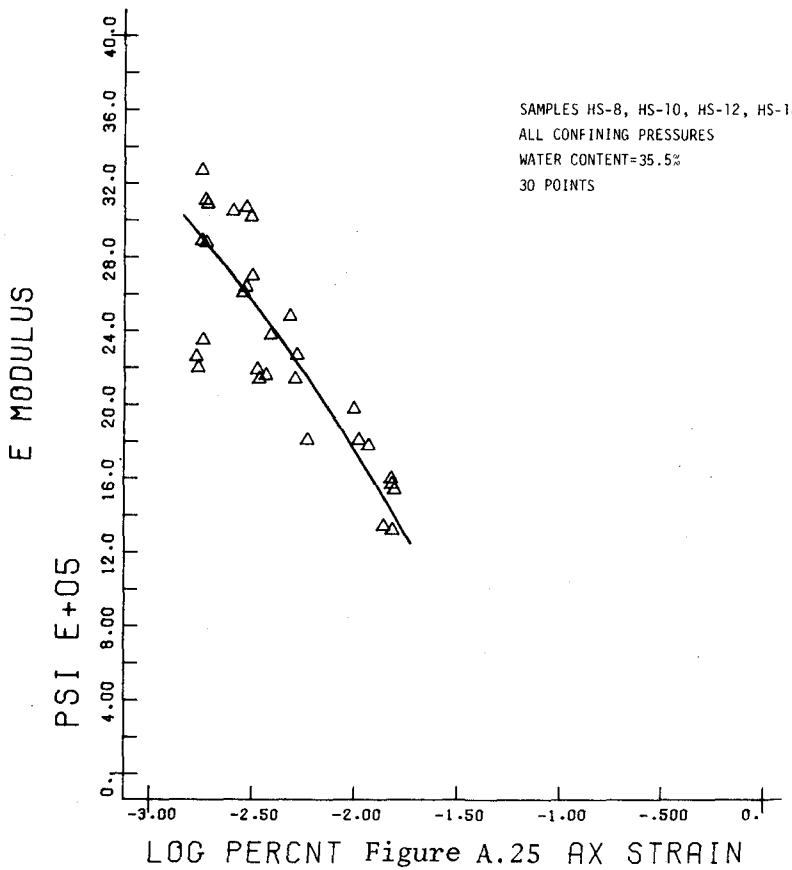

Figure A.25

H-SILTT-4F10

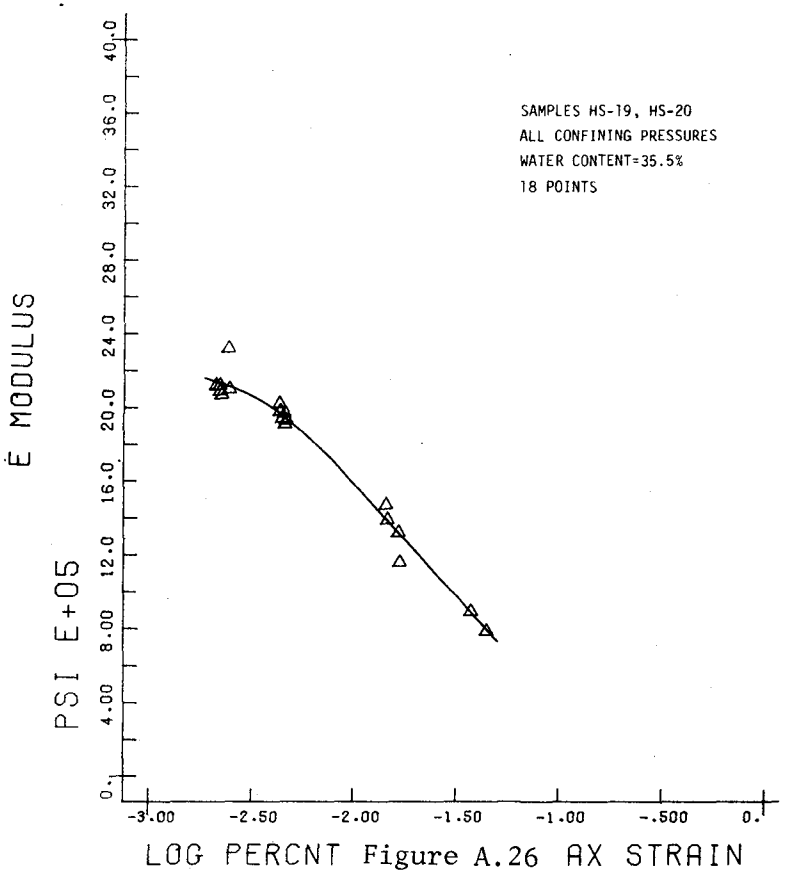

Figure A.26

H-SILTT-10F05

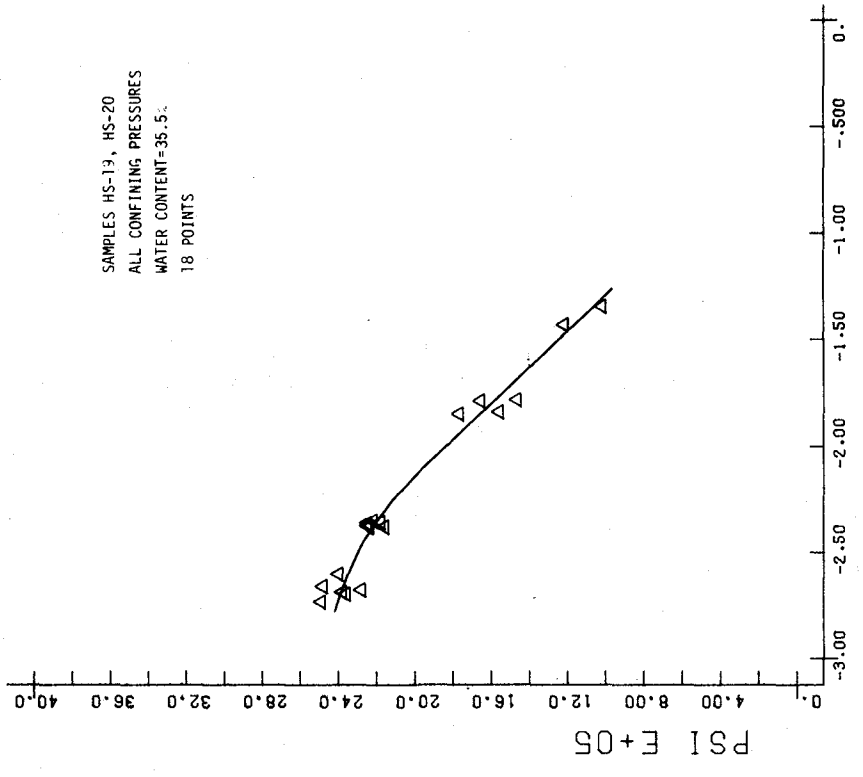

Figure A.28 AX STRAIN

H-SILTT-1OF1

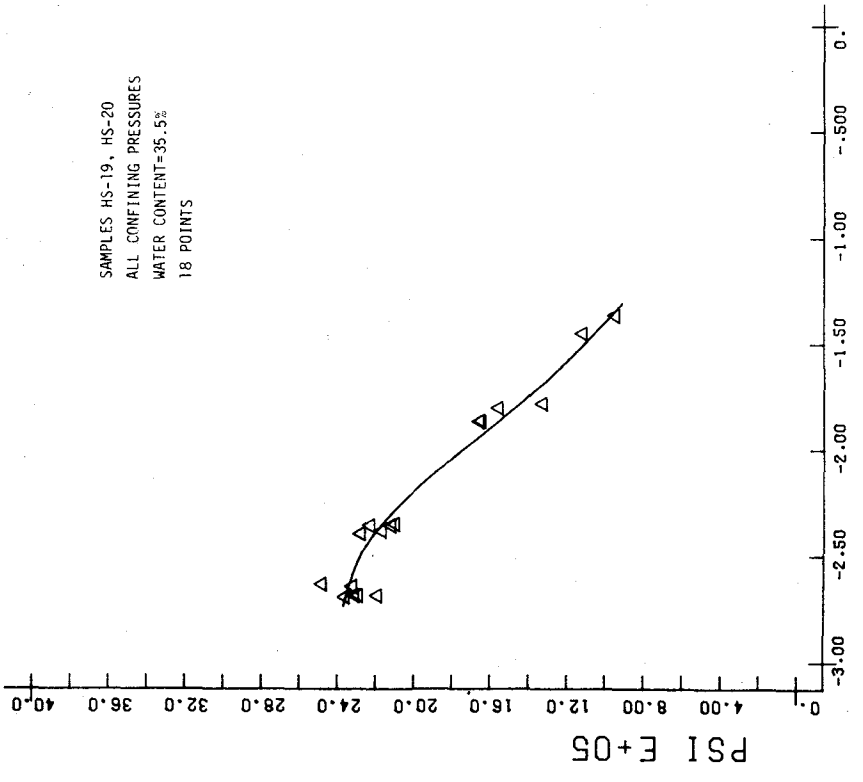

Figure A.27 AX STRAIN

H-SILTT-1OF3

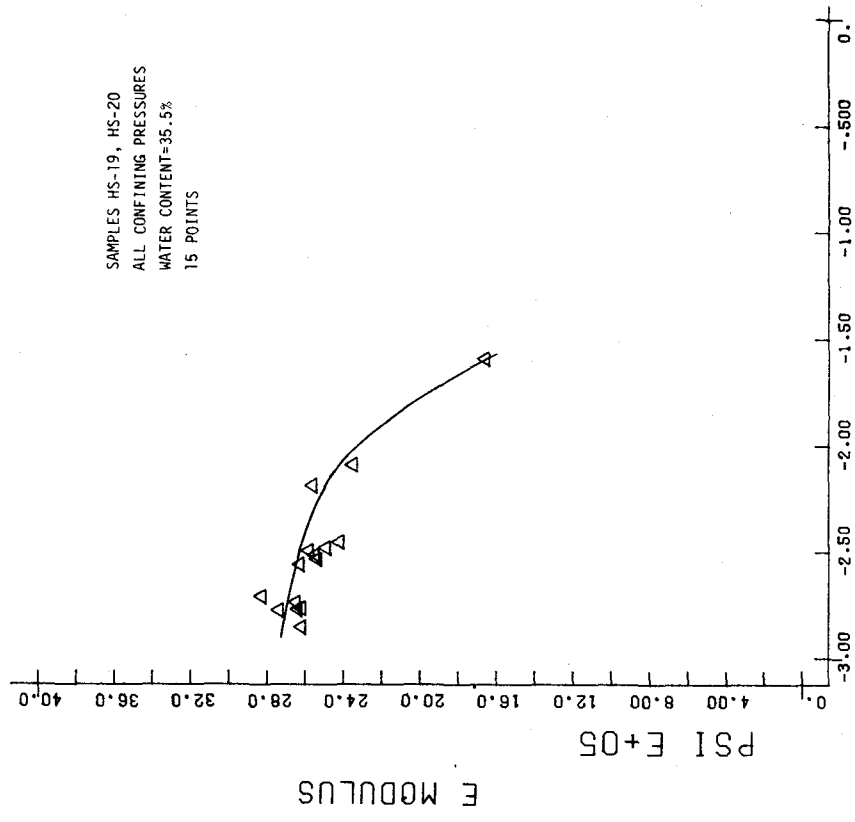

Figure A.30 AX STRAIN

H-SILTT-10F10

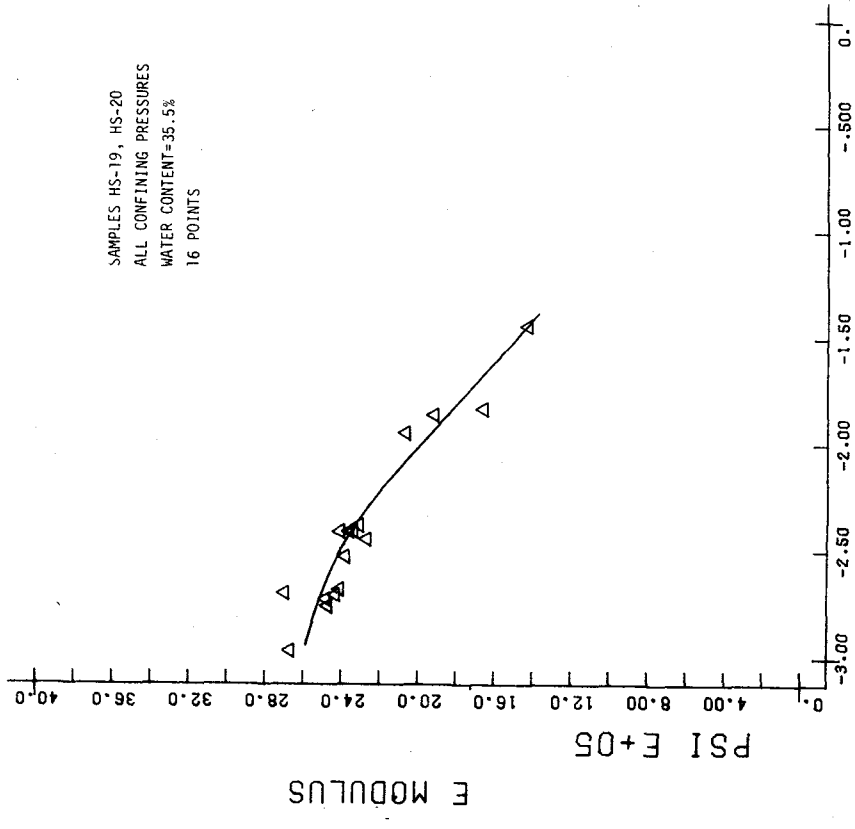

Figure A.29 AX STRAIN

H-SILTT-10F5

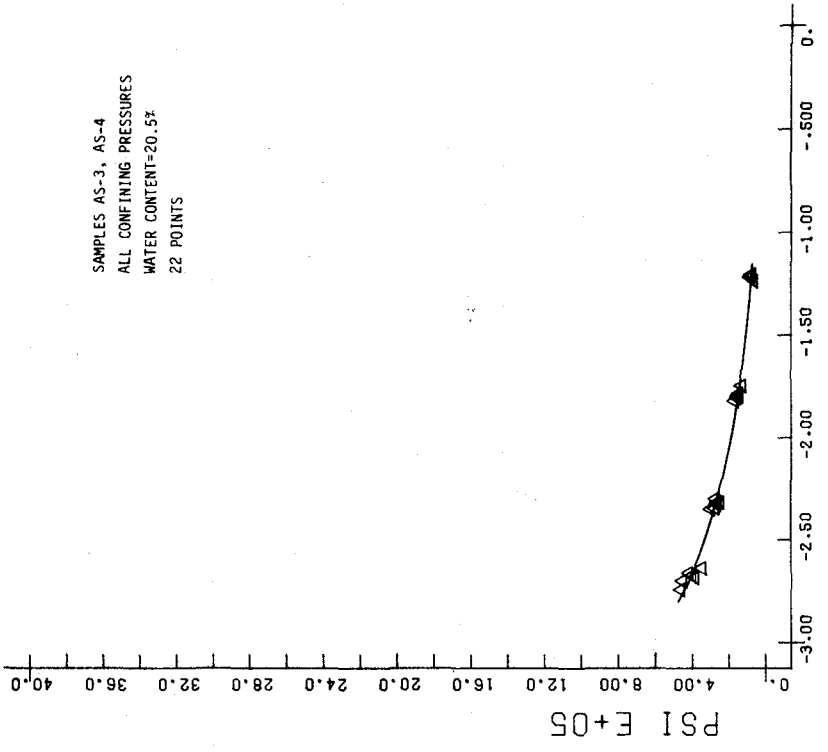
SAMPLES AS-3, AS-4
ALL CONFINING PRESSURES
WATER CONTENT=20.5%
22 POINTS
E MODULUS
PSI E+05
0.
4.00
8.00
12.0
16.0
20.0
24.0
28.0
32.0
36.0
40.0
-3.00
-2.50
-2.00
-1.50
-1.00
-.500
0.
LOG PERCNT Figure A.32 AX STRAIN
A-SILTT-1F3

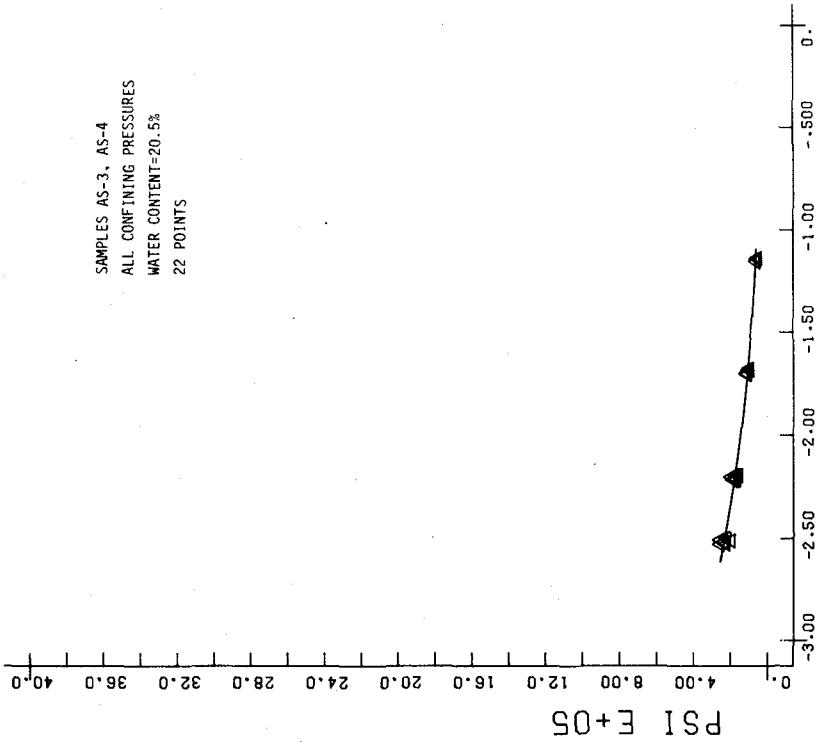
SAMPLES AS-3, AS-4
ALL CONFINING PRESSURES
WATER CONTENT=20.5%
22 POINTS
E MODULUS
PSI E+05
0.
4.00
8.00
12.0
16.0
20.0
24.0
28.0
32.0
36.0
40.0
-3.00
-2.50
-2.00
-1.50
-1.00
-.500
0.
LOG PERCNT Figure A.31 AX STRAIN
A-SILTT-1F05

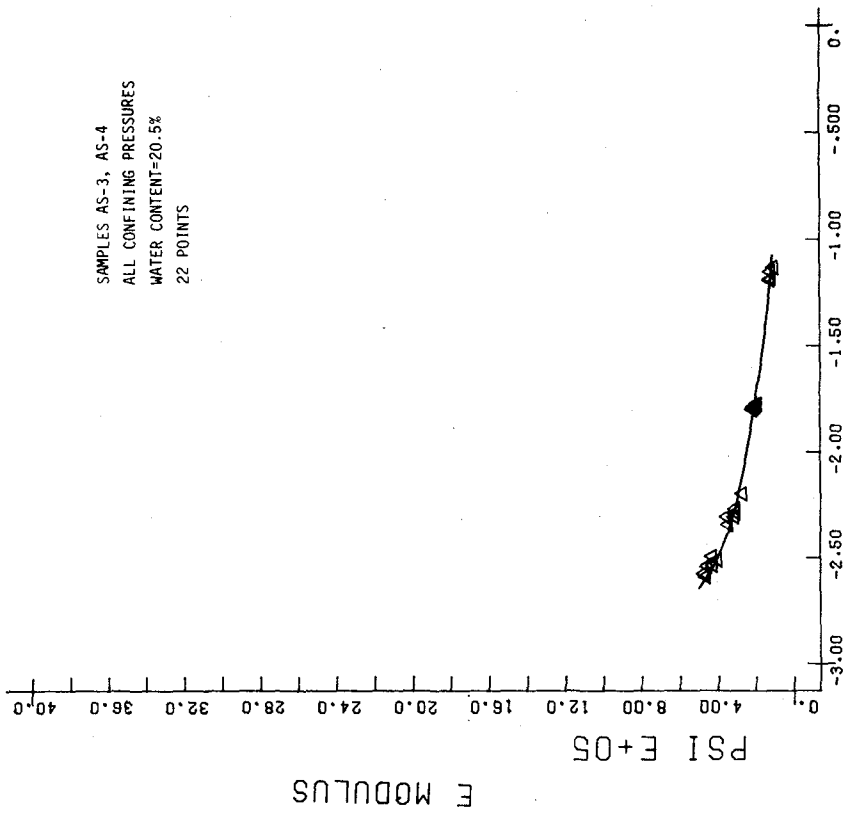
SAMPLES AS-3, AS-4
ALL CONFINING PRESSURES
WATER CONTENT=20.5%
22 POINTS
E MODULUS
PSI E+05
0
4.00
8.00
12.0
16.0
20.0
24.0
28.0
32.0
36.0
40.0
-3.00
-2.50
-2.00
-1.50
-1.00
-.500
0.
LOG PERCNT Figure A.34 AX STRAIN
A-SILTT-1F5

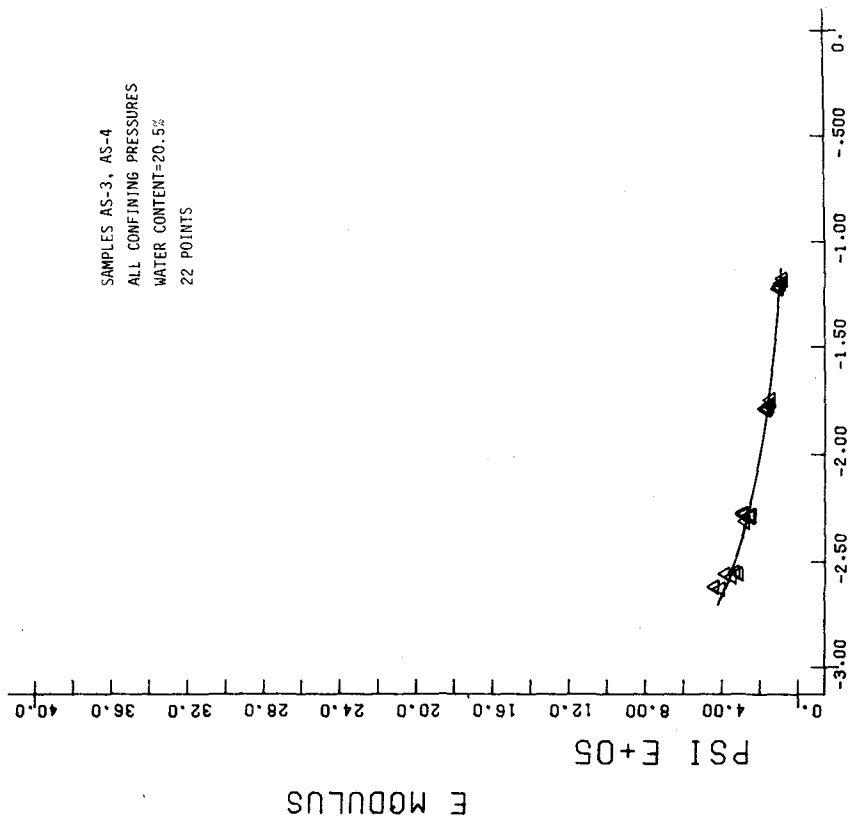
SAMPLES AS-3, AS-4
ALL CONFINING PRESSURES
WATER CONTENT=20.5%
22 POINTS
E MODULUS
PSI E+05
0
4.00
8.00
12.0
16.0
20.0
24.0
28.0
32.0
36.0
40.0
-3.00
-2.50
-2.00
-1.50
-1.00
-.500
0.
LOG PERCNT Figure A.33 AX STRAIN
A-SILTT-1F1

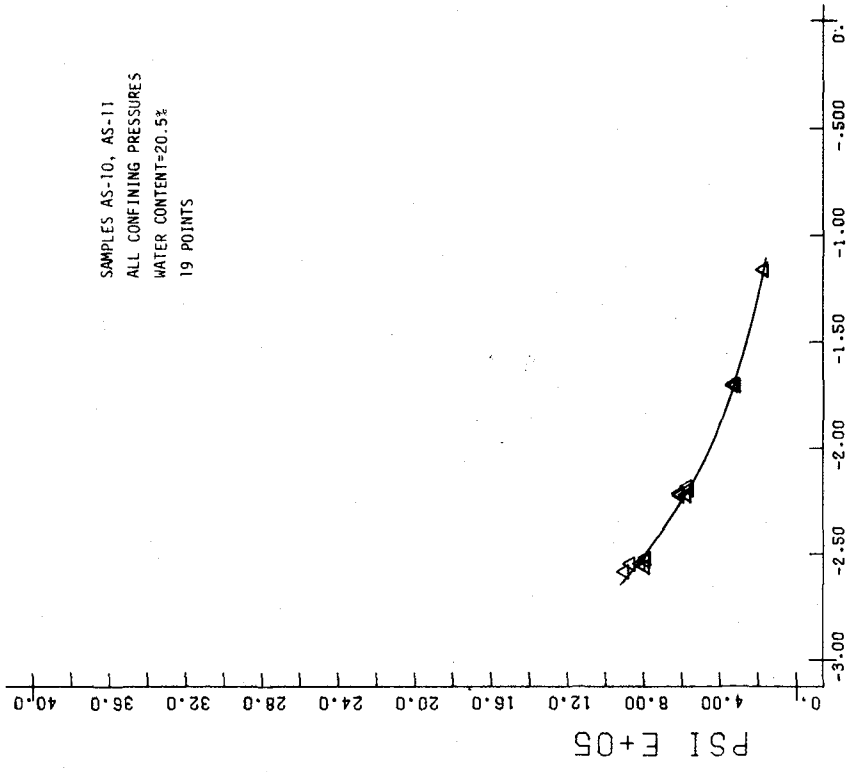

Figure A.36 AX STRAIN

A-SILTT-4F05

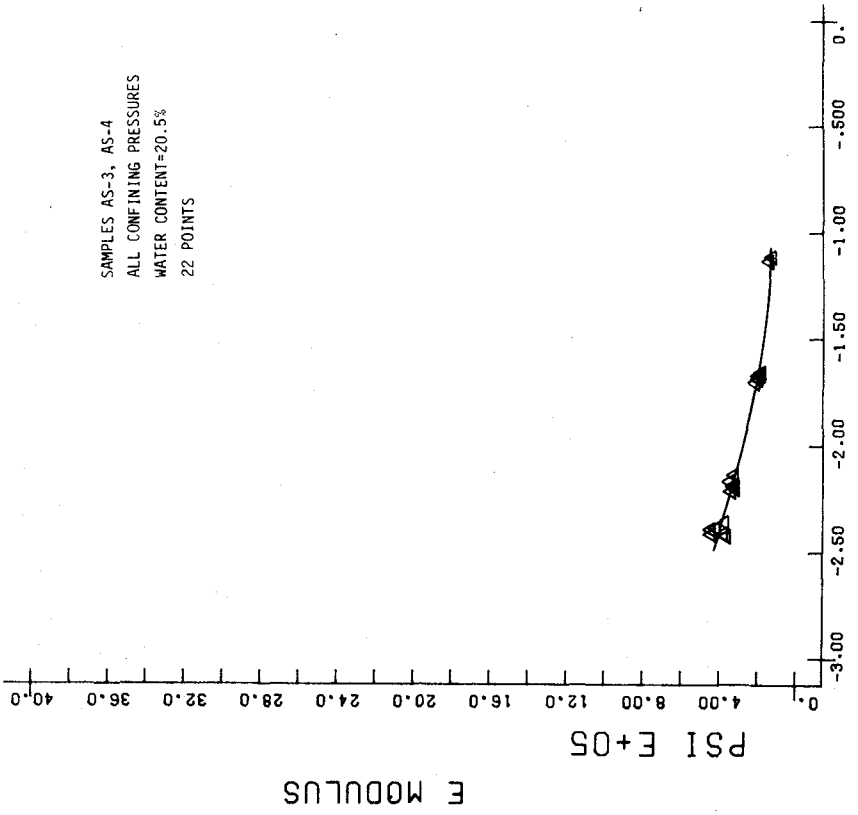

Figure A.35 AX STRAIN

A-SILTT-1F10

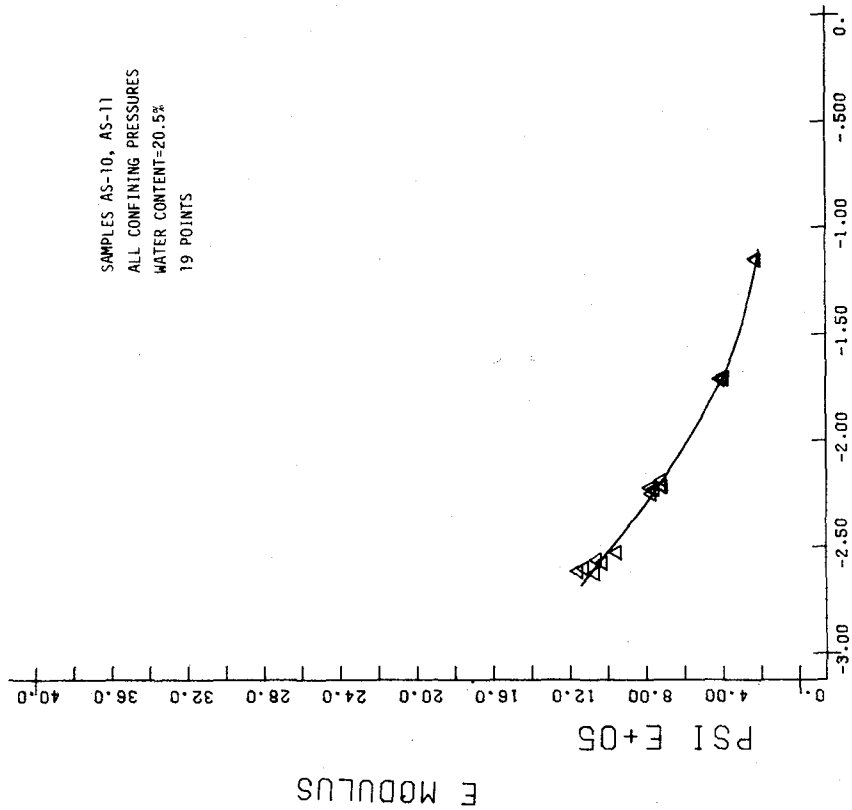

Figure A.38 A-SILTT-4F1

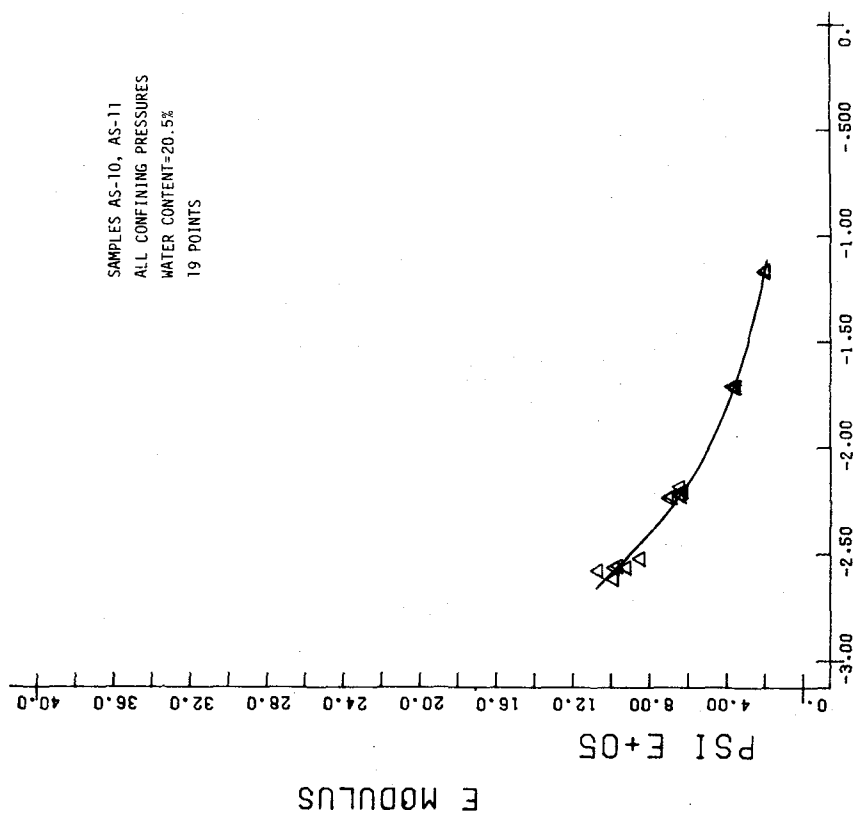

Figure A.37 A-SILTT-4F3

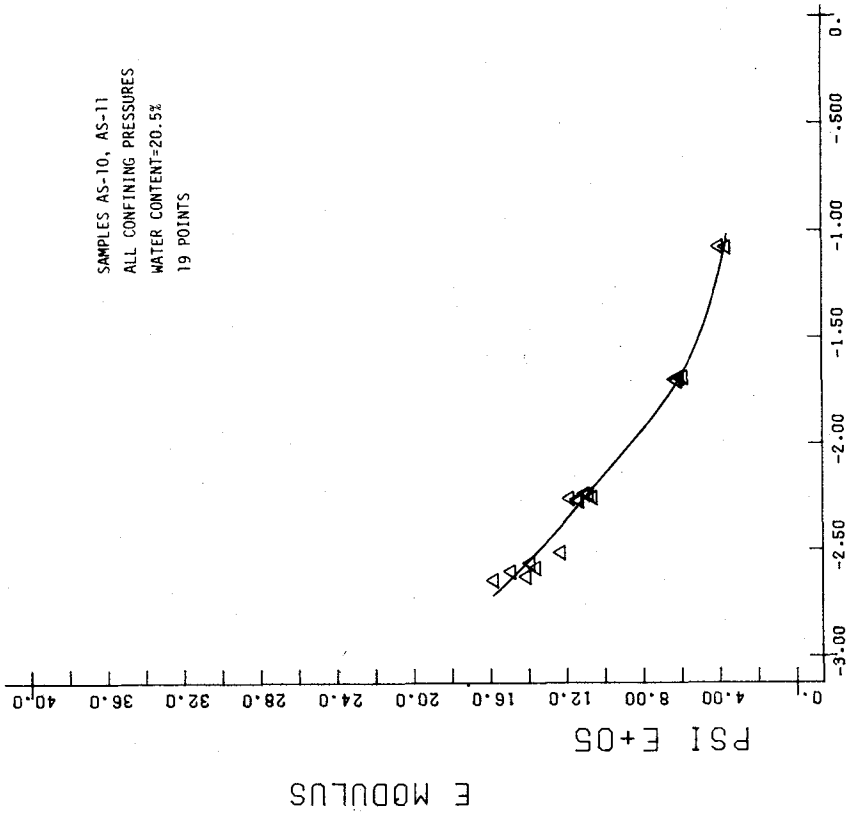
SAMPLES AS-10, AS-11
ALL CONFINING PRESSURES
WATER CONTENT=20.5%
19 POINTS
E MODULUS
PSI E+05
0.
4.00
8.00
12.0
16.0
20.0
24.0
28.0
32.0
36.0
40.0
-3.00
-2.50
-2.00
-1.50
-1.00
-.500
0.
LOG PERCNT Figure A.40 AX STRAIN
A-SILTT-4F10

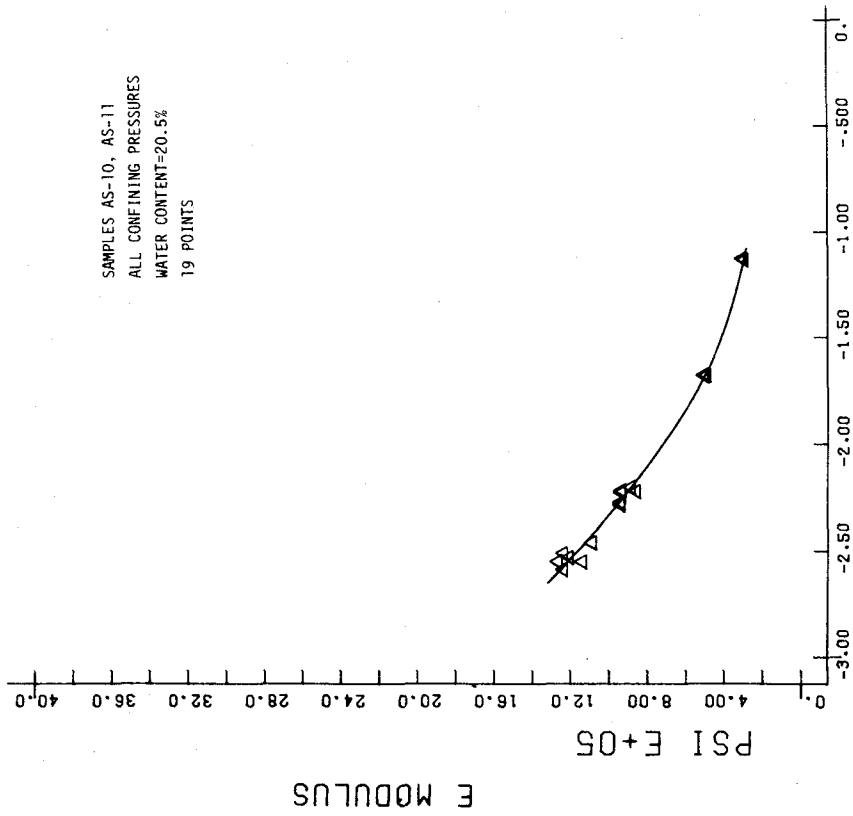
SAMPLES AS-10, AS-11
ALL CONFINING PRESSURES
WATER CONTENT=20.5%
19 POINTS
E MODULUS
PSI E+05
0.
4.00
8.00
12.0
16.0
20.0
24.0
28.0
32.0
36.0
40.0
-3.00
-2.50
-2.00
-1.50
-1.00
-.500
0.
LOG PERCNT Figure A.39 AX STRAIN
A-SILTT-4F5

SAMPLES AS-13, AS-15
ALL CONFINING PRESSURES
WATER CONTENT=20.5%
18 POINTS
E MODULUS
PSI E+05
0.
4.00
8.00
12.0
16.0
20.0
24.0
28.0
32.0
36.0
40.0
-3.00
-2.50
-2.00
-1.50
-1.00
-.500
0.
LOG PERCNT Figure A.42 AX STRAIN
A-SILTT-10F3

SAMPLES AS-13, AS-15
ALL CONFINING PRESSURES
WATER CONTENT=20.5%
19 POINTS
E MODULUS
PSI E+05
0.
4.00
8.00
12.0
16.0
20.0
24.0
28.0
32.0
36.0
40.0
-3.00
-2.50
-2.00
-1.50
-1.00
-.500
0.
LOG PERCNT Figure A.41 AX STRAIN
A-SILTT-10F.05

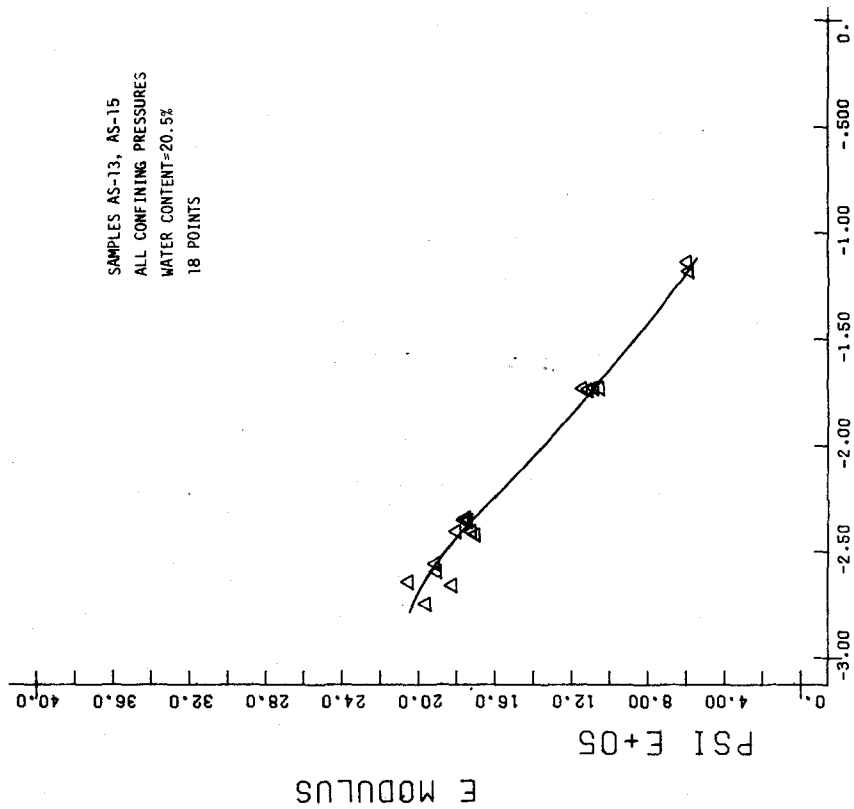

Figure A.44 AX STRAIN

A-SILTT-10F5

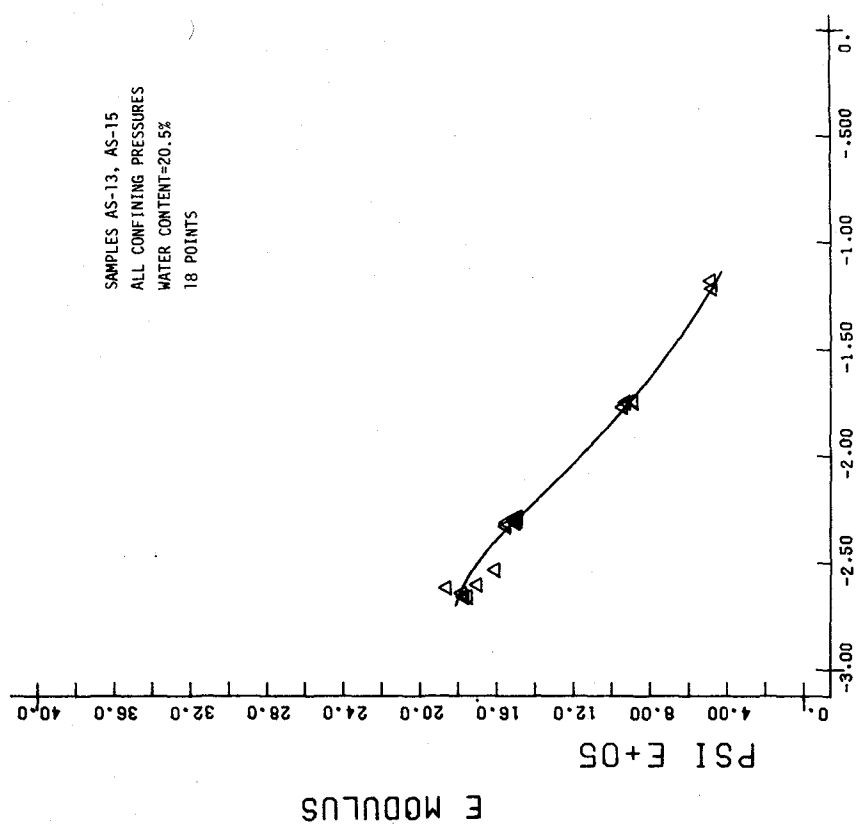

Figure A.43 AX STRAIN

A-SILTT-10F1

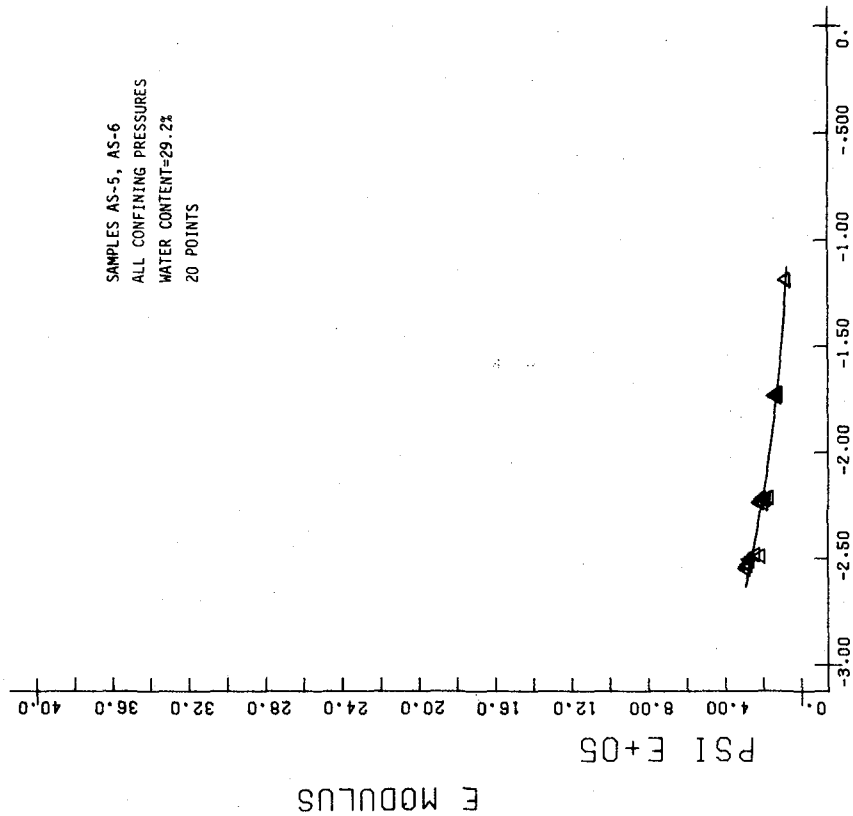

Figure A.46 A-SILTT-1F.05

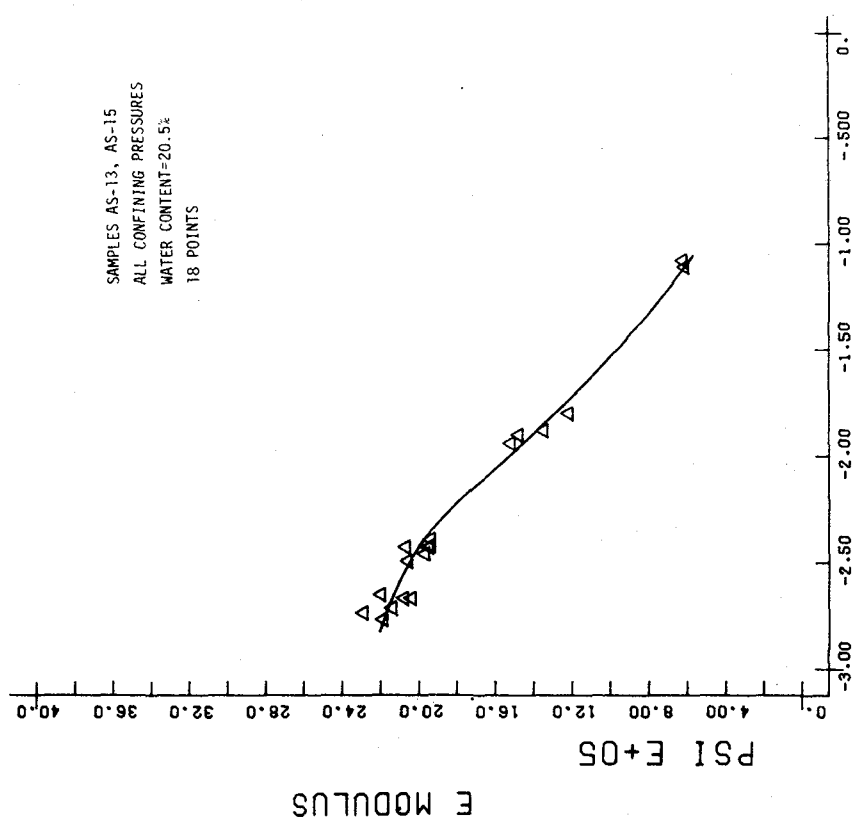

Figure A.45 A-SILTT-10F10

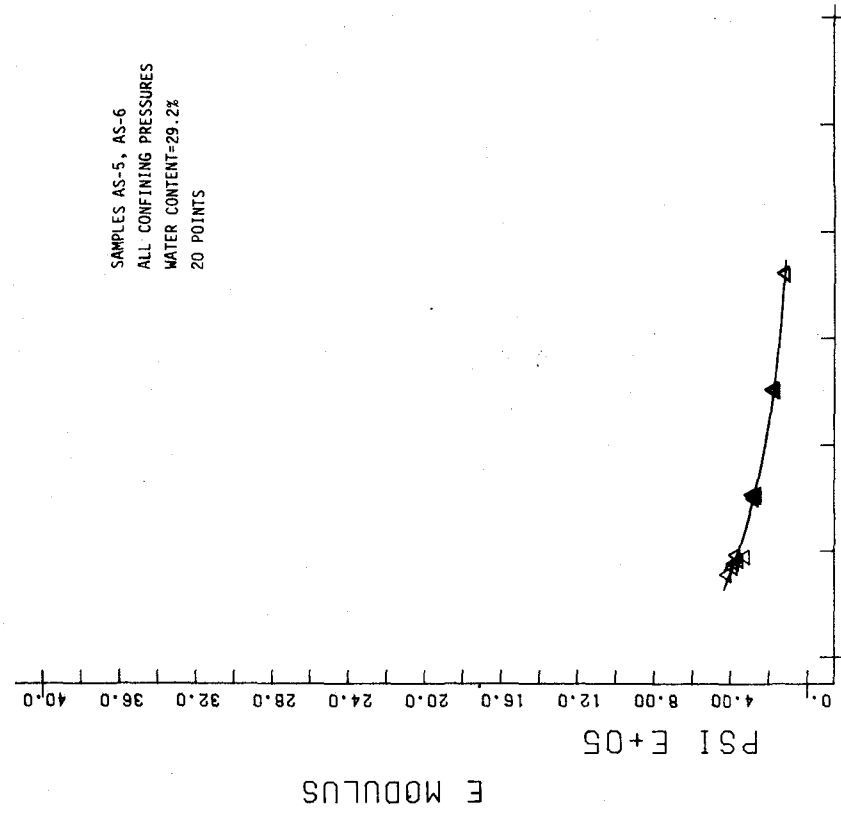

Figure A.48 A-SILTT-1F1

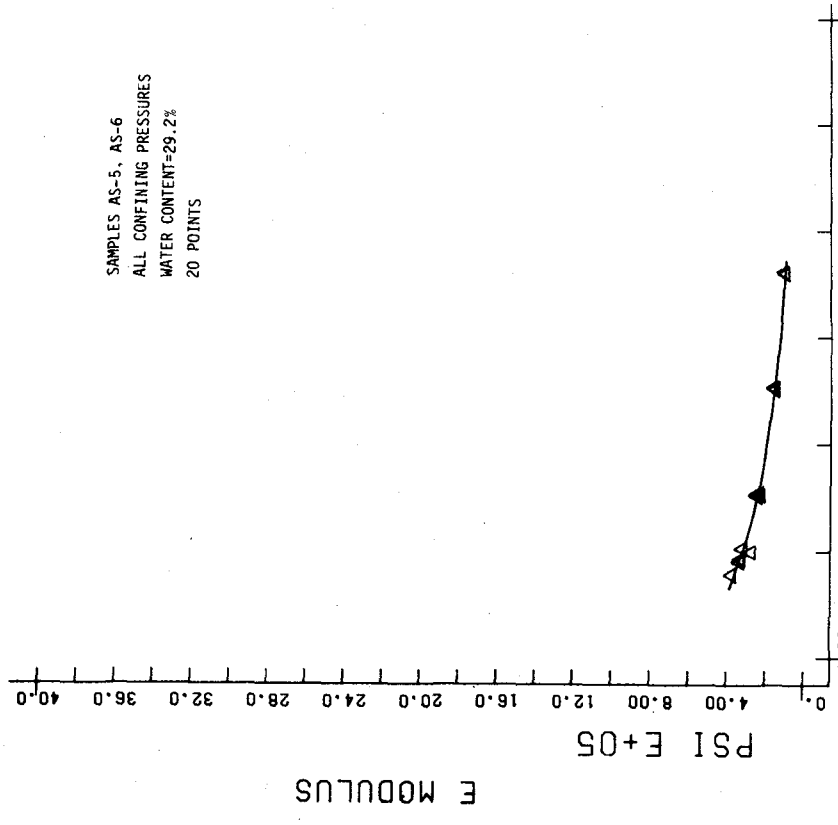

Figure A.47 A-SILTT-1F3

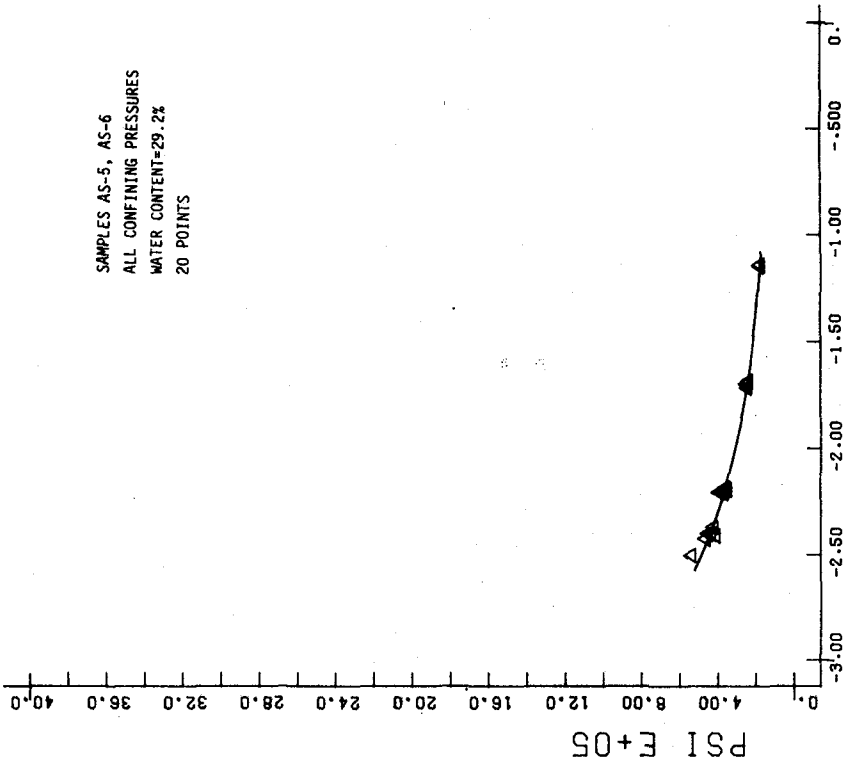

Figure A.50 A-SILTT-1F10

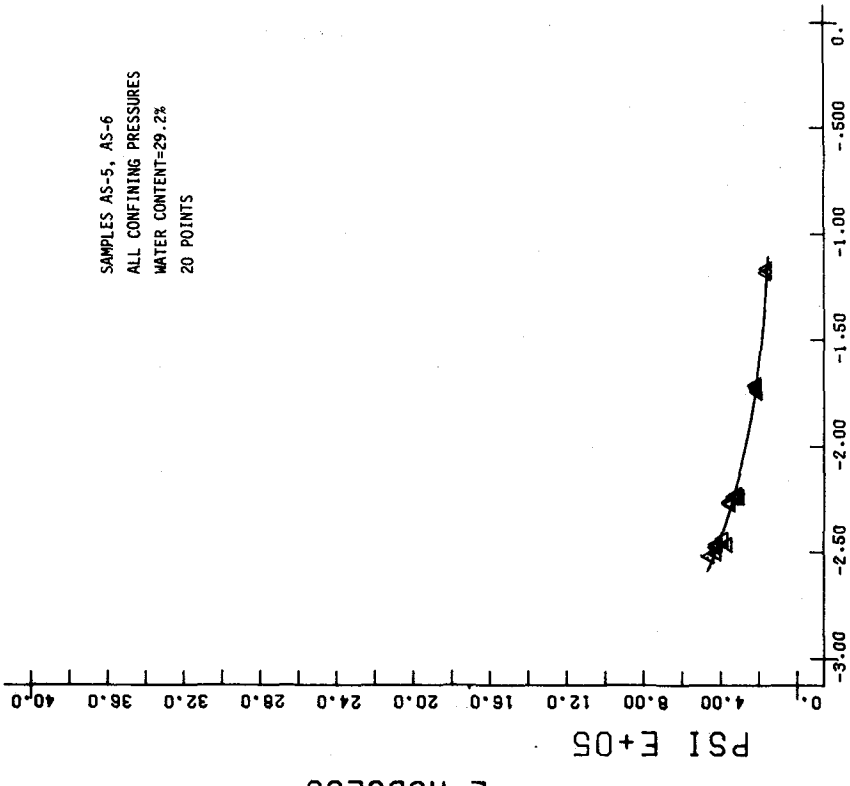

Figure A.49 A-SILTT-1F5

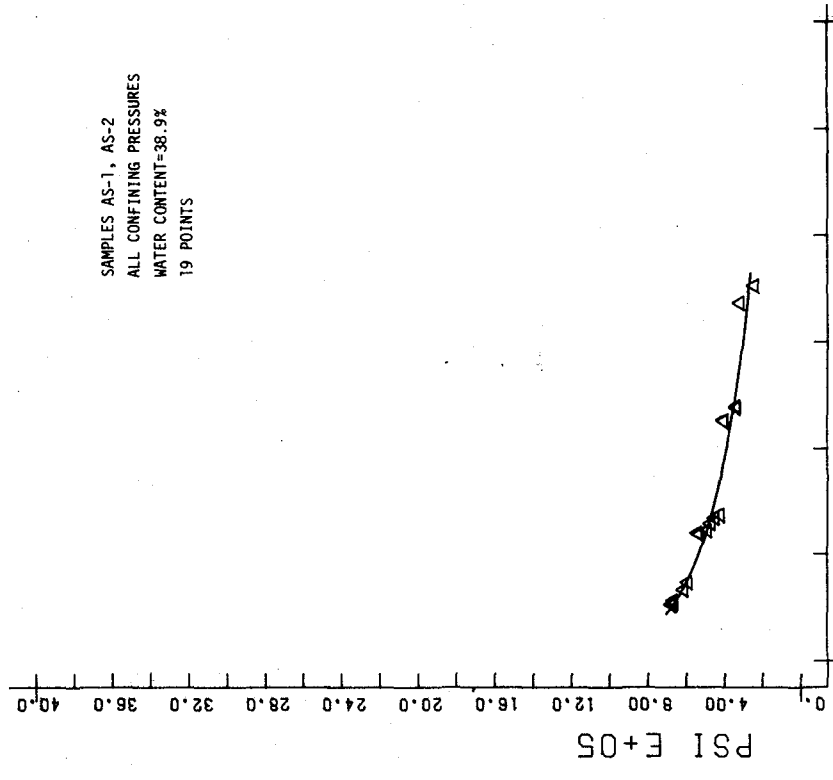
SAMPLES AS-1, AS-2
ALL CONFINING PRESSURES
WATER CONTENT=38.9%
19 POINTS
E MODULUS
PSI E+05
0.
4.00
8.00
12.0
16.0
20.0
24.0
28.0
32.0
36.0
40.0
-3.00
-2.50
-2.00
-1.50
-1.00
-.500
0.
LOG PERCNT Figure A.52 AX STRAIN
A-SILTT-1F3

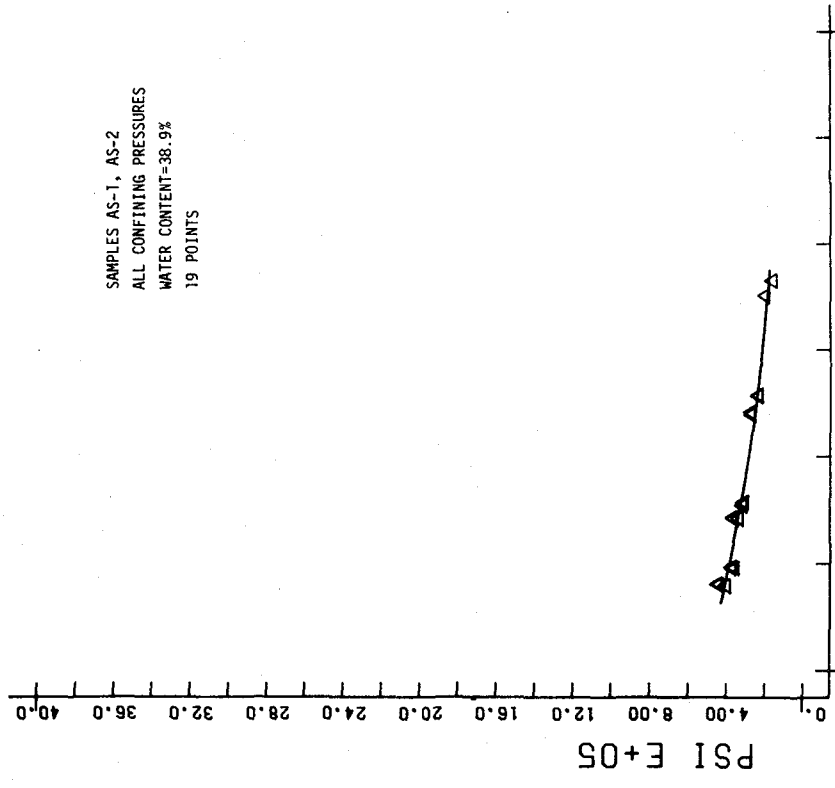
SAMPLES AS-1, AS-2
ALL CONFINING PRESSURES
WATER CONTENT=38.9%
19 POINTS
E MODULUS
PSI E+05
0.
4.00
8.00
12.0
16.0
20.0
24.0
28.0
32.0
36.0
40.0
-3.00
-2.50
-2.00
-1.50
-1.00
-.500
0.
LOG PERCNT Figure A.51 AX STRAIN
A-SILTT-1F05

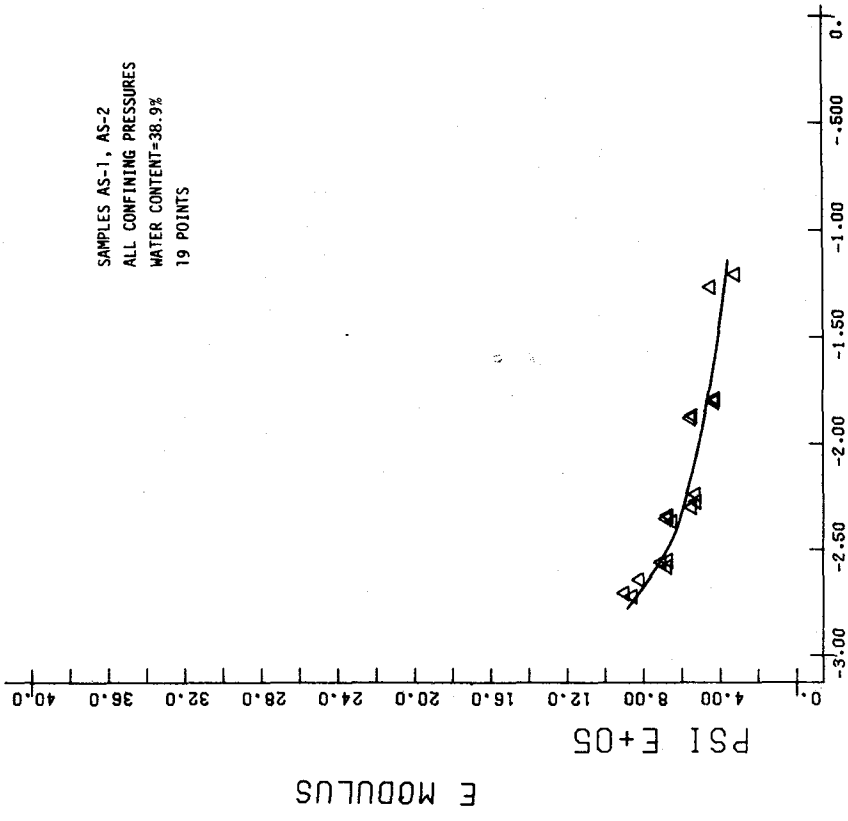

Figure A.54 A-SILTT-1F5

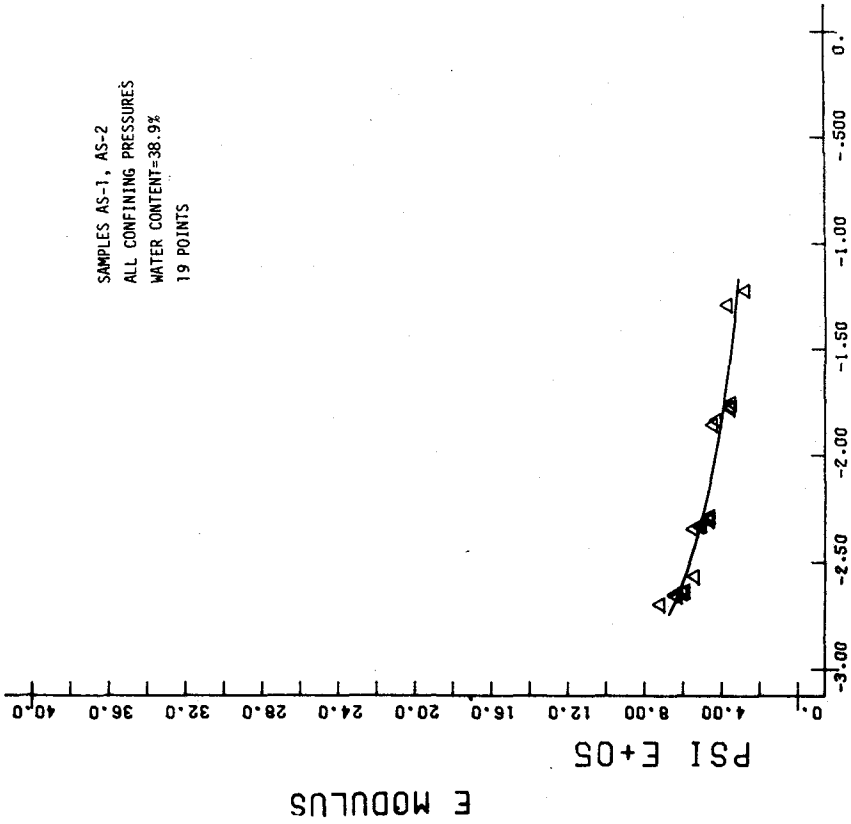

Figure A.53 A-SILTT-1F1

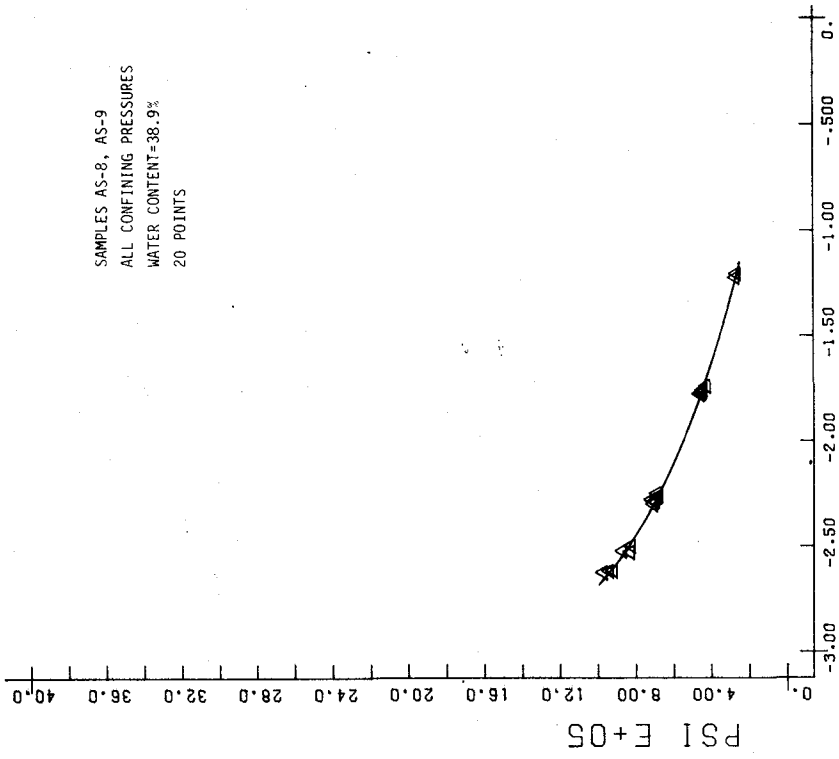

Figure A.56 A-SILTT-4F05

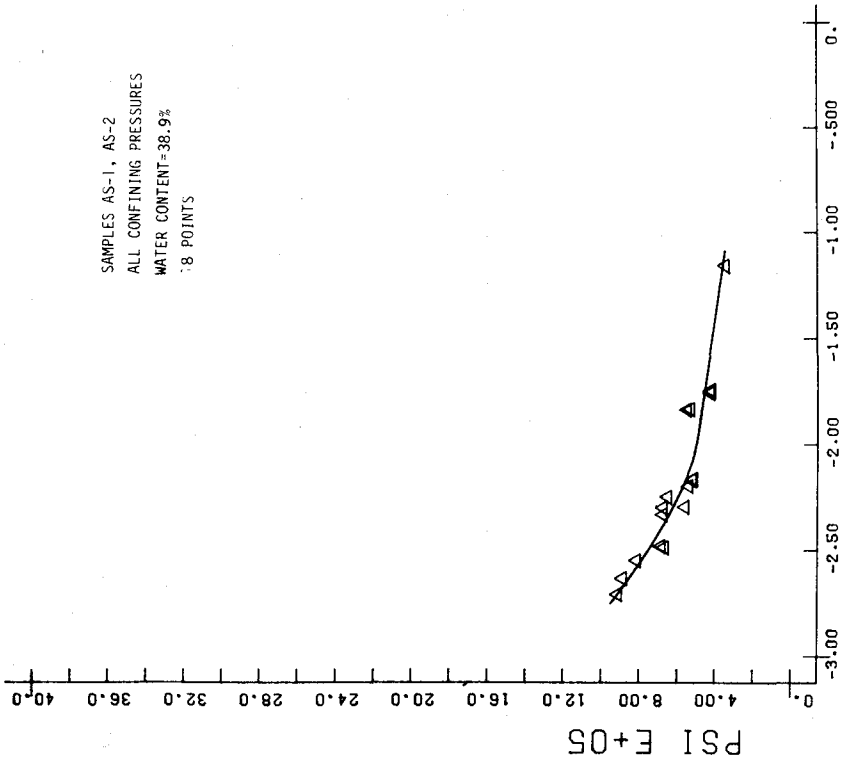

Figure A.55 A-SILTT-1F10

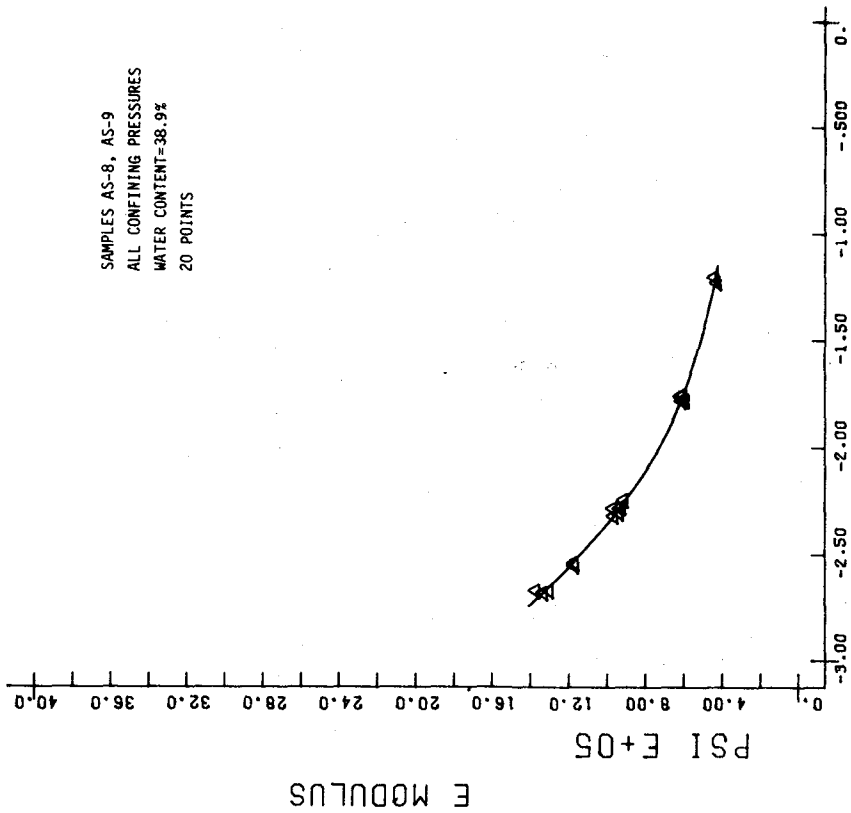

Figure A.58 AX STRAIN

A-SILTT-4F1

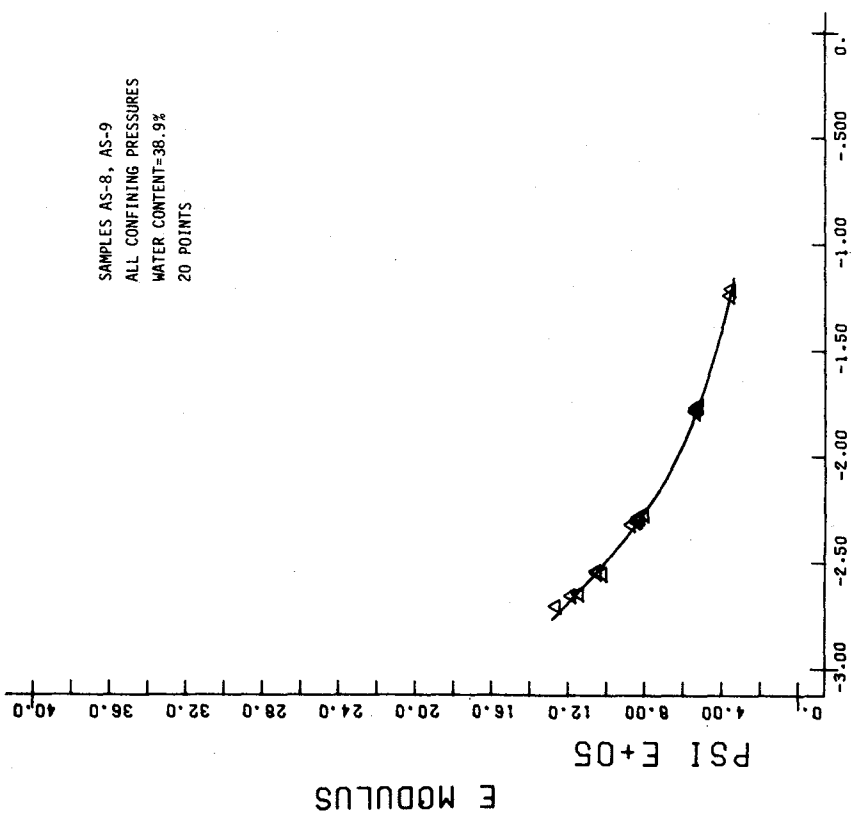

Figure A.57 AX STRAIN

A-SILTT-4F3

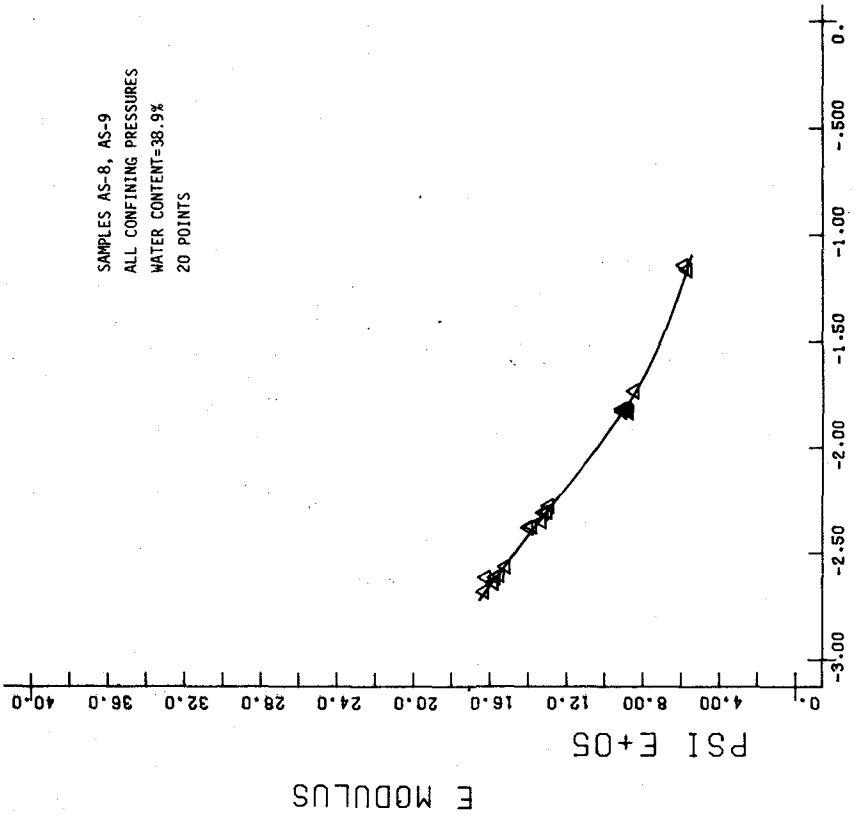

Figure A.60 AX STRAIN

A-SILTT-4F10

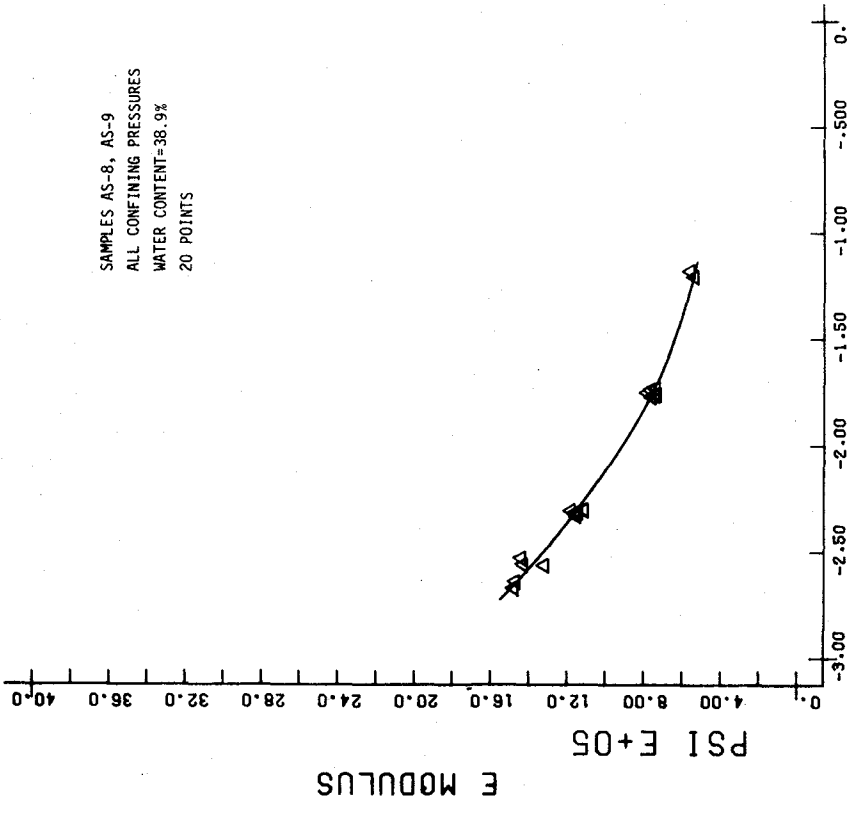

Figure A.59 AX STRAIN

A-SILTT-4F5

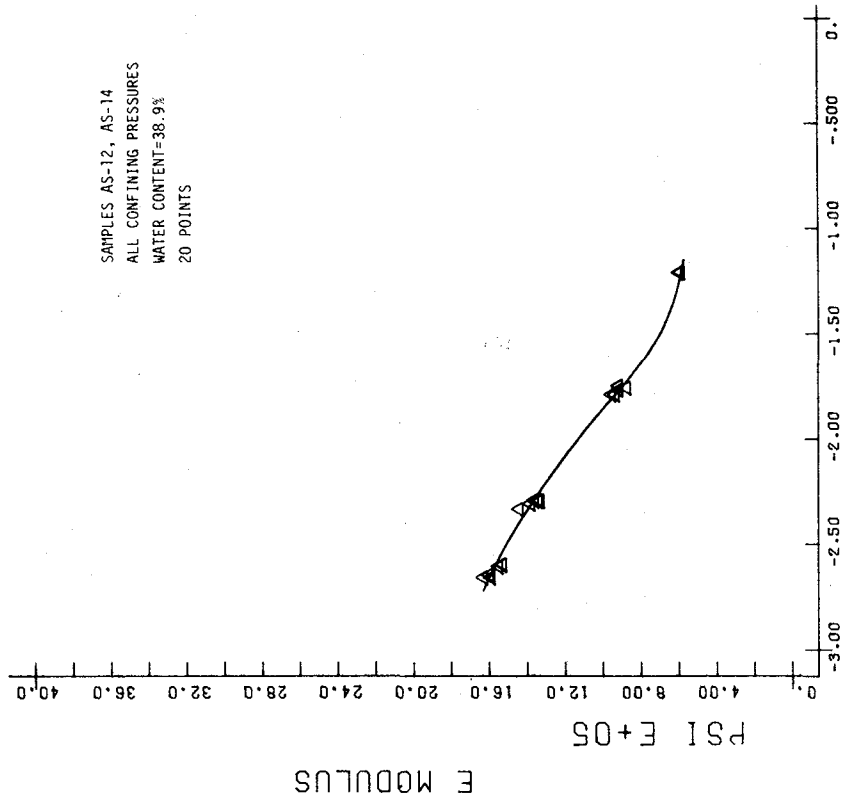

Figure A.62 A-SILTT-10F3

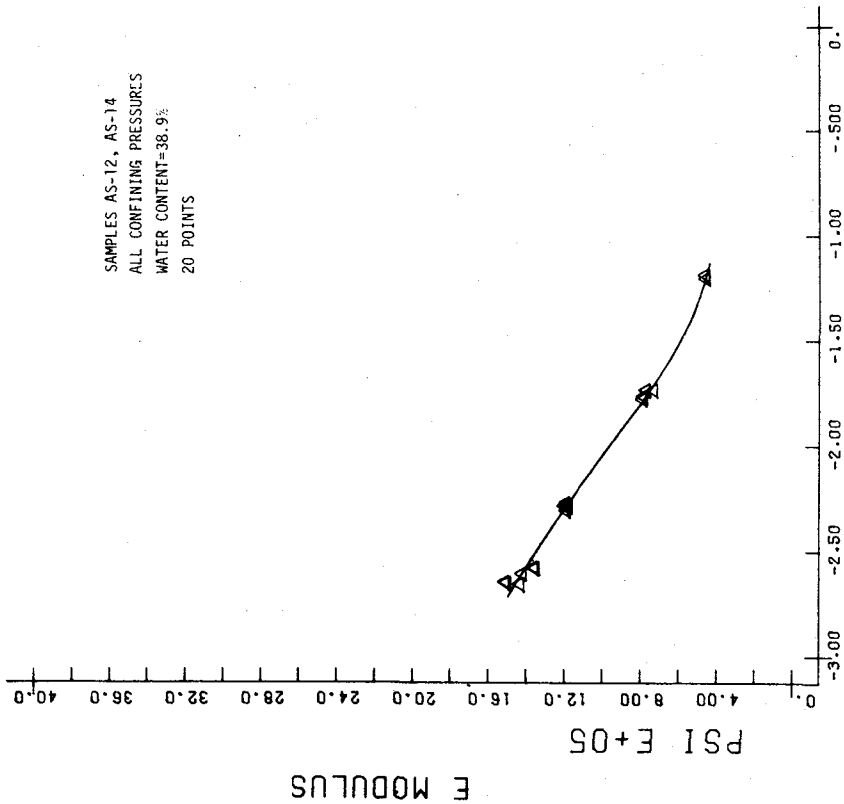

Figure A.61 A-SILTT-10F.05

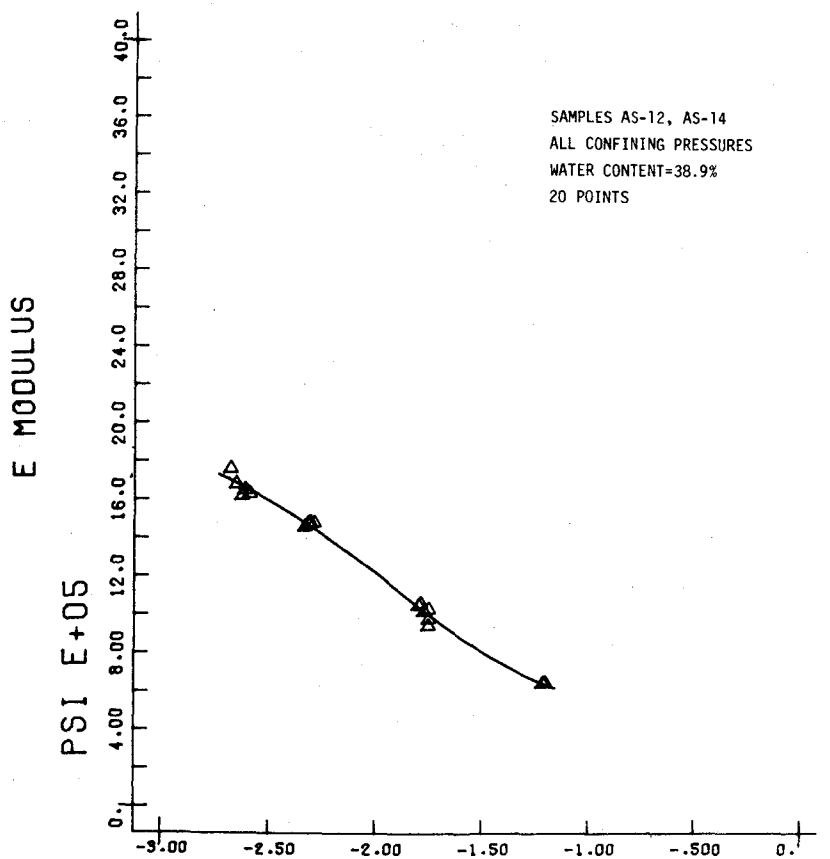

Figure A.63

A-SILTT-10F1

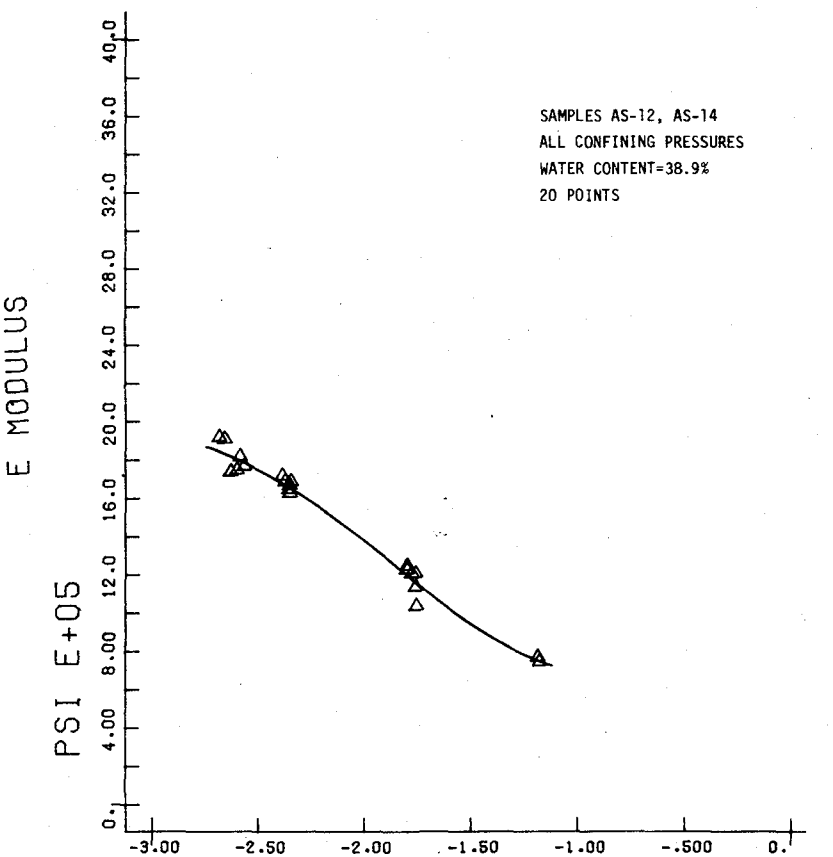

Figure A.64

A-SILTT-10F5

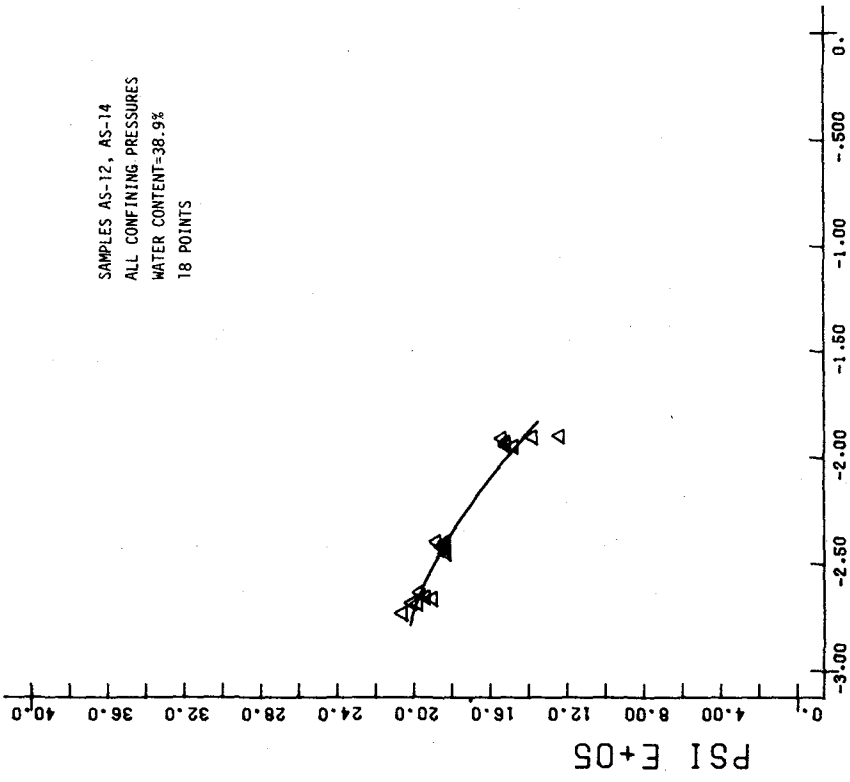

A-SILTT-10F10

APPENDIX B

CYCLIC TRIAXIAL TESTS RESULTS: DAMPING RATIO OF FROZEN SILT

Test results for Hanover silt are shown in Figures B.1 to B.30. Test results for Alaska silt are shown in Figures B.31 to B.65.

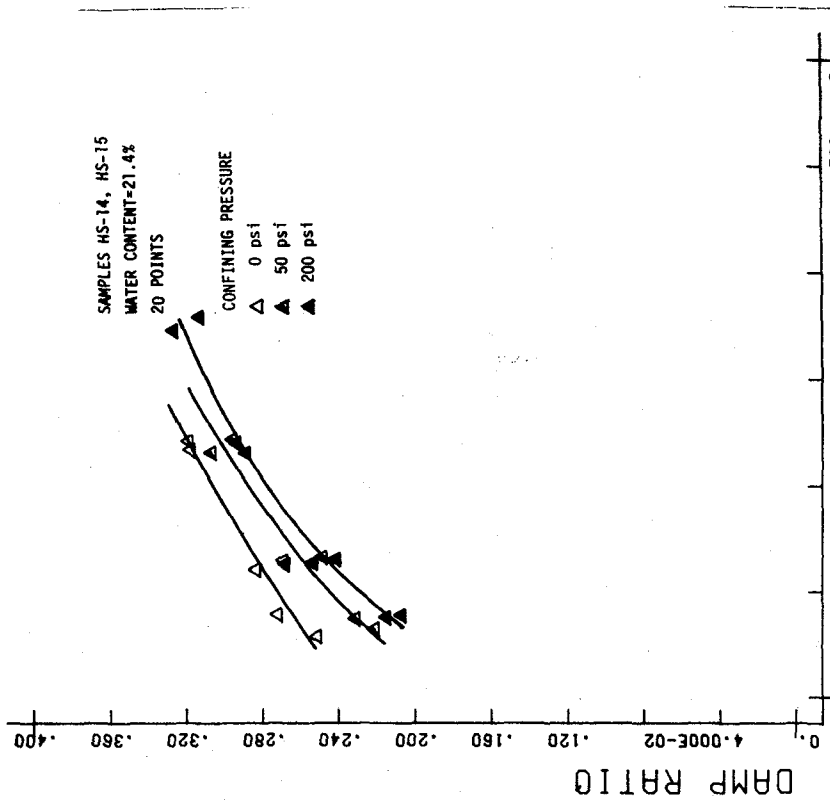

Figure B.2 H-SILTT-1F3

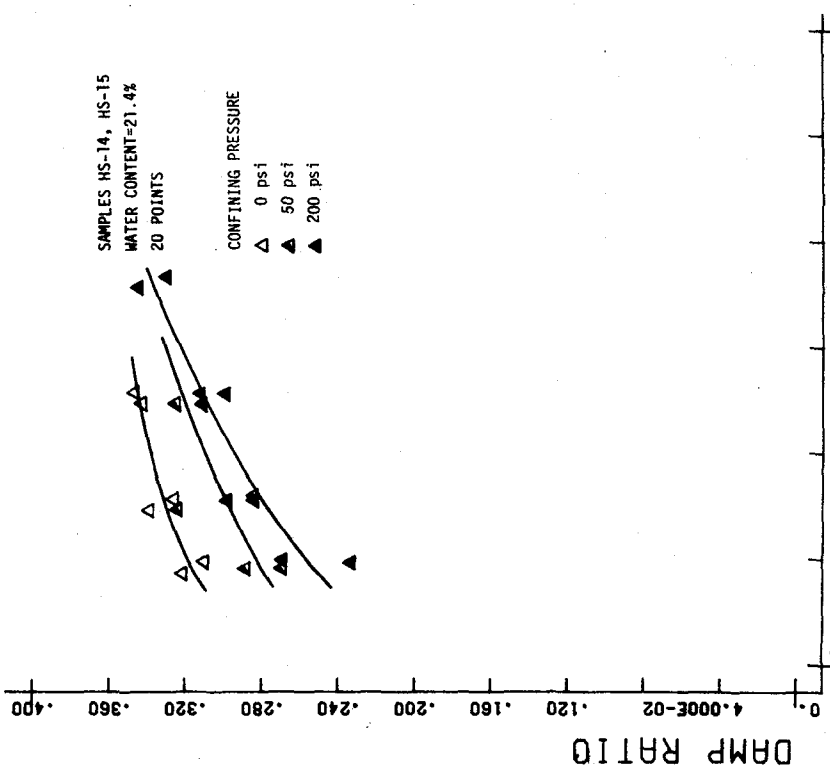

Figure B.1 H-SILTT-1F.05

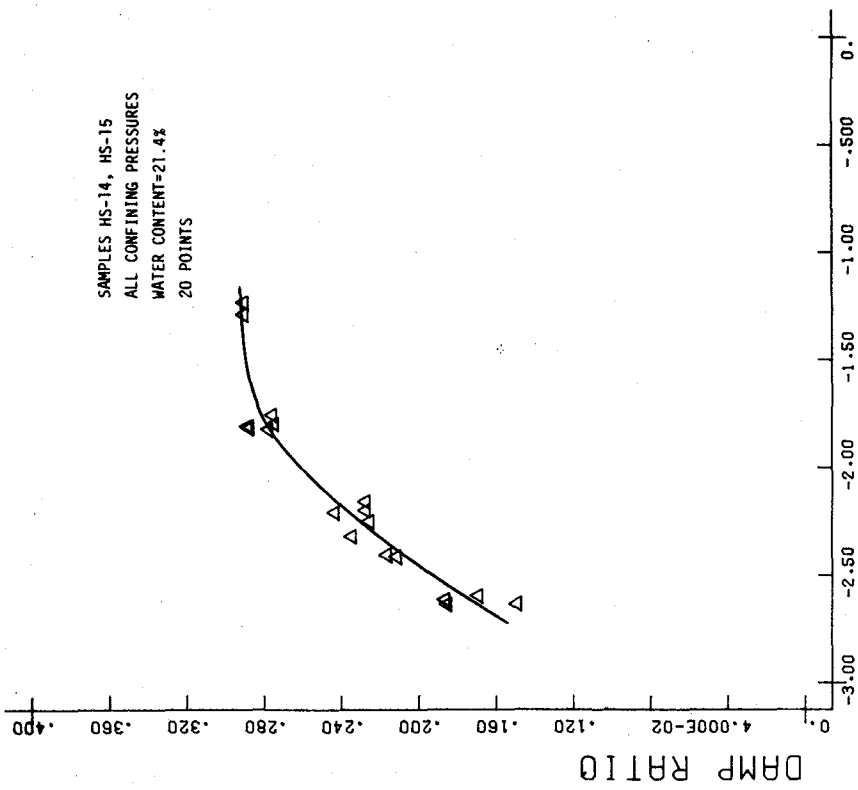

Figure B.4 H-SILTT-1F5

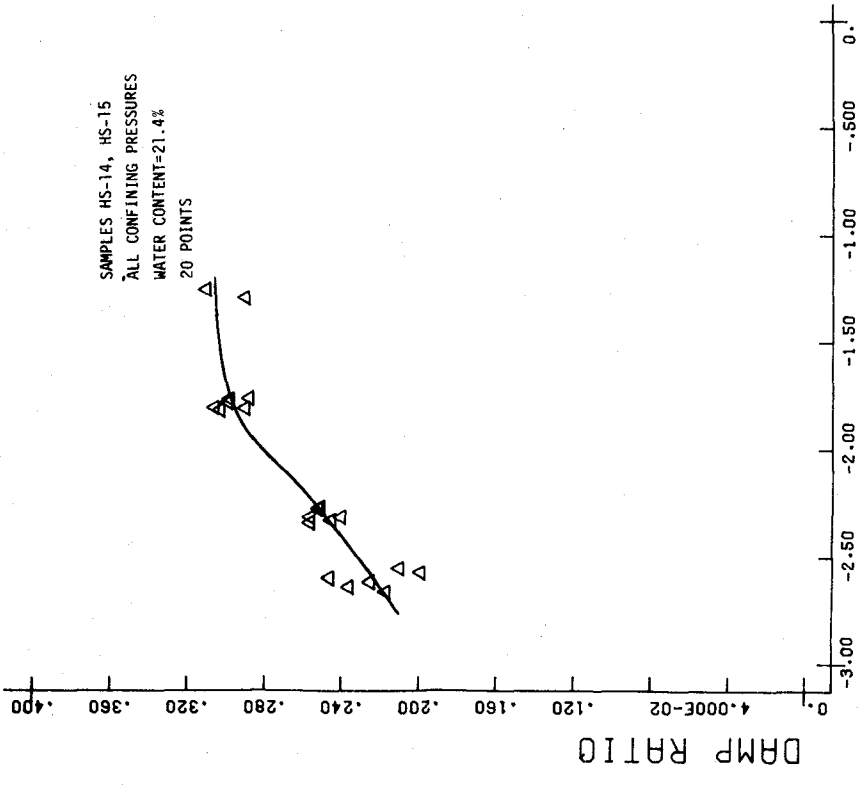

Figure B.3 H-SILTT-1F1

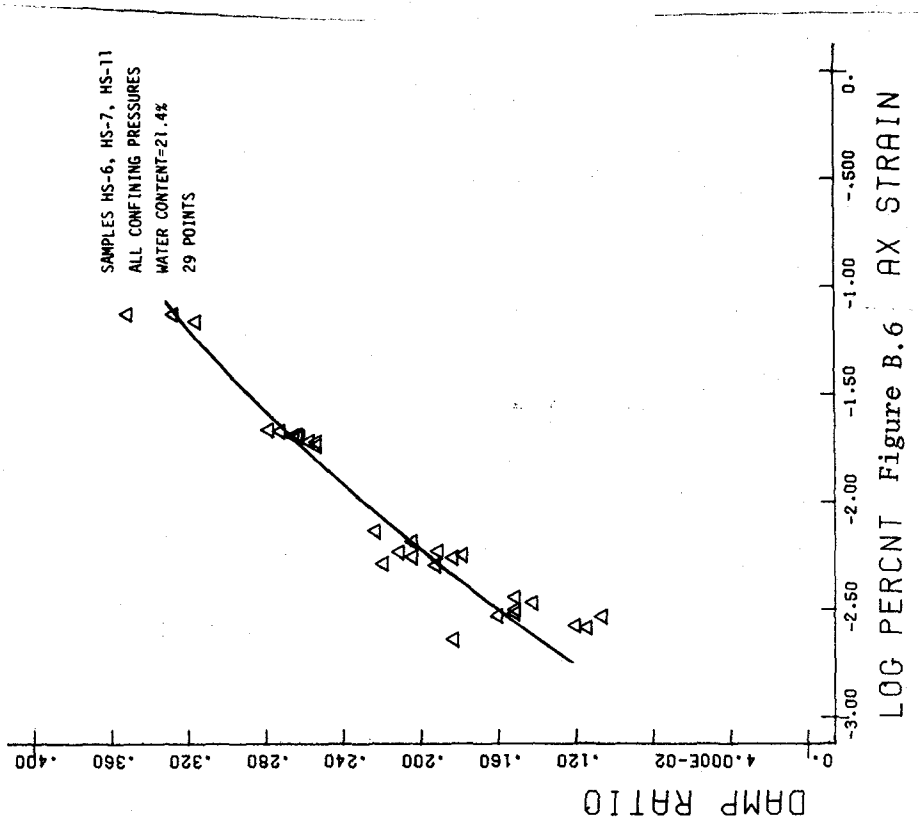

Figure B.6 H-SILTT-4F05

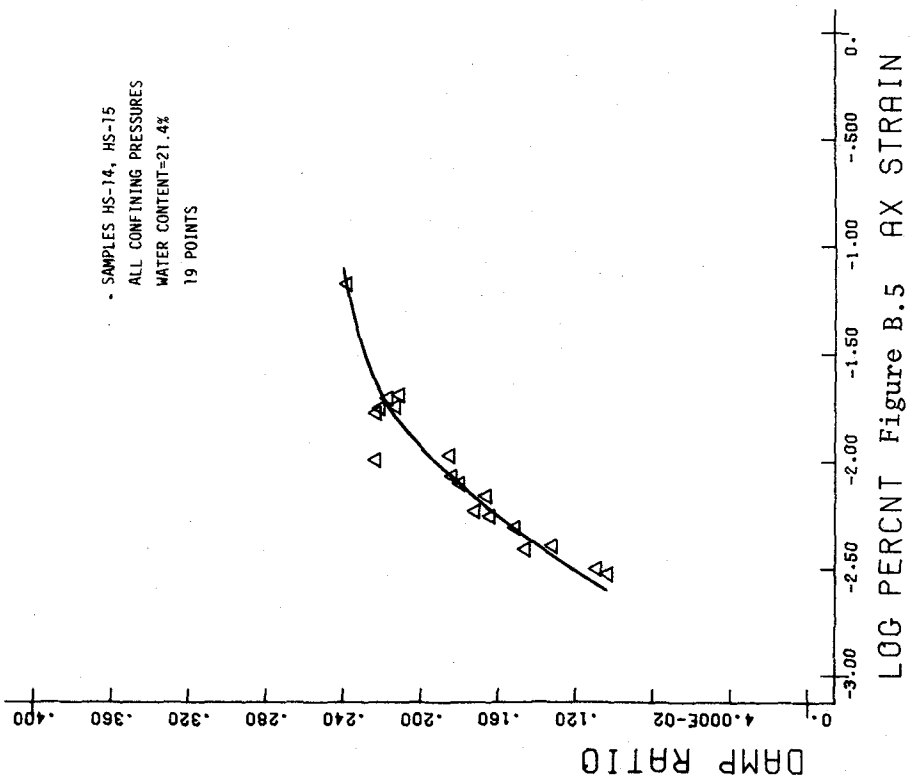

Figure B.5 H-SILTT-1F10

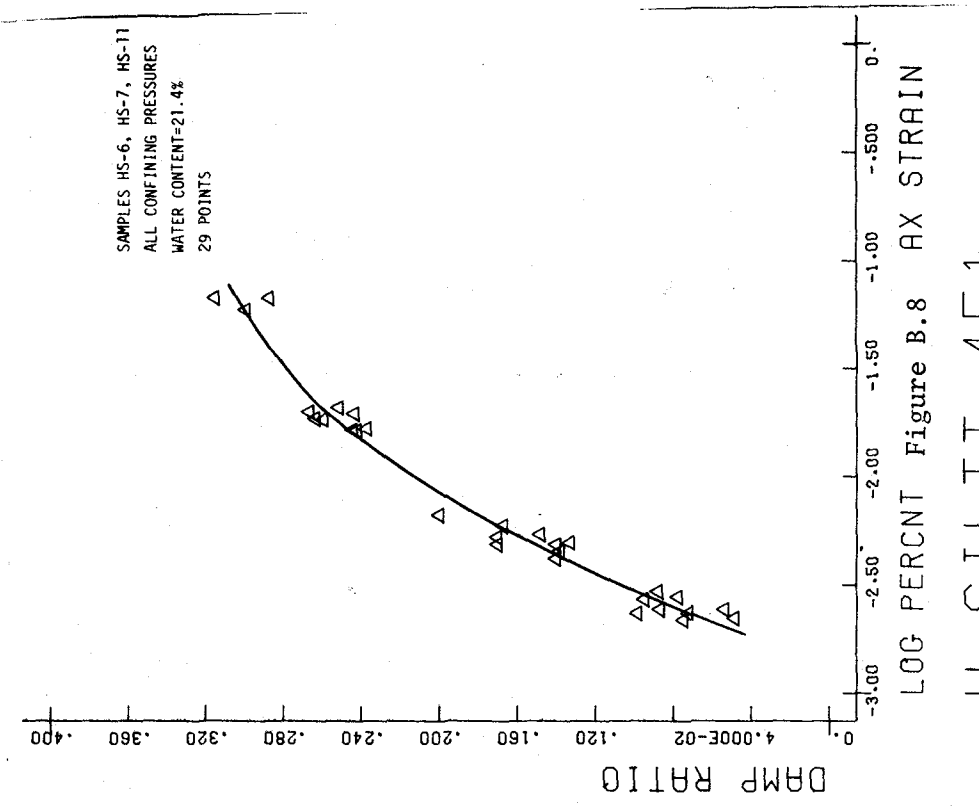

H-SILTT-4F1

Figure B.8

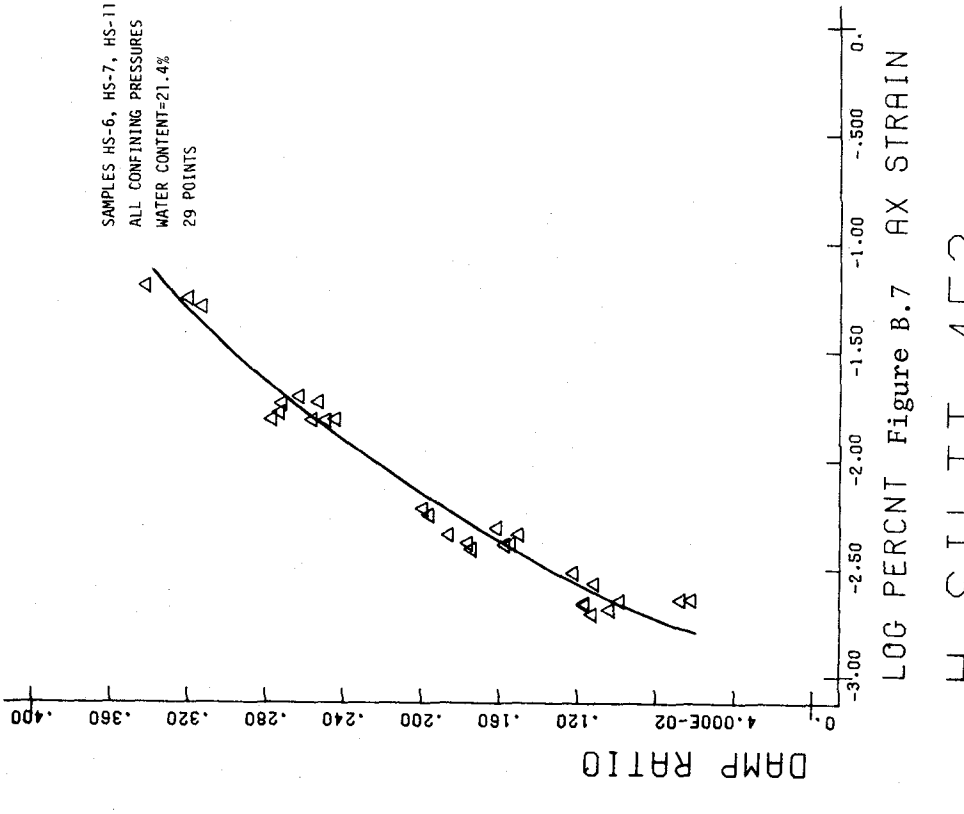

H-SILTT-4F3

Figure B.7

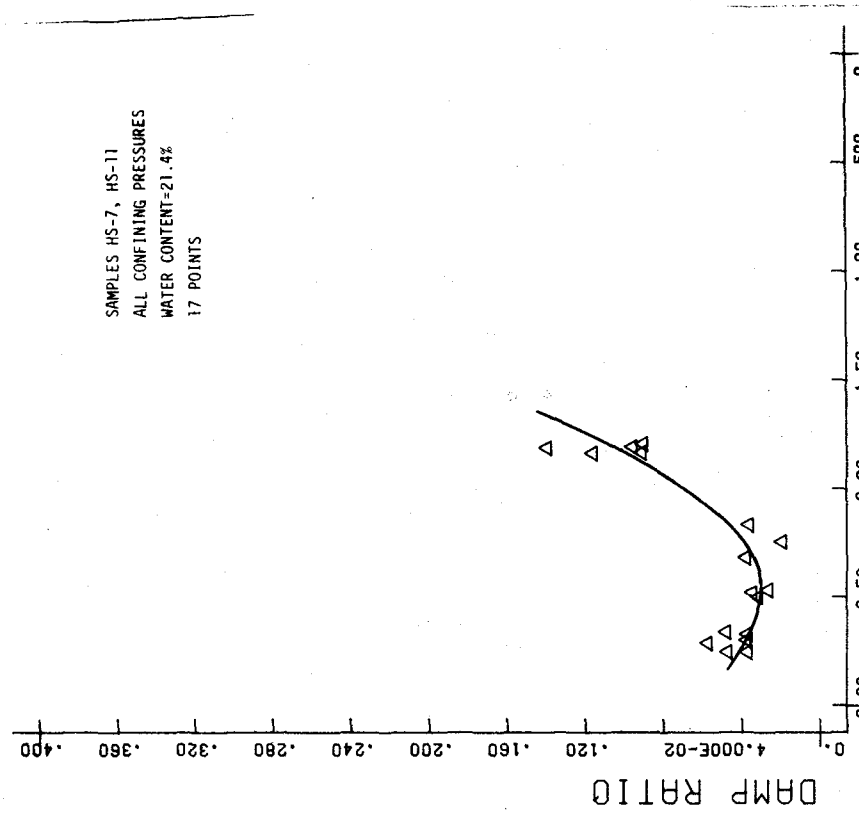

Figure B.10 AX STRAIN

H-SILTT-4F10

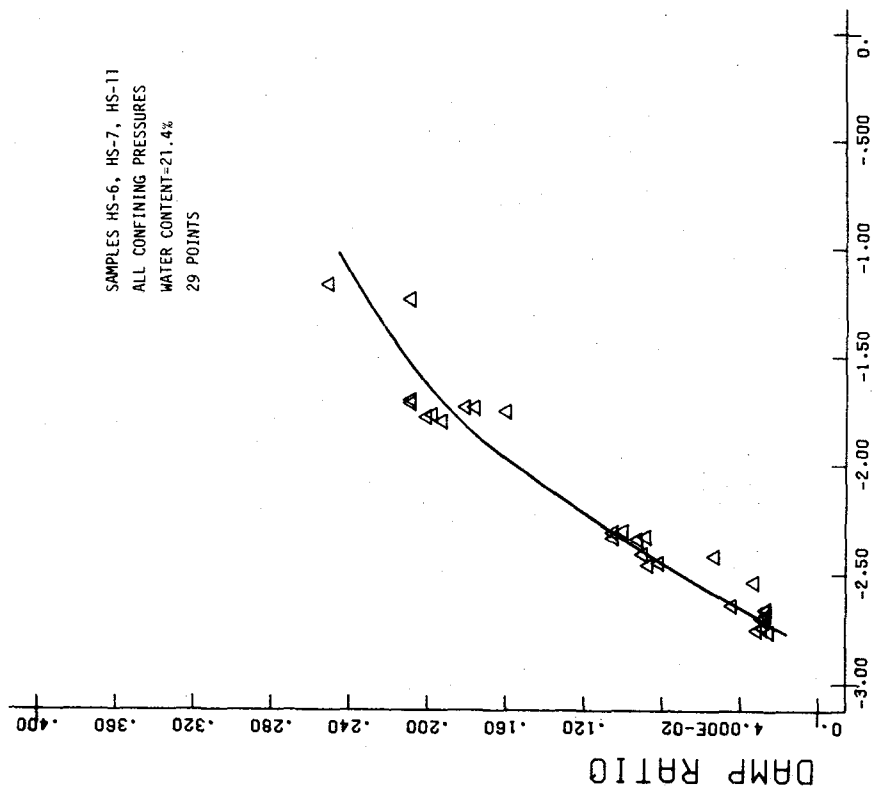

Figure B.9 AX STRAIN

H-SILTT-4F5

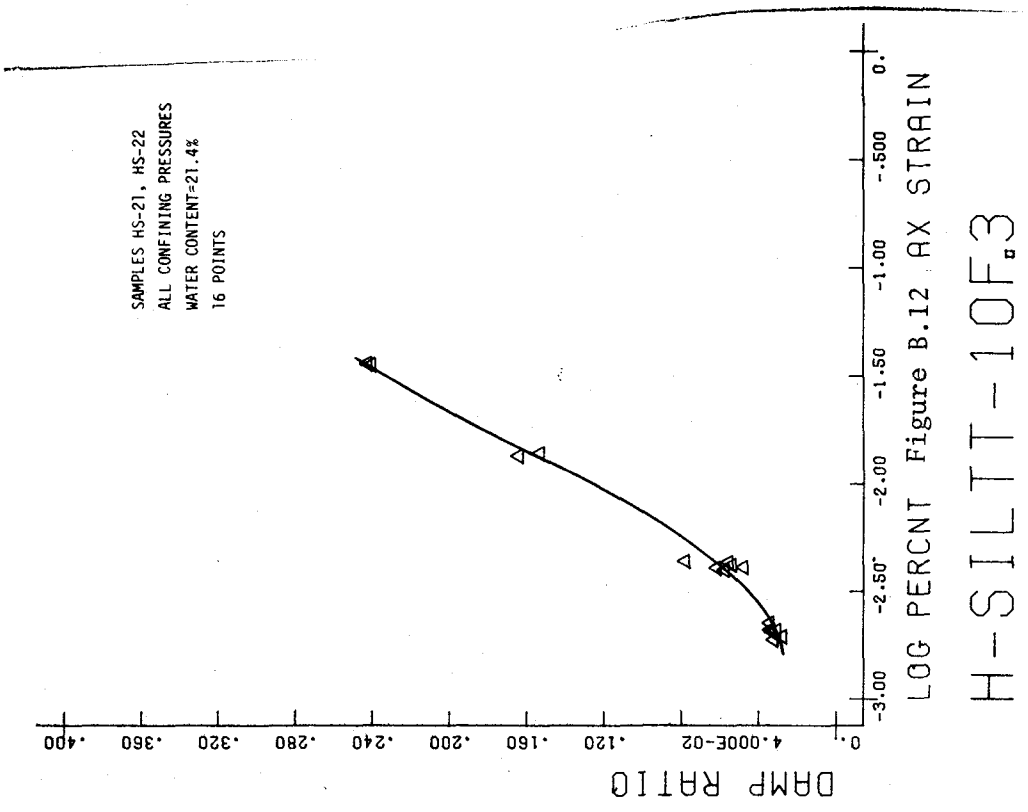

Figure B.12 H-SILTT-10F3

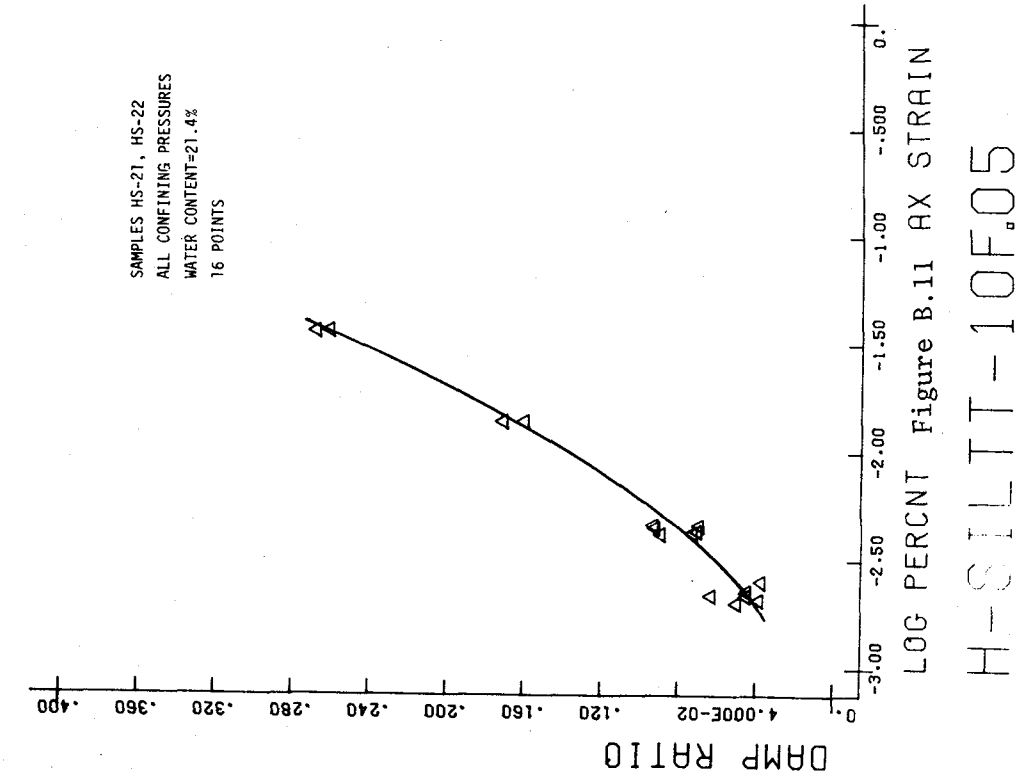

Figure B.11 H-SILTT-10F05

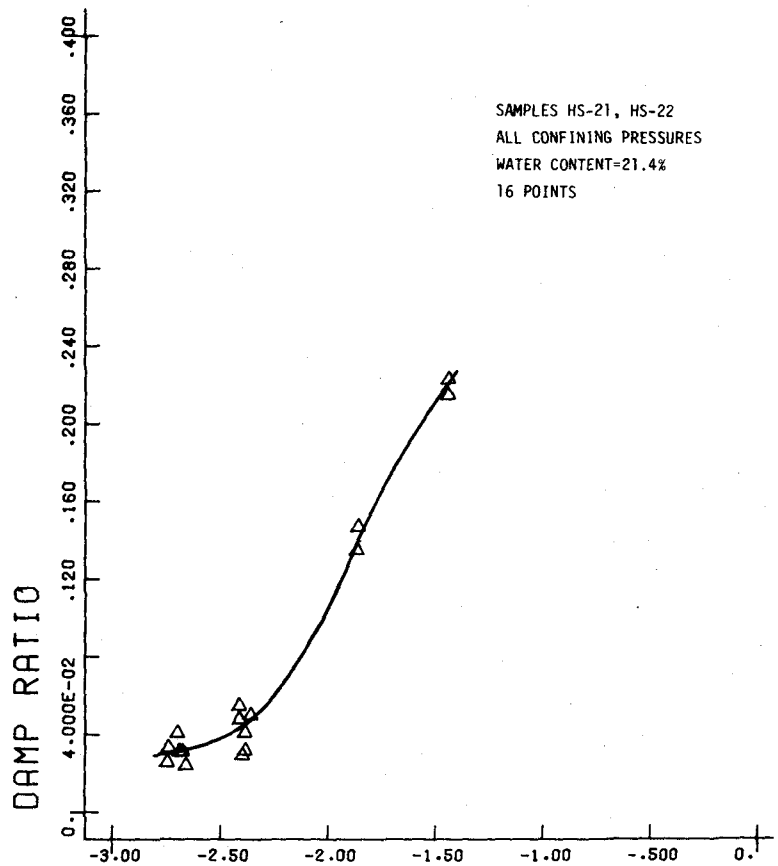

Figure B.13

H-SILTT-10F1

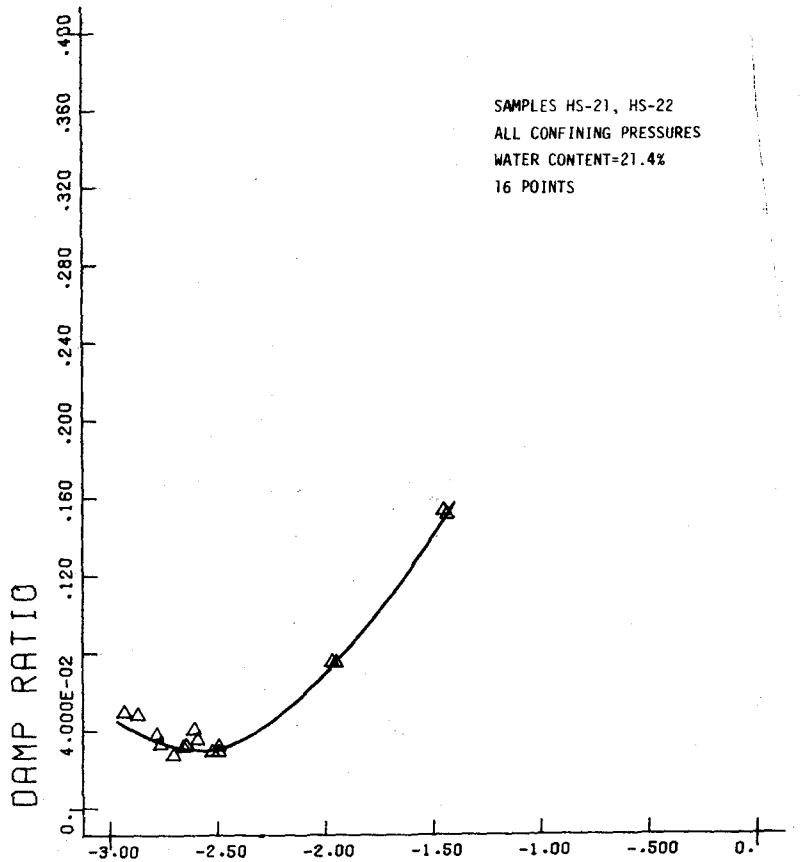

Figure B.14

H-SILTT-10F5

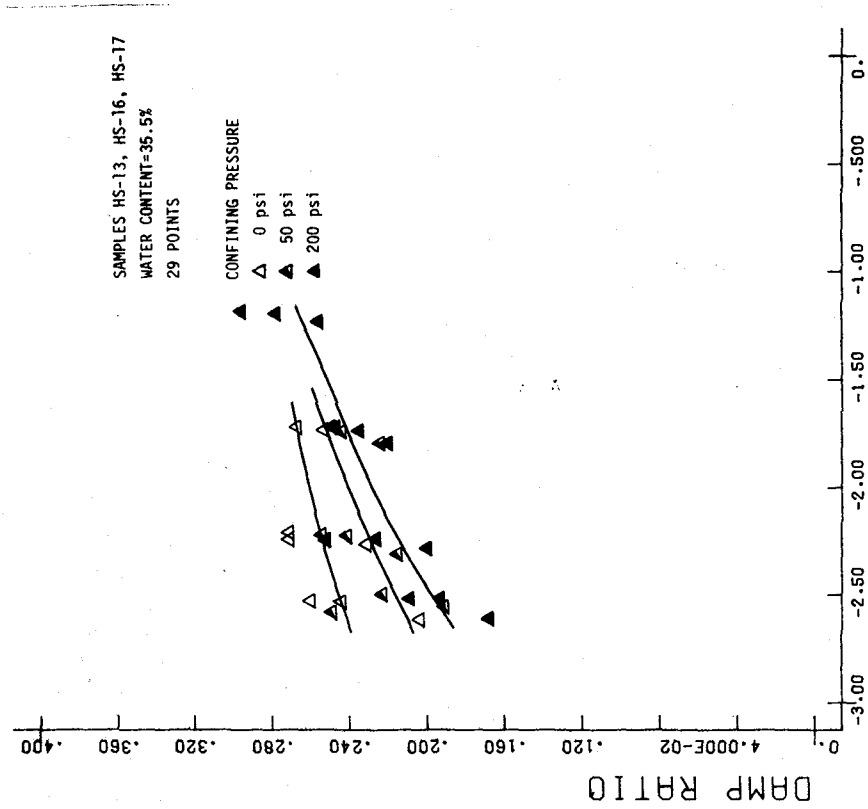

H-SILTT-1F.05

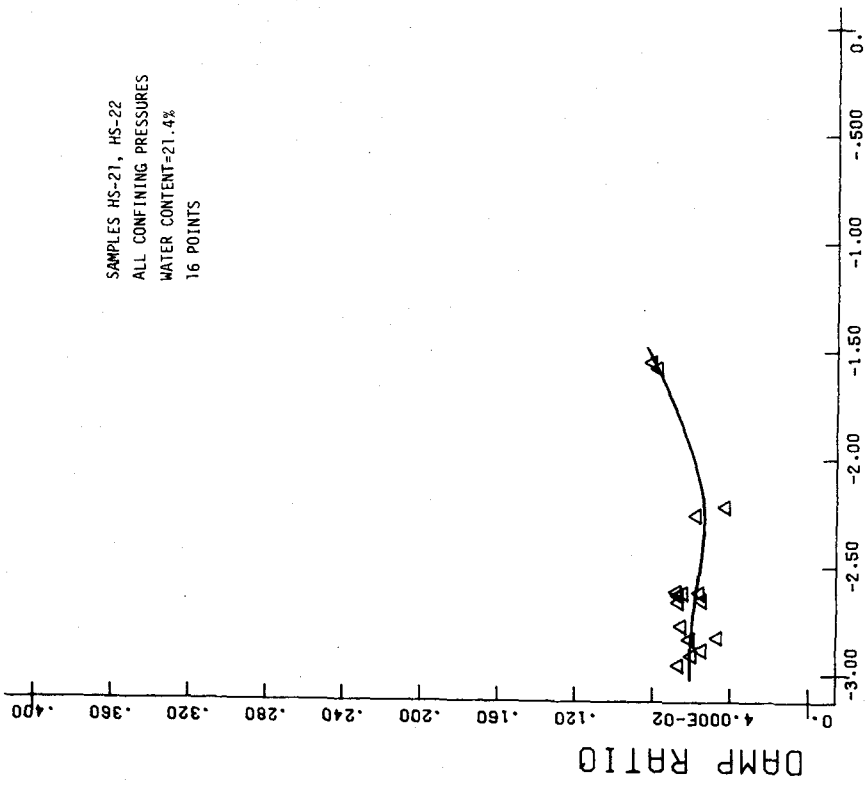

H-SILTT-10F10

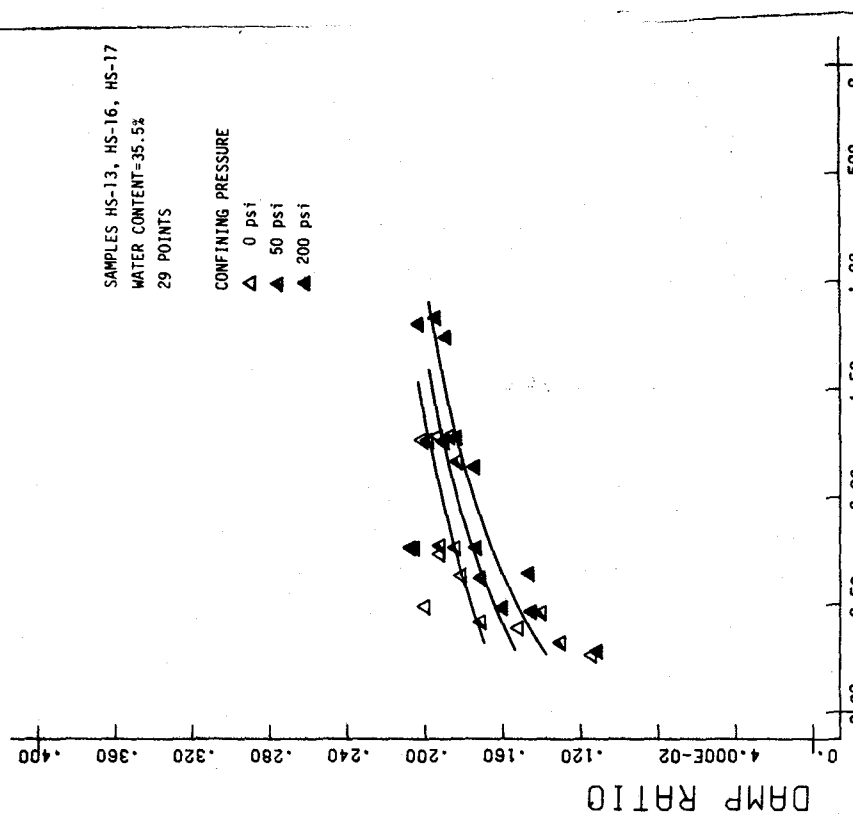

Figure B.18 H-SILTT-1F1

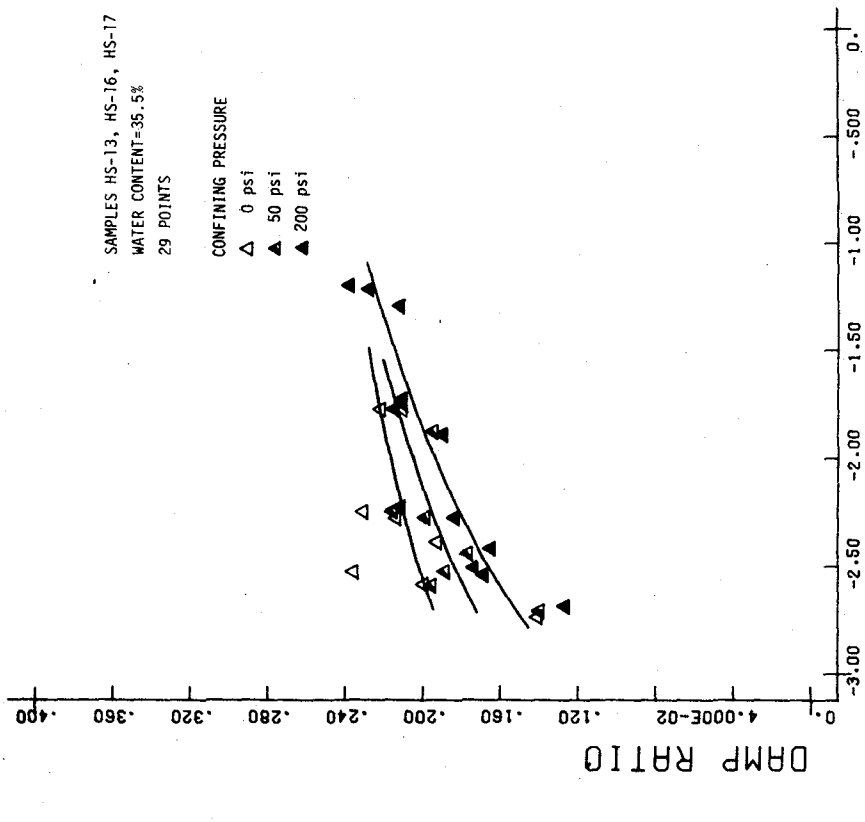

Figure B.17 H-SILTT-1F3

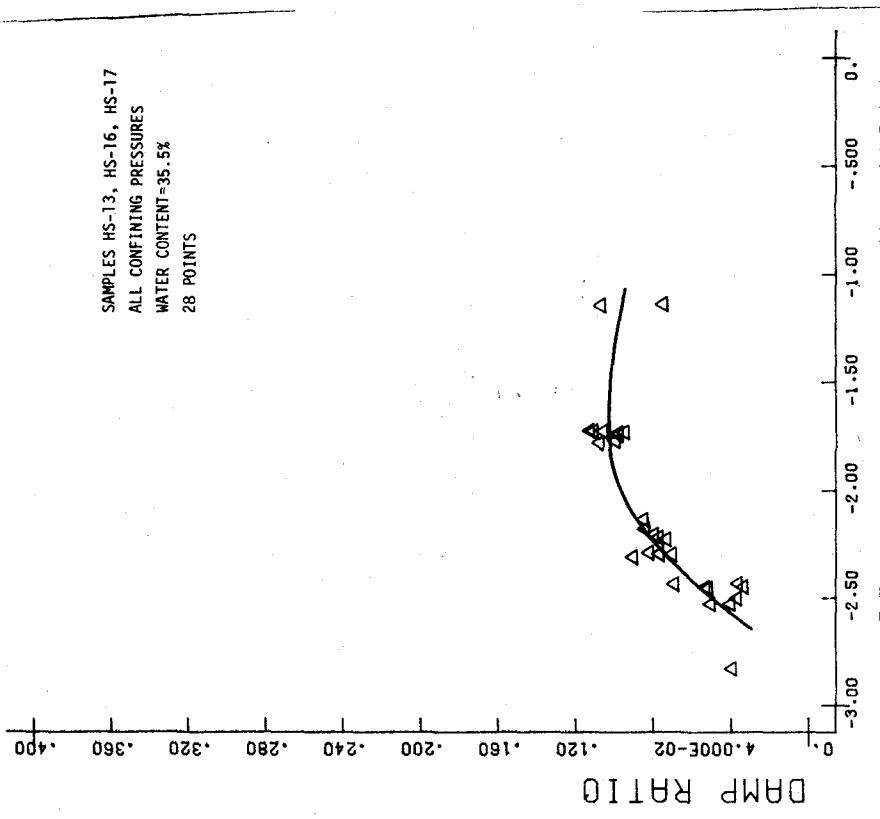

H-SILTT-1F10

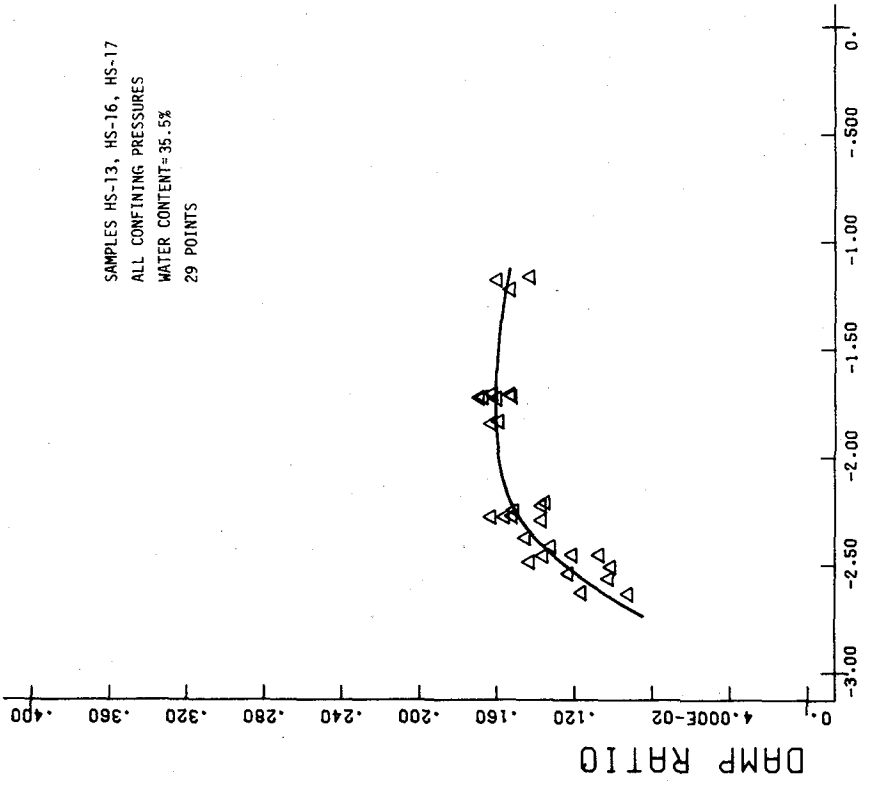

H-SILTT-1F5

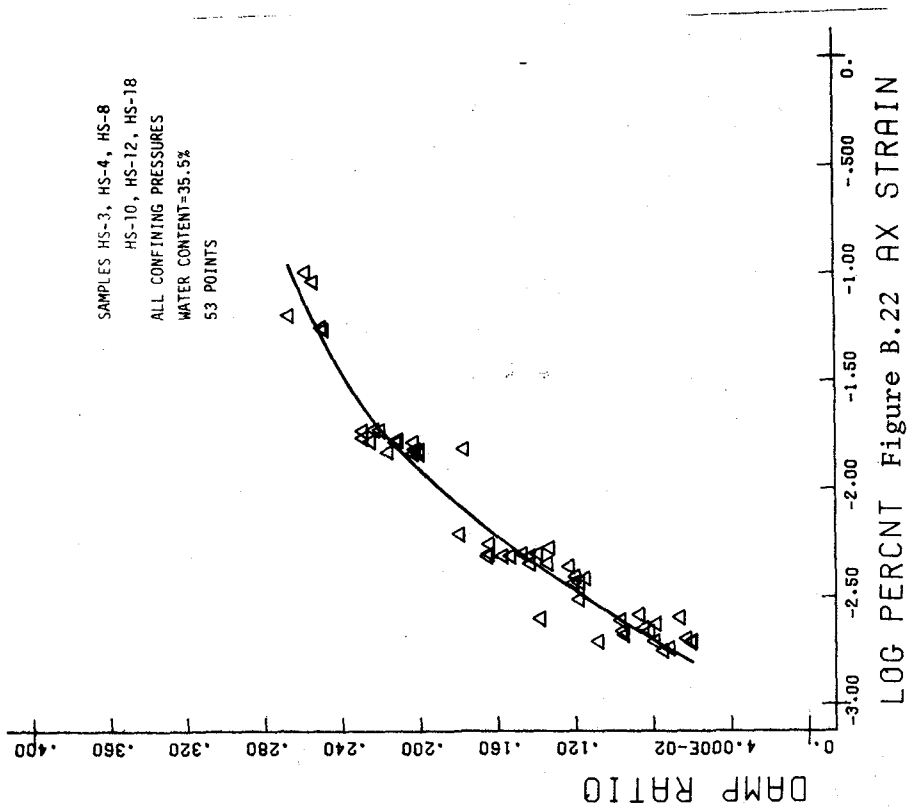

Figure B.22 AX STRAIN

H-SILTT-4F3

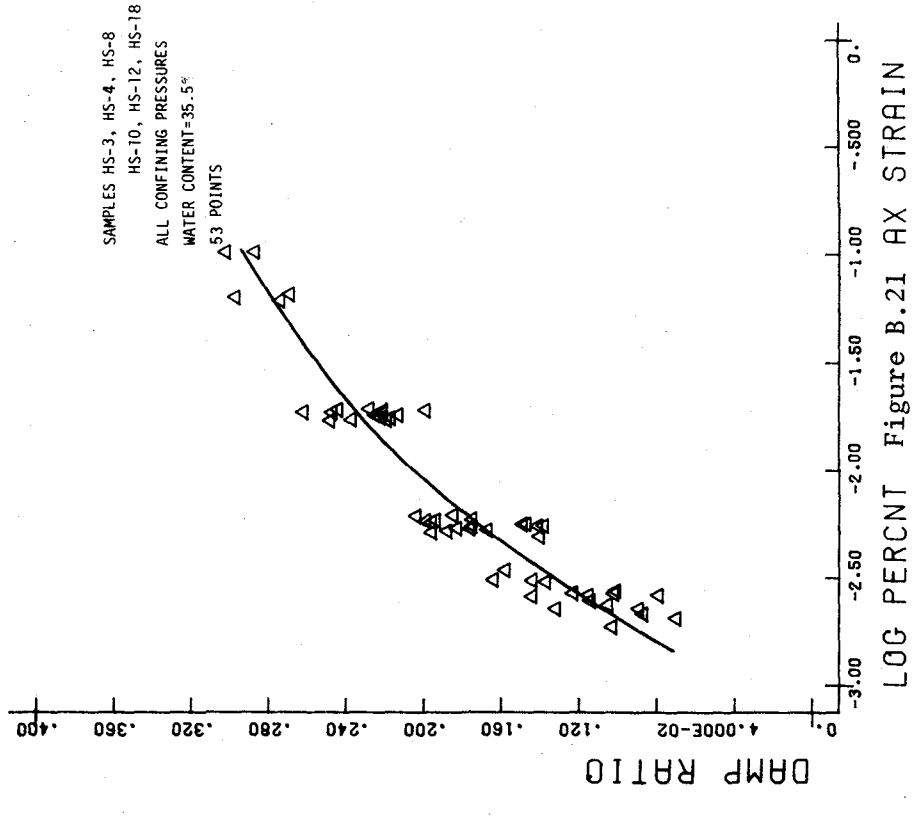

Figure B.21 AX STRAIN

H-SILTT-4F05

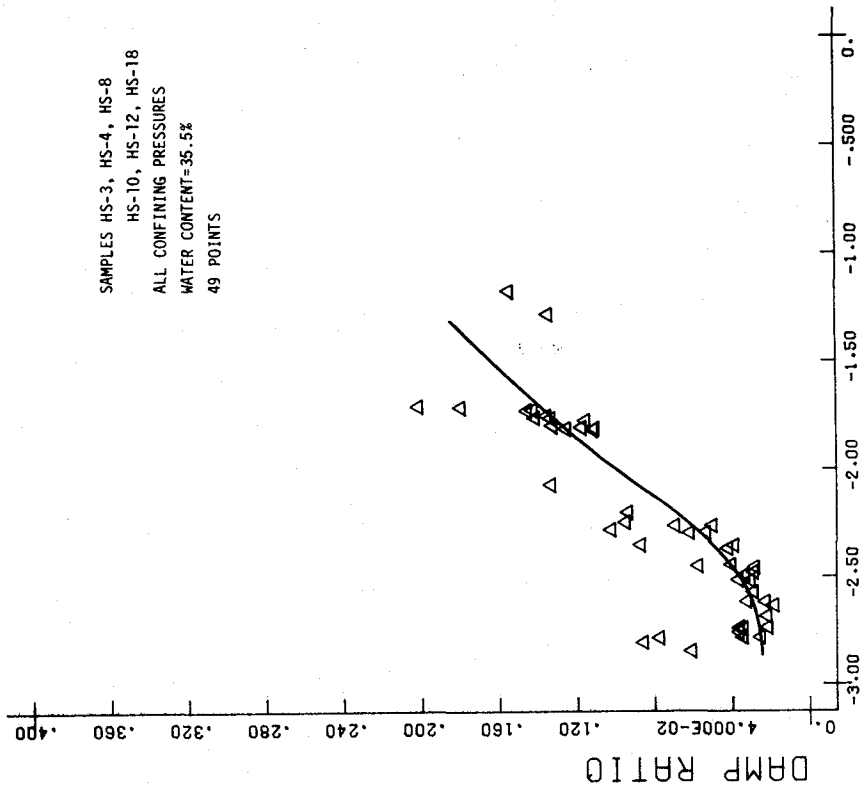

H-SILTT-4F5

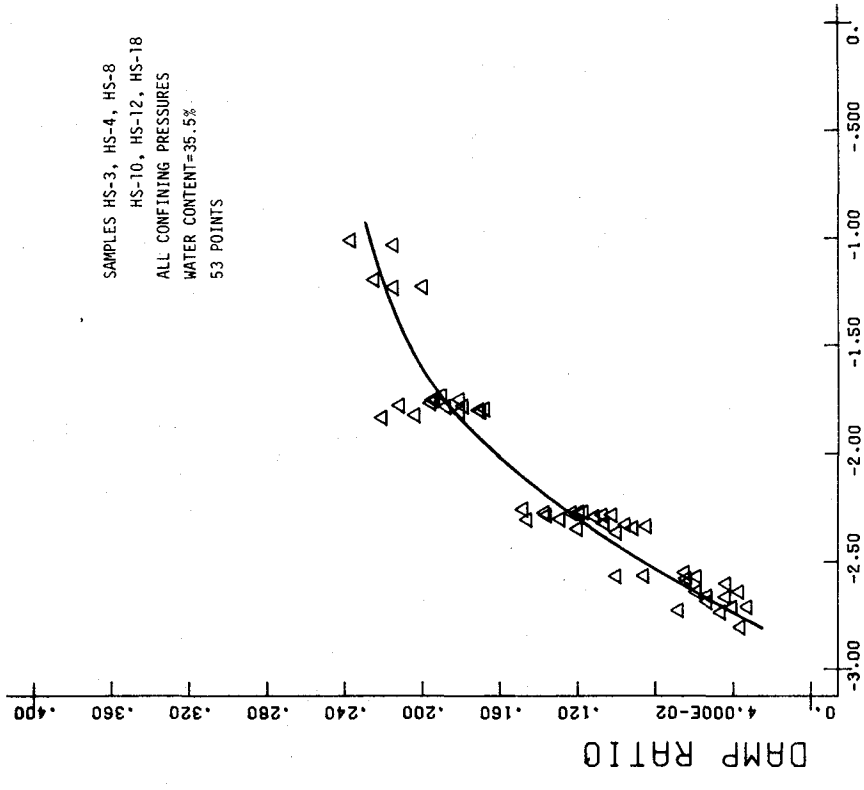

H-SILTT-4F1

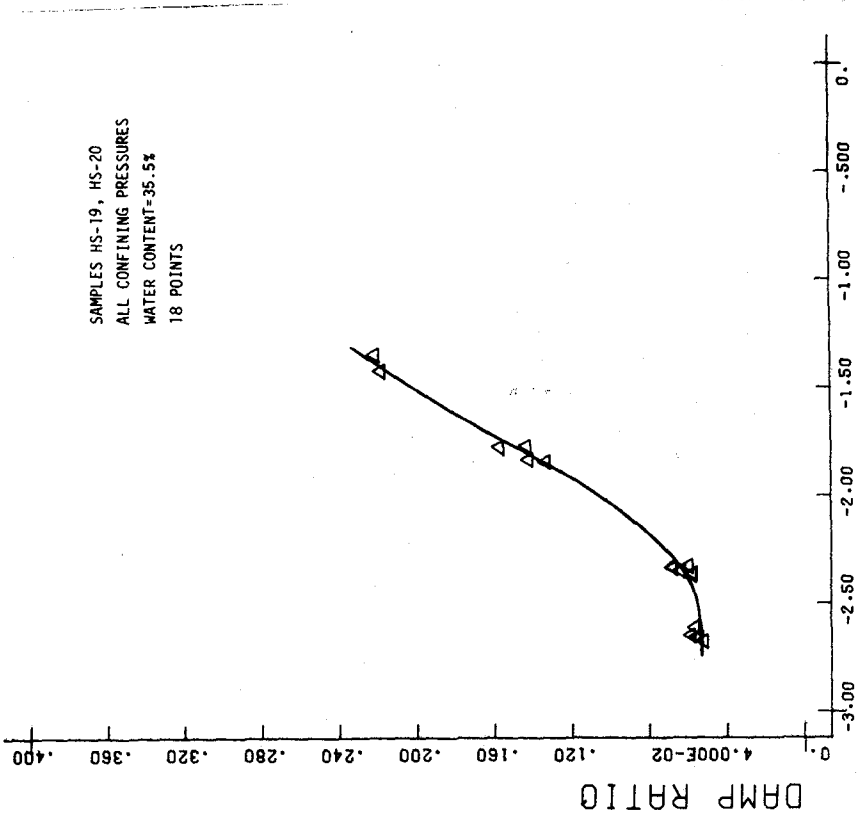

Figure B.26 H-SILTT-10F05

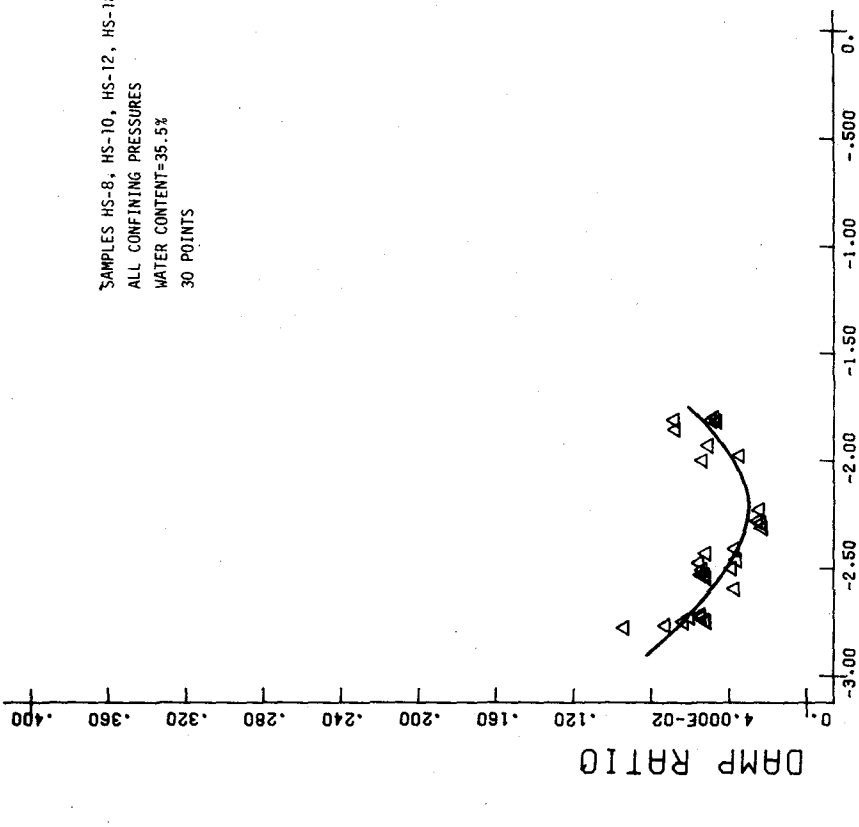

Figure B.25 H-SILTT-4F10

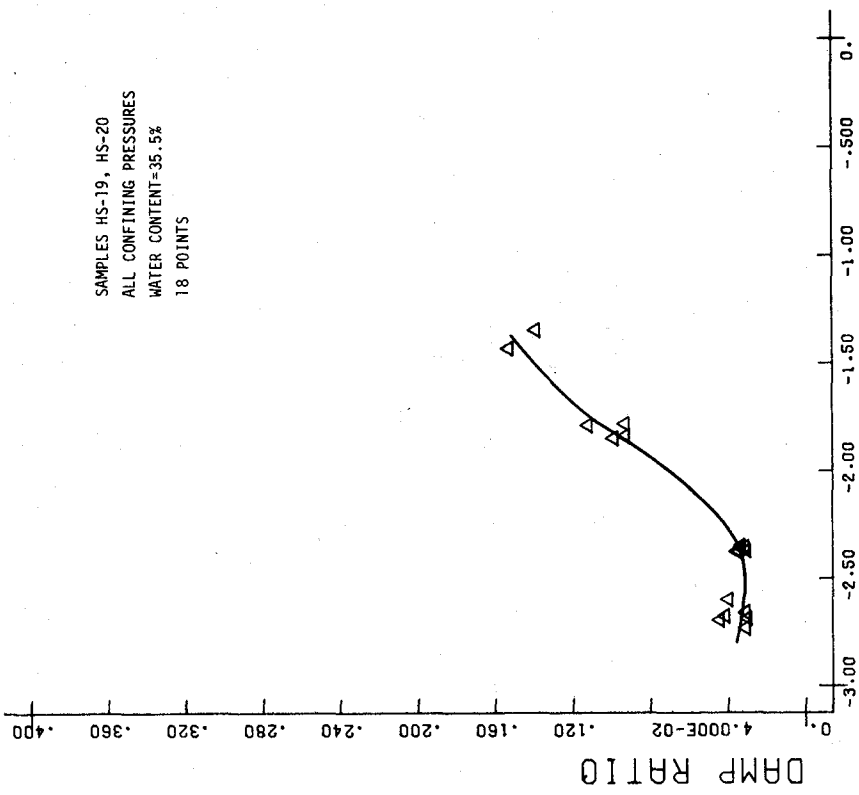

Figure B.28 AX STRAIN

H-SILTT-10F1

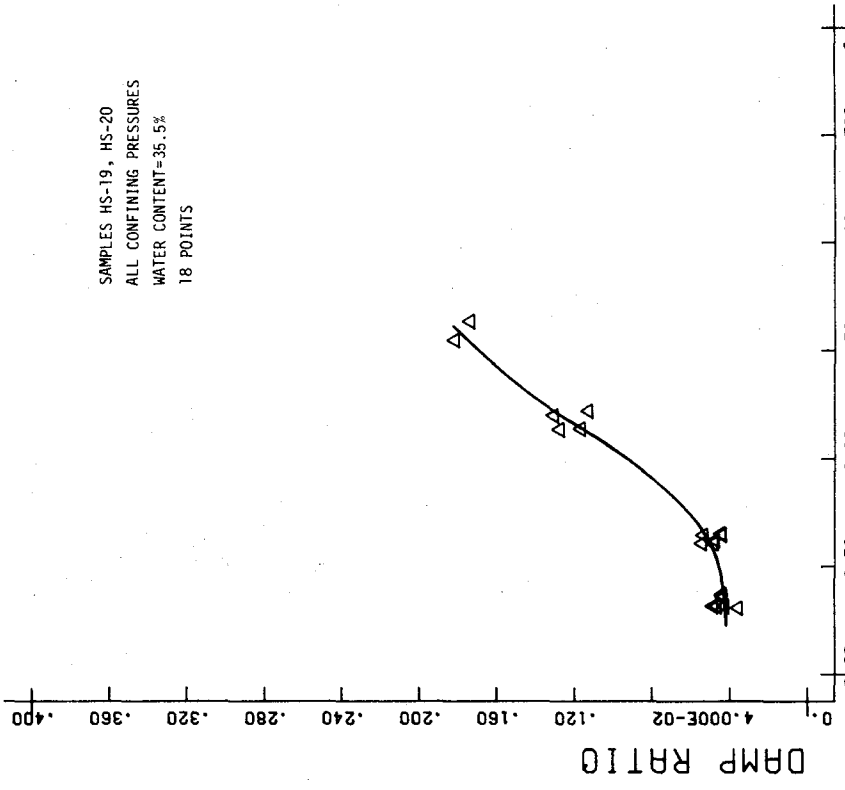

Figure B.27 AX STRAIN

H-SILTT-10F3

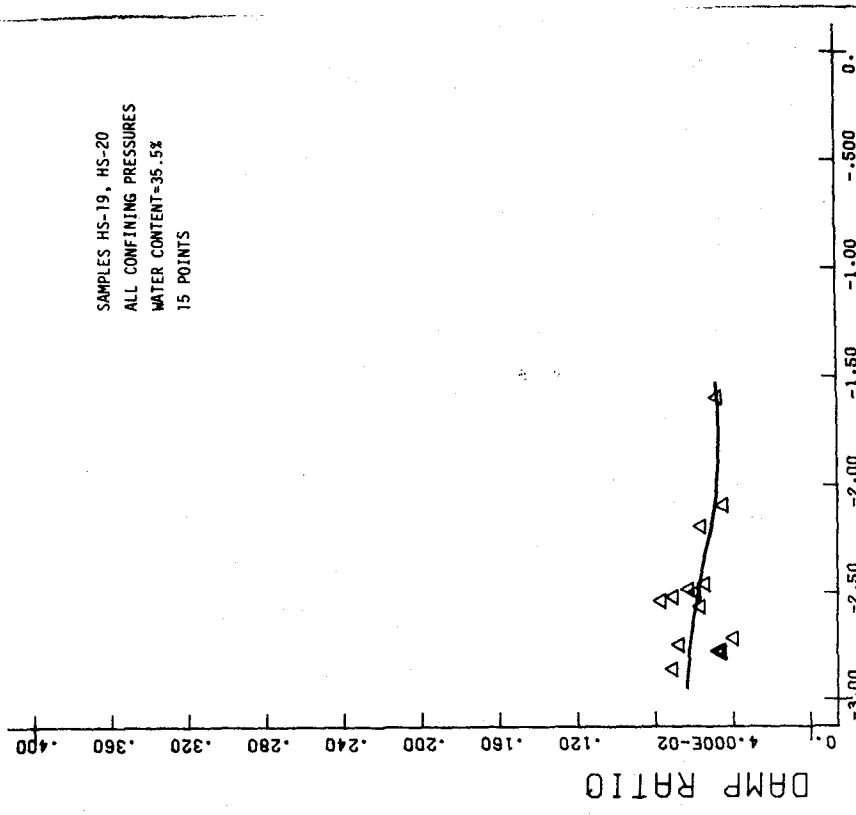

Figure B.30 H-SILTT-10F10

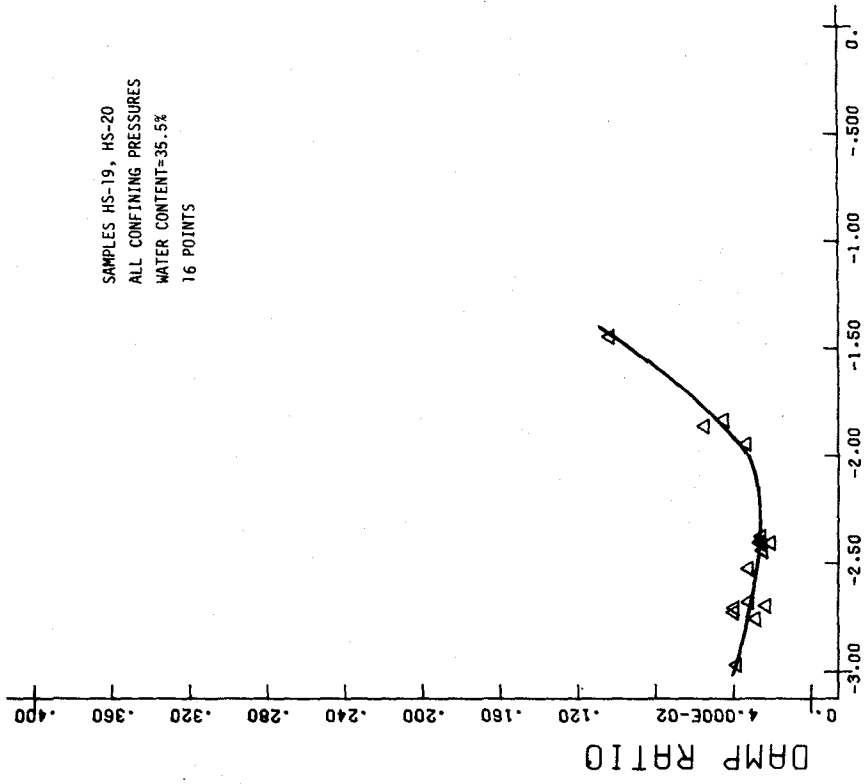

Figure B.29 H-SILTT-10F5

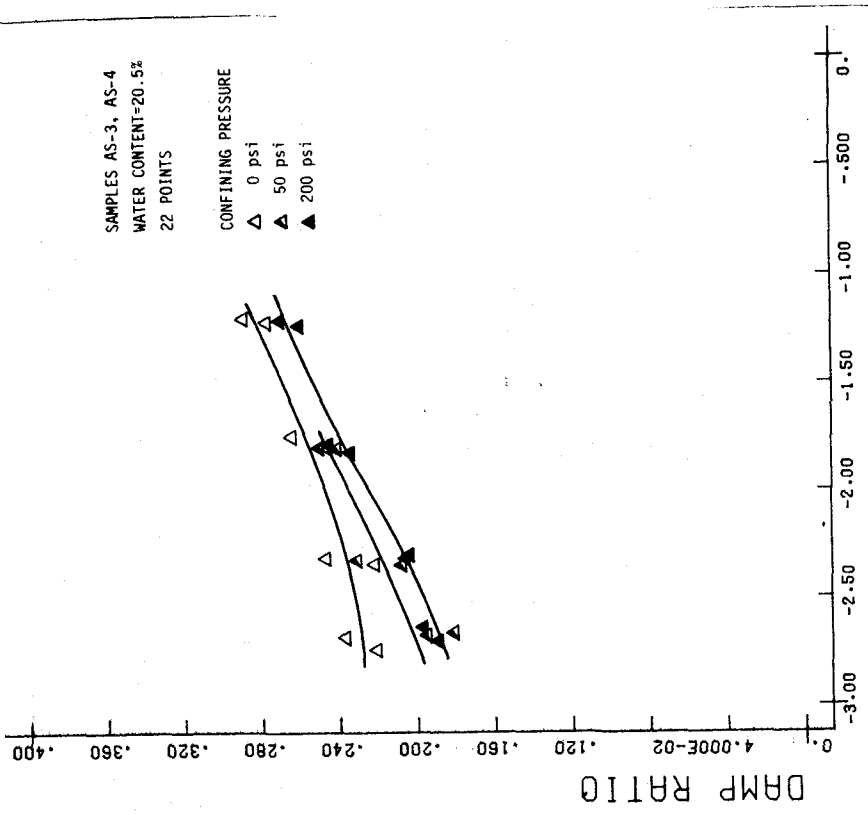

Figure B.32 A-SILTT-1F3

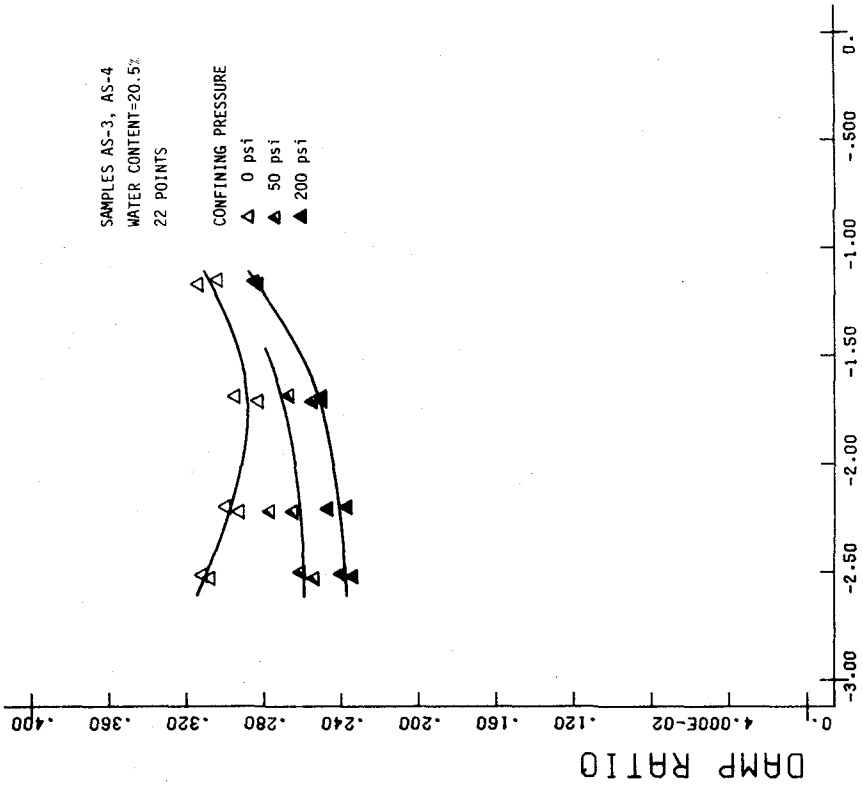

Figure B.31 A-SILTT-1F05

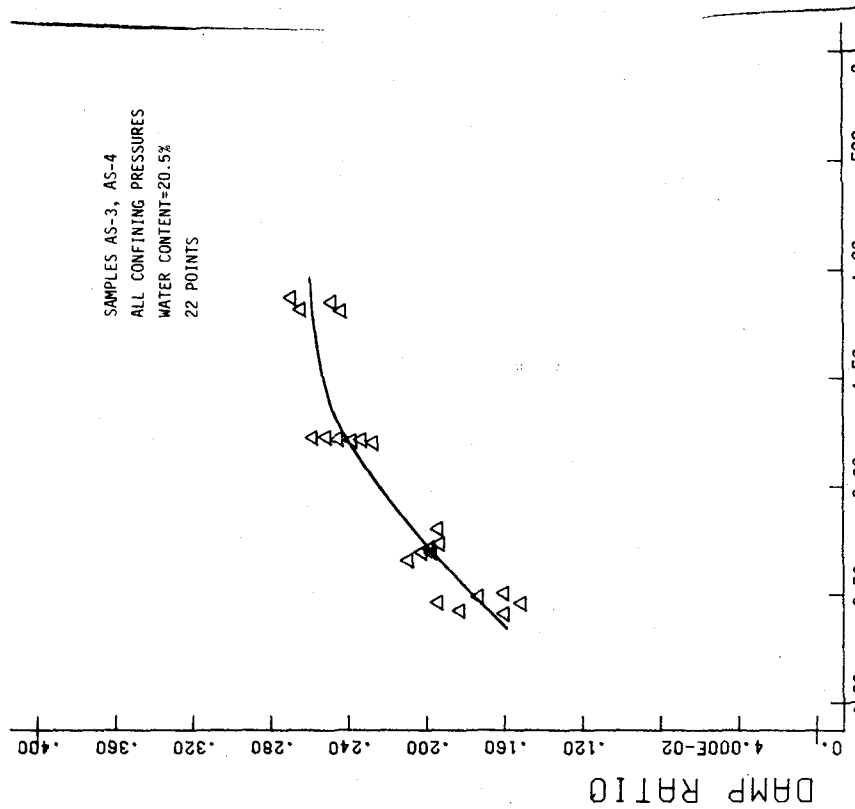

Figure B.34

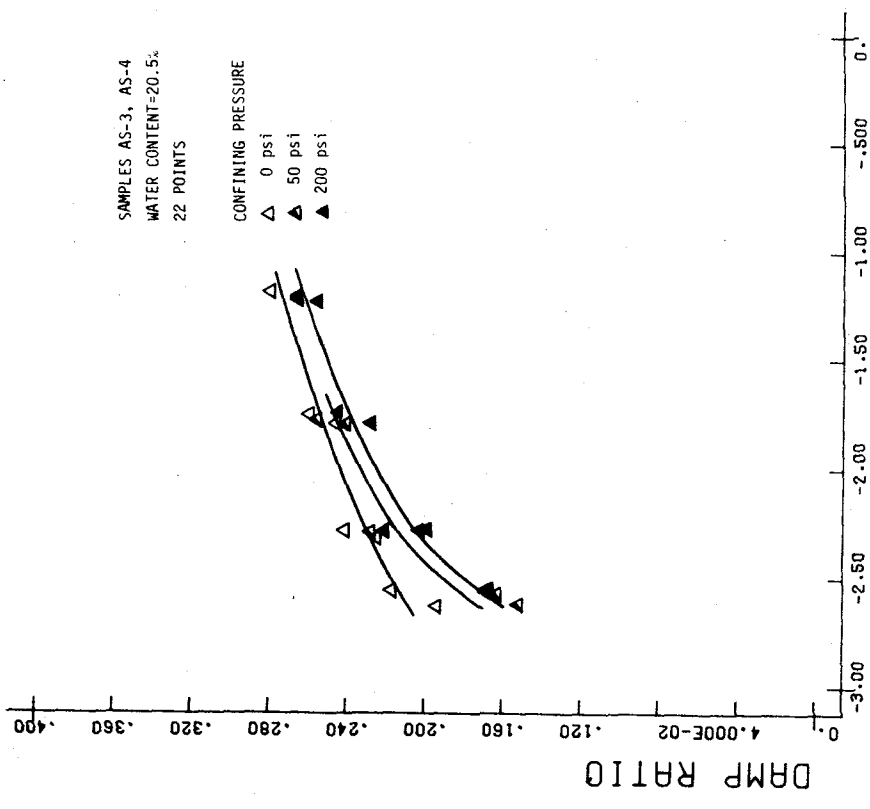

Figure B.33

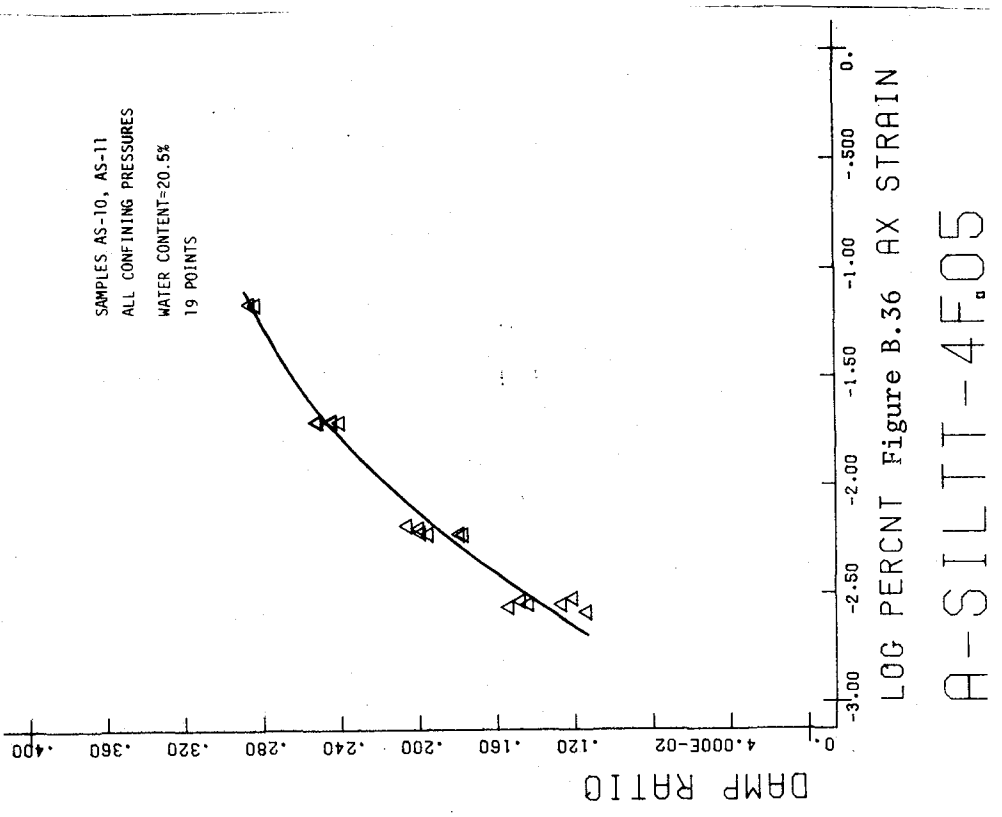

Figure B.36 A-SILTT-4F05

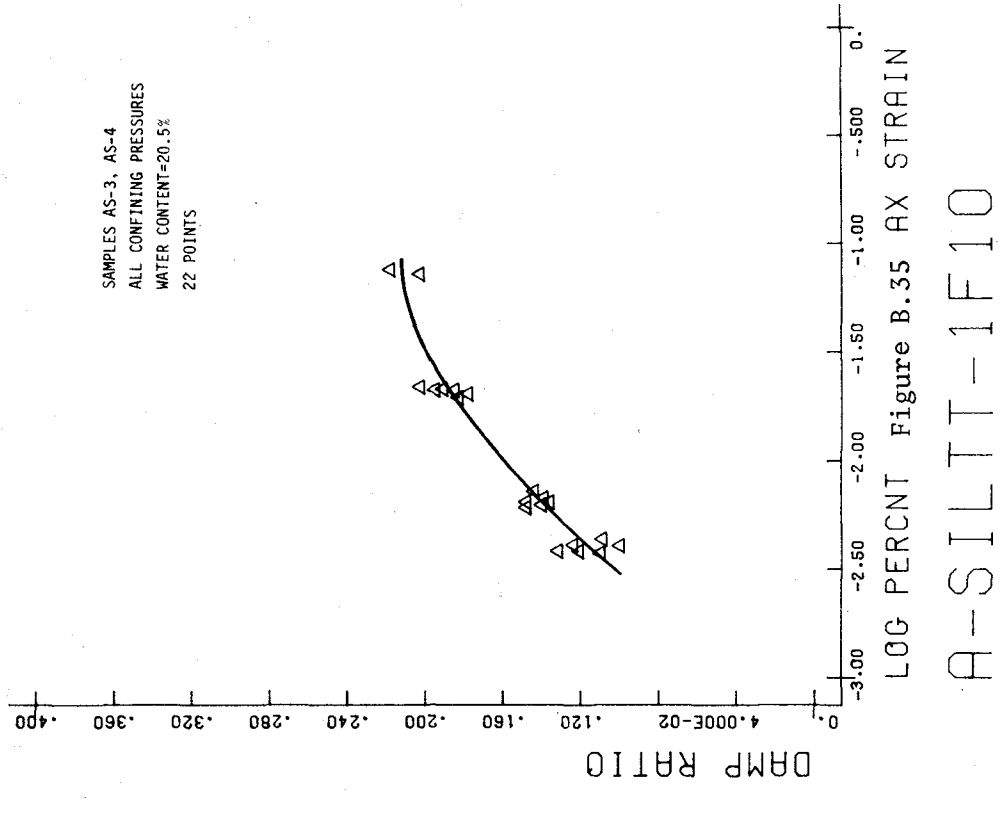

Figure B.35 A-SILTT-1F10

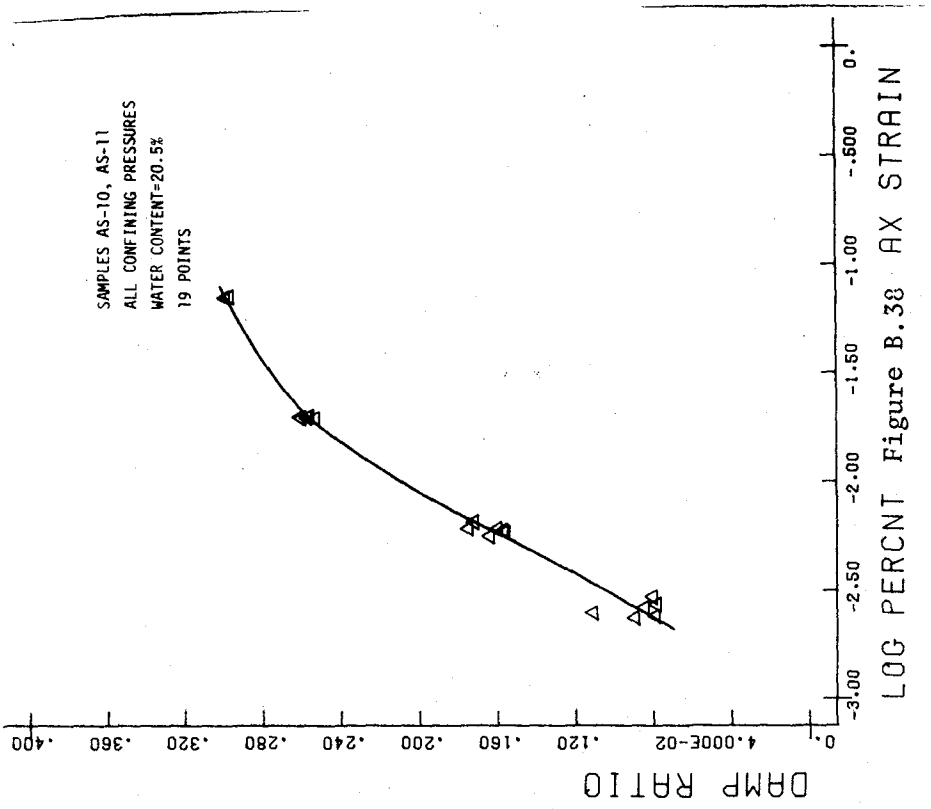

Figure B.38 A-SILTT-4F1

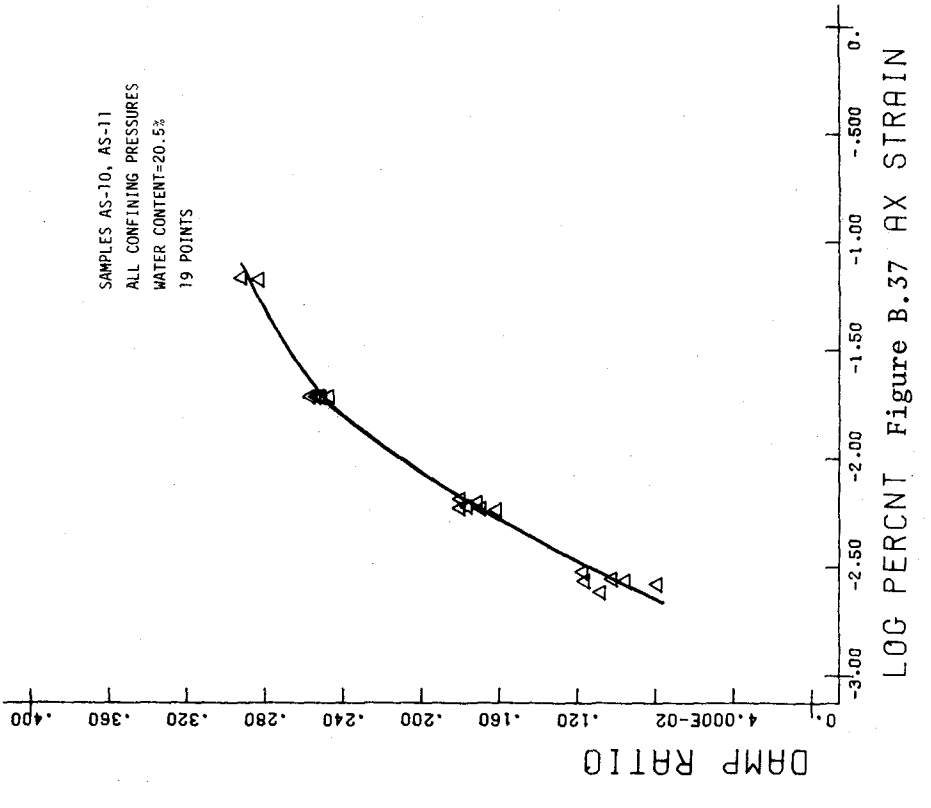

Figure B.37 A-SILTT-4F3

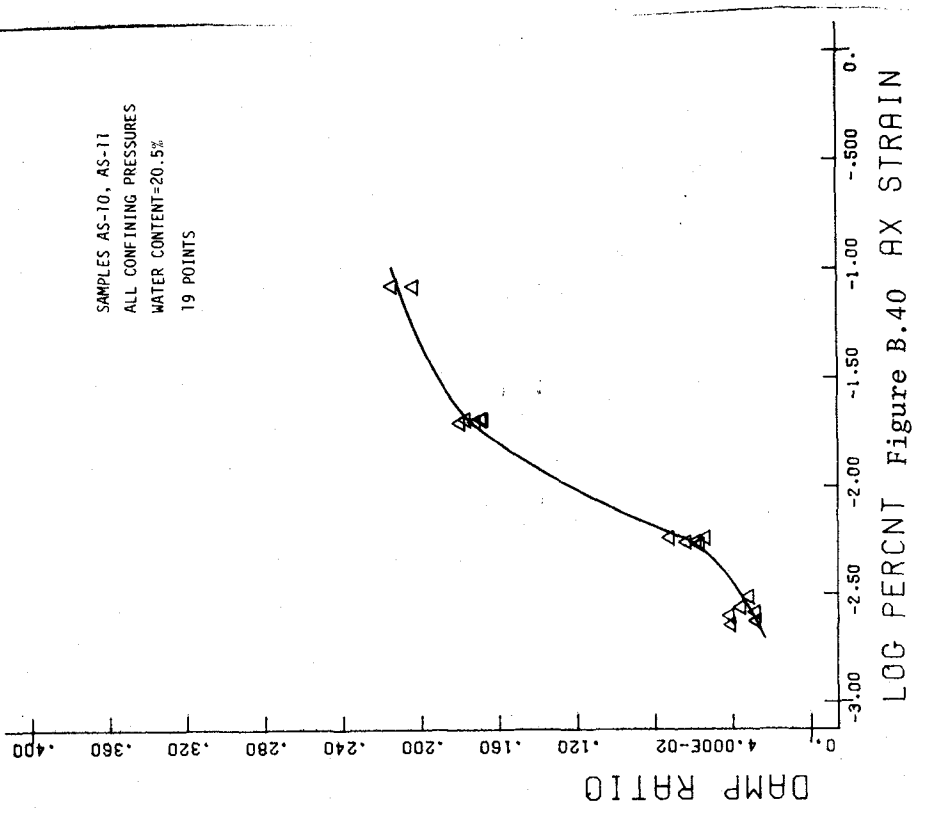

Figure B.40 A-SILTT-4F10

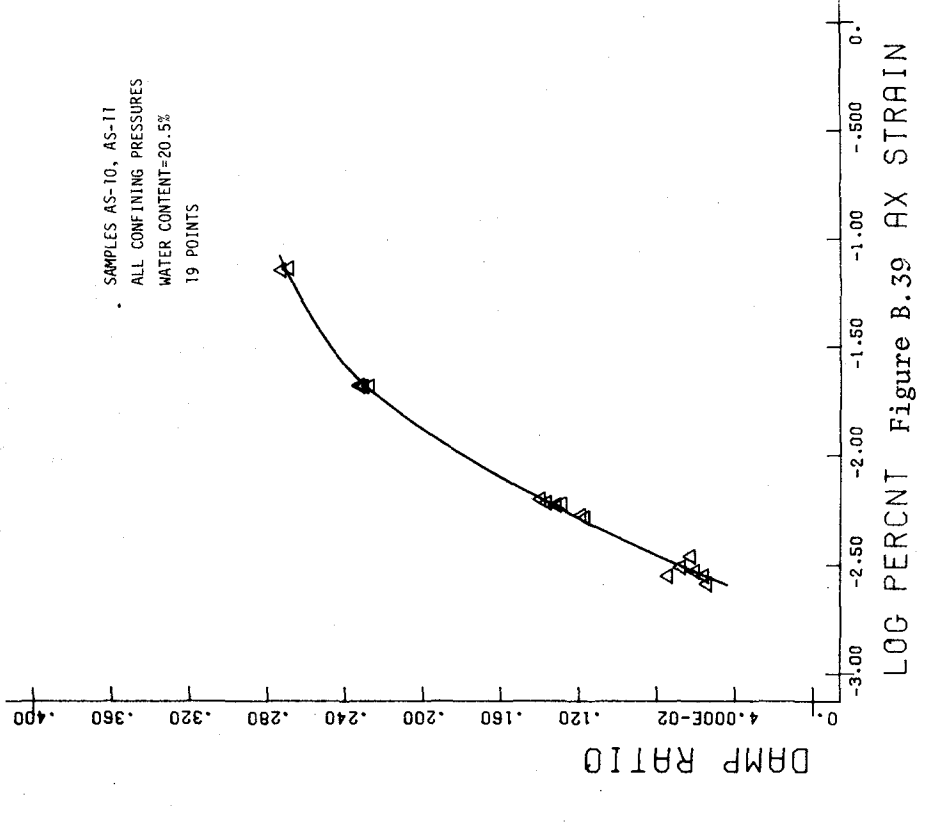

Figure B.39 A-SILTT-4F5

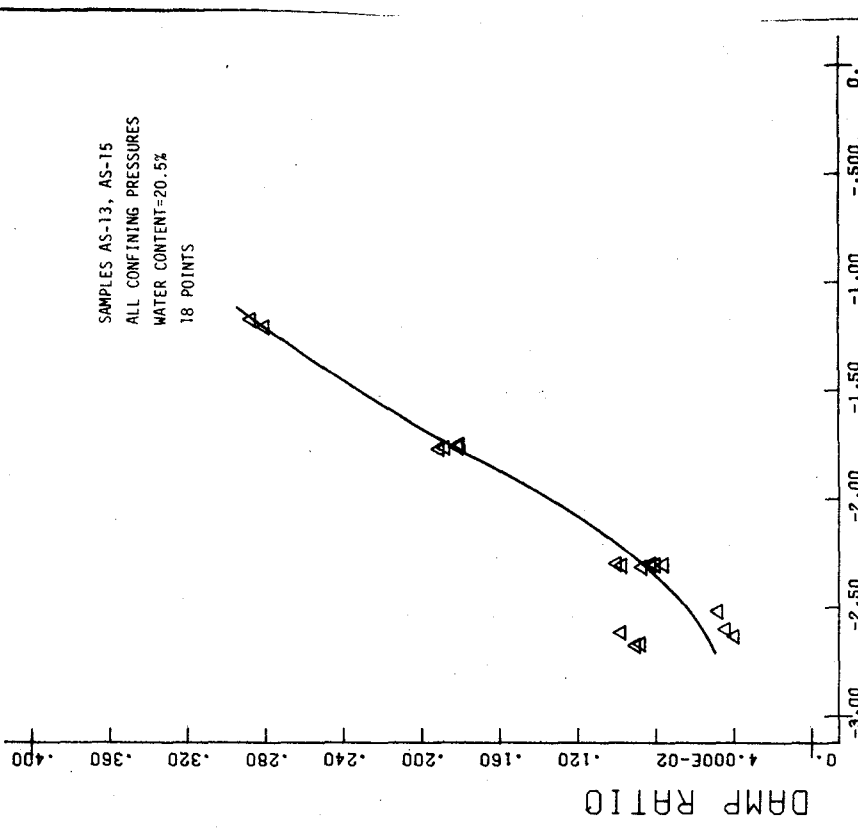

Figure B.42 A-SILTT-10F3

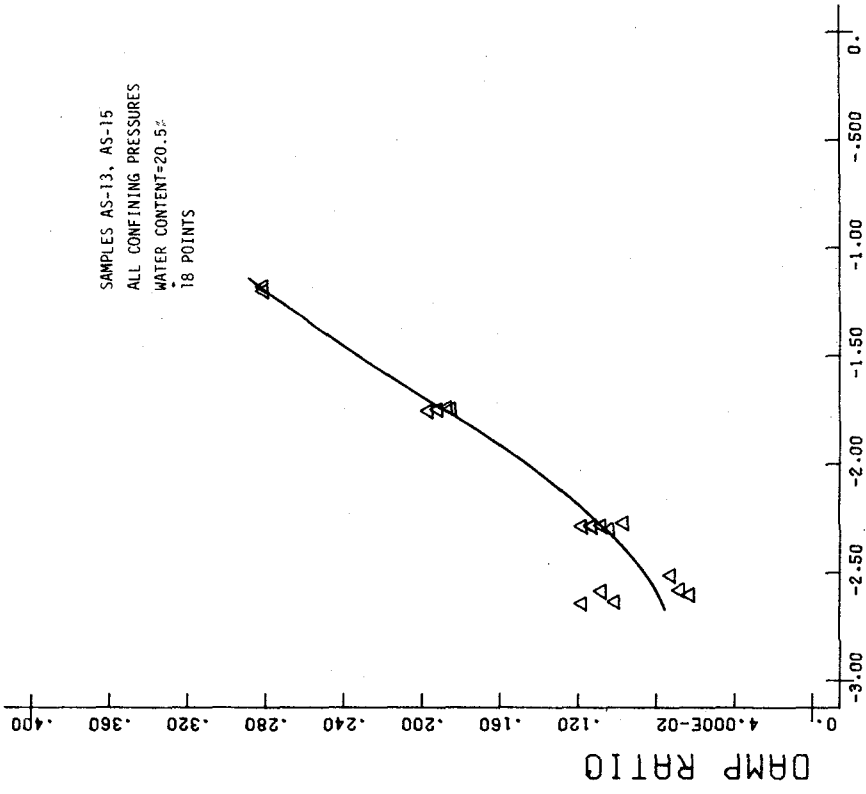

Figure B.41 A-SILTT-10F.05

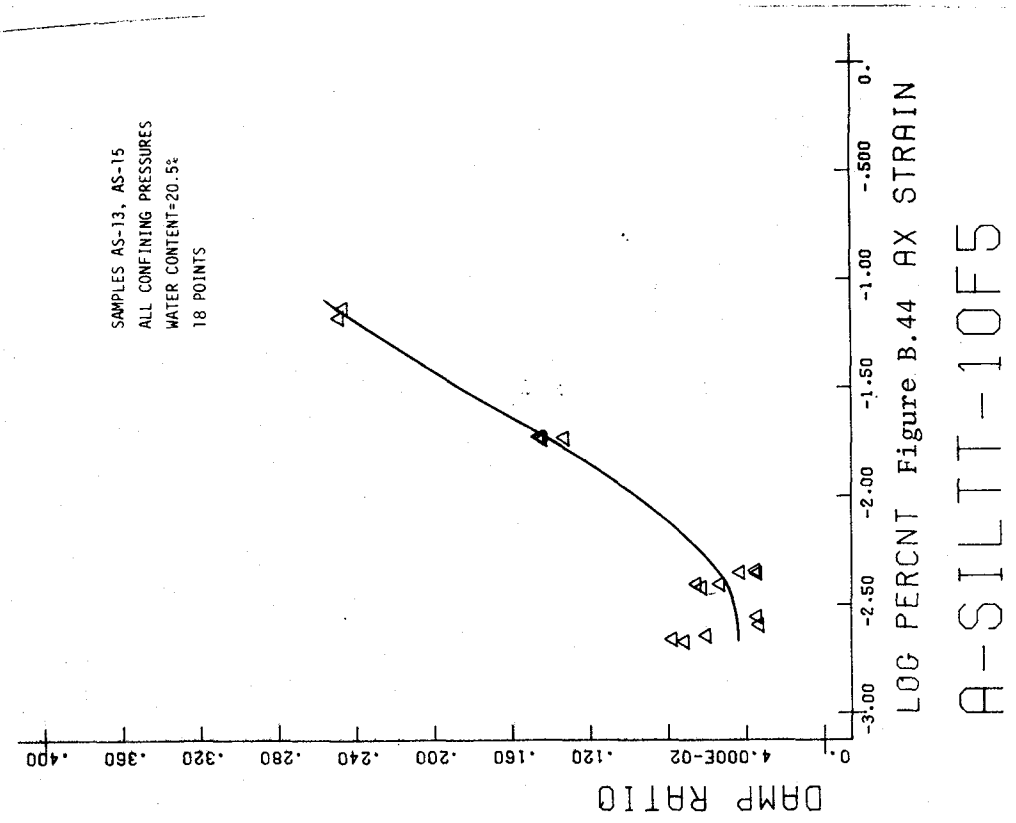

Figure B.44 A-SILTT-10F5

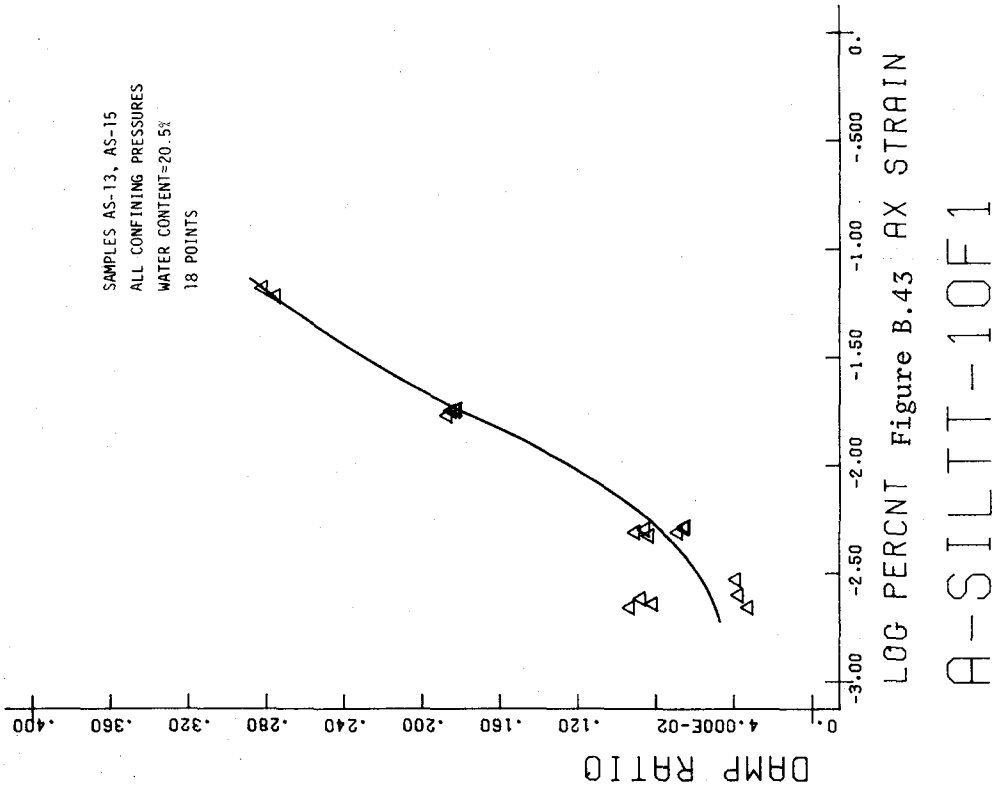

Figure B.43 A-SILTT-10F1

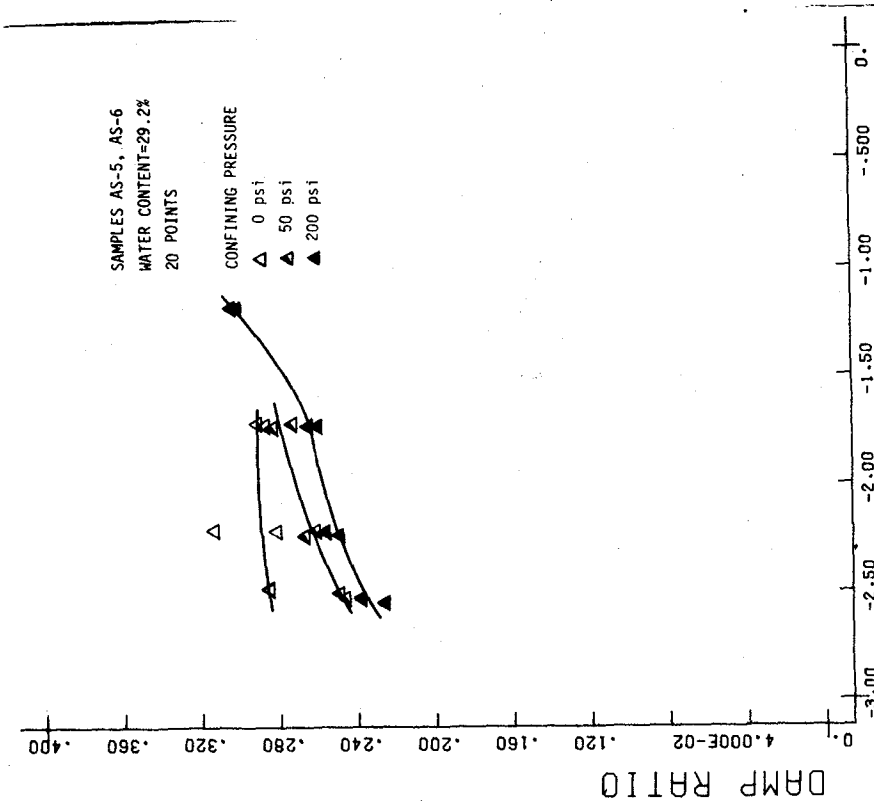

Figure B.46 A-SILTT-1F05

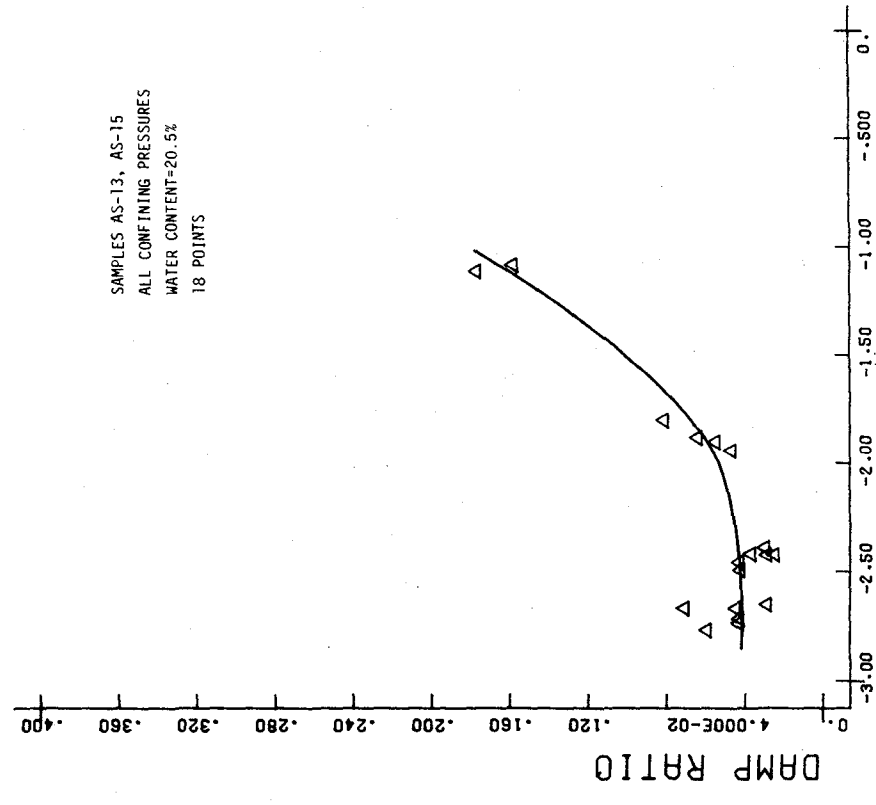

Figure B.45 A-SILTT-10F10

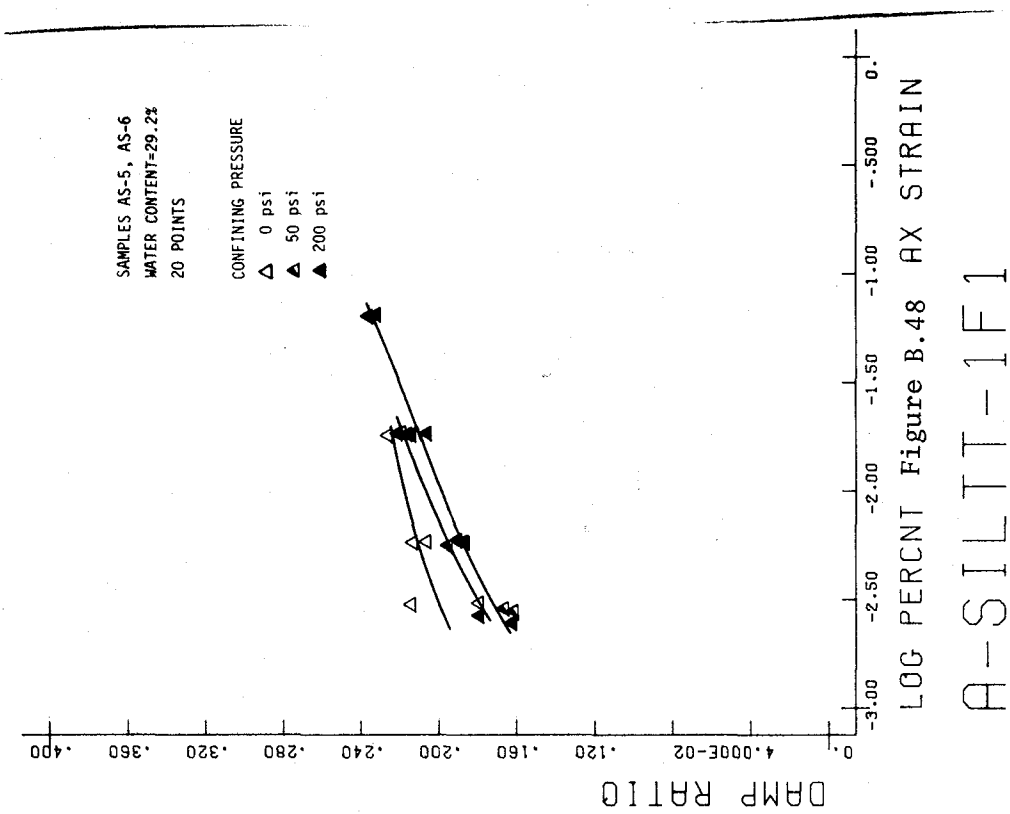

Figure B.48 A-SILTT-1F1

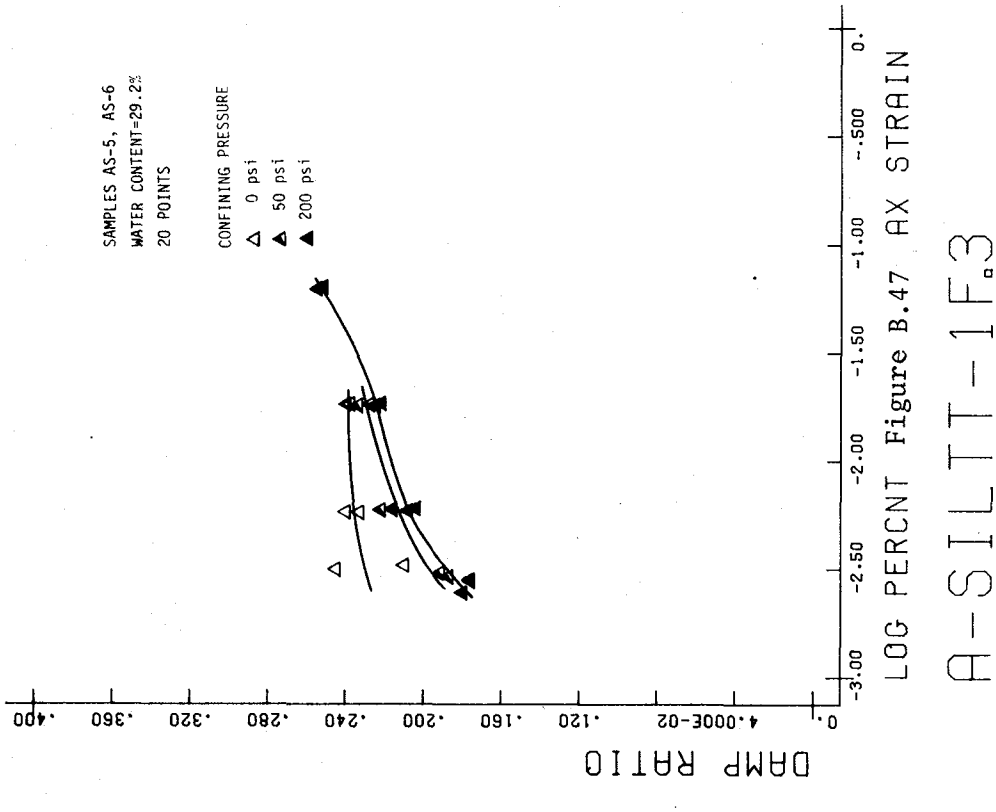

Figure B.47 A-SILTT-1F3

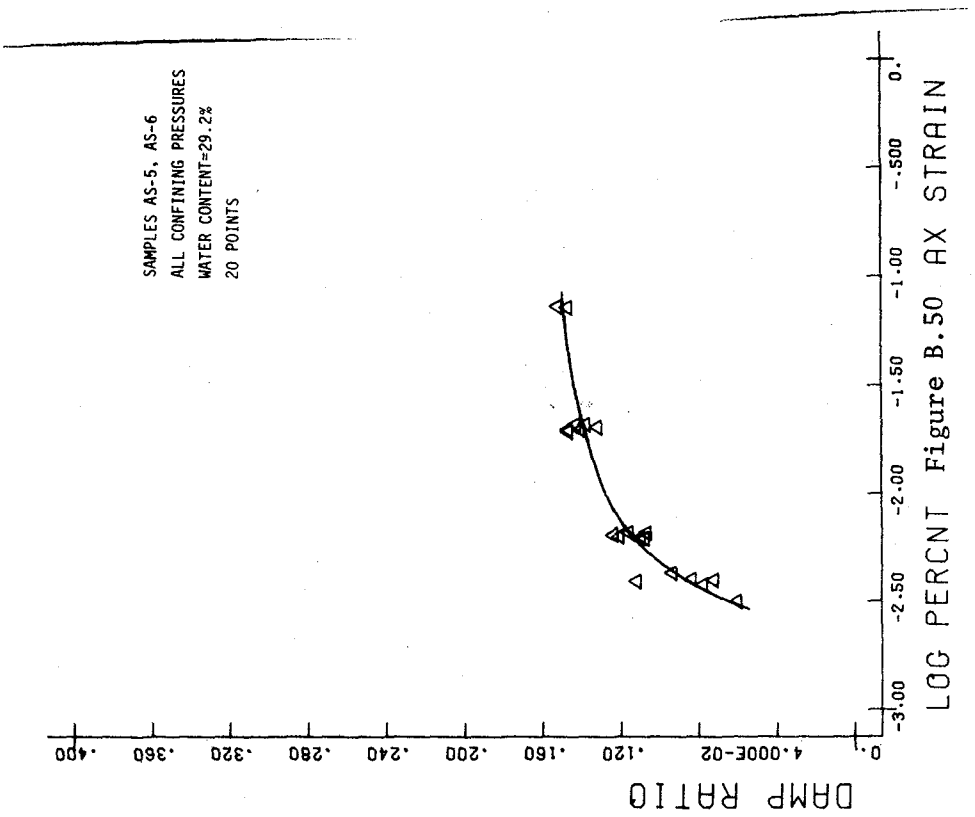

Figure B.50 A-SILTT-1F10

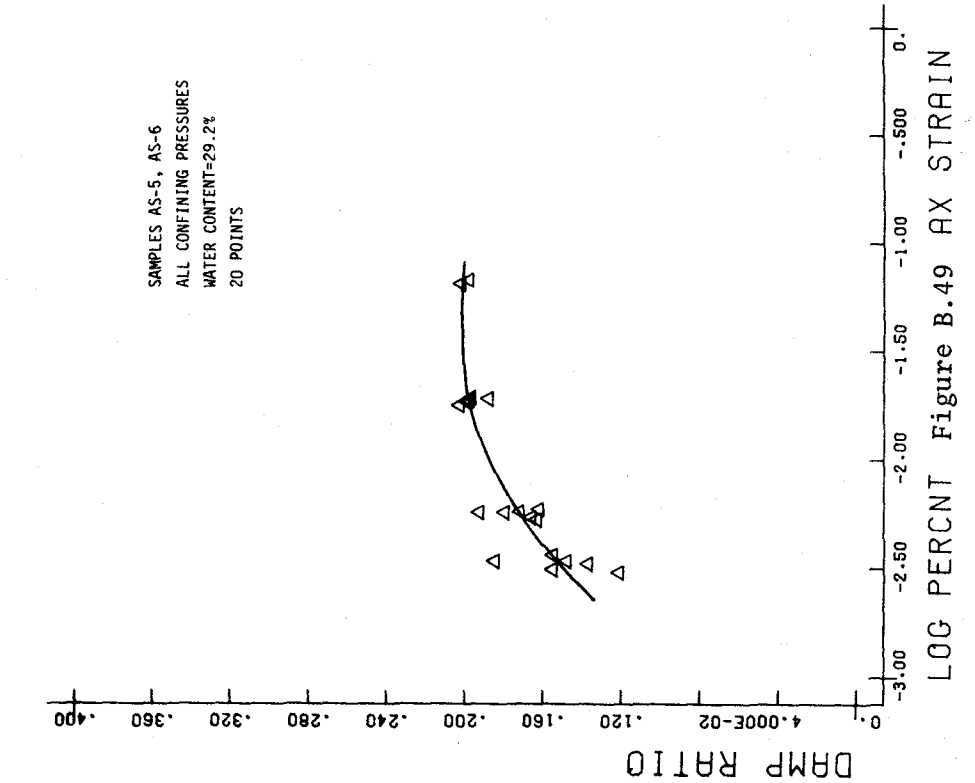

Figure B.49 A-SILTT-1F5

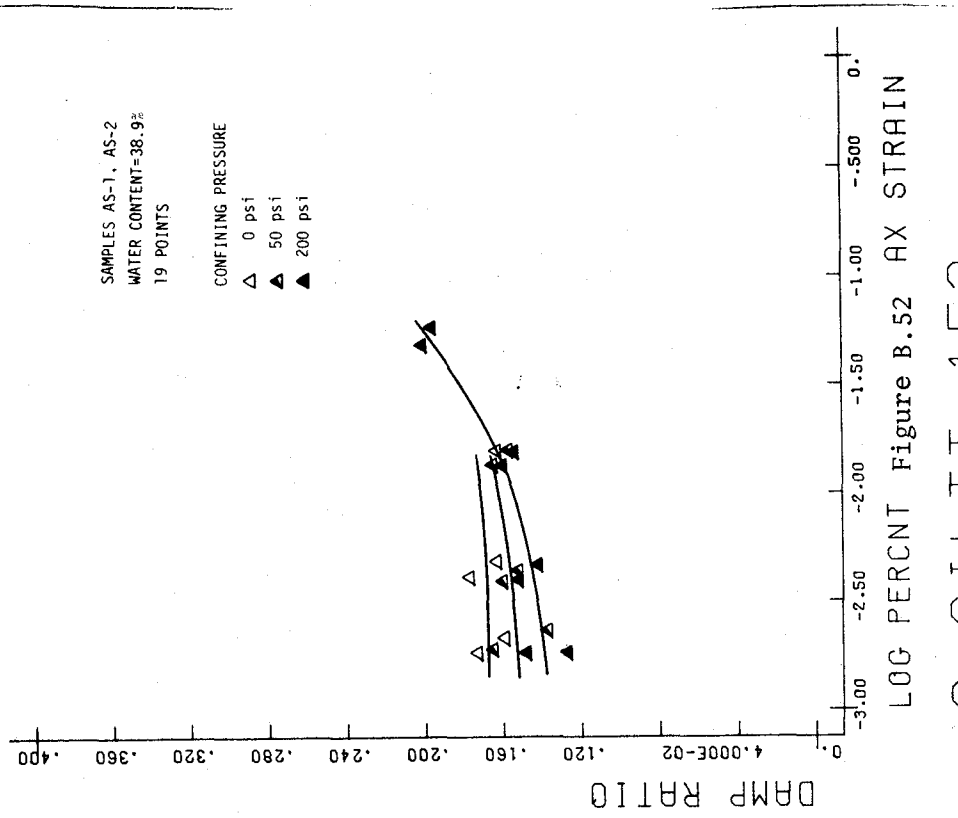

Figure B.52 A-SILTT-1F3

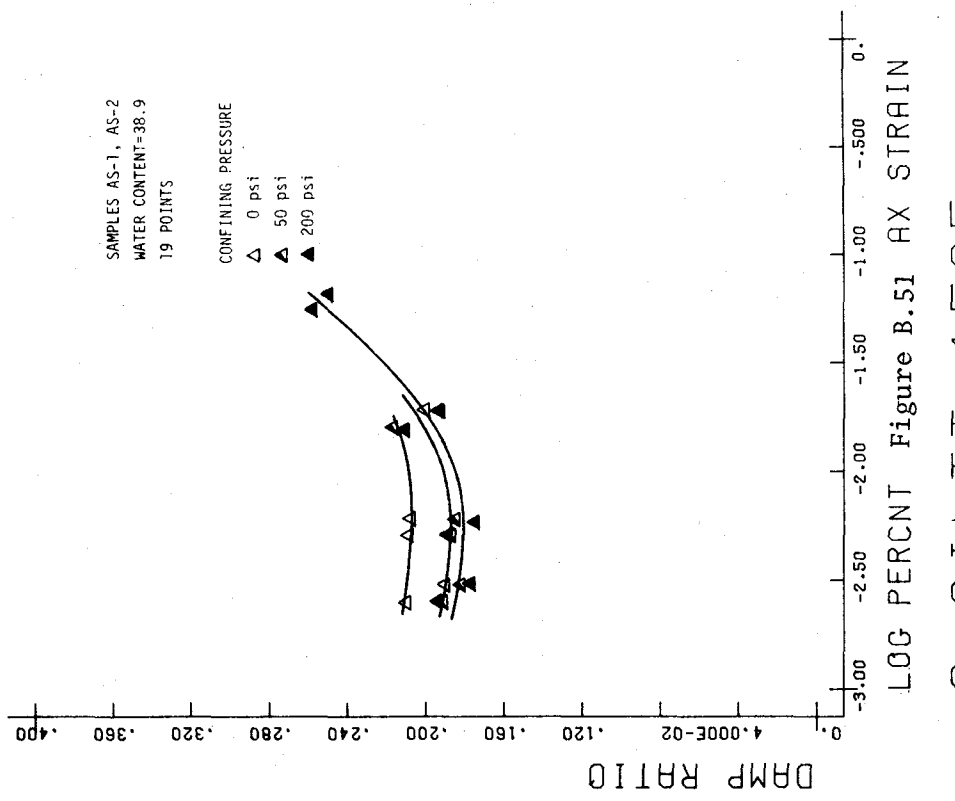

Figure B.51 A-SILTT-1F.05

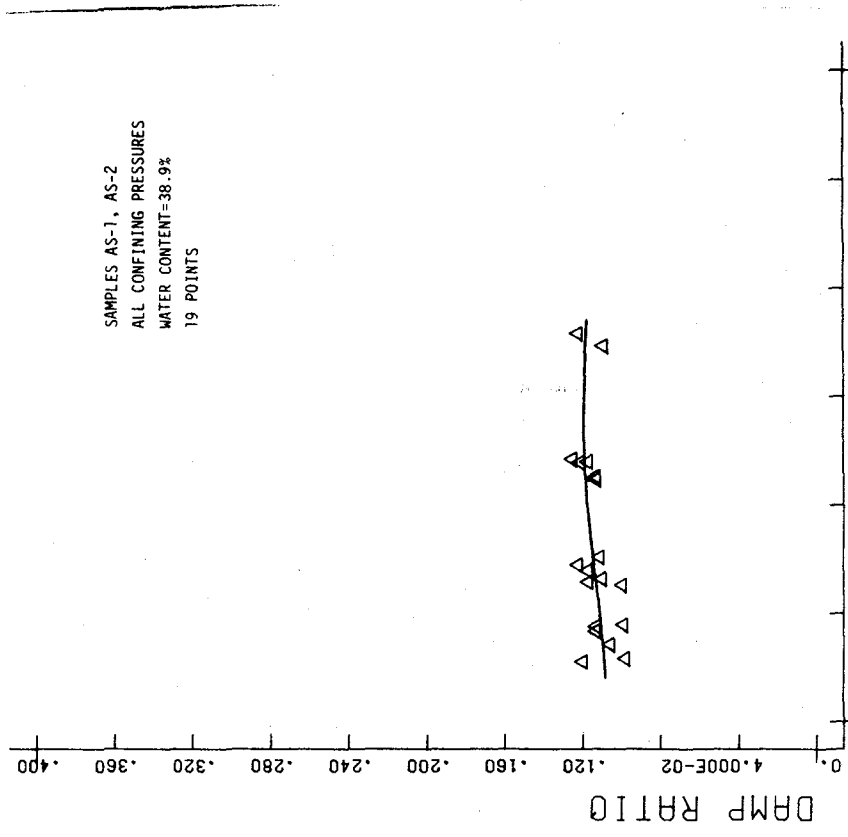

Figure B.54 A-SILTT-1F5

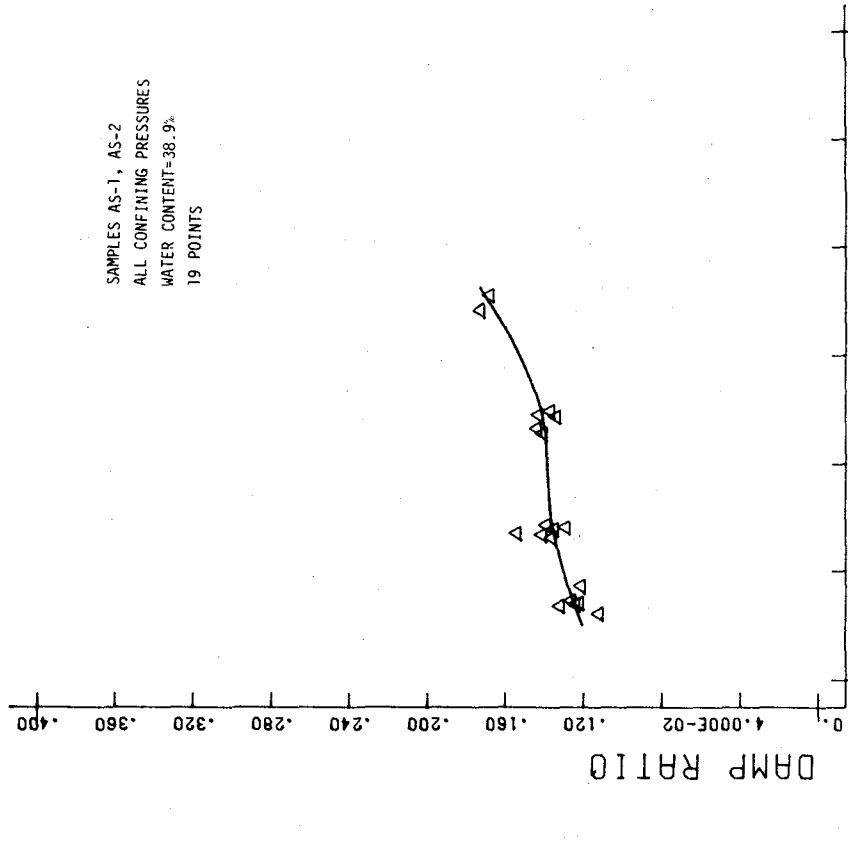

Figure B.53 A-SILTT-1F1

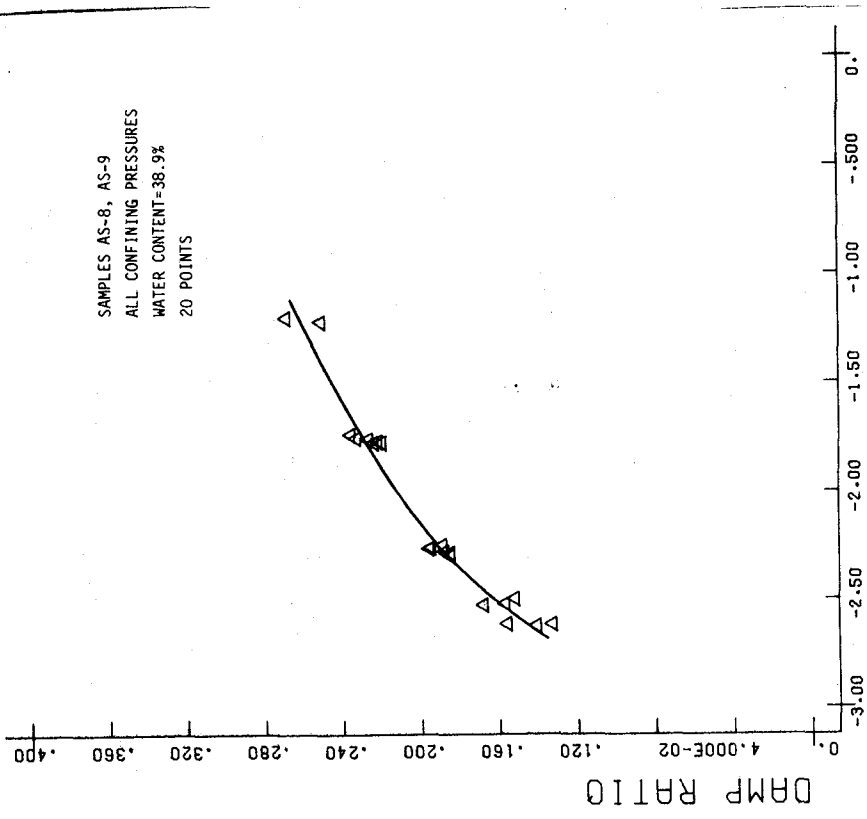

Figure B.56 A-SILTT-4F05

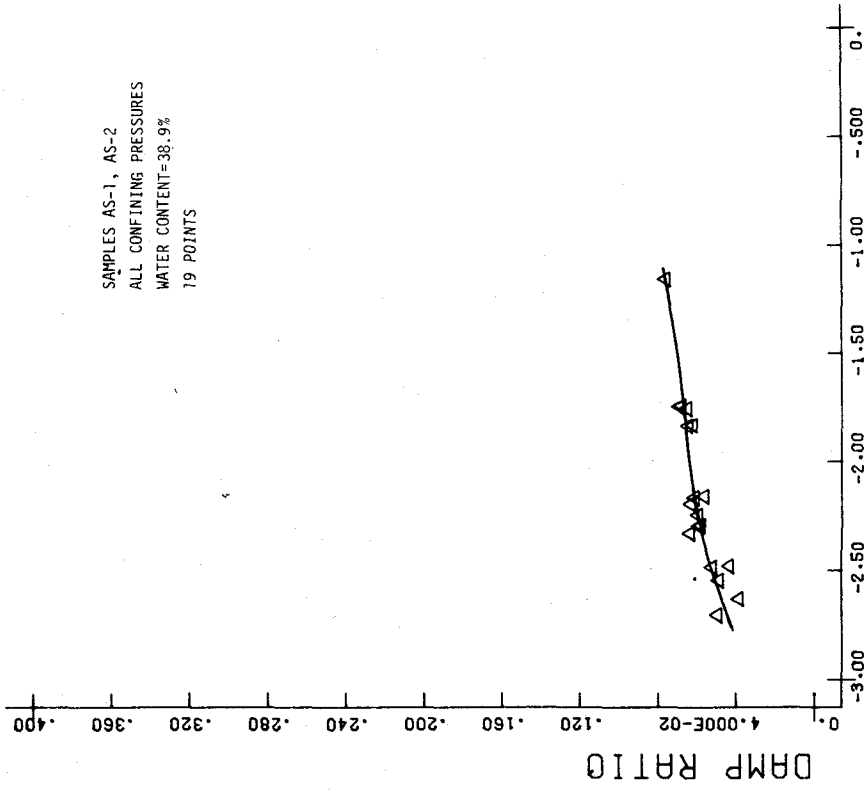

Figure B.55 A-SILTT-1F10

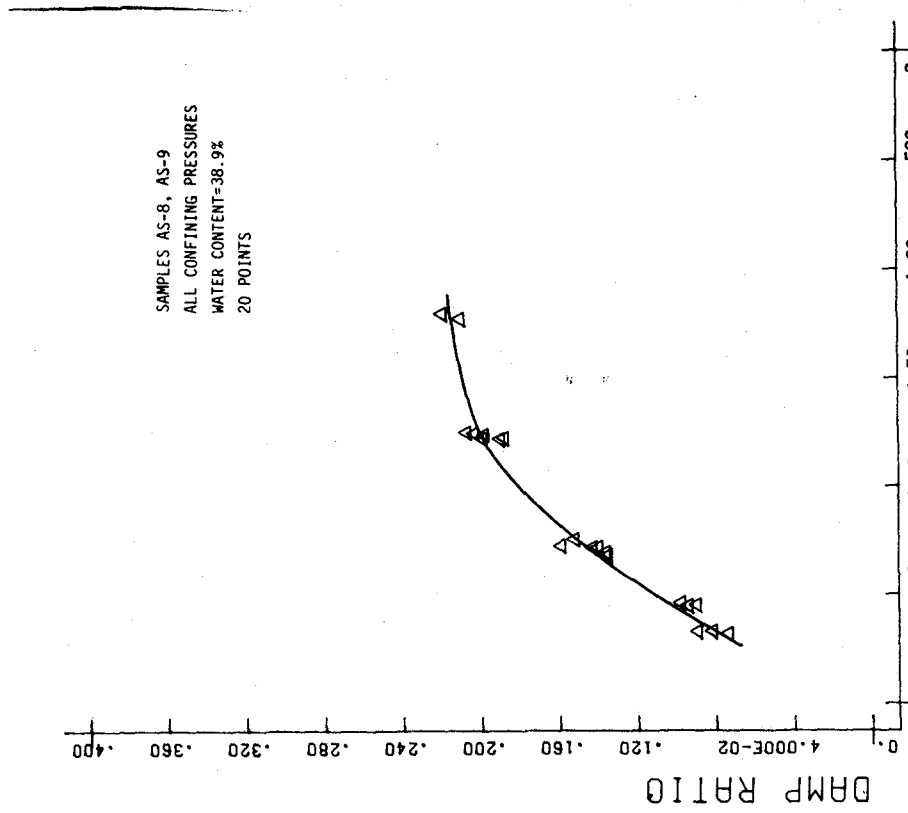

Figure B.58 AX STRAIN

A-SILTT-4F1

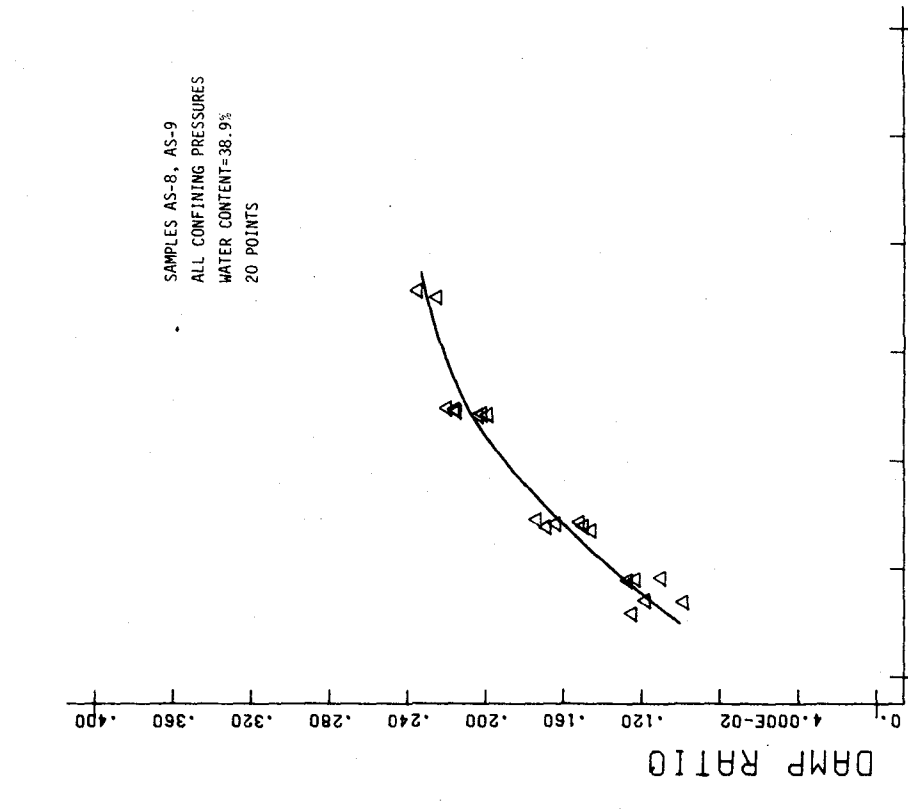

Figure B.57 AX STRAIN

A-SILTT-4F3

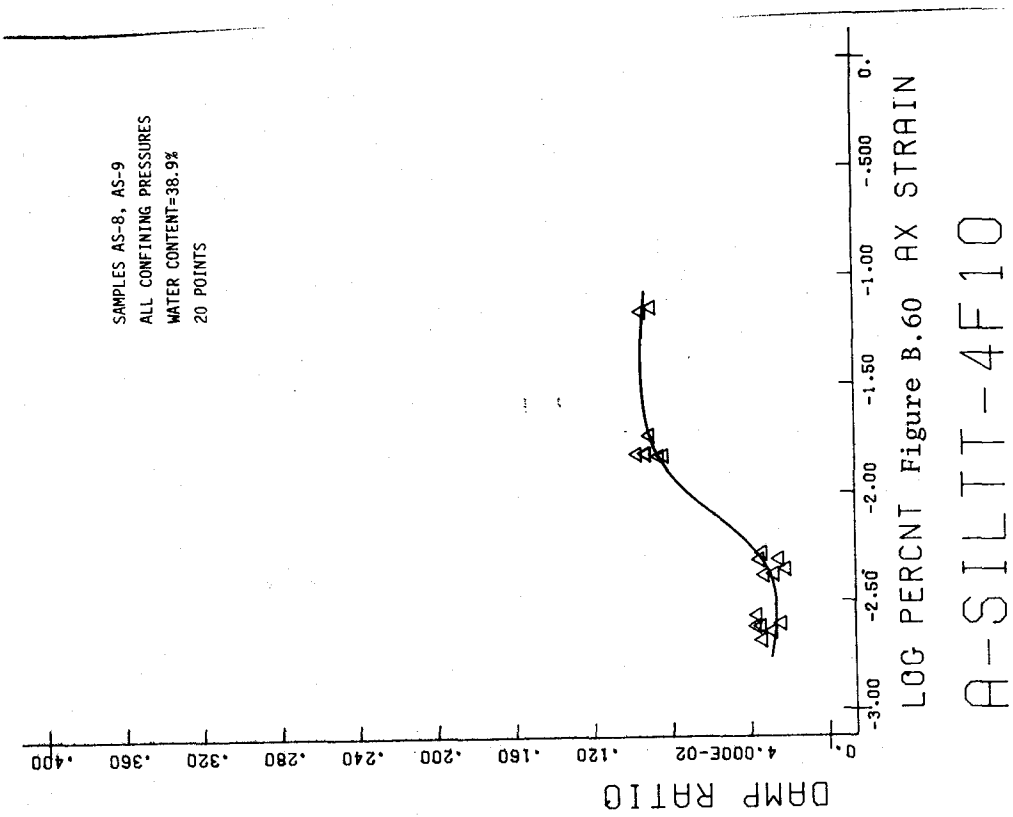

Figure B.60 A-SILTT-4F10

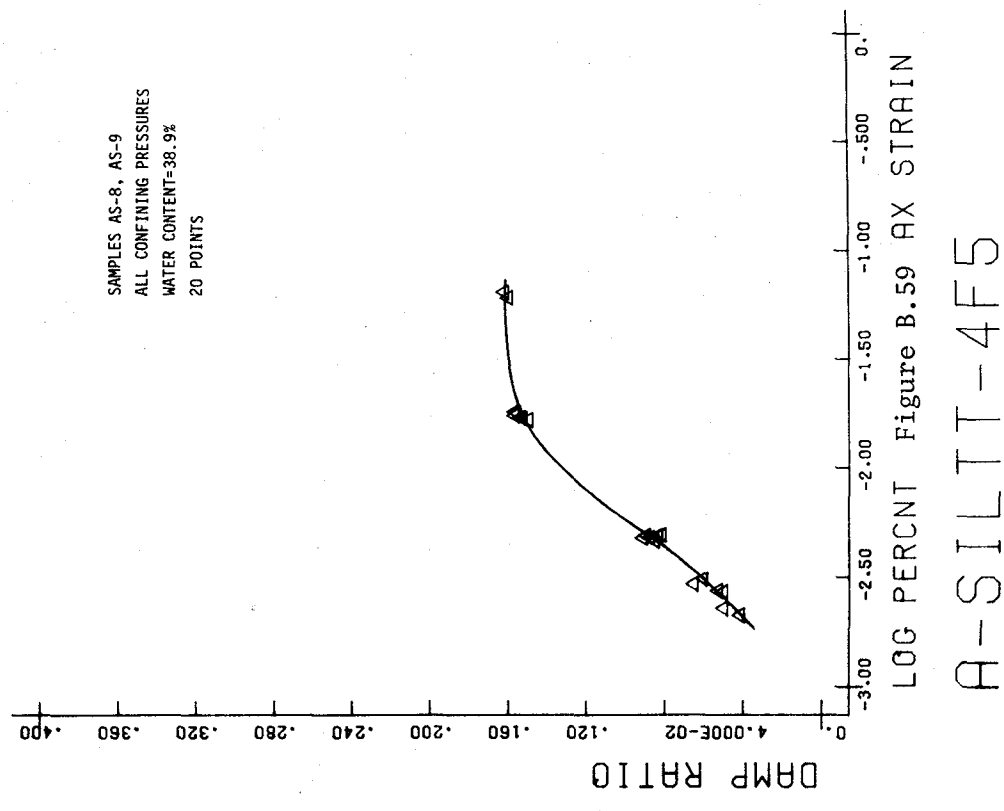

Figure B.59 A-SILTT-4F5

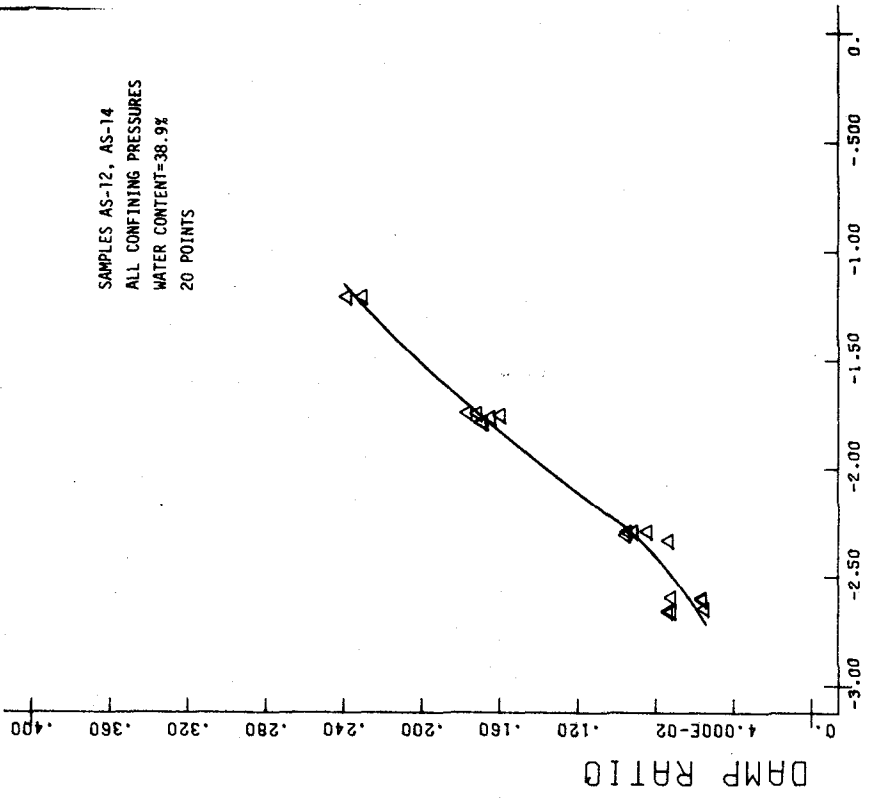

Figure B.62 A-SILTT-10F.3

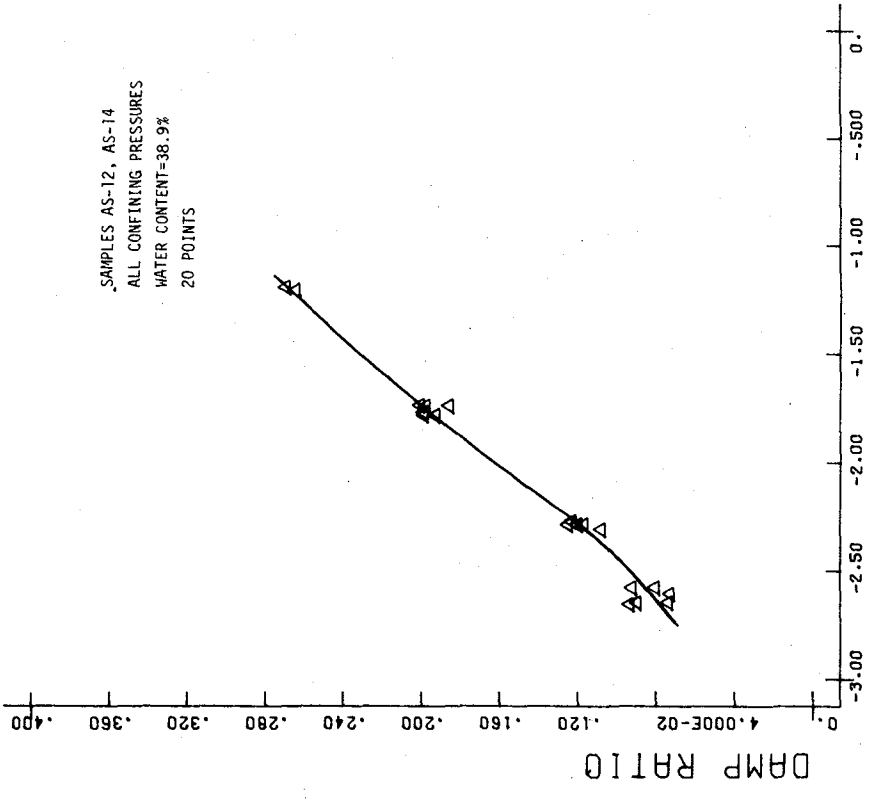

Figure B.61 A-SILTT-10F.05

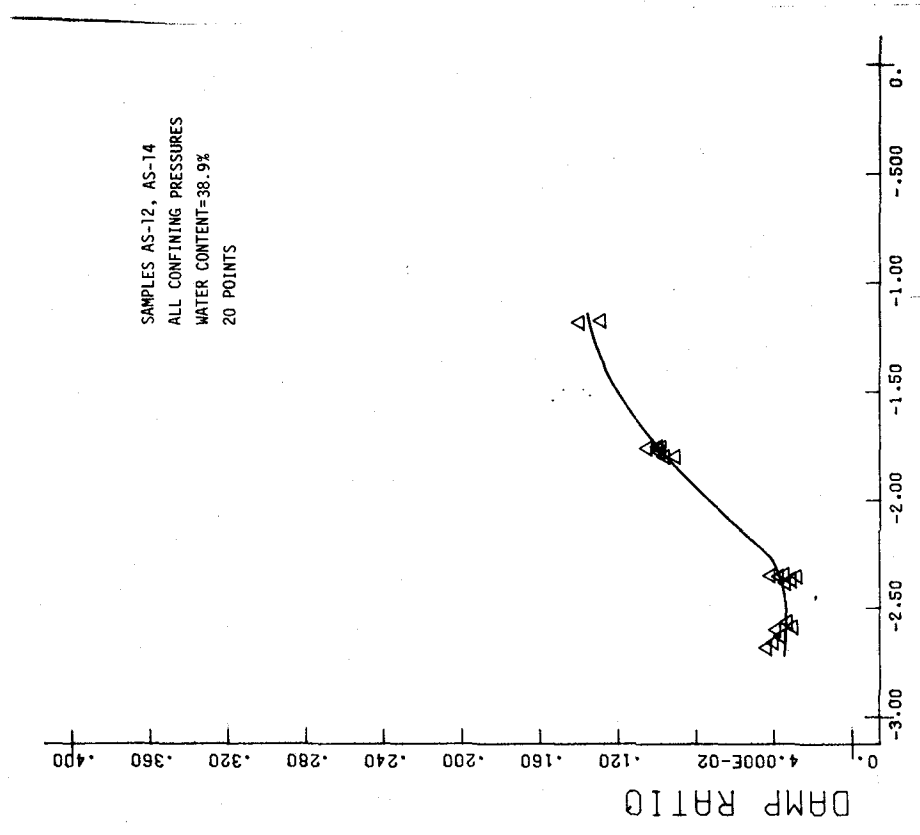

Figure B.64

A-SILTT-10F5

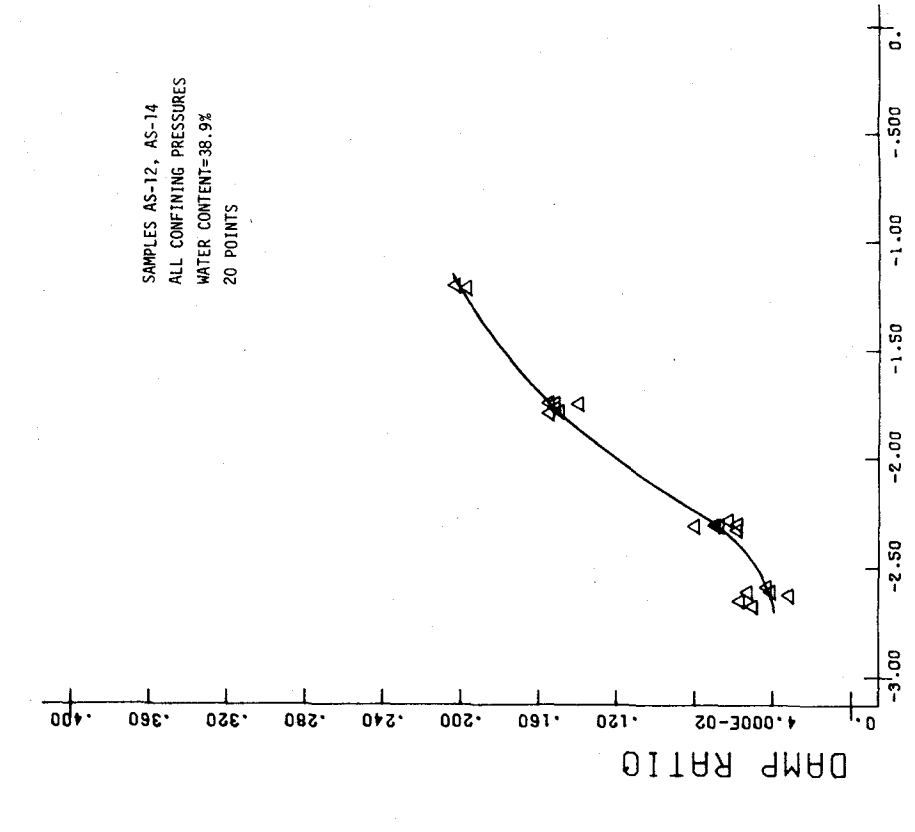

Figure B.63

A-SILTT-10F1

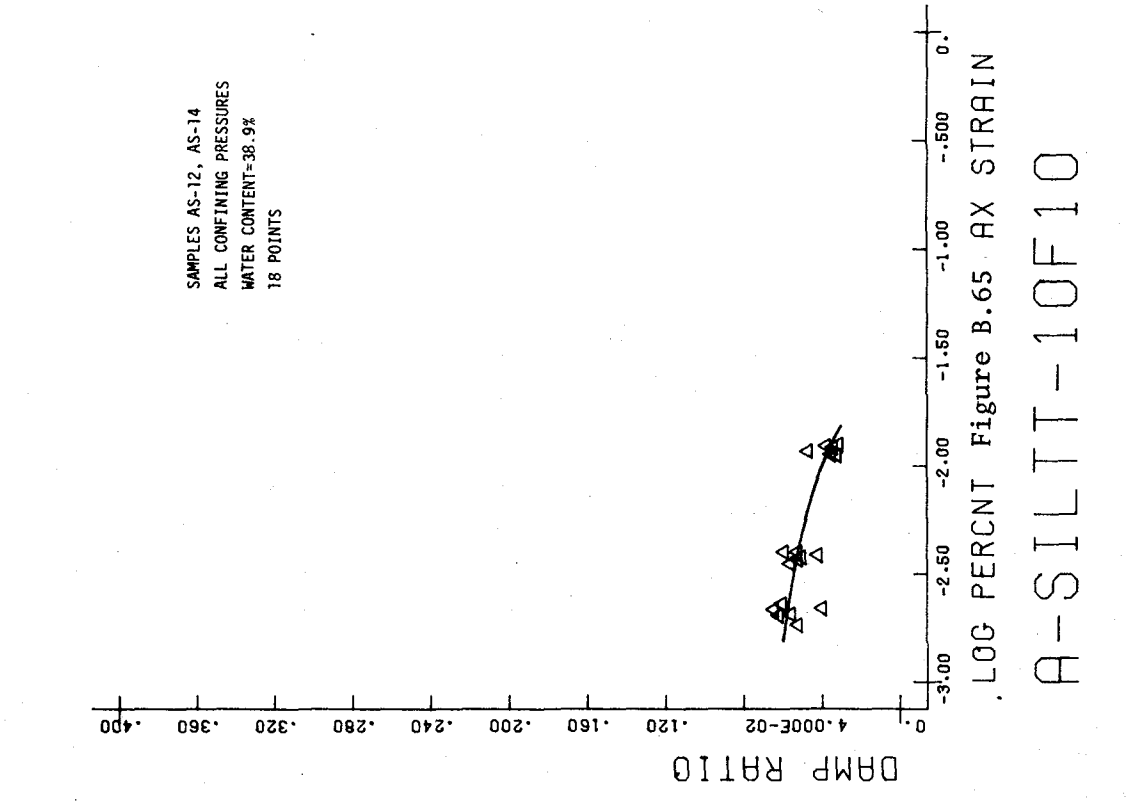
A-SILTT-10F10
SAMPLES AS-12, AS-14
ALL CONFINING PRESSURES
WATER CONTENT=38.9%
18 POINTS
DAMP RATIO
LOG PERCNT AX STRAIN
0.
4.000E-02
.120
.160
.200
.240
.280
.320
.360
.400
-3.00
-2.50
-2.00
-1.50
-1.00
-.500
0.

Figure B.65

APPENDIX C

CYCLIC TRIAXIAL TEST RESULTS: DYNAMIC YOUNG'S MODULUS OF FROZEN SAND

Test results for Ottawa sand at sand contents of 20%, 45%, and 65% are shown in Figures C.1 to C.36; Figures C.37 to C.72; and Figures C.73 to C.108, respectively.

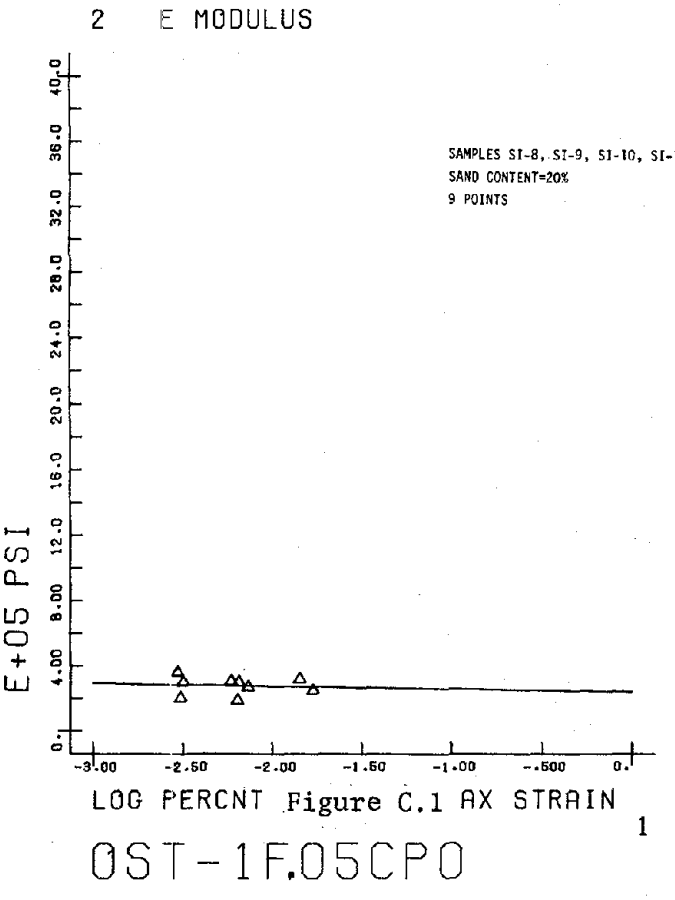

Figure C.1

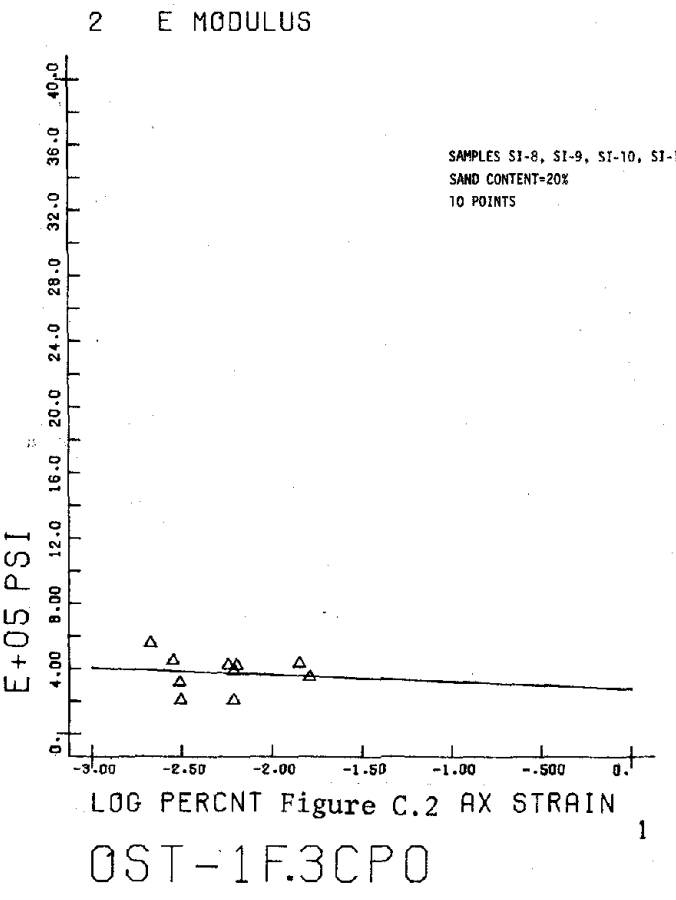

Figure C.2

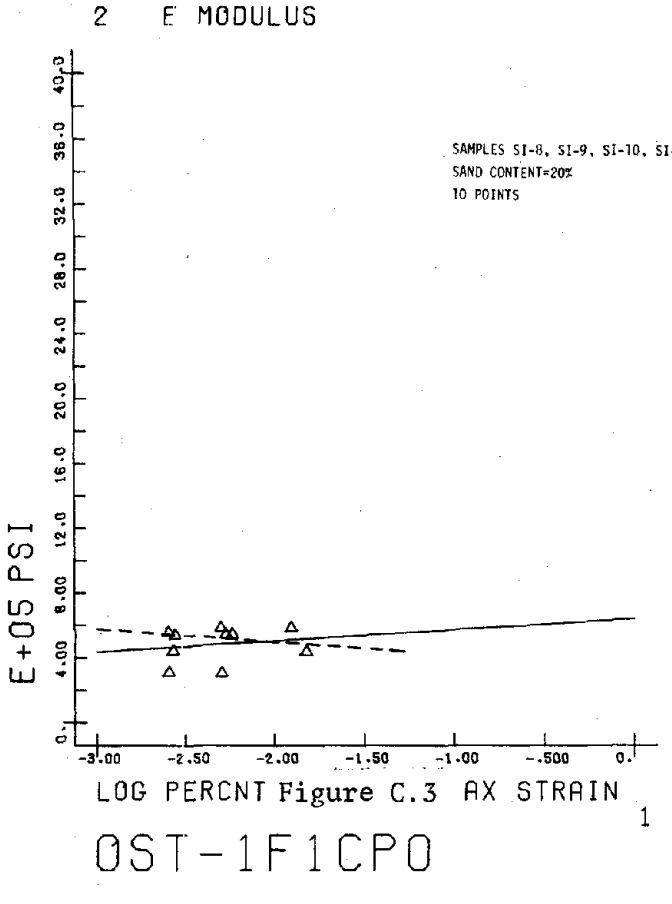

Figure C.3

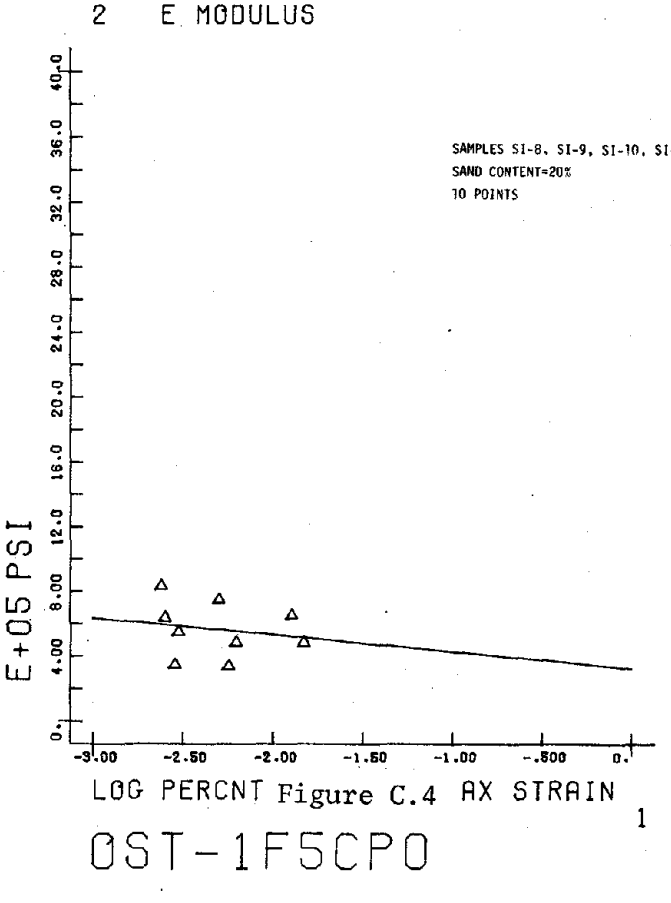

Figure C.4

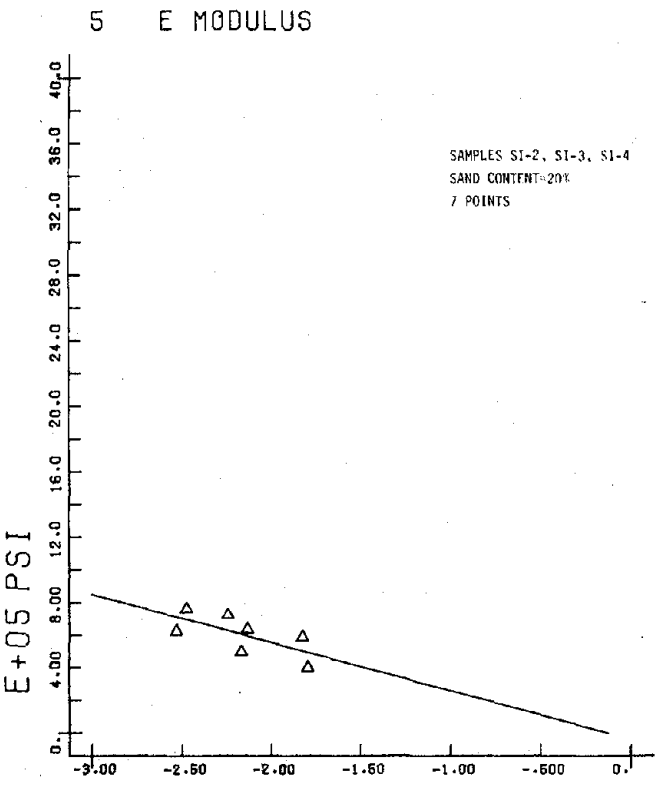

Figure C.5

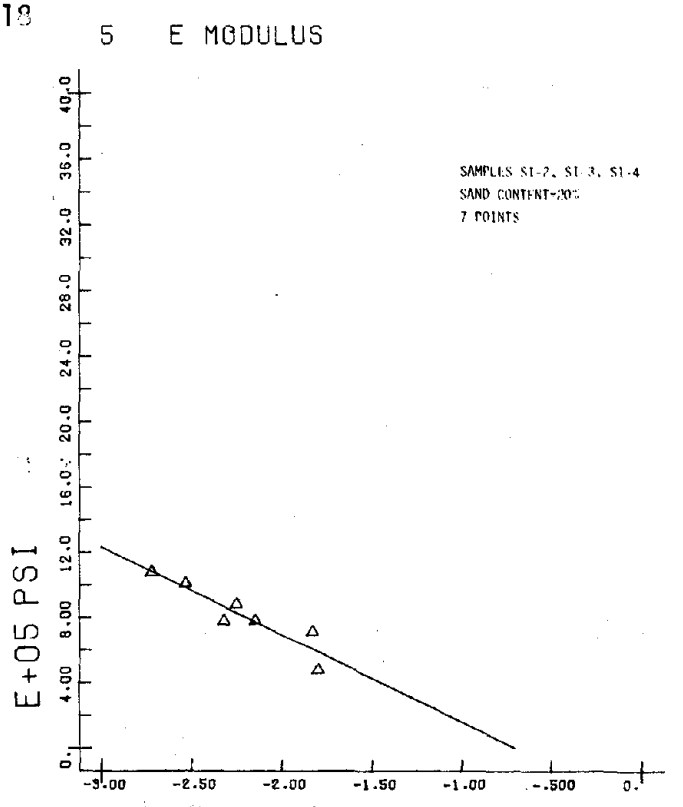

Figure C.6

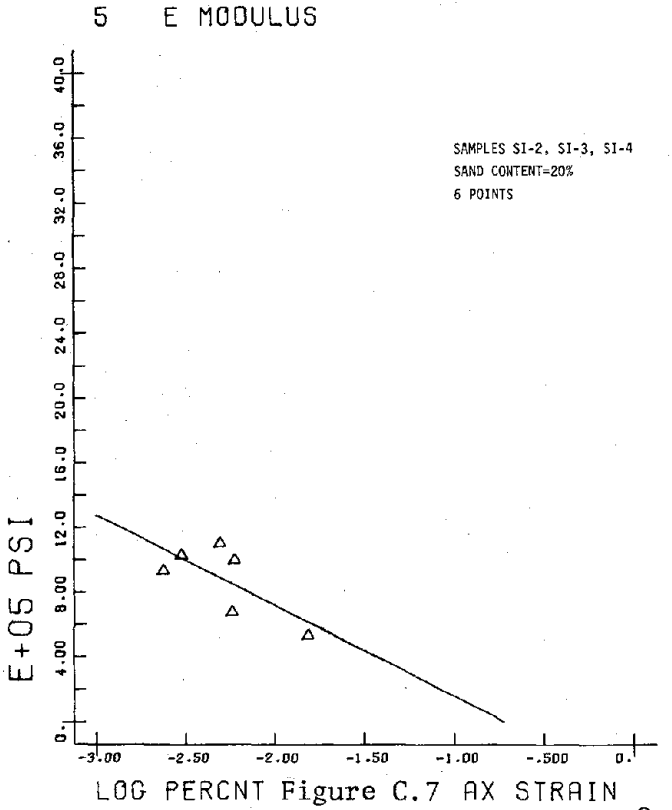

Figure C.7

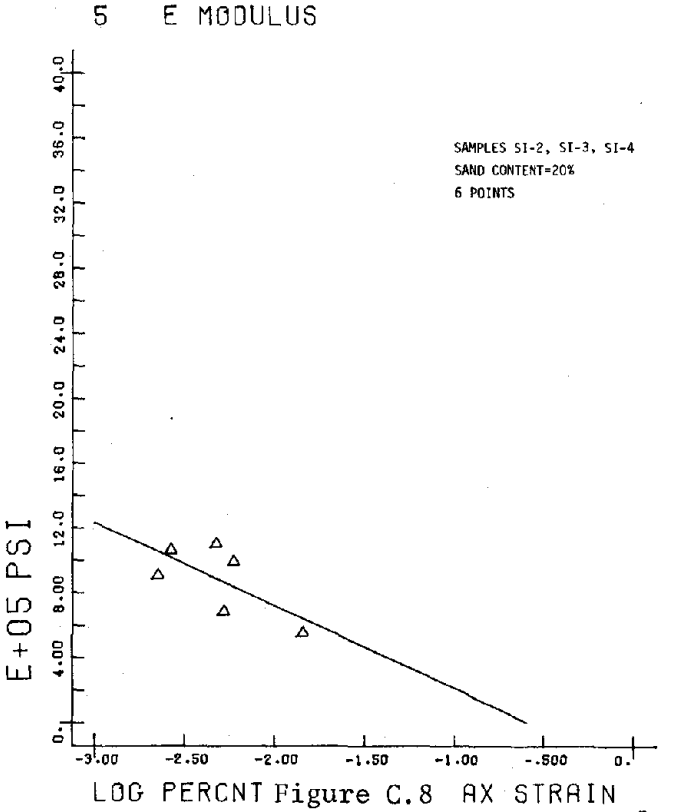

Figure C.8

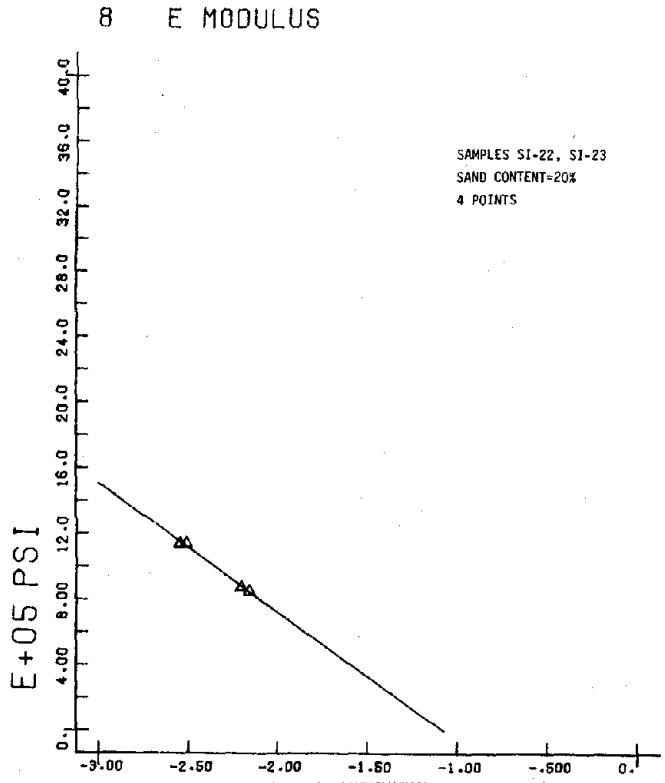

Figure C.9

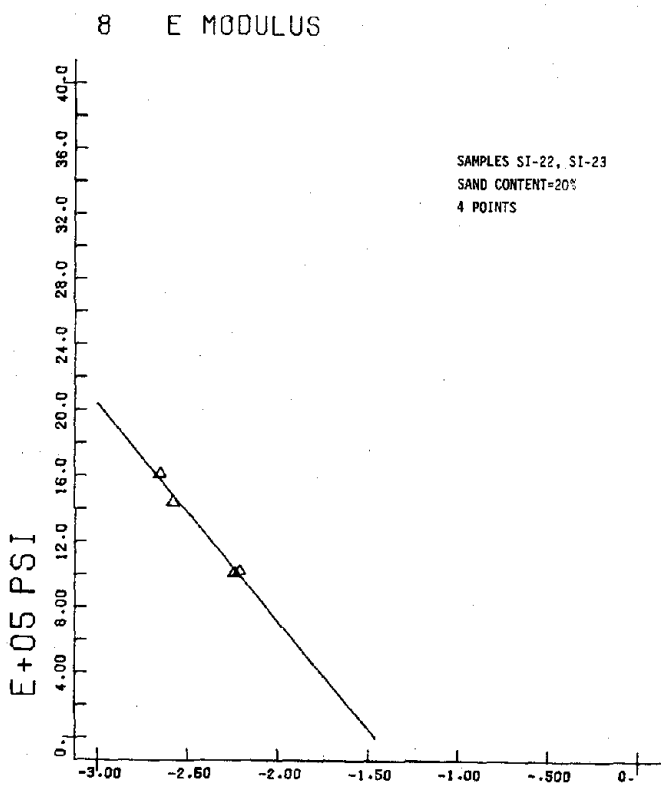

Figure C.10

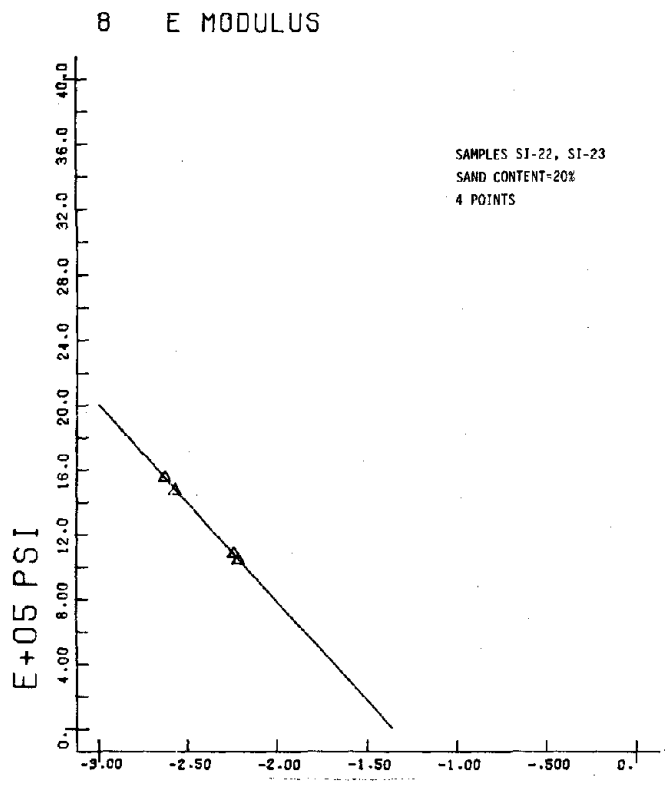

Figure C.11

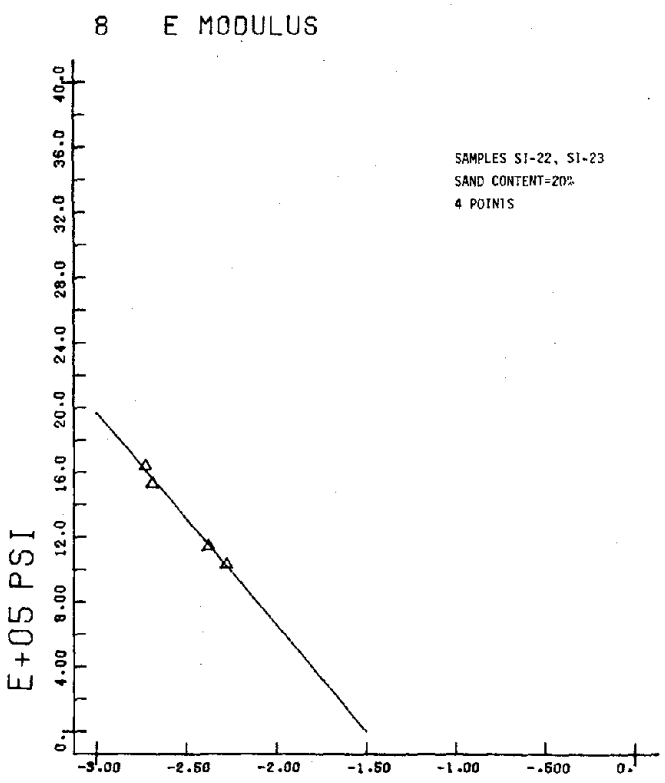

Figure C.12

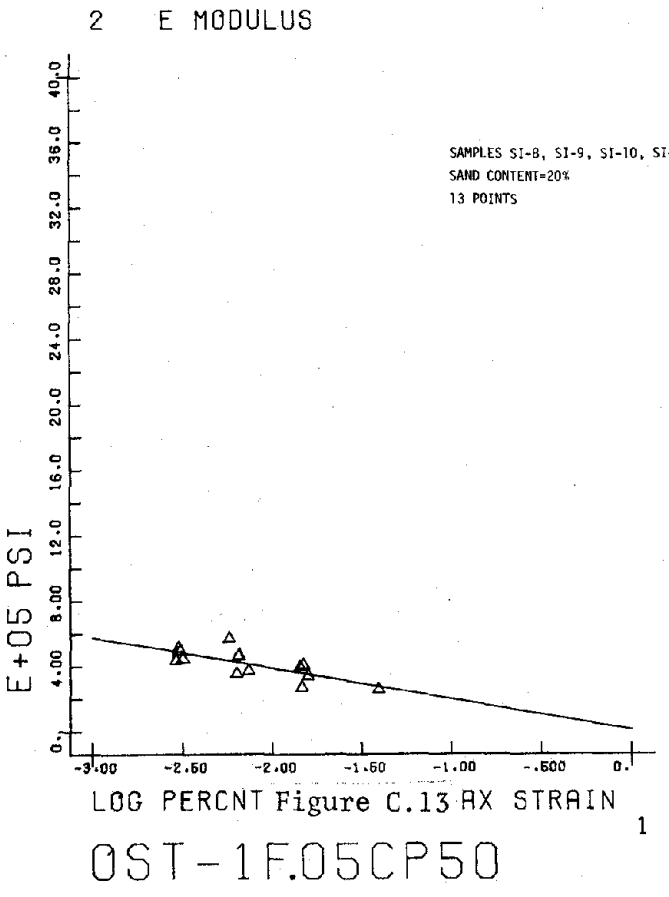

Figure C.13

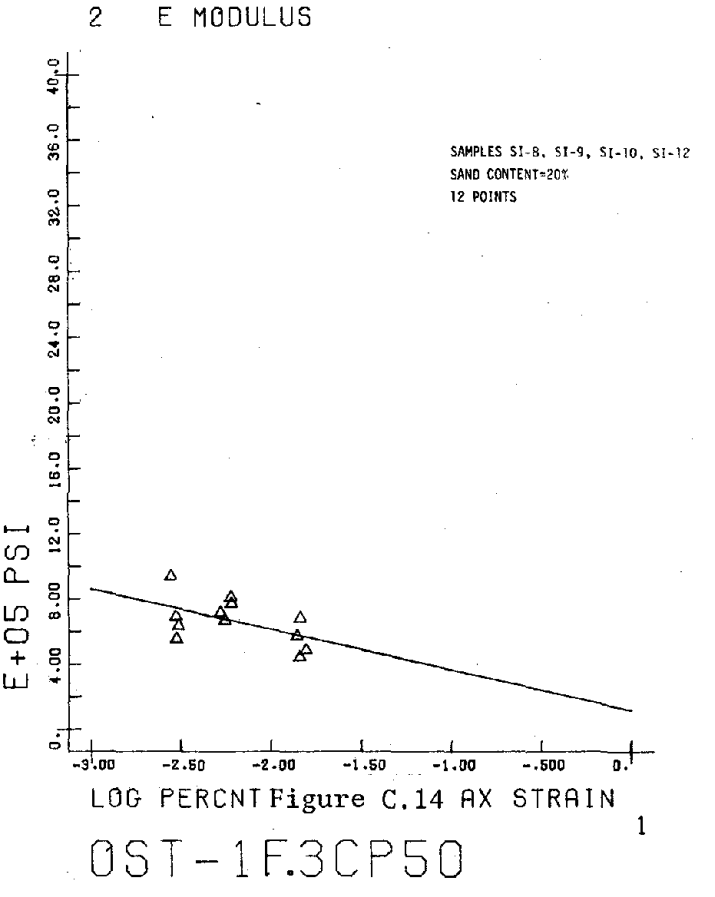

Figure C.14

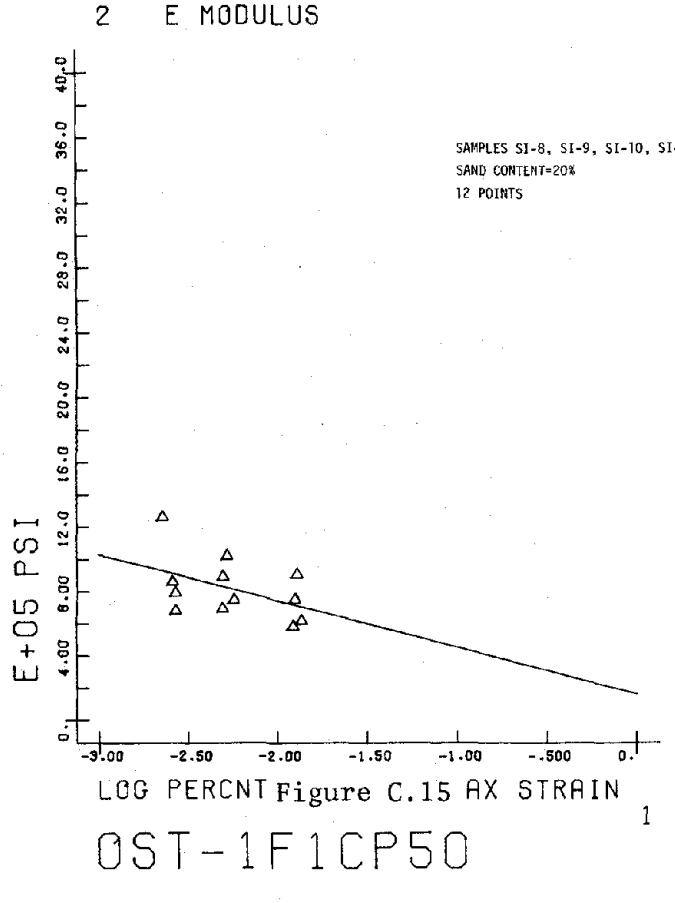

Figure C.15

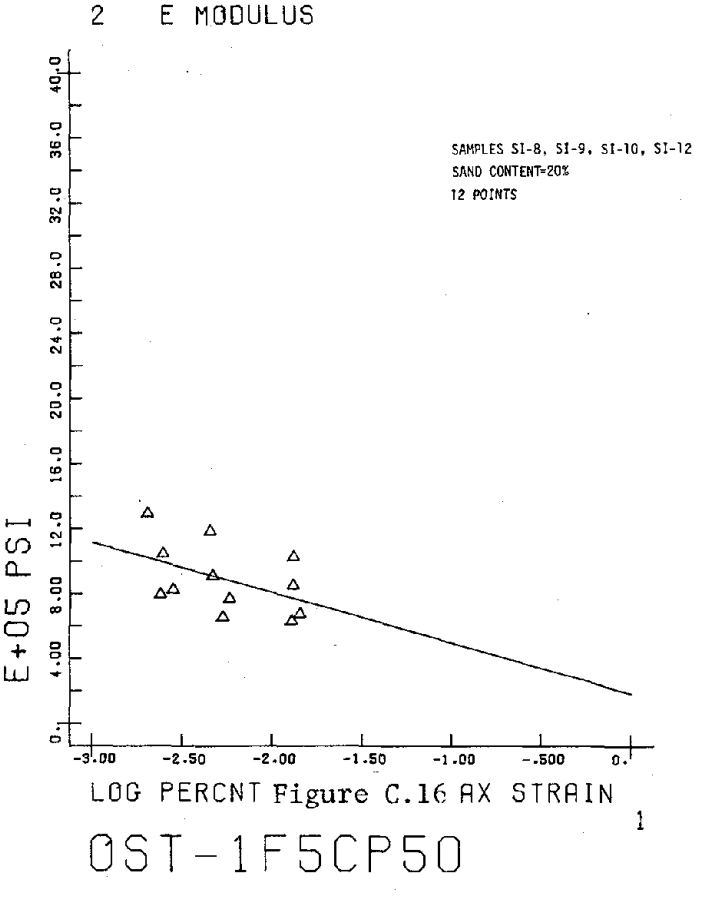

Figure C.16

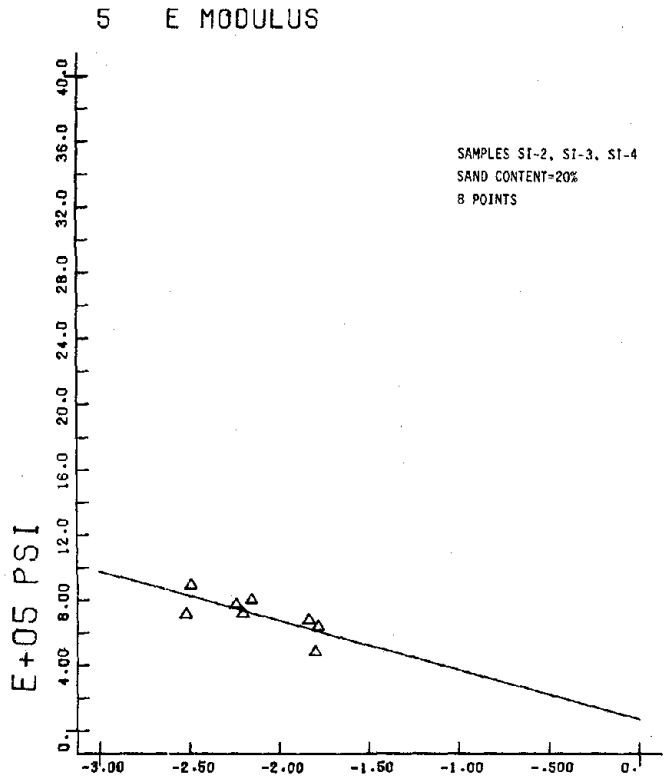

Figure C.17

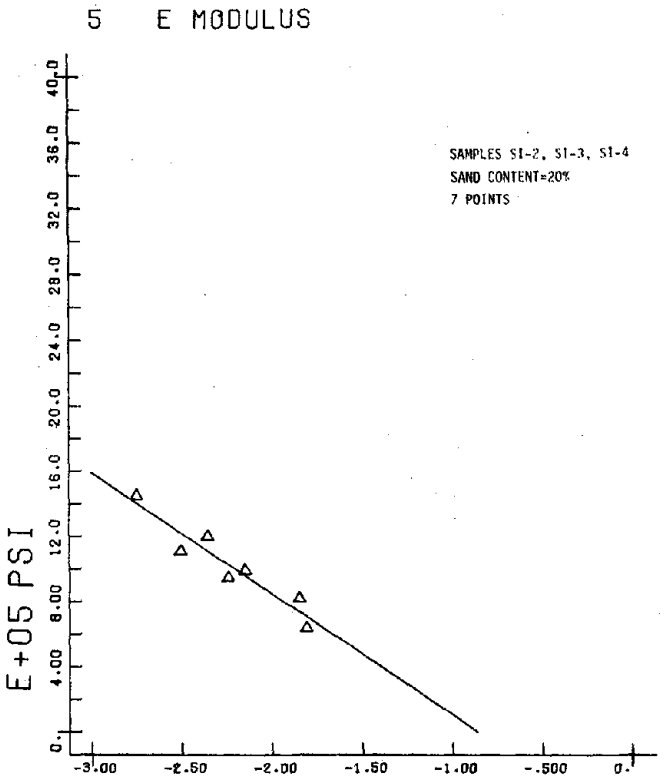

Figure C.18

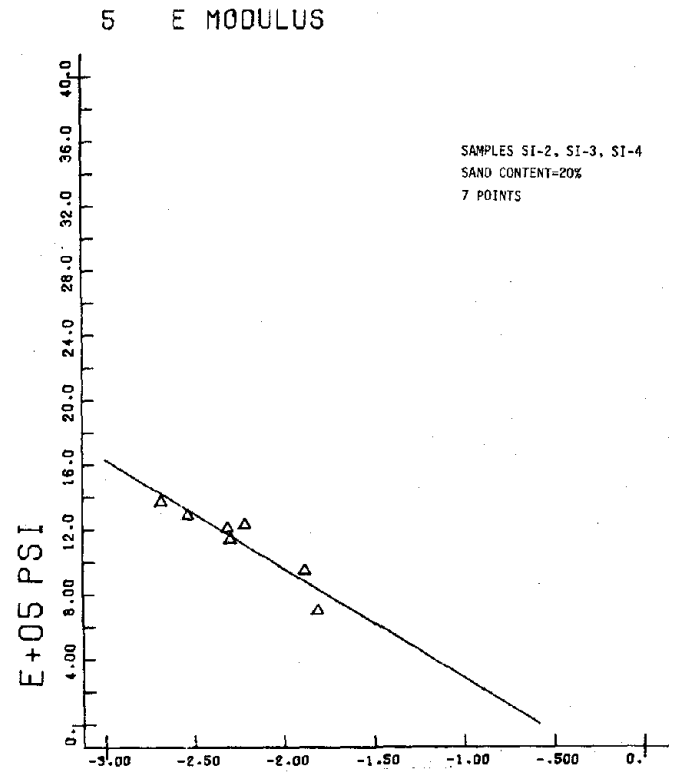

Figure C.19

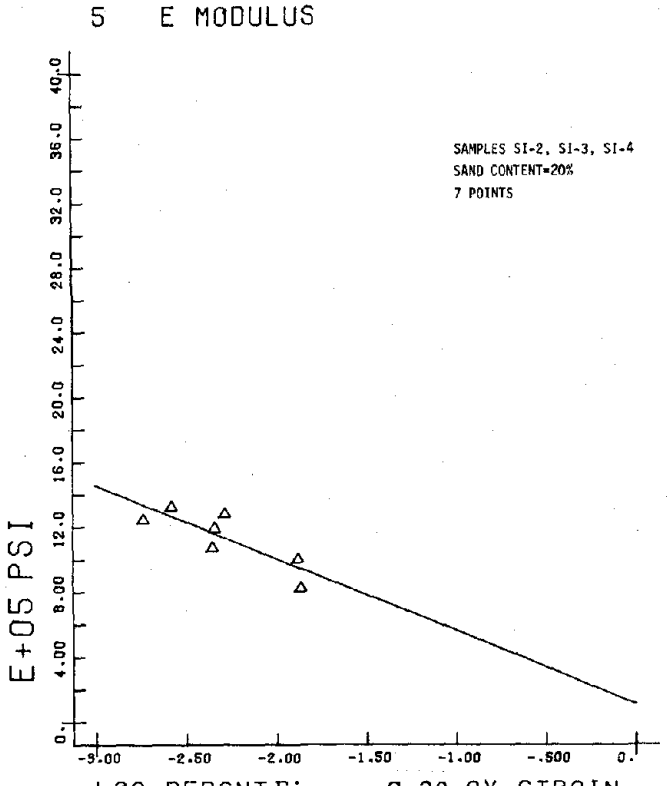

Figure C.20

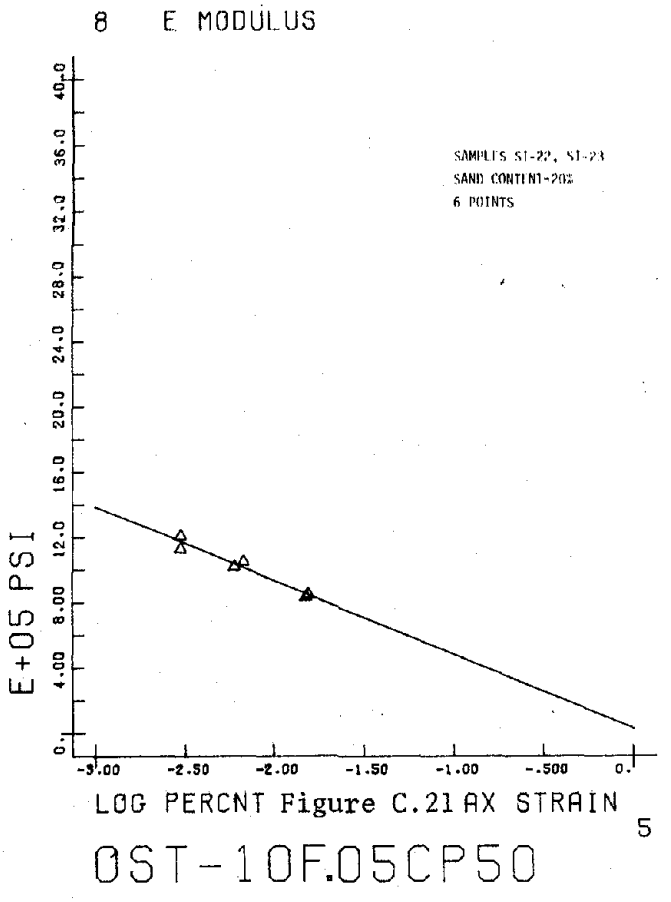

Figure C.21

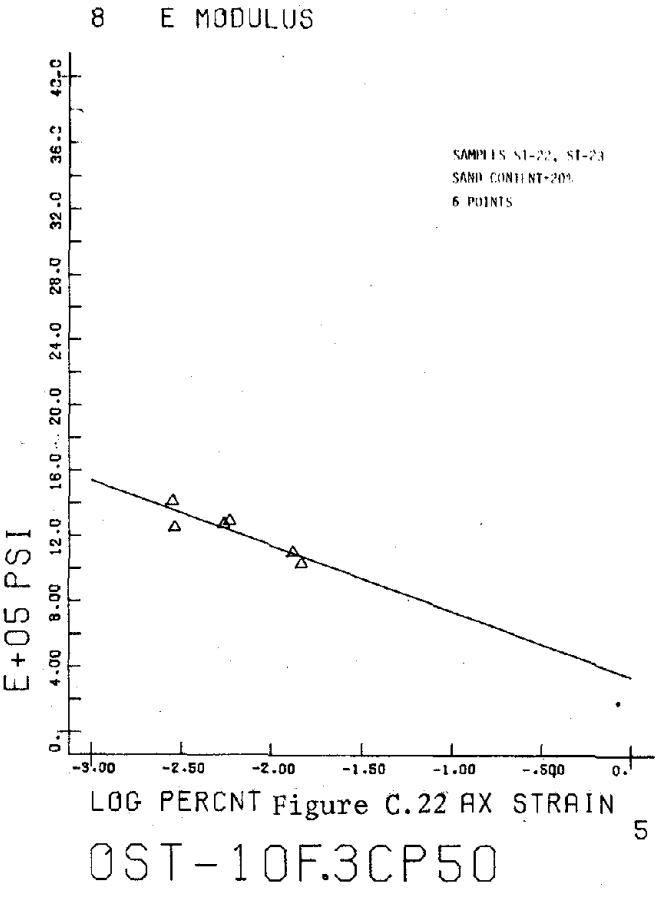

Figure C.22

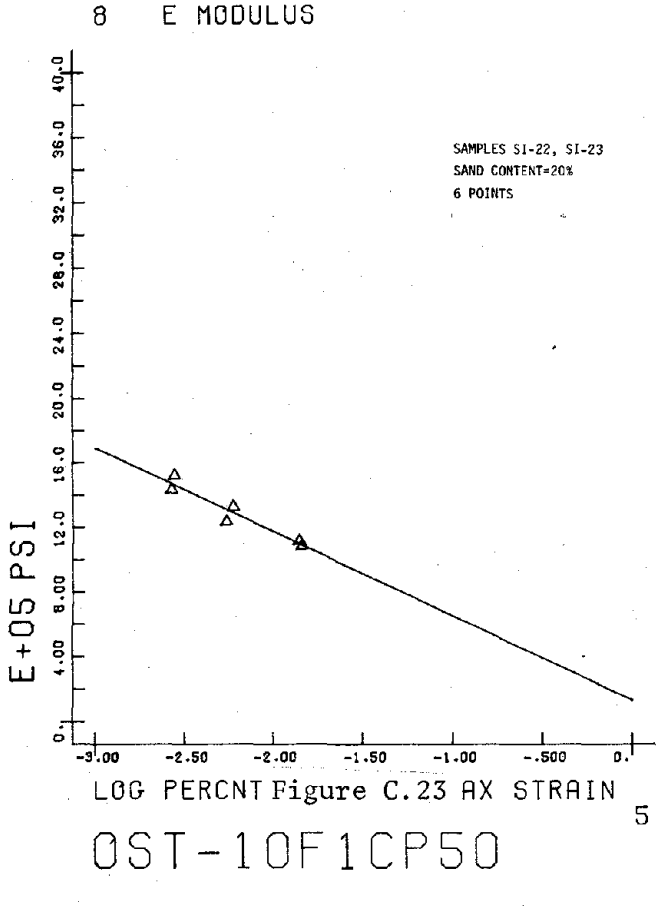

Figure C.23

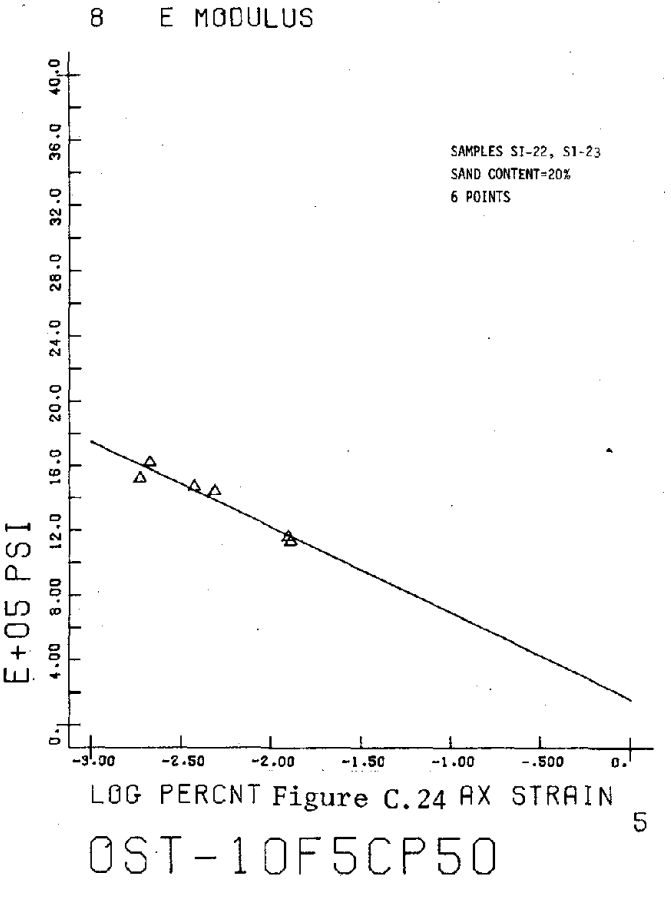

Figure C.24

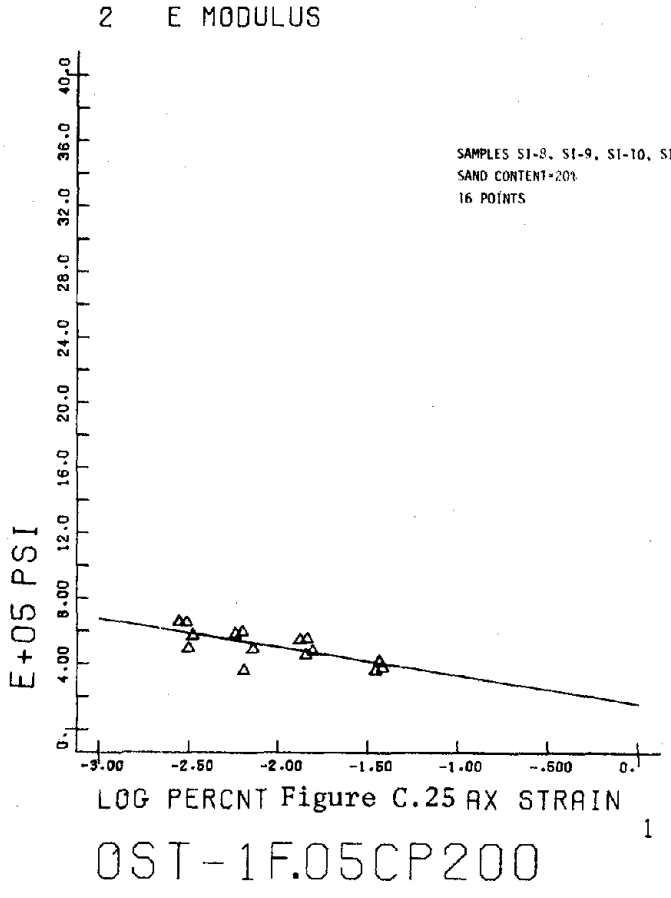

Figure C.25 OST-1F.05CP200

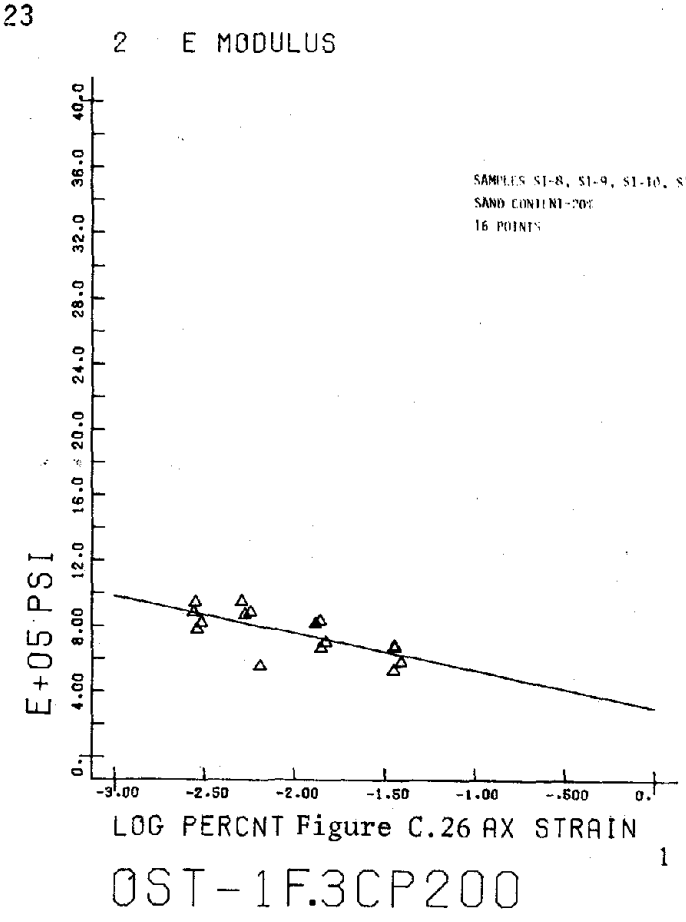

Figure C.26 OST-1F.3CP200

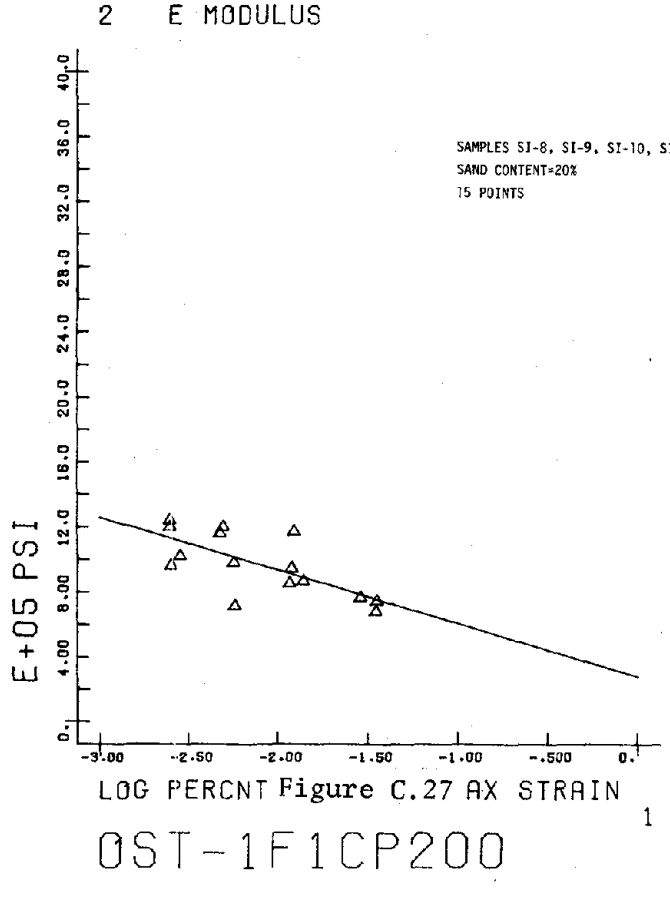

Figure C.27 OST-1F1CP200

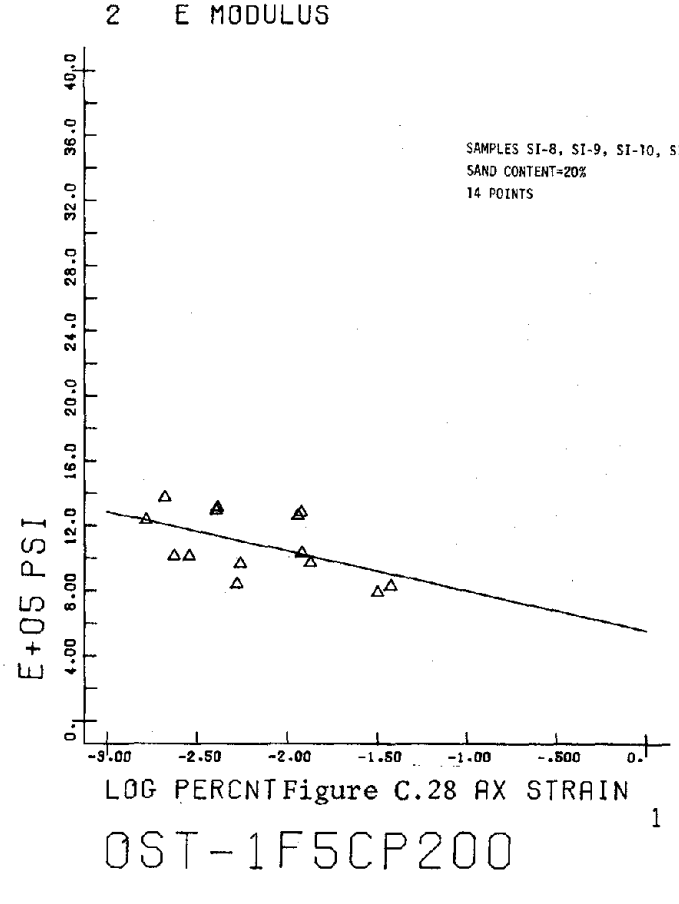

Figure C.28 OST-1F5CP200

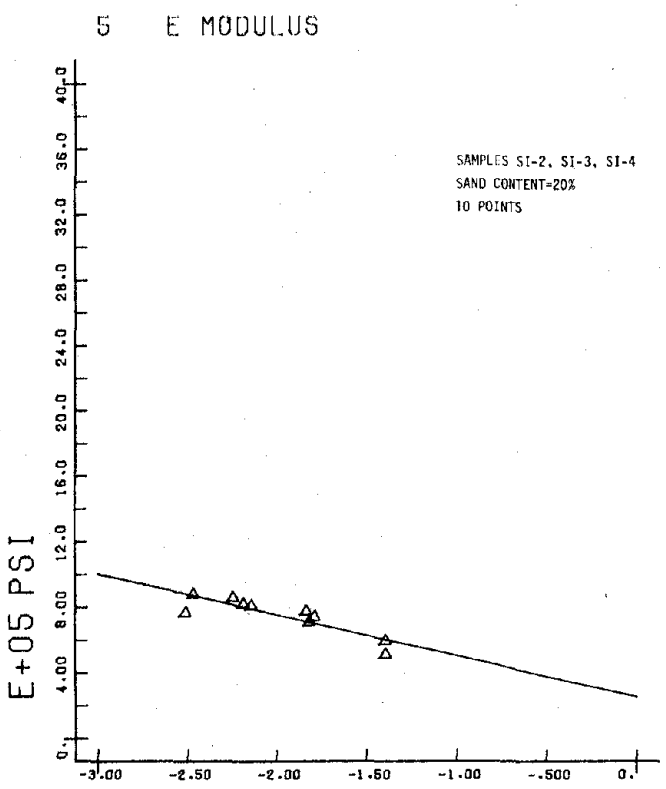

Figure C.29 OST-4F.05CP200

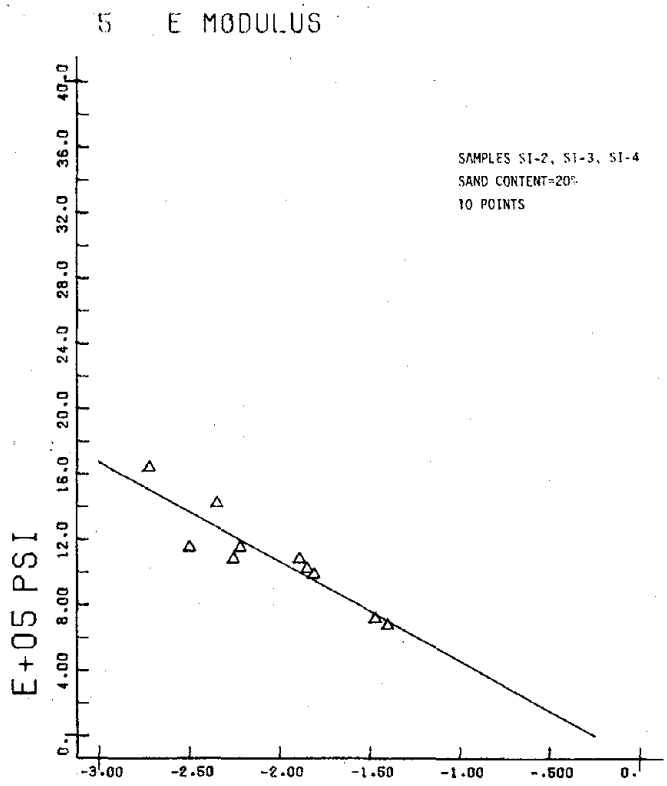

Figure C.30 OST-4F.3CP200

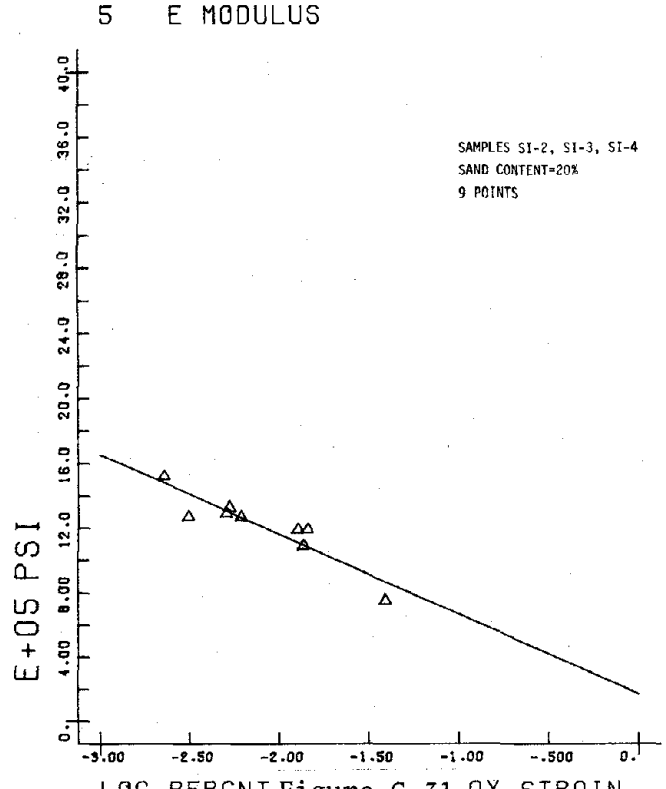

Figure C.31 OST-4F1CP200

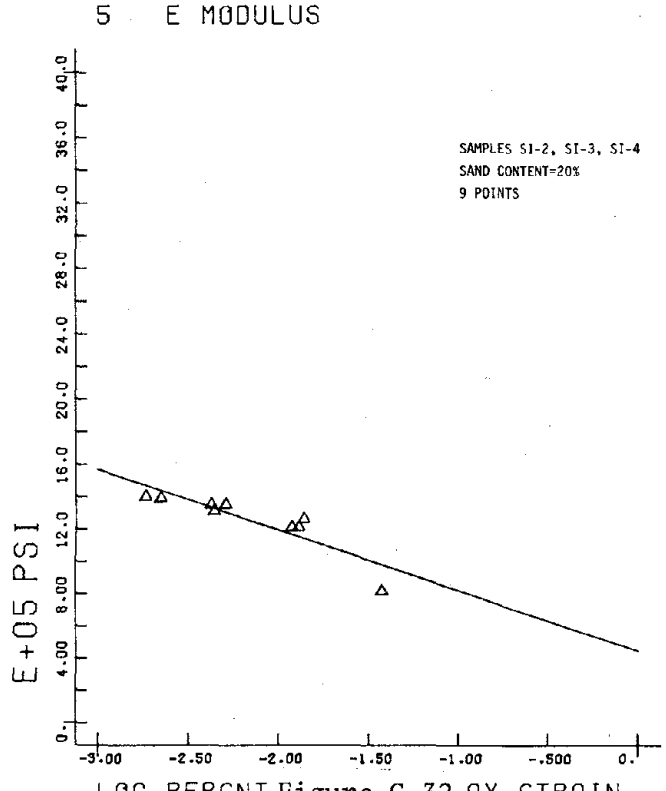

Figure C.32 OST-4F5CP200

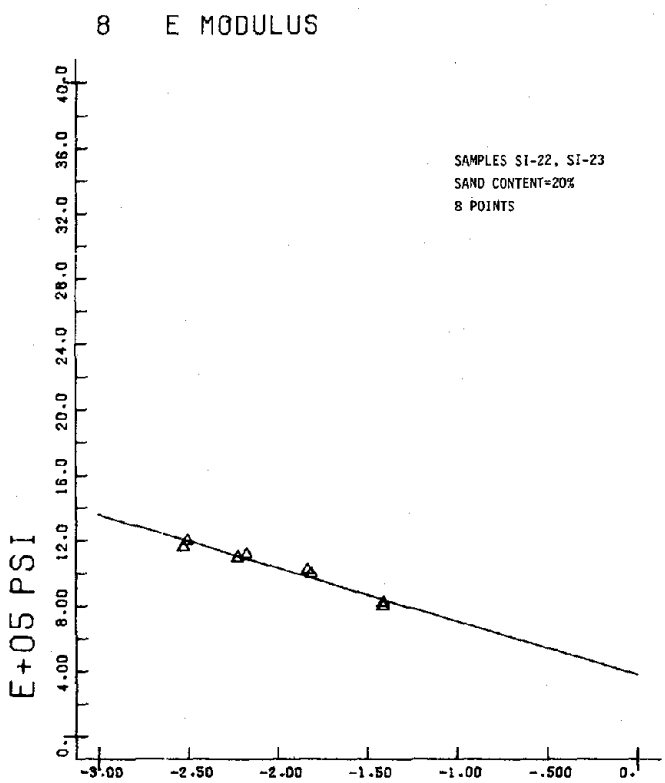

Figure C.33 OST-10F.05CP200

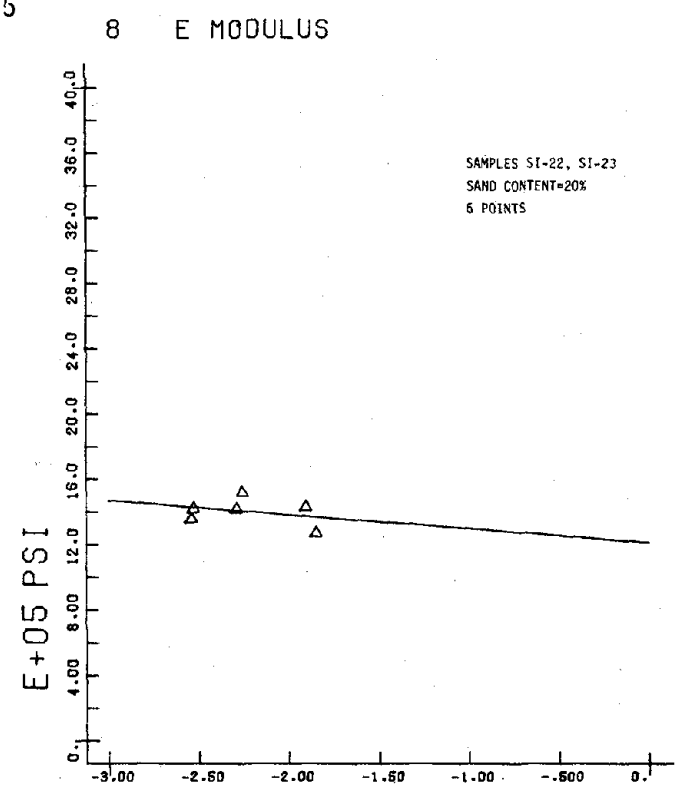

Figure C.34 OST-10F.3CP200

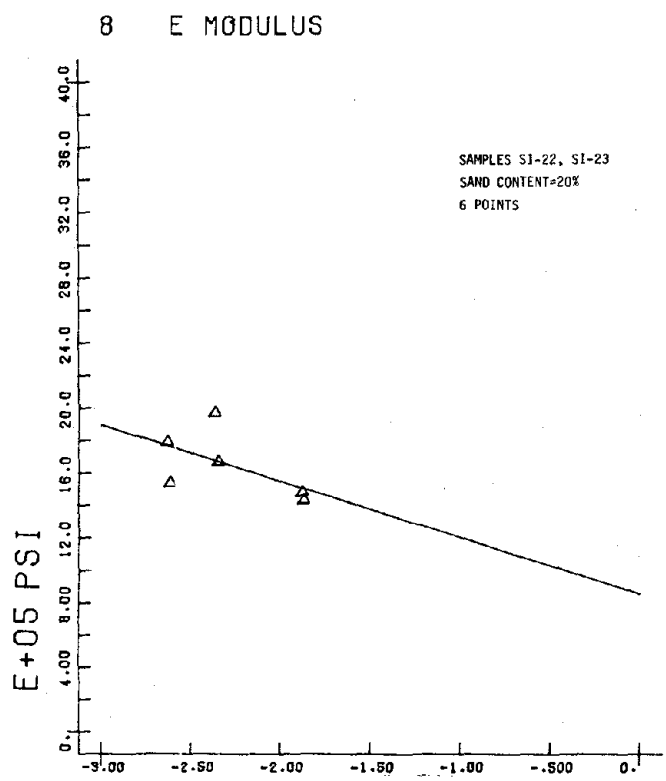

Figure C.35 OST-10F1CP200

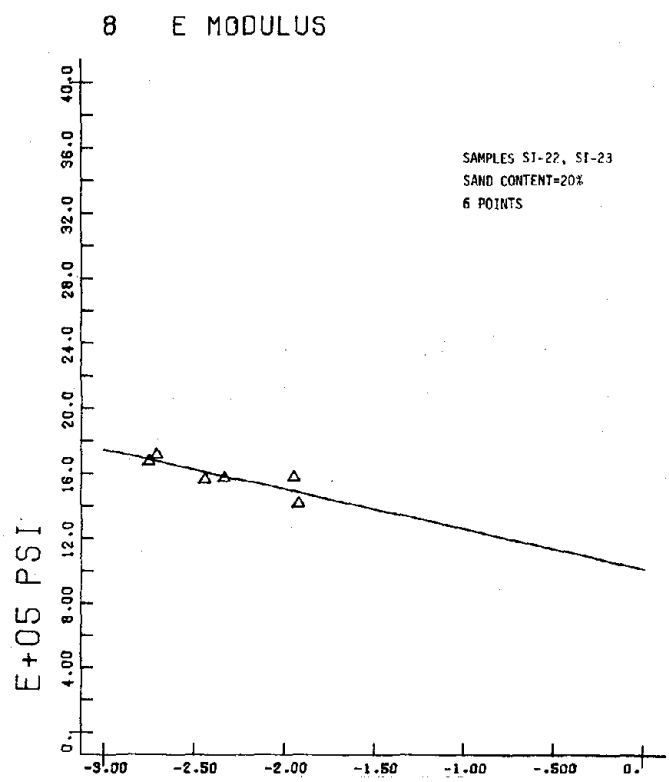

Figure C.36 OST-10F5CP200

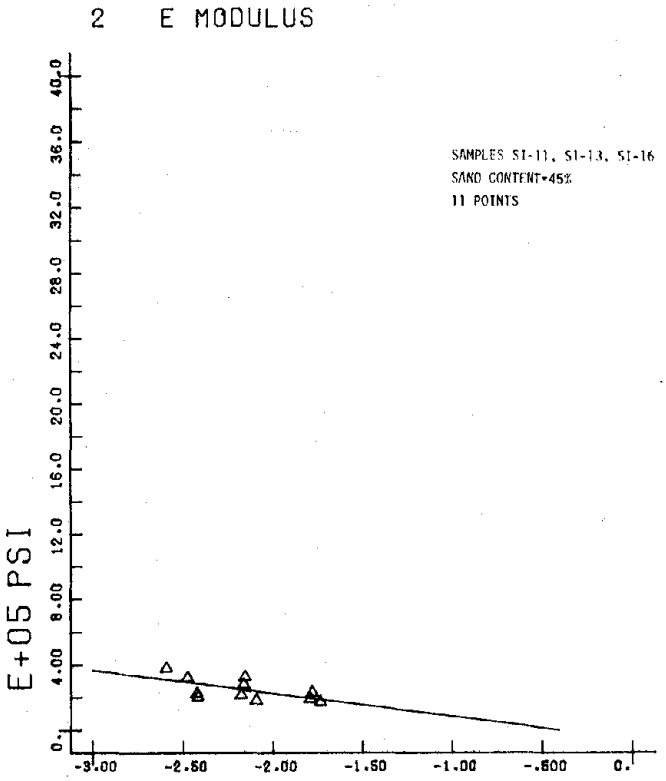

Figure C.37

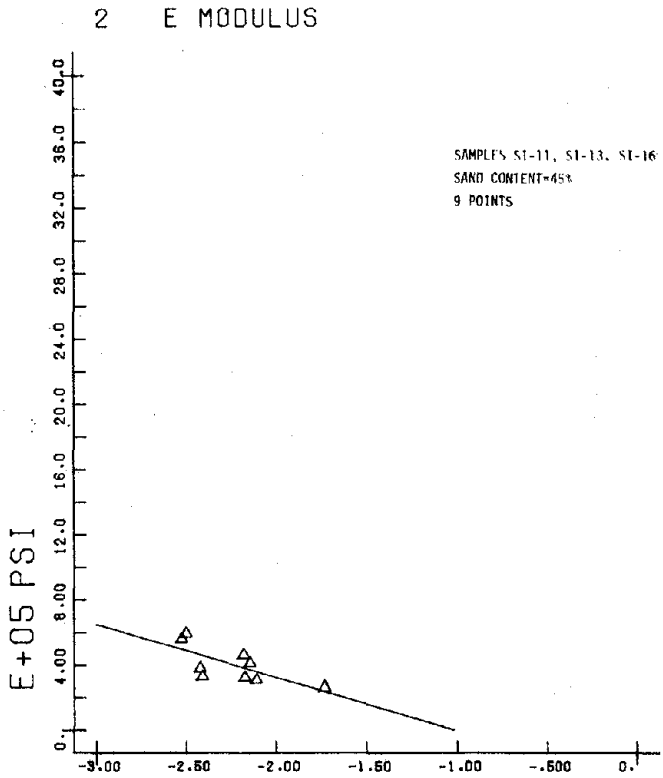

Figure C.38

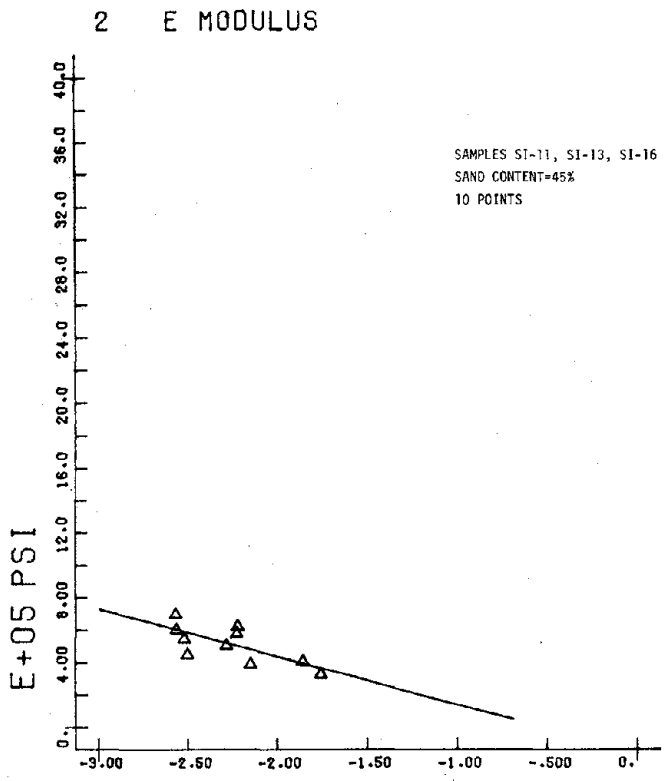

Figure C.39

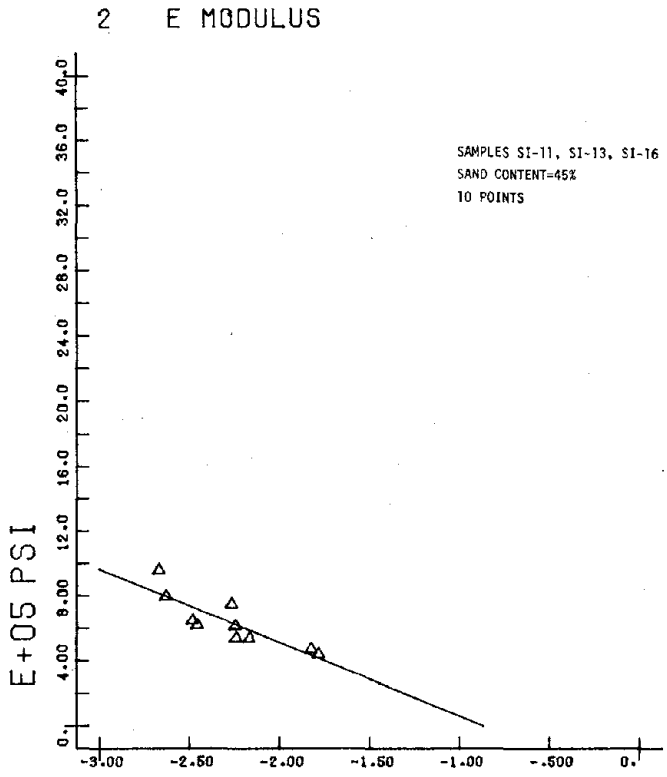

Figure C.40

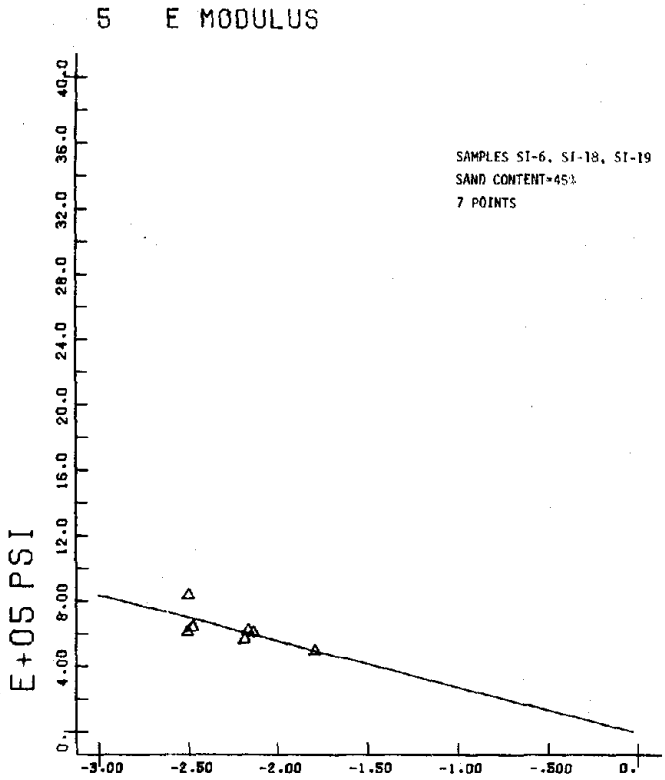

Figure C.41 OST-4F.05CPO

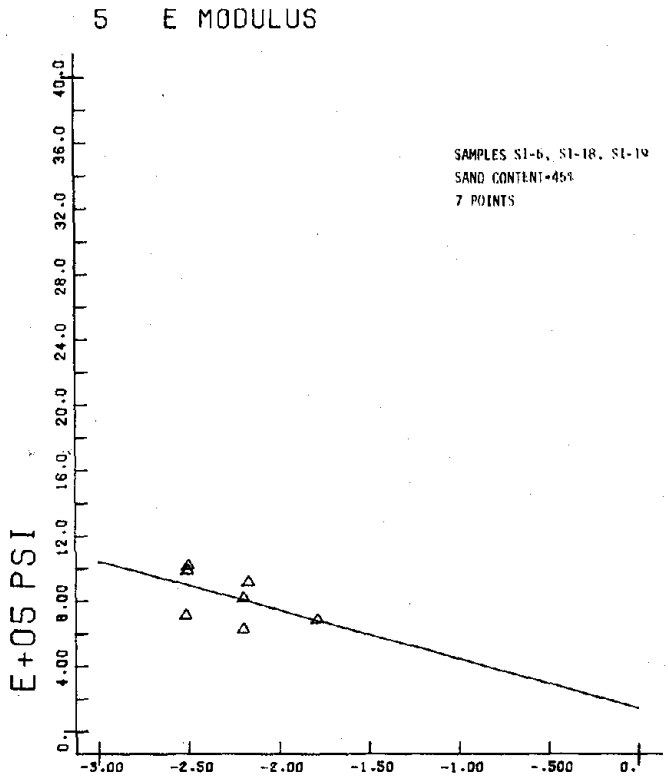

Figure C.42 OST-4F.3CPO

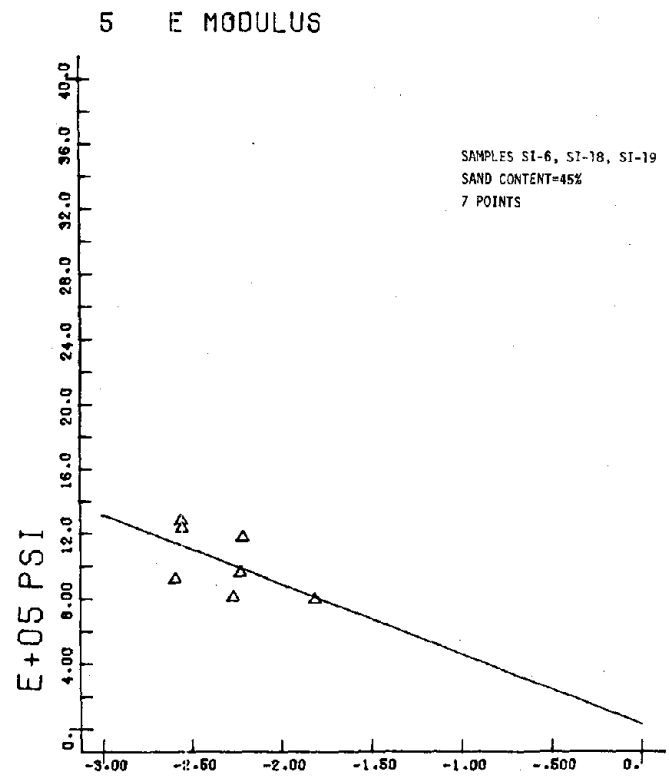

Figure C.43 OST-4F1CPO

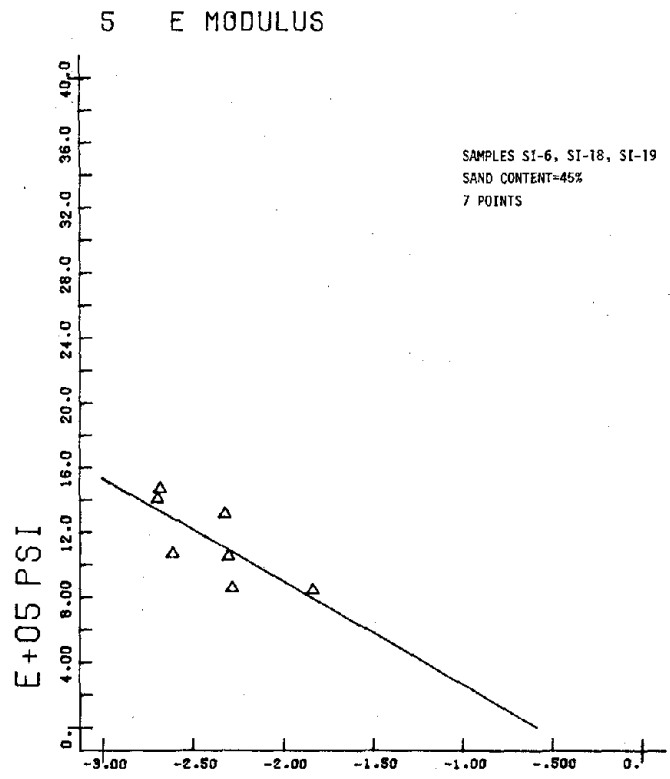

Figure C.44 OST-4F5CPO

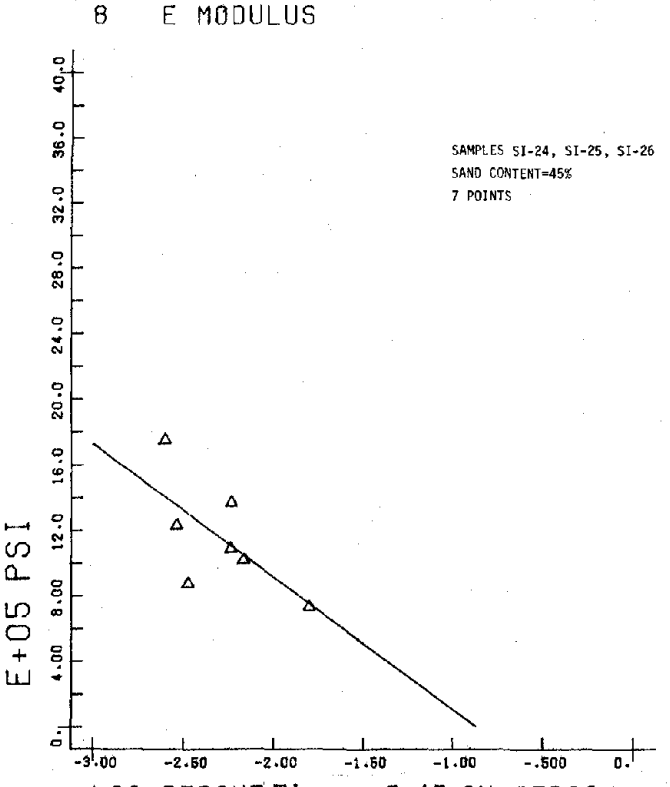

Figure C.45 AX STRAIN 1

OST-10F.05CPO

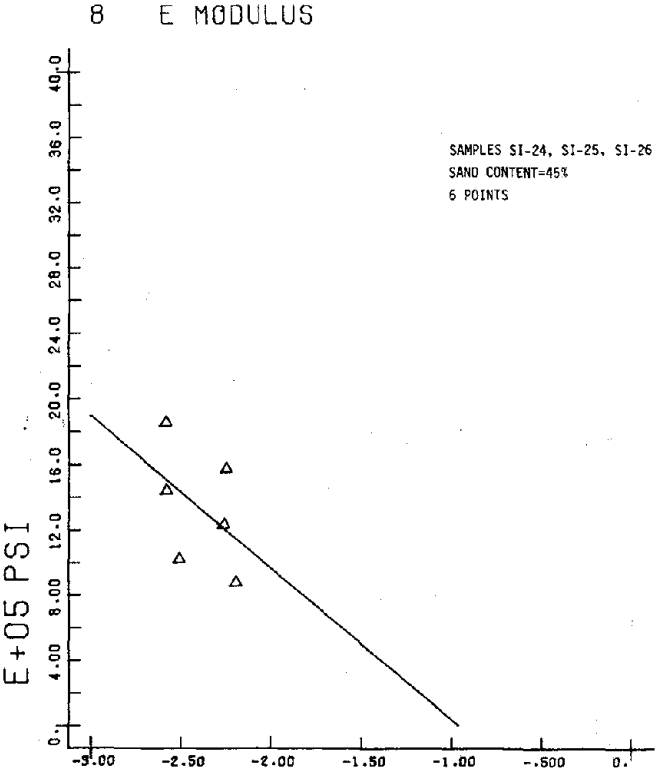

Figure C.46 AX STRAIN 5

OST-10F.3CPO

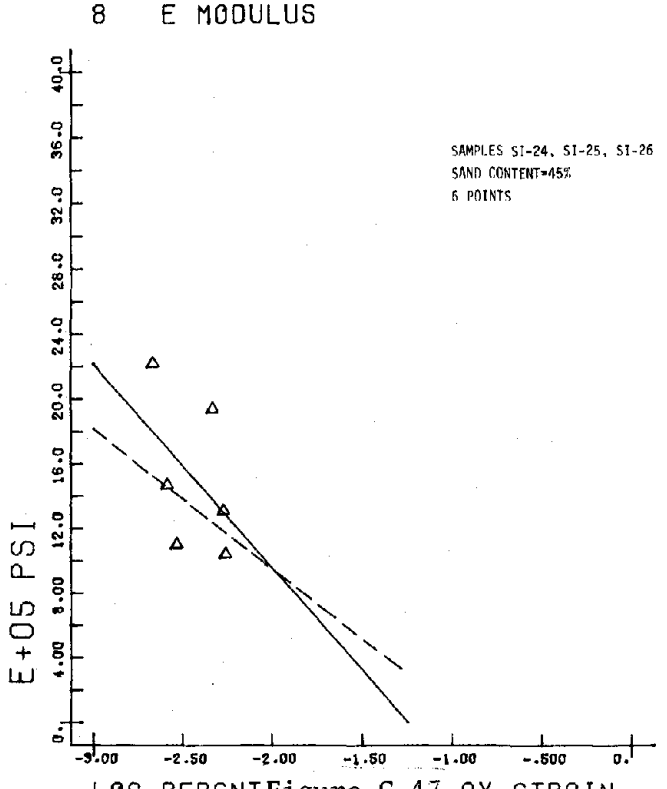

Figure C.47 AX STRAIN 5

OST-10F1CPO

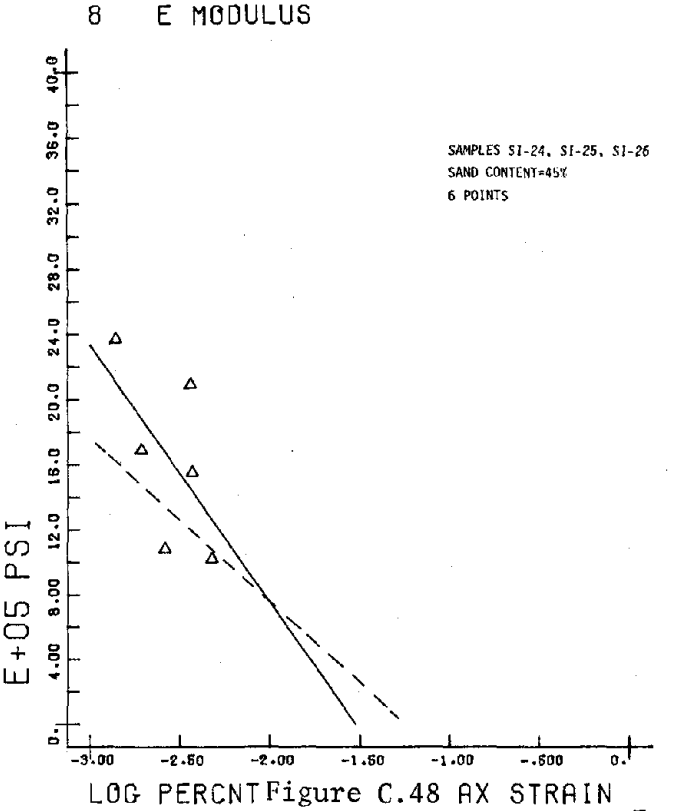

Figure C.48 AX STRAIN 5

OST-10F5CPO

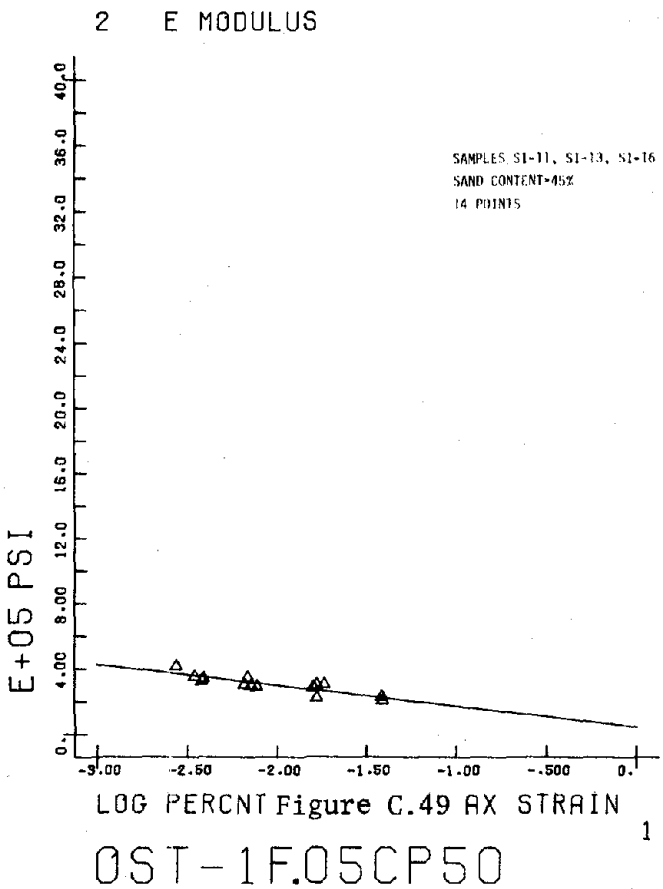

Figure C.49

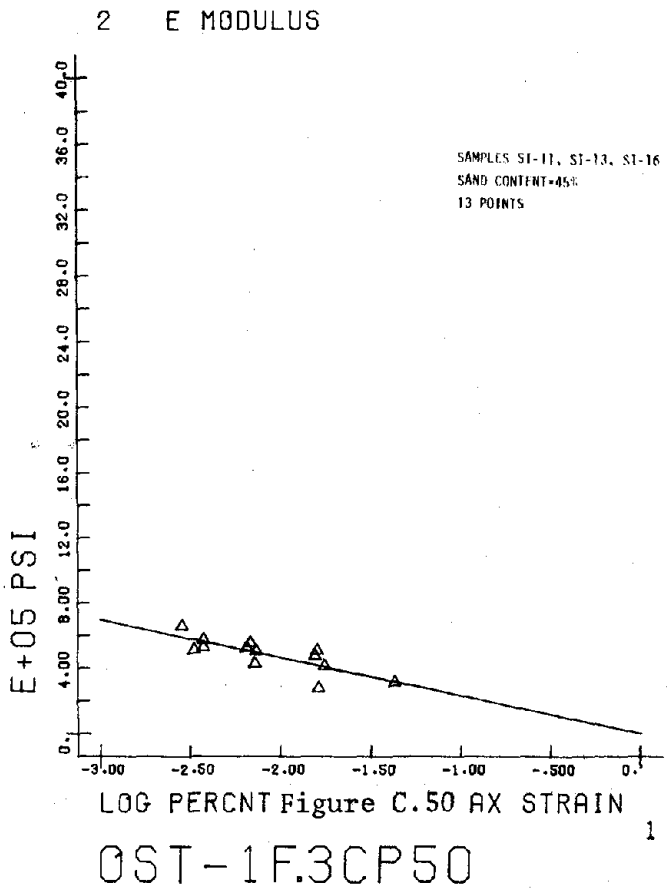

Figure C.50

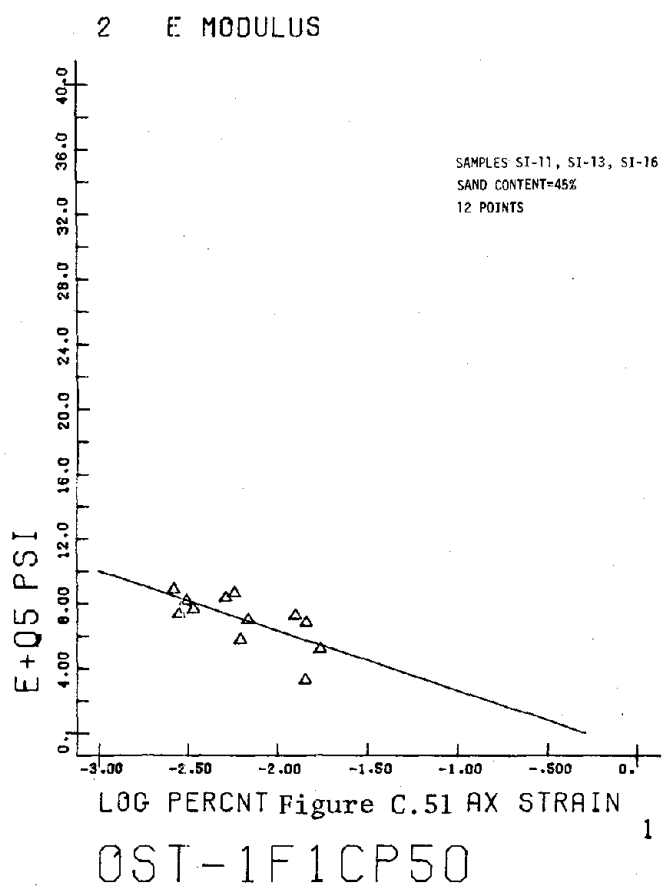

Figure C.51

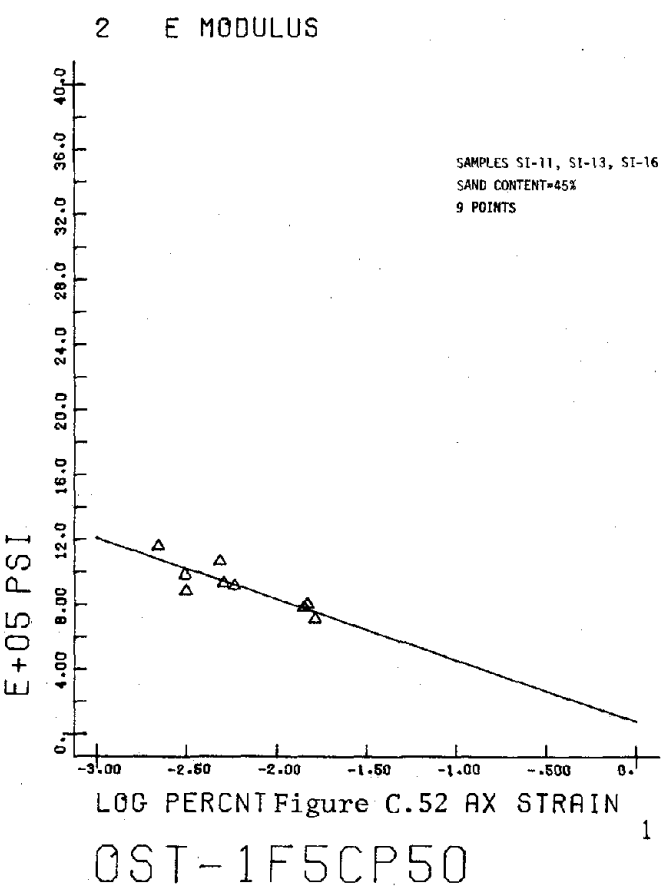

Figure C.52

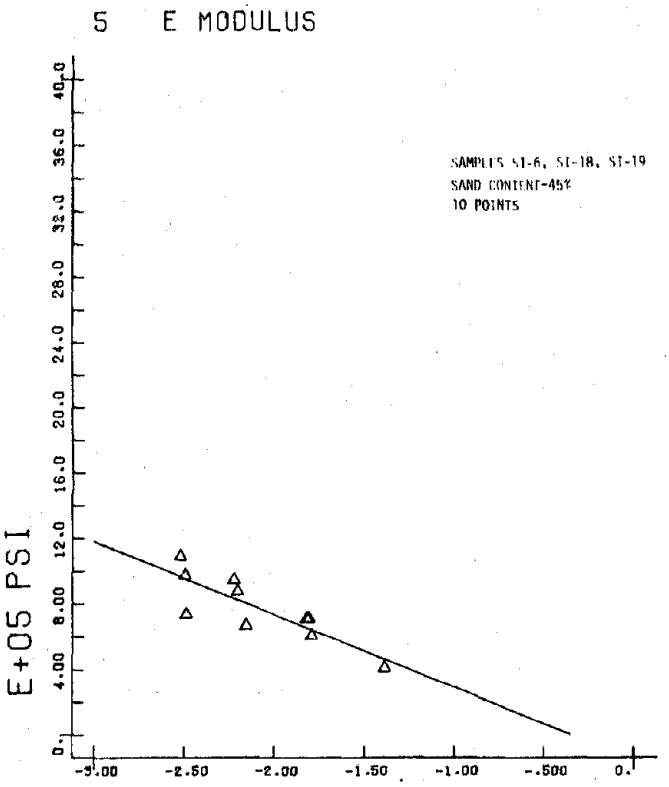

Figure C.53

OST-4F.05CP50

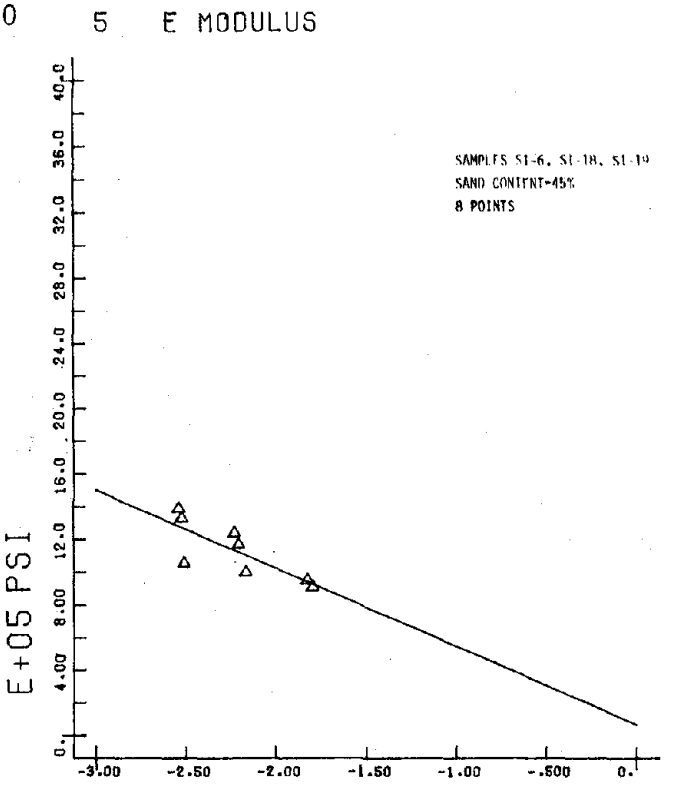

Figure C.54

OST-4F.3CP50

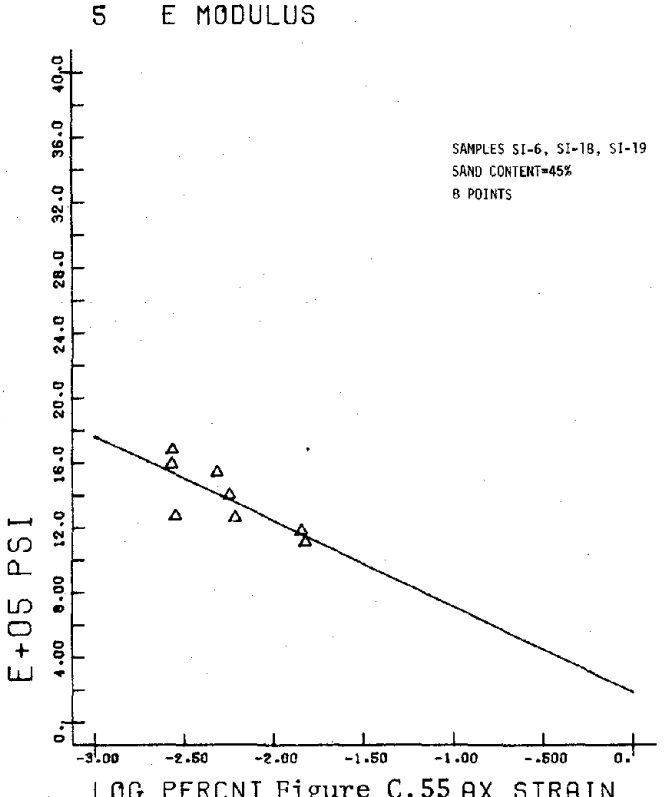

Figure C.55

OST-4F1CP50

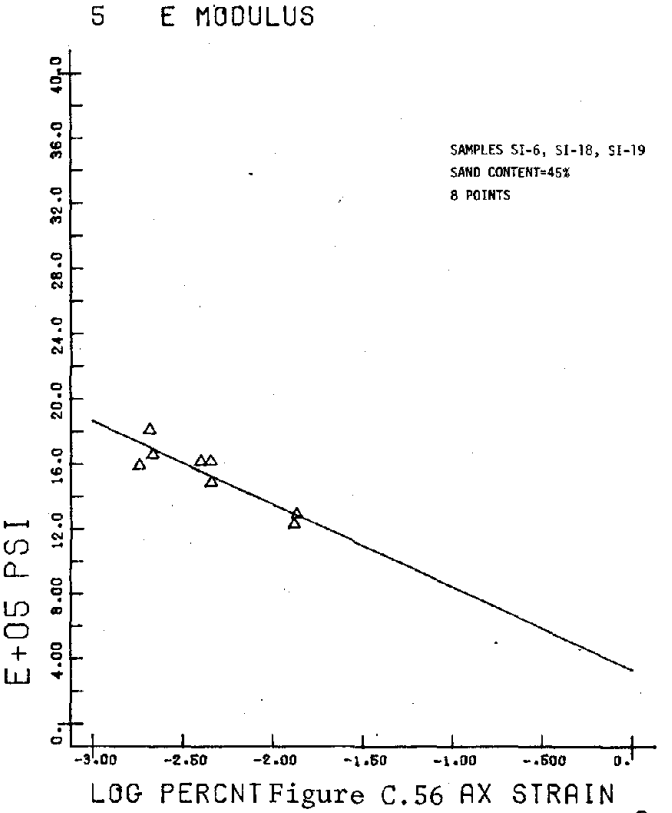

Figure C.56

OST-4F5CP50

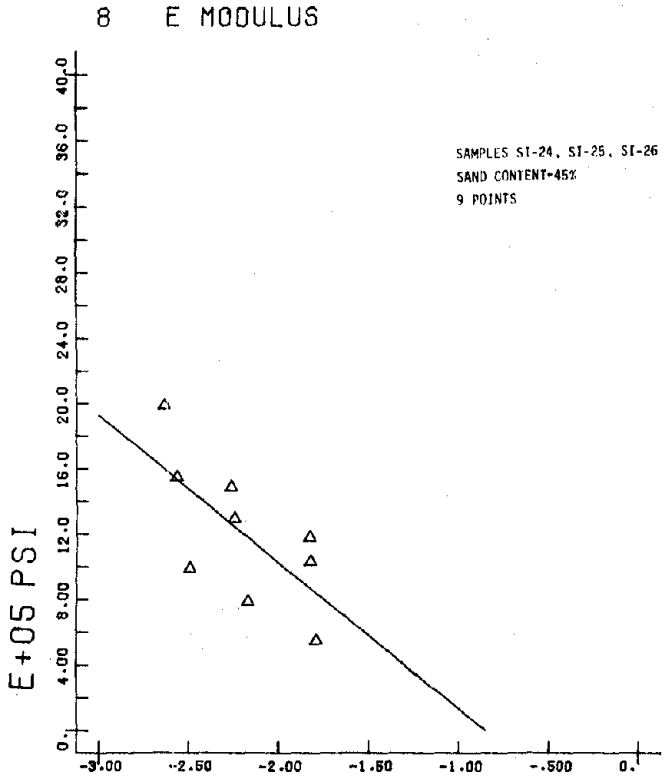

Figure C.57

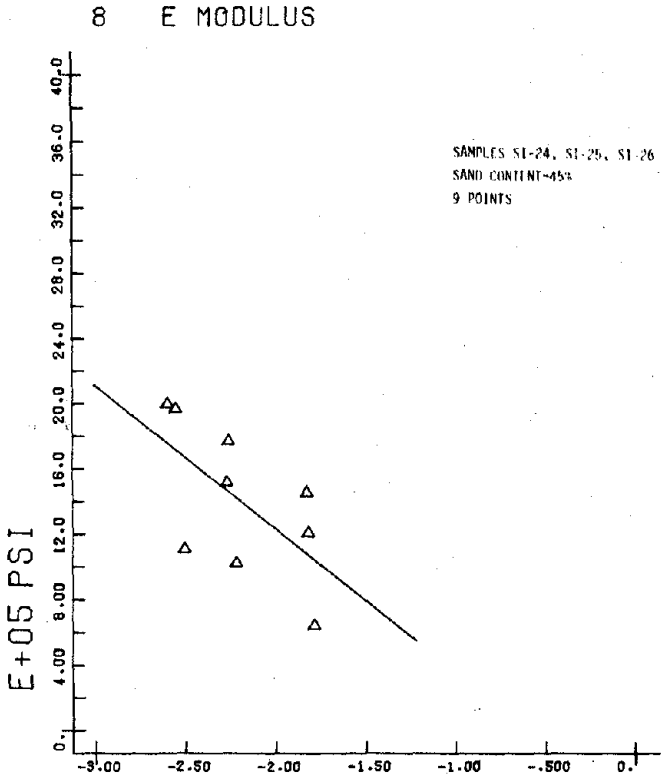

Figure C.58

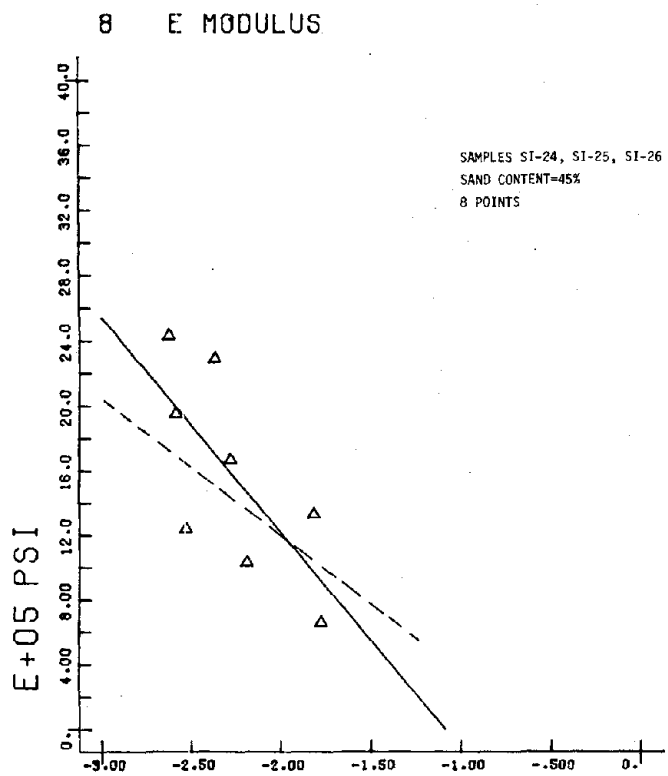

Figure C.59

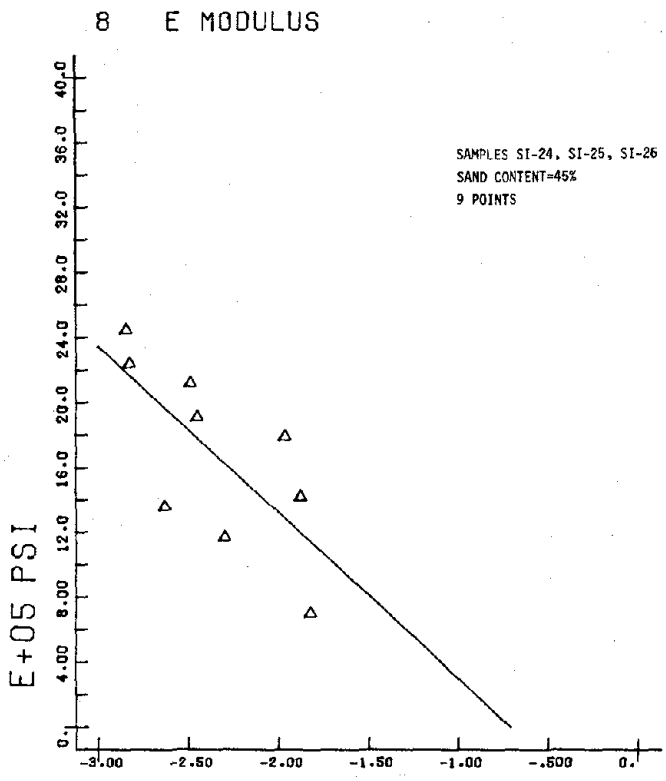

Figure C.60

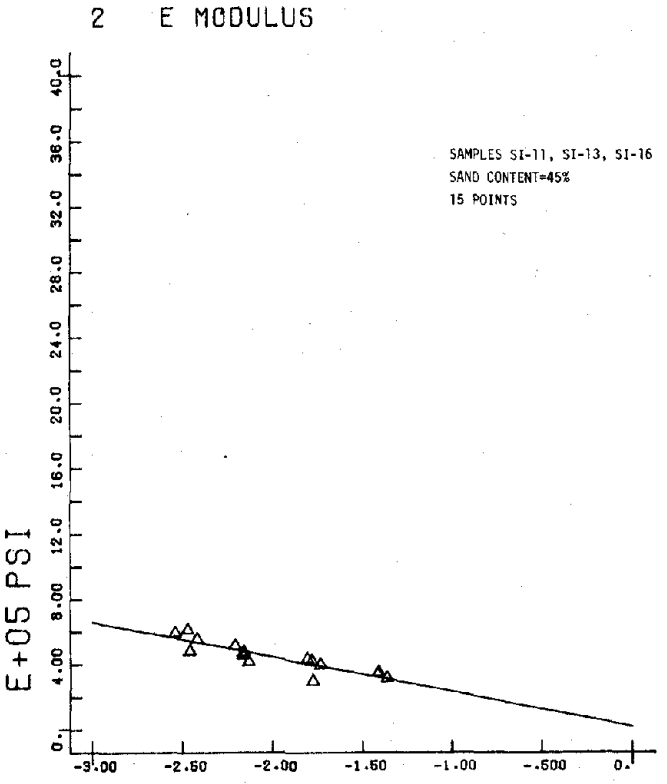
2 E MODULUS
SAMPLES SI-11, SI-13, SI-16
SAND CONTENT=45%
15 POINTS
E+05 PSI
LOG PERCNT Figure C.61 AX STRAIN
1
OST-1F.05CP200

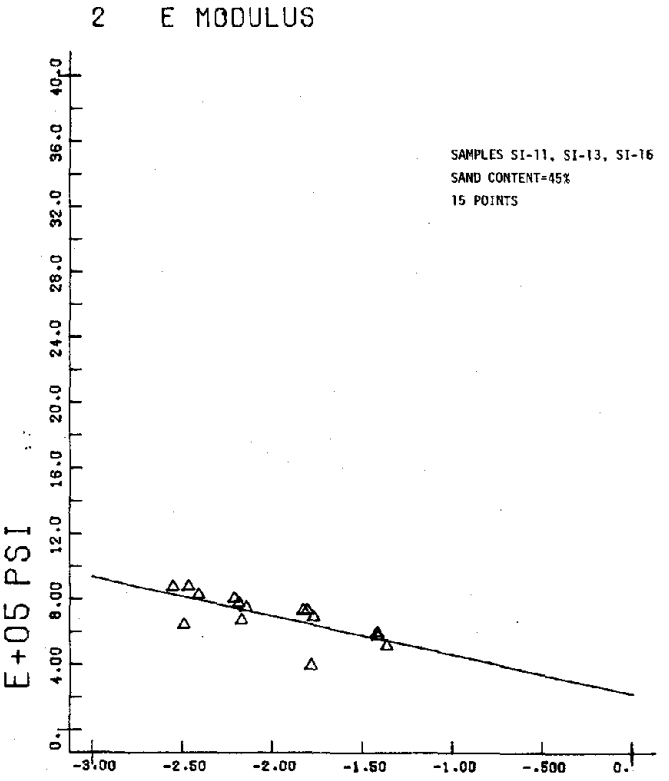
2 E MODULUS
SAMPLES SI-11, SI-13, SI-16
SAND CONTENT=45%
15 POINTS
E+05 PSI
LOG PERCNTFigure C.62 AX STRAIN
1
OST-1F.3CP200

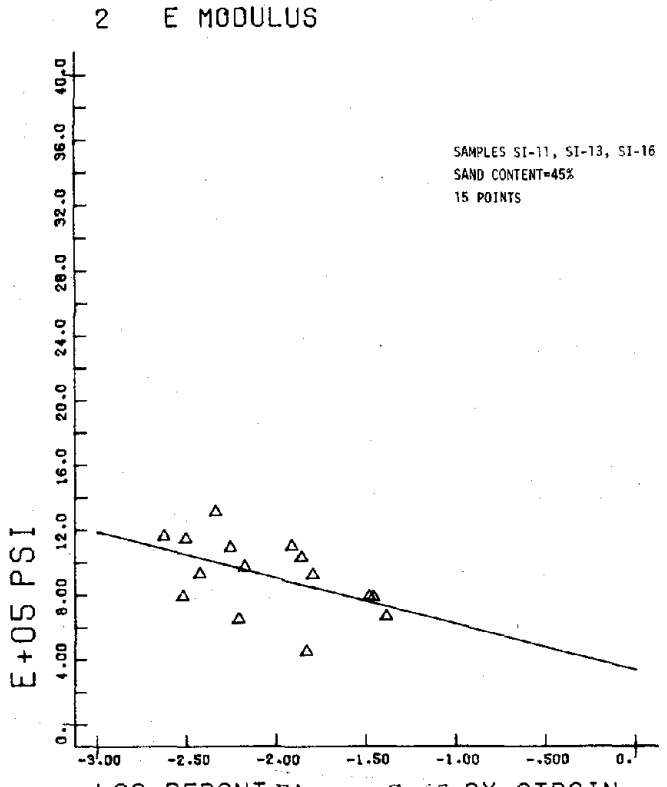
2 E MODULUS
SAMPLES SI-11, SI-13, SI-16
SAND CONTENT=45%
15 POINTS
E+05 PSI
LOG PERCNT Figure C.63 AX STRAIN
1
OST-1F1CP200

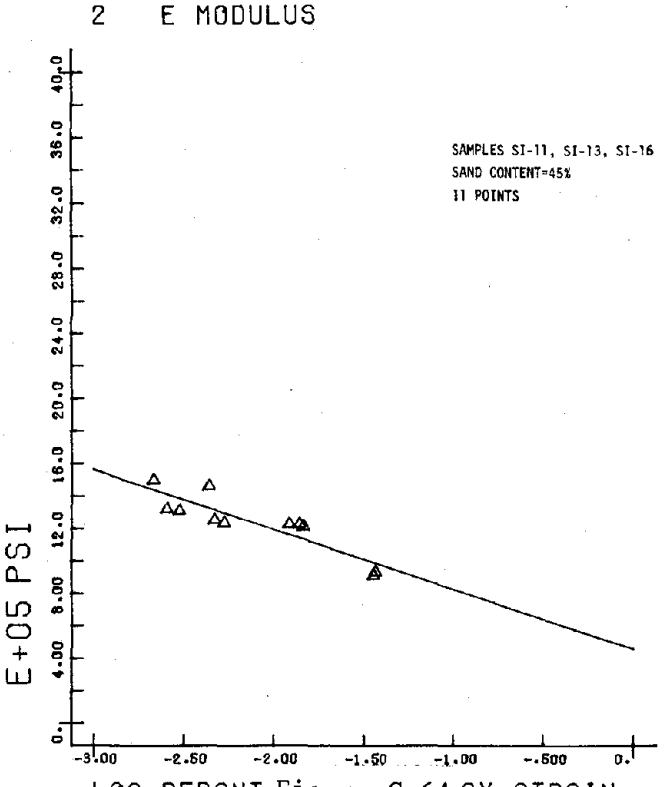
2 E MODULUS
SAMPLES SI-11, SI-13, SI-16
SAND CONTENT=45%
11 POINTS
E+05 PSI
LOG PERCNT Figure C.64 AX STRAIN
1
OST-1F5CP200

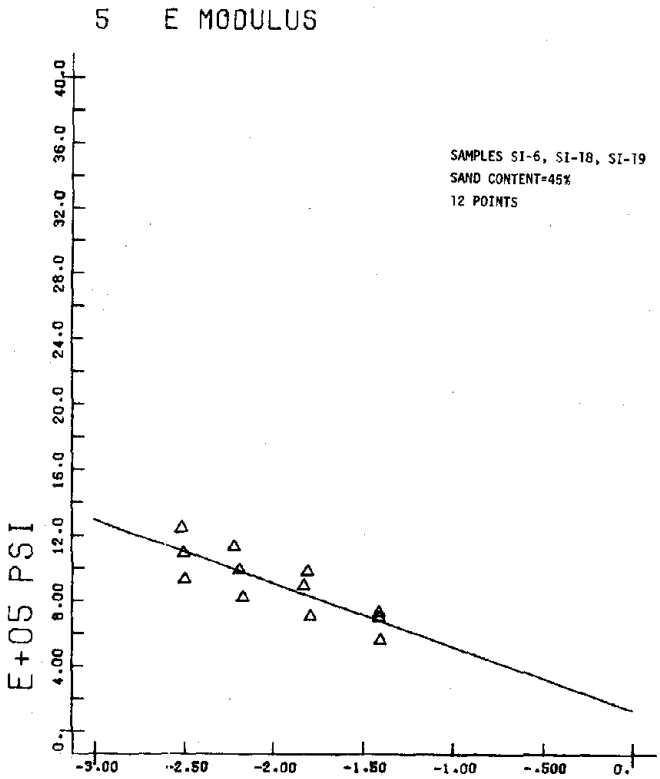

Figure C.65

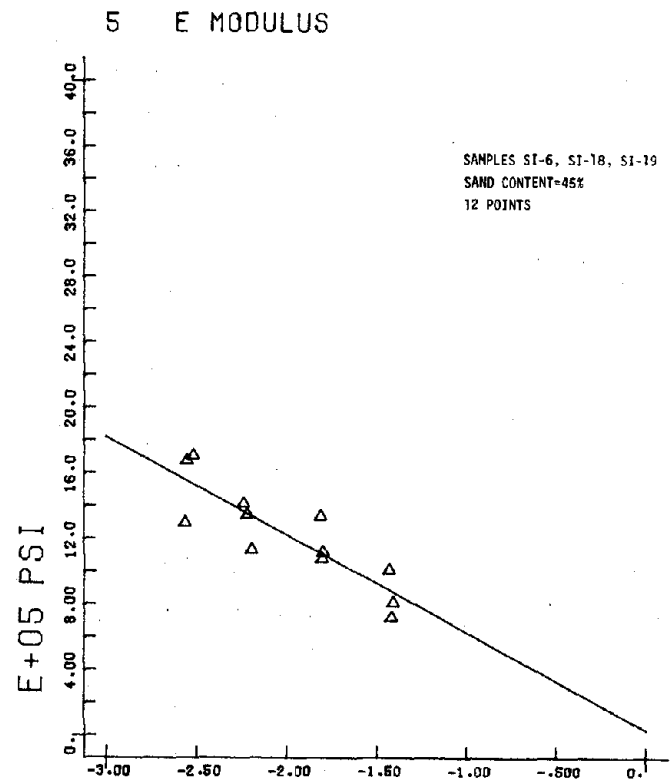

Figure C.66

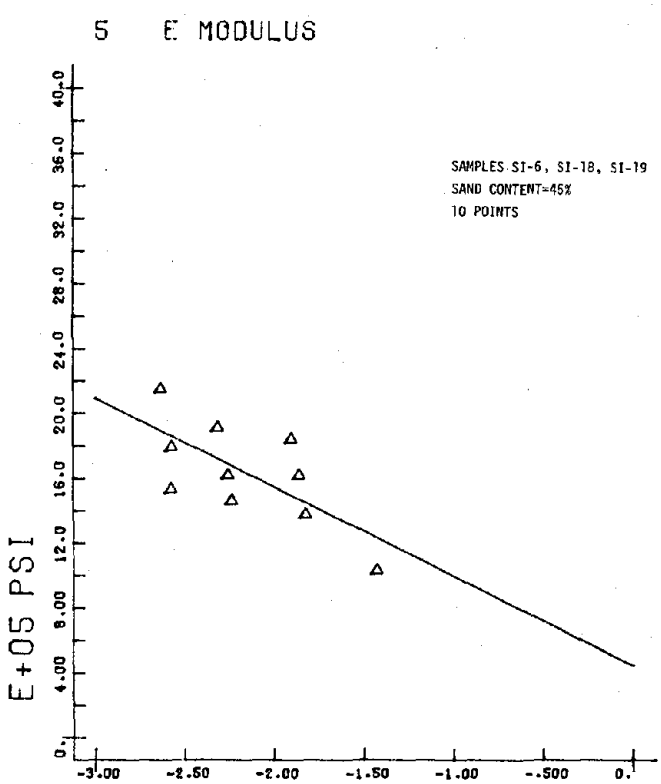

Figure C.67

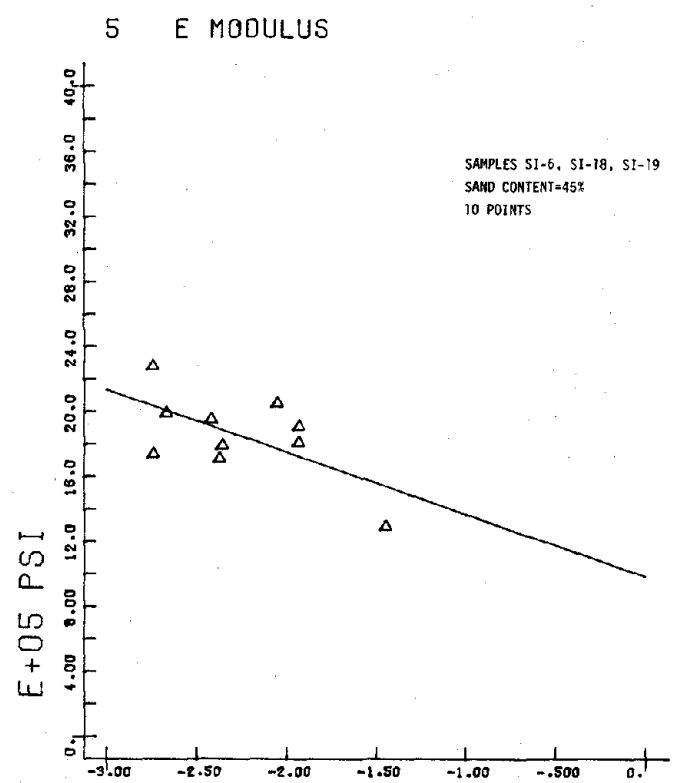

Figure C.68

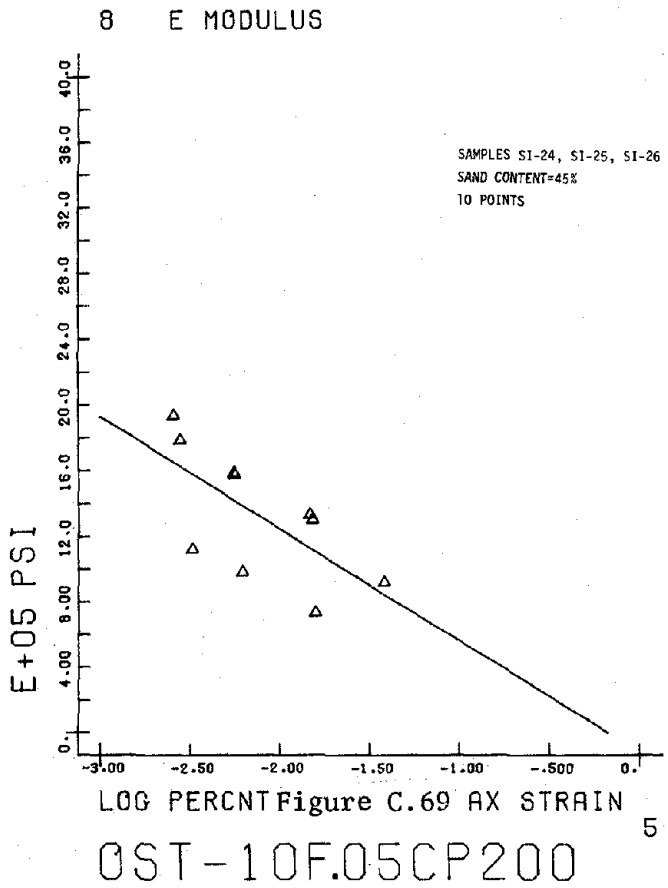

Figure C.69 AX STRAIN

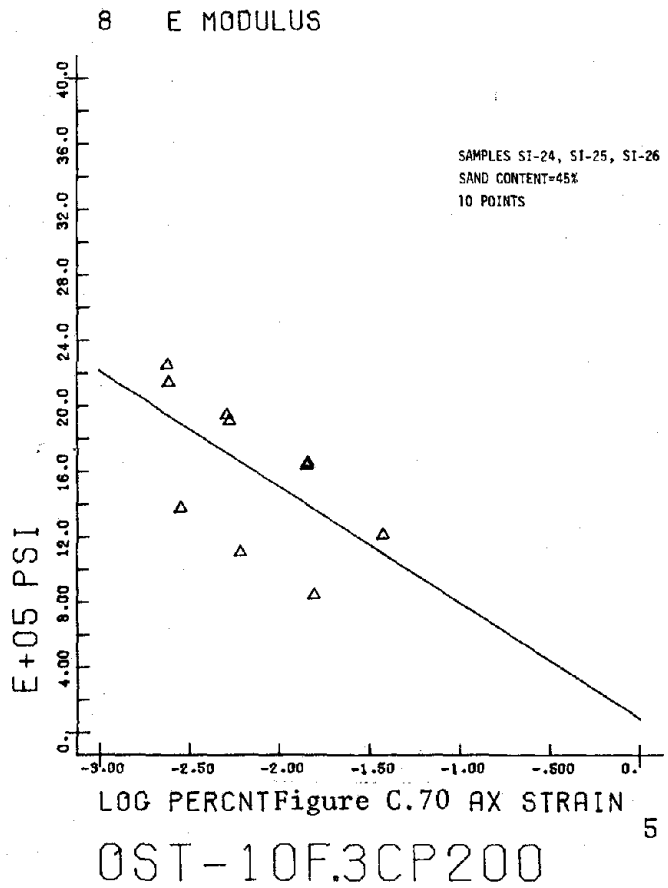

Figure C.70 AX STRAIN

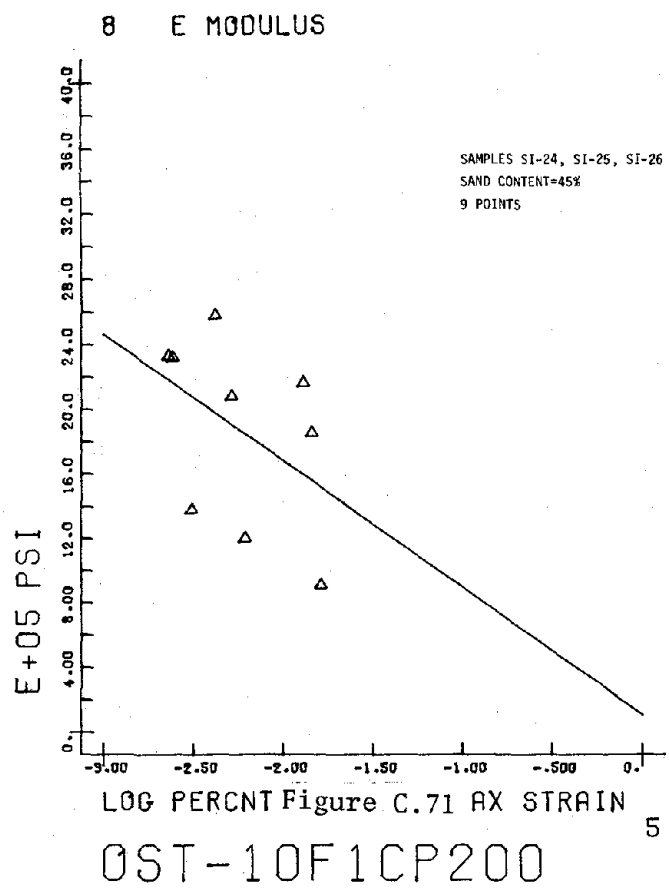

Figure C.71 AX STRAIN

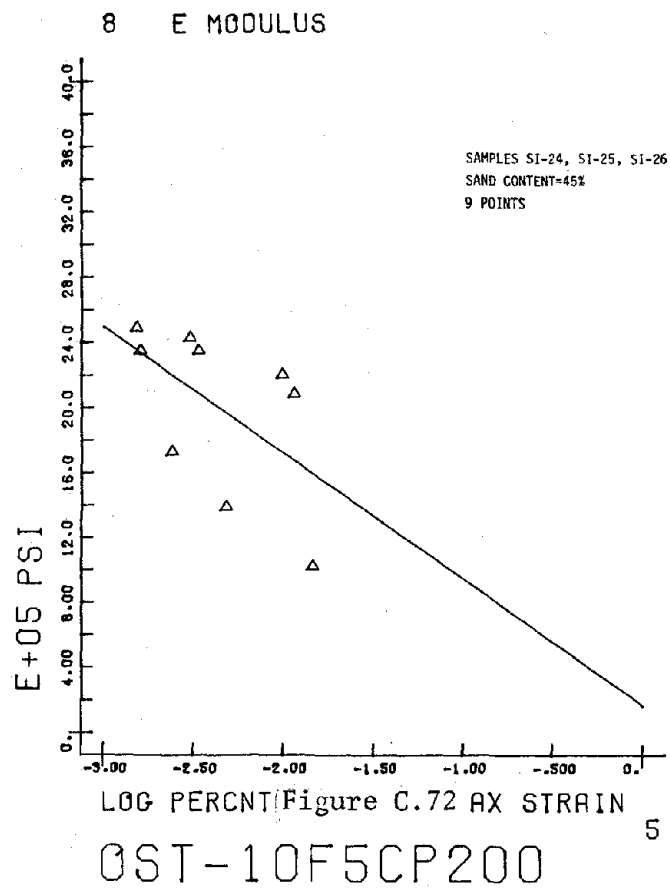

Figure C.72 AX STRAIN

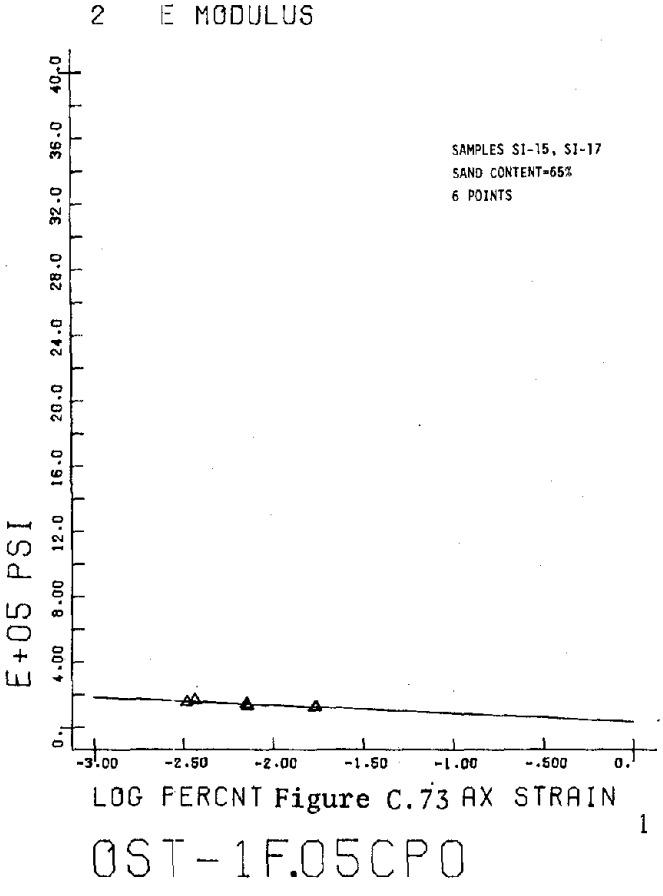

Figure C.73

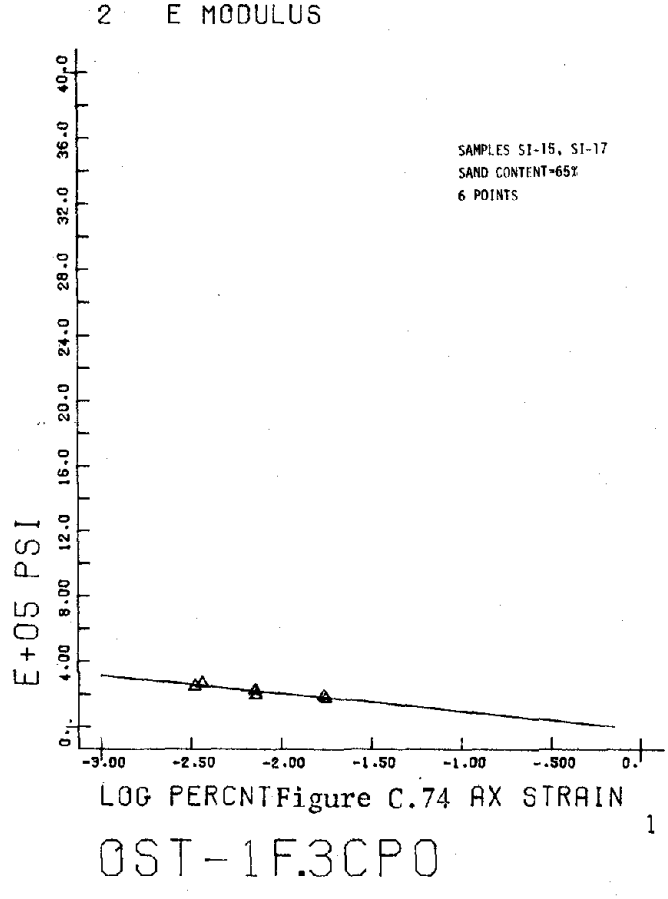

Figure C.74

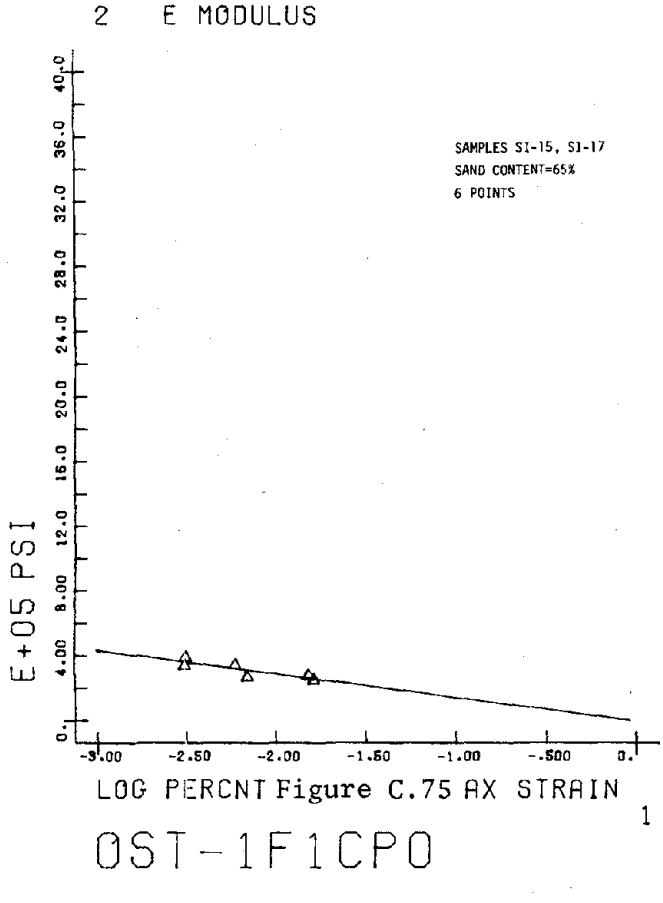

Figure C.75

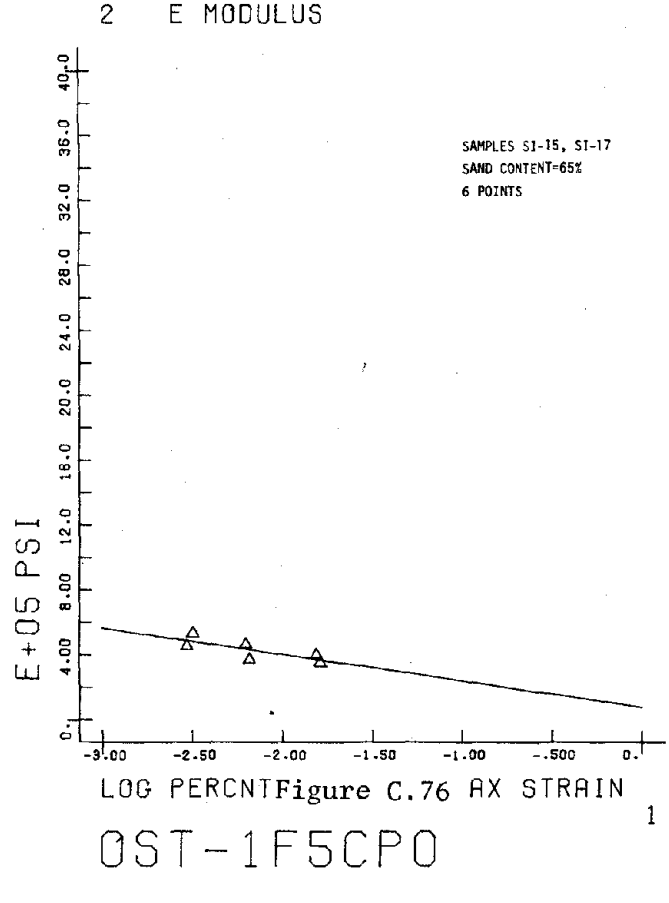

Figure C.76

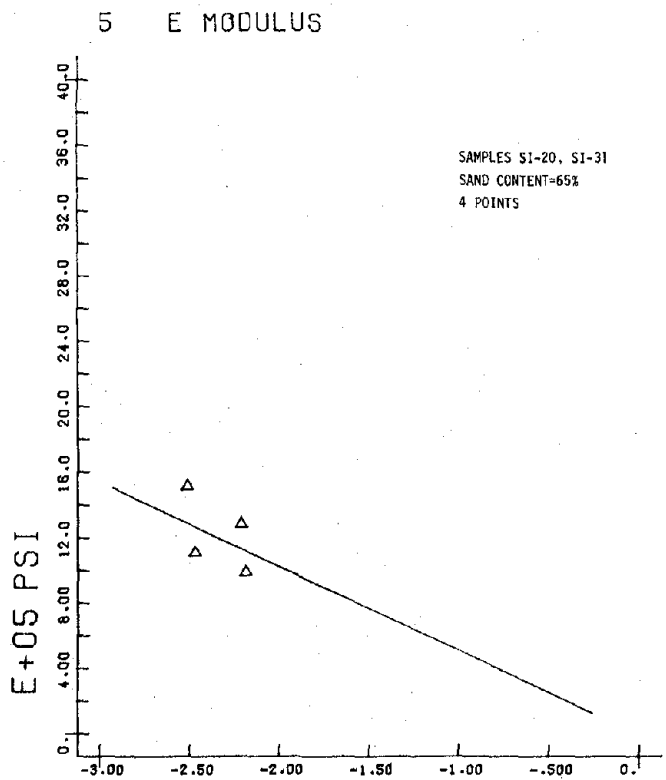

Figure C.77

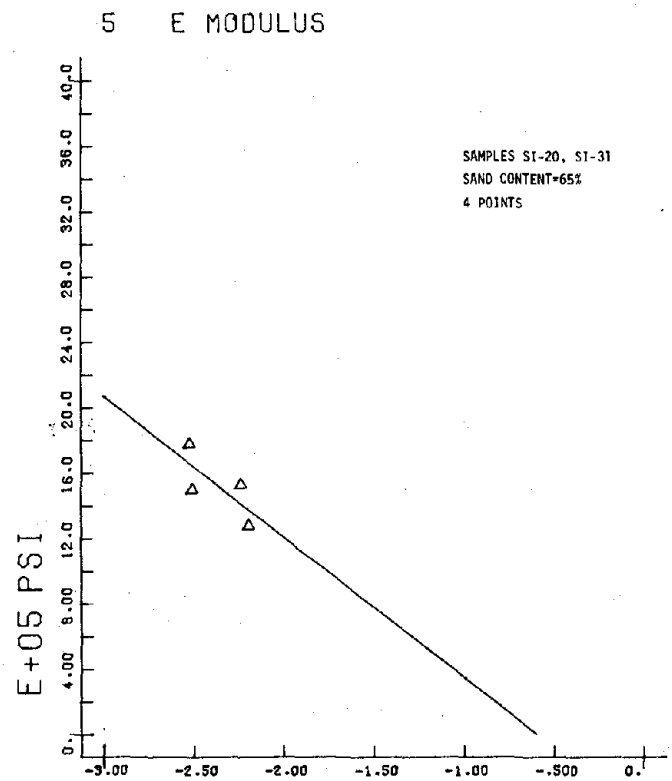

Figure C.78

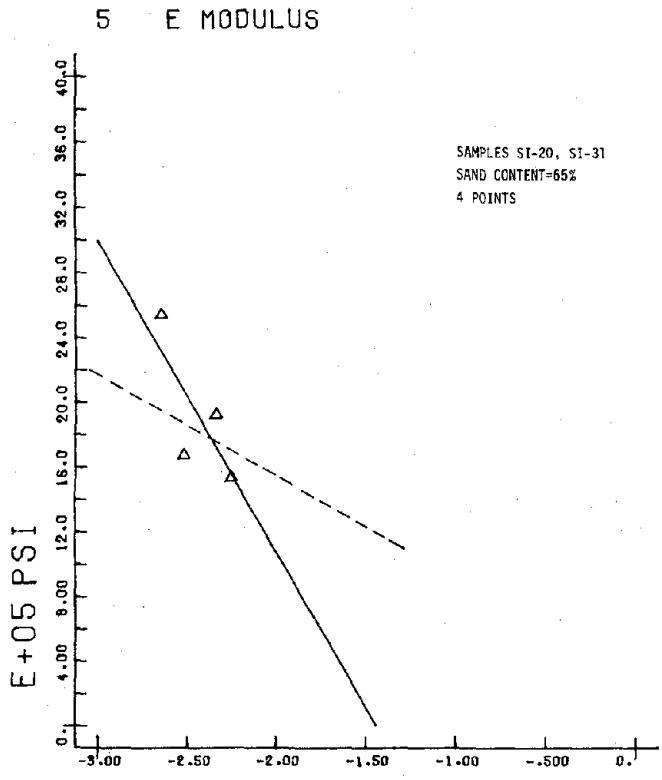

Figure C.79

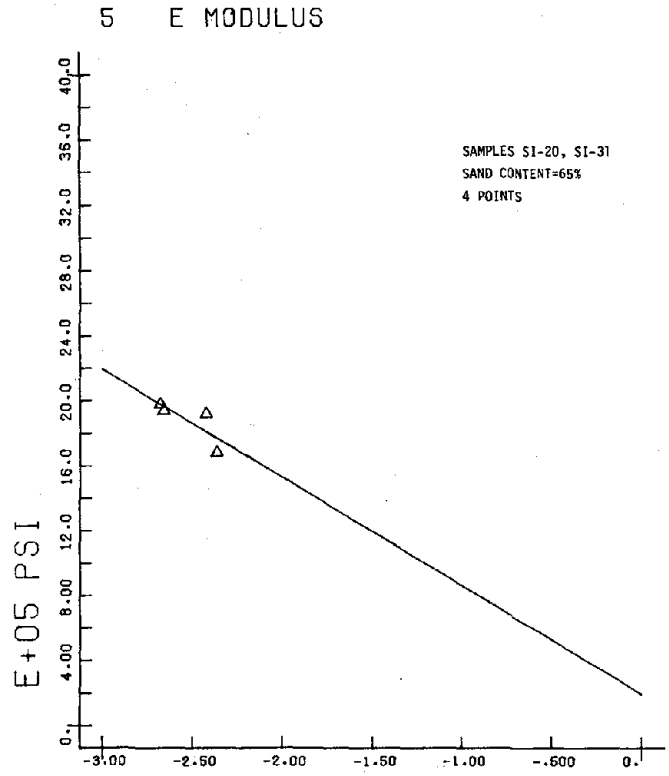

Figure C.8C

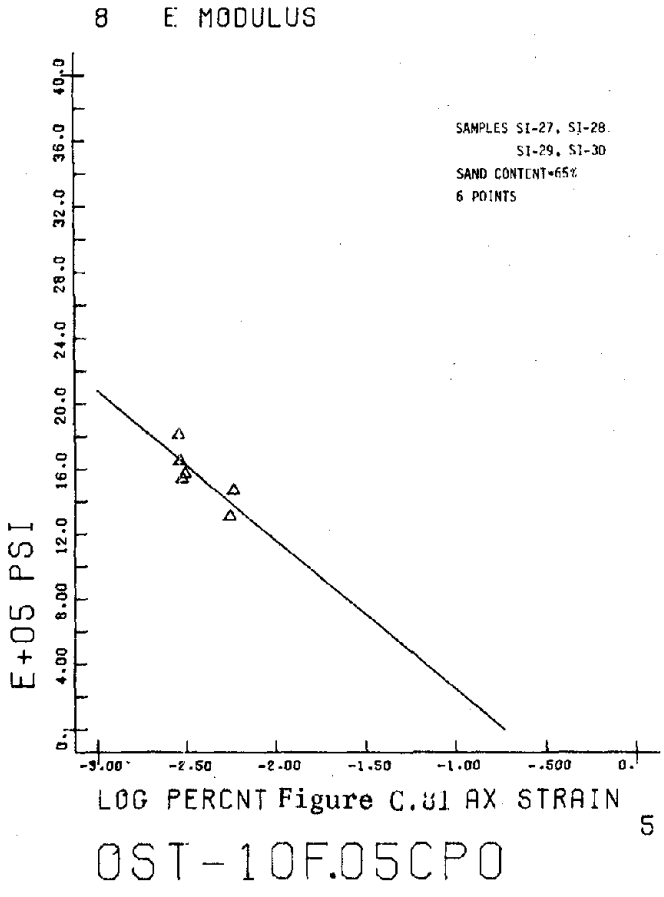

Figure C.81

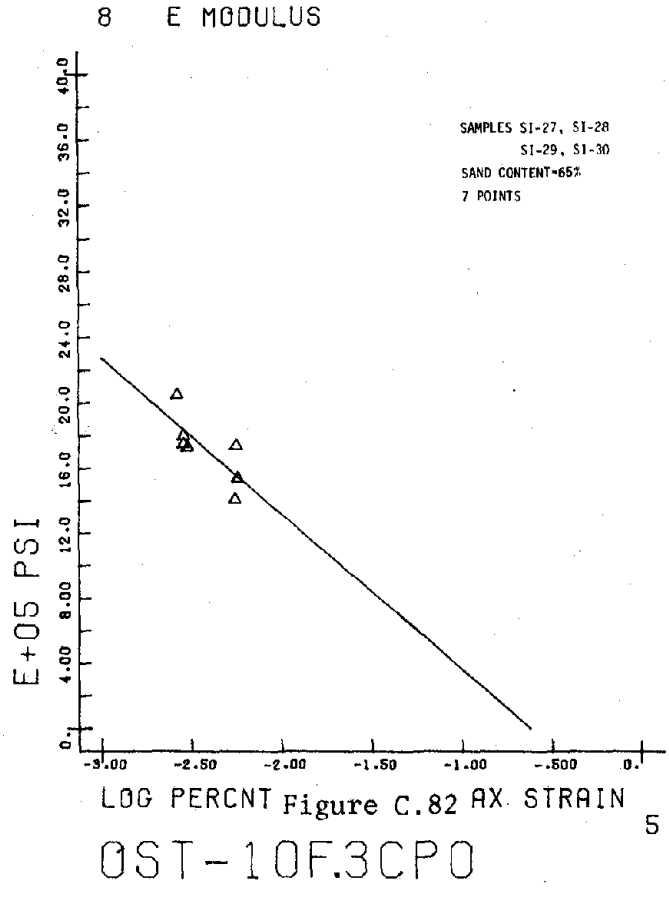

Figure C.82

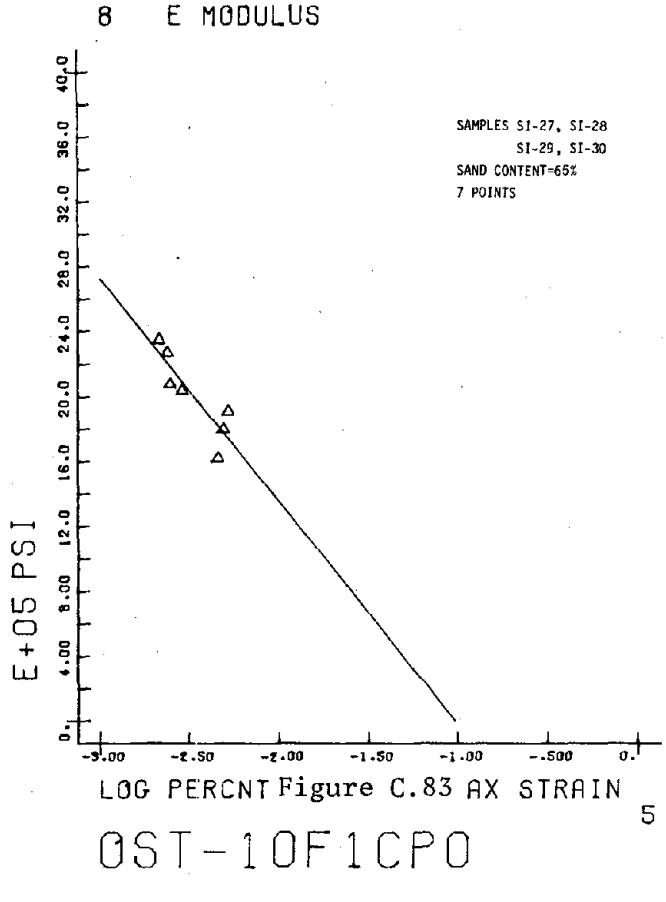

Figure C.83

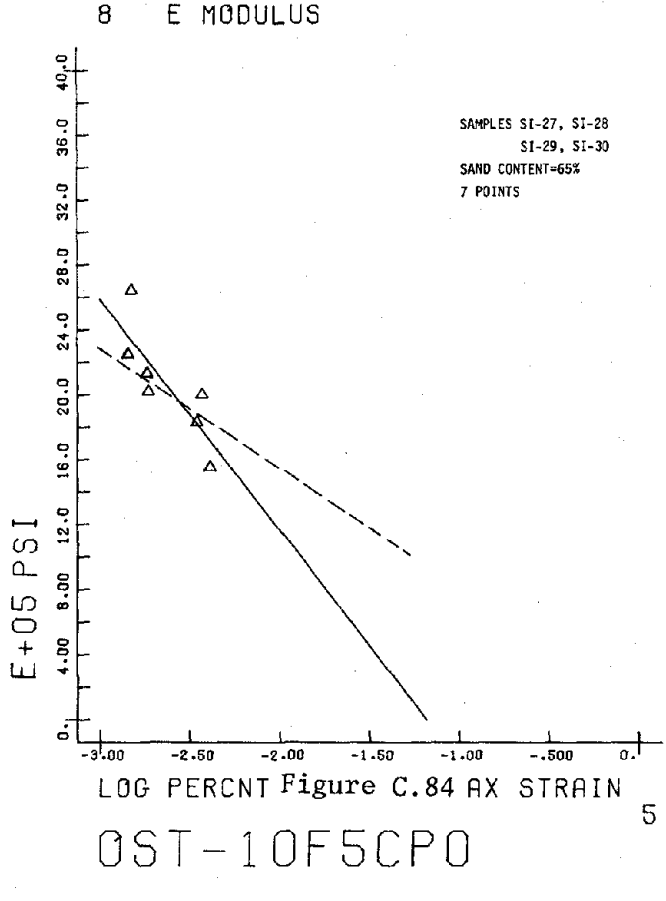

Figure C.84

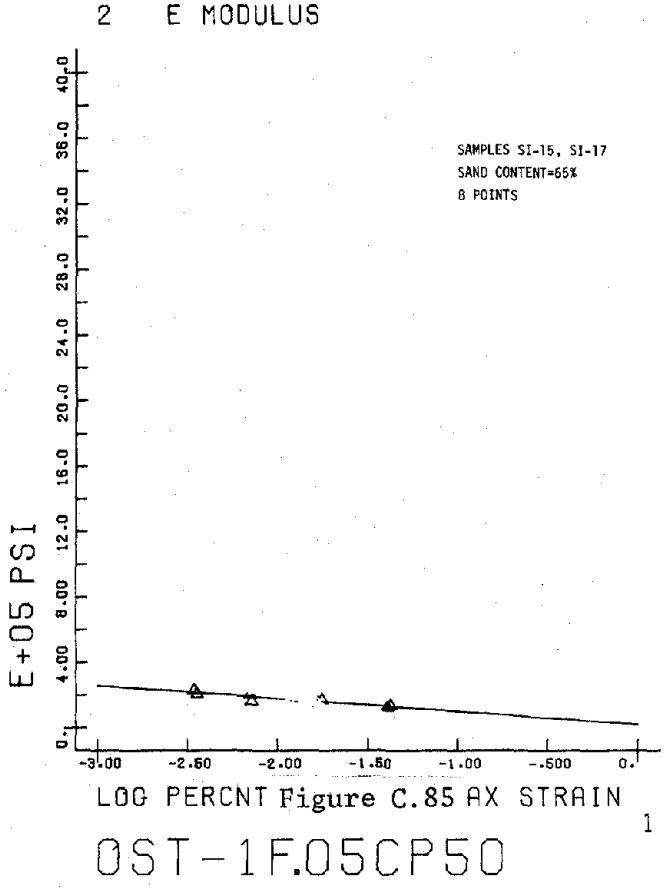

Figure C.85

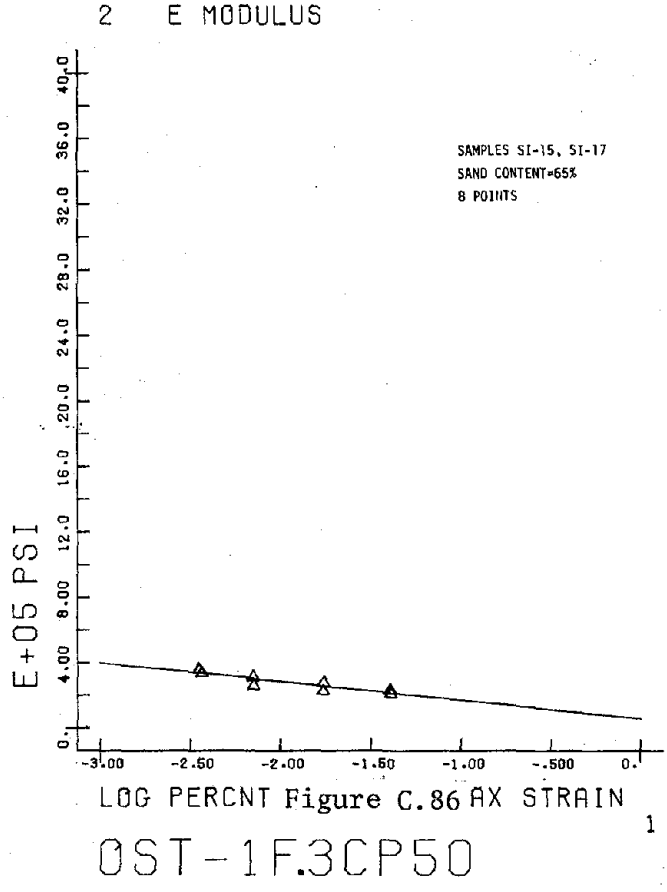

Figure C.86

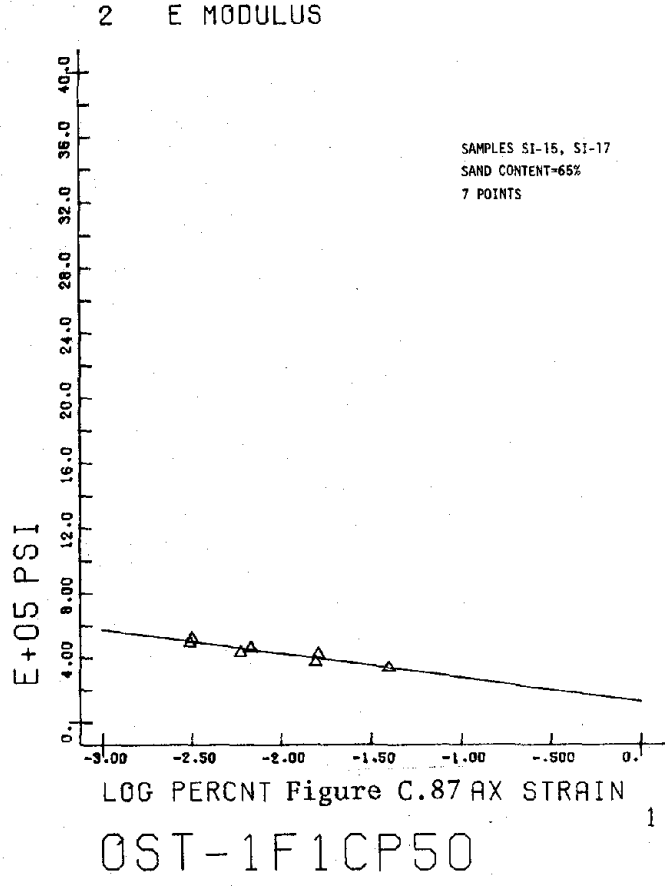

Figure C.87

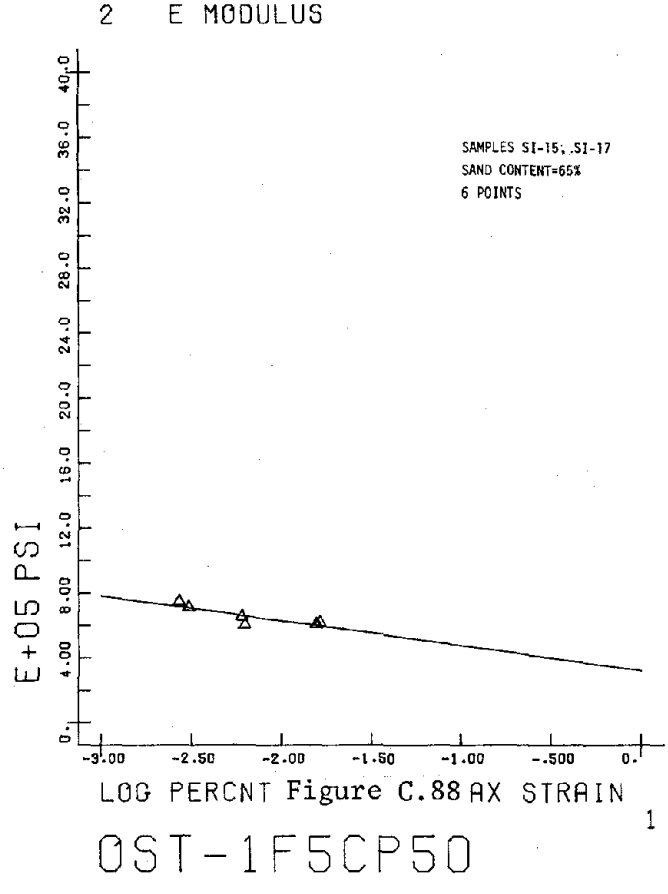

Figure C.88

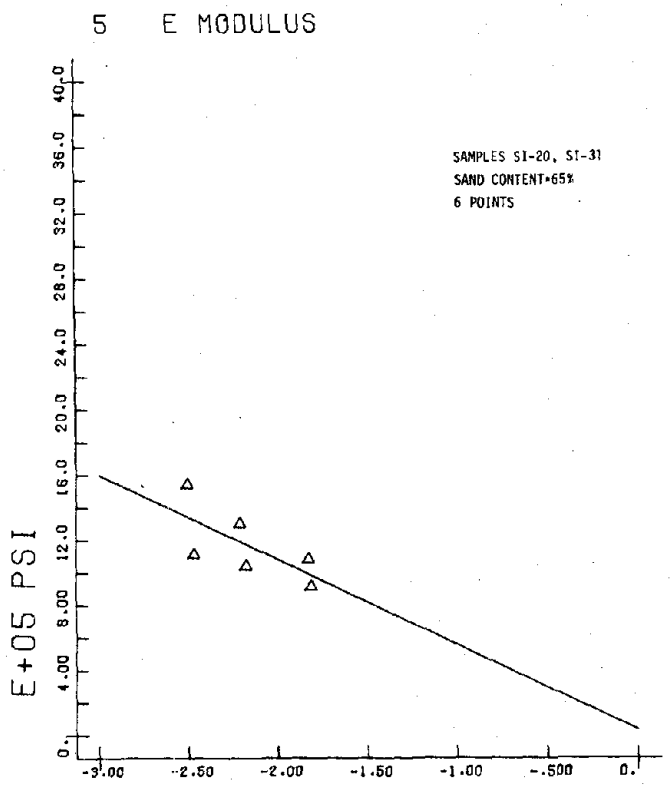

Figure C.89

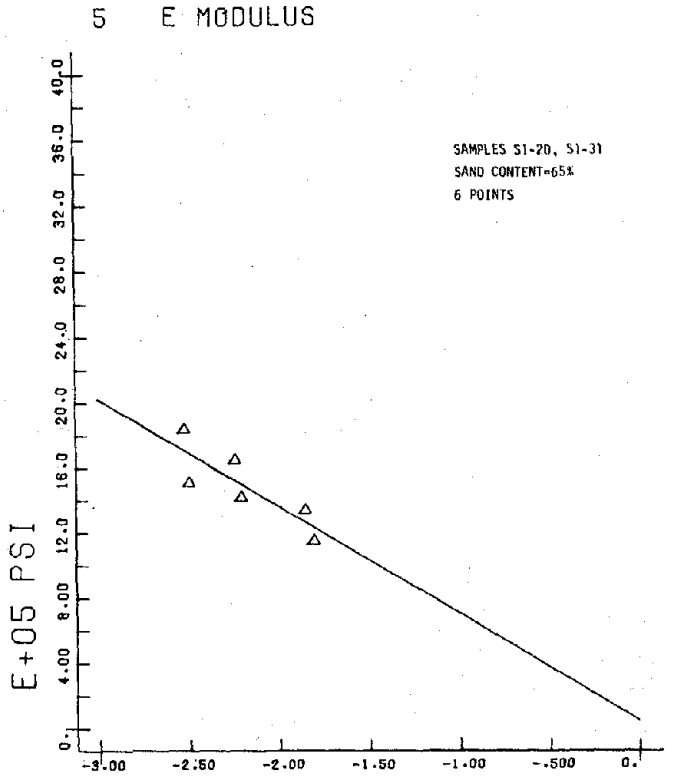

Figure C.90

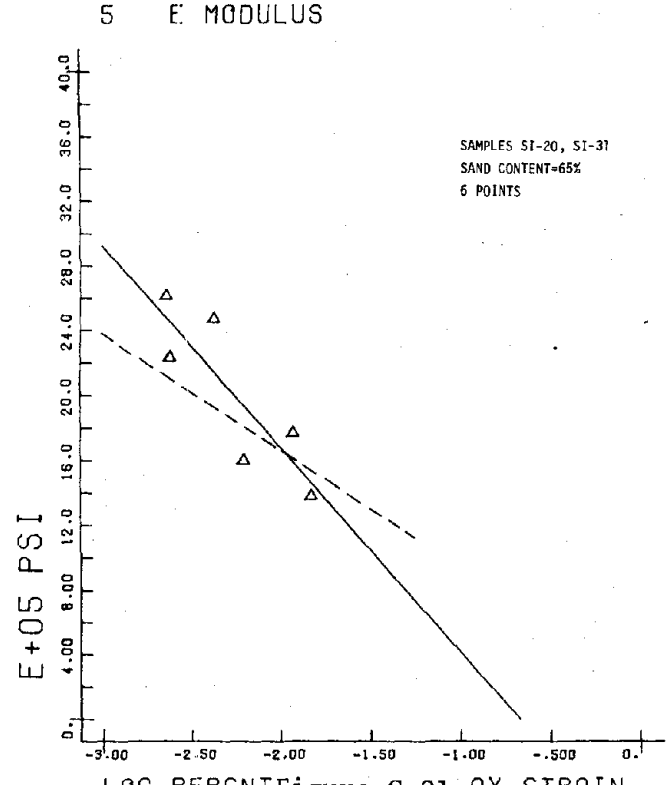

Figure C.91

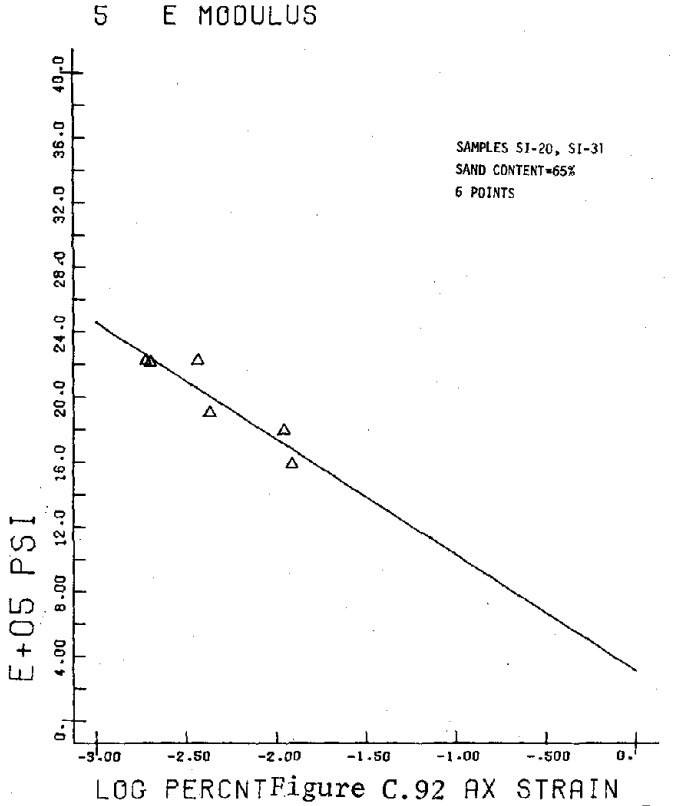

Figure C.92

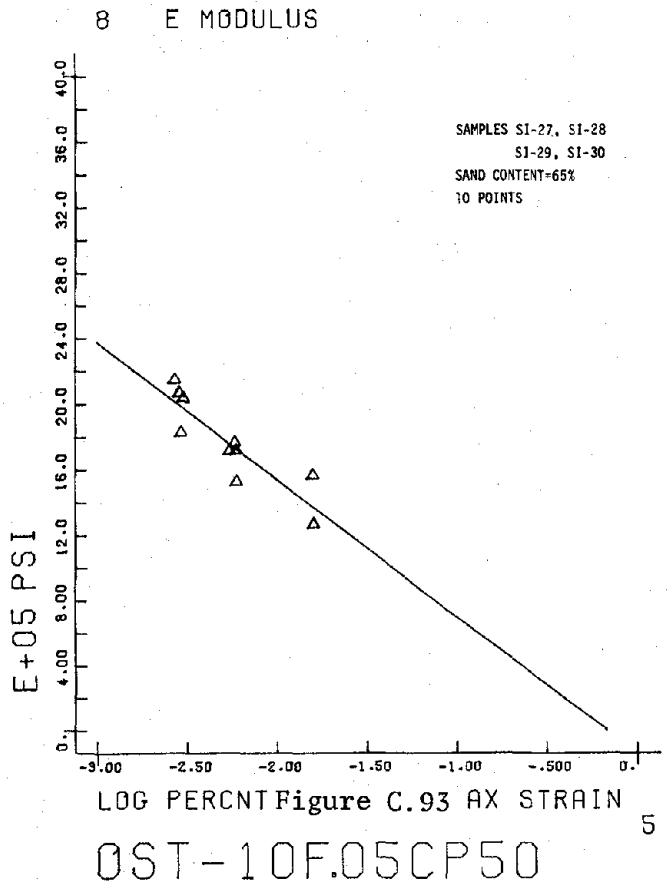

Figure C.93

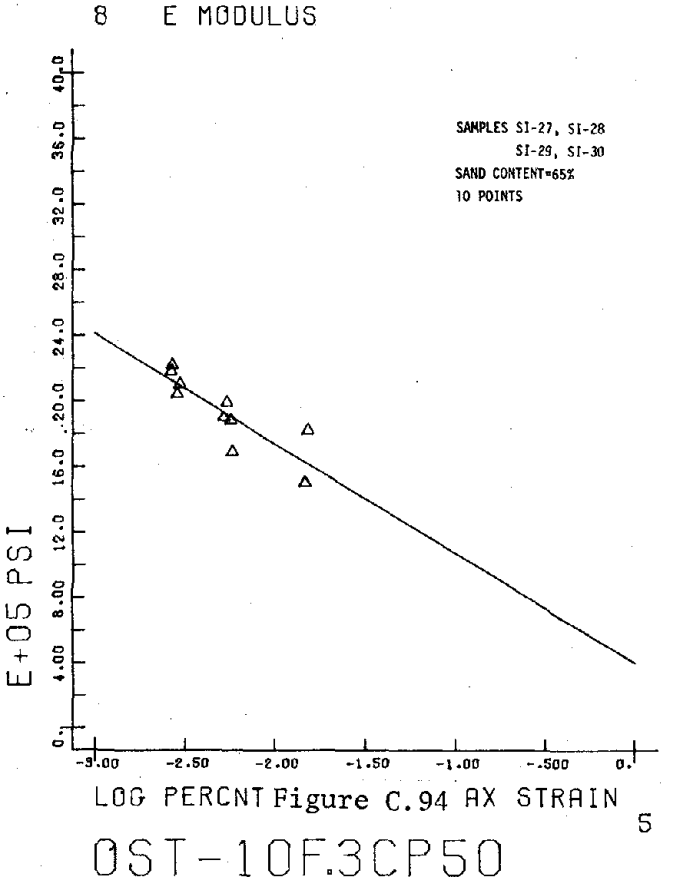

Figure C.94

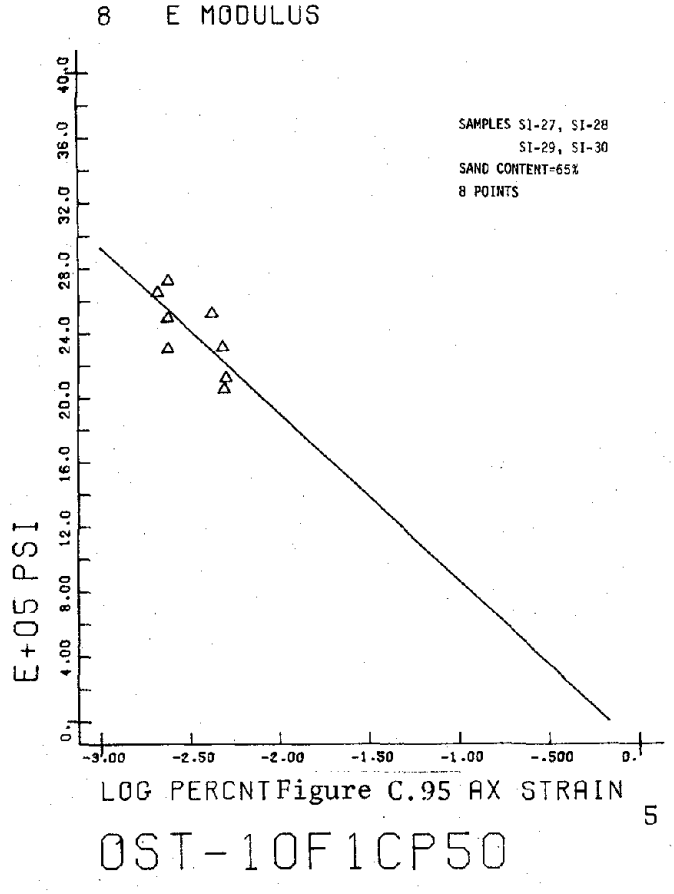

Figure C.95

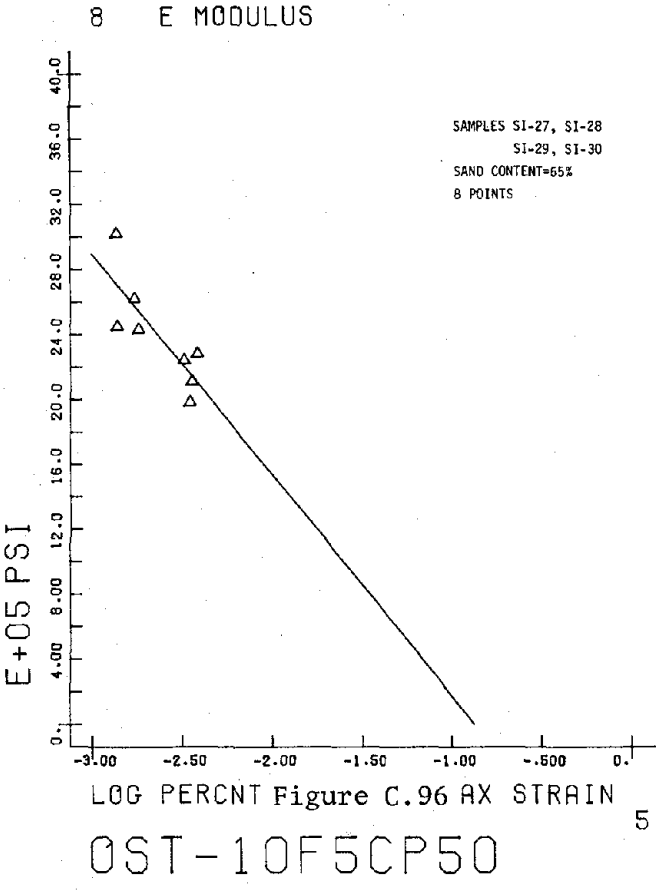

Figure C.96

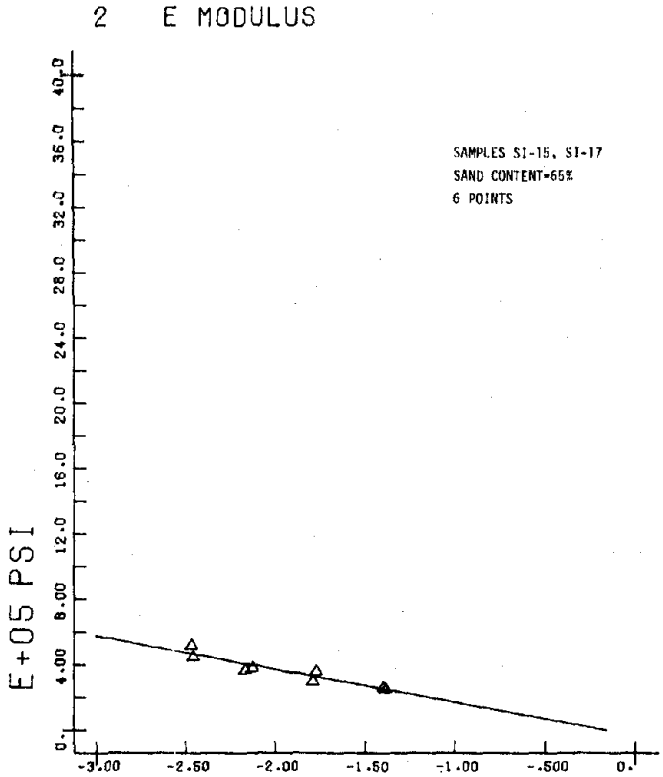

Figure C.97

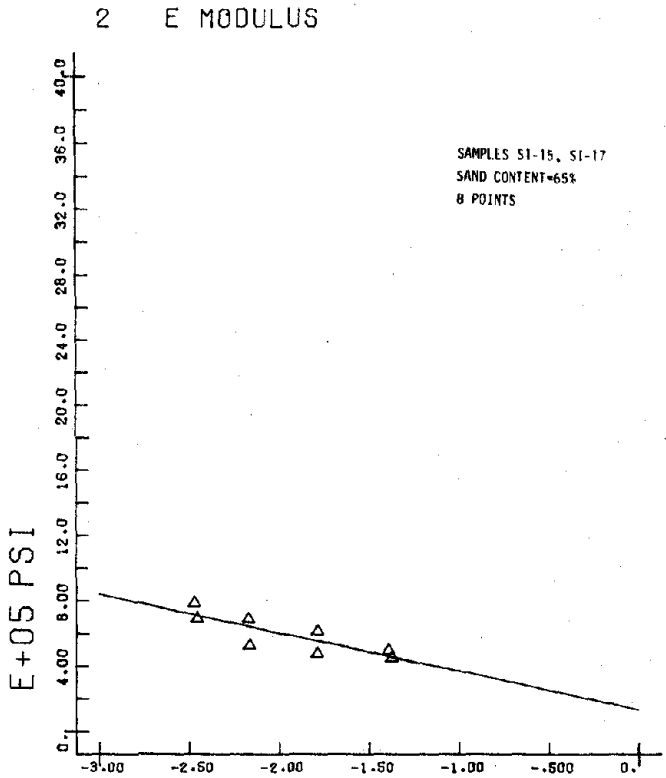

Figure C.98

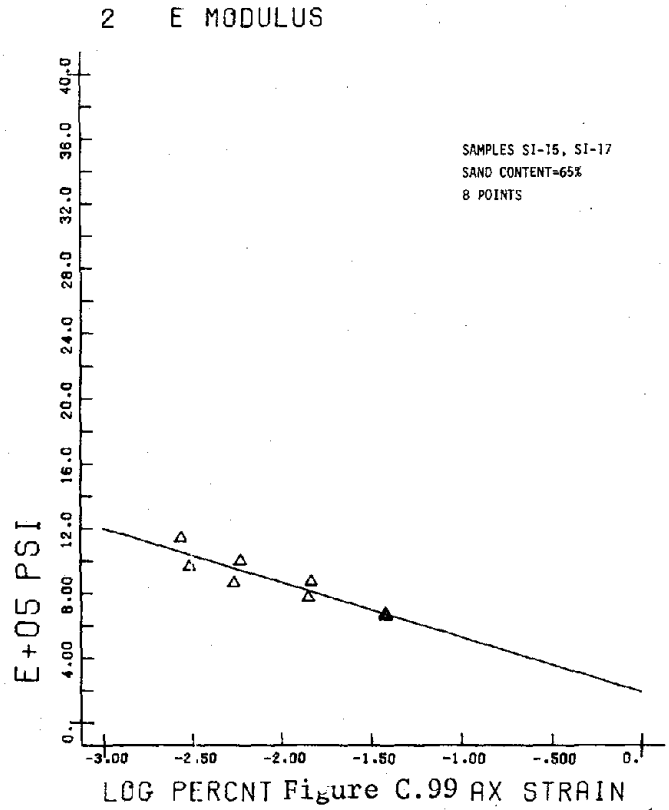

Figure C.99

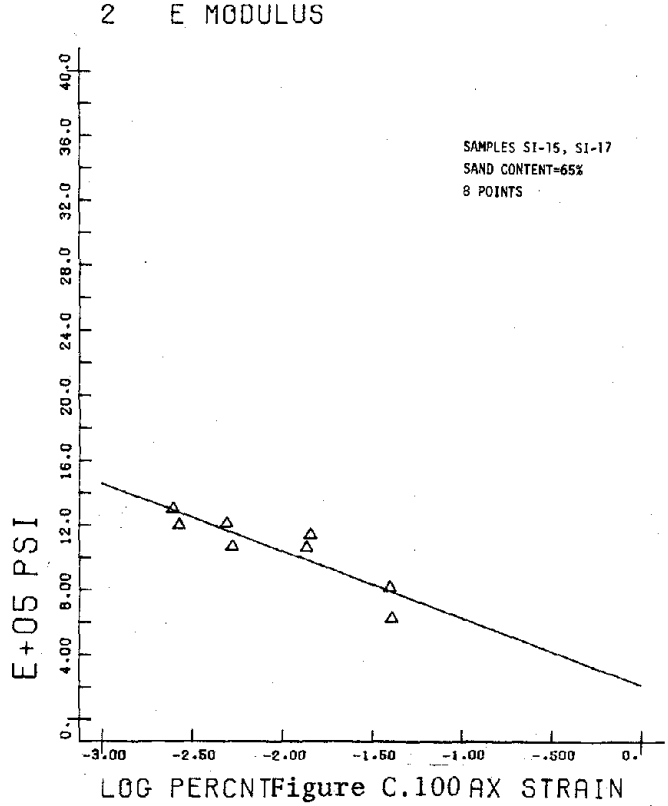

Figure C.100

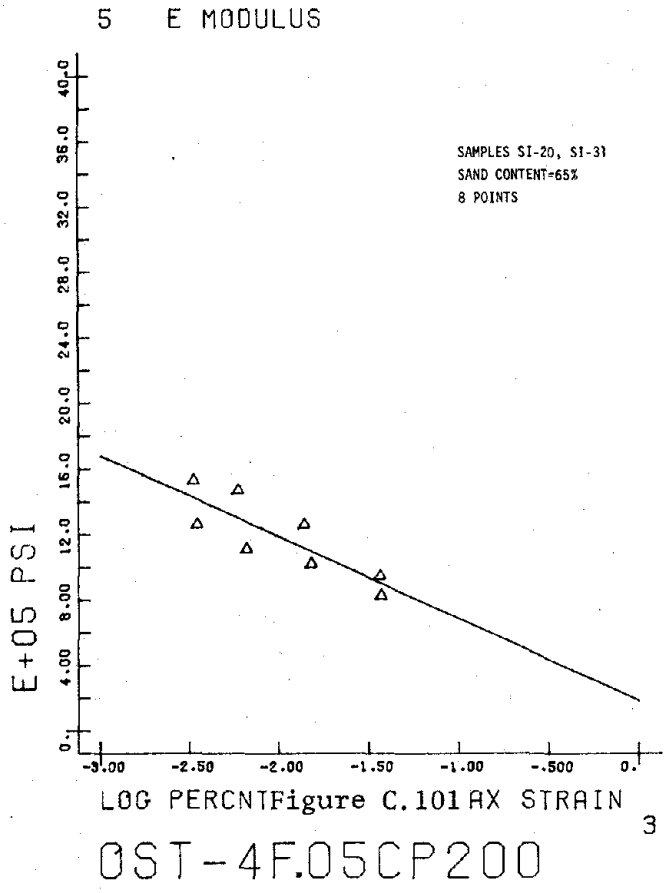

Figure C.101

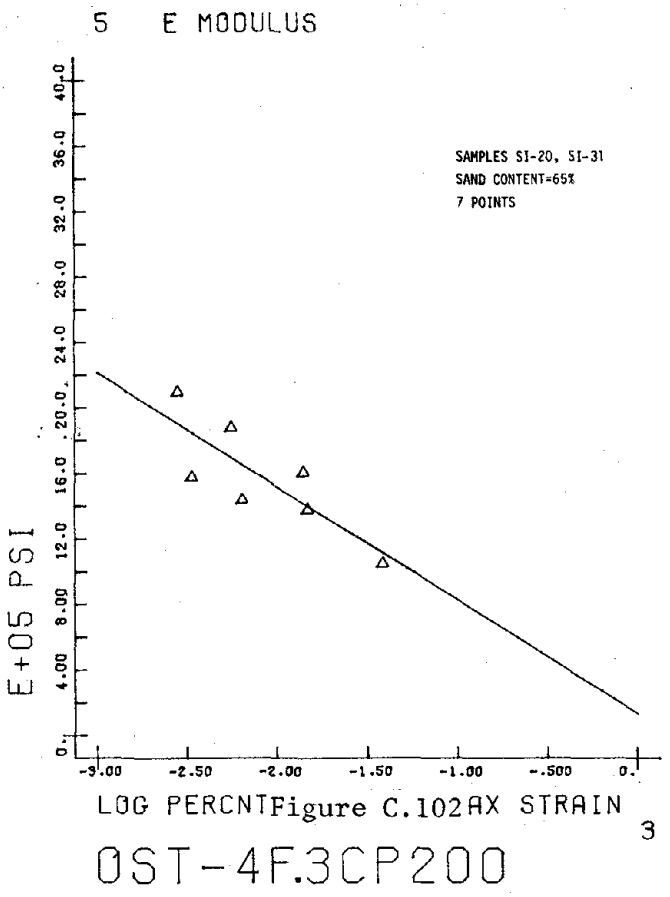

Figure C.102

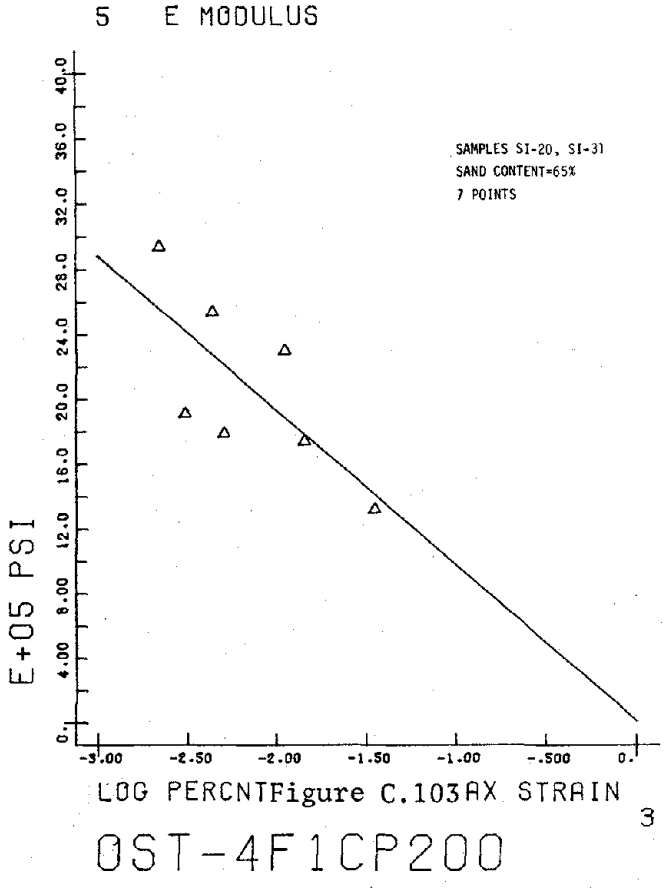

Figure C.103

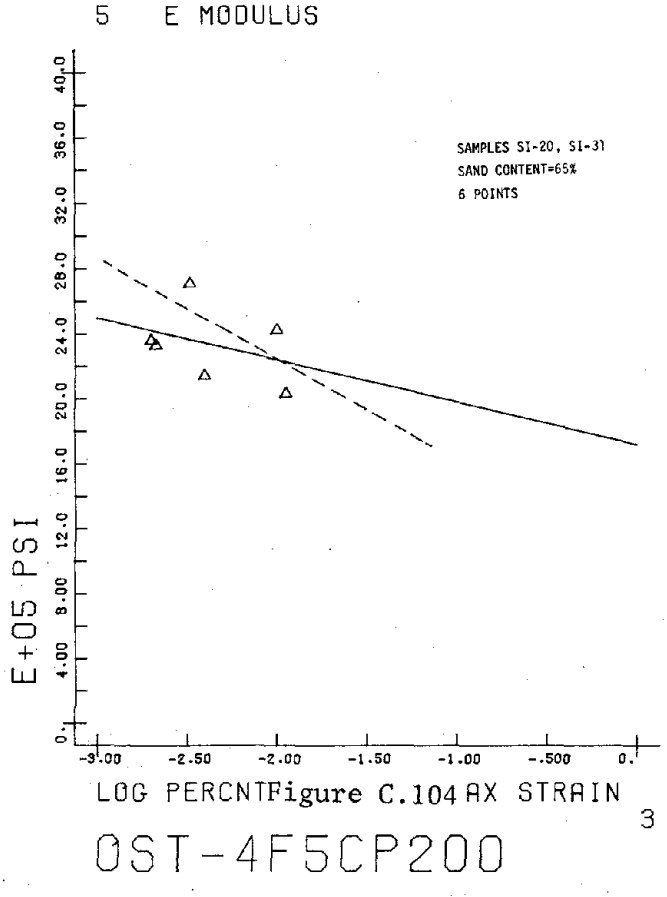

Figure C.104

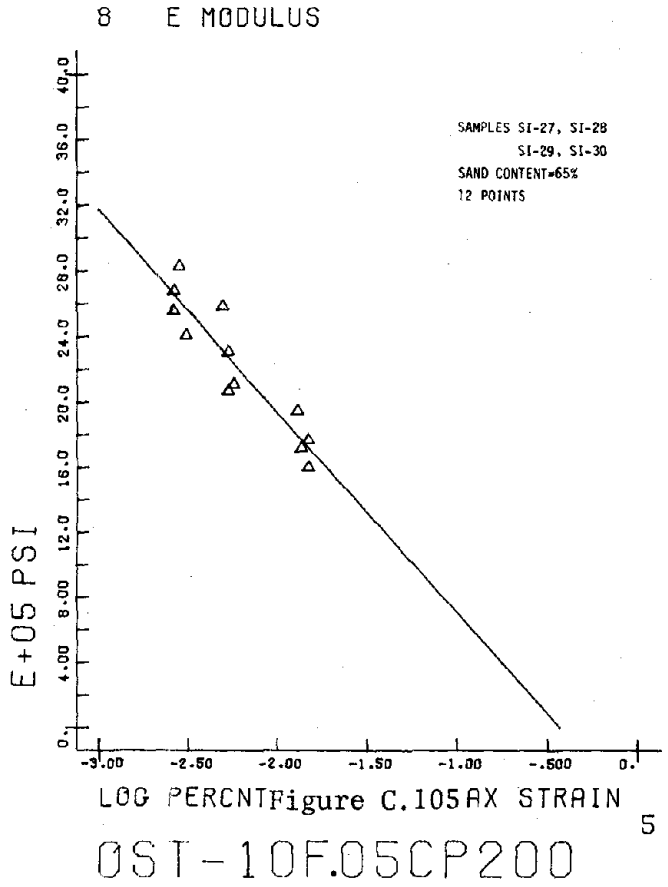

Figure C.105

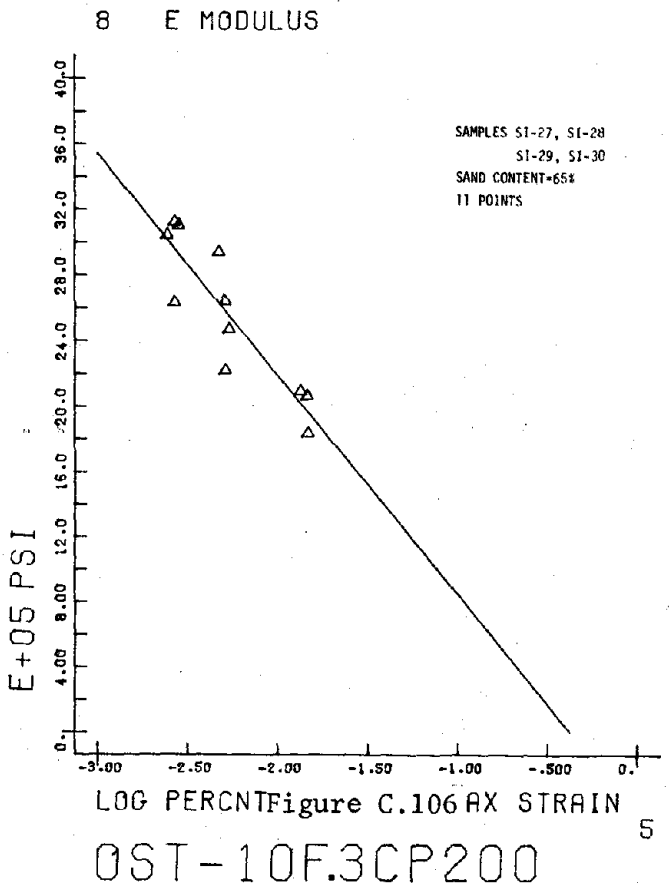

Figure C.106

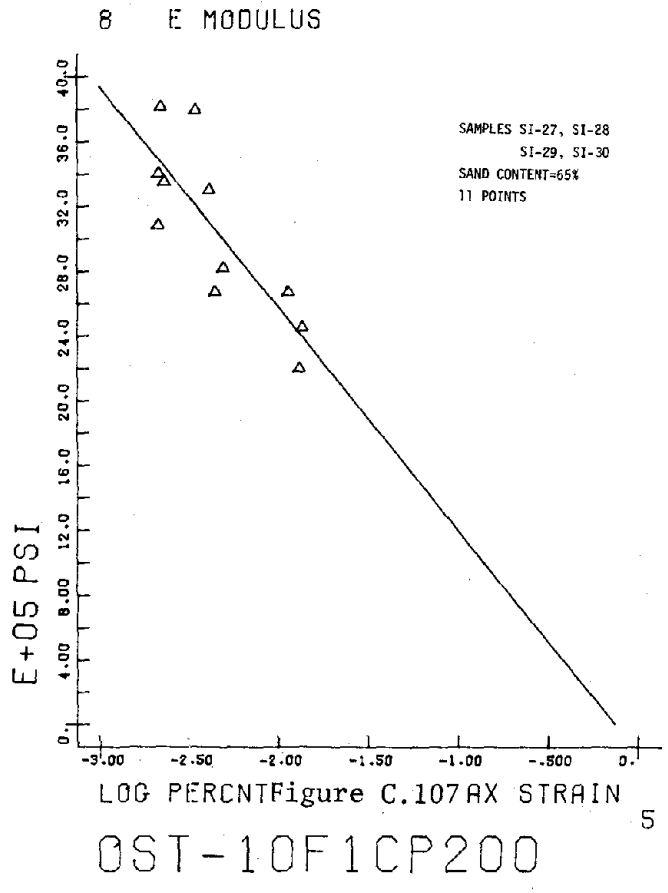

Figure C.107

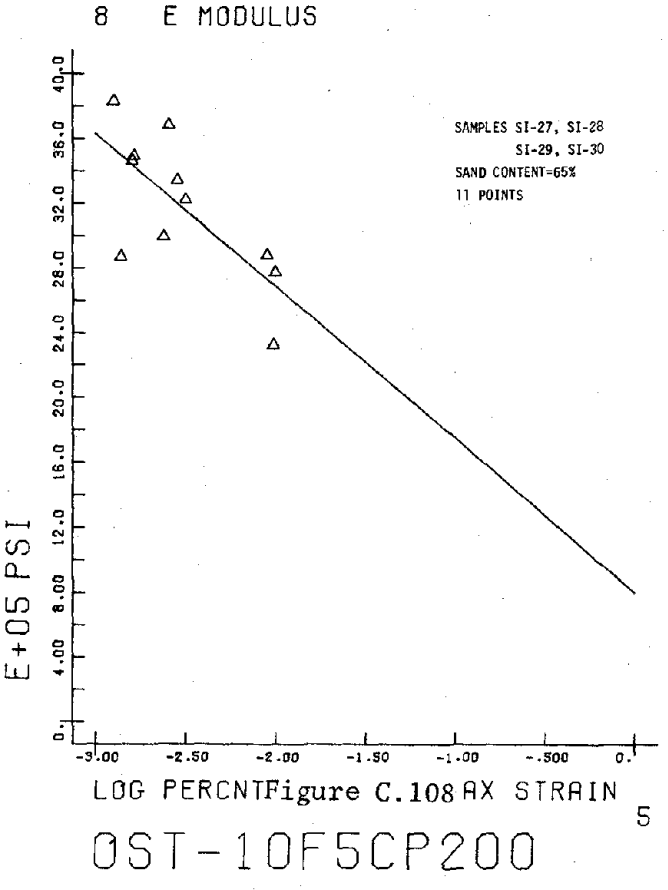

Figure C.108

APPENDIX D

CYCLIC TRIAXIAL TEST RESULTS: DAMPING RATIO OF FROZEN SAND- SEPARATE CONFINING PRESSURES

Test results for Ottawa sand at sand contents of 20%, 45%, and 65% are shown in Figures D.1 to D.36; Figures D.37 to D.72; and Figures D.73 to D.108, respectively.

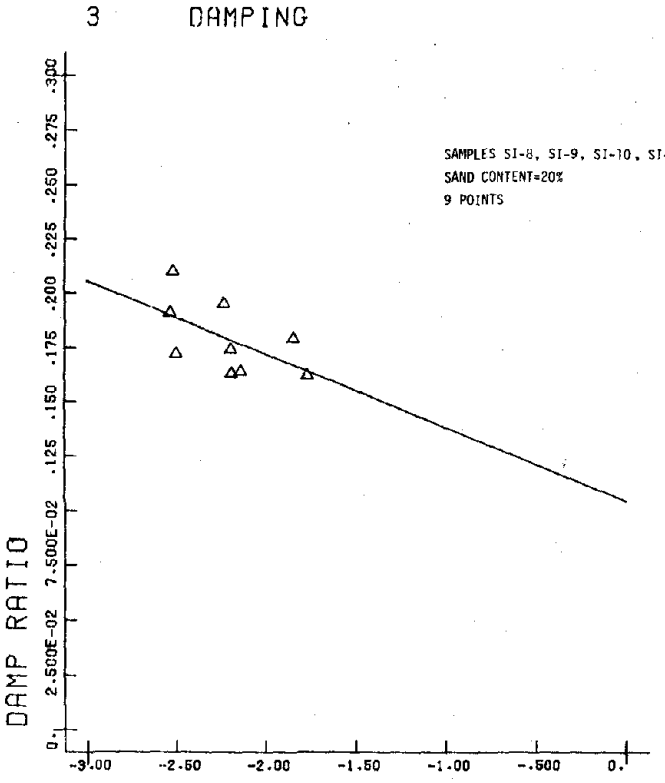

Figure D.1

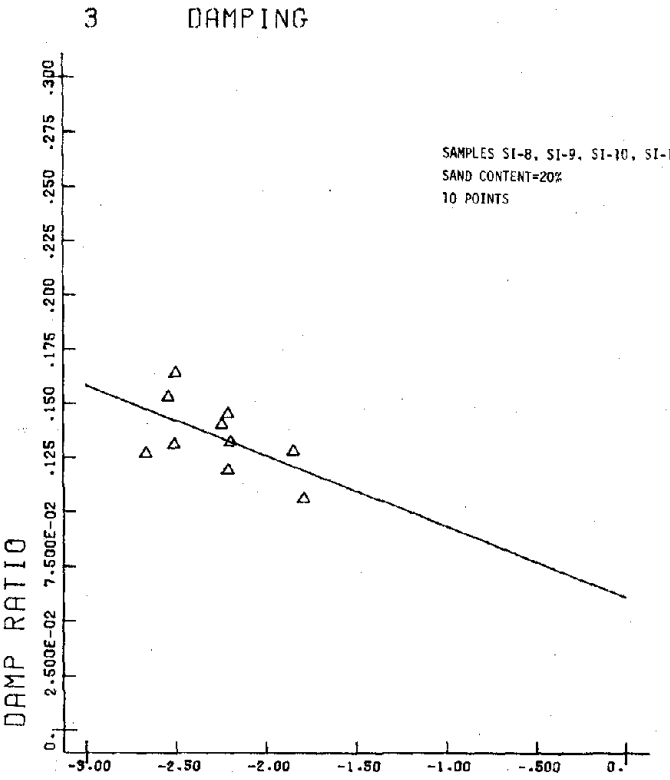

Figure D.2

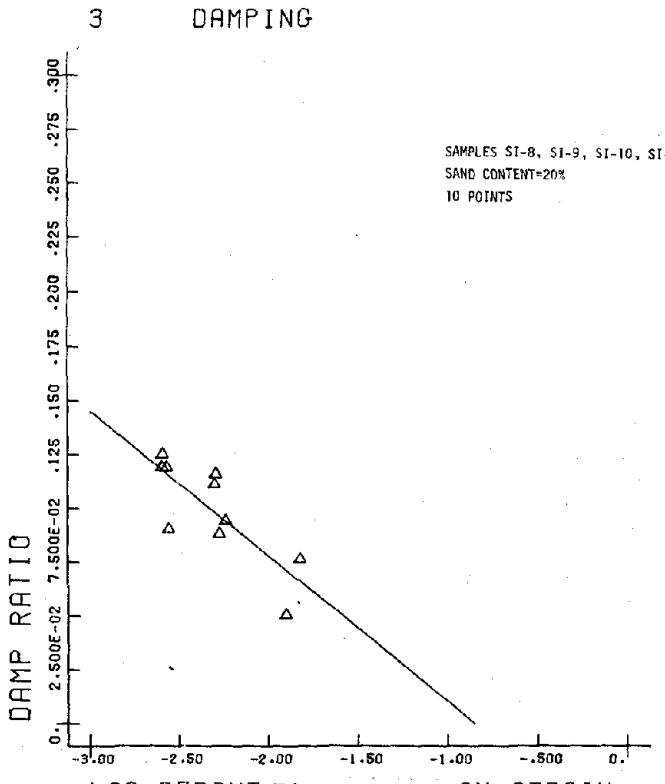

Figure D.3

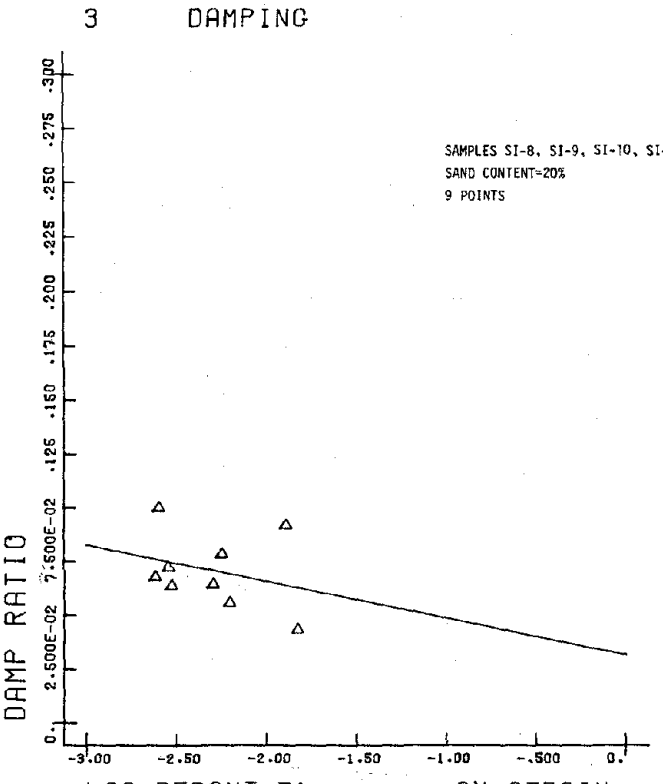

Figure D.4

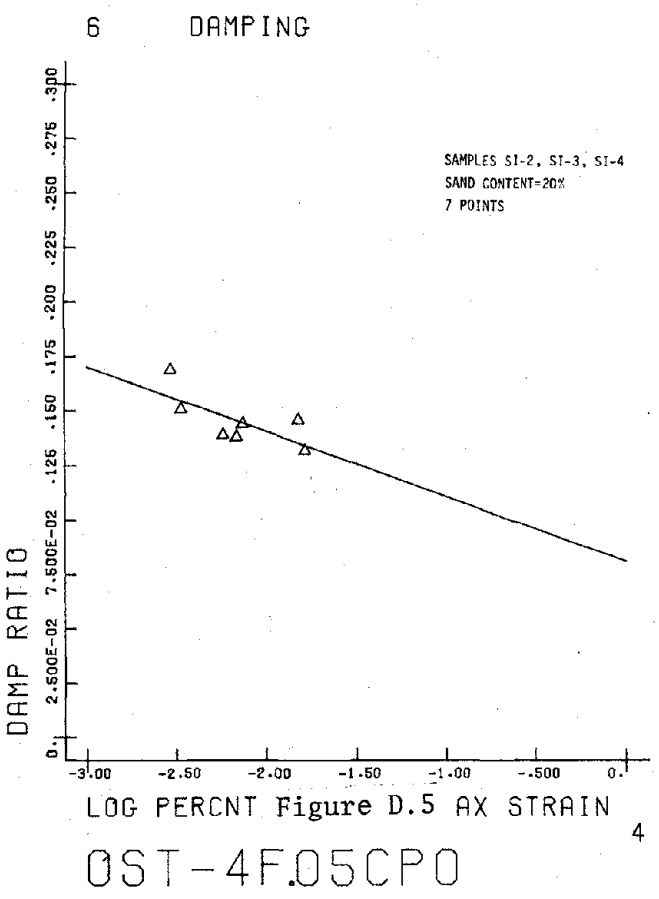

Figure D.5

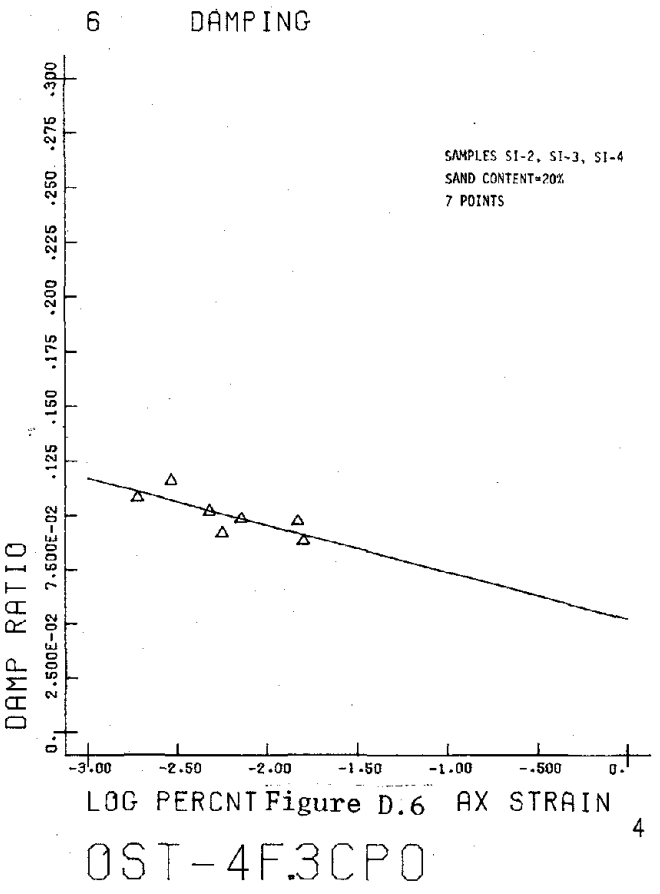

Figure D.6

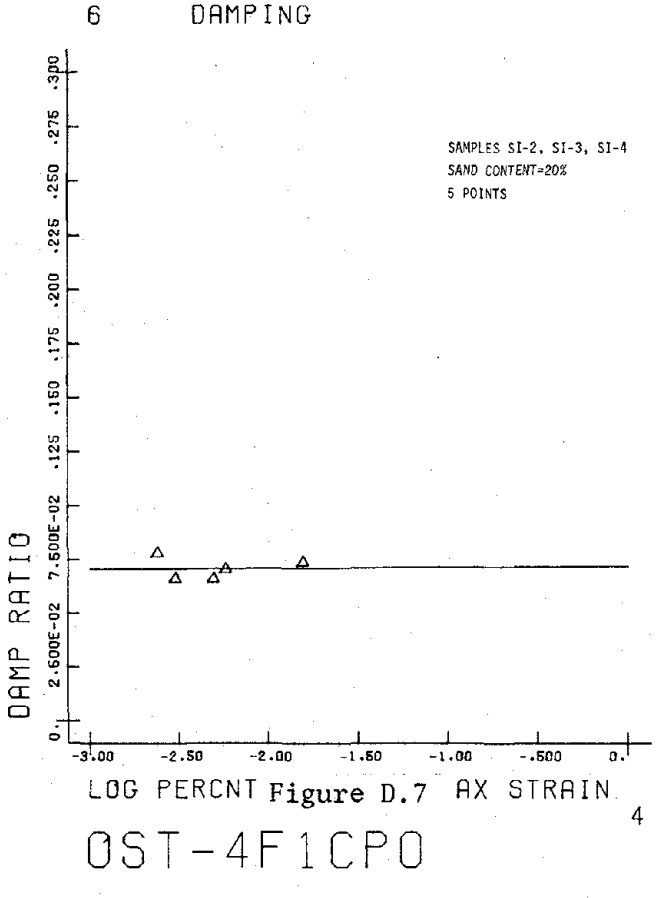

Figure D.7

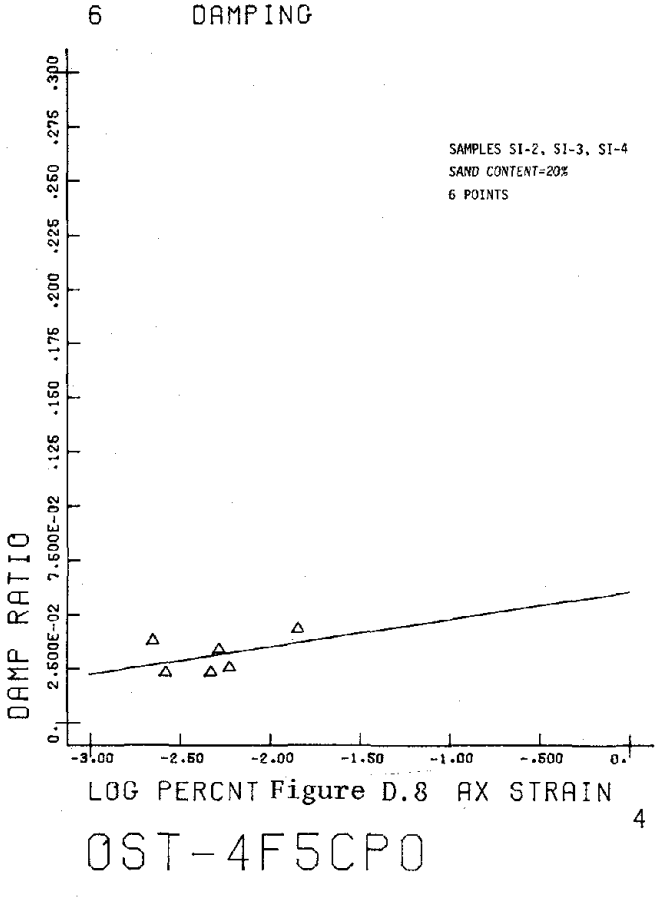

Figure D.8

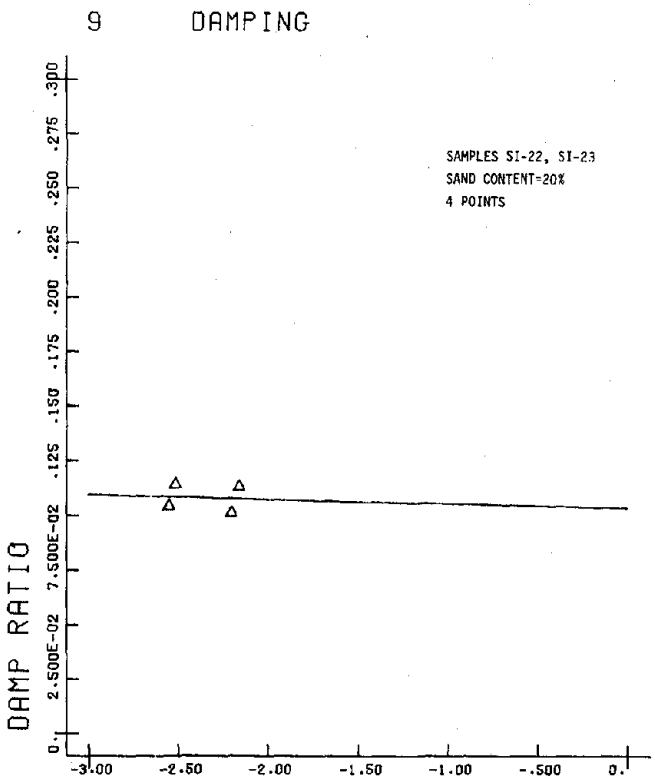

Figure D.9

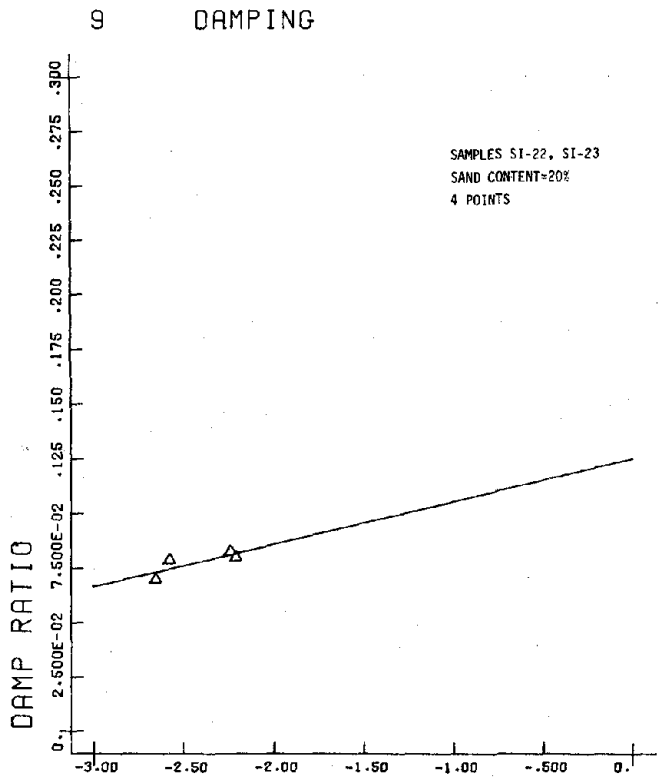

Figure D.10

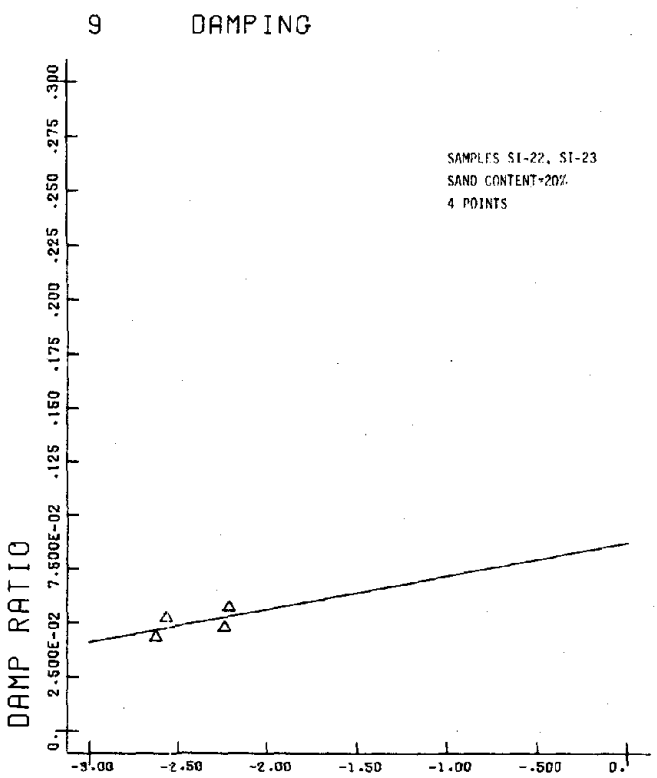

Figure D.11

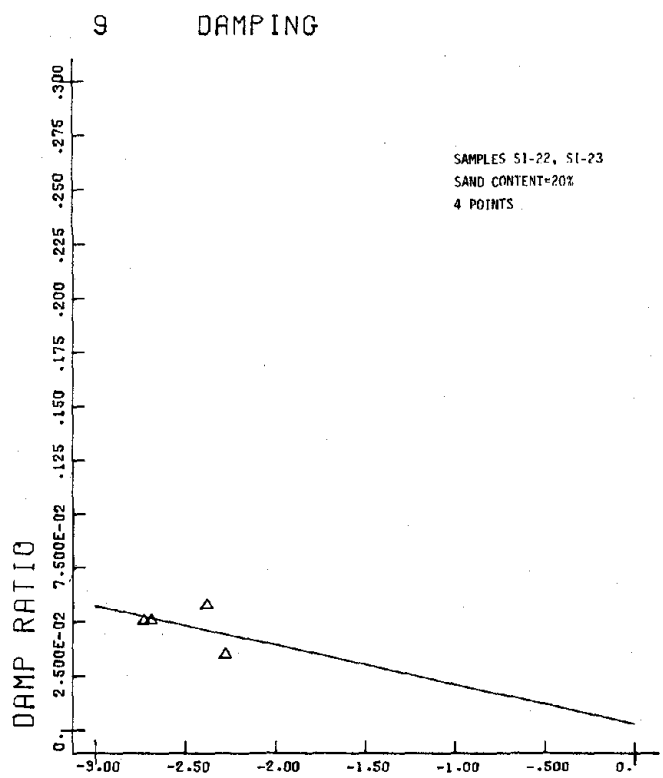

Figure D.12

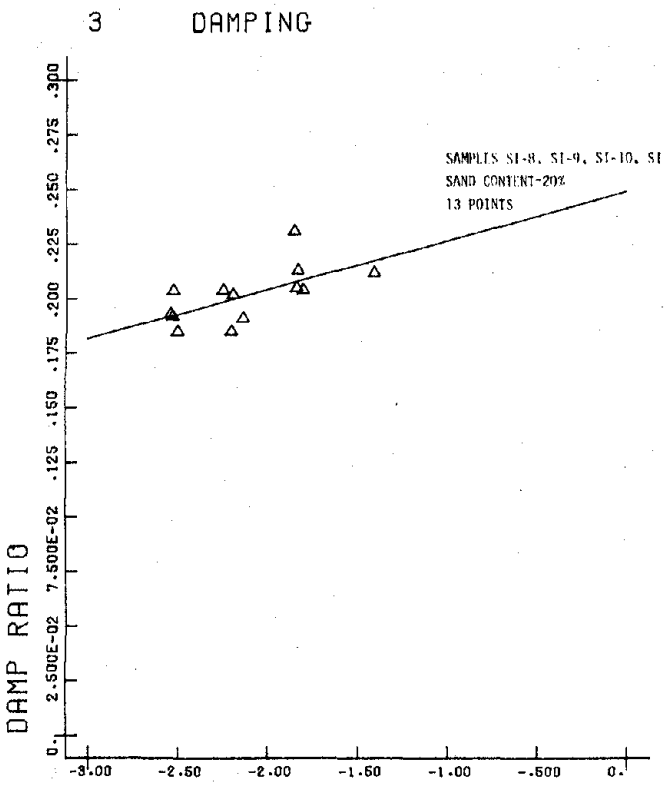

Figure D.13

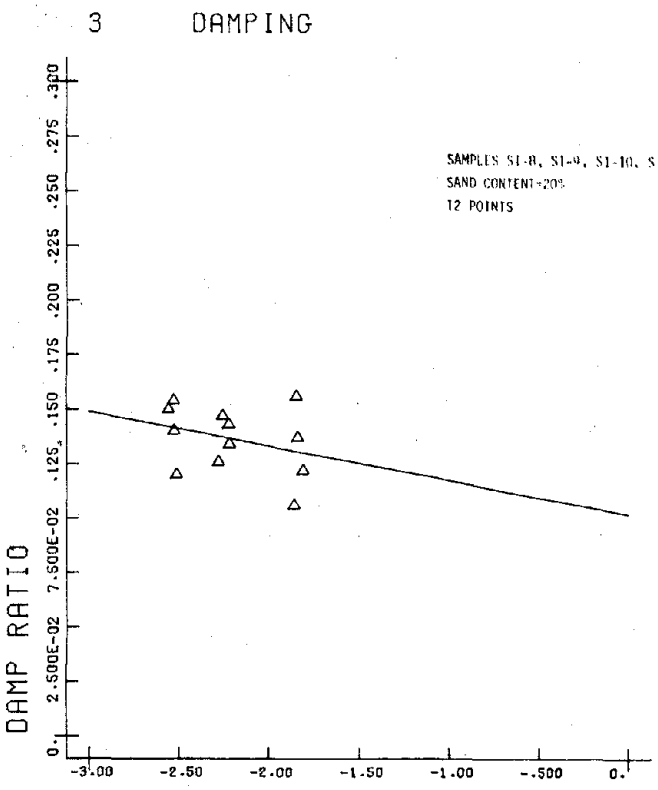

Figure D.14

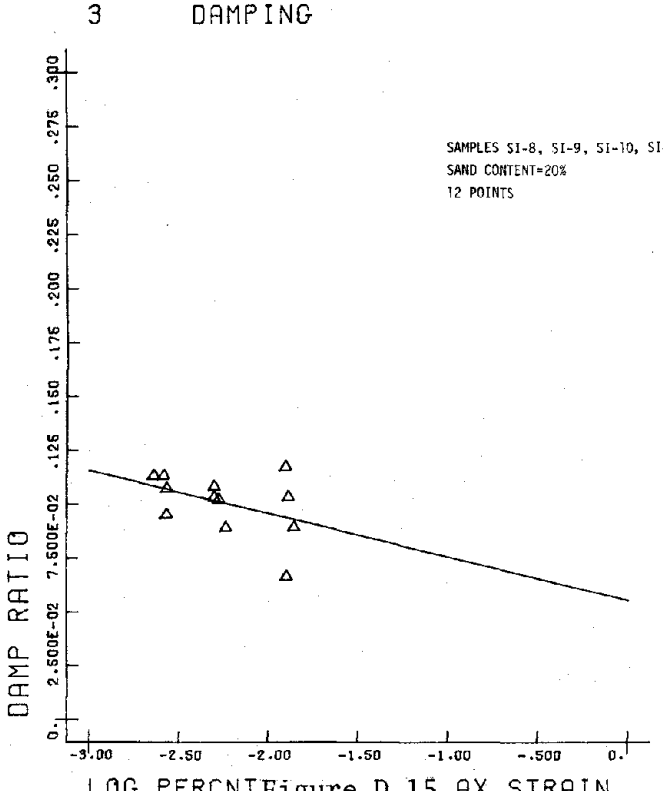

Figure D.15

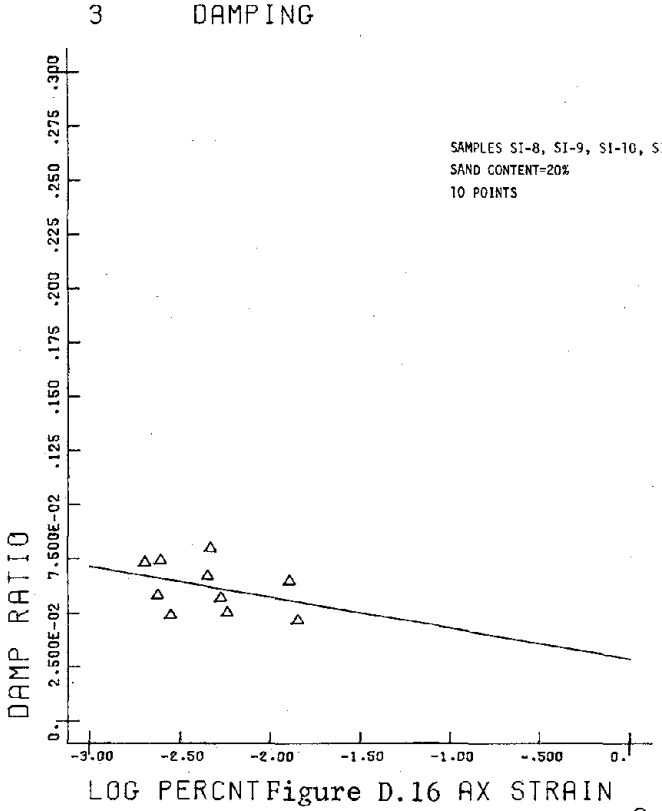

Figure D.16

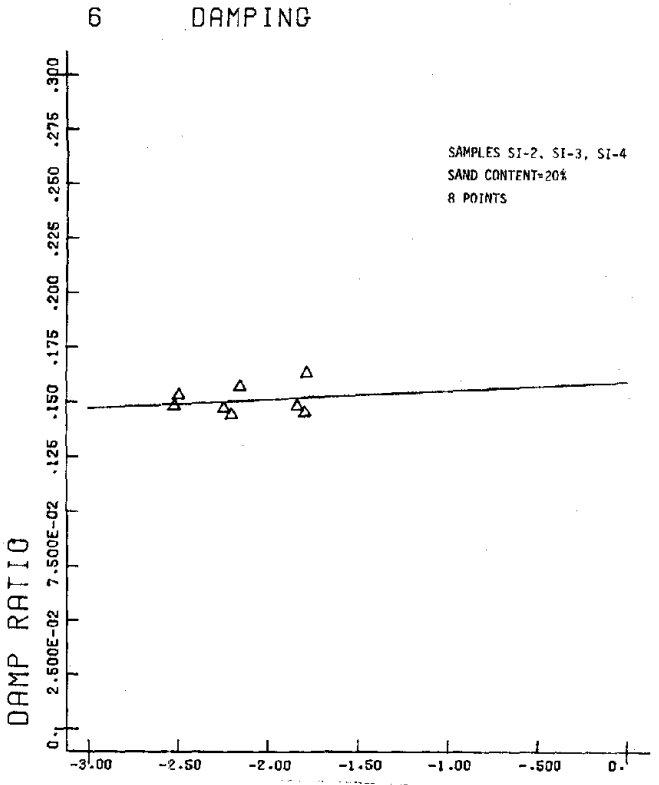

Figure D.17

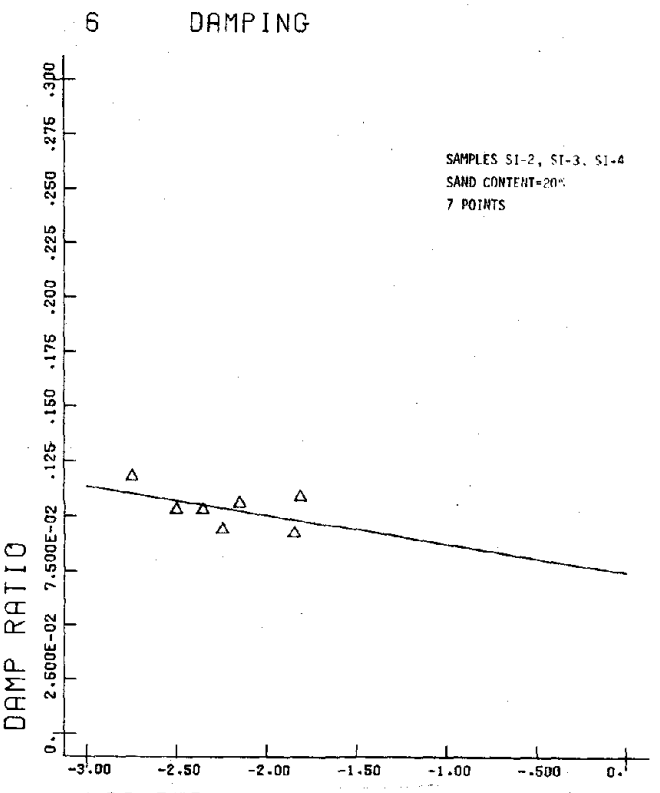

Figure D.18

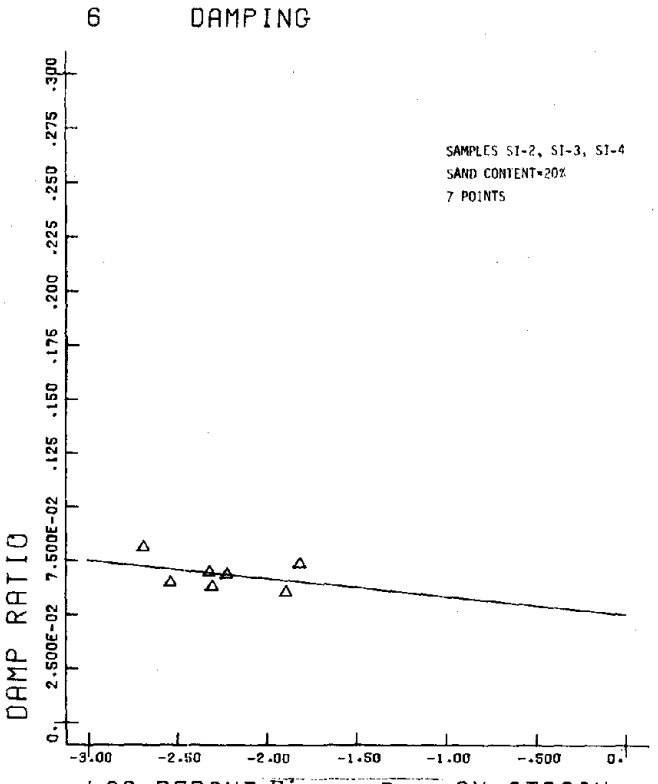

Figure D.19

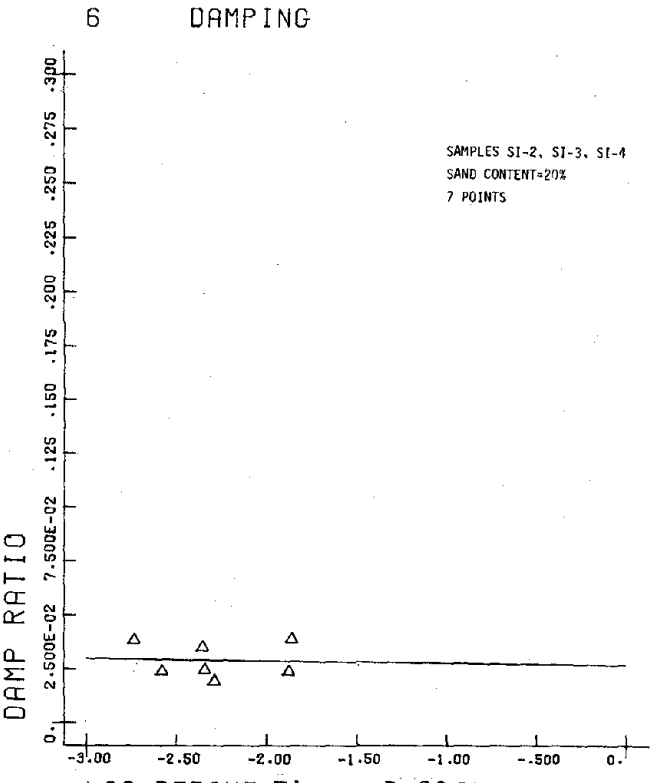

Figure D.20

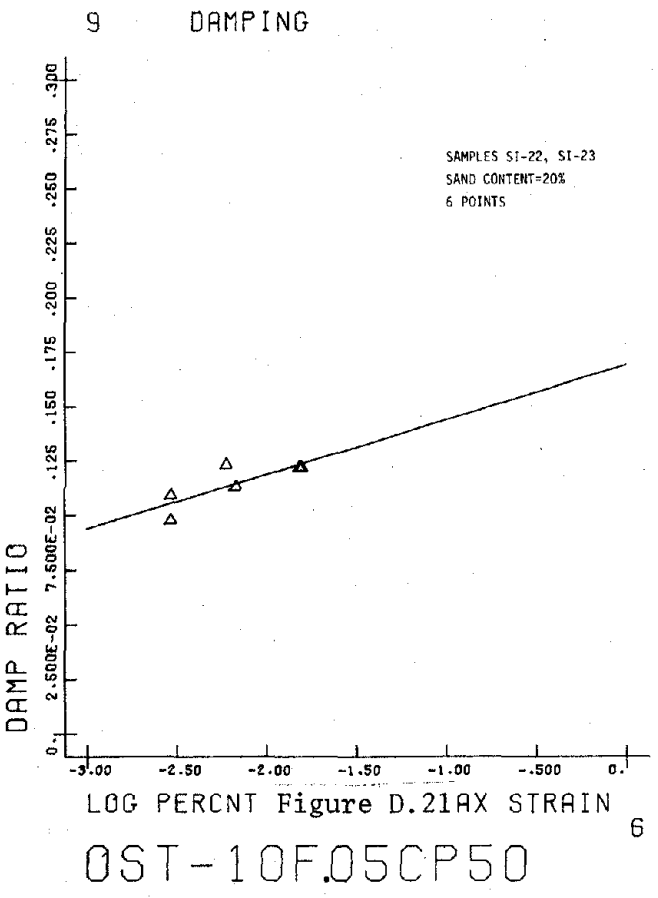

Figure D.21

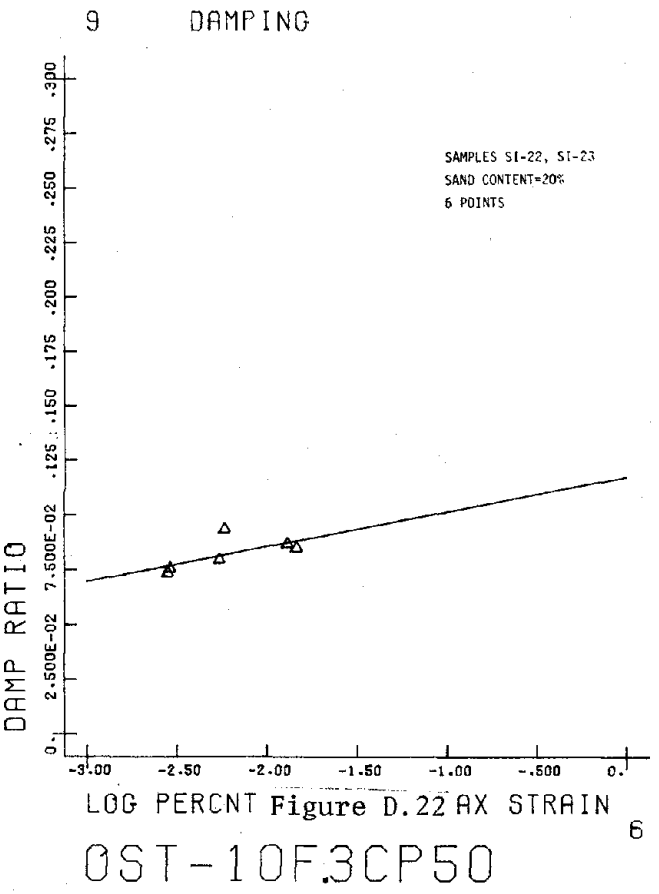

Figure D.22

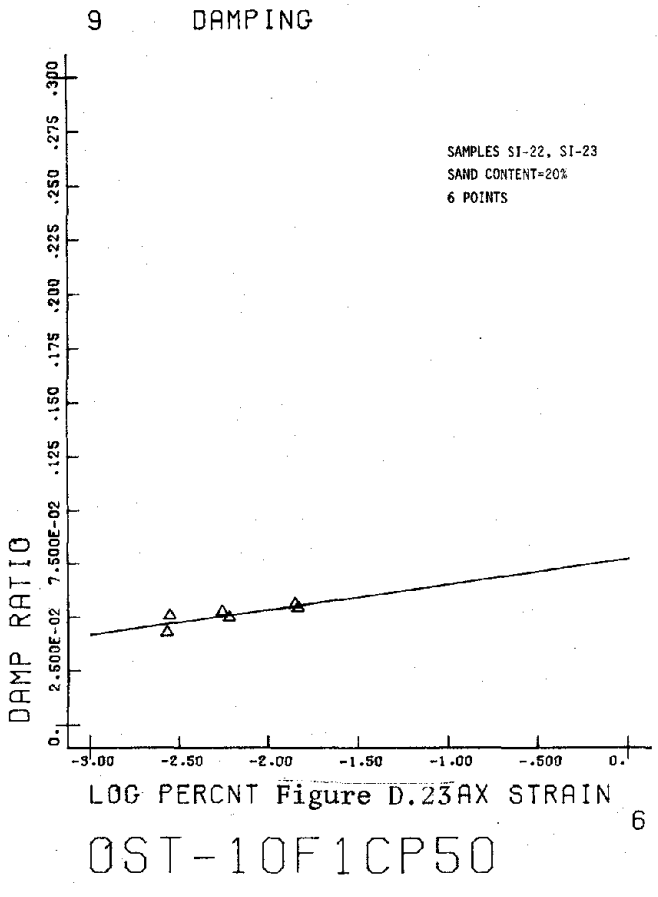

Figure D.23

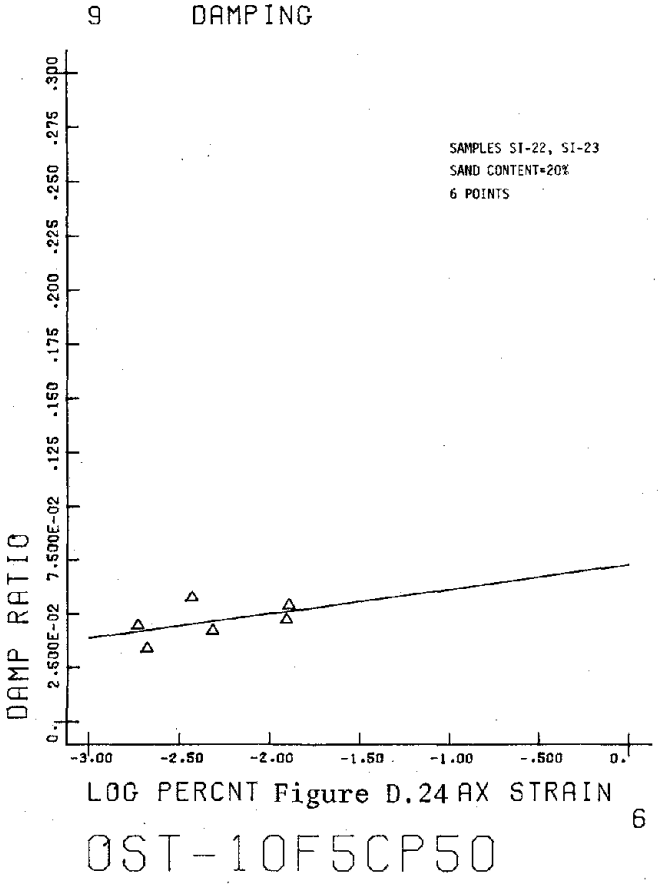

Figure D.24

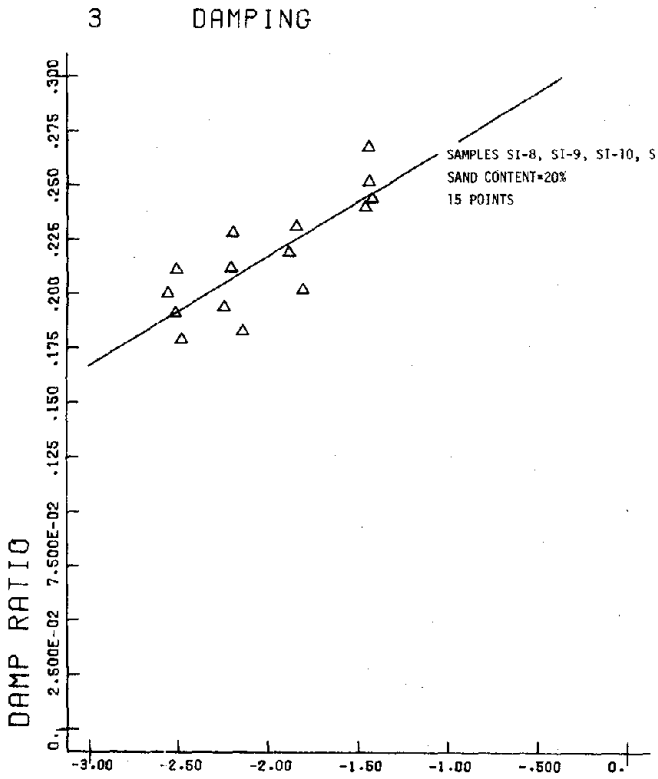

Figure D.25

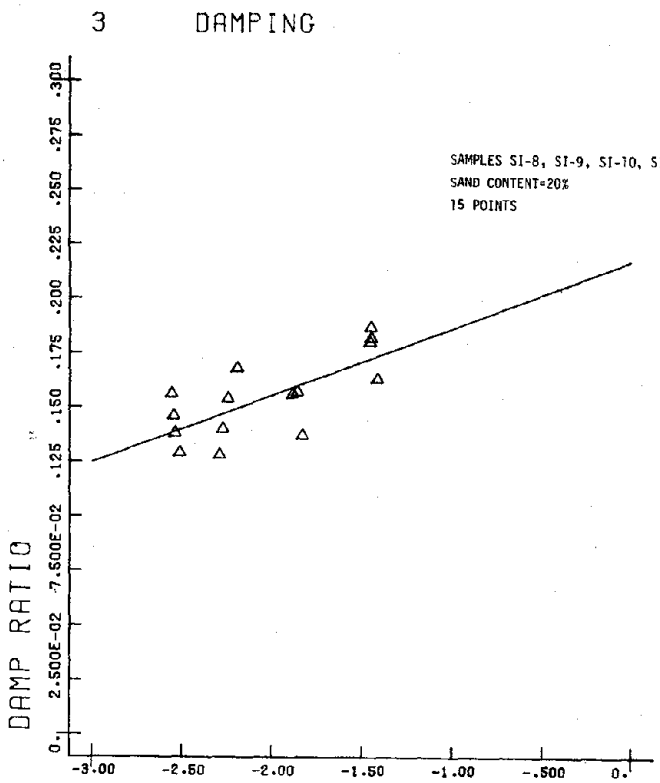

Figure D.26

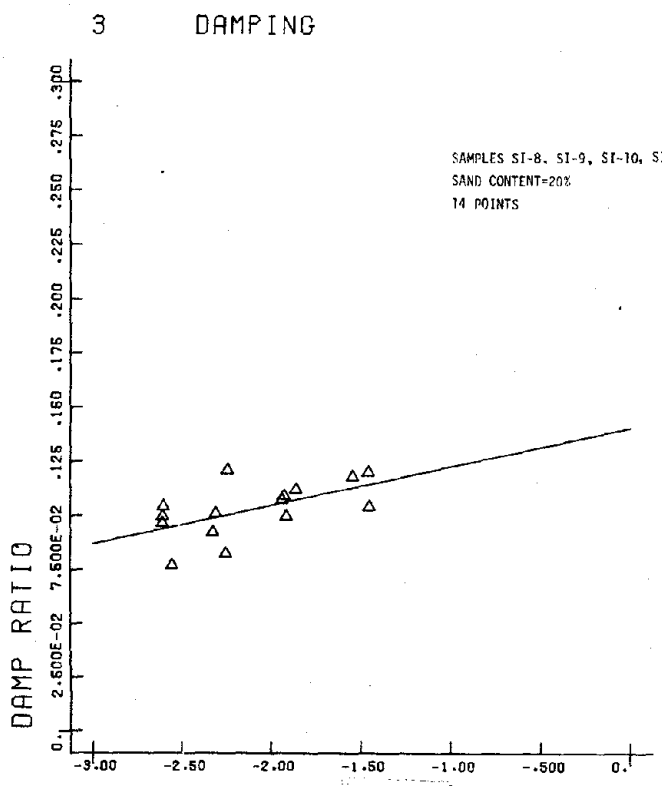

Figure D.27

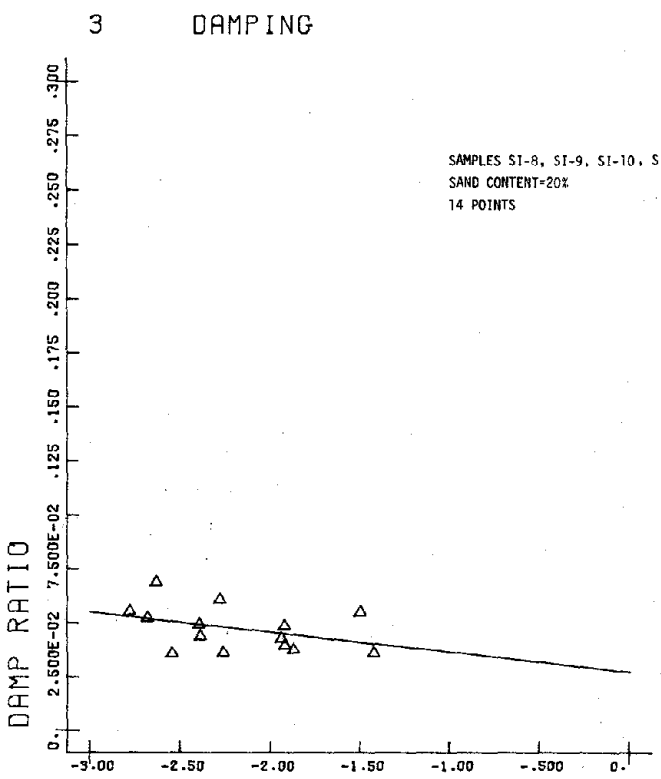

Figure D.28

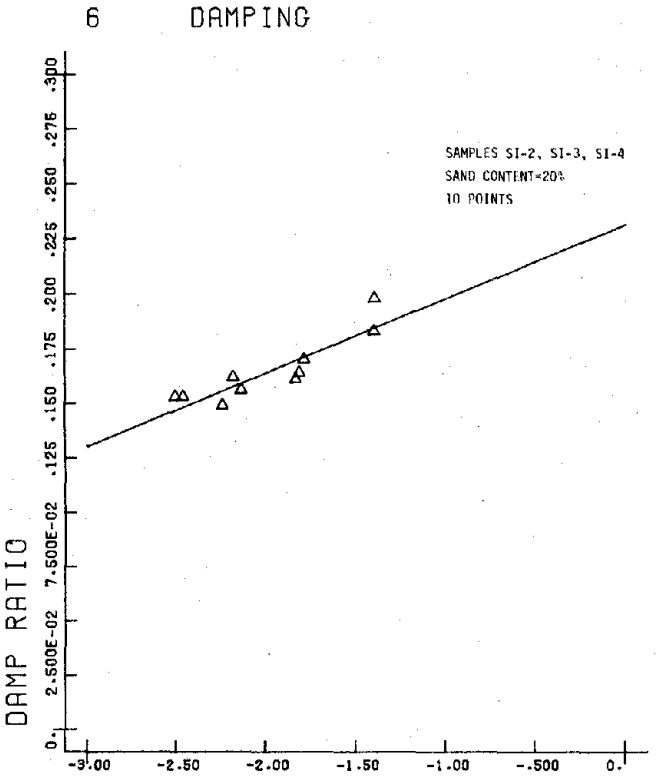

Figure D.29

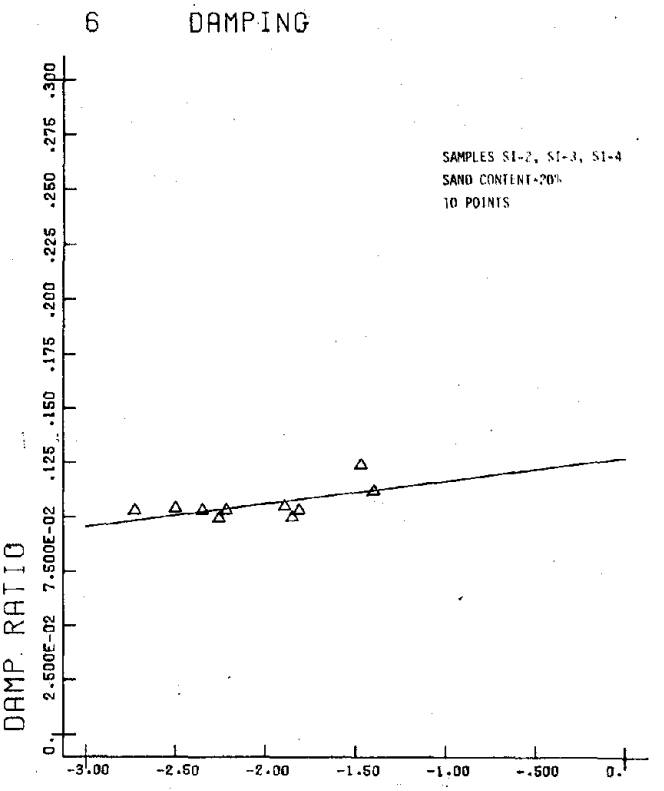

Figure D.30

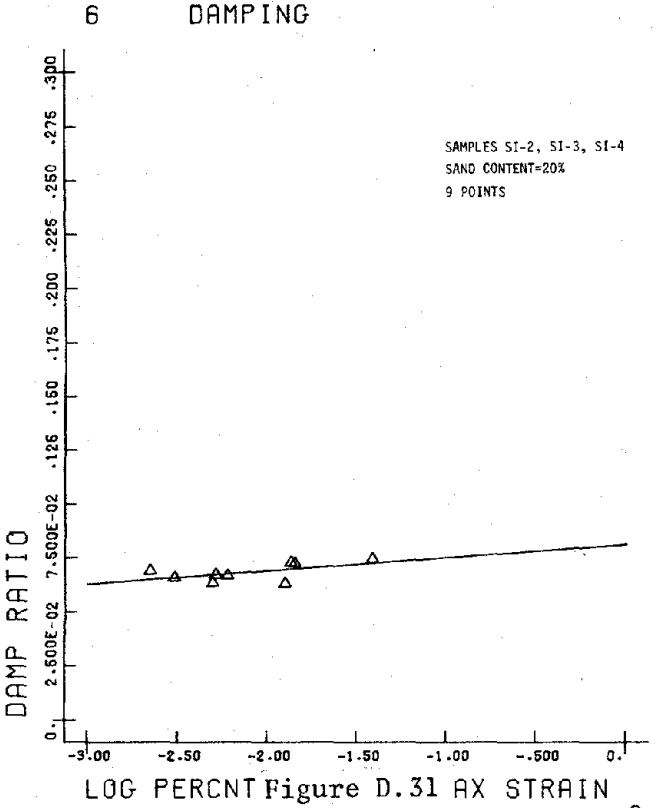

Figure D.31

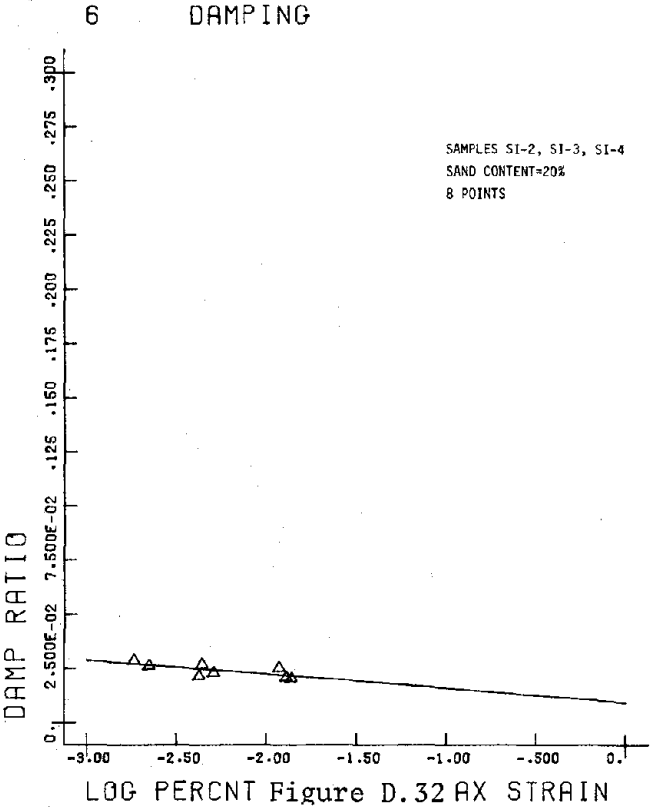

Figure D.32

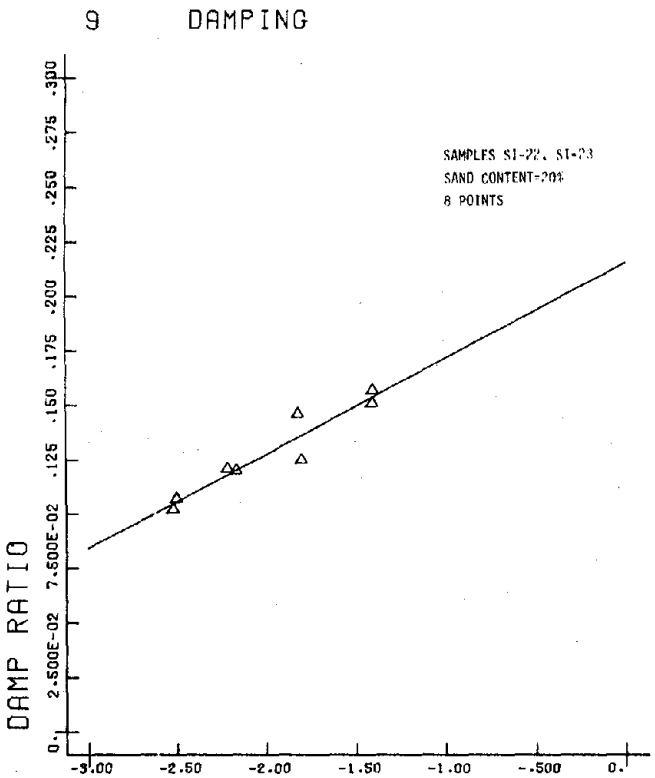

Figure D.33 OST-10F.05CP200

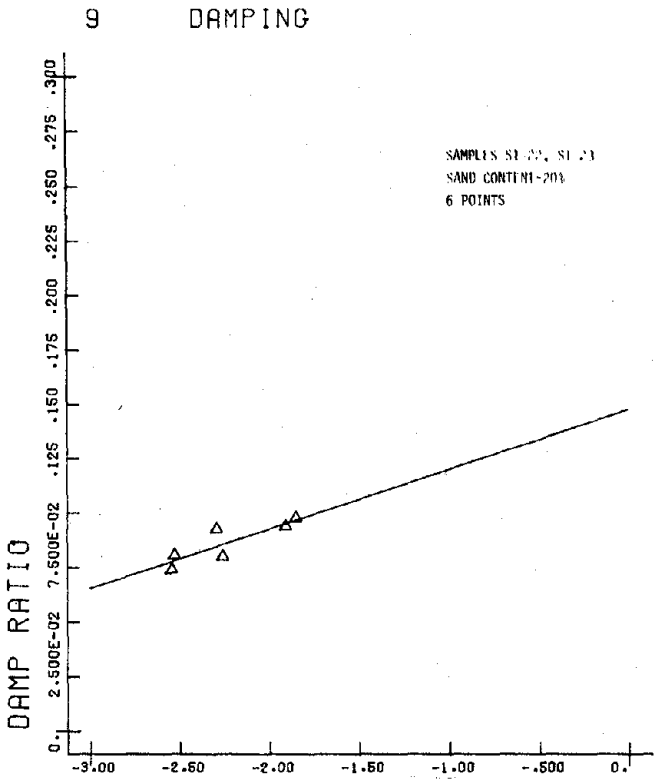

Figure D.34 OST-10F.3CP200

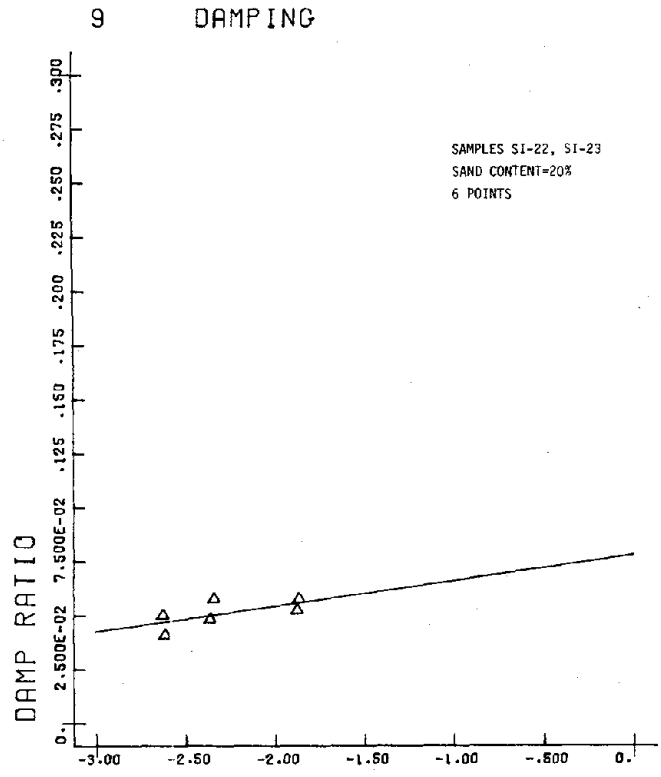

Figure D.35 OST-10F1CP200

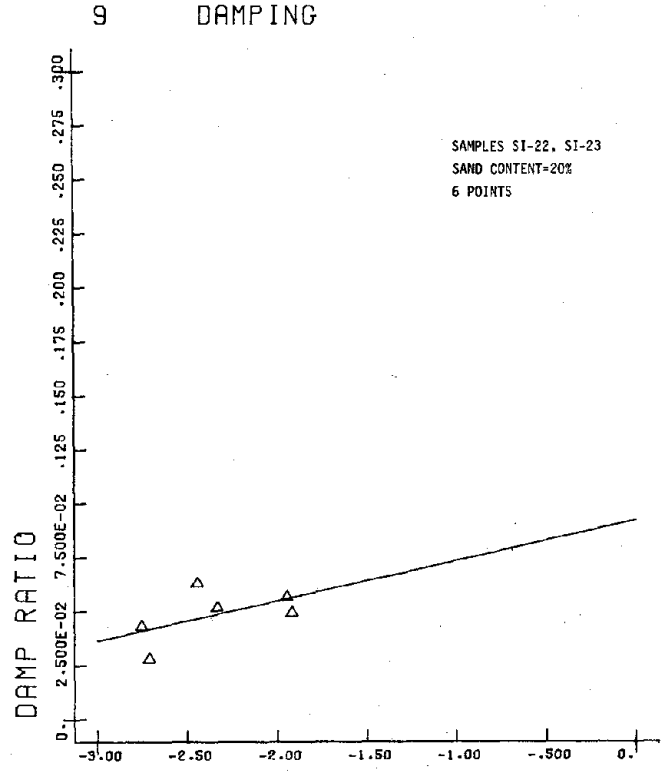

Figure D.36 OST-10F5CP200

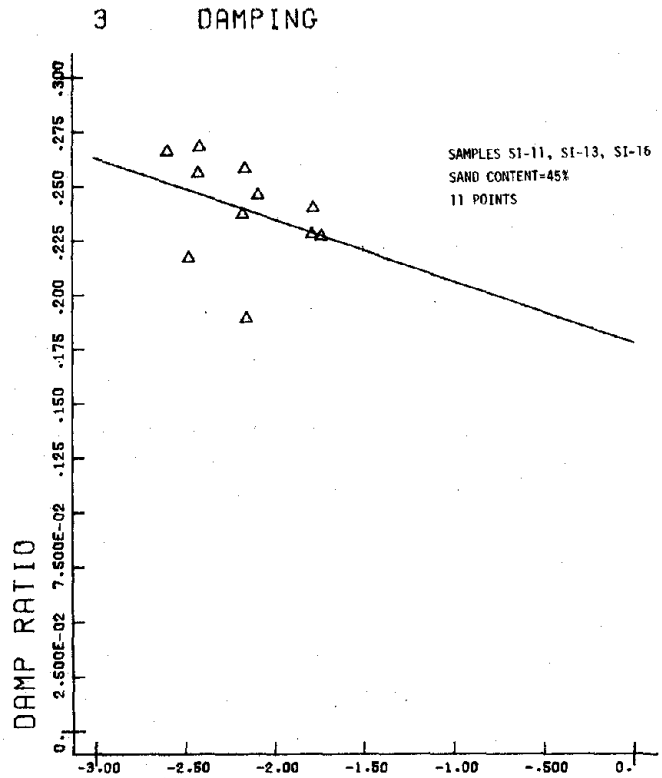
3 DAMPING
SAMPLES SI-11, SI-13, SI-16
SAND CONTENT=45%
11 POINTS
DAMP RATIO
0.
2.500E-02
7.500E-02
.125
.150
.175
.200
.225
.250
.275
.300
-3.00
-2.50
-2.00
-1.50
-1.00
-.500
0.
LOG PERCNT Figure D.37 AX STRAIN
2
OST-1F.05CPO

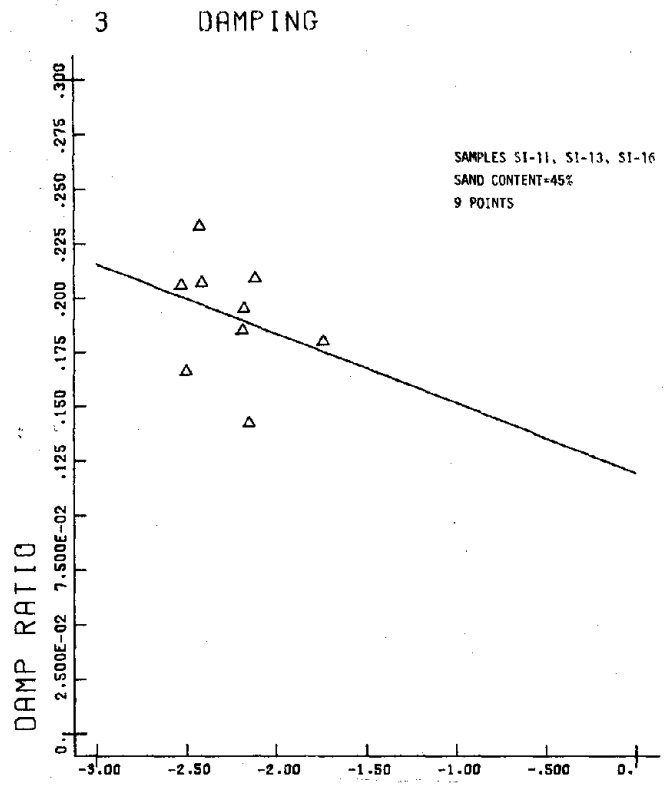
3 DAMPING
SAMPLES SI-11, SI-13, SI-16
SAND CONTENT=45%
9 POINTS
DAMP RATIO
0.
2.500E-02
7.500E-02
.125
.150
.175
.200
.225
.250
.275
.300
-3.00
-2.50
-2.00
-1.50
-1.00
-.500
0.
LOG PERCNT Figure D.38 AX STRAIN
2
OST-1F.3CPO

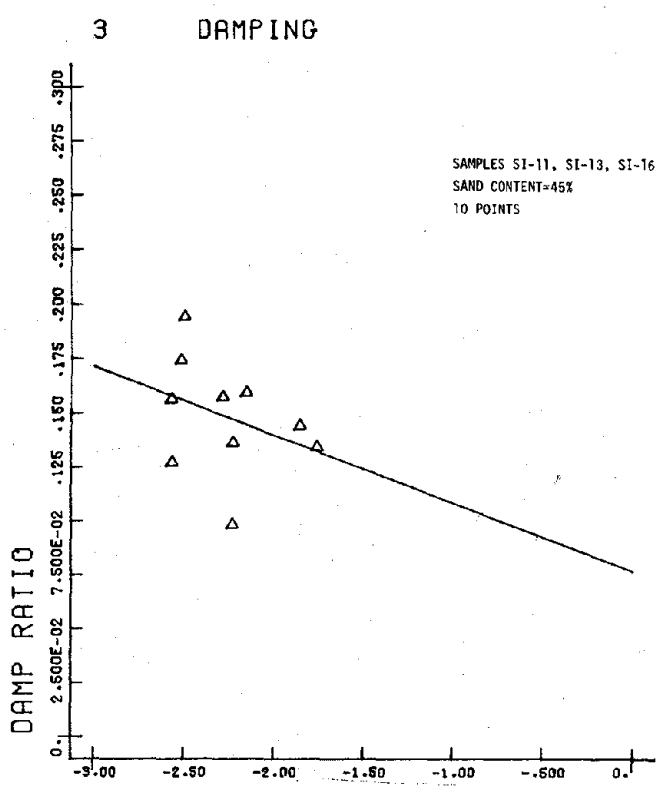
3 DAMPING
SAMPLES SI-11, SI-13, SI-16
SAND CONTENT=45%
10 POINTS
DAMP RATIO
0.
2.500E-02
7.500E-02
.125
.150
.175
.200
.225
.250
.275
.300
-3.00
-2.50
-2.00
-1.50
-1.00
-.500
0.
LOG PERCNT Figure D.39 AX STRAIN
2
OST-1F1CPO

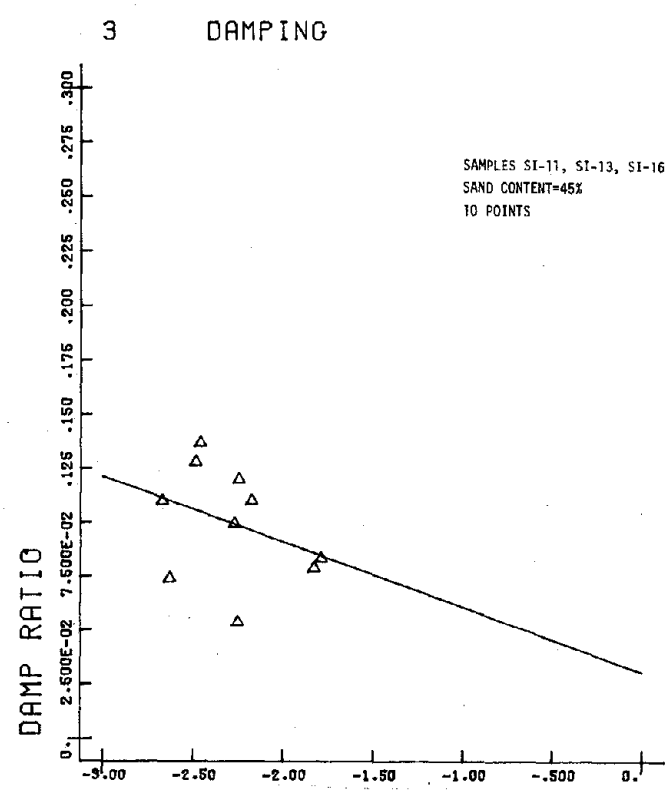
3 DAMPING
SAMPLES SI-11, SI-13, SI-16
SAND CONTENT=45%
10 POINTS
DAMP RATIO
0.
2.500E-02
7.500E-02
.125
.150
.175
.200
.225
.250
.275
.300
-3.00
-2.50
-2.00
-1.50
-1.00
-.500
0.
LOG PERCNT Figure D.40 AX STRAIN
2
OST-1F5CPO

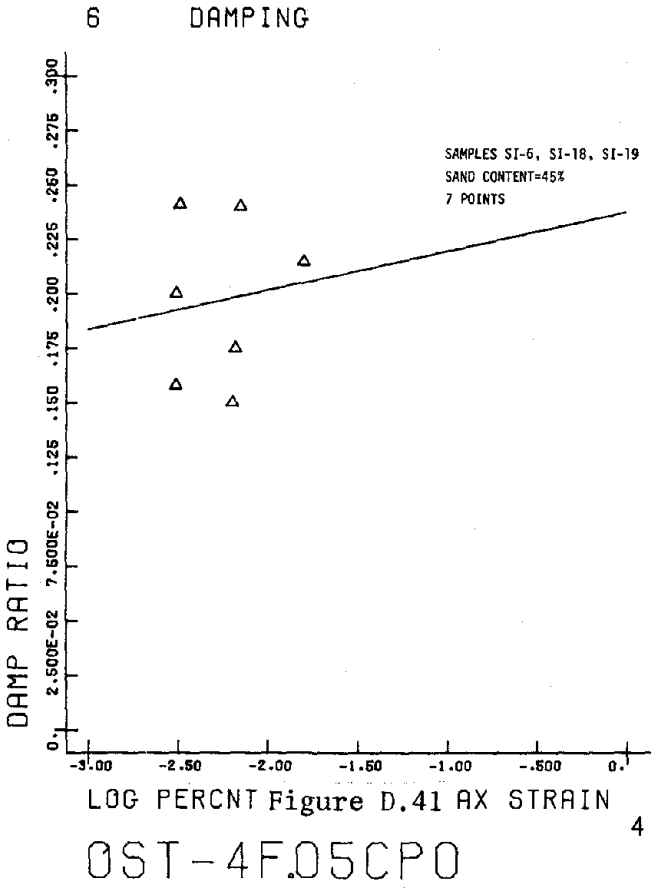

Figure D.41

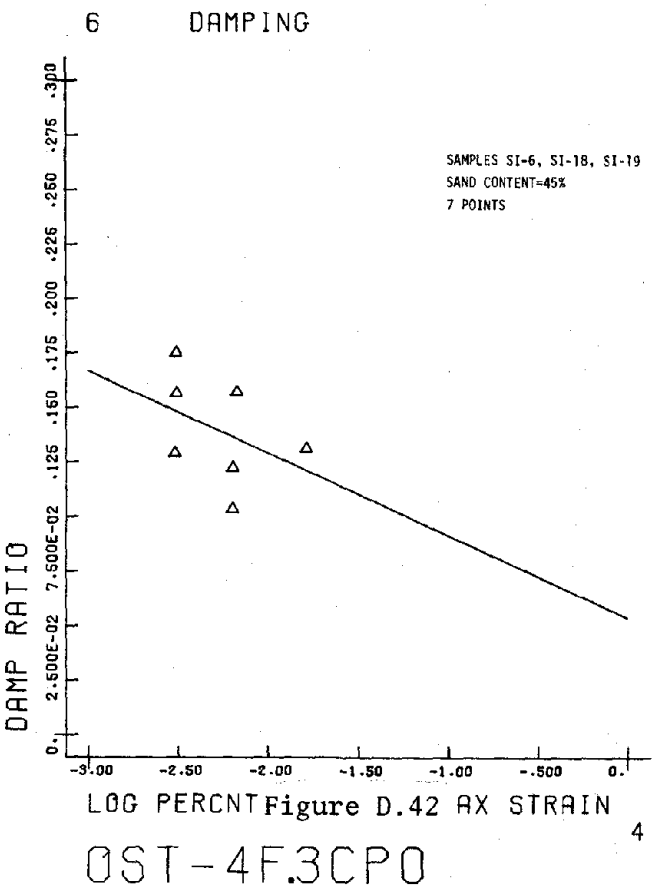

Figure D.42

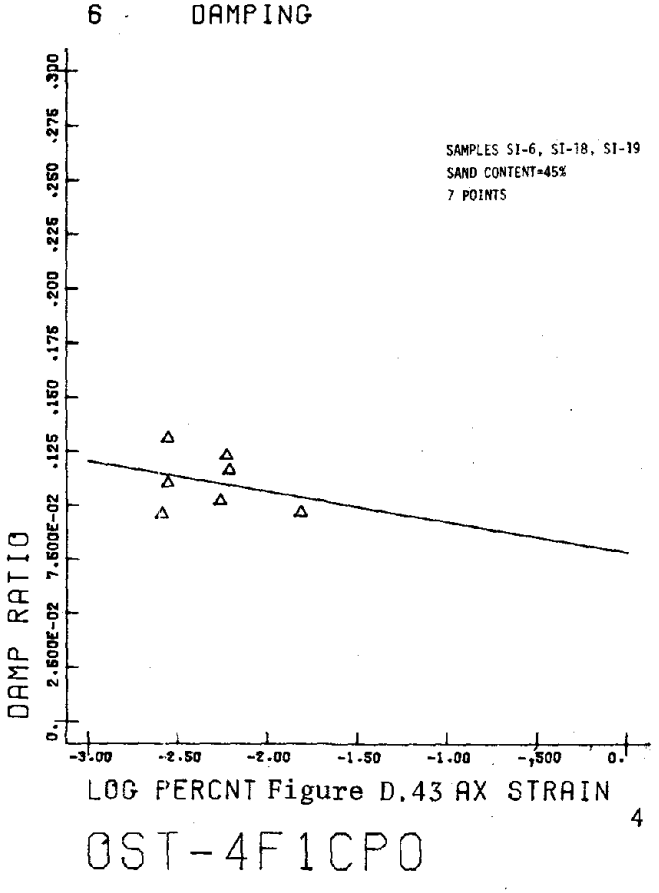

Figure D.43

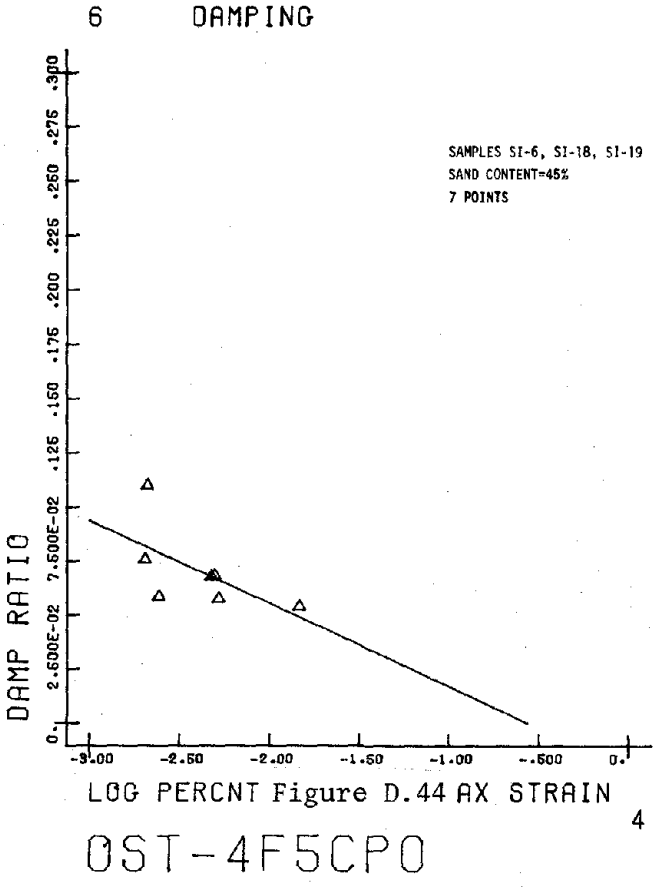

Figure D.44

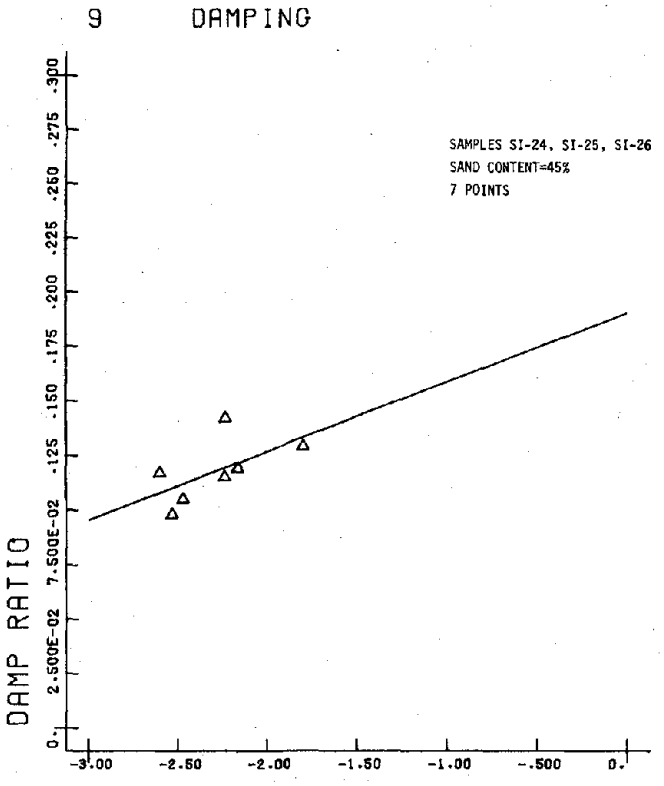
9 DAMPING
SAMPLES SI-24, SI-25, SI-26
SAND CONTENT=45%
7 POINTS
DAMP RATIO
0.
2.500E-02
7.500E-02
.125
.150
.175
.200
.225
.250
.275
.300
-3.00
-2.50
-2.00
-1.50
-1.00
-.500
0.
LOG PERCNT Figure D.45 AX STRAIN
2
OST-10F.05CP0

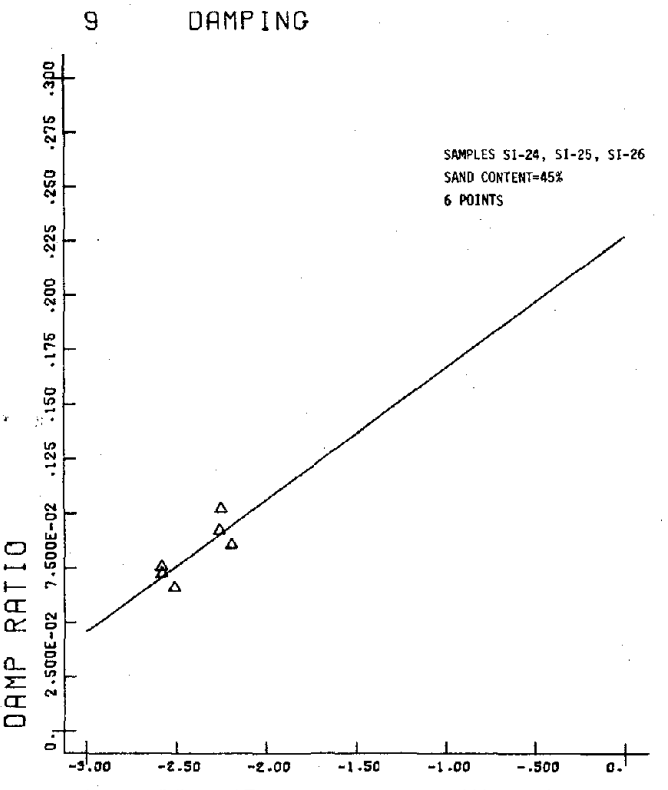
9 DAMPING
SAMPLES SI-24, SI-25, SI-26
SAND CONTENT=45%
6 POINTS
DAMP RATIO
0.
2.500E-02
7.500E-02
.125
.150
.175
.200
.225
.250
.275
.300
-3.00
-2.50
-2.00
-1.50
-1.00
-.500
0.
LOG PERCNT Figure D.46 AX STRAIN
6
OST-10F.3CP0

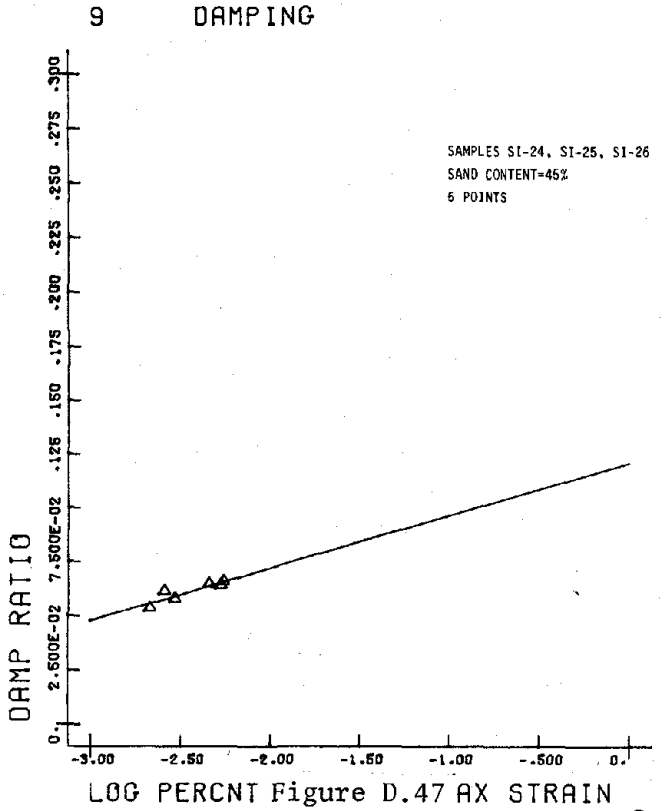
9 DAMPING
SAMPLES SI-24, SI-25, SI-26
SAND CONTENT=45%
6 POINTS
DAMP RATIO
0.
2.500E-02
7.500E-02
.125
.150
.175
.200
.225
.250
.275
.300
-3.00
-2.50
-2.00
-1.50
-1.00
-.500
0.
LOG PERCNT Figure D.47 AX STRAIN
6
OST-10F1CP0

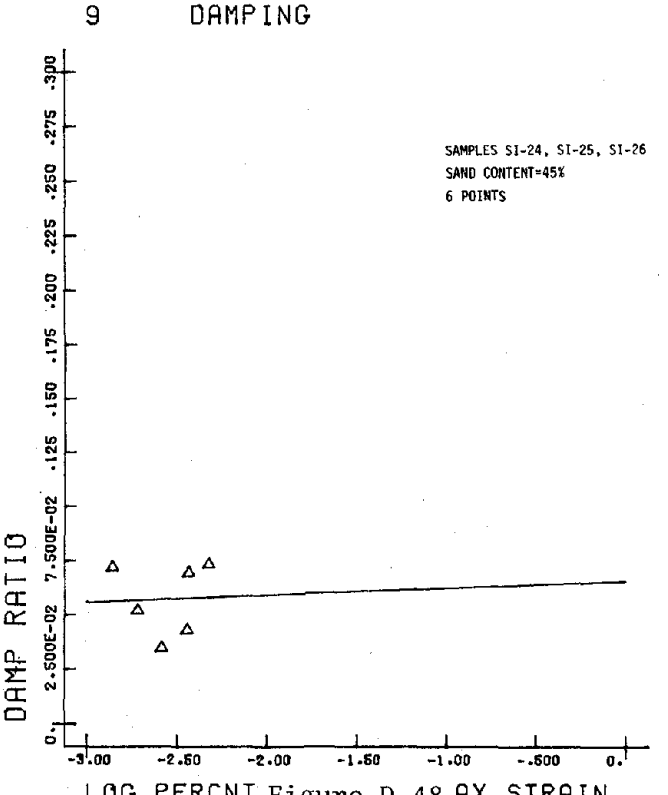
9 DAMPING
SAMPLES SI-24, SI-25, SI-26
SAND CONTENT=45%
6 POINTS
DAMP RATIO
0.
2.500E-02
7.500E-02
.125
.150
.175
.200
.225
.250
.275
.300
-3.00
-2.50
-2.00
-1.50
-1.00
-.500
0.
LOG PERCNT Figure D.48 AX STRAIN
6
OST-10F5CP0

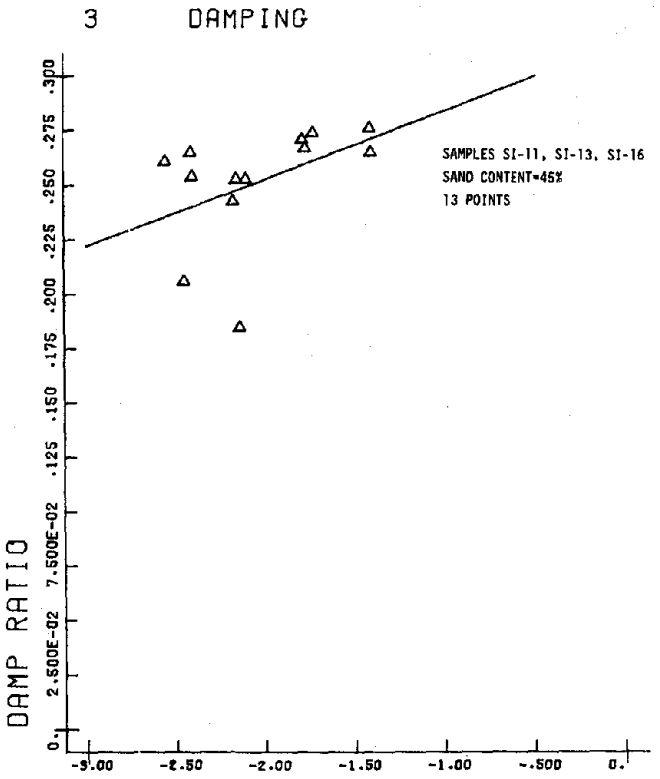

Figure D.49 AX STRAIN 2

OST-1F.05CP50

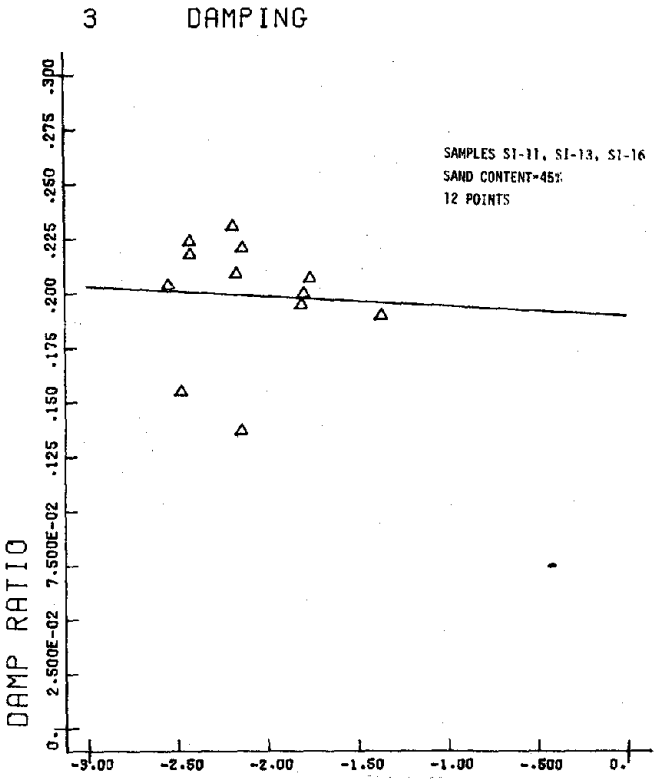

Figure D.50 AX STRAIN 2

OST-1F.3CP50

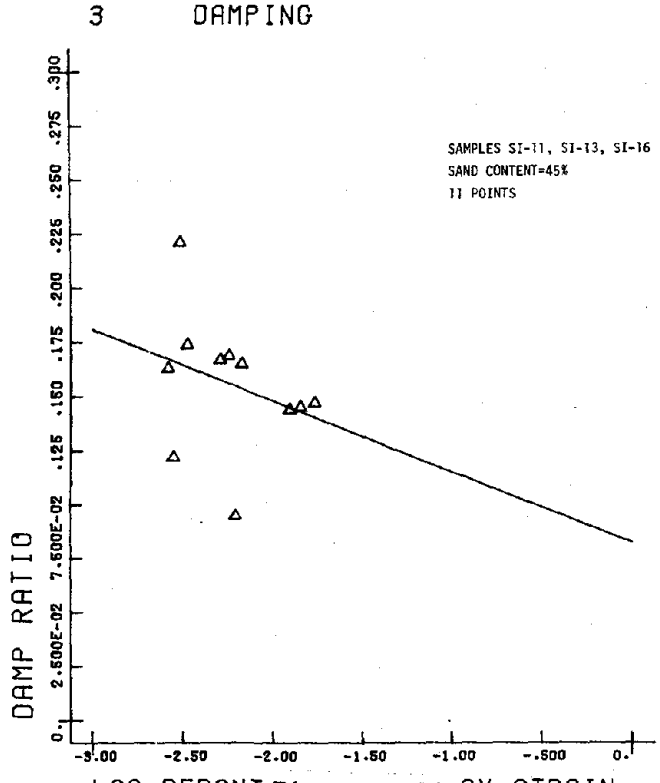

Figure D.51 AX STRAIN 2

OST-1F1CP50

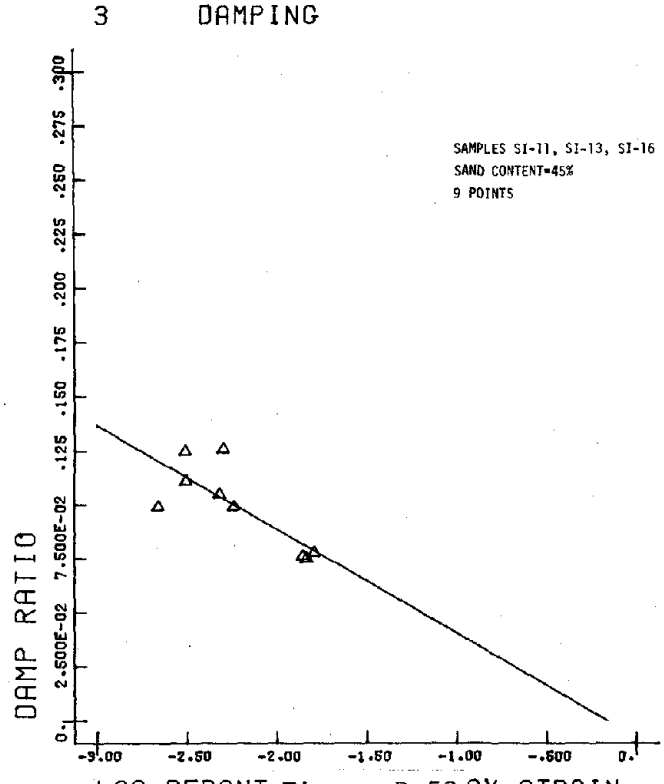

Figure D.52 AX STRAIN 2

OST-1F5CP50

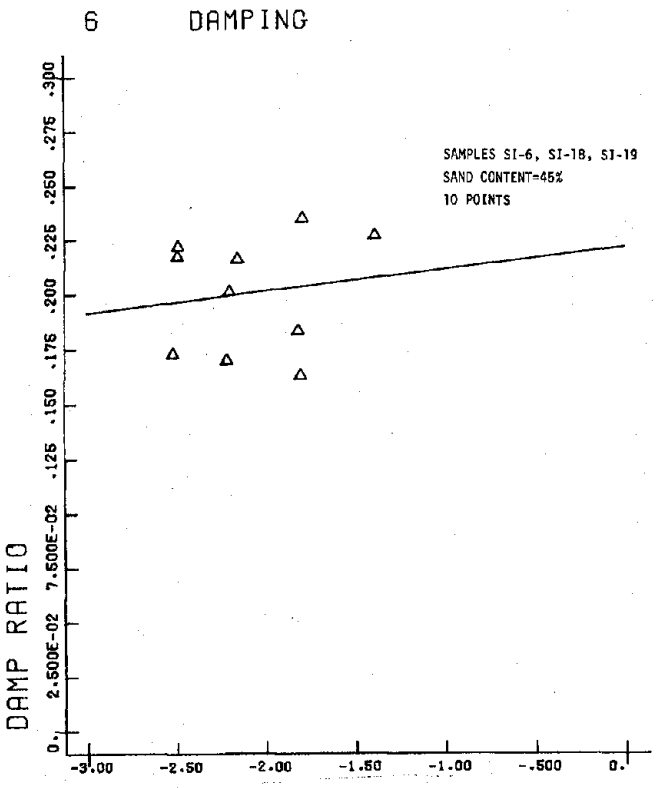

Figure D.53

OST-4F.05CP50

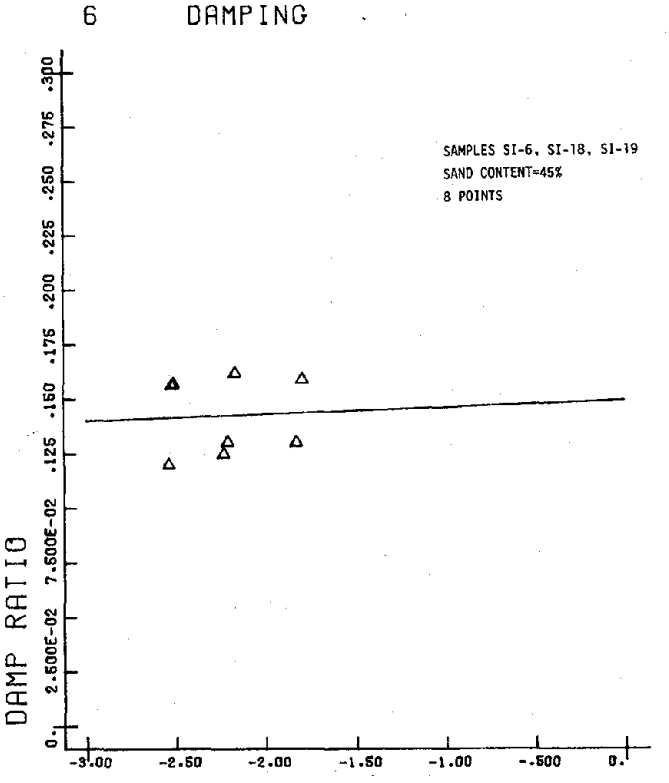

Figure D.54

OST-4F.3CP50

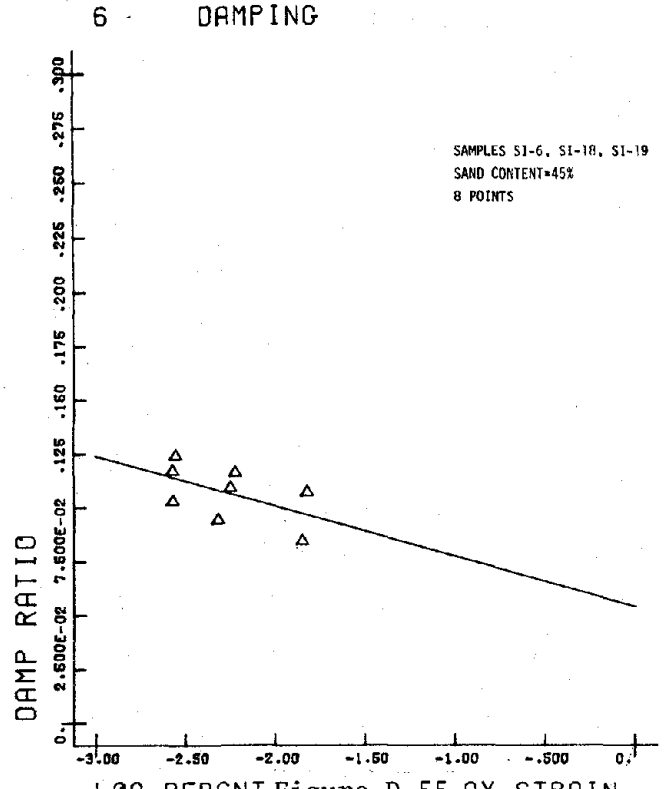

Figure D.55

OST-4F1CP50

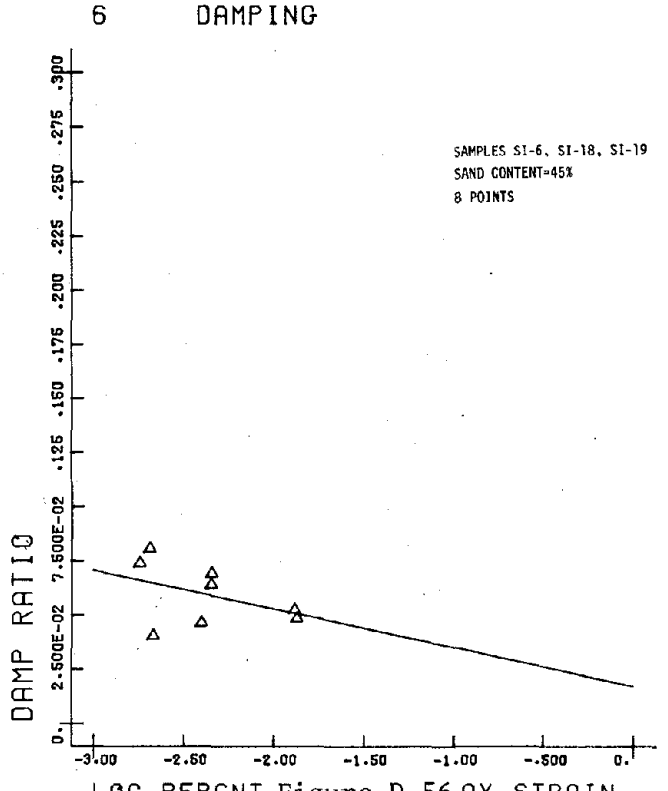

Figure D.56

OST-4F5CP50

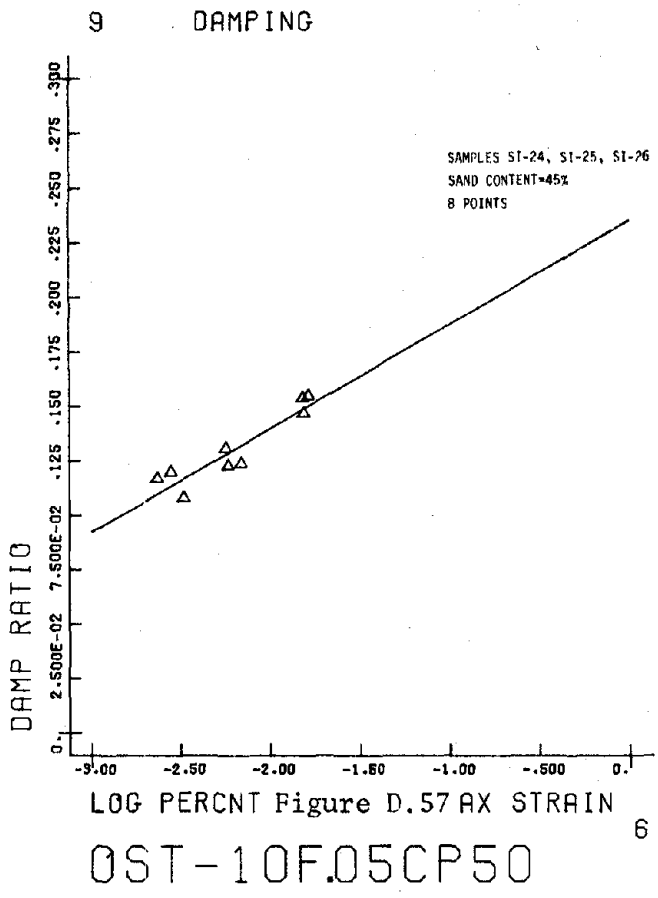

Figure D.57 OST-10F.05CP50

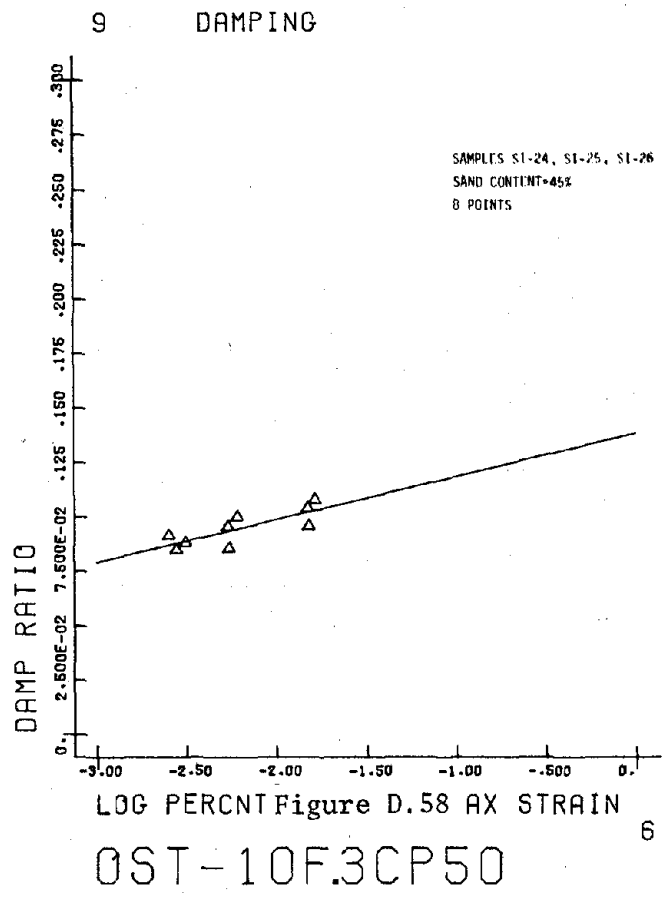

Figure D.58 OST-10F.3CP50

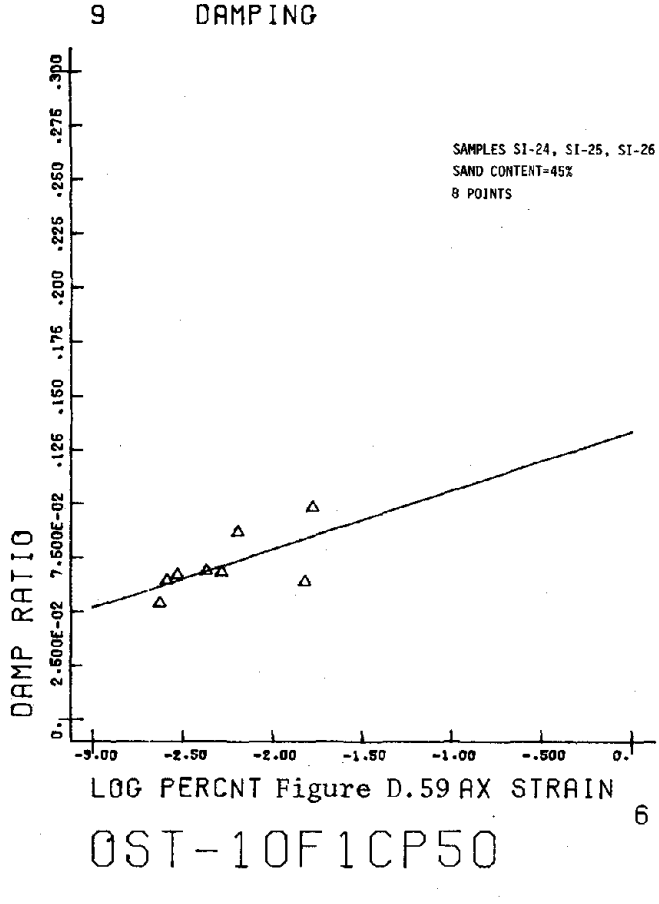

Figure D.59 OST-10F1CP50

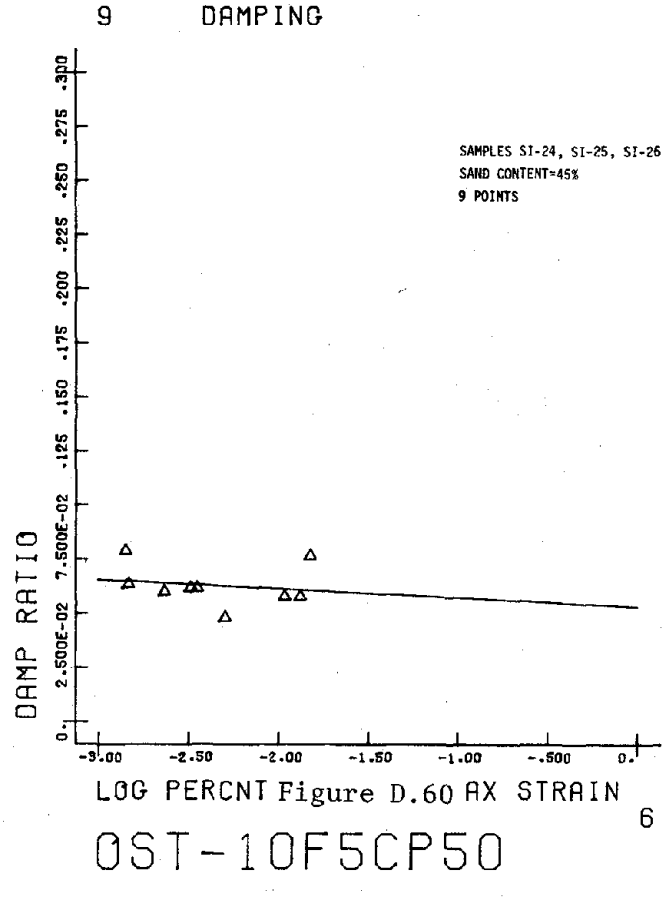

Figure D.60 OST-10F5CP50

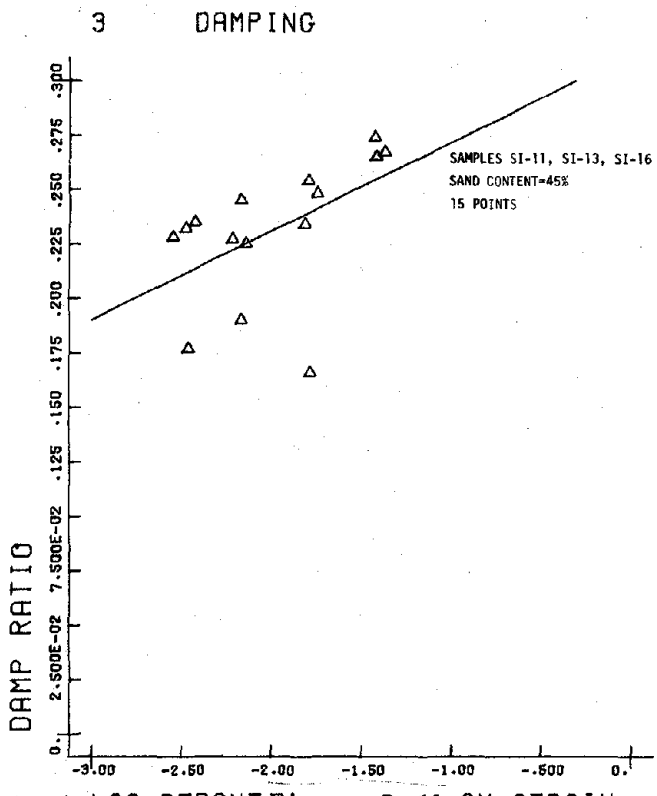

Figure D.61

OST-1F.05CP200

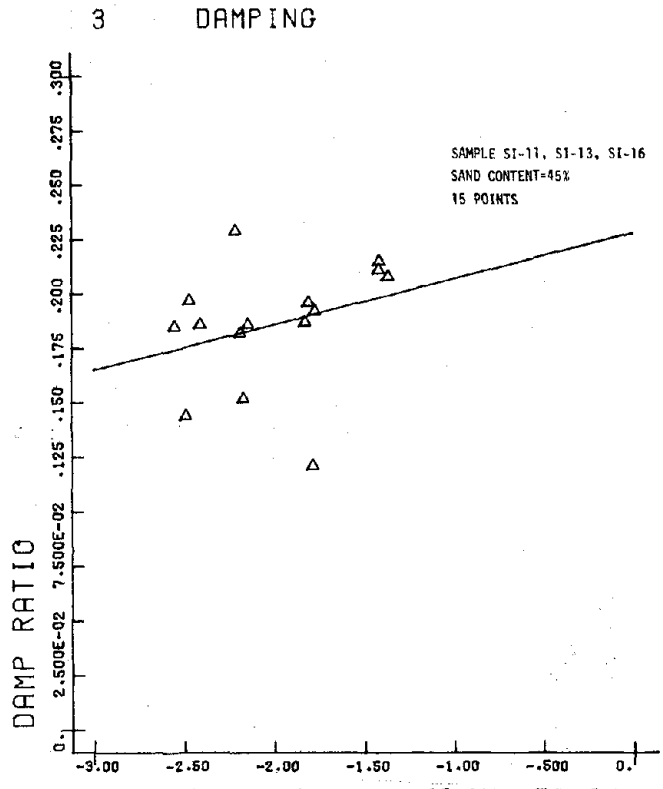

Figure D.62

OST-1F.3CP200

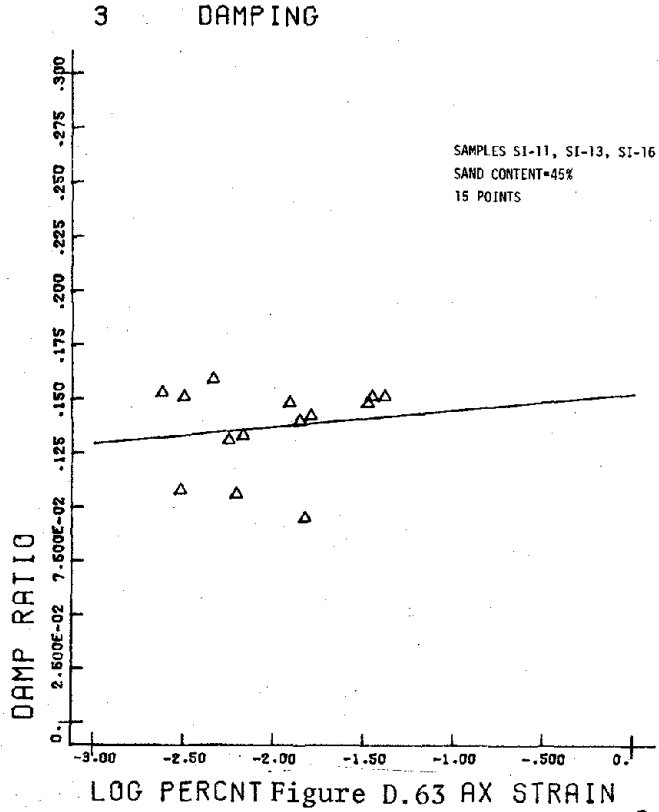

Figure D.63

OST-1F1CP200

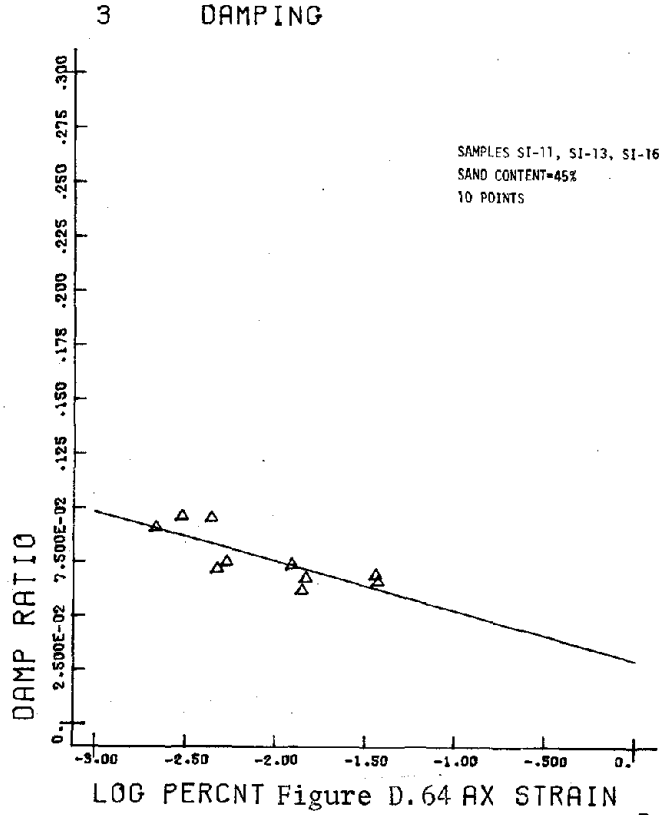

Figure D.64

OST-1F5CP200

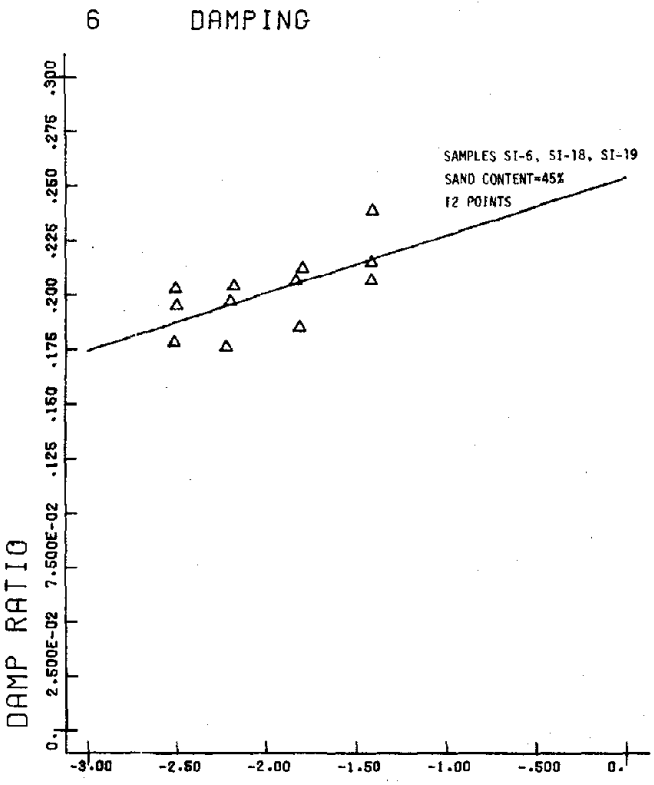

Figure D.65

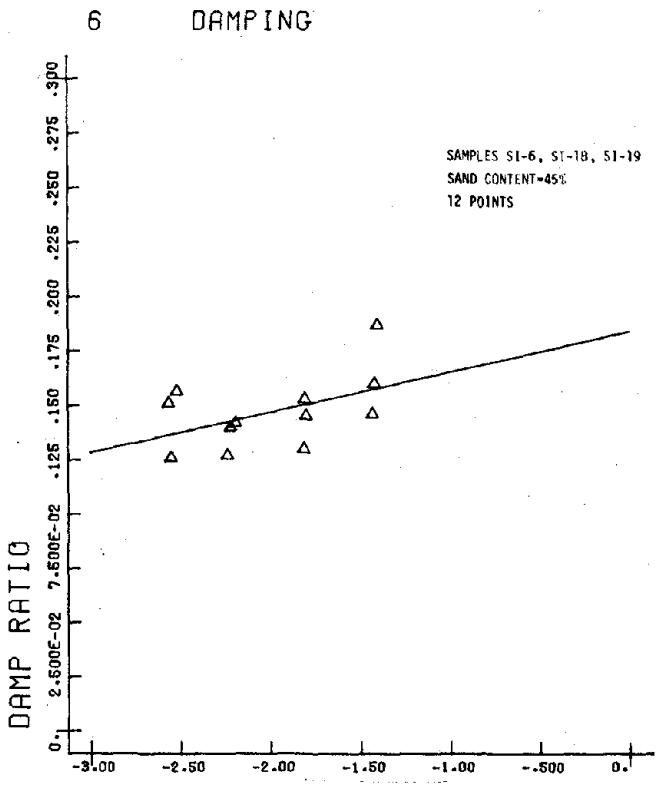

Figure D.66

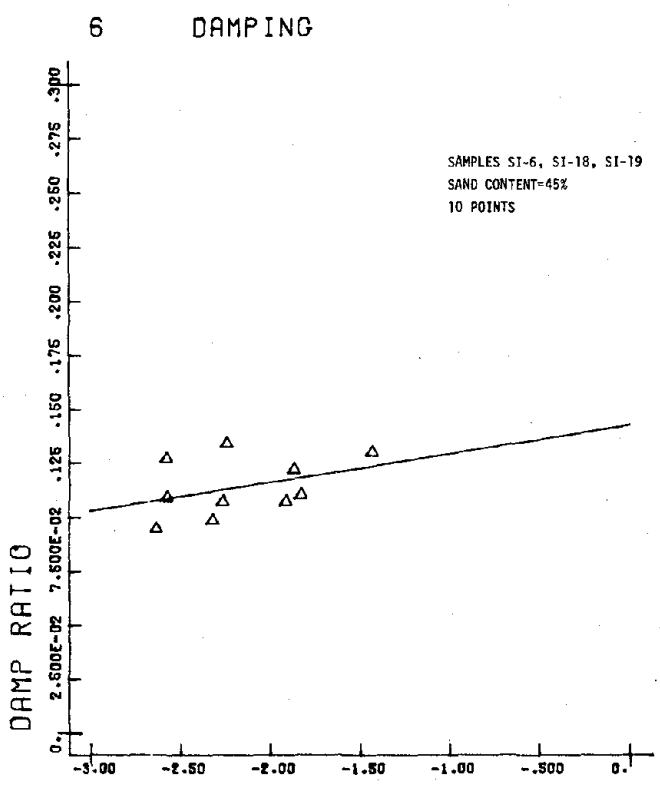

Figure D.67

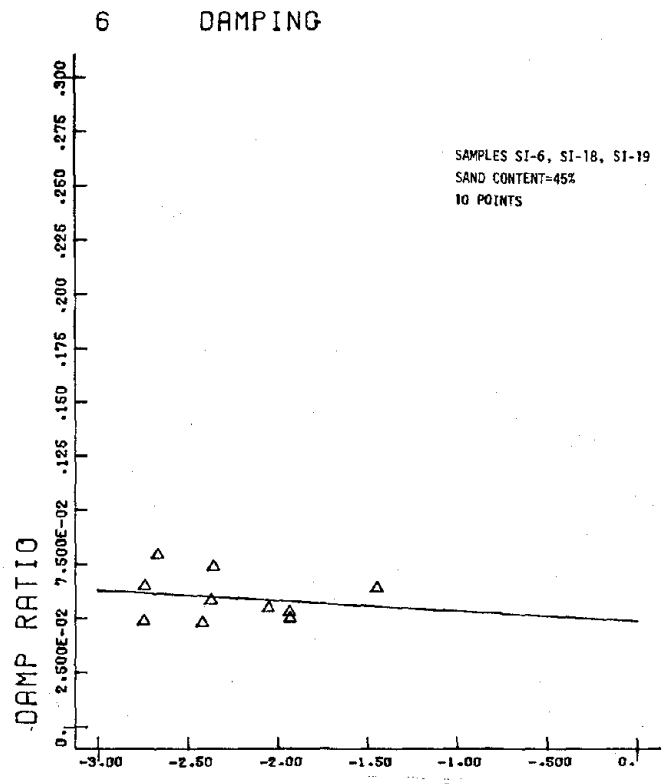

Figure D.68

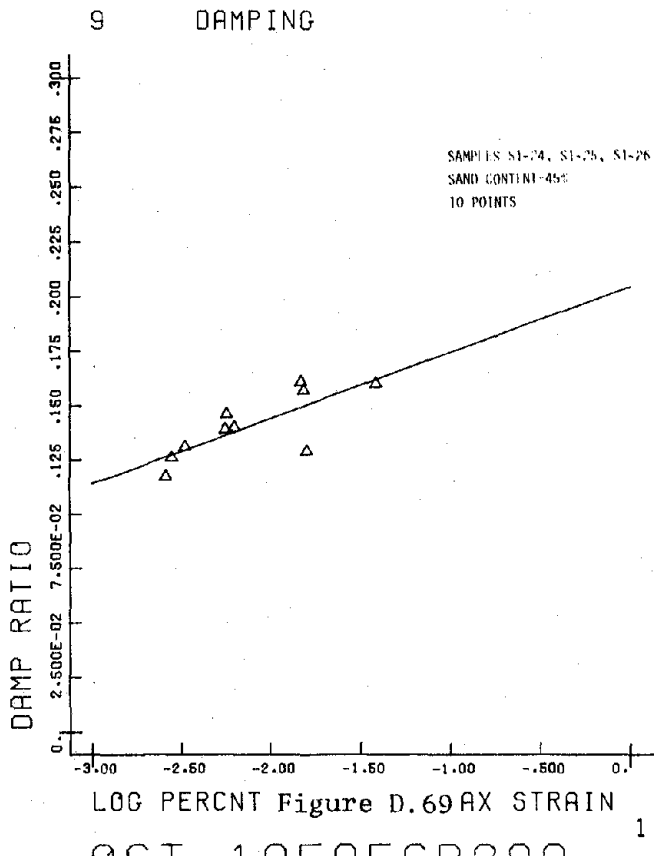

Figure D.69

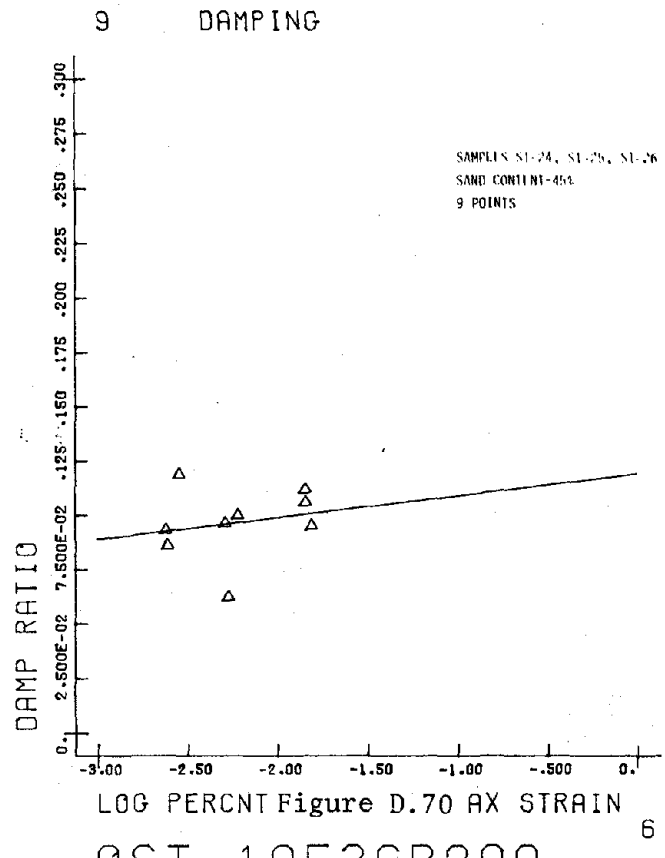

Figure D.70

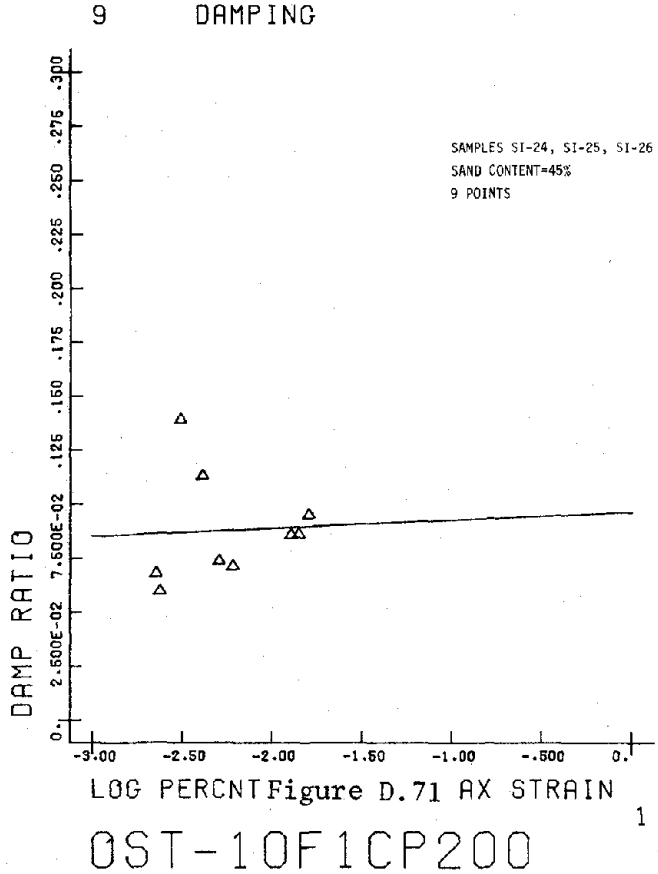

Figure D.71

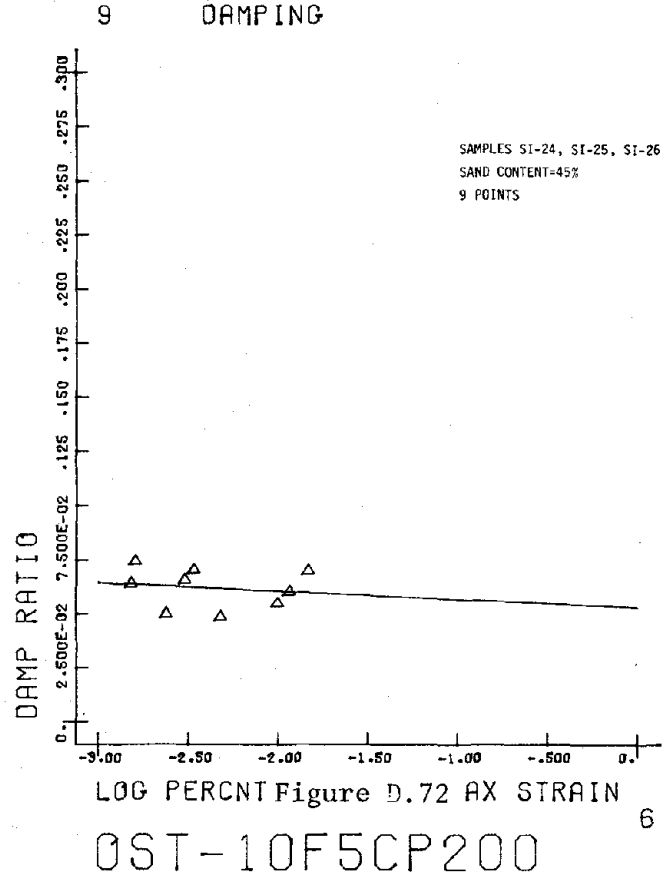

Figure D.72

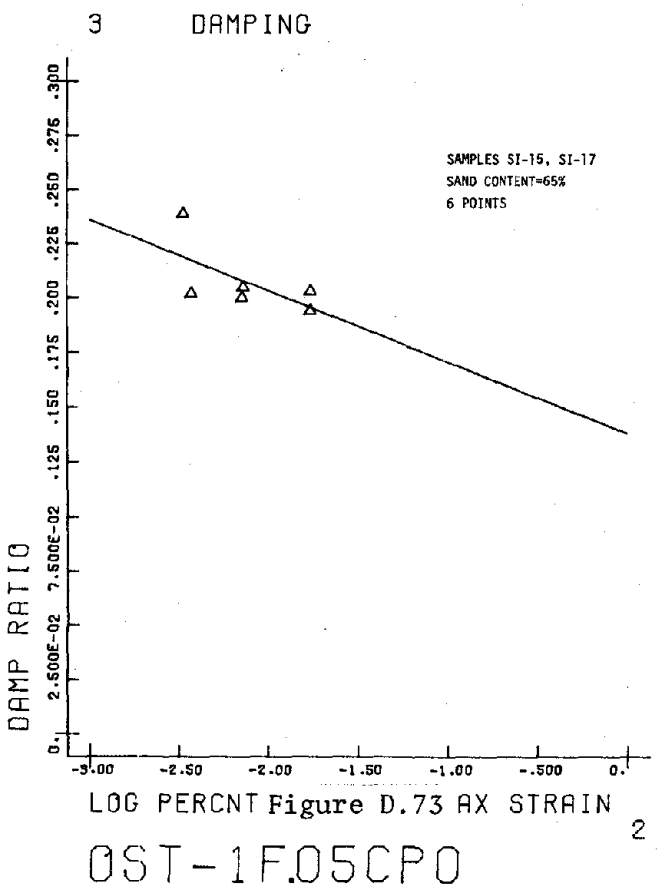

Figure D.73

OST-1F.05CP0

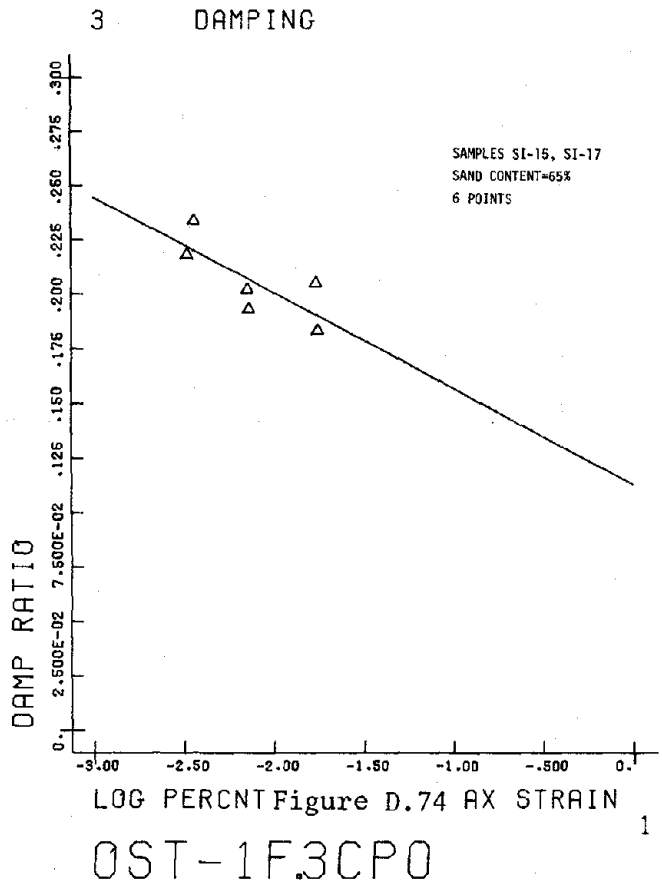

Figure D.74

OST-1F.3CP0

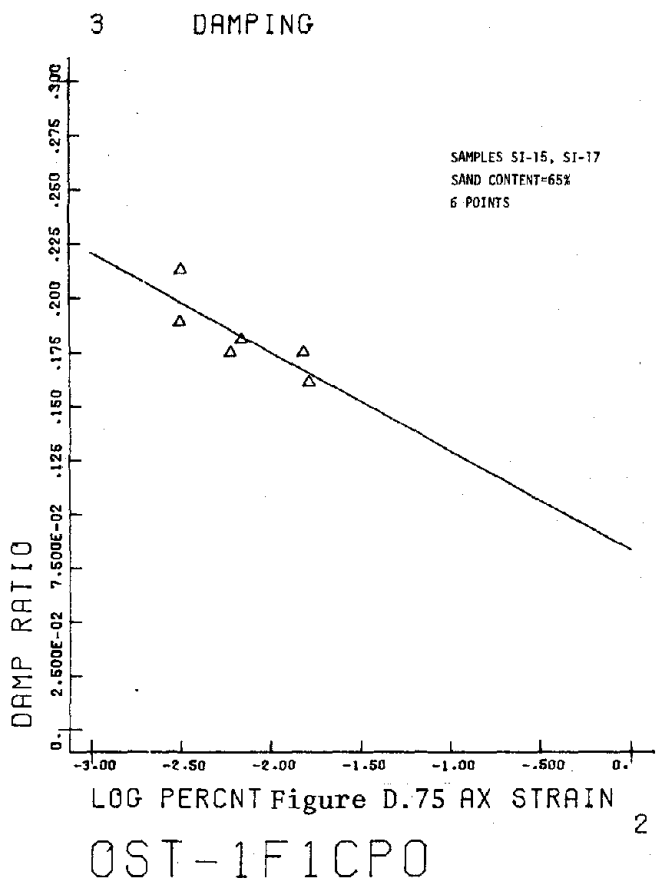

Figure D.75

OST-1F1CP0

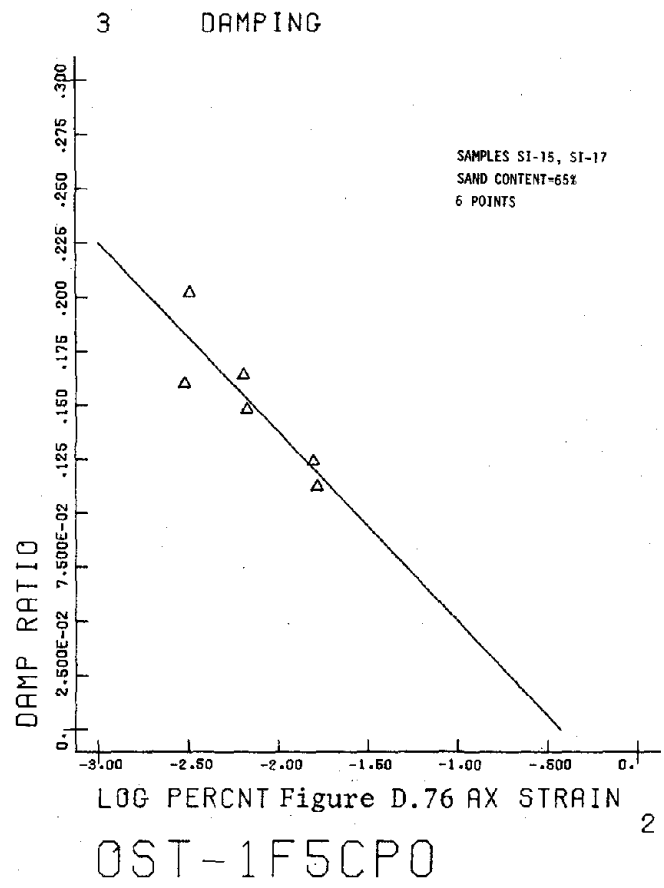

Figure D.76

OST-1F5CP0

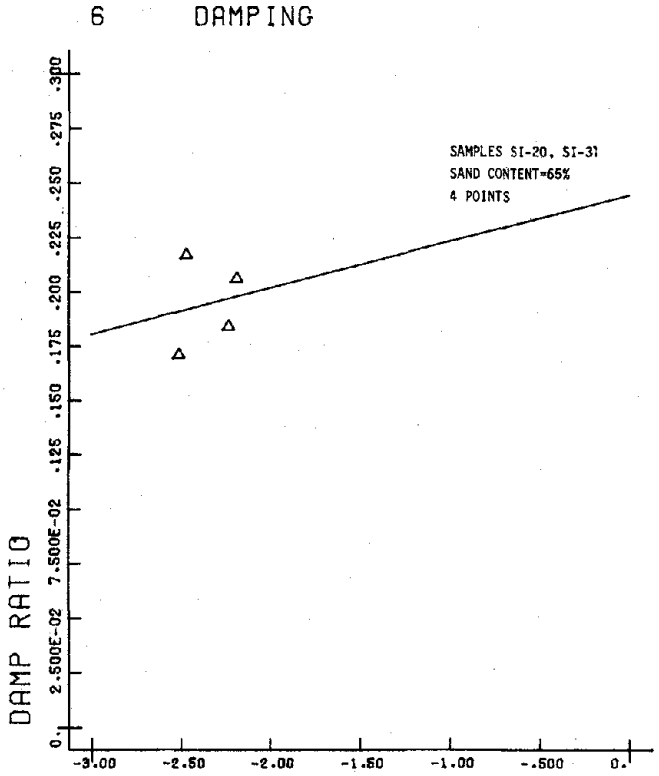

Figure D.77

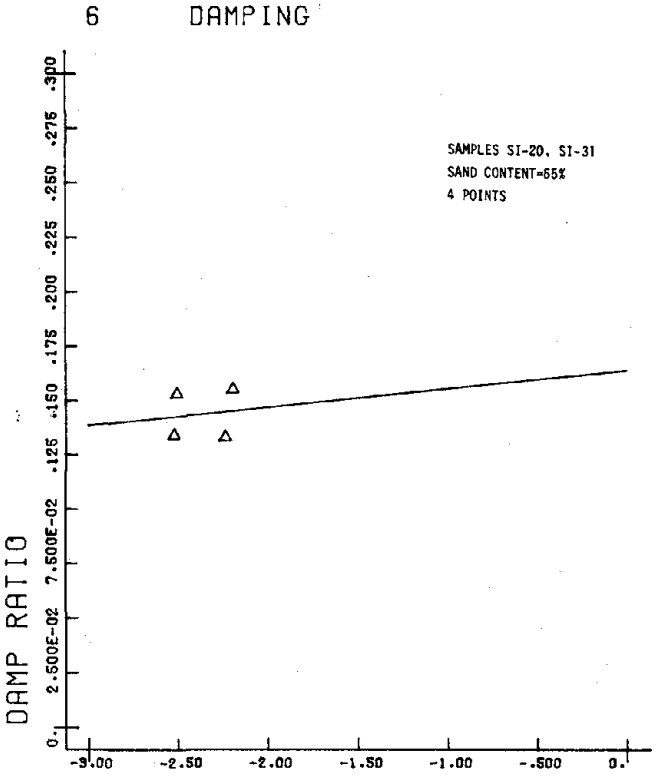

Figure D.78

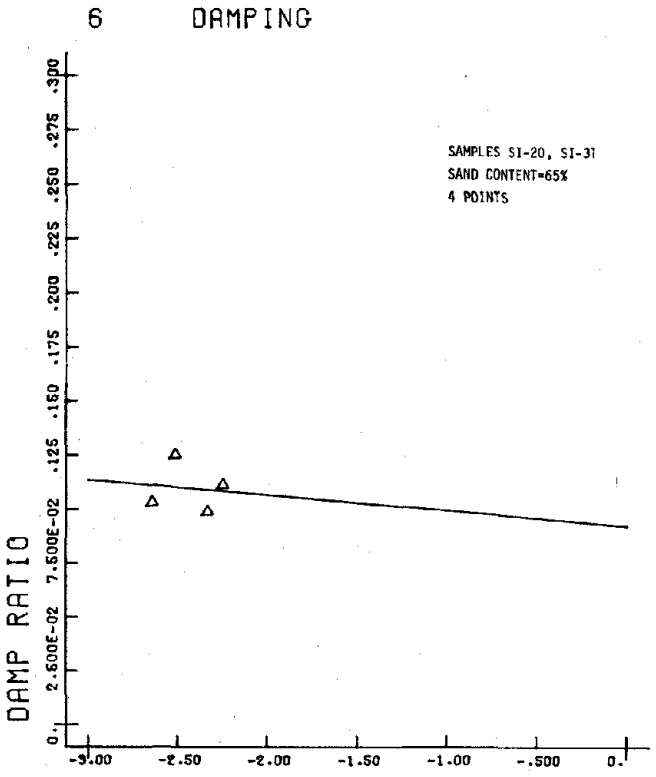

Figure D.79

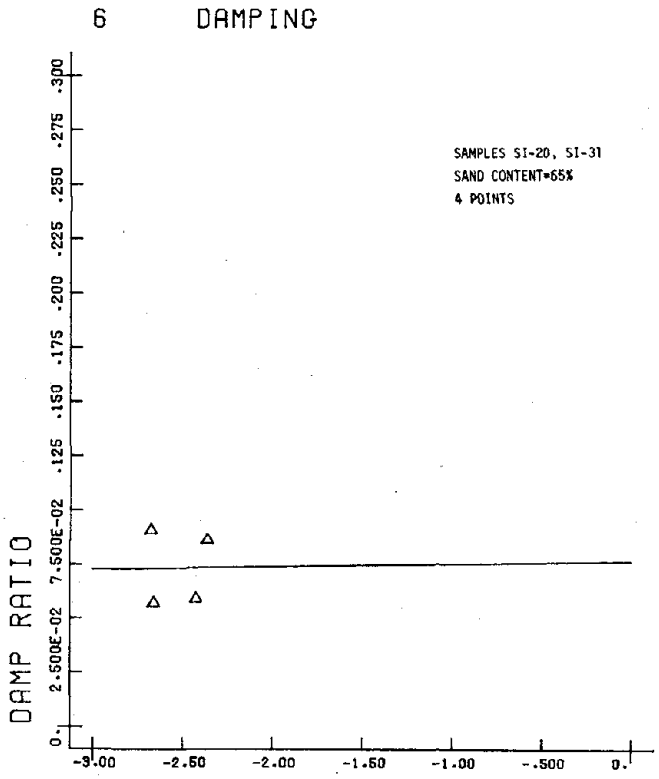

Figure D.80

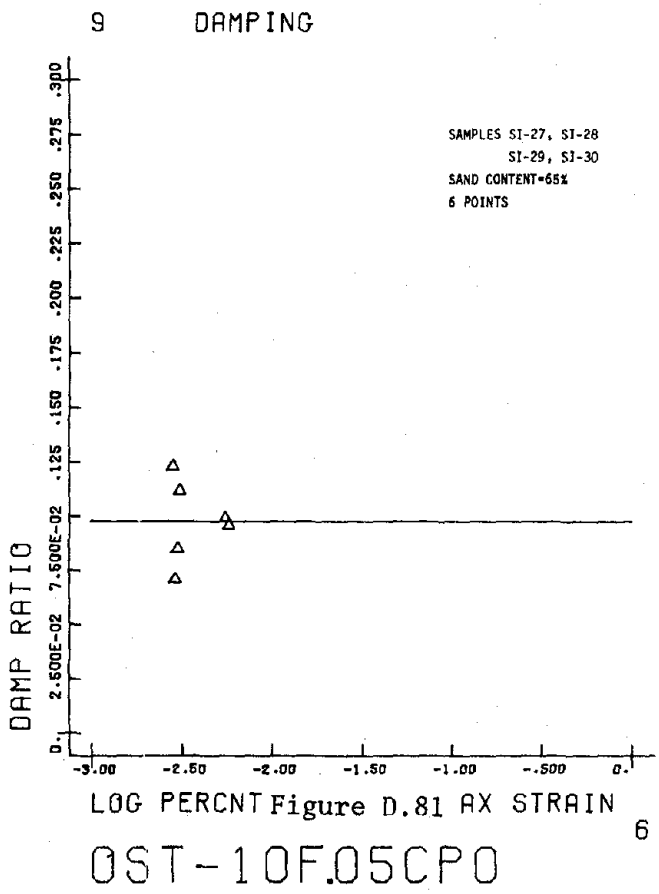

Figure D.81

OST-10F.05CPO

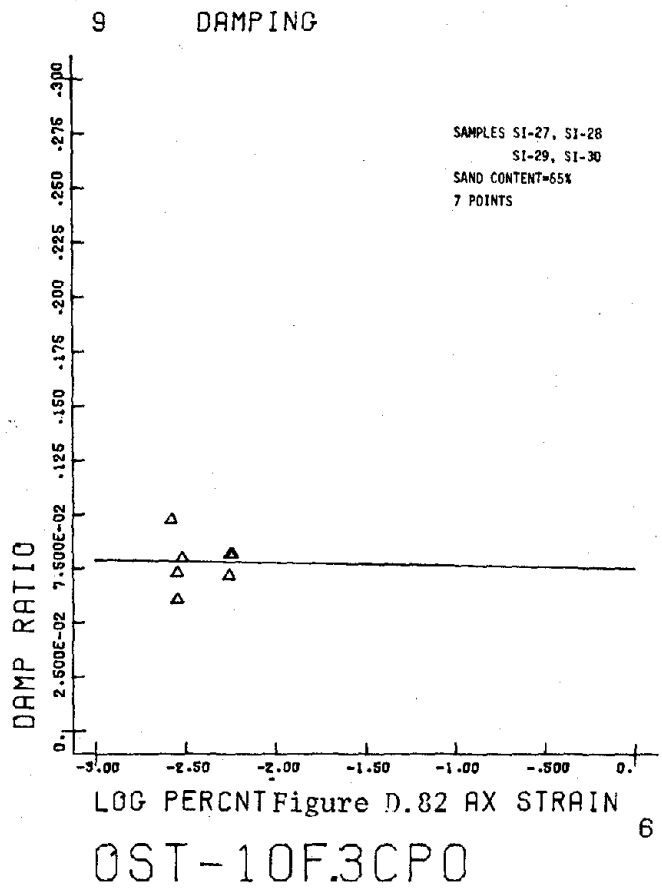

Figure D.82

OST-10F.3CPO

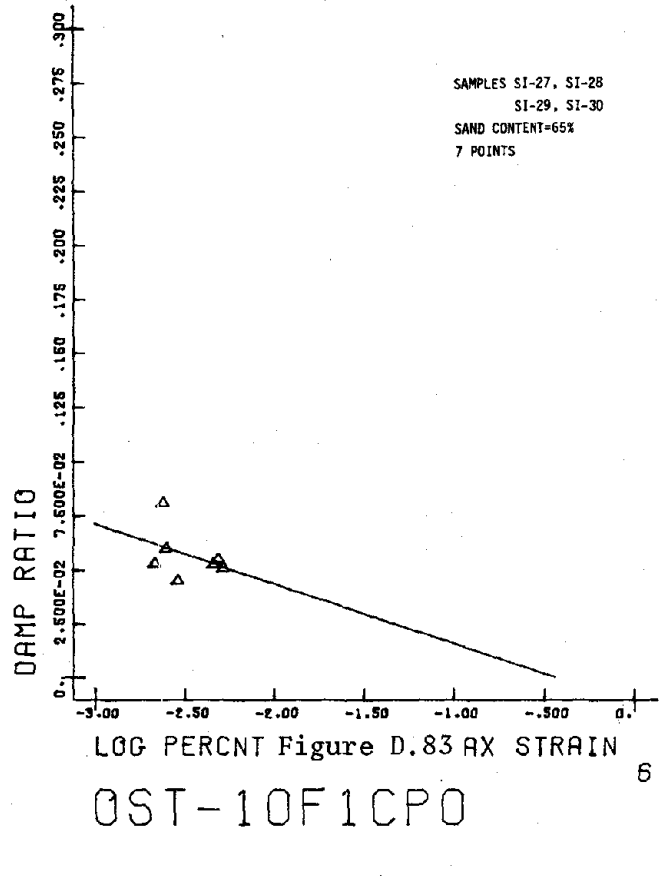

Figure D.83

OST-10F1CPO

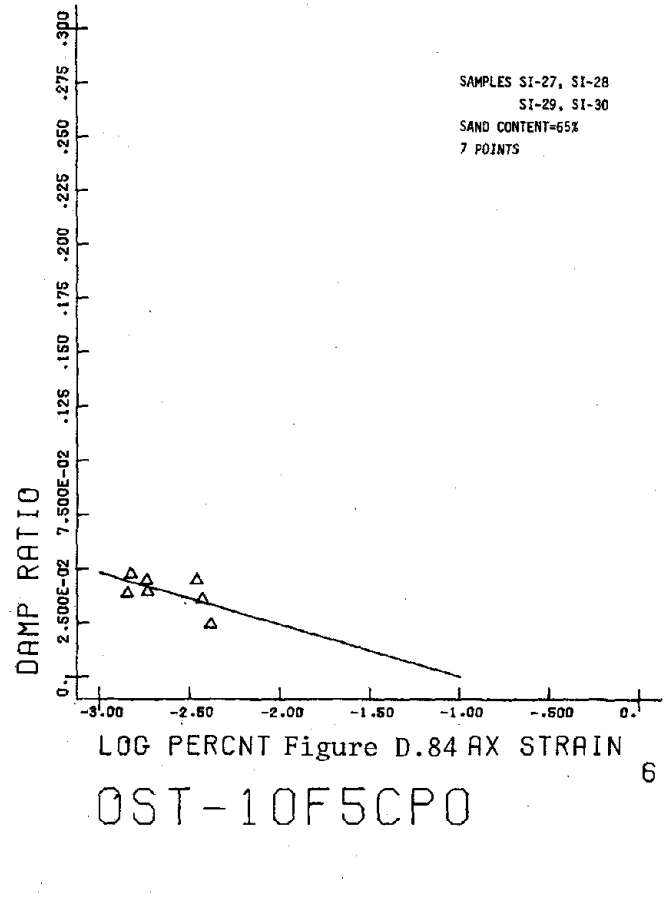

Figure D.84

OST-10F5CPO

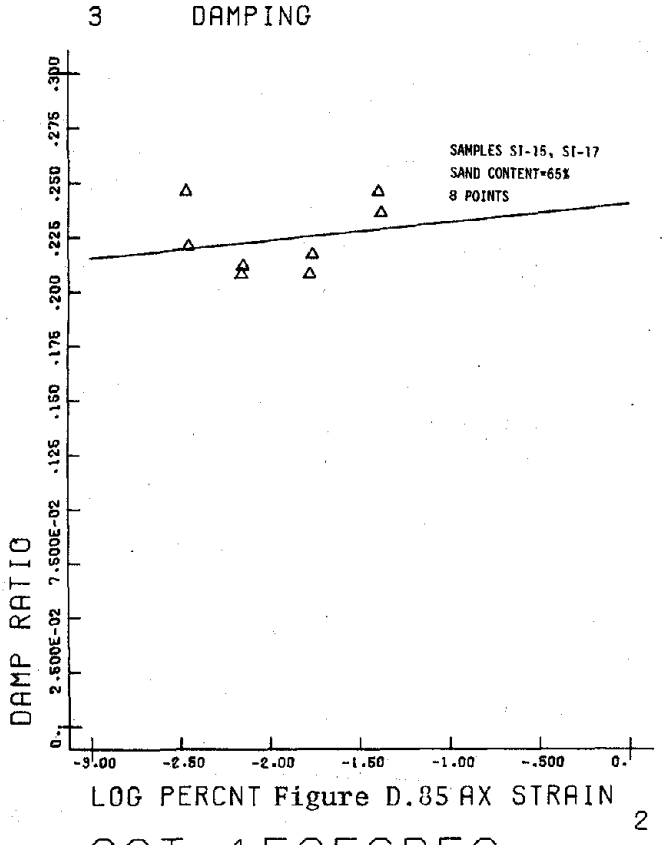

Figure D.85

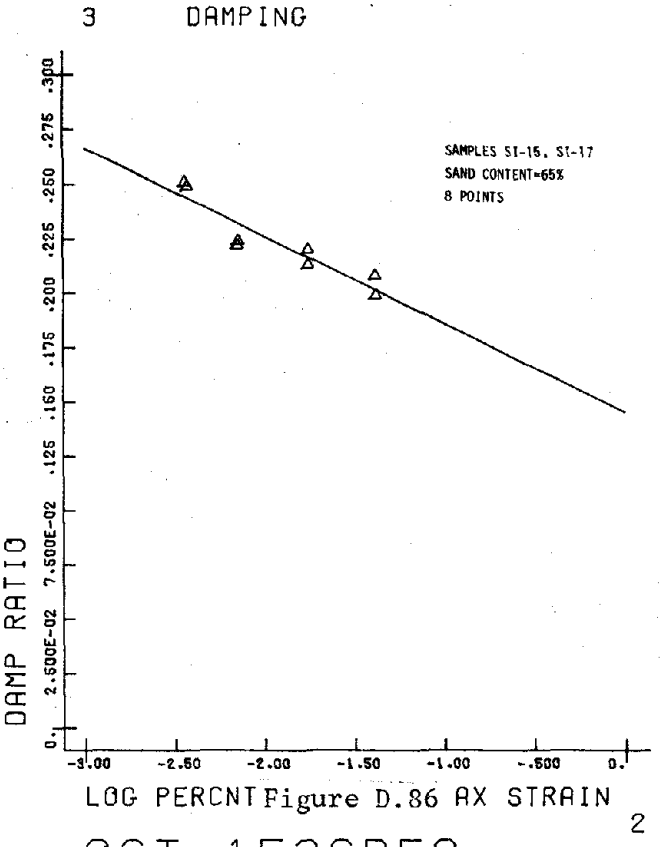

Figure D.86

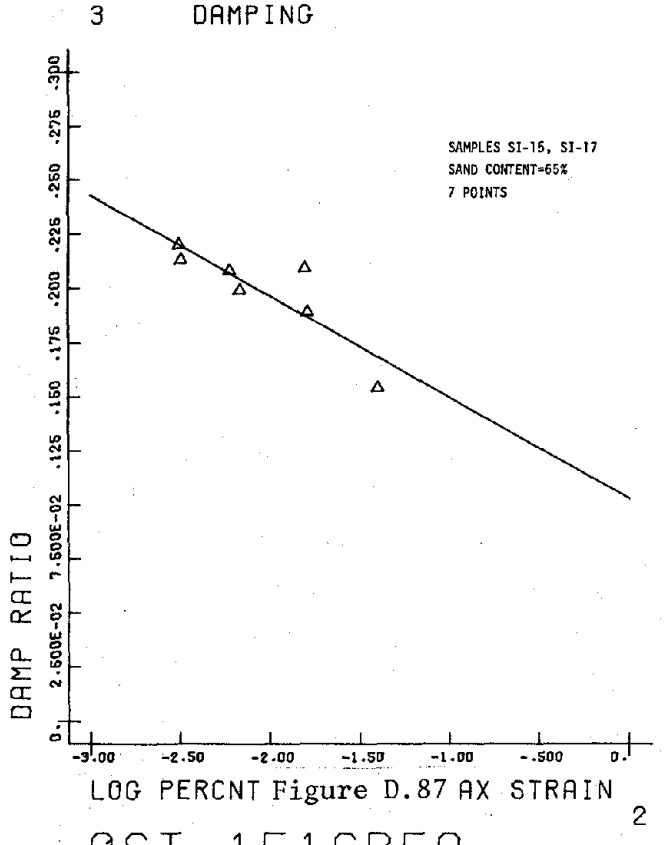

Figure D.87

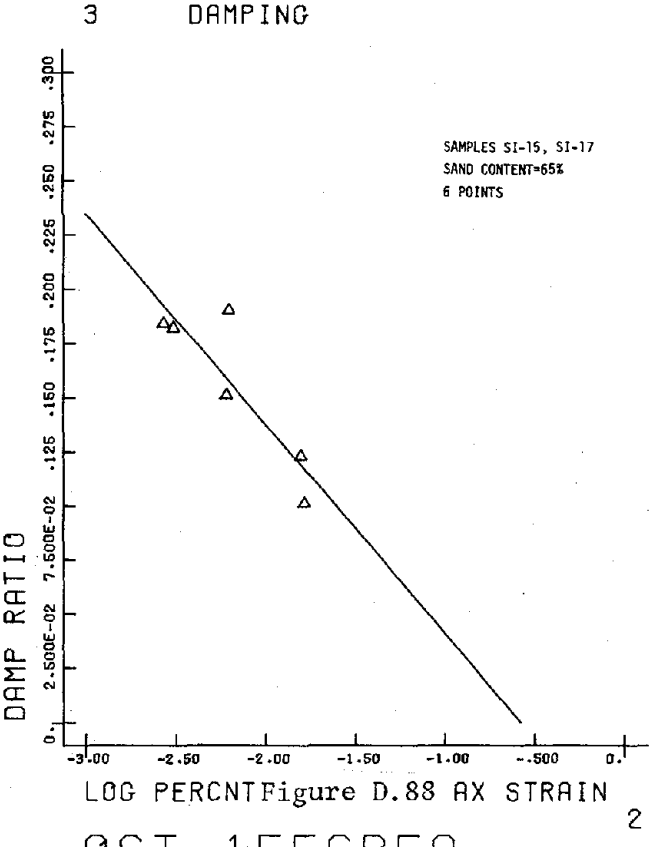

Figure D.88

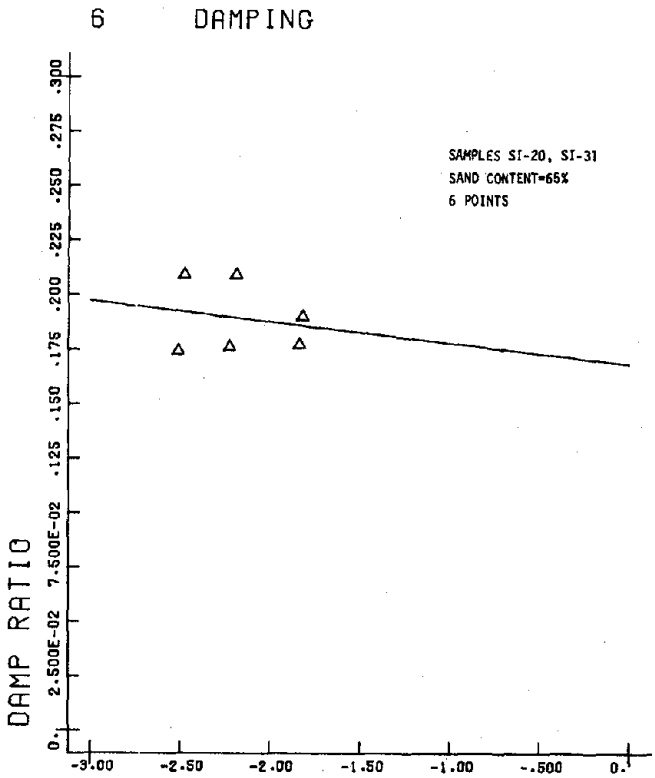

Figure D.89 AX STRAIN

OST-4F.05CP50

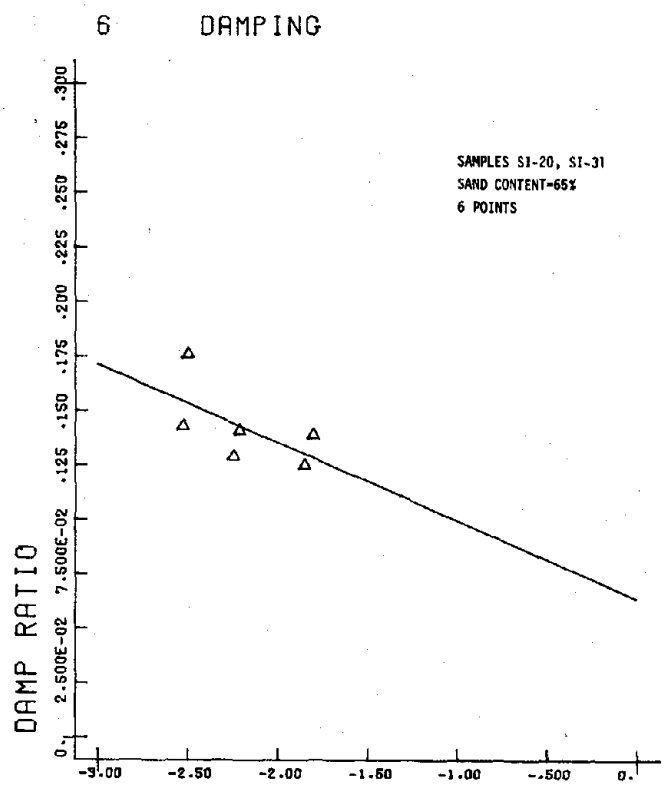

Figure D.90 AX STRAIN

OST-4F.3CP50

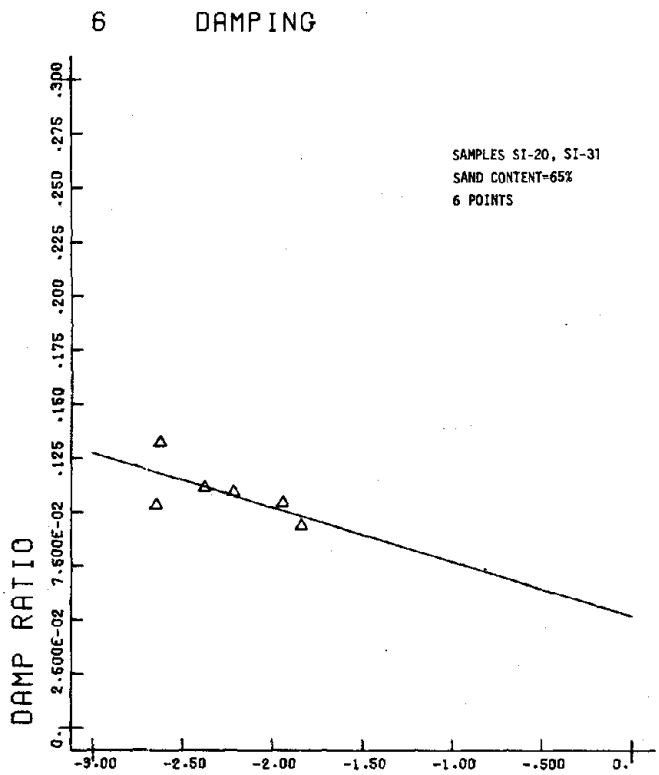

Figure D.91 AX STRAIN

OST-4F1CP50

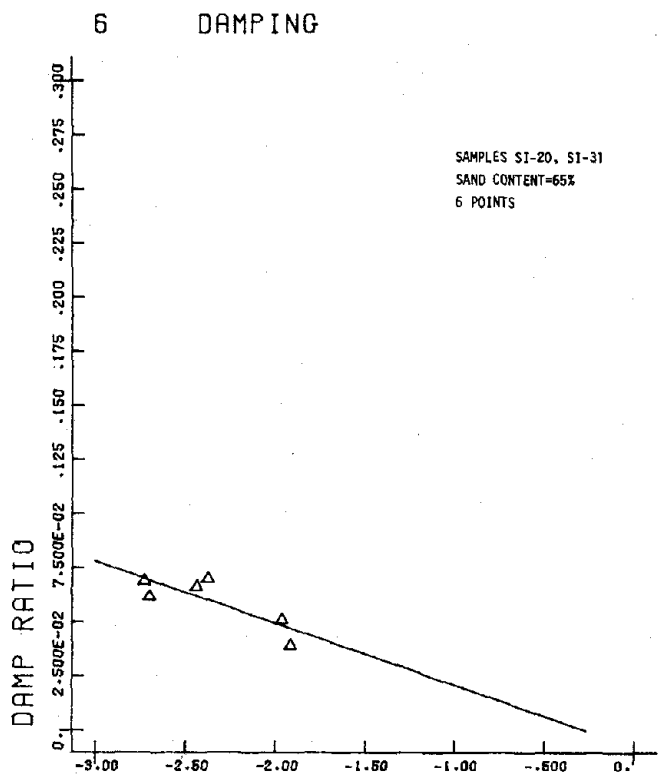

Figure D.92 AX STRAIN

OST-4F5CP50

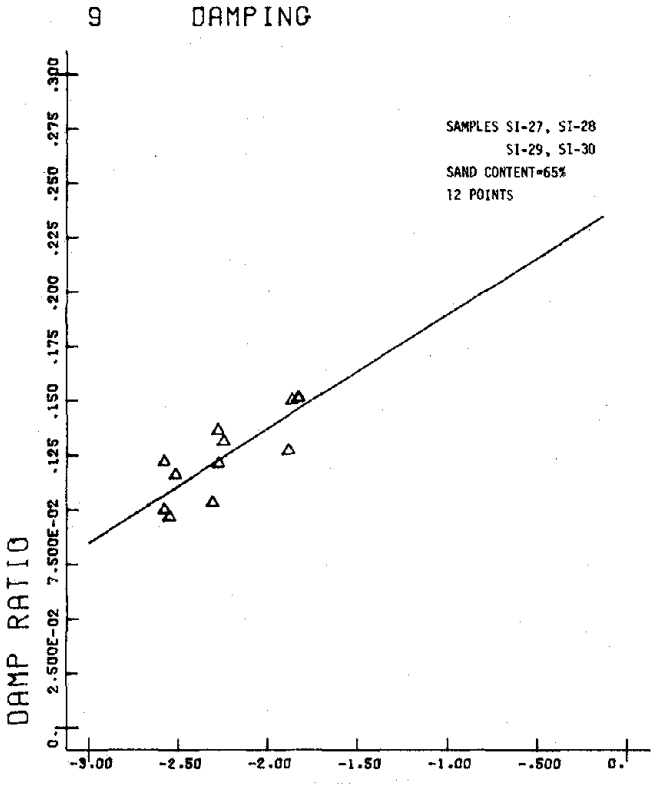

Figure D.93

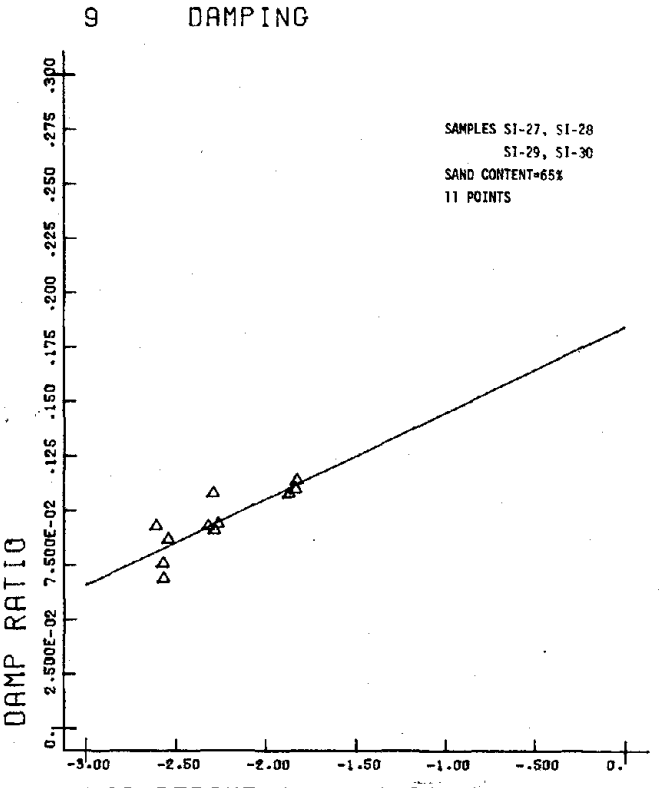

Figure D.94

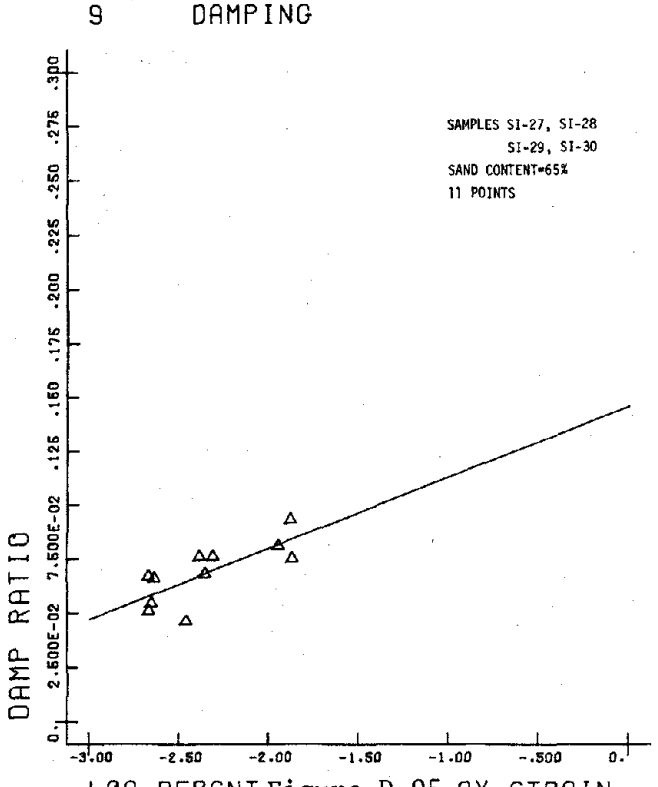

Figure D.95

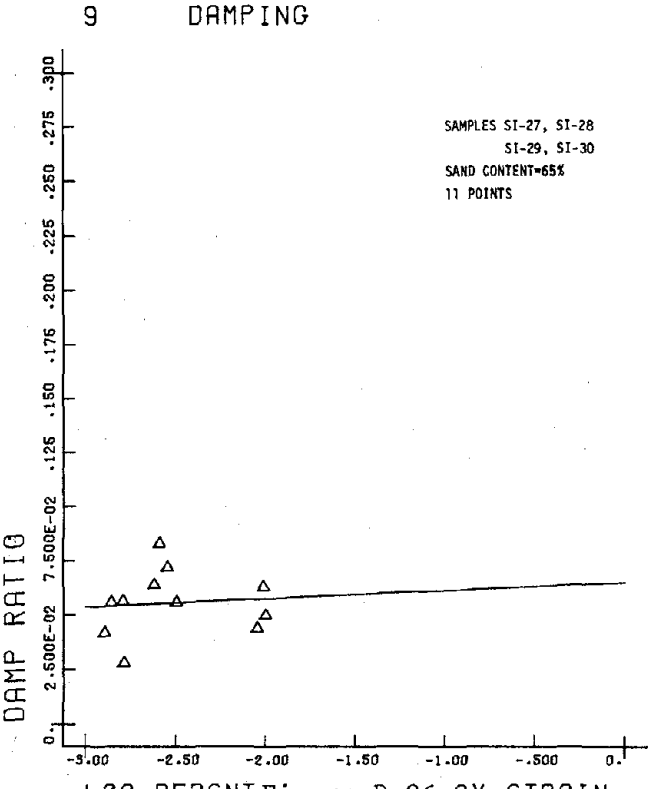

Figure D.96

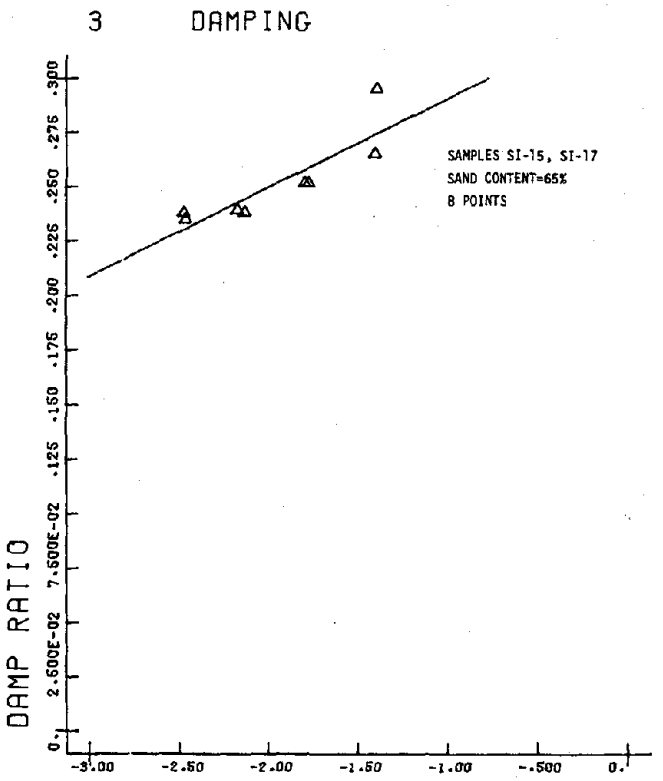
3 DAMPING
SAMPLES SI-15, SI-17
SAND CONTENT=65%
8 POINTS
DAMP RATIO
0.
2.600E-02
7.600E-02
.125
.150
.175
.200
.225
.250
.275
.300
-3.00
-2.50
-2.00
-1.50
-1.00
-.500
0.
LOG PERCNT Figure D.97 AX STRAIN 2
OST-1F.05CP200

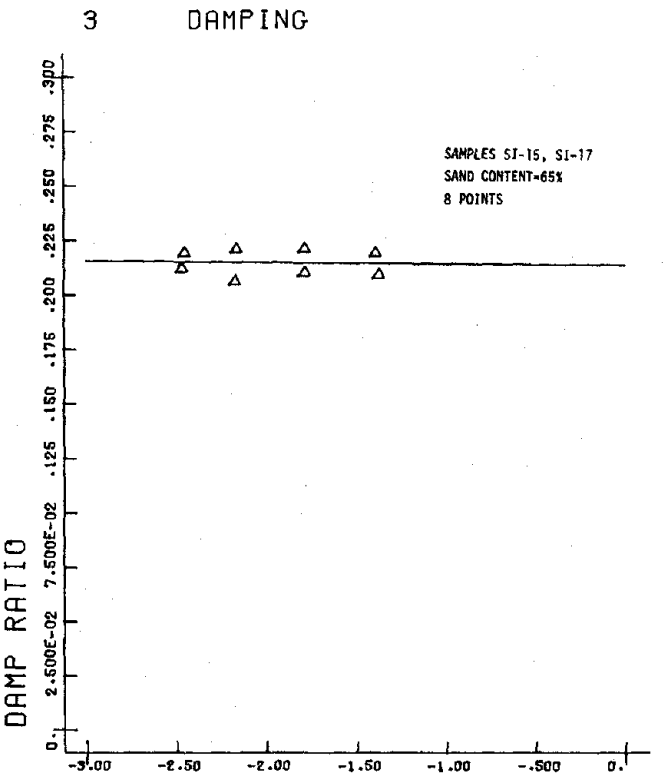
3 DAMPING
SAMPLES SI-15, SI-17
SAND CONTENT=65%
8 POINTS
DAMP RATIO
0.
2.600E-02
7.600E-02
.125
.150
.175
.200
.225
.250
.275
.300
-3.00
-2.50
-2.00
-1.50
-1.00
-.500
0.
LOG PERCNT Figure D.98 AX STRAIN 2
OST-1F.3CP200

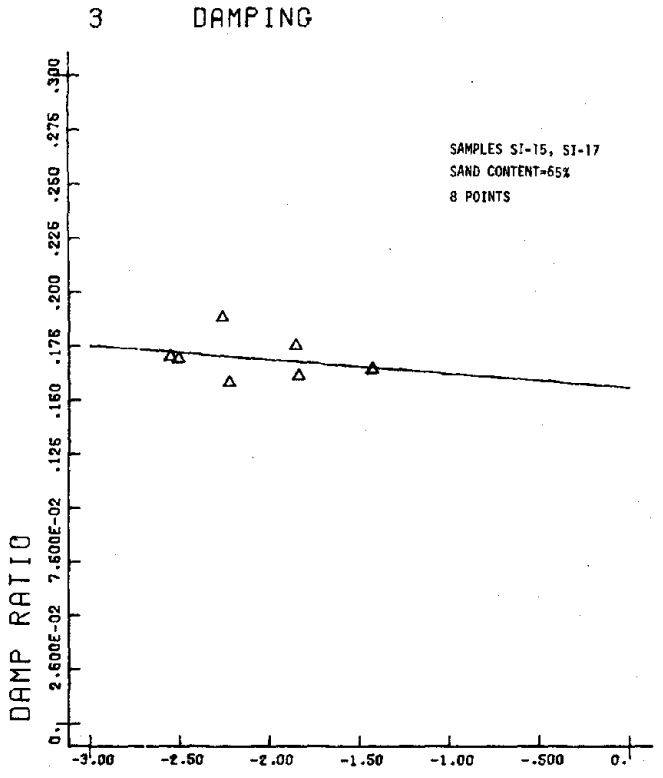
3 DAMPING
SAMPLES SI-15, SI-17
SAND CONTENT=65%
8 POINTS
DAMP RATIO
0.
2.600E-02
7.600E-02
.125
.150
.175
.200
.225
.250
.275
.300
-3.00
-2.50
-2.00
-1.50
-1.00
-.500
0.
LOG PERCNT Figure D.99 AX STRAIN 2
OST-1F1CP200

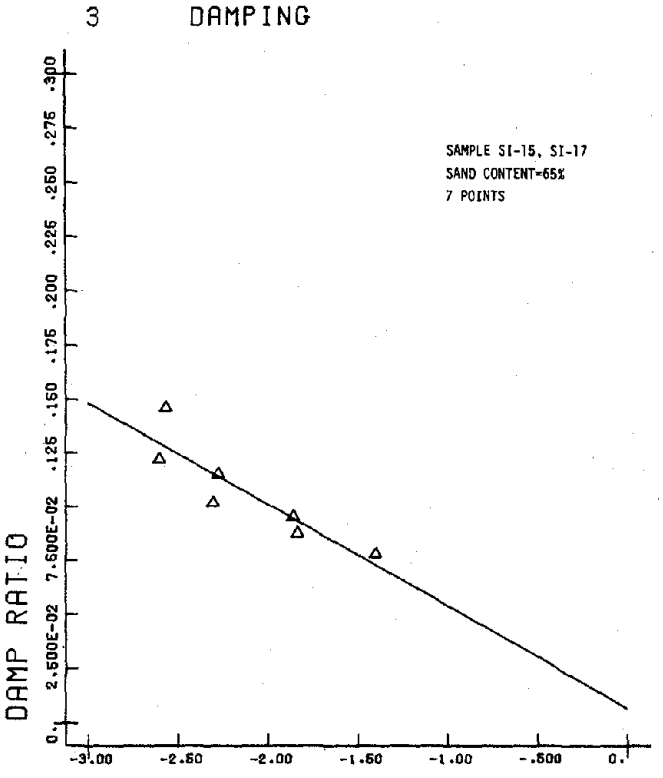
3 DAMPING
SAMPLE SI-15, SI-17
SAND CONTENT=65%
7 POINTS
DAMP RATIO
0.
2.600E-02
7.600E-02
.125
.150
.175
.200
.225
.250
.275
.300
-3.00
-2.50
-2.00
-1.50
-1.00
-.500
0.
LOG PERCNTFigure D.100AX STRAIN 1
OST-1F5CP200

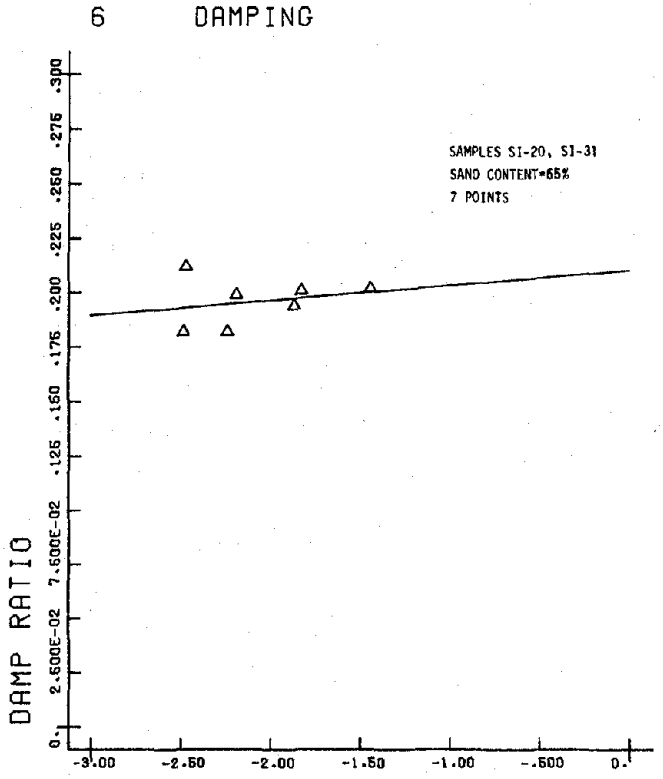

Figure D.101AX 1

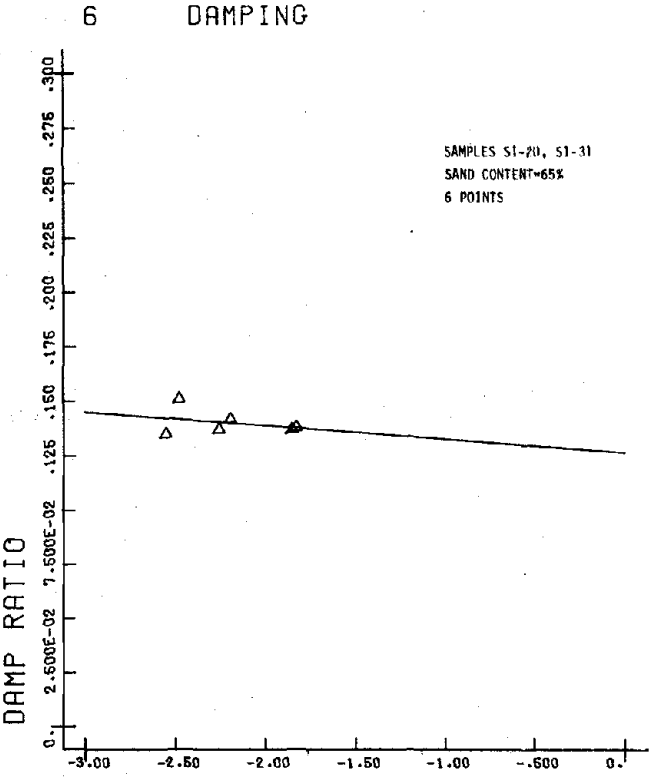

Figure D.102AX 1

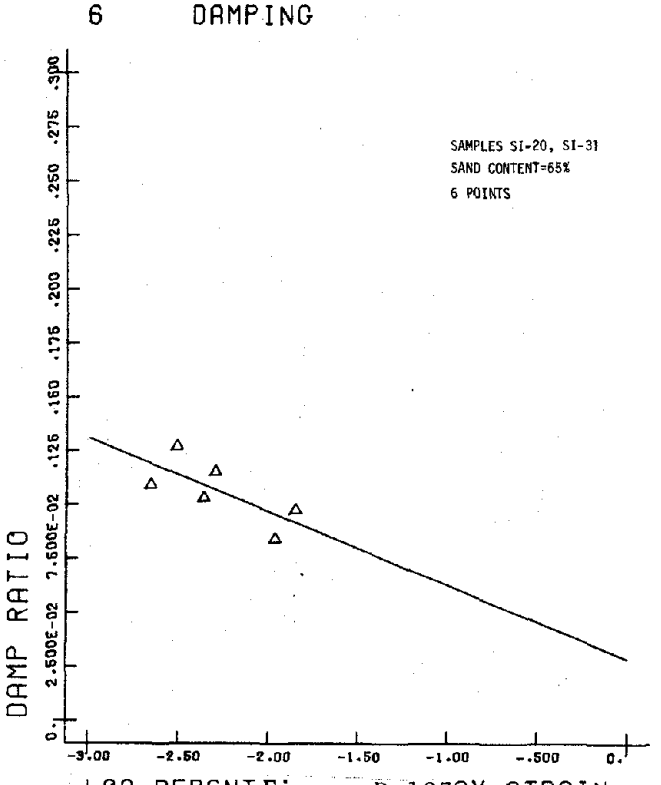

Figure D.103AX 2

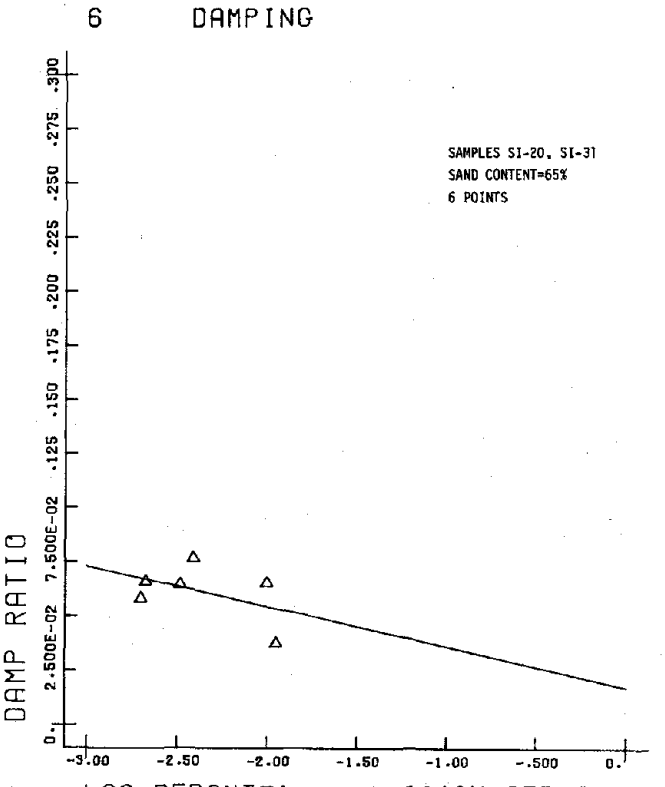

Figure D.104AX 4

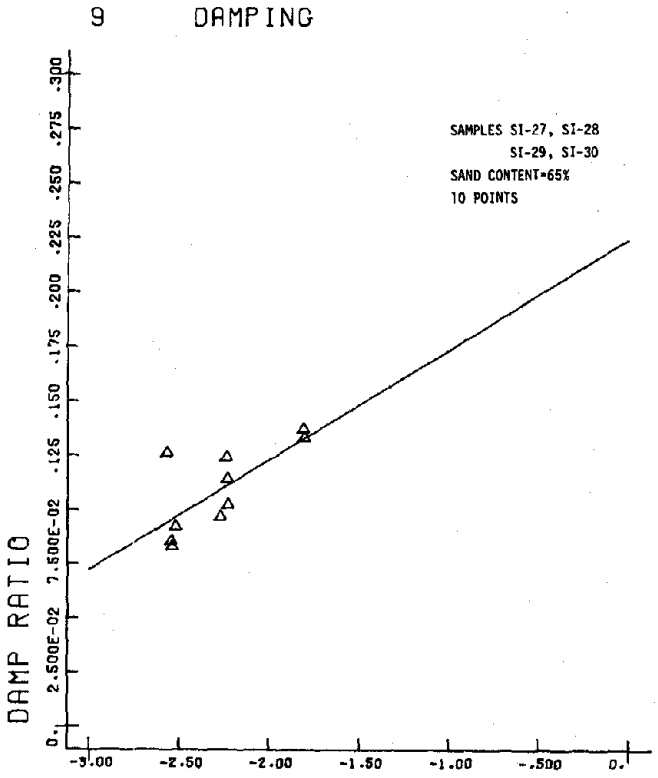

Figure D.105

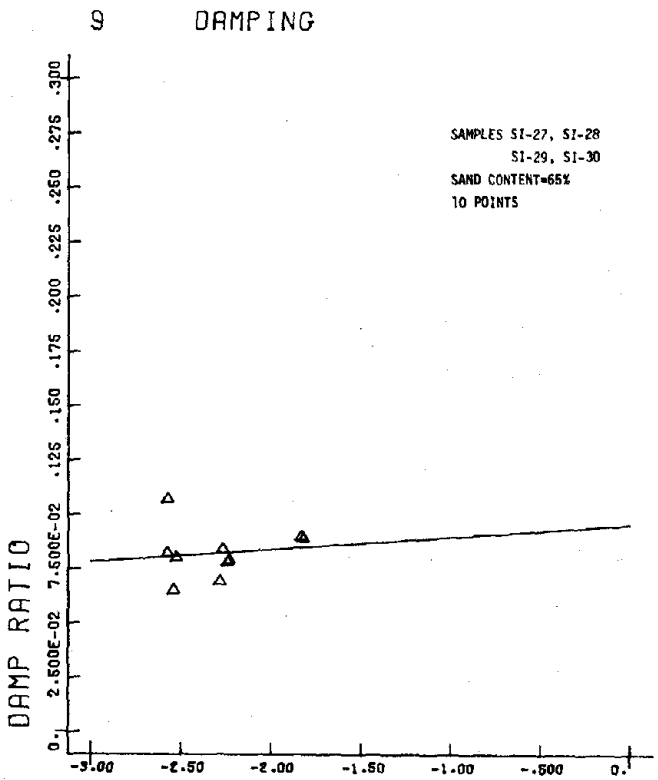

Figure D.106

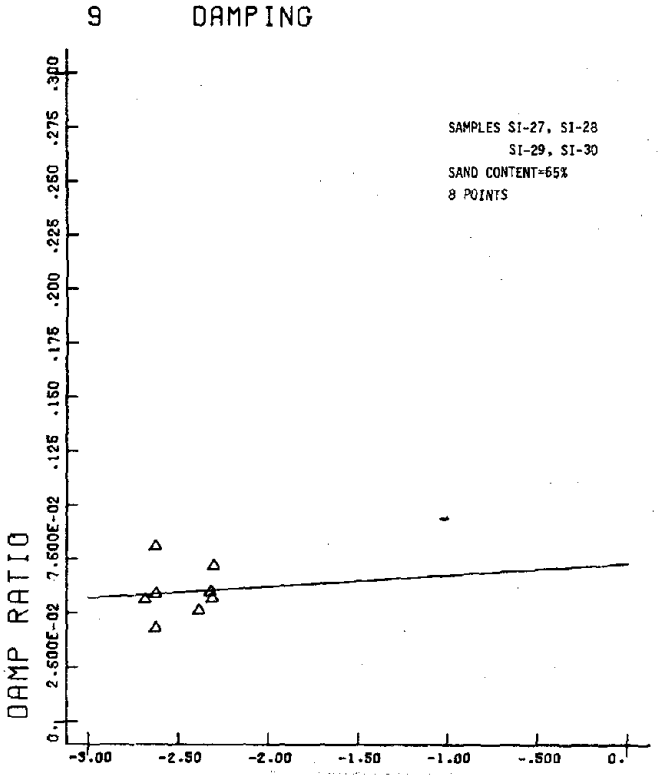

Figure D.107

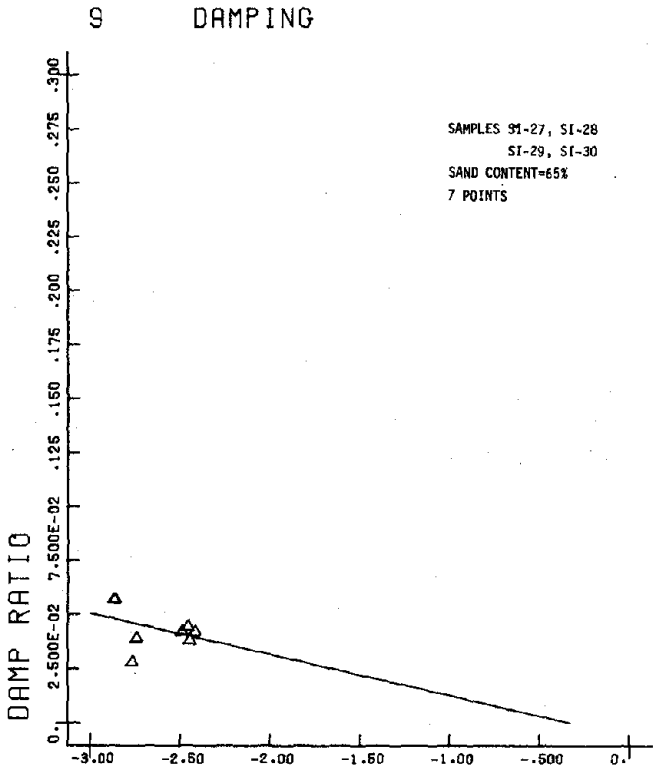

Figure D.108

APPENDIX E

CYCLIC TRIAXIAL TEST RESULTS: DAMPING RATIO OF FROZEN SAND- ALL CONFINING PRESSURES

Test results for Ottawa sand at sand contents of 20%, 45%, and 65% are shown in Figures E.1 to E.2; Figures E.13 to E.24; and Figures E.25 to E.36, respectively.

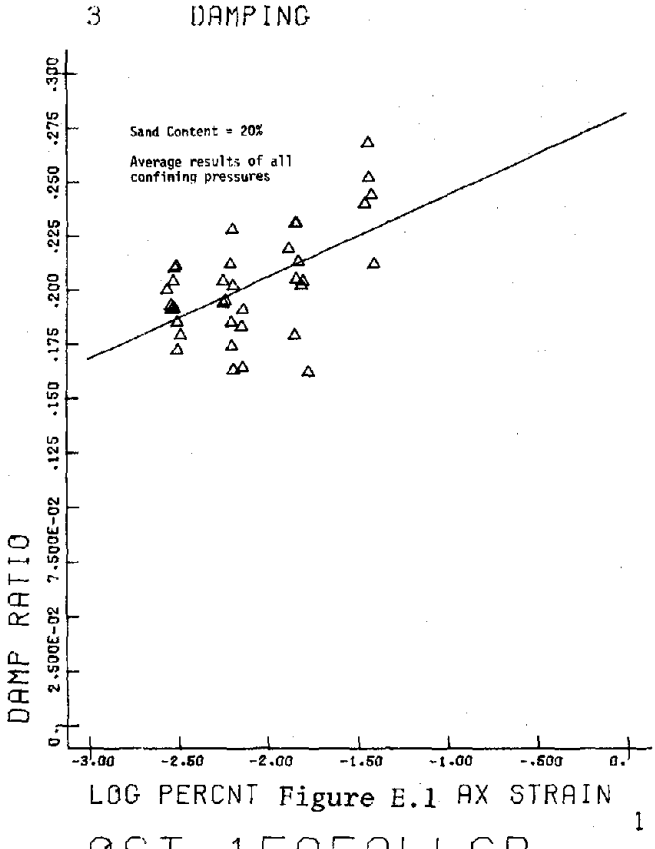

Figure E.1

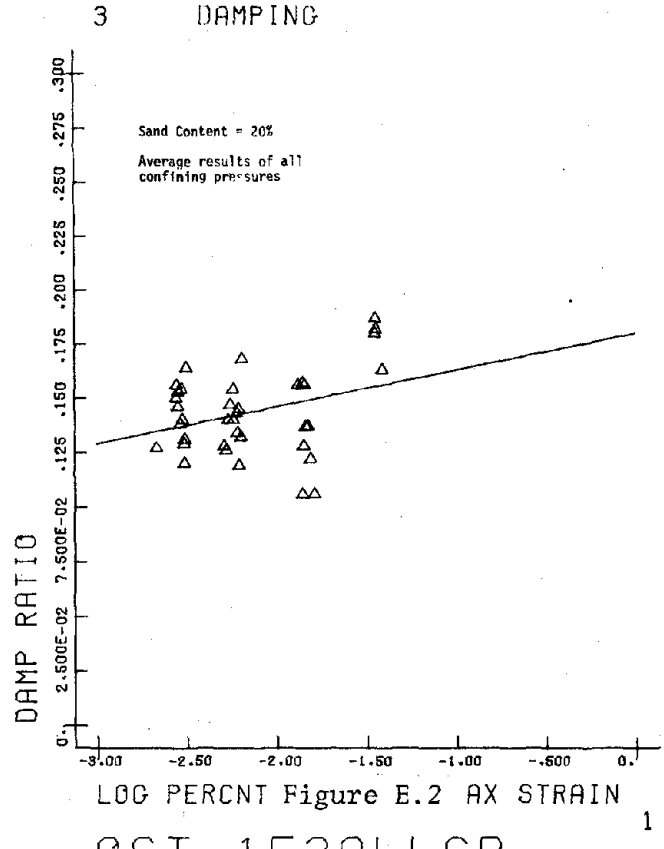

Figure E.2

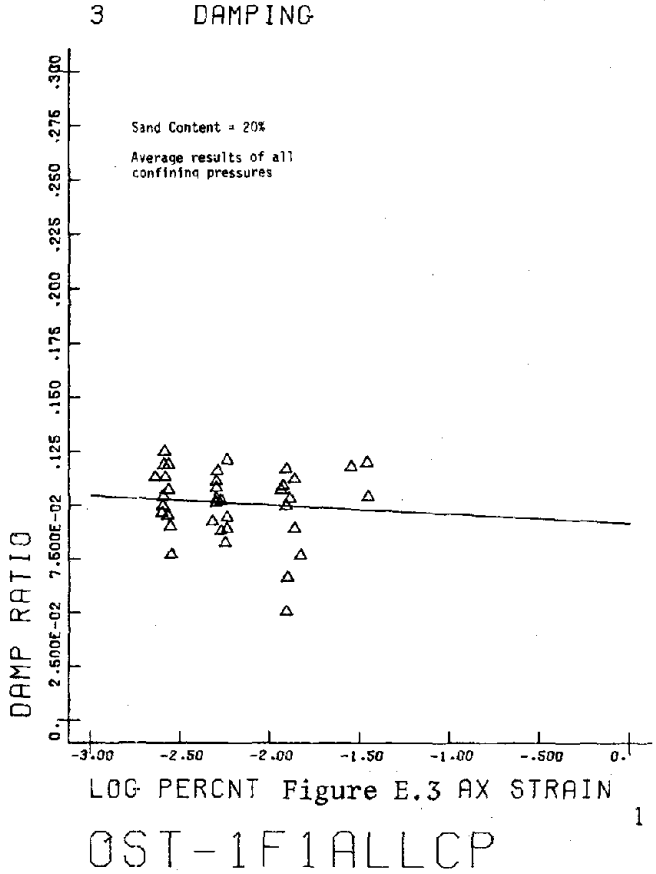

Figure E.3

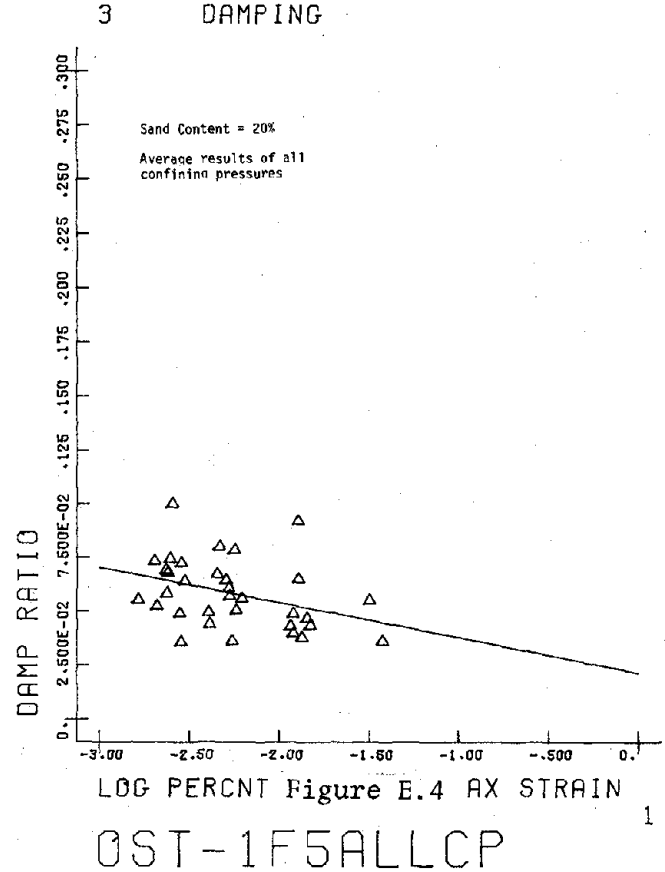

Figure E.4

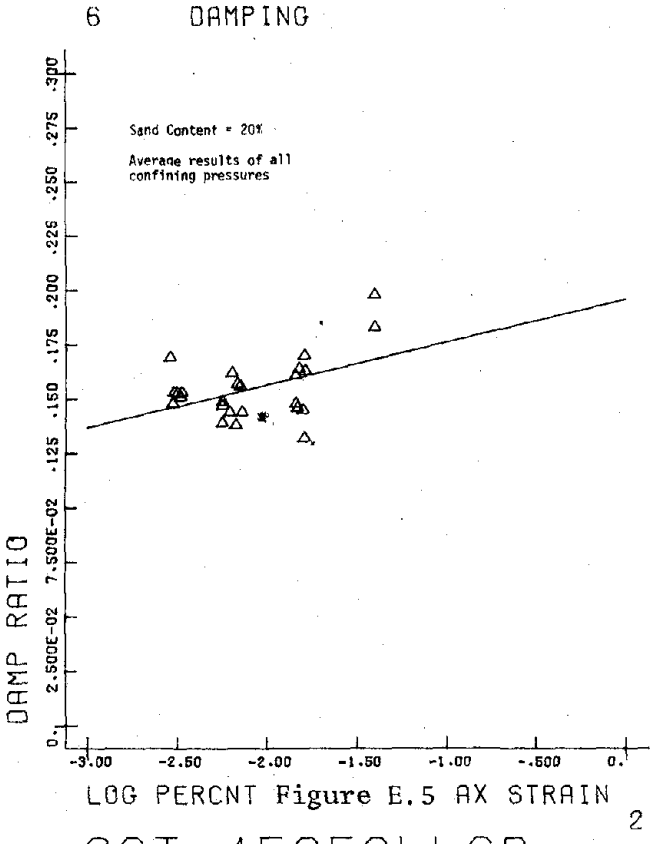

Figure E.5

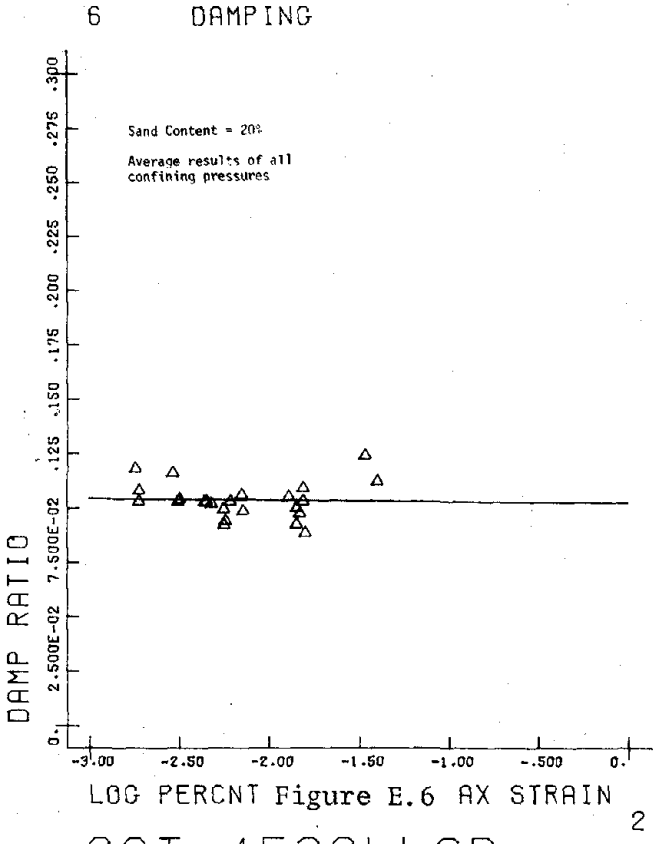

Figure E.6

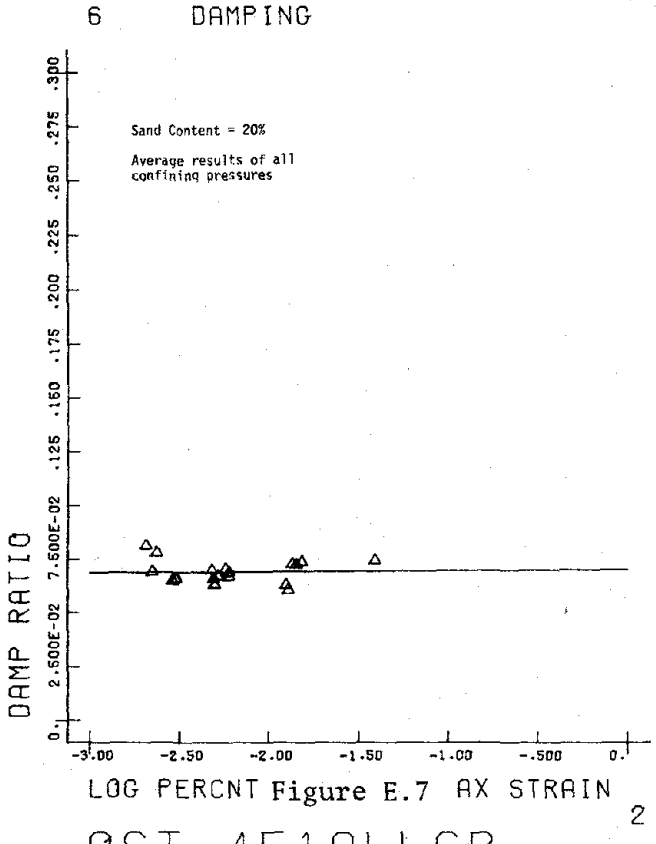

Figure E.7

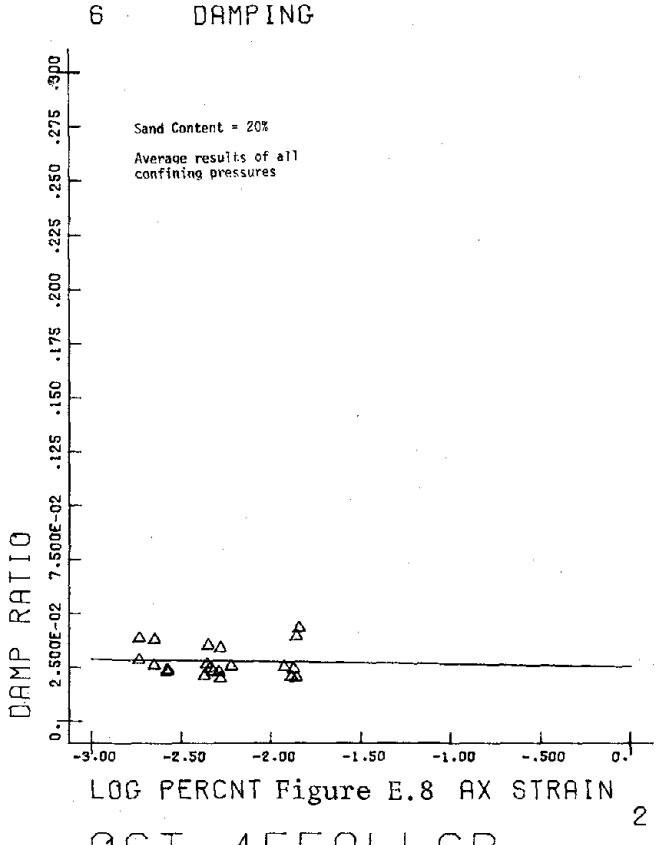

Figure E.8

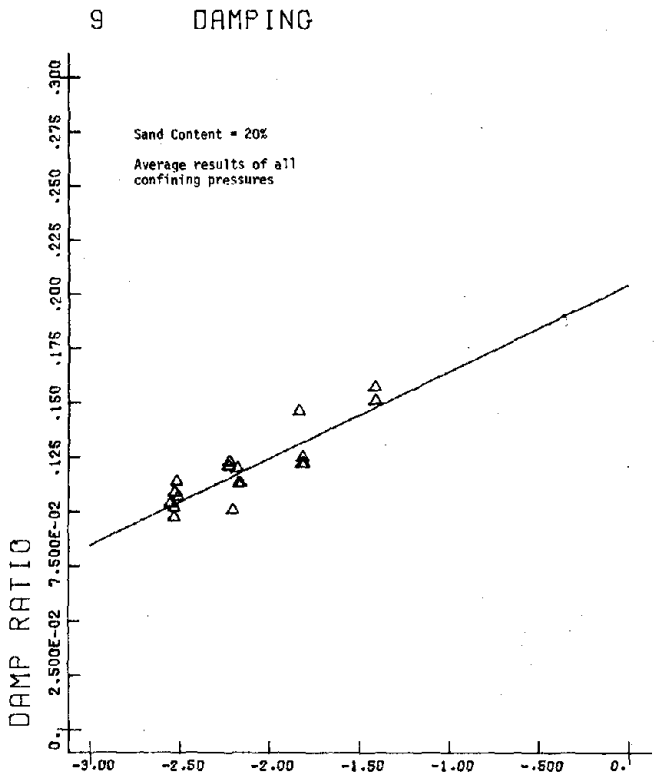

Figure E.9

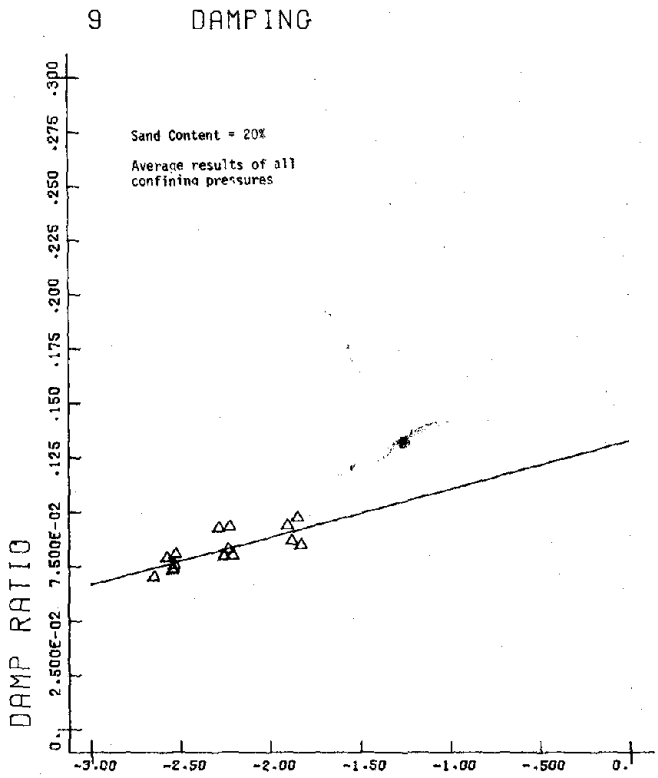

Figure E.10

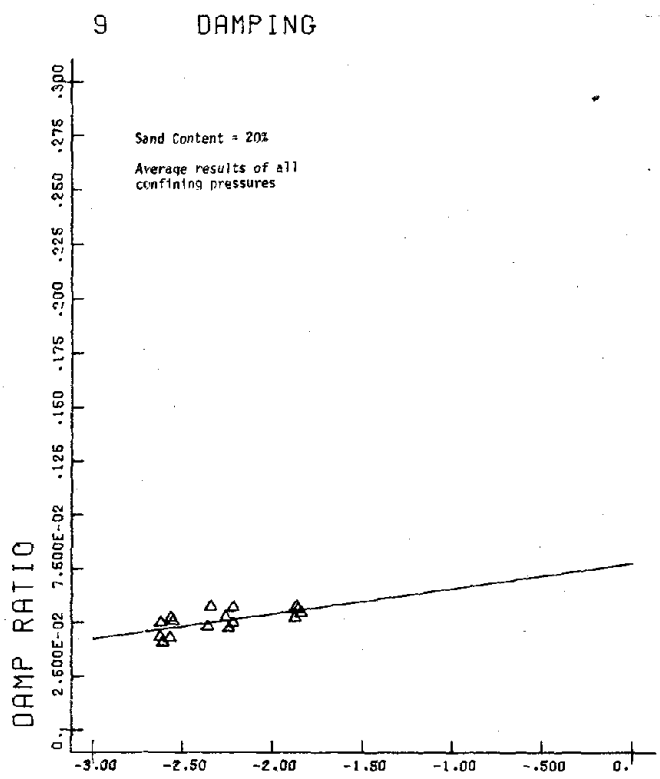

Figure E.11

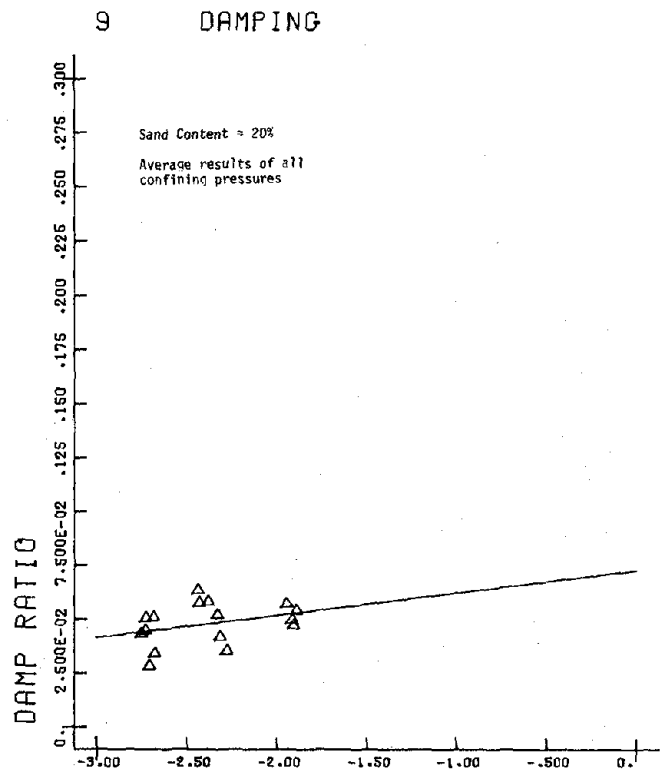

Figure E.12

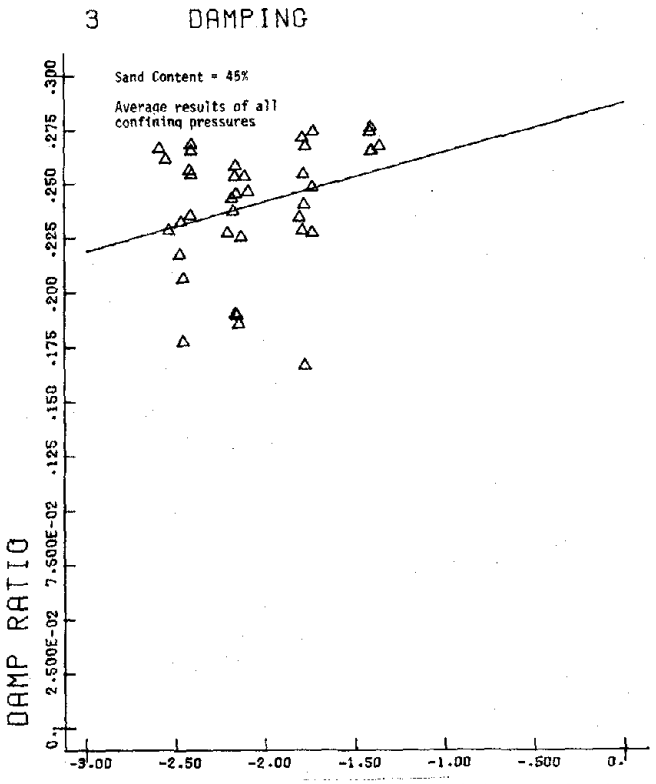

Figure E.13

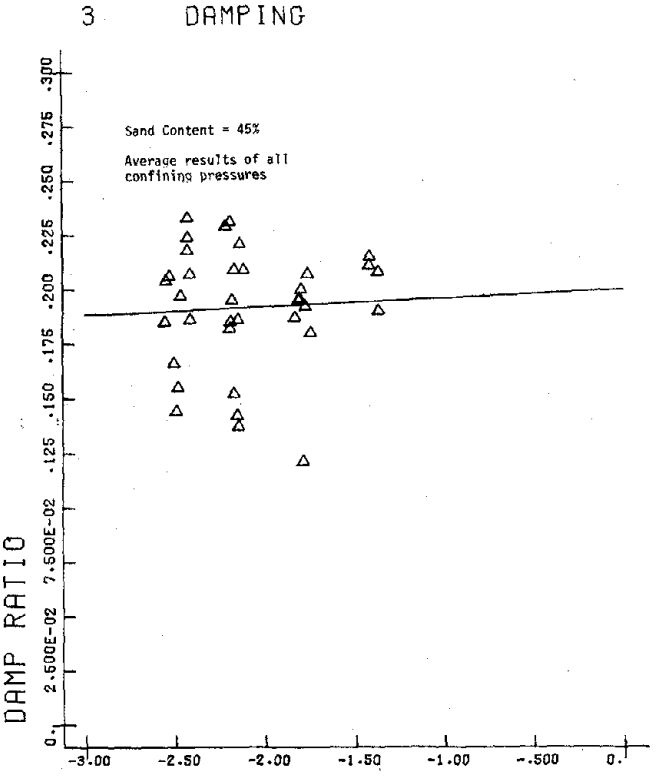

Figure E.14

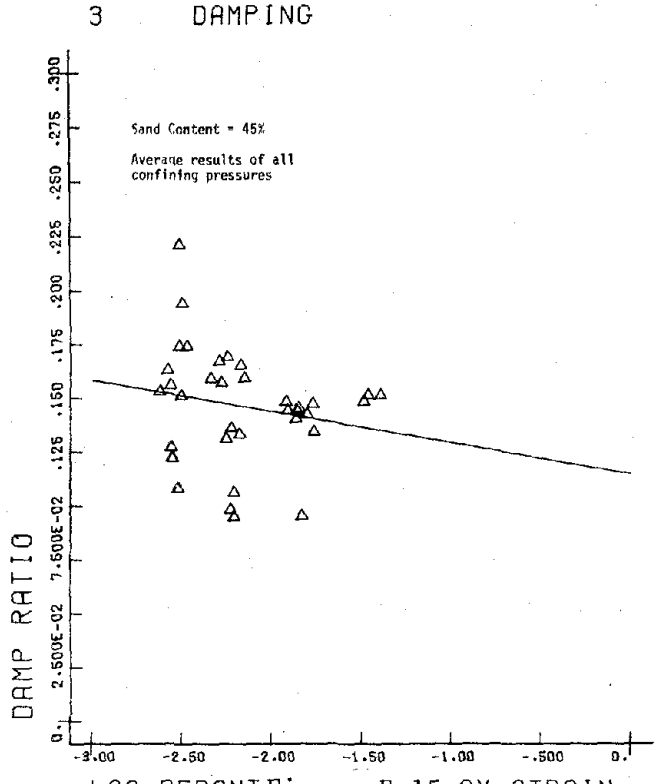

Figure E.15

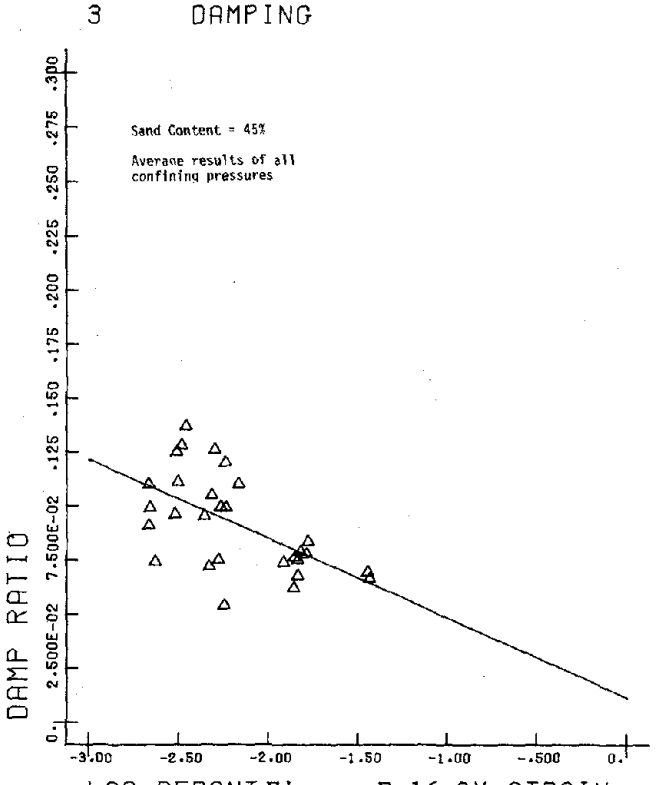

Figure E.16

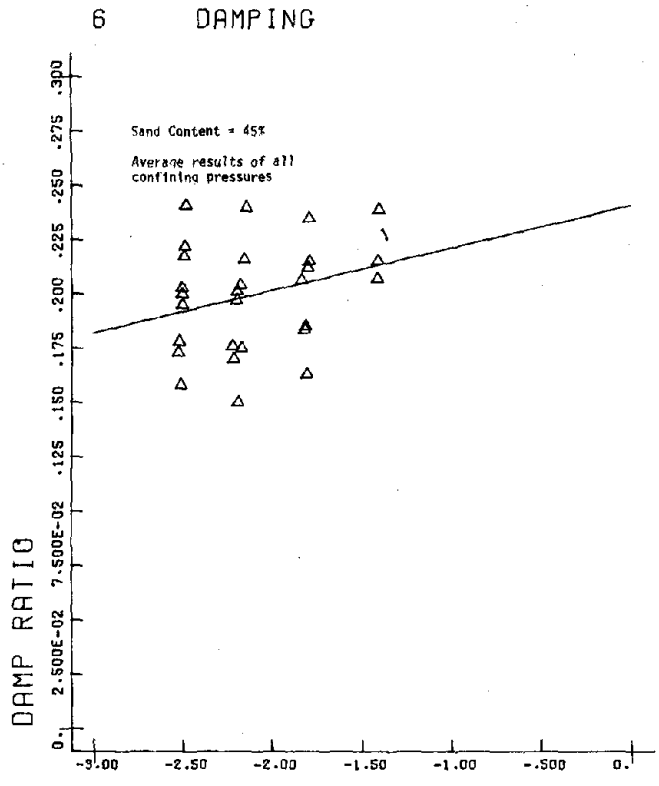

Figure E.17

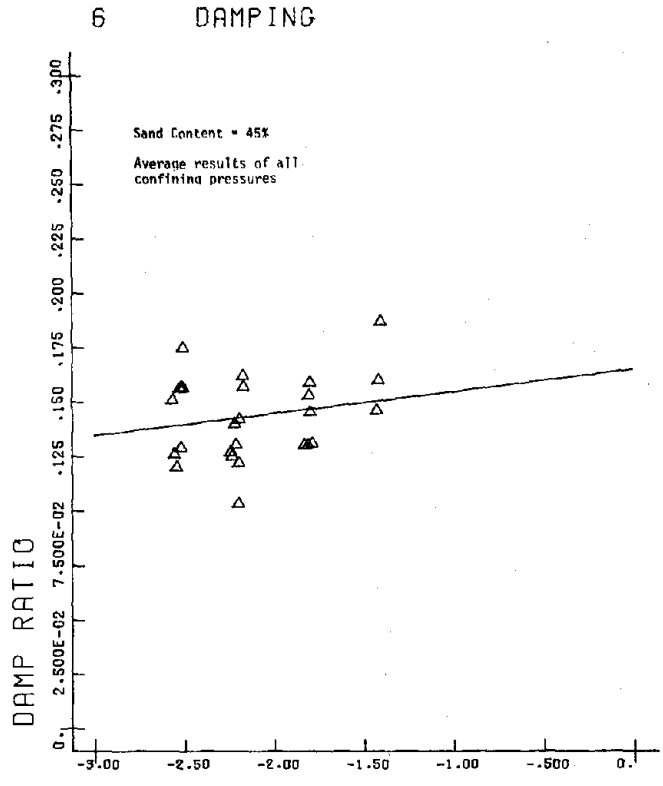

Figure E.18

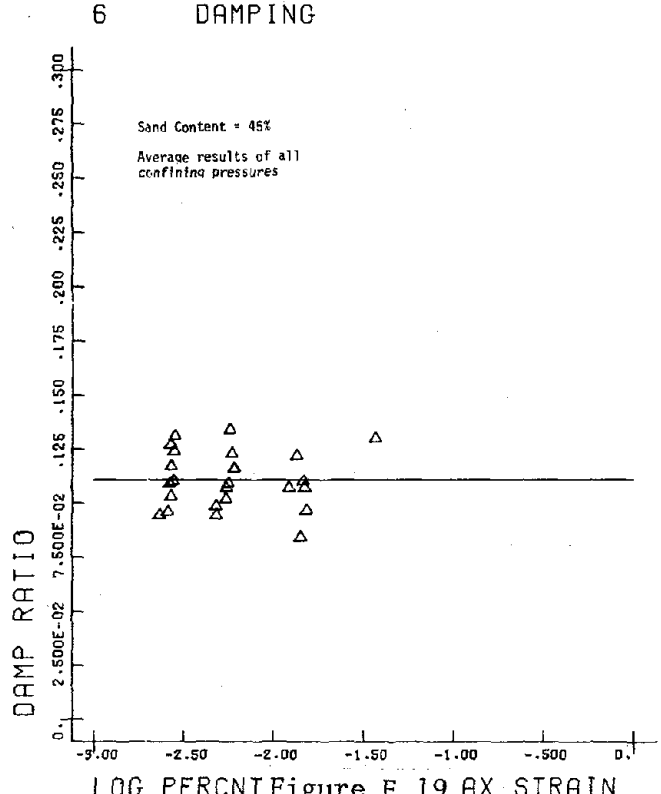

Figure E.19

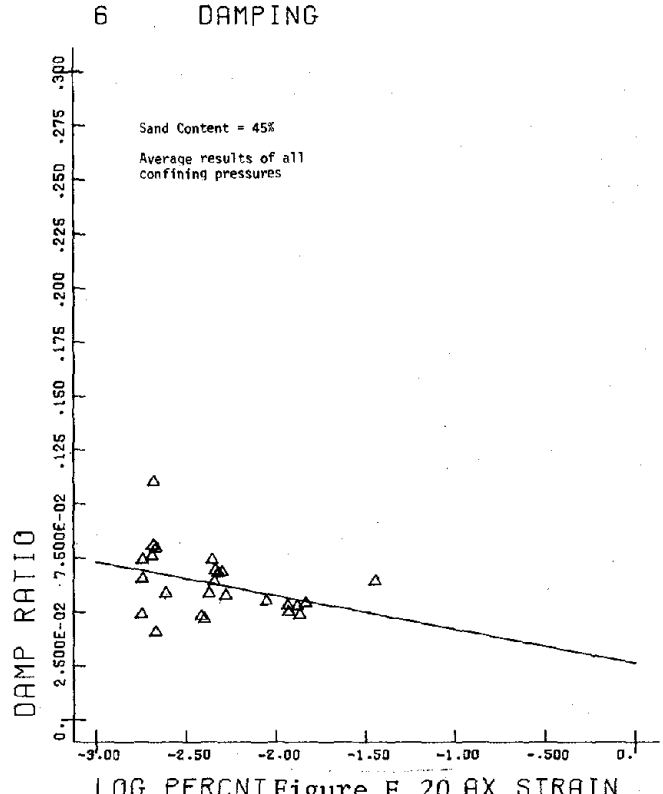

Figure E.20

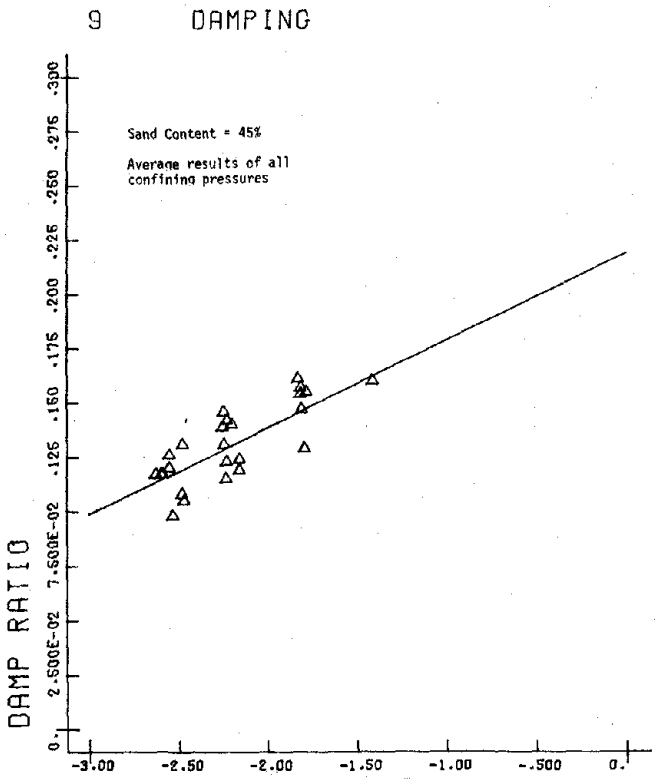

Figure E.21

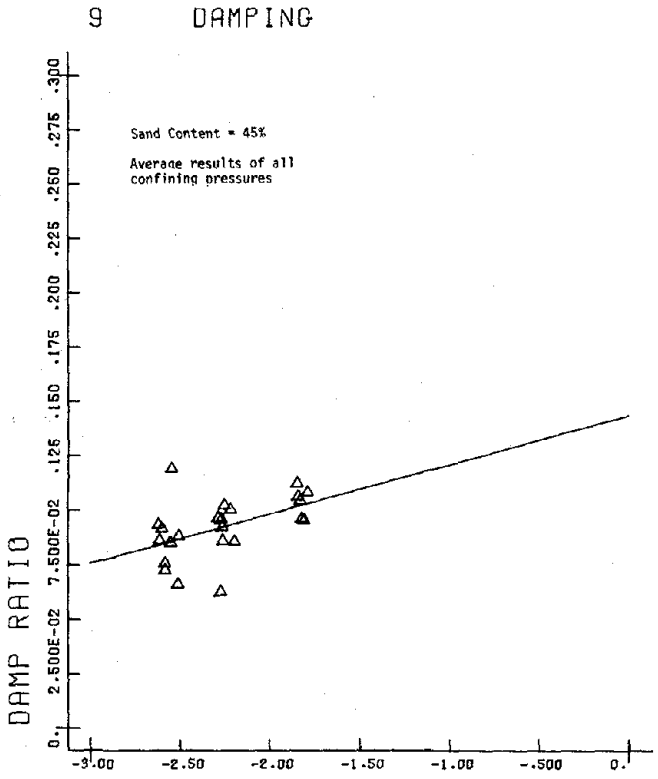

Figure E.22

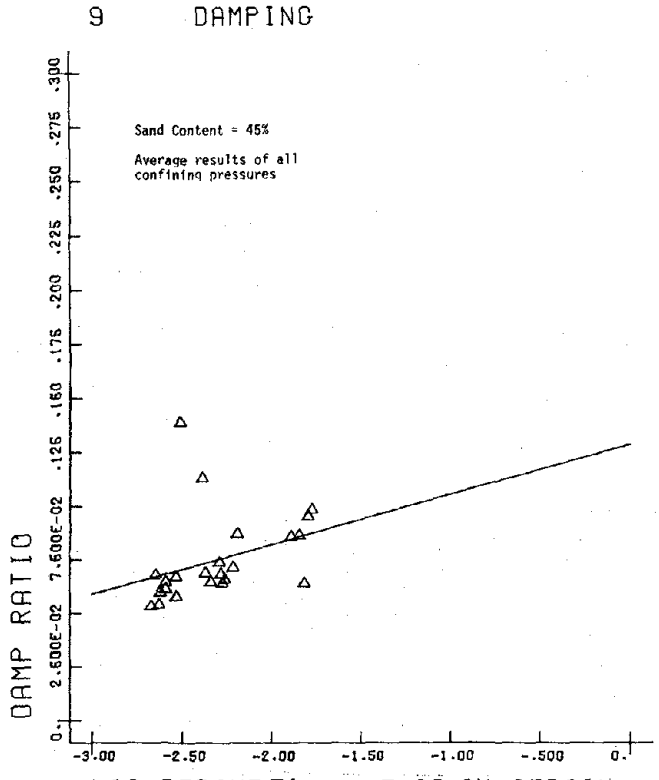

Figure E.23

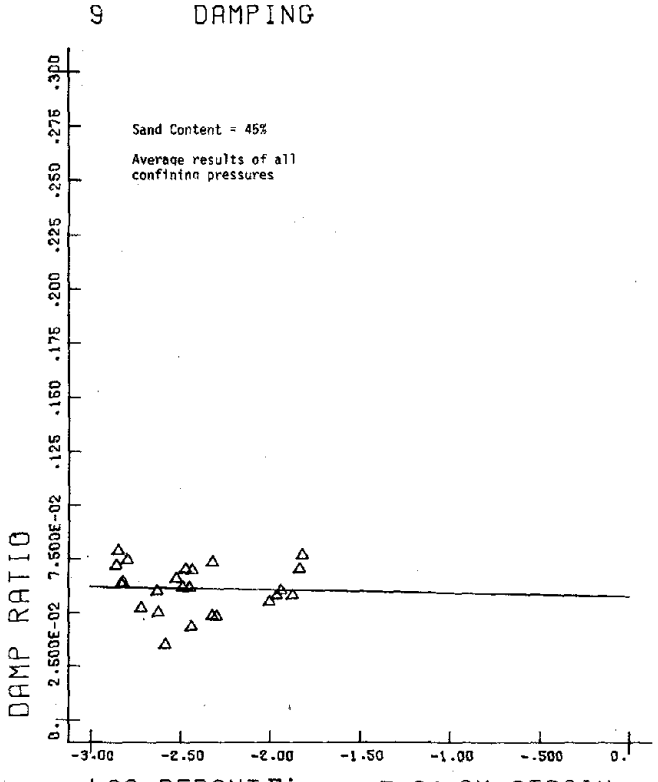

Figure E.24

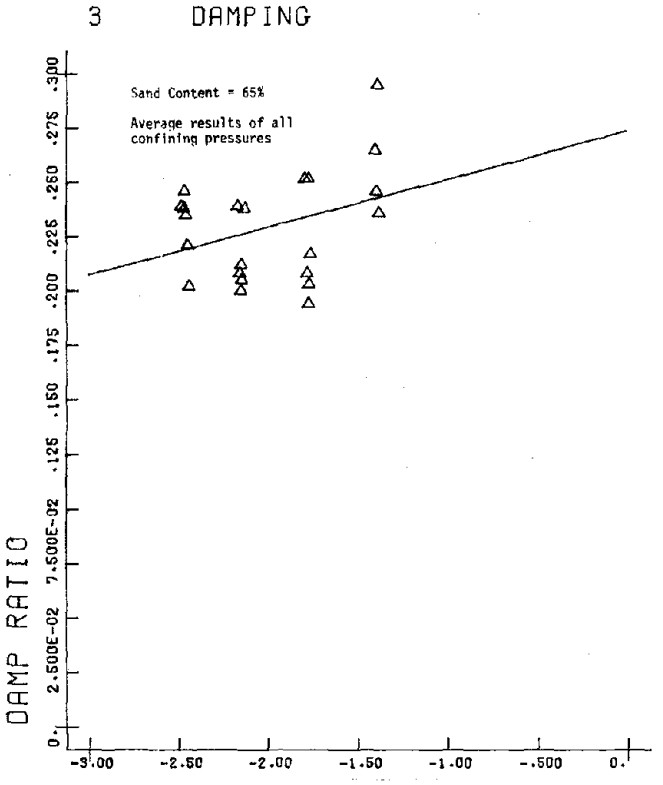

Figure E.25

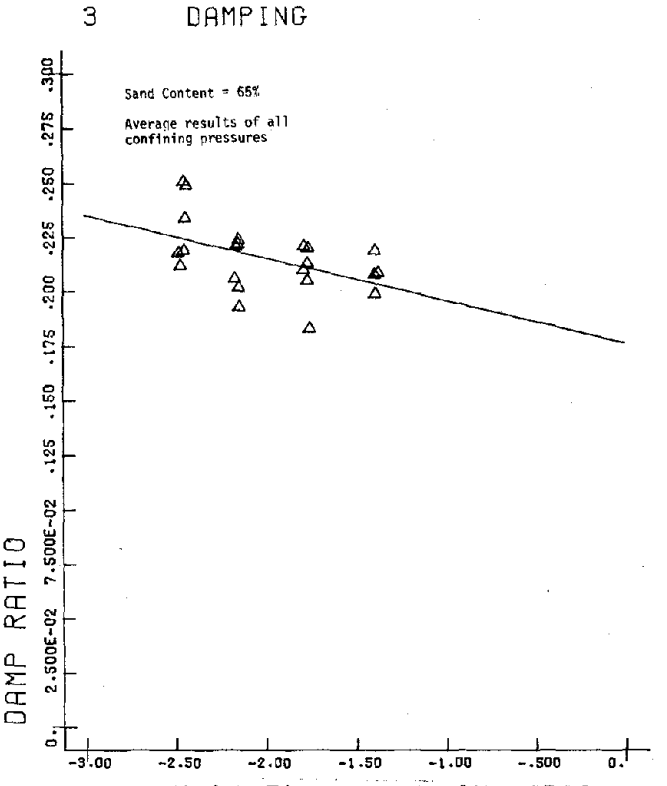

Figure E.26

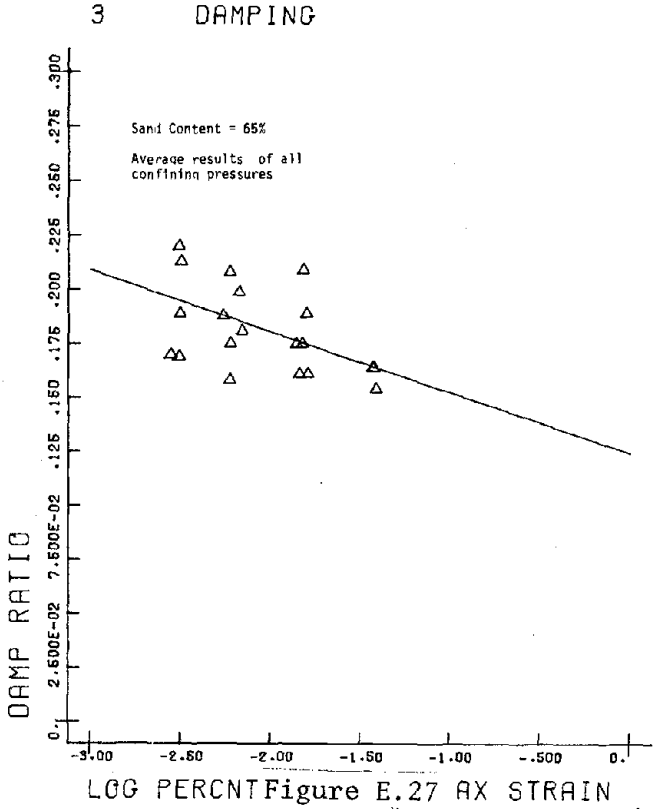

Figure E.27

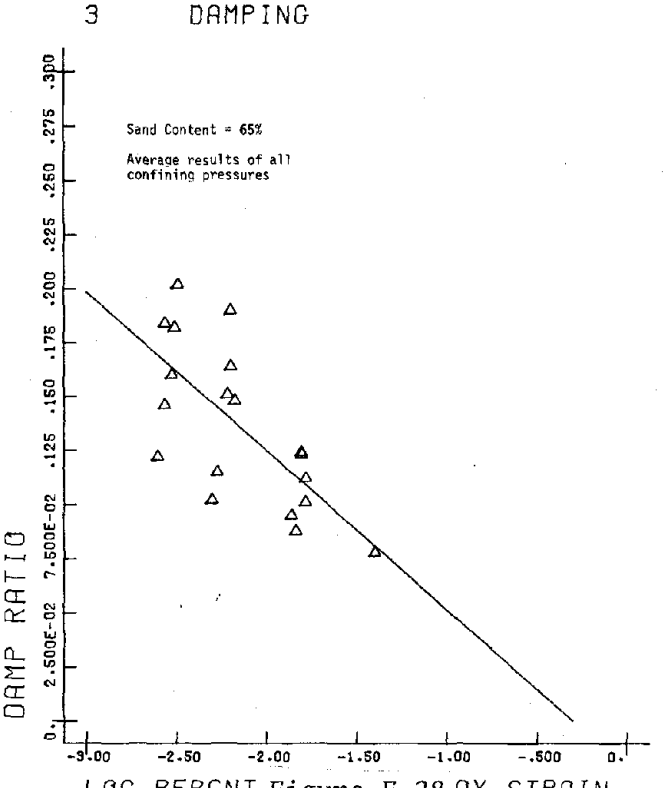

Figure E.28

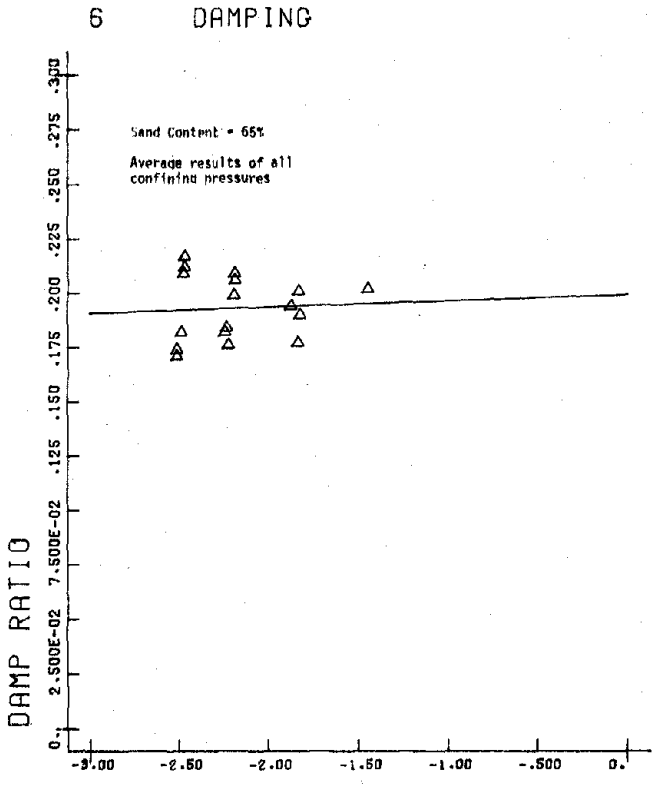

Figure E.29

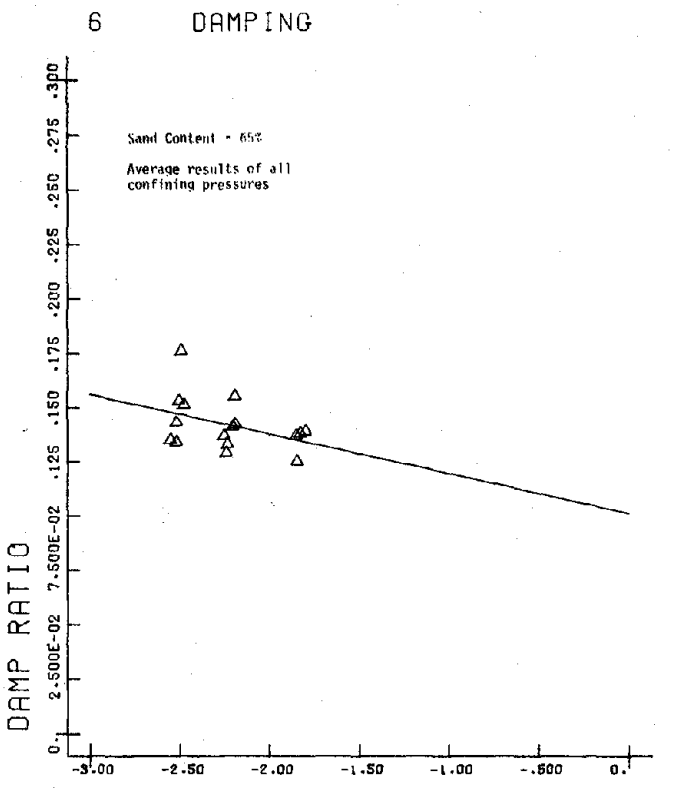

Figure E.30

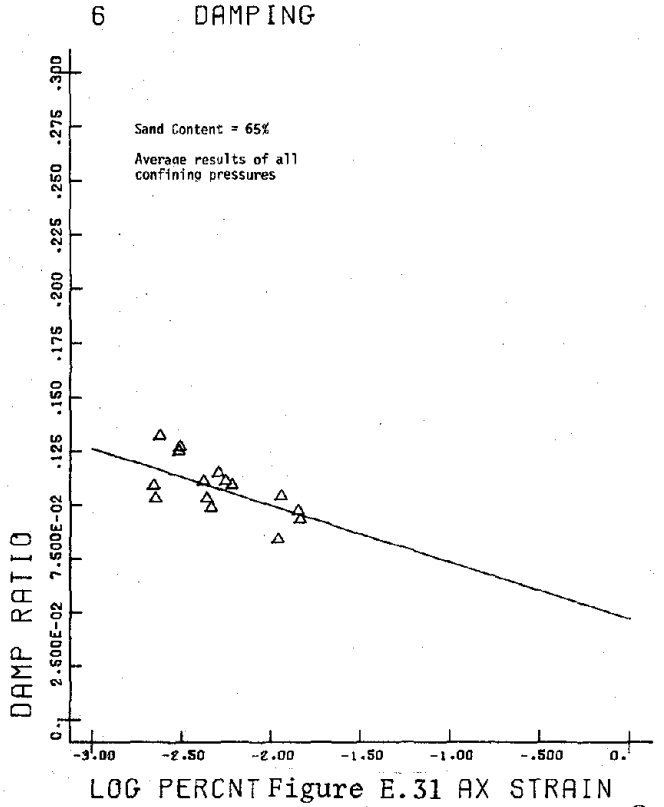

Figure E.31

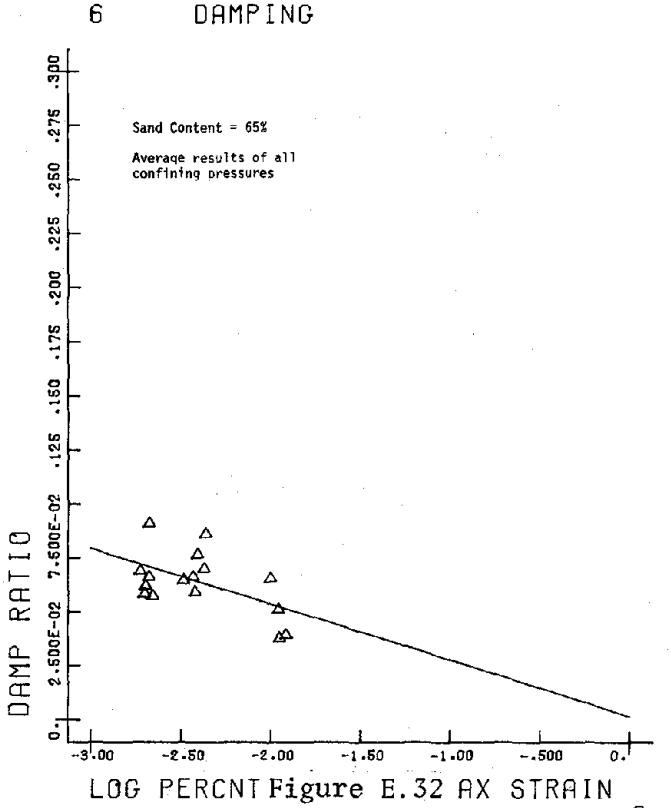

Figure E.32

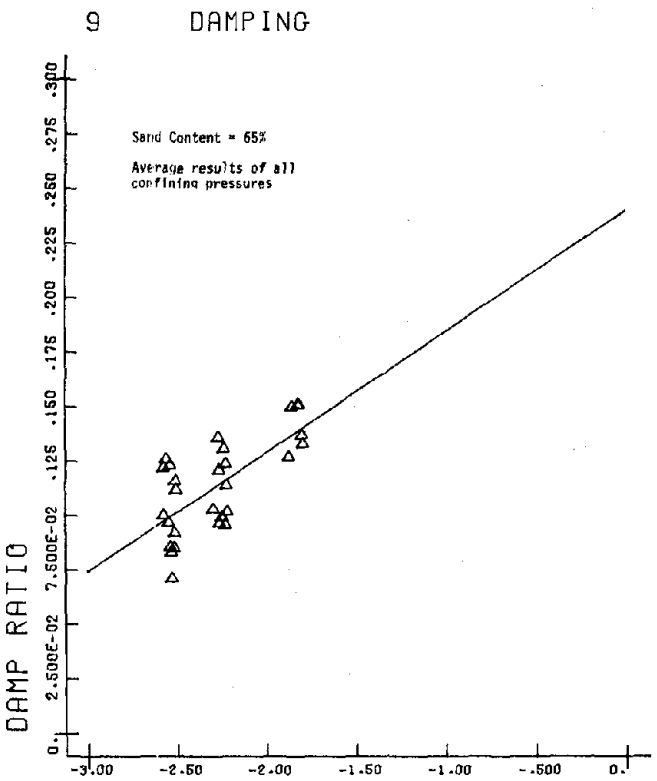

Figure E.33

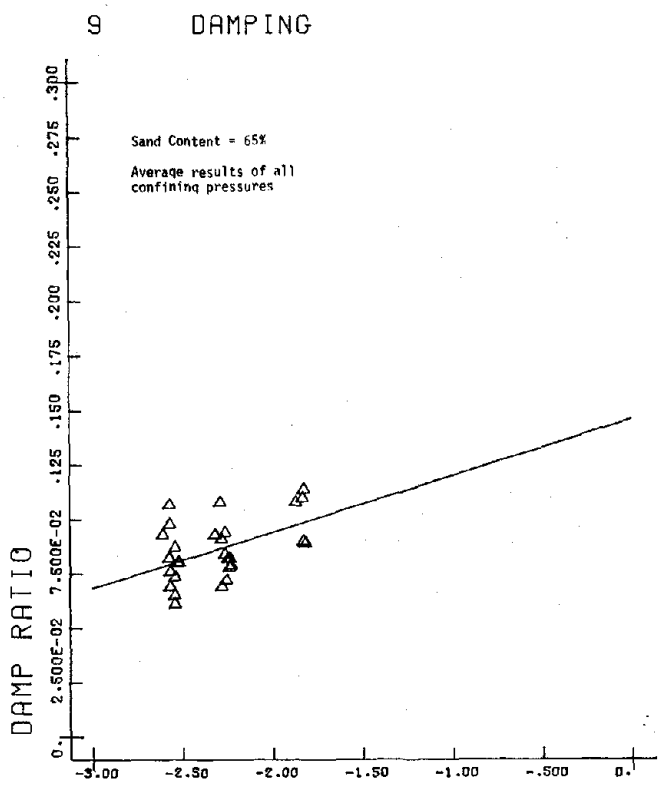

Figure E.34

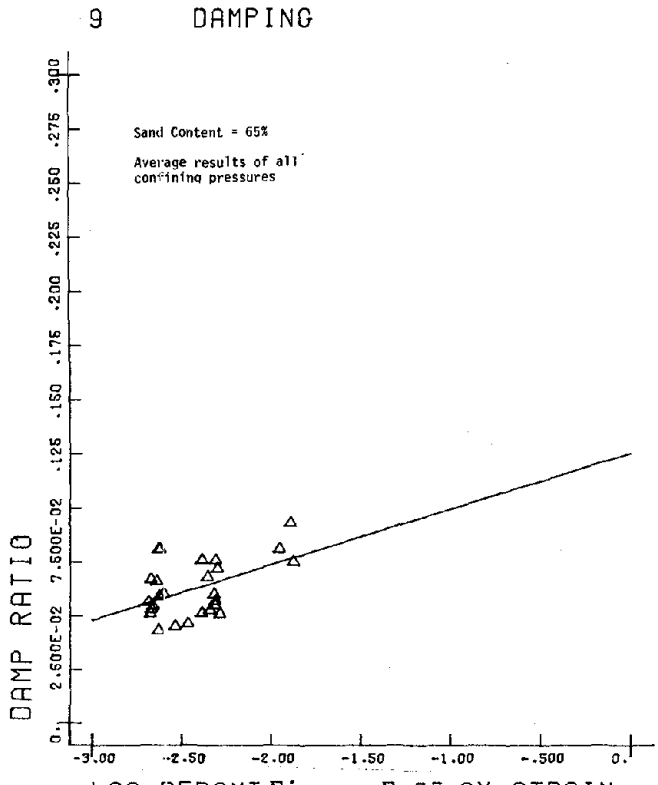

Figure E.35

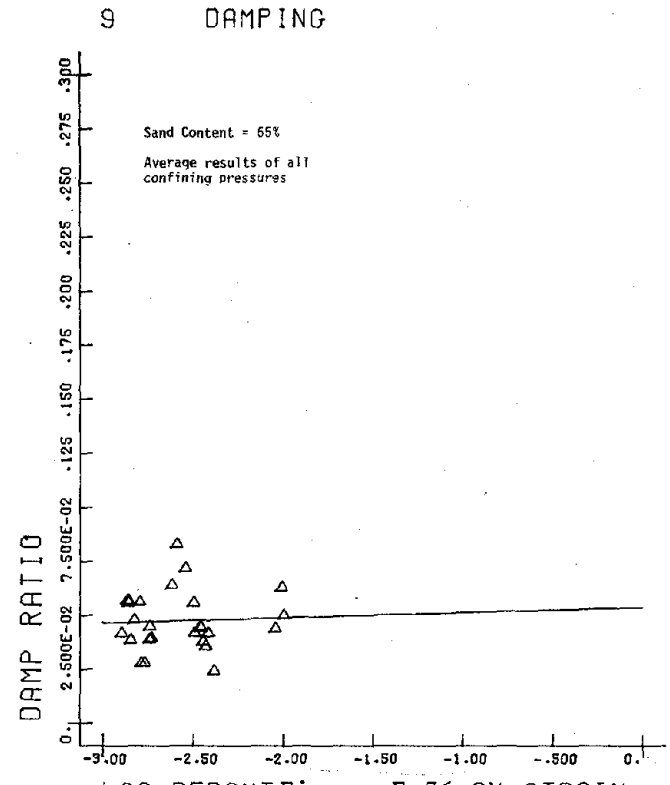

Figure E.36